SPE REPRINT SERIES

NO. 52

GAS RESERVOIR ENGINEERING

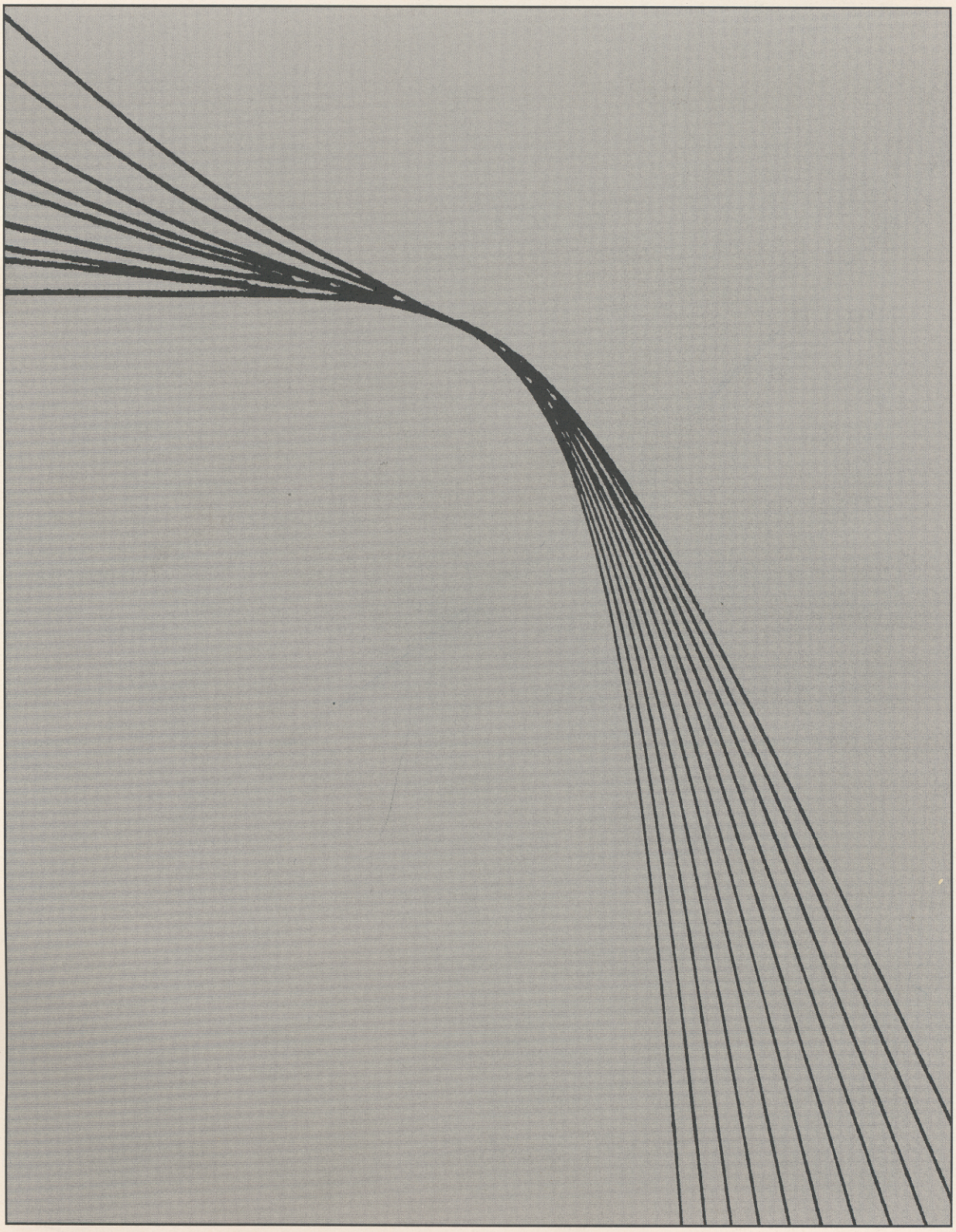

Published by the Society of Petroleum Engineers

SPE REPRINT SERIES NO. 52

GAS RESERVOIR ENGINEERING

1999 Edition

Published by the
Society of Petroleum Engineers
Richardson, Texas

GAS RESERVOIR ENGINEERING SPECIAL REPRINT COMMITTEE

John P. Spivey, Chairman
Holditch-Reservoir Technologies
College Station, Texas

Tom Blasingame
Texas A&M U.
College Station, Texas

Matt Mavor
Tesseract Corp.
Park City, Utah

Lonnie Murphy
DeGolyer and McNaughton
Dallas

Dave Reese
Phillips Petroleum
Bartlesville, Oklahoma

George Voneiff
MGV Energy Inc.
Calgary

ISBN 1-55563-084-7

FOREWORD

At the end of 1996, there were approximately 36,000 dry gas reservoirs in the U.S., according to the U.S. Energy Information Admin. 1997 Annual Energy Review. During 1996, U.S. dry-gas production totaled 18,800 Bcf, while gas reserves were estimated to be 175,000 Bcf. In more than 50 countries worldwide, 81,700 Bcf was produced from reserves estimated at 5,176,000 Bcf. Gas reservoirs may occur at depths of less than 1,000 ft or greater than 25,000 ft. Average reservoir pressure may range from less than 100 to more than 15,000 psi. The economic importance of gas and the technical challenges associated with the limitless variety of its occurrence have led to the development of an extensive body of literature on the topic of gas reservoir engineering.

Because of the breadth of the topic, the committee found it necessary to limit the scope of this volume. Three recent reprint volumes, SPE Reprint Volume 35, *Coalbed Methane* (1992), SPE Reprint Volume 45, *Production From Fractured Shales* (1996), and SPE Reprint Volume 50, *Gas Storage* (1999), cover special topics in gas reservoir engineering. We felt that these topics were more than adequately covered and did not need to be included in the present volume. We also decided not to include papers on gas-condensate reservoirs; this topic is the focus of an upcoming reprint volume.

In selecting the 20 papers to be included in this volume, the committee considered relevance, technical content, utility, and readability. The papers were also selected with a view to covering a variety of aspects of gas reservoir engineering. Finally, in addition to the topical papers, the committee selected a number of case histories to illustrate the application of technology to specific field situations.

In addition to the 20 papers reprinted in full, this volume includes an Annotated Bibliography with 39 papers and a bibliography with more than 200 papers.

On a personal note, I would like to thank all the committee members for their work and patience throughout this project. I would like to express special thanks to Dave Reese and his colleague Ram Jayaraman at Phillips Petroleum for conducting the initial literature search and to Ann Callaway, librarian for Holditch-Reservoir Technologies, for her work on this project.

John P. Spivey
Chairman

CONTENTS

Rock and Fluid Properties

An Analysis of High-Velocity Gas Flow Through Porous Media 7
by Abbas Firoozabadi and Donald L. Katz, *JPT* (February 1979) 211.

A Laboratory Study of Low-Permeability Gas Sands 13
by F.O. Jones and W.W. Owens, *JPT* (September 1980) 1631.

Compressibility Factors for Naturally Occurring Petroleum Gases 23
by L.D. Piper, W.D. McCain Jr., and J.H. Corredor, paper SPE 26668 presented at the 1993 SPE Annual Technical Conference and Exhibition, Houston, 3–6 October.

Material Balance and Water Influx

The Effect of Water Influx on p/z-Cumulative Gas Production Curves 34
by J.R. Bruns, M.J. Fetkovich, and V.C. Meitzen, *JPT* (March 1965) 287.

Depletion Performance of Layered Reservoirs Without Crossflow 39
by Michael J. Fetkovich, Mark D. Bradley, Adonna M. Works, and Thomas S. Thrasher, *SPEFE* (September 1990) 310; *Trans.*, AIME, **289**.

Application of a General Material Balance for High-Pressure Gas Reservoirs 48
by Michael J. Fetkovich, Dave E. Reese, and C.H. Whitson, paper SPE 22921 presented at the 1991 SPE Annual Technical Conference and Exhibition, Dallas, 6–9 October.

Using Short-Term Pressure Buildup Tests for Reserves Estimation in Tight Gas Reservoirs 59
by S.A. Sullivan, S.W. Poston, and L.D. Piper, paper SPE 17707 presented at the 1988 SPE Gas Technology Symposium, Dallas, 13–15 June.

Application of Variable Formation Compressibility for Improved Reservoir Analysis 66
D.P. Yale, G.W. Nabor, J.A. Russell, H.D. Pham, and Mohamed Yousef, paper SPE 26647 presented at the 1993 SPE Annual Technical Conference and Exhibition, Houston, 3–6 October.

Deliverability and Pressure Transient Testing

Analysis of Modified Isochronal Tests To Predict the Stabilized Deliverability Potential of Gas Wells Without Using Stabilized Flow Data 82
by G.S. Brar and K. Aziz, *JPT* (February 1978) 297; *Trans.*, AIME, **265**.

Discussion of Analysis of Modified Isochronal Tests To Predict the Stabilized Deliverability Potential of Gas Wells Without Using Stabilized Flow Data 90
by Fred H. Poettmann, *JPT* (October 1986) 1122.

Authors' Reply to Discussion of the Analysis of Modified Isochronal Tests to Predict the Stabilized Deliverability Potential of Gas Wells Without Using Stabilized Flow 93
by G.S. Brar and L. Mattar, *JPT* (January 1987) 89.

Further Discussion of The Analysis of Modified Isochronal Tests to Predict the Stabilized Deliverability of Gas Wells Without Using Stabilized Flow Data 97
by S.B. Hinchman, H. Kazemi, and F.H. Poettmann, *JPT* (January 1987) 93.

Applying Gas-Well Load-Up Technology 101
by Steve B. Coleman, Hartley B. Clay, David G. McCurdy, and H. Lee Norris III, *JPT* (March 1991) 344; *Trans.*, AIME, **291**.

Characterization of Tight Reservoirs 107
by W.J. Lee and C.W. Hopkins, *JPT* (November 1994) 956; *Trans.*, AIME, **297**.

Estimating Formation Permeability From Single-Point Flow Data 116
By W.J. Lee, T.B. Kuo, S.A. Holditch, and D.A. McVay, paper SPE/DOE/GRI 12847 presented at the 1984 SPE/DOE/GRI Unconventional Gas Recovery Symposium, Pittsburgh, Pennsylvania, 13–15 May.

Production Data Analysis

Evaluation and Performance Prediction of Low-Permeability Gas Wells Stimulated by Massive Hydraulic Fracturing 127
by R.G. Agarwal, R.D. Carter, and C.B. Pollock, *JPT* (March 1979) 362; *Trans.*, AIME, **267**.

Type Curves for Finite Radial and Linear Gas-Flow Systems: Constant-Terminal-Pressure Case 142
by Robert D. Carter, *SPEJ* (October 1985) 719.

Useful Concepts for Decline-Curve Forecasting, Reserve Estimation, and Analysis 152
by M.J. Fetkovich, E.J. Fetkovich, and M.D. Fetkovich, *SPERE* (February 1996) 13.

Gas Reservoir Decline-Curve Analysis Using Type Curves With Real Gas Pseudopressure and Normalized Time 168
by M.L. Fraim and R.A. Wattenbarger, *SPEFE* (December 1987) 671.

Case Histories

Accelerated Blowdown of a Strong Water-Drive Gas Reservoir 180
by J.L. Lutes, C.P. Chiang, R.H. Rossen, and M.M. Brady, *JPT* (December 1977) 1533.

A Tight Gas Field Study: Carthage (Cotton Valley) Field 186
by W.D. McCain, G.W. Voneiff, E.R. Hunt, and M.E. Semmelbeck, paper SPE 26141 presented at the 1993 SPE Gas Technology Symposium, Calgary, 28–30 June.

3-D Reservoir Simulation Results of a 25-Square-Mile Study Area in the Kansas Hugoton Gas Field 201
by R.J. Oberst, P.P. Bansal, M.F. Cohen, and T.C. Ryan, paper SPE 27931 presented at the 1994 SPE Mid-Continent Gas Symposium, Amarillo, Texas, 22–24 May.

Reserves Determination Using Type-Curve Matching and EMB Methods in the Medicine Hat Shallow Gas Field 212
by S.L. West and P.J.R. Cochrane, paper SPE 28609 presented at the 1994 SPE Annual Technical Conference and Exhibition, New Orleans, 25–28 September.

Annotated Bibliography 219

Bibliography 225

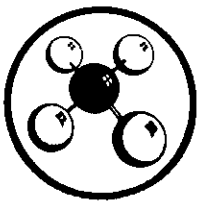

An Analysis of High-Velocity Gas Flow Through Porous Media

Abbas Firoozabadi, Abadan Institute of Technology
Donald L. Katz, SPE-AIME, U. of Michigan

Introduction

Much research has been conducted to understand flow through porous media. Regarding high velocity, suitable correlations and nomenclature are the subject of controversy because of different views on the mechanism causing pressure drop.[1-14]

This study tries to improve the understanding of high-velocity flow through porous media. Using available data and this research, the best correlation is sought to permit the calculation of high-velocity flow based on permeability, porosity, and character of the rock. We hope that a nomenclature can be suggested that is acceptable to both reservoir engineers and fluid mechanics research scientists. The results should be useful for improving correlations of gas-well flow data and for predicting well flow from core data, fluid properties, and specified conditions.

Early Work on High-Velocity Flow

Fancher *et al.*[1] measured pressure drop during flow through a large number of unconsolidated and consolidated porous media. They correlated the data by using the friction factor and Reynolds number, with grain diameter as a characteristic length. They showed that for flow through porous media, an increased pressure drop at high velocity is beyond that proportional to velocity. Data taken at the USBM[2] were correlated using a quadratic equation of pressure drop with the second term of velocity to the nth power. Green and Duwez[4] increased the understanding of high-velocity gas flow data when studying sintered metals. They adapted the equation with a velocity term squared that Forchheimer[15] had developed:

$$-\frac{dp}{dL} = \frac{\mu v}{k} + \beta \rho v^2. \quad \ldots\ldots\ldots\ldots\ldots\ldots (1)$$

Cornell and Katz[5,20] measured the porosity, permeability, and β factors for cores, resulting in a correlation of β with permeability.[16] The term β was called a "turbulence factor," but the expression was unacceptable to several researchers.[14]

Language Used in Literature

Space limitations prohibit quoting completely the language used when describing the mechanism that consumes energy at more than a linear rate with velocity. The term used in flow equations (generally the β in a quadratic flow equation) also has been given various names according to the author's view of the flow mechanism.

Table 1 assembles selected typical titles and statements quoted from published works. After the flow mechanism has been reviewed, a more appropriate language will be submitted to agree with the concepts developed here.

Mechanism for Consumption of Pressure Drop Energy

Here, we try to understand the mechanism by which

0149-2136/79/0002-6827$00.25

Darcy's law is inadequate for representing high-velocity gas flow in porous media, such as near the wellbore. An analysis of pressure lost during flow through conduits of alternating cross sections suggests more appropriate words for describing the mechanism for energy loss and terms in the flow equation. Updated correlations are presented for the coefficient of the velocity-squared term.

increased velocity results in a pressure drop greater than that proportional to velocity increase. The mechanism of consuming pressure drop energy in pipe flow is well understood. In Fig. 1, the cylinders of fluid are flowing at different velocities. Work energy overcomes the longitudinal shear stresses between the cylinders flowing at different velocities. In the case of unidirectional flow for a constant cross section, there is a single term in the resistance equation that includes the velocity of the fluid. The increased energy consumed at higher velocities is directly proportional to the velocity increase for streamline flow, as shown by Poiseuille's law.

TABLE 1—LANGUAGE USED IN LITERATURE FOR HIGH-VELOCITY GAS FLOW

Reference	Comments
Fancher *et al.*[1] (1933)	". . . the flow of fluids through these porous materials closely resembles that through pipes; that there is a condition of flow in porous systems which resembles viscous flow, another which corresponds to turbulence."
Elenbaas and Katz[3] (1948)	"A Radial Turbulent Flow Formula"
Green and Duwez[4] (1951)	"The inertial coefficient β . . . may be interpreted as a measure of the tortuosity of the flow channels, perhaps as an average curvature of the streamline determining the acceleration experienced by the fluid."
Hubbert[17] (1956)	". . . we have seen that the cause of the failure of Darcy's Law is the distortion that results in the flow lines when the velocity is great enough that the inertial force become significant."
Tek[6] (1957)	"The generalized Darcy equation may be referred to as the 'non-Darcy flow' regime. The transition from Darcy to non-Darcy flow is a gradual one."
Katz *et al.*[8] (1959)	"If one includes extra motion of the fluid to consume the extra pressure loss, then the term 'turbulent flow' here is justified."
Houpeurt[7] (1959)	". . . we do not think, the flow can be really turbulent . . . , we consider the kinetic energy losses are responsible for the deviation . . . from Darcy's Law."
Tek *et al.*[23] (1962)	"The Effect of Turbulence on Flow of Natural Gas. . . ."
Swift and Kiel[18] (1962)	"Prediction of Gas-Well Performance Including the Effect of Non-Darcy Flow" "Analysis of data . . . to give direct "in situ" information for . . . turbulence or non-Darcy coefficients."
Wright[10] (1968)	". . . Four regimes of flow for water in an unconsolidated bed. 1) a laminar regime 2) a steady inertia regime 3) a turbulent transition regime 4) a fully turbulent regime."
Gewers and Nichol[12] (1969)	"Gas Turbulence Factor in a Microvugular Carbonate."
Geertsma[14] (1974)	"Coefficient of Inertial Resistance" "The flow regime of concern is usually fully laminar. The observed departure from Darcy's Law is the result of convective accelerations and decelerations of the fluid particles on their way through the pore space."

Now consider the flow in the interstices of a porous solid, as idealized in Fig. 2. In flow through pores, there are two variations from the horizontal cylindrical flow. First, the cross section of the flow channel is increasing and decreasing alternately. Then, there is the displacement from a straight line when moving through a network of pores. Each deviation from the direction of fluid movement now has two components of the viscous resistance: (1) longitudinal shear *e-f* in the direction of flow and (2) longitudinal tension or a normal stress component *f-g* during the expansion and, correspondingly, *i-j* and *h-i* during contractions, commonly written as Eqs. 2 and 3.[19]

$$\tau_{xy} = \mu \left(\frac{\partial v_y}{\partial y} + \frac{\partial v_x}{\partial x} \right)$$

longitudinal shear stress, ... (2)

$$\sigma_{xx} = \mu \left(\frac{\partial v_y}{\partial x} + \frac{\partial v_x}{\partial y} \right)$$

longitudinal tension stress. . . . . (3)

Now consider the effect of velocity on the resistances. The flowlines with increased velocity are no longer constant in length and are believed to increase the shear and tension areas with increased velocity (Figs. 3a and 3b). At still higher velocities, separation or reversed flow occurs in the enlarged cross sections to increase the viscous resistance (Fig. 3c). Here, the recirculating portion may be considered laminar. All these transverse effects are characteristics of irregular alternating cross-section flow paths and are not present in cylinders.

Porous media (such as sandstones or carbonates with only matrix porosity and free from irregular solution processes) no doubt are always in the regimes in Figs. 3a and 3b. In some porous solids (such as vugular carbonates, reefs, and conglomerates), there are interstices large enough to allow the regimes in Fig. 3c and even in Fig. 3d to be described as turbulence. A student working with Katz observed that this turbulence occurred in pipes when an ink filament was used in a liquid flowing at increasing velocities through a bed of glass beads with about 3/16 in. diameter. Regarding porous solids characterized by Figs. 3a and 3b, the term turbulence is unacceptable. However, flow through such

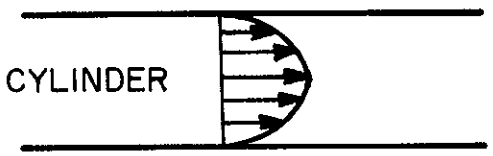

Fig. 1—Flow in a cylindrical conduit.

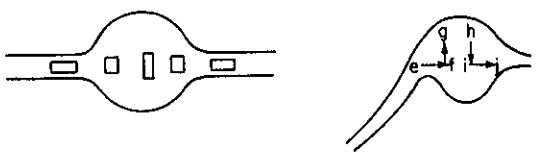

(a) Change of shape of fluid element.

(b) Longitudinal shear and longitudinal tension forces.

Fig. 2—Flow in an idealized pore.

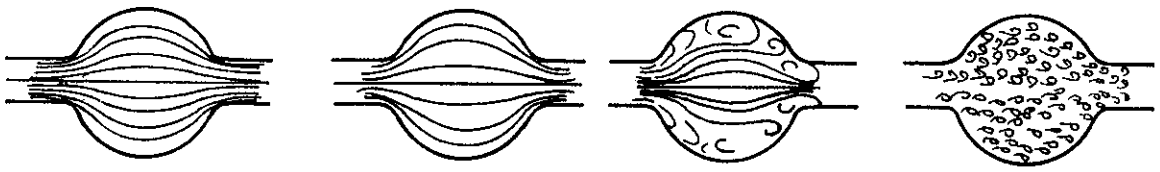

Fig. 3—Idealized flow through alternating cross sections.

solids has a continuous function between pressure drop and flow rate since there is no change in mechanism between low and high flow rates.

Mathematical Representation of High-Velocity Flow

When correlating the data for the high-velocity water flow through porous media, Forchheimer[15] found that a relationship of the type presented by Eq. 1 described his data best. In some cases another velocity term seemed better:

$$-\frac{dp}{dL} = \frac{\mu v}{k} + \beta\rho v^2 + \gamma\rho^2 v^3. \quad \ldots\ldots\ldots\ldots (4)$$

To use Eq. 1 for gases, it should be changed to the following form.[8]

$$\frac{(p_1^2 - p_2^2)Mg_c}{2\mu zRTGL} = \frac{1}{k} + \frac{\beta u}{\mu}. \quad \ldots\ldots\ldots\ldots (5)$$

A plot of $(p_1^2 - p_2^2)Mg_c/2\mu zRTGL$ vs u/μ results in a straight line for many cores. The slope of the straight line is β; the inverse of the intercept with the y axis is the permeability, k. In many cases, Eq. 5 deviates from a straight line. This deviation is attributed to two factors.

One factor, which appears predominantly in the lower portion of the line for flow of gases, results from the slip effect.[21] The slip could be interpreted as the bouncing of the gas molecules on the wall at low pressures when the mean free path of the molecules becomes the same order of magnitude as the pore diameter. In low-velocity gas flow, where the Darcy equation describes the flow behavior, Klinkenberg[21] demonstrated that the slip effect can be taken into the Darcy equation by Eq. 6:

$$k_a = k\left(1 + \frac{b}{\bar{p}}\right) \quad \ldots\ldots\ldots\ldots\ldots\ldots (6)$$

The other factor causing deviation from straight-line behavior results from the inadequacy of Eq. 1 to represent high-velocity gas flow. In other words, in addition to the v^2 quadratic term, a third term of the form $\gamma\rho^2 v^3$ is necessary, as noted by Forchheimer, for high-velocity water flow. One might also represent this type of deviation by substituting an exponent n instead of 2 for v in the second term, as was done by Johnson and Taliaferro.[2]

Permeability Limit at Zero or Low Velocity

From the analysis of the mechanism of energy consumption for fluid flowing in alternating size conduits and from Eq. 1, one would expect that the high-velocity term, $\beta\rho v^2$, should apply over the entire range of velocity. To illustrate that the data do not deny this statement, the data are plotted to demonstrate that a constant value of permeability in reality is a limiting value.

Fig. 4 shows data on a consolidated sandstone with nitrogen flowing at high pressure at both outlet and inlet, as plotted by Iffly[22] according to an equation similar to Eq. 5. The straight line represents the prior concept of Darcy's law and the curve represents measured values. Accepting that the curve becomes tangent to the line at zero flow rate demonstrates that the constant value of k applies at the limit of zero velocity. Forchheimer's data on water describe a similar relationship. This behavior would be expected when the velocity is the variable that changes the flowline length (Figs. 2 and 3).

In normal measurements of core permeability (in millidarcies), the results are valid as the limiting value since $\beta\rho v^2$ is less than the experimental error when measuring the flow rate or pressure drop. When gases near atmospheric pressure are used to measure permeability, the slip may err more than when neglecting the velocity effect.

Nomenclature

The introduction of the β factor by Cornell and Katz[5] as the turbulence factor, although defined as "extra fluid motion consuming extra energy," was unacceptable to many researchers. This concept overlooked the stages of progress for the growth of shear and tension components in laminar mode before random movement that is typical of turbulence. Equally valid objections are made now to the terms "non-Darcy" and "inertial" flow.

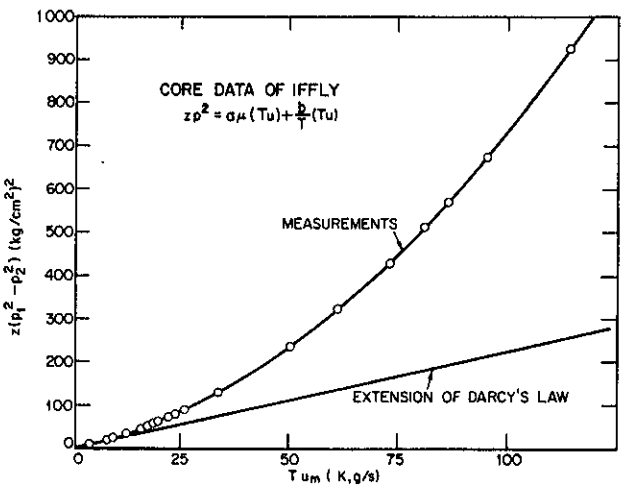

Fig. 4—Pressure drop and flow rate data of Iffly[22] illustrating that Darcy's law applies as a limit. Nitrogen flow through a sandstone of 21.4% porosity is 73.5 md.

Since there is a continuous function between pressure drop and flow rate for porous media with alternating cross sections in the flow path, the term "non-Darcy flow" is out of place because it implies two different flow mechanisms. The same can be said for using "Darcy flow" at low velocities and "inertia regime" for higher velocities; the inertia effects are always present. There is a spectrum of velocities in the various flow channels at a given flow rate. Any implication that there is one type of flow mechanism at low velocities and another regime at high velocities (short of true turbulence) disregards the nature of the mechanism by which the pressure-loss energy is consumed in porous media.

A simple concept is to characterize the flows as "low velocity" and "high velocity" to distinguish conditions for which $\beta\rho v^2$ may be ignored and where it should be used. High velocity becomes the velocity for which neglecting $\beta\rho v^2$ gives an error in computed pressure drop more than the unreliability of the permeability measurement.

Continued use of the term "Darcy flow" to characterize low velocity is recommended. This concept is ingrained in our past and implies that permeability is constant with a range of pressure drops.

For flow rates where neglecting $\beta\rho v^2$ calculates significantly less pressure drop than would occur, the term "high-velocity flow" would be used to describe the condition.

What to Call β?

The term β is used in flow equations for gas wells and even for high flow-rate oil wells. Objections to the turbulence factor and inertial coefficient are clear; they denote changes in flow regimes.

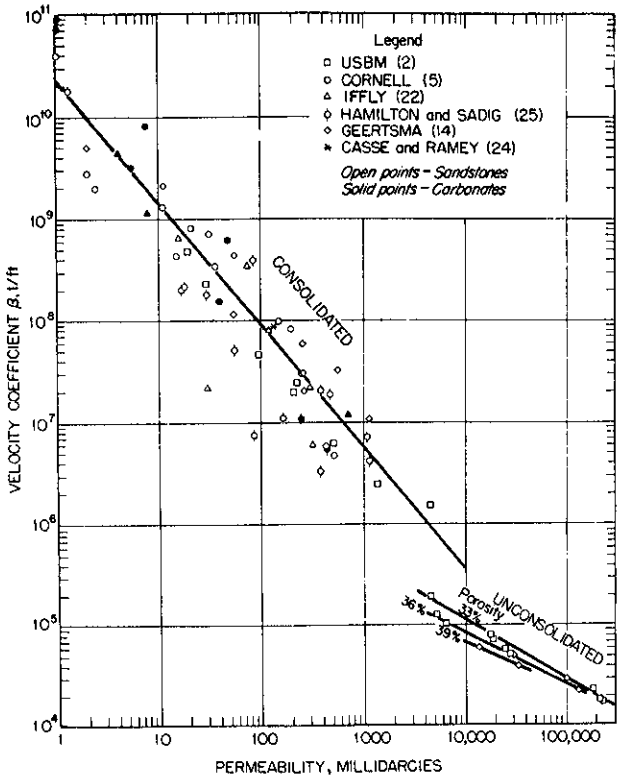

Fig. 5—Correlation of β from Eq. 9.

TABLE 2—CORRELATIONS OF VELOCITY COEFFICIENTS (β)

Correlation Equation Tested	Standard Error of Estimate for β	Equation
$\log\beta = m \log k + b$**		7
$m = -1.101$; $b = 23.33$	±0.85*	
$m = -1.201$; $b = 23.83$	±0.89	
$\log\beta = m \log (k^{0.5}\phi^{1.5}) + b$		8
$m = 1.695$; $b = 17.89$	±0.99	
$\log\beta = m \log \left(\frac{1}{k^{0.5}\phi^{5.5}}\right) + b$		9
$m = 0.810$; $b = 12.66$	±2.30	
$\log\beta = m \log (k^{0.1}\phi) + b$		10
$m = 0.991$; $b = 19.92$	±3.07	
$\log\beta = m \log (k\phi) + b$		11
$m = -1.074$; $b = 21.42$	±0.87	
$m = -1.01$; $b = 21.2$	±0.85*	
$\log\beta = m \log \phi + b$		12
$m = -5.148$; $b = 9.70$	±1.91	

*Sandstones only, after values are for all data.
**b = a correlating constant.

The term "velocity coefficient" seems appropriate for β and is used here. When the flow rate or velocity reaches the magnitude where accuracy during prediction requires using the velocity-squared term, the velocity coefficient is required. Should high velocity cause the data plotted according to Eq. 5 to be a curve, Eq. 4 applies and a value of γ is found.

Correlation of Data for Velocity Coefficient, β

Six sets of data were selected for correlating the velocity coefficient with permeability or porosity. The data were on dry cores with gas-flow measurements that were believed to eliminate the Klinkenberg slip interference. Table 2 presents the relationships used in regression analysis of the data. The constants in the equations are given, and the standard error of deviation for predicting β is listed. From this analysis, the data were plotted following the preferred relationships in Figs. 5 and 6. The difference between the correlation for sandstones only and all data including carbonates was nominal. Therefore, only one relationship is given for all data.

The data for unconsolidated sands are plotted in Fig.

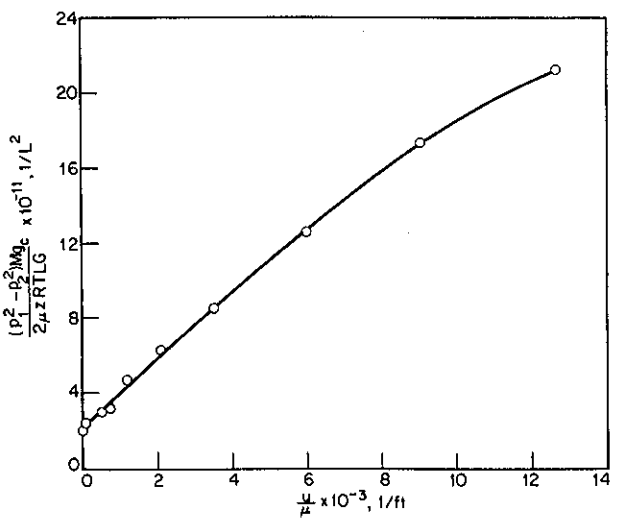

Fig. 6—Correlation of β from Eq. 13.

TABLE 3—ADDED FLOW DATA ON SANDSTONE CORES

Rock	k (md)	ϕ (fraction)	$\beta\left(\frac{1}{ft}\right)$	$k\phi$	Correlation Value of β Read from Fig. 6	Correlation Value of β Read from Fig. 5 (k only)
St. Peter	2,087	0.267	3.17×10^{6}	557.	2×10^{6}	2.3×10^{6}
	1,158	0.266	7.3×10^{6}	308.	4×10^{6}	5×10^{6}
	614	0.24	1.59×10^{7}	147.	9×10^{6}	9×10^{6}
	178	0.201	4.94×10^{7}	36.	4×10^{7}	5×10^{7}
Jordan	248	0.20	3.94×10^{6}	50.*	3×10^{7}	3×10^{7}
	811	0.233	7.33×10^{7}	189.*	7×10^{6}	7×10^{6}
	1,232	0.214	4.46×10^{6}	264.	5×10^{6}	4.5×10^{6}
	63	0.217	1.05×10^{8}	13.7	1.2×10^{8}	1.5×10^{8}
Lower Franconia	16	0.183	2.24×10^{9}	2.9	5.5×10^{8}	8×10^{8}
	1,049	0.255	3.46×10^{6}	268.	5×10^{6}	5×10^{6}
	117	0.211	1.17×10^{8}	24.7	6×10^{7}	8×10^{7}
Mt. Simon	40	0.142	3.56×10^{8}	5.7	3×10^{8}	2.7×10^{8}
	240	0.153	9.38×10^{7}	37.	3×10^{7}	3×10^{7}
	665	0.255	1.24×10^{7}	170.	8×10^{6}	9×10^{6}

*Deviation from correlation larger than by previous data.
Data taken by Core Laboratories Inc. and transmitted to authors by Dan Slagle of Northern Natural Gas Co.

5, the k vs β chart. The correlation lines with porosity as the parameter definitely have slopes quite different from the consolidated data. The correlating curve in Fig. 5 is similar to that presented earlier without the porosity parameter.[8] If porosity is to be a parameter, Fig. 6 is preferred over the porosity lines of Janicek and Katz.[16]

Casse and Ramey[24] note the absence of temperature effect on β for a Berea sandstone. Wong[13] took data on limestone cores and found curvature using Eq. 5; the cores contained connate liquid. Johnson and Taliaferro[2] (Fig. 7) also obtained curvature for data on a dry limestone core. To represent these data, a second term is needed, such as $\gamma\rho^2v^3$ shown in Eq. 4, to represent pressure drop. Then, β could be the first velocity coefficient and γ the second velocity coefficient.

New Data

Since this paper was written, more data were found in the files for 14 cores (Table 3). Twelve of the points scattered in Figs. 5 and 6 were not unlike previous data. Two points were beyond the normal band of point scatter. The data included six to eight data points each, were plotted in the manner of Cornell,[5] and reported k corrected for Klinkenberg effect.

Complexity of Reservoir Flow

The influence of reservoir heterogeneity, fractures, infiltration at the wellbore, and presence of liquids all discount the value of simple flow calculations with Eq. 1. However, such calculations are valuable when designing aquifer gas storage reservoirs. Also, well flow data may be used to obtain in-situ β values. Such data provide some measure of reservoir deviations from the model using core data alone and allow evaluation of the reservoir condition.

Conclusions

A greater variety of high-velocity flow data on oil and gas reservoir rocks would be helpful. The range of predictions could be evaluated better and could be related to well flow characteristics.

We hope the nomenclature used here will be acceptable to both practicing engineers and fluid flow specialists and will help establish language and terms that will eliminate future misunderstandings.

The correlation of β used during the past 20 years has been generally representative of the character of reservoir rocks. The correlations given here demonstrate that more data show only modest improvement in the correlation curve. Additional data show that half the data may fit the correlation, while individual cores may deviate tenfold.

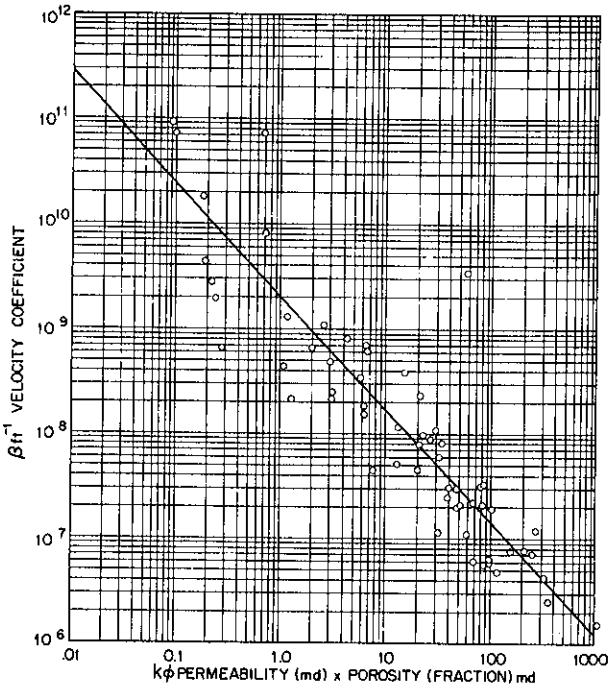

Fig. 7—Plot according to Eq. 7 of USBM data[2] for a limestone core.

Nomenclature

a = a constant
A = cross-sectional area, L^2
b = slip coefficient, m/Lt^2
g_c = unit conversion factor
G = gas gravity, M/29
k = absolute permeability, L^2
k_a = apparent permeability, L^2
L = length, L
m = a correlating constant
M = molecular weight
p = pressure, m/Lt^2
p_1 = inlet pressure, m/Lt^2
p_2 = outlet pressure, m/Lt^2
$\bar{p}$ = arithmetic average pressure, m/Lt^2
R = universal gas constant
T = absolute temperature
u = mass velocity, m/L^2t
v_x = velocity in the x direction, L/t
v_y = velocity in the y direction, L/t
x = coordinate
y = coordinate
z = compressibility factor
β = first velocity coefficient, 1/L
γ = second velocity coefficient, Lt/m
ρ = density, m/L^3
τ = longitudinal shear stress, m/Lt^2
σ = longitudinal tension stress, m/Lt^2
ϕ = porosity

Acknowledgments

The assistance of C. S. Yih, U. of Michigan Mechanics Dept., in clarifying and understanding pressure losses during flow through porous media is appreciated. The correlations of β in Table 3 were performed by J. Azuonye Ironkwe.

References

1. Fancher, G. H., Lewis, J. A., and Barnes, K. B.: "Some Physical Characteristics of Oil Sands," *Bull. 12*, Pennsylvania State C., Minerals Industries Experiment Station, University Park (1933) 65.
2. Johnson, T. W. and Taliaferro, D. B.: "Flow of Air and Natural Gas Through Porous Media," Technical Paper 592, USBM (1938).
3. Elenbaas, J. R. and Katz, D. L.: "A Radial Turbulent Flow Formula," TP 2304, AIME (Jan. 1948) 25-40.
4. Green, L. and Duwez, P.: "Fluid Flow Through Porous Metals: *J. Appl. Mech.* (March 1951) **18,** 39.
5. Cornell, D. and Katz, D. L.: "Flow of Gases Through Consolidated Porous Media," *Ind. and Eng. Chem.* (Oct. 1953) **45,** 2145.
6. Tek, M. R.: "Development of a Generalized Darcy Equation," *Trans.*, AIME (1957) **210,** 376-377.
7. Houpeurt, A.: "On the Flow of Gases in Porous Media," *Revue*, l'Institut Français du Petrole (Nov. 1959) **XIV,** 1468.
8. Katz, D. L., Cornell, D., Kobayashi, R., Poettman, F. H., Vary, J. A., Elenbaas, J. R., and Weinaug, C. F.: *Handbook of Natural Gas Engineering*, McGraw-Hill Book Co. Inc., New York City (1959).
9. Tek, M. R., Coats, K. H., and Katz, D. L.: "The Effect of Turbulence on Flow of Natural Gas Through Porous Reservoirs," *J. Pet. Tech.* (July 1962) 799-806; *Trans.*, AIME, **225.**
10. Wright, D. E.: "Non-Linear Flow Through Granular Media," *J. Hydraulic Div.*, ASCE (1968) **94,** 851.
11. Dranchuk, P. M. and Kolada, L. J.: "Interpretation of Steady Linear Visco-Inertial Gas Flow Data," *J. Cdn. Pet. Tech.* (Jan.-March 1968) 36.
12. Gewers, C. W. W. and Nichol, L. R., "Gas Turbulence Factor in a Microvugular Carbonate," *J. Cdn. Pet. Tech.* (April-June 1969) 51.
13. Wong, S. W.: "Effect of Liquid Saturation on Turbulence Factors for Gas-Liquid Systems,": *J. Cdn. Pet. Tech.* (Oct.-Dec. 1970) 274.
14. Geertsma, J.: "Estimating the Coefficient of Inertial Resistance in Fluid Flow Through Porous Media," *Soc. Pet. Eng. J.* (Oct. 1974) 445-450.
15. Forchheimer, P.: "Wasserbewegung durch Boden," *Zeitz ver deutsch Ing.* (1901) **45,** 1731.
16. Janicek, J. D. and Katz, D. L.: "Application of Unsteady State Gas Flow Calculations," paper presented at a research conference, U. of Michigan, Ann Arbor, June 20, 1955.
17. Hubbert, M. K.: "Darcy's Law and the Field Equations of the Flow of Underground Fluids," *Trans.*, AIME (1956) **207,** 222-239.
18. Swift, G. W. and Kiel, O. G.: "The Prediction of Gas-Well Performance Including the Effect of Non-Darcy Flow," *J. Pet. Tech.* (July 1962) 791-798; *Trans.*, AIME, **225.**
19. Yih, C. S.: *Fluid Mechanics: A Concise Introduction to the Theory*, McGraw-Hill Book Co., Inc., New York City (1969).
20. Cornell, D.: "Flow of Gases Through Consolidated Porous Media," PhD thesis, U. of Michigan, Ann Arbor (1952).
21. Klinkenberg, L. J.: "The Permeability of Porous Media to Liquids and Gases," *Drill. and Prod. Prac.*, API (1941) 230.
22. Iffly, R.: "Etude de l'Ecoulement des Gas dans les Milieux Poreux — Application à la Determination de la Morphologie des Roches," Faculté des Sciences, l'U. de Paris (March 1956).
23. Tek, M. R., Coats, K. H., and Katz, D. L.: "The Effect of Turbulence on Flow of Natural Gas Through Porous Reservoirs," *J. Pet. Tech.* (1962) 799-806; *Trans.*, AIME, **225.**
24. Casse, F. S. and Ramey, H. J. Jr.: "The Effect of Temperature and Confining Pressure on Single Phase Flow in Consolidated Rocks," paper SPE 5877 presented at the SPE-AIME 46th Annual California Regional Meeting, Long Beach, April 8-9, 1976.
25. Sadig, S.: "The Inertial Resistance Coefficient and Other Rock Properties," MS thesis. U. of Alberta, Edmonton (1965). **JPT**

Original manuscript received in Society of Petroleum Engineers office Sept. 20, 1977. Paper accepted for publication May 26, 1978. Revised manuscript received Aug. 10, 1978. Paper (SPE 6827) first presented at the SPE-AIME 52nd Annual Fall Technical Conference and Exhibition, held in Denver, Oct. 9-12, 1977.

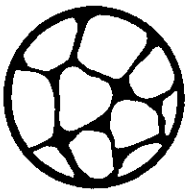

A Laboratory Study of Low-Permeability Gas Sands

F.O. Jones, SPE, Amoco Production Co.
W.W. Owens, SPE, Amoco Production Co.

Introduction

Yearly compilations of U.S. oil and gas reserves by the American Gas Assn.[1] show that U.S. gas reserves reached a maximum in 1967 of nearly 290 Tcf (8×10^{12} m^3). With the exception of the year 1970 when Prudhoe Bay reserves were added, gas reserves have declined at a near-constant rate of 10 Tcf (2.8×10^{11} m^3) per year since then. To help moderate or reverse this trend, the industry is extending its exploration and development efforts to include horizons with permeabilities in about the same range as common cement – i.e., microdarcies. The design of stimulation treatments to achieve commercial rates of production and reliable assessment of potential reserves in such low-permeability rocks demands accurate knowledge of their permeability, porosity, and flow properties. Though meager, there is sufficient information already available in the literature to suggest that some of the flow properties of these rocks differ markedly from those of more permeable rocks and, thus, require closer study.

Results of several different studies of the properties of low-permeability gas-producing horizons have been published previously. A study by Thomas and Ward[2] showed that the permeability of cores from the Pictured Cliffs and Fort Union formations were affected significantly by confining pressure. Porosities, however, were not altered greatly. They also reported that the presence of a simulated connate water saturation (about 50%) reduced gas permeabilities to only 10% to 20% of the specific gas permeability. Vairogs *et al.*[3] concluded that very low-permeability rocks are affected by stress to a greater degree than those having higher levels of permeability. This agreed with results reported earlier by McLatchie *et al.*[4]

Tannich[5] mathematically studied liquid removal from fractured gas wells in low-permeability horizons and concluded that in very low-permeability rocks, cleanup times could be extensive but that permanent formation damage was not likely. The study, however, provided no measured experimental data of the flow properties of low-permeability rocks.

Early wells drilled and cored by Amoco Production Co. in the Wattenberg field of Colorado in the Union Pacific Railroad Lease Area indicated the need for further laboratory studies of tight gas sands. Large differences in formation permeabilities, as derived from core and pressure buildup analyses, were not entirely explainable from data available in the literature. In addition, developments in stimulation design showed the need for reliable reservoir permeability values to prevent overdesign

0149-2136/80/0009-7551$00.25

Editor's Note: This paper won the 1980 Award for Outstanding Applied Research presented May 29 by the U.S. National Committee for Rock Mechanics of the National Research Council.

Routine permeabilities of tight gas sands are shown to be greater than under reservoir conditions, often by more than a hundred-fold, because of the great relief of stress, absence of connate water, and increased gas slippage. Correlations are presented that can be used to estimate in-situ permeability from routine data.

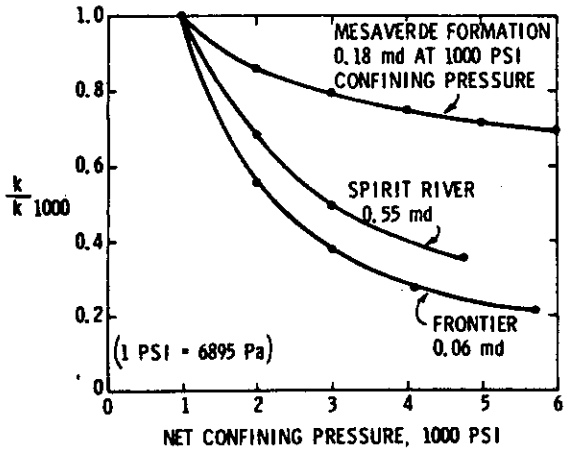

Fig. 1 – Effect of confining pressure on tight gas sand permeability.

(and cost) of massive hydraulic fracturing treatments. In addition, concern existed over the proper choice of drilling and stimulation fluids to minimize formation damage. This study is part of an ongoing Amoco study to provide answers to these and other problems that arise in the development of tight gas sand reserves.

Reported here are the results of selected laboratory tests that were designed to (1) study the factors that cause routine core-analysis permeability values to be different from those that exist in the reservoir, (2) study the range of the influence of these factors in low permeability producing horizons of interest to Amoco, (3) develop, if possible, correlations for predicting reservoir values of permeability from core analysis results, and (4) evaluate the effects of invasion of fluids of different salinities on the rate of regainment of permeability to gas.

Apparatus and Experimental Procedure

Plug samples ¾ in. (1.9 cm) in diameter and 1 in. (2.5 cm) long drilled parallel to formation bedding planes were tested in Hassler sleeve holders capable of exerting up to 10,000 psi (69 MPa) confining pressure uniformly in all directions ("hydrostatic" test conditions). Permeability to either gas or water could be measured at injection pressures up to 1,000 psi (6.9 MPa) and were measured at flow rates sufficiently low to avoid turbulence. Vacuum deaerated liquids, passing through line filters, were supplied to the cores at constant pressure by nitrogen-driven transfer cylinders designed to prevent diffusion of nitrogen into the driven liquid. Flowing pressures were measured with Bourdon gauges for gas and variable reluctance diaphragm transducers and indicators for liquid. Confining pressures were exerted by oil and were adjusted to compensate for average pore pressure to obtain a given net confining pressure.

Flow rates of liquids were measured by timing their travel in pipets. Flow rates lower than 10^{-6} cm^3/s could be measured to allow measuring permeabilities down to 10^{-6} md. Low gas flow rates were measured by timing the passage of the meniscus when displacing oil from a horizontal pipet whose tip was bent downward to discharge under oil. This arrangement – with its constant, slightly negative oil head – insured instant displacement of oil by gas and avoided complications from the action of interfacial forces at either the meniscus or pipet tip. Pipets of 1- to 2-cm^3 capacity with 0.01-cm^3 subdivisions ordinarily were used. It is important that the meniscus travel horizontally; if the oil head changes during flow measurement, gas between the core and meniscus will change volume sufficiently to introduce significant error when using small-bore pipets. However, 10-cm^3 pipets can be operated vertically with less than 1% error if volume between the core and pipet is less than 5 cm^3. Samples were liquid-saturated by evacuating them in pressure chambers for 4 hours at pressures less than 1 mm Hg (130 Pa), after which deaerated liquid was admitted and then pressured at 1,000 psi (6.9 MPa) for 16 hours to dissolve remaining traces of gas. Pore volume compressibilities were determined using the Hassler cells and measuring the liquid displaced into calibrated pipets (0.001-cm^3 subdivisions) with time allowed to obtain equilibrium at each step.

Effects of confining pressure on permeability ordinarily were measured in gas flow tests using dry cores. Permeabilities were measured at increasing confining pressure levels up usually to the reservoir net overburden pressure. [Net overburden pressure is taken to be the difference between gross overburden pressure, assumed to increase at 1.0 psi/ft (22.6 kPa/m), and reservoir fluid pressure.] Klinkenberg (no gas slippage) permeabilities were determined at the highest confining pressures by the conventional method of measuring permeabilities at more than one average flowing pressure; preliminary investigations indicated that measurements at two injection pressures provided sufficient data. Gas drive tests were performed using cores which had been saturated with formation water and whose permeability to water had been determined. For reasons discussed in a later section, nitrogen was injected, usually at 1,000 psi (6.9 MPa) (sometimes lower, if needed, to avoid turbulence) until 3,500 cm^3 (at ambient pressure) had emitted downstream. Permeability was monitored throughout the test. Holdup volumes were too great to permit measuring the rate of water production; consequently, saturation data for determining relative permeabilities could not be collected except for end points.

Results

Effect of Confining Pressure on Permeability

The large effect of confining pressure on the permeability of tight gas sands documented earlier[2-4] also was found in this study. Hydrostatically applied confining pressures equaling reservoir net overburden pressure [5,000 to 6,000 psi (34 to 41 MPa)] reduced permeability nearly 10-fold below the routine values measured under surface conditions in which confining pressure is 150 to 250 psi (1 to 1.7 MPa). Reductions ranged from less than threefold to

more than 20-fold. Typical results are shown in Fig. 1. The reason that confining pressure has greater effects on tighter sands than on more permeable ones is not well established. A popular conjecture holds that rock compression is distributed as greater fractional changes of the smaller apertures of the tight sands, the effect of which is further increased by the fact that flow depends on a higher power of the aperture dimension (round capillaries vary as the fourth power and slits by the cube of the dimension).

The experimental data were plotted in a number of ways in search of linear relationships to facilitate data handling, correlation, and, ultimately, to simplify testing. For representing behavior between 1,000 psi (6.9 MPa) and reservoir net overburden conditions, a plot of the cube root of permeability vs. the logarithm of confining pressure was found well-suited. Fig. 2 shows plots of the cube root of permeability against the logarithm of confining pressure using the data presented in Fig. 1 to illustrate the linear character of this relation. Permeability values are normalized on the basis of permeability measured at 1,000 psi (6.9 MPa) net confining pressure to allow direct comparison of the influence of confining pressure independent of permeability level; the slopes of the lines are measures of this influence. A convenient form of the equation for the relation is

$$k = k_{1,000}\left(1 - S\log\frac{P_k}{1,000}\right)^3, \quad \ldots\ldots\ldots\ldots (1)$$

where S, the magnitude of the negative slope, is given by

$$S = \frac{1-\left(\frac{k}{k_{1,000}}\right)^{1/3}}{\log\frac{P_k}{1,000}} \quad \ldots\ldots\ldots\ldots\ldots\ldots (2)$$

Use of the straight-line relation simplifies both testing and handling of data. Permeabilities need be measured at only two confining pressures to fix the slope parameter of the equation well enough for most engineering purposes. Measurements usually are made at 1,000 psi (6.9 MPa) and at the reservoir net overburden pressure. The S factor, the absolute value of the slope, embodies the effect of confining pressure in a single number convenient for conceptual and correlation purposes. Increasing values of S imply increasing effects of confining pressure. Moderate effects of stress, such as seen in testing higher permeability rocks, produce S factors in the vicinity of 0.1 to 0.2. Significant effects, as obtained in most tight gas sand tests, yielded S factors in the range of 0.3 to 0.6 with factors greater than 0.7 indicating large reductions. A rock decreased 10-fold in permeability below routine permeability by reservoir overburden pressure would have an S factor of approximately 0.4.

Generally, the lower the core permeability the more it is affected by confining pressure. This is illustrated in the top half of Fig. 3, a plot of S factors of Frontier formation samples against the logarithms of permeabilities measured at 1,000-psi (6.9-MPa)

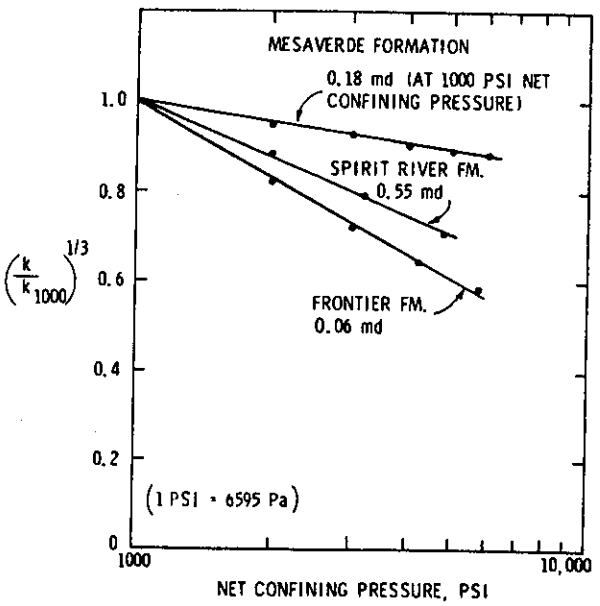

Fig. 2 – The cube root of permeability as a linear function of the logarithm of confining pressure.

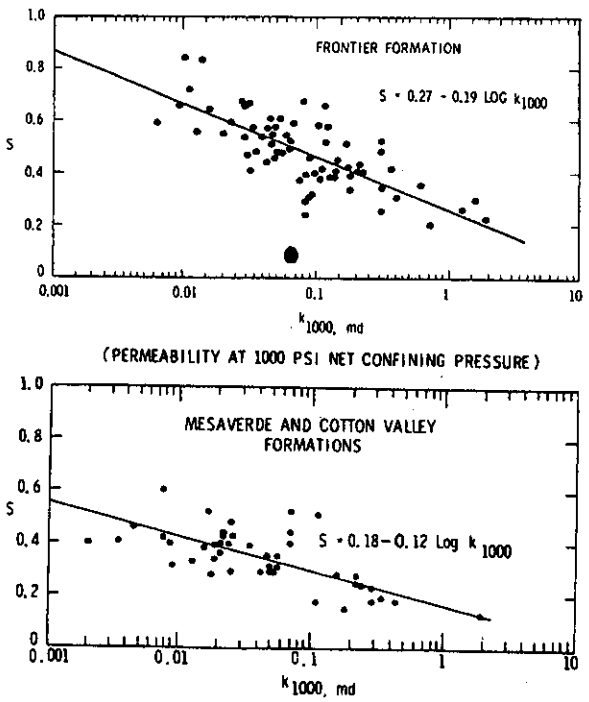

Fig. 3 – Correlation of permeability stress factor S with permeability.

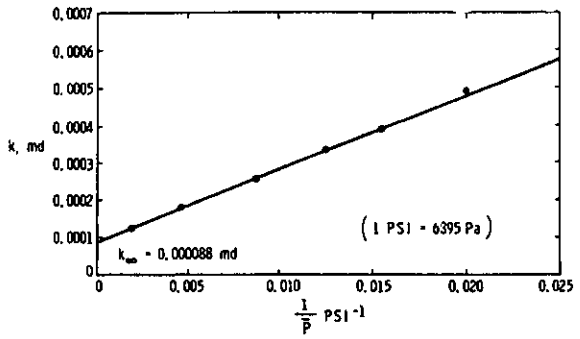

Fig. 4 – Determination of Klinkenberg permeability.

TABLE 1 – COMPARISON OF KLINKENBERG AND OIL PERMEABILITIES

Formation	Net Confining Pressure (psi)	k_∞ (md)	k_o (md)
Mesaverde	5,100	0.0092	0.0092
Mesaverde	5,200	0.0040	0.0032
Frontier	5,400	0.0018	0.0013
Frontier	5,500	0.0018	0.0010
Frontier	5,500	0.0039	0.0037
Frontier	5,500	0.0026	0.0023
Frontier	5,700	0.0066	0.0050

net confining pressure. Note also that the data, although scattered, have a linear trend. A best-fit straight line through the data affords a compact description of the average effect of confining pressure on permeability of cores from this formation. Fig. 3 shows plots of this type. Frontier formation data plotted in the upper half of the figure show effects of stress on permeability which are greater than those for the Mesaverde and Cotton Valley formations shown in the lower half.

No correlation between permeability and reduction due to confining stress was found which extended down to the 150- to 250-psi (1- to 1.7-MPa) net confining pressure condition commonly used in routine core testing; such correlations evidently must be made on an individual formation basis. Permeability measured at 1,000-psi (6.9-MPa) net confining pressure usually is between 0.4 to 0.75 times the routine permeability.

Above 2,000-psi (14-MPa) net confining pressure the logarithm of permeability vs. the logarithm of confining pressure produces fairly linear plots that possibly may be the best correlative relation for use in predicting effects by confining pressure on permeability as reservoirs are depleted.

Gas Slippage

Gas slippage, or Klinkenberg[6] effects, are large in tight gas sands. As an example, a sample with 0.001-md true, or Klinkenberg, permeability typically would exhibit about 0.003 md with gas injected at 100 psig (0.69 MPa) and exiting at atmospheric pressure, and more than 0.007 md if upstream pressure were 15 psig (103 kPa). Effective pore radii of sands with less than 0.1 md are indicated by mercury injection data and by gas slippage theory to range downward from 1 micron (1 μm) into the size realm of the mean free paths of the gas molecules. Because of this, there was concern that the conventional extrapolative procedure (in which permeability plotted vs. reciprocal arithmetic mean pressure is extrapolated to zero reciprocal pressure) for determining Klinkenberg permeability might not yield a straight line for the very low-permeability tight gas sands. The reason for this concern was that Warburg's model,[7] on which Klinkenberg based his development, assumed mean free path length was small compared with capillary radius. Klinkenberg ascribed depressions in b factors (the slope of the line connecting a data point to the Klinkenberg permeability in the above plot) determined at reduced pressure to this departure from Warburg's model. In this study, however, very good straight-line Klinkenberg plots were obtained for rocks with Klinkenberg permeabilities even less than 0.0001 md. An example is given in Fig. 4, showing the results of a test on an 0.000 088-md sample in which upstream pressures ranged from 50 to 1,000 psig (0.34 to 6.9 MPa). Both dry Klinkenberg permeabilities and specific permeabilities to a 1.3 cp (1.3 mPa·s) refined oil (Soltrol 130) were measured in tests on a series of cores in the 0.001- to 0.01-md range; the results are given in Table 1. Oil permeabilities were equal to or lower than Klinkenberg permeability in every case, averaging 25% less. The agreement is sufficiently close, however, to assume that Klinkenberg permeabilities obtained by the extrapolation procedure are satisfactory for practical application. It is not known which, if either, of the permeabilities is "correct." Oil permeabilities might be low because of interactions between the oil and rock, or Klinkenberg values may trend higher because of departure from the Warburg model.

For this study, Klinkenberg permeabilities and b factors were calculated from permeabilities measured usually at 100- and 1,000-psig (0.7- and 6.9-MPa) upstream pressure and atmospheric pressure downstream. Lower pressures were used when necessary during tests of the more-permeable samples to avoid turbulence. The measurements were made at net confining pressures equaling reservoir net overburden pressures. Confining pressure was increased sufficiently to offset average increase in pore pressure to keep confining pressure essentially constant during determination of the Klinkenberg permeability. Klinkenberg's b factor was calculated from the data using the Klinkenberg equation:

$$k_a = k_\infty \left(1 + \frac{b}{\bar{P}}\right). \quad \ldots\ldots\ldots\ldots\ldots\ldots (3)$$

As indicated by the equation, the b factor is an index of the magnitude of the gas slippage effect. It often is regarded as the fractional increase in apparent permeability which would be observed when

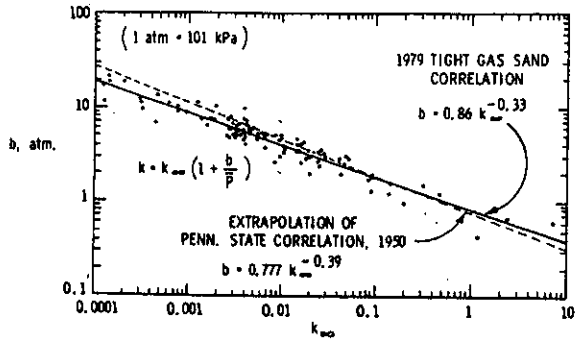

Fig. 5 – Klinkenberg b factor as a function of Klinkenberg permeability.

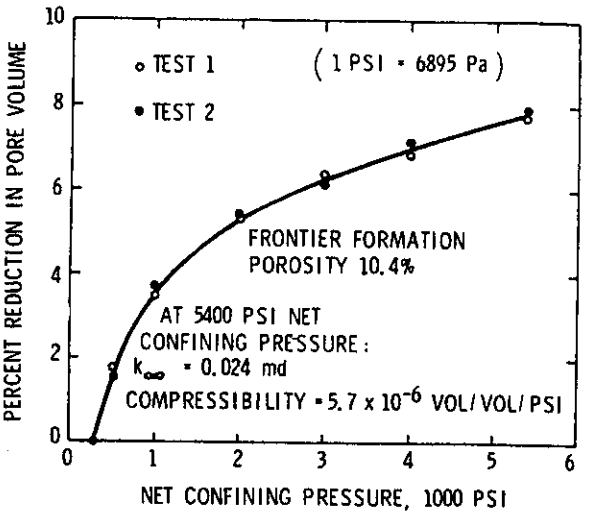

Fig. 6 – Pore volume compressibility of typical tight gas sand sample.

measuring permeability with gas at atmospheric pressure.

The results of measurements made on more than 100 tight gas sand samples are given in Fig. 5 as a plot of the logarithm of b factor against the logarithm of Klinkenberg permeability, a method used by Heid *et al.*[8] for presenting results of the 1950 study of Pennsylvania State U. for the API. The tight gas sand data are scattered closely about a straight line not greatly different from an extrapolation of the best-fit straight line through the higher-permeability 1950 Penn State data, the equation for which is

$$b = 0.777\, k_\infty^{-0.39} \quad \ldots\ldots\ldots\ldots\ldots\ldots\ldots\ldots (4)$$

The best line through the tight gas sand data given in this study is

$$b = 0.86\, k_\infty^{-0.33} \quad \ldots\ldots\ldots\ldots\ldots\ldots\ldots\ldots (5)$$

As discussed in the 1950 Penn State study, for ideal cases consisting of a parallel capillary bundle, b should vary inversely as the square root of permeability, which would yield a slope of -0.5 cycles/cycle. The -0.39 slope was regarded as nearly corresponding to this idealized view. The -0.33 slope obtained in this tight gas sand study is reminiscent of the cube root relation arising from Lamb's[9,10] expression for flow through ducts and suggests that apertures controlling flow in the tight gas sands may be slit-like rather than round.

The tight gas sand correlation (Eq. 5) yields values of the b factor sufficiently accurate for many practical purposes. The correlative power function may be substituted for b in Klinkenberg's equation as follows.

$$k_a = k_\infty \left(1 + \frac{0.86\, k_\infty^{-0.33}}{\bar{P}}\right). \quad \ldots\ldots\ldots\ldots (6)$$

This expression can be used as a starting point for generating graphs or numerical solutions for calculating Klinkenberg permeabilities and b factors from ordinary permeability data, provided the pressures used in the measurements are known. An expression originating from Eq. 6 from which k_∞ may be estimated from permeabilities k_a measured at 100-psig (0.69-MPa) upstream pressure is

$$k_\infty = 10^{(-0.0398 \log^2 k_a + 1.067 \log k_a - 0.0825)}, \quad 0.0001 \text{ md} < k_a < 1 \text{ md}, \quad \ldots\ldots\ldots\ldots\ldots\ldots\ldots\ldots (7)$$

which agrees with Eq. 6 within a few percent over the k_a range of 0.0001 to 1 md.

Pore Volume Compressibility

The chief reason for measuring pore volume compressibility was to determine if porosity values measured in routine tests were significantly greater than under reservoir conditions. It was found that the behavior of tight gas sands was similar to higher-permeability consolidated rocks and that the porosity measured at the surface was not appreciably greater than at depth. Pore volume diminished usually between 5 and 10%; a rock exhibiting 10% porosity under surface conditions would have 9.0 to 9.5% porosity in the reservoir. For many purposes, the effect of overburden pressure on porosity can be ignored. Multiplying porosity by a factor of 0.95 will correct most data sufficiently close to reservoir-condition porosity for all but the most exacting purposes. Pore volume compressibility averages about 6×10^{-6} vol/vol/psi (vol/vol/6895 Pa).

Results of a typical test are shown in Fig. 6. The percent decrease in pore volume is given as a function of increasing confining pressure. The pore volume compressibility at reservoir stress level is calculated from the slope of the curve at the reservoir net overburden pressure, taking also into account the pore volume decrease up to that point. Table 2

TABLE 2 – PORE VOLUME COMPRESSIBILITY

Formation	Porosity (%)	Net Confining Pressure (psi)	Permeability to H_2O (md)	Pore Volume Decrease (%)	Pore Volume Compressibility (vol/vol/psi × 10^6)
Mesaverde	12.8	5,200	–	5.7	5.4
Mesaverde	12.1	5,200	0.00057	5.8	5.0
Mesaverde	10.6	5,200	0.0025	6.6	6.0
Mesaverde	13.6	5,200	–	3.8	5.1
Mesaverde	13.4	5,200	0.0015	5.6	4.3
Frontier	13.2	5,400	0.0073	7.8	5.7
Frontier	14.3	5,700	0.00029	9.5	5.7
Frontier	11.6	5,700	0.012	10.4	3.5
Frontier	7.0	5,500	0.00091	4.3	2.7
Frontier	10.0	5,500	–	8.5	6.1
Frontier	11.1	5,500	–	10.4	9.0
Frontier	10.8	5,500	0.000069	9.8	9.1
Frontier	12.1	5,500	0.00041	4.6	3.2
Frontier	13.6	5,500	–	9.6	7.7
Frontier	13.8	5,500	–	7.1	5.9
Frontier	13.5	6,700	–	8.1	3.3
Frontier	14.0	5,700	0.00052	7.0	5.5
Muddy "J"	10.8	4,000	0.0012	8.3	9.2
Spirit River	10.2	4,000	0.0099	8.1	15.7

presents the data from a number of such tests, showing both pore volume compressibility and total effect on pore volume.

Effect of Water on Core Permeability

Water greatly reduces permeability of tight gas sands and in a manner different from its effect on higher-permeability sands. Brine causes almost as great a reduction in permeability as fresh water. For example, a 60,000-mg/L NaCl solution will reduce permeability typically 85% below Klinkenberg permeability of the dry core; introduction of distilled water will cause further reduction but only in the order of another 10% for a total reduction of about 95%. Examples of such test results are given in Table 3. A more permeable water-sensitive sand, such as Berea, would lose about 50% permeability upon introducing the above brine but would lose more than 49% additional permeability upon exposure to distilled water for a total reduction of more than 99%. Fresh water has a lesser proportionate effect on tight gas sands possibly because otherwise dispersible clays or mineral fines may tend to be mechanically locked or wedged in place in the smaller pores of the fine-textured rocks and, thereby, are inhibited from moving to form obstructions. However, the reason that even highly saline solutions can reduce permeability severely is not explained easily. There are several existing theories that alone or in combination may offer explanation. The most popular theory, although subject to much controversy concerning the magnitude of the effects, holds that water adjacent to high-energy surfaces becomes ordered to result in viscosity increase or even solidification sufficient to

TABLE 3 – EFFECT OF FRESH WATER ON PERMEABILITY

Formation	Net Confining Pressure (psi)	k_∞* (md)	k_w** (md)	k_{H_2O}† (md)
Lewis	2,000	0.0077	0.00094	0.00027
Lewis	2,000	0.0070	0.00094	0.00034
Mesaverde	5,300	0.0031	0.00032	0.00010
Mesaverde	5,300	0.0063	0.0021	0.00080
Mesaverde	5,300	0.014	0.0040	0.00064
Mesaverde	6,000	0.0039	0.00055	0.00036
Mesaverde	6,000	0.091	0.076	0.041
Mesaverde	6,000	0.0040	0.0011	0.00037
Frontier	2,000	–	0.0026	0.0009
Frontier	2,000	0.092	0.016	0.0047
Frontier	2,000	0.089	0.033	0.0090
Frontier	2,000	0.0090	0.00029	0.00013
Frontier	6,700	0.010	0.00084	0.00051
Frontier	5,700	0.0065	0.0010	0.00026
Spirit River	4,000	0.033	0.011	0.0037
Spirit River	4,000	0.0068	0.0010	0.00091
Spirit River	4,000	0.0011	0.000031	0.000022

*Klinkenberg permeability of dry core at indicated confining pressure.
**Specific permeability to formation water at indicated confining pressure.
†Specific permeability to distilled water at indicated confining pressure following flow of 60,000-mg/L NaCl solution to sensitize clays.

reduce effective pore diameter significantly. Calculations based on Poiseuille's and Lamb's laws applied to pore radii calculated from Klinkenberg b factor[6,8] indicate that fixed layers of water would need to be in the order of 100 Å (0.01 μm) or more to account for the minimum reduction observed in 0.001- to 0.1-md samples of this study.

Smectites exfoliate and most clays and many other mineral fines associate with water in going from the dry to the moistened state (even in brine) to increase the volumes of aggregates. Apertures could be reduced by this mechanism sufficient to impede flow.

The specific permeabilities to formation water of more than 100 tight gas sand samples were measured. Klinkenberg permeabilities were measured with the samples dry prior to the water flow tests. All tests were made at net confining pressure equaling reservoir net overburden pressures. The results are given in Fig. 7 as a plot of the logarithm of water permeability vs. the logarithm of Klinkenberg permeability. Two features are evident: the trend is linear and the lower the permeability the more water reduces permeability. A line centered in this data is the power function

$$k_w = k_\infty^{1.32}, \quad k < 1 \text{ md} \quad \ldots\ldots\ldots\ldots\ldots\ldots\ldots\ldots (8)$$

This correlative function may be used to calculate the average effect of water on permeability. Plots such as these of data from single formations or rock types may be less scattered, meaning that, in particular cases, laboratory data from samples selected from a range of permeabilities can be used to determine the exponent applicable for use in the water-effect power equation for that formation. Examination of Fig. 7 shows that the boundary of minimum effect appears well defined; a line along this boundary has a slope of about 1.13 cycles/cycle. A line bounding most of the data below 0.1-md dry Klinkenberg permeability on the side of maximum effect has a slope of about 1.5 cycles/cycle. This function can be used in conjunction with the correlations describing effects of stress and slippage to obtain estimates of in-situ gas permeability from routine permeability values. This is discussed in a later section.

Clay content was not found to correlate with effect of water on permeability. Large clay content usually forecasts large effects of water, but low clay content does not forecast low effects. Cores with large amounts of clay probably were affected most because of the low permeability resulting from the presence of clay rather than by effects of the clay itself.

The fact that water of even high salinity can seriously affect tight gas sand permeability but that, in contrast, fresh water has relatively less additional effect has obvious practical significance. Limiting entry of water during drilling or stimulation should help preserve reservoir permeability and hasten cleanup time. Filtrate invasion from muds can be reduced by maintaining mud weights close to balance, or even underbalanced, with respect to reservoir pressure. Minimizing postfracture shut-in times might also reduce fracturing-fluid invasion and

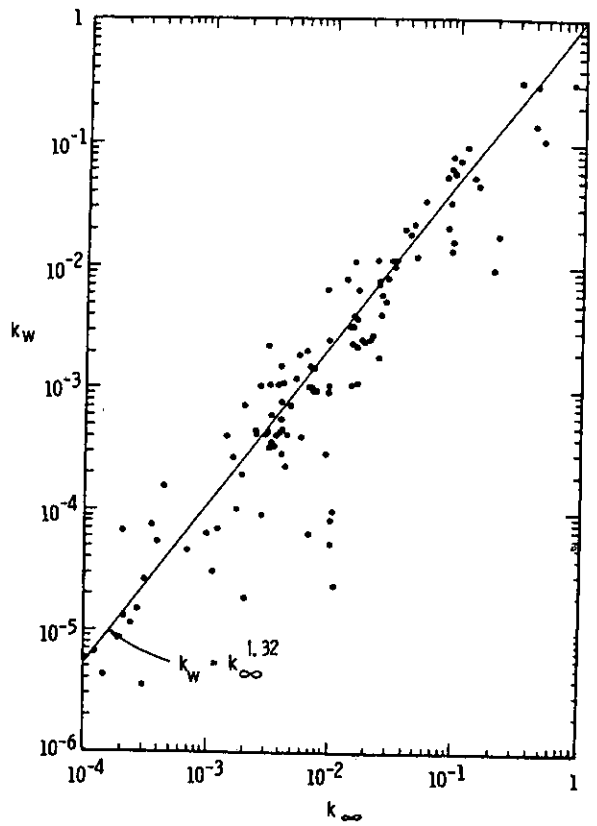

Fig. 7 – Specific water permeability as a function of Klinkenberg permeability.

prove beneficial. Another point implied, since fresh water is not a great deal more harmful than brines, is that less concern is needed regarding the chemical composition of fracturing fluids or mud filtrates.

Effect of Partial Water Saturation on Gas Permeability

Those tight gas sands whose specific water permeabilities are a great deal less than the Klinkenberg permeabilities of the dry samples also have correspondingly low gas permeabilities in the presence of simulated connate water saturations. As a first approximation, effective gas permeability under reservoir conditions can be taken as equal to specific permeability to water measured under reservoir stress conditions. Experiments demonstrating this observation are discussed as follows.

Relative permeability apparatus suitable for testing tight gas sands was not available at the initiation of the study. Exploratory gas drive experiments showed, however, that gas injected usually at 1,000 psi (6.9 MPa) into the plug samples [¾-in. (1.9-cm) diameter and 1-in. (2.5-cm) long] for a time sufficient to produce 3,500 cm^3 downstream at atmospheric pressure reduced water saturations to an average of 40% pore space. Under these conditions most of the water is removed by displacement; not more than 10% pore space of the water was evaporated. No attempt was made to measure or account for saturation gradients which may have existed. An example of the development of permeability with

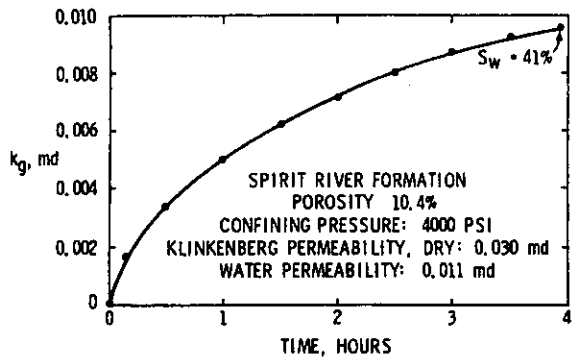

Fig. 8 – Establishment of gas permeability during displacement of water by gas.

time in a gas drive test of this type is shown in Fig. 8. Results of 22 gas drive tests are given in Table 4 in which are compared Klinkenberg permeabilities of the dry cores, specific permeabilities to water, and effective gas permeabilities at the indicated water saturations. There is a degree of bias in that testing of higher-permeability samples was favored because of the inordinate length of time required for tests of samples with less than 0.001-md permeability. Examination of the data shows that effective gas permeability in every case is nearer the specific water permeability, most often by a large margin, than to the Klinkenberg permeability of the dry sample. In more than three-fourths of the cases, effective gas permeability is within a factor of two of the specific permeability to formation water. Effective gas permeability averaged about 35% higher than specific water permeability. This suggests, as mentioned earlier, that the more easily obtained water permeability values could be used for estimating formation gas permeability. Gas drive tests are lengthy and must be attended closely, while, on the other hand, several specific water permeability tests may be conducted simultaneously by one person, usually faster than a sample per cell per day.

Combined Effects of Confining Pressure, Gas Slippage, and Water on Permeability

The individual effects of stress, gas slippage, and water on tight gas sand permeability have been described in the preceding sections. Also, the measurement of specific formation water permeability under reservoir stress conditions was suggested as a core test for estimating effective gas permeabilities under reservoir conditions. This section deals with methods of estimating reservoir-condition gas permeability using routine core analysis data.

Routine permeabilities are inexpensive and consequently plentiful, but because they are measured on dry cores at low stress levels and low flowing gas pressures, they poorly represent in-situ tight gas sand permeabilities. Routine values range from ten to more than a thousand times too high. Also, because of variability in response, routine values cannot be depended upon for comparison purposes. Frontier sand samples compared with Mesaverde sand samples, for example, commonly exhibit higher routine values but lower effective gas permeabilities under reservoir conditions of stress, presence of water saturation, and elimination of slippage. Methods for correcting routine permeability values to reservoir-condition permeability must, therefore, not only compensate for the large changes but also for the wide range of rock variability.

Two methods for estimating reservoir-condition gas permeability are suggested. The first involves

TABLE 4 – COMPARISON OF EFFECTIVE GAS PERMEABILITY TO SPECIFIC WATER PERMEABILITY

Formation	Net Confining Pressure (psi)	k_∞ (md)	k_w (md)	k_g (md) @	S_w (%)
Mesaverde	5,100	0.0092	0.0050	0.0028	40
Mesaverde	5,200	0.0032	0.00057	0.00079	29
Mesaverde	5,200	0.0035	0.00041	0.00010	29
Mesaverde	5,200	0.0096	0.0025	0.0033	34
Mesaverde	5,200	0.0068	0.0015	0.0020	34
Frontier	5,100	0.0067	0.000065	0.000054	44
Frontier	5,400	0.0017	0.00010	0.000070	47
Frontier	5,400	0.024	0.0073	0.0083	60
Frontier	5,700	0.0039	0.00029	0.00071	33
Frontier	5,700	0.047	0.012	0.029	60
Frontier	5,500	0.0027	0.00091	0.00075	43
Frontier	5,500	0.0012	0.000069	0.000073	49
Frontier	5,500	0.0043	0.00041	0.0011	33
Frontier	6,700	0.016	0.0011	0.0028	40
Frontier	5,700	0.010	0.00052	0.0015	52
Muddy "J"	4,000	0.0050	0.0012	0.0015	38
Cotton Valley	4,900	0.0014	0.00040	0.00026	45
Cotton Valley	4,900	0.044	0.022	0.018	32
Spirit River	4,000	0.030	0.011	0.010	41
Spirit River	4,000	0.023	0.011	0.010	38
Spirit River	4,000	0.033	0.0037*	0.0063	40
Spirit River	4,000	0.0068	0.00091*	0.0011	39

*Distilled water following 60,000-mg/L NaCl solution.

correcting sequentially for stress, slippage, and presence of connate water and is the more flexible of the two because adjustments can be made for the individual effects. The second method is derived from the first in which all effects are compounded into a single "stadium" equation (providing "ballpark" values) with two parameters that are varied simultaneously over the range from minimum to very large effects of stress, water, and slippage. Neither method, at least at present, appears capable of high precision, but the two methods do provide more reasonable values for reservoir gas permeability than the routine permeability values.

The first method requires five steps: (1) correction of routine permeability to that at 1,000-psi (6.9-MPa) confining pressure, (2) calculation of S factor (influence of pressure), (3) calculation of effect of overburden pressure using the S factor, (4) correction for gas slippage, and (5) calculation of the effect of water. Core tests over a range of permeability values for each rock type can be used to evaluate necessary parameters that then may be applied to existing routine results. For scoping studies, values of the necessary parameters may be assumed. Only three estimates are necessary: (1) the correction of routine permeability to 1,000-psi (6.9-MPa) confining pressure (a factor usually of 0.4 to 0.75), (2) selection of an S factor equation between defined upper and lower limits, S = (0.1 to 0.3) − (0.1 to 0.23) log $k_{1,000}$, and (3) selection of a water-effect exponent for Eq. 8 that also lies within the reasonably well-defined limits of 1.13 to 1.5; k_w then is assumed equal to k_g.

This method was used to generate a series of curves ranging from minimum to maximum effect of stress and water, assuming that rocks most affected by stress were also most affected by water. These calculations all generated gently curving, almost linear curves in plots of the logarithms of routine permeability against the logarithms of the calculated reservoir-condition gas permeability. Straight lines were fitted by eye to these curves, which lay within a few percent of the calculated value over the range of 0.02- to 0.55-md routine permeability. The intercepts and the slopes of these lines are the coefficients and exponents used in the stadium equation:

$$k_g = a\,k^b,$$
$$0.02 \text{ md} < k < 0.55 \text{ md} \quad \ldots\ldots\ldots\ldots\ldots (9)$$

k_g is effective gas permeability under reservoir conditions, and k is routine permeability. The coefficient a varies from 1/5 to 1/20 and the exponent c varies from 1.5 to 2.7 as the effect of stress and water increases.

Severity of Effects of Stress and Water	a	c
Minimum	1/5	1.5
Moderate	1/7.5	1.9
Great	1/12	2.3
Very great	1/20	2.7

Examples of formations having lower effect of stress and water are clean Mesaverde and Cotton Valley sands. Those moderately affected are shaly Cotton Valley sand samples and cleaner Frontier sands. Most Frontier samples studied exhibited large effects, and some experienced very large effects. Lesser effects tend to accompany increased induration, while increased clay content appears associated with larger effects. Parameters of a = 1/7.5 and c = 1.9 are reasonable values for use as first approximations in the absence of other information.

Conclusions

Results of compressibility and flow tests on more than 100 tight gas sand core samples from five formations indicate the following.

1. Confining pressure simulating net reservoir overburden pressure reduces permeability of tight gas sands two to more than 10 times, depending on permeability and rock type. The cube root of permeability was found to be a linear function of the logarithm of confining pressure; the slope of the line indicative of the intensity of the effect of stress and was found correlatable with permeability, with correlations varying with rock type. Lower permeability rocks were more affected by stress than higher permeability ones.

2. Gas slippage (Klinkenberg) effects were found to be substantial, as would be anticipated for lower permeability rocks. Slippage effects were found correlatable with an expression not greatly different from an earlier expression derived from more permeable rocks.

3. Water (including brine) severely reduced permeability with the effect more pronounced in the lower permeability rocks. This indicates that preservation of permeability in an invaded zone in a reservoir would be assisted by minimizing invasion of water during drilling and fracturing. Water permeability was found correlatable with Klinkenberg permeability.

4. Specific water permeability measured at the reservoir level of confining pressure was found useful as an approximation of effective gas permeability under conditions of reservoir stress, gas slippage, and partial water saturation.

5. Despite large permeability reductions caused by brine, reducing salinity has comparatively less additional effect, to suggest that the chemical composition of mud filtrates or fracture fluids is ordinarily of secondary importance in preventing permeability impairment.

6. Pore volume compressibility of tight gas sands is of the same order as more permeable sands. Pore volume under reservoir overburden conditions was indicated to average 93% of that under no stress for the samples tested.

7. Effects of stress, gas slippage, and water were found correlatable with permeability but not directly with clay content. Lower permeability rocks experienced large effects with both low and high clay contents. These results suggest that the large effects observed with clay-laden rocks are attributable to the low permeabilities accompanying the high clay content, not to the fact that the fine material was clay.

8. Correlations were found to enable estimating in-situ effective gas permeability from routine core analysis data by taking into account the separate effects of stress, gas slippage, and partial water saturations.

Nomenclature

a = coefficient for stadium equation
b = Klinkenberg b factor, atm
c = exponent for stadium equation
k = permeability, md
k_a = apparent gas permeability, md
k_g = effective permeability to gas, partial water saturation present, md
k_o = specific permeability to oil, md
k_w = specific permeability to water, md
k_∞ = Klinkenberg (no gas slippage) permeability, md
$k_{1,000}$ = permeability measured of dry core at 1,000-psi (6.9-MPa) net confining pressure, md
$\bar{P}$ = arithmetic mean of gas pressure in core during flow of gas, atm (Pa)
P_k = confining pressure, psi (Pa)
S = stress factor defined in text

References

1. "Reserves of Crude Oil, Natural Gas Liquids, and Natural Gas in the United States and Canada as of December 31, 1977," AGA and API (June 1978) 39.
2. Thomas, R.D. and Ward, D.C.: "Effect of Overburden Pressure and Water on Gas Permeability of Tight Sandstone Cores," *J. Pet. Tech.* (Feb. 1972) 120-124.
3. Vairogs, J., Hearn, C.L., Dareing, D.W., and Rhoades, V.W.: "Effect of Rock Stress on Gas Production from Low-Permeability Reservoirs," *J. Pet. Tech.* (Sept. 1971) 1161-1167; *Trans.*, AIME 251.
4. McLatchie, A.S., Hemstock, R.A., and Young, J.W.: "The Effective Compressibility of Reservoir Rock and Its Effects on Permeability," *J. Pet. Tech.* (June 1958) 49-51; *Trans.* AIME, 213.
5. Tannich, J.D.: "Liquid Removal From Hydraulically Fractured Gas Wells," *J. Pet. Tech.* (Nov. 1975) 1309-1317.
6. Klinkenberg, L.J.: "The Permeability of Porous Media to Liquids and Gases," *Drill. and Prod. Prac.*, API (1941) 200-213.
7. Warburg, E.: *Annalen der Physik,* Halle, Leipzig (1876) Series 2, 159, 499.
8. Heid, J.G., McMahon, J.J., Nielsen, R.F., and Yuster, S.T.: "Study of the Permeability of Rocks to Homogeneous Fluids," *Drill. and Prod. Prac.*, API (1950) 230-246.
9. Lamb, H.: *Hydrodynamics*, sixth edition, Cambridge U. Press, New York City (1932) 582.
10. Jones, F.O.: "A Laboratory Study of the Effects of Confining Pressure on Fracture Flow and Storage Capacity in Carbonate Rocks," *J. Pet. Tech.* (Jan. 1975) 21-27.

SI Metric Conversion Factors

atm	×	1.013 250*	E+02	= kPa
L	×	1*		= dm^3
psi	×	6.894 757	E−03	= MPa
torr (mm Hg, 0°C)	×	1.333 224	E−01	= kPa

*Conversion factor is exact.

JPT

Original manuscript received in Society of Petroleum Engineers office March 9, 1979. Paper accepted for publication Dec. 21, 1979. Revised manuscript received July 7, 1980. Paper (SPE 7551) first presented at the SPE 1979 Symposium on Low-Permeability Gas Reservoirs, held in Denver, May 20-22.

SPE 26668

Compressibility Factors for Naturally Occurring Petroleum Gases

L.D. Piper, Texas A&M U.; W.D. McCain Jr., S.A. Holditch & Assocs. Inc.; and J.H. Corredor, Intera Petroleum Production Div.

SPE Members

This paper was prepared for presentation at the 68th Annual Technical Conference and Exhibition of the Society of Petroleum Engineers held in Houston, Texas, 3-6 October 1993.

ABSTRACT

The Sutton gas specific gravity correlation gives values of pseudocritical properties which, when used with the Dranchuk and Abou-Kassem (DAK) representation of the Standing and Katz (SK) chart, currently provide the most accurate estimates of compressibility factors for naturally occurring petroleum gases. However, other correlations must be used to account for the presence of acid gases. A new gas specific gravity correlation is presented which takes into account the effects of the acid gases and nitrogen. The new correlation provides more accurate estimates of the compressibility factor than can be obtained by current methods and also eliminates the need for involving additional correlations to correct for the presence of acid gases and nitrogen. The new correlation was developed using a set of 1482 data points, ranging in composition from lean sweet to rich acid gases.

INTRODUCTION

Knowledge of the pressure-volume-temperature (PVT) behavior of natural gases is necessary to solve many petroleum engineering problems. Gas reserves, gas metering, gas pressure gradients, pipeline flow and compression of gases are some of the problems requiring the gas compressibility factor, or z factor. Typically, the z factor is determined by laboratory measurement. However, laboratory data is only applicable for the compositions and conditions investigated. When conditions of interest are different from those of the laboratory studies or data is not available, correlations must be used.

The basic methods for estimating the gas compressibility factor are relatively simple and well known.[1] The principle of corresponding states, Kay's pseudocritical point, and the SK chart are commonly used. If the composition of the gas is known, the pseudocritical temperature and pressure may be calculated using Kay's rules--molar averages of the critical properties of the mixture's components. Otherwise, the pseudocritical temperature and pressure may be estimated using correlations based on gas specific gravity. Then, the reduced temperature and pressure may be calculated and the SK chart or its representation by the DAK equation of state may be used to determine the z factor.

Sutton[2] presented more accurate methods for both cases. His method for calculating the pseudocritical temperature and pressure when the composition of the gas is known is based on the Stewart, Burkhardt, and Voo (SBV) equations given by:

$$T_{pc} = \frac{K^2}{J} \text{ and } p_{pc} = \frac{T_{pc}}{J}, \quad \ldots\ldots\ldots\ldots (1a)$$

where,

$$J = \frac{1}{3}\sum_j y_j\left(\frac{T_c}{p_c}\right)_j + \frac{2}{3}\left[\sum_j y_j\left(\frac{T_c}{p_c}\right)_j^{0.5}\right]^2$$

$$\text{and } K = \sum_j y_j\left(\frac{T_c}{\sqrt{p_c}}\right)_j. \quad \ldots\ldots (1b)$$

His gas specific gravity correlation for estimating the pseudocritical temperature and pressure when the composition of the gas is known, based on 634 compositions from 275 PVT reports, is given by:

$$T_{pc} = 169.2 + 349.5\,\gamma_g - 74.0\,\gamma_g^2,$$

and

$$p_{pc} = 756.8 - 131.0\,\gamma_g - 3.6\,\gamma_g^2. \quad \ldots\ldots (2)$$

References and illustrations at end of paper.

If the gas contains hydrogen sulfide or carbon dioxide, the Wichert and Aziz correlation:

$$T'_{pc} = T_{pc} - \varepsilon,$$

where,

$$\varepsilon = 120\cdot\left[(y_{H_2S} + y_{CO_2})^{0.9} - (y_{H_2S} + y_{CO_2})^{1.6}\right] + 15\cdot\left[(y_{H_2S})^{0.5} - (y_{H_2S})^{4}\right],$$

and,

$$p'_{pc} = \frac{p_{pc}\,T'_{pc}}{T_{pc} + y_{H_2S}(1 - y_{H_2S})\varepsilon}, \qquad \ldots\ldots\ldots\ldots\ldots (3)$$

should be used to adjust the pseudocritical constants.[2-3] However, Ref. 2 is unclear on how Eqs. 3 should be applied to Eqs. 2.

In an earlier paper[4], we discussed Sutton's modification to the SBV rules in detail and presented a new modification which takes into account the effects of the heptane plus fraction, acid gases and nitrogen. This correlation, having a form similar to the SBV equations, was based on 896 data points from 134 PVT reports and is given by:

$$J = \alpha_0 + \sum_{i=1}^{3} \alpha_i y_i \left(\frac{T_c}{p_c}\right)_i + \alpha_4 \sum_j y_j \left(\frac{T_c}{p_c}\right)_j + \alpha_5 \left[\sum_j y_j \left(\frac{T_c}{p_c}\right)_j\right]^2 + \alpha_6 y_{C7+} M_{C7+} + \alpha_7 (y_{C7+} M_{C7+})^2,$$

and,

$$K = \beta_0 + \sum_{i=1}^{3} \beta_i y_i \left(\frac{T_c}{\sqrt{p_c}}\right)_i + \beta_4 \sum_j y_j \left(\frac{T_c}{\sqrt{p_c}}\right)_j + \beta_5 \left[\sum_j y_j \left(\frac{T_c}{\sqrt{p_c}}\right)_j\right]^2 + \beta_6 y_{C7+} M_{C7+} + \beta_7 (y_{C7+} M_{C7+})^2, \qquad \ldots\ldots (4)$$

where $y_i \in \{y_{H_2S}, y_{CO_2}, y_{N_2}\}$, $y_j \in \{y_{C_1}, y_{C_2}, \ldots, y_{nC_6}\}$, and the α_i and β_i were shown in Table 3 of Ref. 4. Eqs. 4, used with Eqs. 1a and the DAK representation of the SK chart, provided more accurate estimates of the compressibility factor, simplified the prodedures, and included the effects of nitrogen.

This paper reports on further studies using a larger data base. We present an update for the coefficients of Eqs. 4, based on the expanded data base, and a new gas specific gravity correlation. Both Eqs. 4 and the new correlation eliminate the need for Eqs. 3 and include the effects of nitrogen; and can be used with Eqs. 1a to calculate more accurate estimates of the compressibility factor.

EXPANDED DATA BASE

Our previous work on gas compressibility correlations used a data base with a limited number of high specific gravity gases and gases with high impurities content. The data set has been expanded by about 60 %, with emphasis on adding gases to correct these deficiencies. For this study, we added 586 data points from 37 PVT reports from the literature[5-13] and other sources[14-15]. **Table 1** shows the range of composition, physical properties, and conditions of the resulting data base. Our expanded data base contains significantly more gases with specific gravities ranging from 1.3 to 1.8. Additionally, it contains significantly more gases with impurities than the data base used by Sutton. While the maximum concentrations of hydrogen sulfide and carbon dioxide are quite large, only ten percent of the samples had an acid gas concentration greater than twelve percent.

Updated Coefficients for Eqs. 4. Our previous analysis was repeated using the expanded data base to develop the new coefficients for Eqs. 4 shown in **Table 2**. We then evaluated the SBV rules, Sutton's modification to the SBV rules (SSBV) and Eqs. 1a and 4 using the expanded data base. The average absolute errors of the calculated compressibility factors were 2.23, 1.53, and 1.07 percent, respectively. These results were consistent with those in Ref. 4 and are shown in **Table 3**, for four different subsets of the data, ranging from lean sweet gases to rich acid gases, and **Figs. 1** through **4**. **Figs. 2** and **4** show the distribution of the errors with the experimental z factor. Higher errors occurred at lower z factors. Even though the gases in Sutton's data base contained no hydogen sulfide and only limited amounts of carbon dioxide and nitrogen, the z factors calculated using his modification fitted the expanded data base very well. This fact gives a great deal of confidence in the theoretical basis of the form of the SBV equations.

EVALUATION OF SPECIFIC GRAVITY CORRELATIONS

To evaluate the current gas specific gravity correlations, we first assumed that the amount of impurites in the mixture was known. The technique given by Standing[3] for applying the Wichert and Aziz correlation, Eqs. 3, was used to correct for the presence of acid gases. We evaluated Standing's reservoir gas correlation and Sutton's correlation, Eqs. 2. The results of these calculations using our data base are shown in **Table 3** and **Fig. 5**. The average absolute error was 1.99 and 1.42 percent, respectively. We then assumed that the amount of impurites in the mixture was unknown. As may be seen in **Fig. 6**, the error was as large as 27 percent and the maximum error varied linearly with the amount of impurities in the mixture.

DEVELOPMENT OF THE NEW METHOD

Our objective was a method for estimating the pseudocritical constants when composition is not known which, if used with the DAK representation of the SK chart, more accurately reproduces the experimental compressibility factors. The data discussed above was used with the DAK equation of state and a minimization procedure to determine the inferred pseudocritical constants. This set of inferred pseudocritical values was then used with multiple regression analysis to develop a new correlation for J and K to be used with Eqs. 1a in calculating values for the pseudocritical point. We later refer to the new method as the proposed gas specific gravity correlation.

Procedure. A multidimensional conjugate gradient algorithm[16] was used to find the point on the z-p_{pr}-T_{pr} surface given by the

DAK representation of the SK chart which minimized the difference between experimental and calculated z factors. The experimental compressibility factor, pressure and temperature, and pseudocritical constants calculated using Sutton's modification to SBV rules were used as initial guesses. The algorithm converged for all the data points and returned values for the inferred pseudocritical temperature and pressure. Based on our previous finding, that much of the scatter in comparing calculated to inferred values of pseudocritical temperature and pressure, ocurred at the last steps of a depletion study--a difficult laboratory procedure, 121 data points were not used in our correlations. We attempted but were unable to correlate the inferred pseudocritical temperature and pressure with gas specific gravity because of the large amount of impurities in the gases of our data base.

Inferred Values of J and K. The 1482 remaining pairs of the inferred pseudocritical constants and Eqs. 1a were used to find the inferred values for the SBV parameters J and K, as shown below:

$$J_{(inferred)} = \frac{T_{pc(inferred)}}{p_{pc(inferred)}}, \text{ and}$$

$$K_{(inferred)} = \frac{T_{pc(inferred)}}{\sqrt{p_{pc(inferred)}}}. \quad \ldots\ldots (5)$$

After finding that the inferred values of J and K were strongly related to the specific gravity of the gas mixture as can be observed in **Figs. 7** and **8**, we decided to use a regression model similar to Eqs. 4, which was originally developed by Corredor[17]. Notice the data points in the lower right half of both figures. These two samples, which contain very high concentrations of carbon dioxide, obviously are outliers with respect to the relationships between J and K and specific gravity. The correlations can be improved by omitting them; however, they were retained in the data base because they were correlatable by the model discussed below.

Proposed Specific Gravity Correlation. Multiple regression techniques were used with the 1482 pairs of inferred J and K as dependent variables to empirically find a correlation incorporating the first four terms of Eqs. 4 and the gas specific gravity. The new correlations are given by Eqs. 6.

$$J = \alpha_0 + \sum_{i=1}^{3} \alpha_i y_i \left(\frac{T_c}{p_c}\right)_i + \alpha_4 \gamma_g + \alpha_5 \gamma_g^2,$$

and,

$$K = \beta_0 + \sum_{i=1}^{3} \beta_i y_i \left(\frac{T_c}{\sqrt{p_c}}\right)_i + \beta_4 \gamma_g + \beta_5 \gamma_g^2, \quad \ldots\ldots (6)$$

where $y_i \in \{y_{H_2S}, y_{CO_2}, y_{N_2}\}$, and the α_i and β_i are shown in **Table 4**. Eqs. 6 directly account for the effects of hydrogen sulfide, carbon dioxide, and nitrogen, eliminating the need for Eqs. 3. The new method for calculating the z factor uses only Eqs. 1a and 6 and the DAK representation of the SK chart. Note that the new method is simplier than current methods. While Eqs. 6 contains terms similar to those in Eqs. 1b, the introduction of terms for nonhydrocarbon gases is a departure from the current method.

Results. To evaluate Eqs. 1a and 6, we again assumed that the amount of impurites in the mixture was known. **Figs. 9 and 10** compare values of the pseudocritical constants calculated using Eqs. 1a and 6 with the inferred values. The results of z factor calculations are shown in **Table 3** and **Fig. 11**. The average absolute error of the calculated z factor was 1.30 percent using the proposed correlation. We then assumed that the amount of impurites in the mixture was unknown. As indicated in **Fig. 12**, the error was again as large as 27 percent and the maximum error varied linearly with the amount of impurities in the mixture. **Table 5** shows a comparison of errors made in using the gas specific gravity correlations when the amount of impurities are unknown. Notice that the errors are relatively small if the gas is lean and sweet. However, the errors can be large if the gas contains more than five percent acid gas and is at a high pressure. The right half of **Fig. 12** shows results from several samples containing a large amount of impurities. The large errors are attributable to high concentrations of acid gas alone. The large range in error at a constant composition is attributable to variation in pressure. Generally, the larger errors occurred at the higher pressures.

CONCLUSIONS

1. A set of z factors, temperatures, pressures, and gas compositions covering a very wide range of naturally occurring petroleum gases and nonhydrocarbon impurities has been used to develop two new pseudocritical property correlations for use in calculating z factors. These correlations may be used with confidence for any naturally occurring petroleum gas with an acid gas content as high as 50 percent and nitrogen content as high as ten percent.

2. One proposed correlation, based on gas composition, is a modification of the SBV mixing rules, which does not require the use of other correlations for the properties of the heptanes plus fraction or the effect of acid gas and nitrogen. This correlation resulted in z factors which fitted the data base with an average absolute error of 1.1 percent and a maximum error of 5.8 percent.

3. The other proposed correlation, based on gas specific gravity and the amounts of nonhydrocarbon impurities in the gas, also does not require the use of other correlations for the effect of acid gas and nitrogen. This correlation resulted in z factors which fitted the data base with an average absolute error of 1.3 percent and a maximum error of 7.3 percent.

4. The presence of nonhydrocarbon impurities in a gas must be accounted for when using a gas specific gravity correlation. Errors in z factors as high as 27 percent occurred when high concentrations of acid gas were ignored.

NOMENCLATURE

J	= SBV parameter, °R/psia
K	= SBV parameter, °R/psia$^{0.5}$
M	= molar mass, lb-mole
$M_{C_{7+}}$	= molar mass of heptane plus fraction, lb-mole
p	= pressure, psia
p_c	= critical pressure, psia

p_{pc} = pseudocritical pressure, psia
p_{pr} = pseudoreduced pressure
r = correlation coefficient
T = temperature, °R
T_c = critical temperature, °R
T_{pc} = pseudocritical temperature, °R
T_{pr} = pseudoreduced temperature
y_{C7+} = mole fraction of heptane plus fraction
y_i = mole fraction of the i-th component
z = gas compressibility factor
α_i = coefficients of the correlations for J
β_i = coefficients of the correlations for K
γ_g = specific gravity of the gas mixture
ε = Wichert and Aziz pseudocritical temperature adjustment parameter, °R

ACKNOWLEDGMENTS

We thank Core Laboratories Inc. and S. A. Holditch & Associates, Inc. for providing data.

REFERENCES

1. McCain, William D., Jr.: *The Properties of Petroleum Fluids*, 2nd ed., PennWell Books, Tulsa(1990) 104-22, 510-12.
2. Sutton, R. P.: "Compressibility Factors for High Molecular Weight Reservoir Gases," paper SPE 14265 presented at the SPE Annual Technical Meeting and Exhibition, Las Vegas, Sept. 22-25, 1985.
3. Standing, M. B.: *Volumetric and Phase Behavior of Oil Field Hydrocarbon Systems*, 9th Printing, Society of Petroleum engineers of AIME, Dallas(1977) 122.
4. Corredor, J.H., Piper, L.D., and McCain, W.D. Jr.: "Compressibility Factors for Naturally Occurring Petroleum Gases," paper SPE 24864 presented at the SPE Annual Technical Meeting and Exhibition, Washington, D. C., Oct. 4-7, 1992.
5. Wichert, E.: "Compressibility Factor of Sour Natural Gases," MEng Thesis, The University of Calgary, Alberta (1970)
6. Metcalfe, R. S. and Raby, W. J.: "Phase Equilibria for a Rich Gas Condensate-Nitrogen System," *Fluid Phase Equilibria* 29 (1986) 563-73.
7. Firoozabadi, A., Hekim, Y. and Katz, D. L.: "Reservoir Depletion Calculations for Gas Condensates Using Extended Analyses in the Peng-Robinson Equation of State," *J. Cdn. Pet. Tech.*, (Oct., 1978) 610-15.
8. Coats, K. H. and Smart, G. T.: "Application of a Regression-Based EOS PVT Program to Laboratory Data," *SPERE* (May, 1986) 277-99.
9. Kenyon D.E. and Behie, A. : "Third SPE Comparative Solution Project: Gas Cycling of Retrograde Condensate Reservoirs," *JPT* (Aug., 1987) 981-97.
10. Whitson, C. H. and Torp, S. B.: "Evaluating Constant Volume Depletion Data," *JPT* (March, 1983) 610-620.
11. Moses, P. L. : "Engineering Applications of Phase Behavior of Crude Oil and Condensate Systems," *JPT* (July, 1986) 715-23.
12. Coats, K. H.: "Simulation of Gas Condensate Reservoir Performance," paper SPE 10512 presented at the Sixth SPE Symposium on Reservoir Simulation, New Orleans, Jan. 31-Feb. 3, 1982.
13. Kilgren, K. H.. : "Phase Behavior of a High-Pressure Condensate Reservoir Fluid," *JPT* (Aug, 1966) 1001-7.
14. Vrla, F.: personal communication, May 29, 1992.
15. Holditch, S. A.: personal communication, June 7, 1993
16. Press, W. H., Flannery, B. P., Teukolsky, S. A. and Vetterling, W. T.: *Numerical Recipes*, 1st ed., Cambridge University Press, New York, (1986) 301-7.
17. Corredor, J. H.: "Compressibility Factors for Retrograde Gases: A New Correlation," MS Thesis, Texas A&M University, College Station (1991).

TABLE 1--RANGE OF DATA

Variable	Mean	Minimum	Maximum
Hydrogen Sulfide	2.45	0.00	51.37
Carbon Dioxide	3.38	0.00	67.16
Nitrogen	1.87	0.00	15.68
Methane	71.15	19.37	94.73
Ethane	8.21	2.30	18.40
Propane	4.04	0.06	12.74
iso-Butane	0.90	0.00	2.60
n-Butane	1.55	0.00	6.04
iso-Pentane	0.64	0.00	2.24
n-Pentane	0.88	0.00	3.92
Hexane	0.65	0.00	4.78
Heptane Plus	4.28	0.00	14.94
M_{C7+}	135.2	98.0	295.0
γ_{C7+}	0.779	0.710	0.884
z	0.989	0.698	2.099
T, °F	243.8	78.0	326.0
p, psia	3758.6	514.0	12814.0
γ_g (air = 1)	0.972	0.613	1.821

TABLE 2--UPDATED COEFFICIENTS FOR EQS. 4

	J		K	
i	α_i	Standard Error	β_i	Standard Error
0	5.2073E-02	8.8370E-03	-3.9741E-01	2.2271E-01
1	1.0160E+00	2.3018E-02	1.0503E+00	1.5428E-02
2	8.6961E-01	2.1985E-02	9.6592E-01	1.6132E-02
3	7.2646E-01	4.1292E-02	7.8569E-01	4.2227E-02
4	8.5101E-01	1.5402E-02	9.8211E-01	1.5134E-02
5	0.0	0.0	0.0	0.0
6	2.0818E-02	2.10E-04	4.5536E-01	4.546E-03
7	-1.506E-04	7.0E-06	-3.7684E-03	1.73E-04
r^2	0.981		0.979	

TABLE 3--ACCURACY OF COMPRESSIBILITY FACTOR CALCULATIONS

	Pseudocritical Property Correlation					
	Composition Known			Gravity and Impurities Known		
	SBV	SSBV	Eqs. 4	Standing	Sutton	Eqs. 6
Lean Sweet Gases ($0.61 < \gamma_g < 0.99$) - 628 data points ($y_{C_{7+}} < 4$ % & $y_{H_2S} + y_{CO_2} < 5$ %)						
Average Error	-0.023	-0.014	0.001	-0.004	0.001	0.003
Maximum Absolute Error	0.065	0.067	0.054	0.089	0.079	0.076
Average Absolute Error, %	2.508	1.577	1.040	1.293	1.304	1.361
Maximum Absolute Error, %	6.668	4.582	5.831	5.882	6.371	7.280
Lean Acid Gases ($0.63 < \gamma_g < 1.42$) - 369 data points ($y_{C_{7+}} < 4$ % & $y_{H_2S} + y_{CO_2} \geq 5$ %)						
Average Error	-0.010	-0.002	-0.001	-0.006	-0.002	-0.003
Maximum Absolute Error	0.046	0.046	0.030	0.063	0.053	0.035
Average Absolute Error, %	1.627	1.267	1.015	1.295	1.163	1.176
Maximum Absolute Error, %	6.467	6.518	3.647	6.356	6.450	4.386
Rich Sweet Gases ($0.84 < \gamma_g < 1.82$) - 439 data points ($y_{C_{7+}} \geq 4$ % & $y_{H_2S} + y_{CO_2} < 5$ %)						
Average Error	-0.014	0.008	0.003	-0.034	0.009	0.001
Maximum Absolute Error	0.148	0.056	0.053	0.162	0.075	0.061
Average Absolute Error, %	2.556	1.608	1.173	3.070	1.681	1.356
Maximum Absolute Error, %	7.571	5.816	4.410	9.795	7.856	4.709
Rich Acid Gases ($0.84 < \gamma_g < 1.82$) - 167 data points ($y_{C_{7+}} \geq 4$ % & $y_{H_2S} + y_{CO_2} \geq 5$ %)						
Average Error	-0.012	0.011	0.001	-0.032	-0.004	-0.002
Maximum Absolute Error	0.063	0.057	0.048	0.143	0.059	0.043
Average Absolute Error, %	1.656	1.689	1.069	3.307	1.715	1.235
Maximum Absolute Error, %	5.789	7.719	3.674	9.829	6.786	5.350
Total - 1603 data points						
Average Error	-0.016	-0.003	0.001	-0.016	0.002	0.001
Maximum Absolute Error	0.148	0.067	0.054	0.162	0.079	0.076
Average Absolute Error, %	2.230	1.526	1.073	1.990	1.418	1.304
Maximum Absolute Error, %	7.571	7.719	5.831	9.829	7.856	7.280

TABLE 4--PROPOSED GAS SPECIFIC GRAVITY CORRELATION

	J		K	
i	α_i	Standard Error	β_i	Standard Error
0	1.1582E-01	7.450E-03	3.8216E+00	1.7133E-01
1	-4.5820E-01	1.3616E-02	-6.5340E-02	8.684E-03
2	-9.0348E-01	1.5387E-02	-4.2113E-01	1.0812E-02
3	-6.6026E-01	3.9664E-02	-9.1249E-01	4.1073E-02
4	7.0729E-01	1.3878E-02	1.7438E+01	3.1914E-01
5	-9.9397E-02	6.055E-03	-3.2191E+00	1.3925E-01
r^2	0.979		0.975	

TABLE 5--ACCURACY OF GAS SPECIFIC GRAVITY CORRELATIONS WHEN IMPURITIES ARE UNKNOWN

		$y_{H_2S} + y_{CO_2} < 5$ %		$y_{H_2S} + y_{CO_2} \geq 5$ %	
		Sutton	Eqs. 6	Sutton	Eqs. 6
$y_{C_{7+}} < 4$ %	Avg. Abs. Error, %	1.273	1.224	4.133	3.994
	Max. Abs. Error, %	5.359	5.699	27.22	27.03
$y_{C_{7+}} \geq 4$ %	Avg. Abs. Error, %	1.909	1.408	4.012	3.347
	Max. Abs. Error, %	8.048	4.859	24.64	21.99

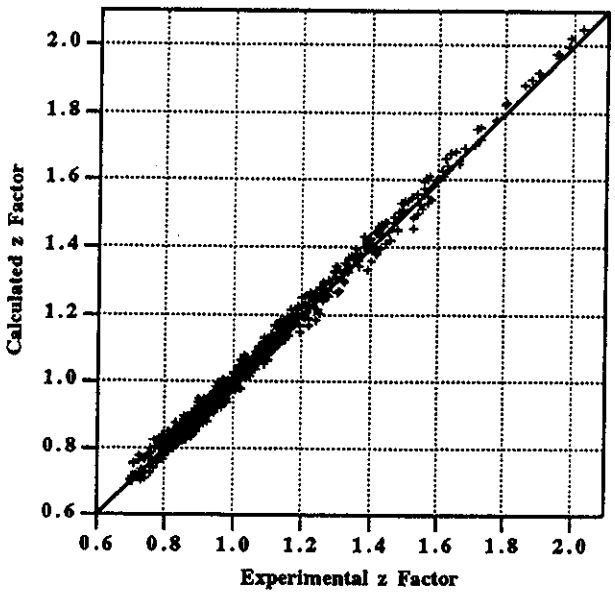

Fig. 1--Calculated z Factor using Sutton's Modification to SBV Rules

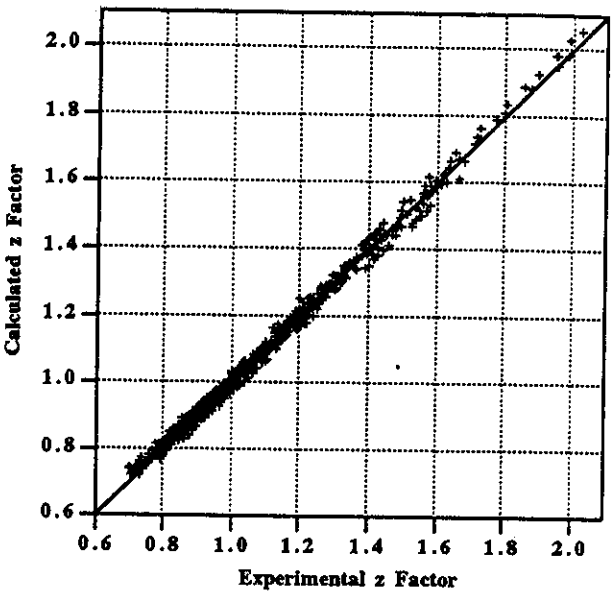

Fig. 3--Calculated z Factor using Proposed Modification to SBV Rules

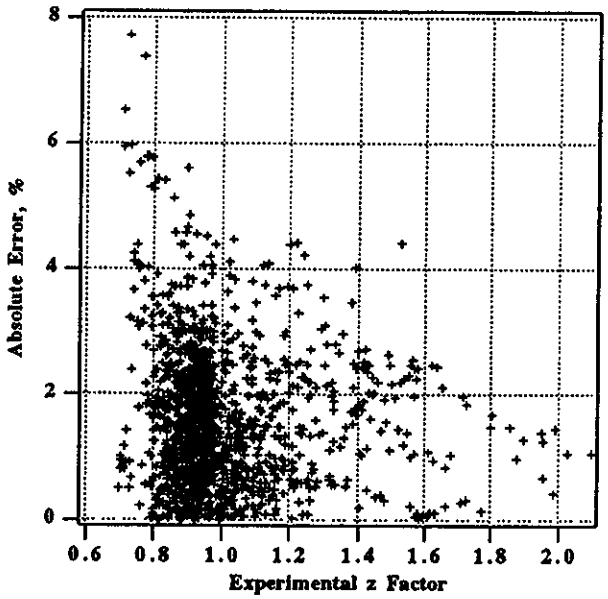

Fig. 2--Error in Calculated z Factor using Sutton's Modification to SBV Rules

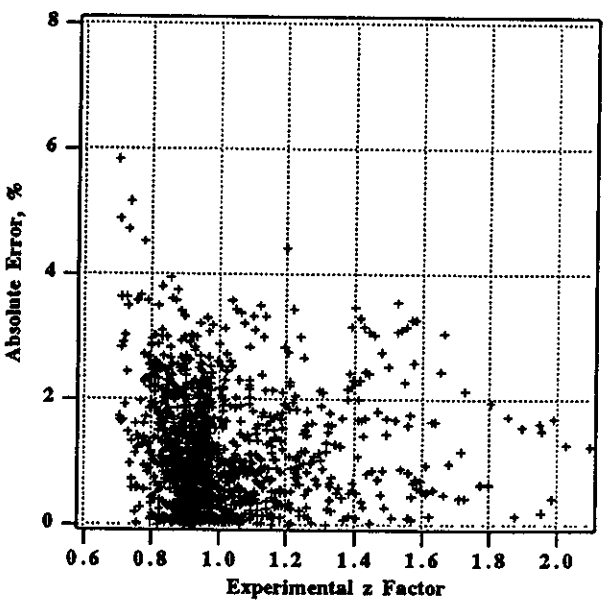

Fig. 4--Error in Calculated z Factor using Proposed Modification to SBV Rules

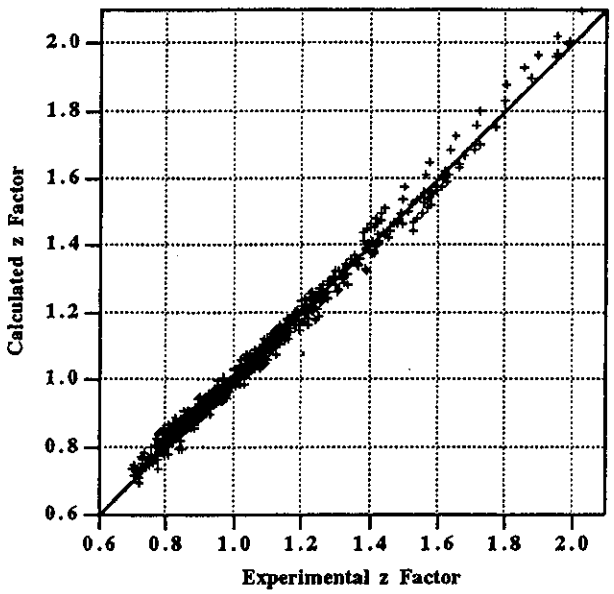

Fig. 5--Calculated z Factor using Sutton's Specific Gravity Correlation with Impurities Known

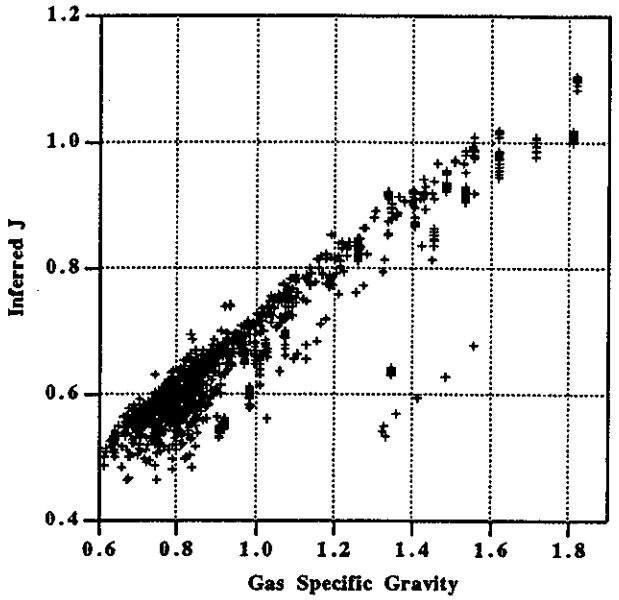

Fig. 7--Variation of the Inferred Value of J with the Specific Gravity of the Gas Mixture

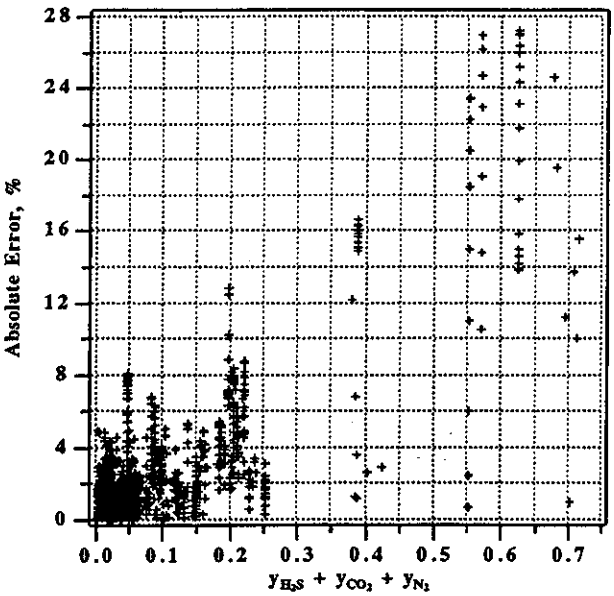

Fig. 6--Error in Calculated z Factor using Sutton's Specific Gravity Correlation with Impurities Unknown

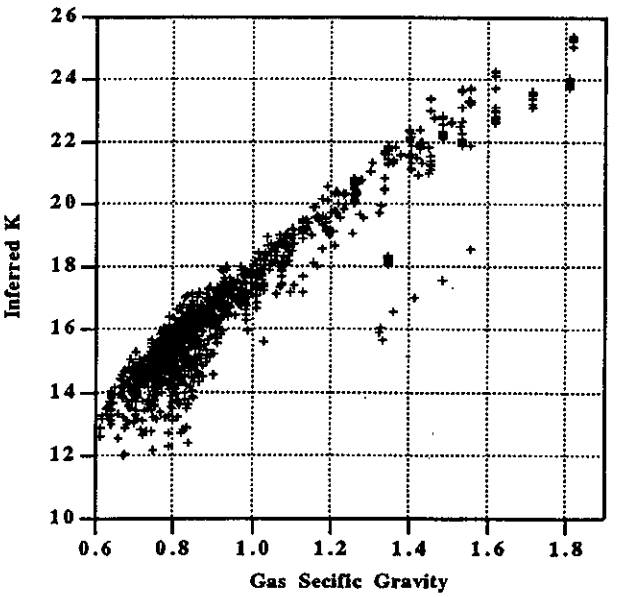

Fig. 8--Variation of the Inferred Value of K with the Specific Gravity of the Gas Mixture

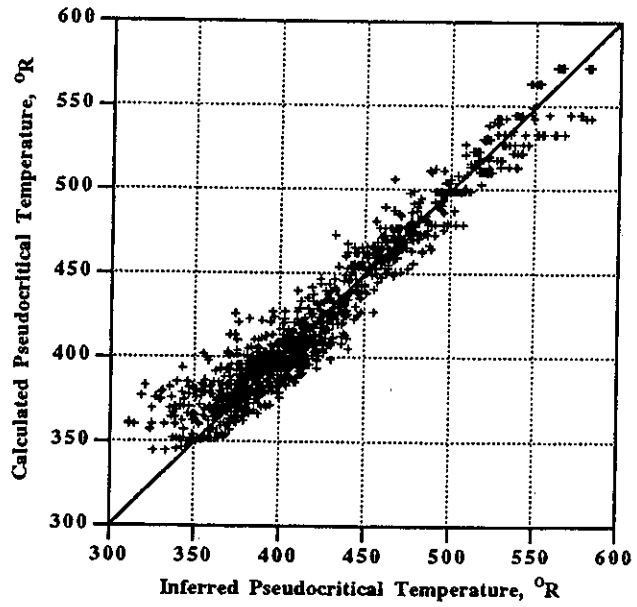

Fig. 9--Calculated Pseudocritical Temperature using Proposed Specific Gravity Correlation

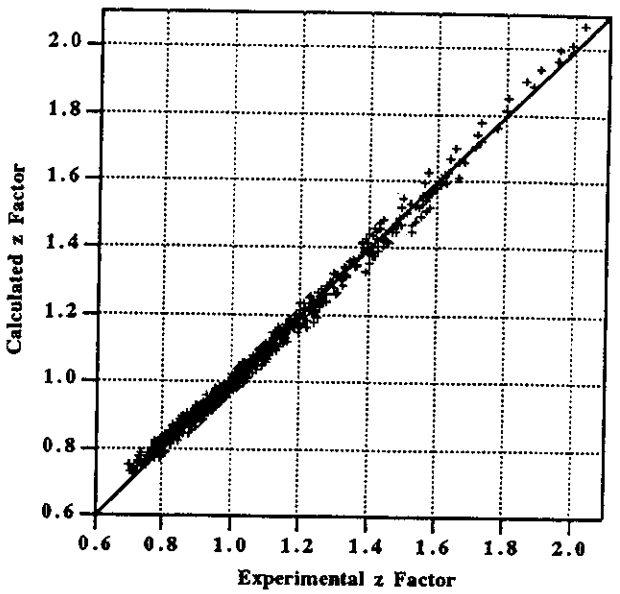

Fig. 11--Calculated z Factor using Proposed Specific Gravity Correlation with Impurities Known

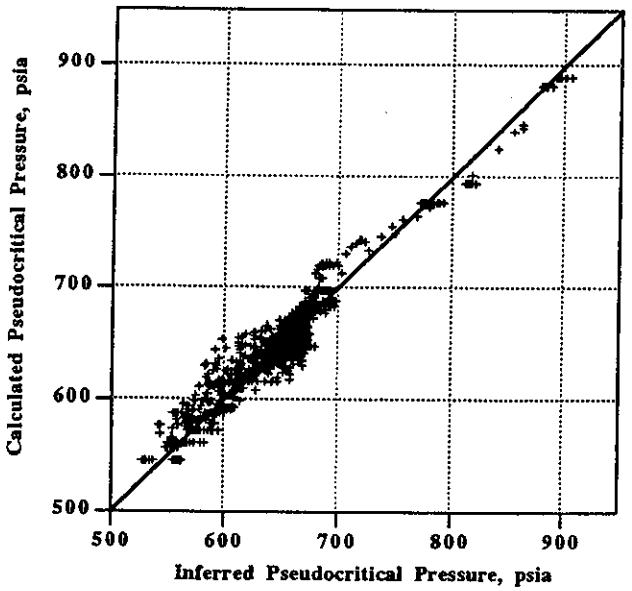

Fig. 10--Calculated Pseudocritical Pressure using Proposed Specific Gravity Correlation

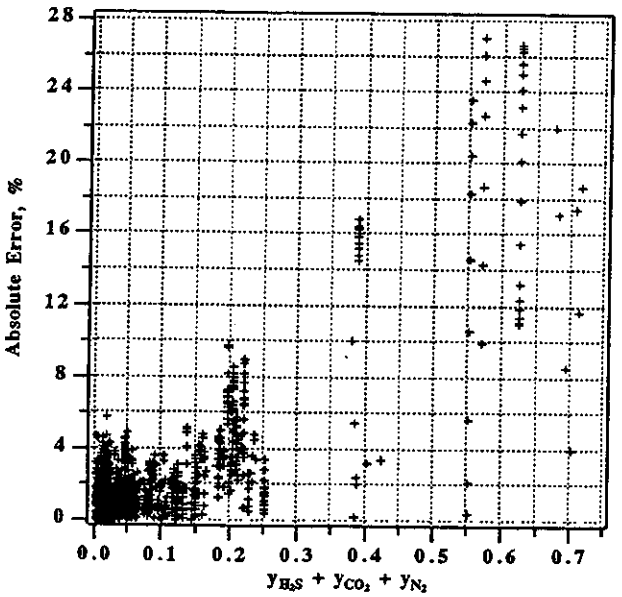

Fig. 12--Error in Calculated z Factor using Proposed Specific Gravity Correlation with Impurities Unknown

J as a Function of Gas Specific Gravity and Amount of Impurities

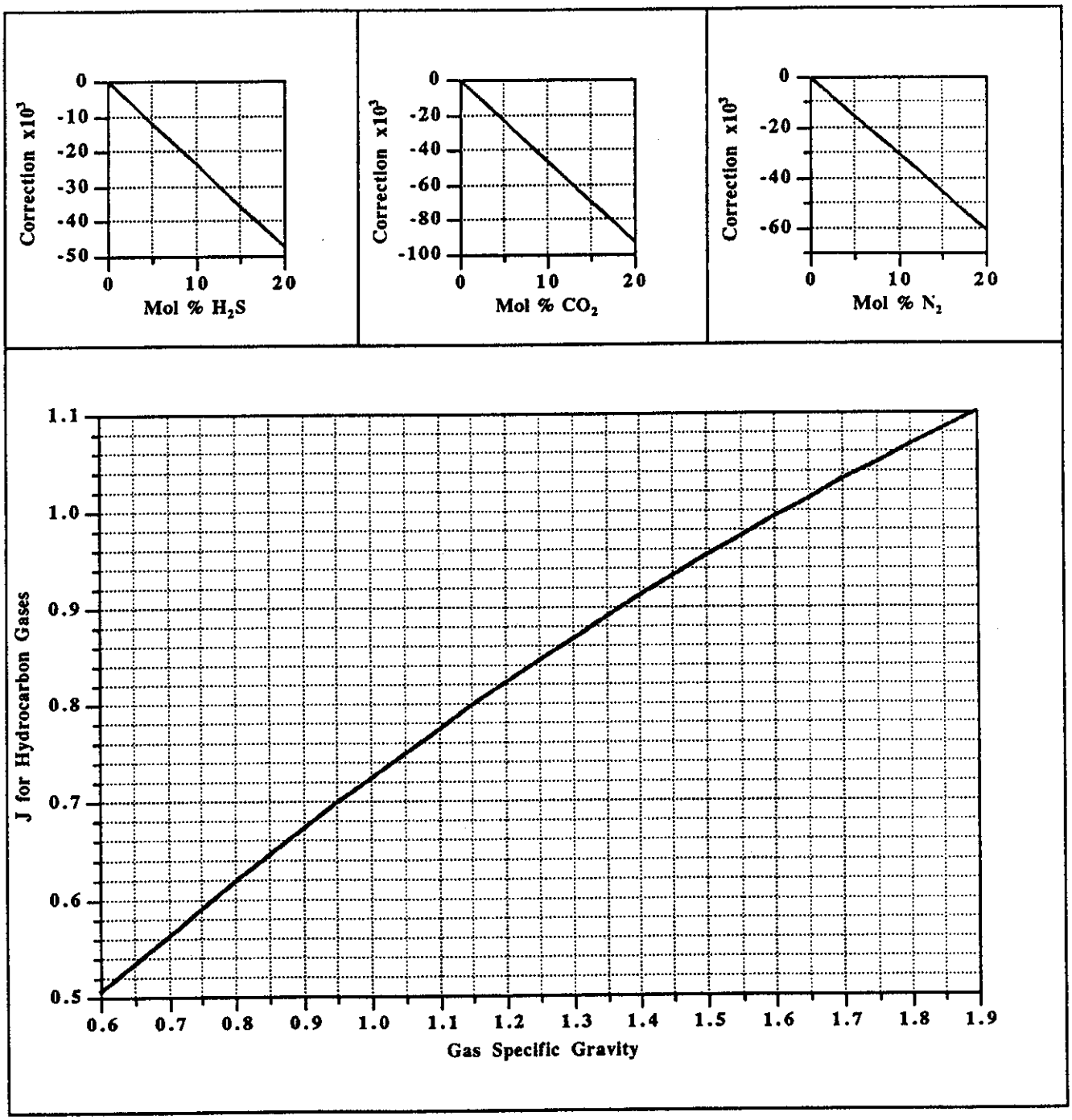

NOTE: Use this chart for J, the companion chart for K, and the Stewart, Burkhardt and Voo equations,

$$T_{pc} = \frac{K^2}{J} \;\&\; p_{pc} = \frac{T_{pc}}{J} \text{ to estimate } T_{pc} \;\&\; p_{pc}.$$

See Piper, McCain, & Corredor, "Compressibility Factors for Naturally Occurring Petroleum Gases", SPE 26668, presented at the 1993 SPE Annual Technical Conference and Exhibition in Houston, Texas, October 3-6, 1993.

K as a Function of Gas Specific Gravity and Amount of Impurities

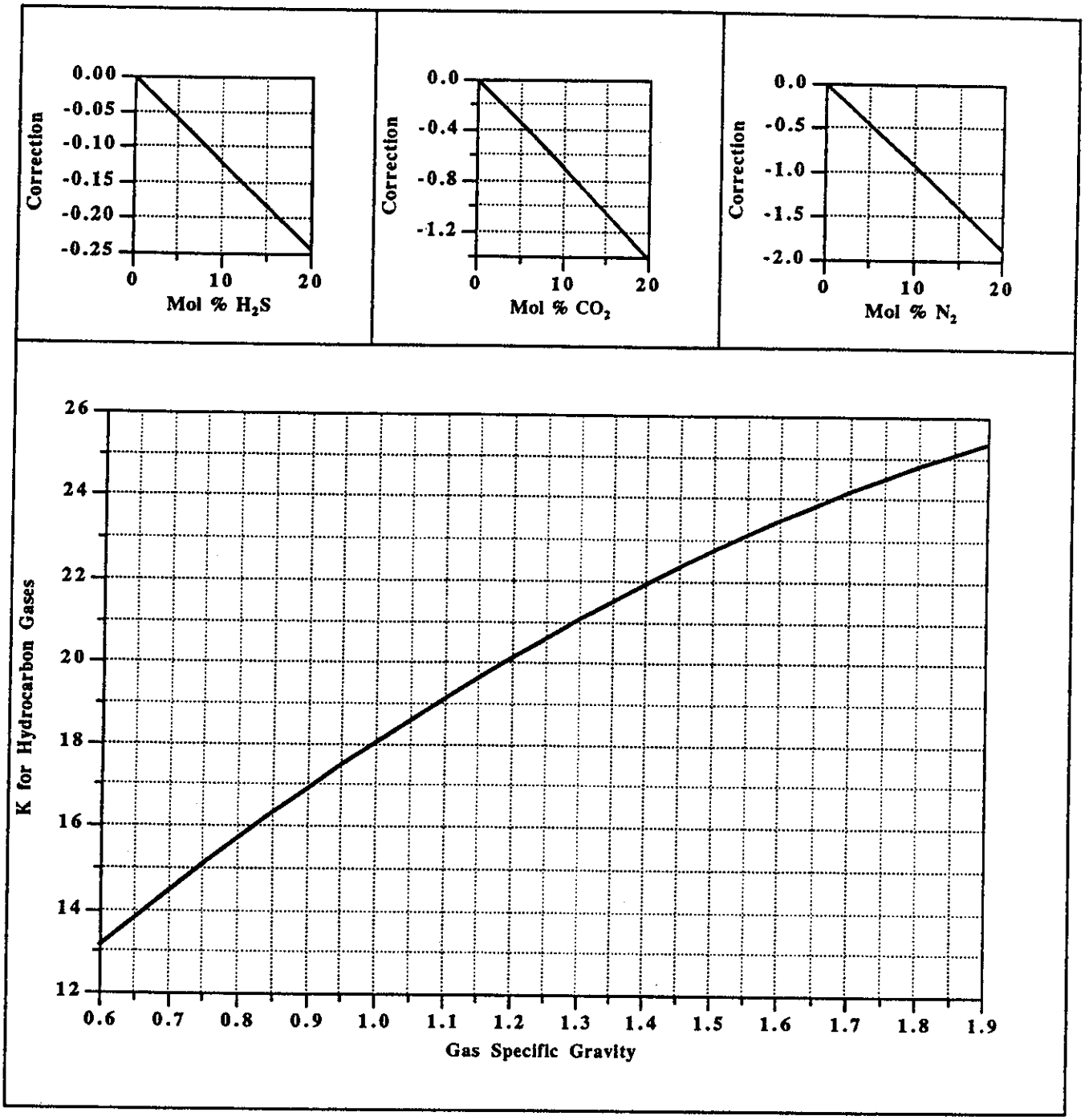

NOTE: Use this chart for K, the companion chart for J, and the Stewart, Burkhardt and Voo equations,

$$T_{pc} = \frac{K^2}{J} \;\&\; p_{pc} = \frac{T_{pc}}{J} \text{ to estimate } T_{pc} \;\&\; p_{pc}.$$

See Piper, McCain, & Corredor, "Compressibility Factors for Naturally Occurring Petroleum Gases", SPE 26668, presented at the 1993 SPE Annual Technical Conference and Exhibition in Houston, Texas, October 3-6, 1993.

The Effect of Water Influx on p/z-Cumulative Gas Production Curves

J. R. BRUNS
MEMBER AIME
M. J. FETKOVICH
JUNIOR MEMBER AIME
V. C. MEITZEN

PHILLIPS PETROLEUM CO.
BARTLESVILLE, OKLA.

Abstract

The relationship between p/z and cumulative gas production for typical gas reservoirs was studied by calculating pressure response to various modes of gas production and water encroachment. Water encroachment methods considered were Schilthuis, Hurst simplified and van Everdingen-Hurst. In the method, the assumptions normally made in water encroachment calculations were accepted. Normally, pressures are measured and the gas reserves and water encroachment found implicitly. Conversely, in this work various encroachment factors, reserves and reservoir-aquifer geometry were assumed and the pressures solved implicitly.

The results show the spectrum of p/z shapes that can be expected for real reservoirs. With normal encroachment rates for closed aquifers the p/z chart exhibits the typical inflection at early times. This has sometimes been interpreted as all measurement error. These studies have shown that a new look should be taken at interpretation. It is rather dangerous to extrapolate "straight-line" p/z charts if encroachment from an aquifer is suspected.

Introduction

A common method of predicting gas reserves is the graphical solution to the gas material balance equation. A special case of the material balance equation is linear in p/z with cumulative gas production (G_p) which predicts the initial in-place gas when p/z is extrapolated to zero. Derivation of this form is based on the equation of state, corrected for compressibility ($pV = znRT$), and, particularly, on the reservoir being closed (no water encroachment). A straight line on the p/z chart results when these conditions hold. However, an apparent straight line on the chart does not assure that the reservoir is closed. Many of the curves show a rapid decline in the early stages of production after which they flatten out. Confusion arises as to whether these characteristics are caused totally by pressure measurements. To answer this question in part, a series of controlled mathematical experiments was performed in which a typical gas field was produced subject to various forms of water encroachment. These runs were specifically designed to eliminate measurement errors by calculating pressures at the inner boundary of the aquifer. The resultant p/z charts were thus made available for study and direction in predicting reserves and to indicate the curvature that can be expected in addition to that caused by normal measurement error.

Original manuscript received in Society of Petroleum Engineers office July 13, 1964. Revised manuscript received Feb. 2, 1965. Paper presented at SPE 39th Annual Fall Meeting held in Houston, Tex., Oct. 11-14, 1964.

Solution of the Basic Equation for p/z

The basic equation solved for p and p/z is derived in Appendix A. It is

$$G_a = G_r + \frac{K_i S(p,t)}{B_g - B_{gi}} \quad . \quad . \quad . \quad . \quad . \quad . \quad . \quad . \quad . \quad (1)$$

G_a and G_r are the apparent and real values of original gas in place and are derived by assuming a closed reservoir for G_a, and one open to an aquifer for G_r. The function $S(p,t)$ is defined by three methods—Schilthuis, Hurst simplified or van Everdingen-Hurst.[1-4] The definitions of these functions are given in Appendix B.

Eq. 1 is the linear function that is commonly plotted (G_a vs $S(p,t)/B-B_i$) with the intercept predicting the original gas in place and slope predicting the water encroachment factor.[5,6] This is a graphical solution of Eq. 1 when histories on pressure and cumulative productions are known. In some cases the equation has been rearranged so a plot can be made such that the encroachment factor is predicted by the intercept and the reserve by the slope.[7]

In the calculations presented in this paper, in-place values, water encroachment factors, rock fluid properties, and cumulative production were set. Eq. 1 was solved implicitly for p/z.

The equivalent of Eq. 1 in terms of p/z is

$$p/z = \frac{p_i}{z_i}\left[\frac{G_r - G_p}{G_r - \frac{z_i T p_{sc}}{T_{sc} p_i K_i S(p,t)}}\right] \quad . \quad . \quad . \quad (2)$$

[1]References given at end of paper.

Setting $K_e S(p,t) = 0$ (no water encroachment), produces the linear form. Obviously, whether the p/z curve is linear or not when $K_e S(p,t) \neq 0$ depends upon the $S(p,t)$ function.

The cumulative productions were determined from production rates calculated from wellhead operating curves subject to the maximum allowables.[8] The wellhead curve is defined by

$$q_g = C(p_{swh}^2 - p_{tf}^2)^n, \quad \ldots\ldots\ldots \quad (3)$$

where q_g = the production rate, Mscf/D
C = the performance coefficient
p_{swh} = the wellhead shut-in pressure, psia
p_{tf} = the tubing flowing pressure
n = the back-pressure exponent.

Shut-in wellhead pressures were determined after the reservoir pressure p was chosen by calculating the static head by the method of Cullender and Smith.[9] The static head was subtracted from p to give p_{swh}.

A general flow scheme of the calculation technique is given in Fig. 1, and the field conditions are given in Table 1.

Compressibilities were interpolated from the 1952 API tables. Tables 2 and 3 list conditions that were varied for individual runs.

Discussion of Results

The results of the calculations are shown in Figs. 2 through 9. All of the curves show p/z as a function of cumulative gas produced and are labeled with the numbers corresponding to the data in Tables 2 and 3. Each plotted point represents two years.

Fig. 2 gives the results when the aquifer was assumed to be unlimited, or when original aquifer pressure was assumed to remain constant at some outer boundary (Schilthuis). As the encroachment factor was increased the pressure was maintained at a higher and higher level. The dotted line at the bottom represents no encroachment and the top dotted line shows complete pressure maintenance by a very active water drive.

Fig. 3 shows the results of increasing the Hurst simplified encroachment factor from 2.5×10^4 to 2.5×10^6 (cu ft) ln (mo)/psi/year.

The van Everdingen-Hurst encroachment factors were assumed for runs shown in Figs. 4 through 9, and the aquifer was assumed closed and radial. Combinations of three variations in relative aquifer size, two water compressibilities and nine aquifer permeabilities were represented in the runs.

Curves with inflections, which have been observed in practice, were produced for the closed aquifers.

In most cases the families of curves appear to approach a common slope at zero time. At zero time this slope will represent the p/z line for no water encroachment.

Runs with the Schilthuis method and Hurst-simplified method converge at or near a horizontal line as water encroachment factors increase. This means that pressure drops in the aquifer are approaching zero.

In the van Everdingen-Hurst runs the curves respond to the mobility (k/μ) and compressibility of the water, and the relative size of the aquifer. For R_a/R_r of 1.5,

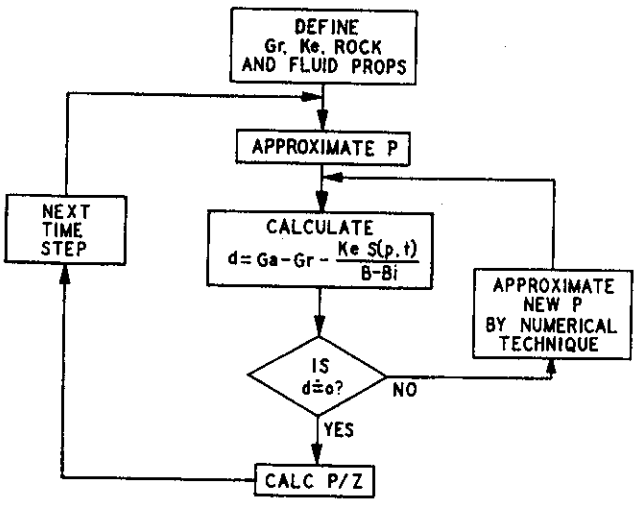

Fig. 1—Solution of Eq. A-12 for p/z.

TABLE 1—FIELD CONDITIONS

Area = 2,500 acres
Pay = 100 ft
Porosity = 0.25
Connate water = 0.3
Original BHP = 5,000 psia
Formation temperature = 250F
Depth = 10,000 ft
Gas Gravity = 0.68 (No N_2, CO_2 or H_2S)
$(\text{Radius})^2 = 34.7\times10^6$ sq ft
Initial wellhead shut-in pressure = 4,200 psia
Wellhead shut-in temperature = 100F
Back-pressure curve slope = 0.7
Open flow potential = 74.4 MM scf/D
Minimum wellhead flowing pressure = 100 psia
Maximum allowable field rate = 47.2 MM scf/D

TABLE 2—VARIABLE CONDITIONS FOR RUNS 1 THROUGH 14

Run No.	Type Encroachment Factor	Encroachment Factor
1	↑	5,900
2		18,000
3	Schilthuis	36,000
4	(cu ft/psi/year)	59,000
5	Radial Infinite	100,000
6	↓	200,000
7		590,000
8	↑	25,000
9		90,000
10	Hurst Simplified	150,000
11	(cu ft in (month)/psi/year)	250,000
12	Radial Infinite	340,000
13	↓	610,000
14		2,500,000

TABLE 3—VARIABLE CONDITIONS FOR RUNS 15 THOUGH 38

Run No.	Type Encroachment Factor	Ratio of Aquifer Radius to Field Radius	Aquifer Permeability (md)	Dimensionless Time to Real Time Ratio (1/year)	Water Compressibility (1/psi)
15		1.5	1	.089	3.0×10^{-6}
16		1.5	10	.89	3.0×10^{-6}
17	↓	1.5	100	8.9	3.0×10^{-6}
18		5.0	1	.089	3.0×10^{-6}
19	van Everdingen	5.0	10	.89	3.0×10^{-6}
20	Hurst Radial Finite	5.0	100	8.9	3.0×10^{-6}
21	16,350 cu ft/psi	5.0	1000	89.	3.0×10^{-6}
22		10.0	1	.089	3.0×10^{-6}
23		10.0	10	.89	3.0×10^{-6}
24		10.0	100	8.9	3.0×10^{-6}
25	↓	10.0	1000	89.	3.0×10^{-6}
26		10.0	10000	890.	3.0×10^{-6}
27		1.5	10	.089	30×10^{-6}
28		1.5	100	.89	30×10^{-6}
29	↓	5.0	10	.089	30×10^{-6}
30		5.0	18	.16	30×10^{-6}
31	van Everdingen	5.0	39.3	.35	30×10^{-6}
32	Hurst Radial Finite	5.0	100	.89	30×10^{-6}
33	163,500 cu ft/psi	10.0	10	.089	30×10^{-6}
34		10.0	15.8	.141	30×10^{-6}
35		10.0	31.5	.28	30×10^{-6}
36		10.0	100	.89	30×10^{-6}
37	↓	10.0	1000	8.9	30×10^{-6}
38		10.0	10000	89.	30×10^{-6}

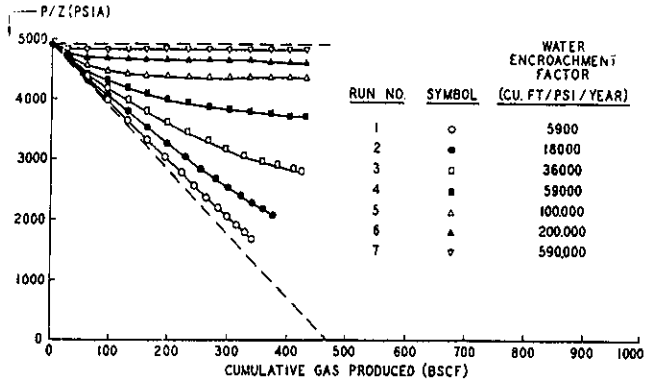

Fig. 2—Curves of p/z for gas reservoirs with water influx, Schilthuis method.

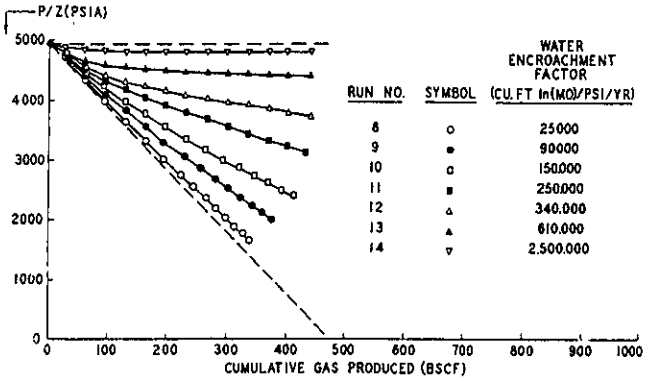

Fig. 3—Curves of p/z for gas reservoirs with water influx, Hurst simplified method.

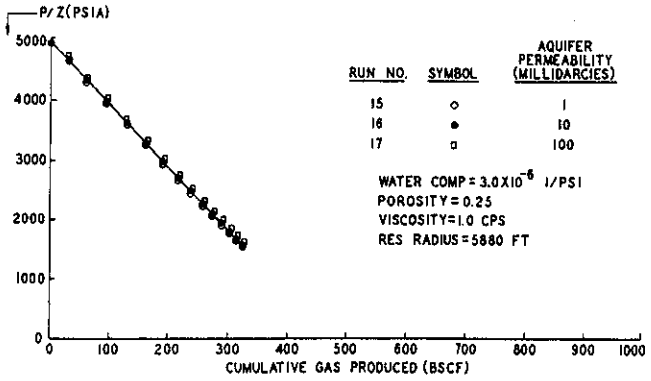

Fig. 4—Curves of p/z for gas reservoirs with water influx, van Everdingen-Hurst, finite, $R_a/R_r = 1.5$.

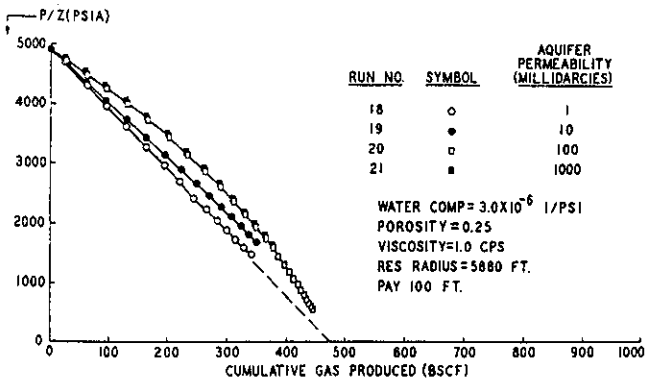

Fig. 5—Curves of p/z for gas reservoirs with water influx, van Everdingen-Hurst method, finite, $R_a/R_r = 5$.

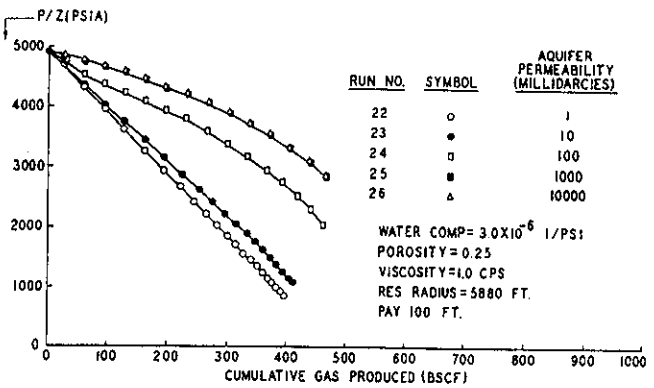

Fig. 6—Curves of p/z for gas reservoirs with water influx, van Everdingen-Hurst method, finite, $R_a/R_r = 10$.

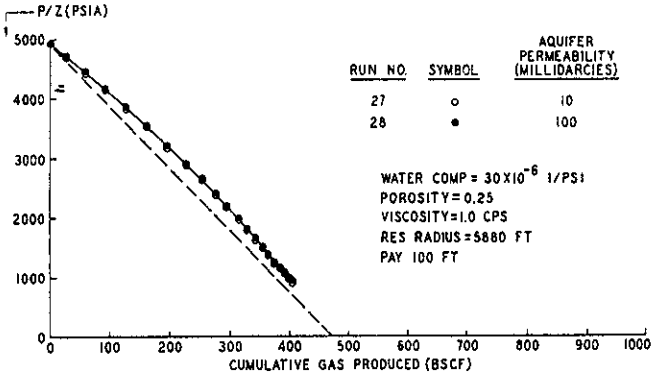

Fig. 7—Curves of p/z for gas reservoirs with water influx, van Everdingen-Hurst method, finite, $R_a/R_r = 1.5$.

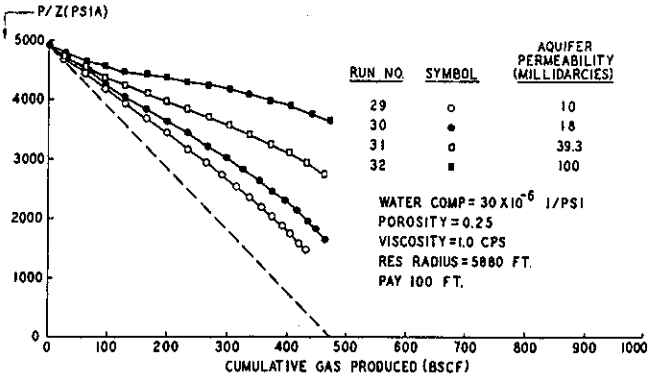

Fig. 8—Curves of p/z for gas reservoirs with water influx, van Everdingen-Hurst method, finite, $R_a/R_r = 5$.

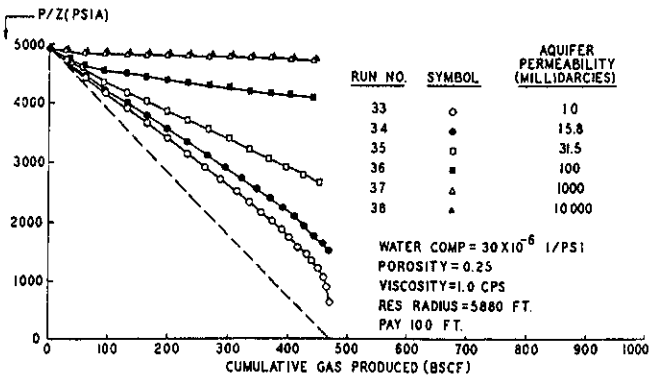

Fig. 9—Curves of p/z for gas reservoirs with water influx, van Everdingen-Hurst method, finite, $R_a/R_r = 10$.

the effect of the aquifer is negligible for a given water compressibility regardless of the permeability (Fig. 4). However, for a higher water compressibility an effect is felt for comparable mobilities (Fig. 7).

In general the pressure is maintained at higher levels as the water compressibility, aquifer size or water mobility is increased. Yet, even with increases in mobility an extreme curve was approached for the closed aquifers (Runs 25 and 26, Fig. 6). In these cases pressure drops in the aquifer were small and the shapes were controlled by the water compressibilities.

Conclusions

Fig. 10 illustrates the increasing error that occurs if a p/z curve is extrapolated with no regard for water encroachment. As the relative size of the aquifer increases from $R_a/R_r = 1.5$ to 10, the error increases from a negligible amount to an estimate of over 100 per cent of the actual initial gas in place. This estimate would be made after 65 per cent of the initial gas in place is produced.

This leads to the principal conclusion that it is dangerous to extrapolate p/z charts on a straight line without considering the possibility of water influx.

Runs performed here eliminated measurement error and the curved portions were produced under realistic production schedules. Thus, curved portions at the start of production history can be caused by the unsteady-state nature of the aquifer and not solely by measurement errors. So, these curved portions should not be neglected, but ought to be regarded as an indication of possible water encroachment.

These results make a case for accelerated early production so that the inflections will be accentuated, permitting better early estimates of gas in place.

Acknowledgment

The authors thank the Phillips Petroleum Co. for permission to publish this work. Special thanks are due R. V. Smith for his cooperation and assistance.

References

1. Schilthuis, R. J.: "Active Oil and Reservoir Energy", *Trans.*, AIME (1936) **118**, 33.
2. van Everdingen, A. F. and Hurst, W.: "The Application of the Laplace Transformation to Flow Problems in Reservoirs", *Trans.*, AIME (1949) **186**, 305.
3. Hurst, W.: "Water Influx Into a Reservoir and Its Application to the Equation of Volumetric Balance", *Trans.*, AIME (1943) **151**, 57.
4. van Everdingen, A. F., Timmerman, E. H. and McMahon, J. J.: "Application of the Material Balance Equation to a Partial Water Drive Reservoir", *Trans.*, AIME (1953) **198**, 51.
5. Pirson, S. J.: *Oil Reservoir Engineering*, 2nd Ed. McGraw-Hill Book Co., Inc., New York (1958) 608.
6. Stanley, L. T.: "Curve-Fitting Cuts Material Balance Calculations", *Pet. Eng.* (Aug., 1961) 90.
7. Hubbard, R. M. and Elenbaas, J. R.: "Determining Gas-Filled Pore Volume in a Water-Drive Gas Storage Reservoir", *Jour. Pet. Tech.* (April, 1964) 383.
8. Frick, T. C.: *Petroleum Production Handbook*, Vol. II, McGraw-Hill Book Co., Inc., New York (1962) 30.
9. Cullender, M. H. and Smith, R. V.: "Practical Solution of Gas-Flow Equations for Wells and Pipelines with Large Temperature Gradients", *Trans.*, AIME (1956) **207**, 281.

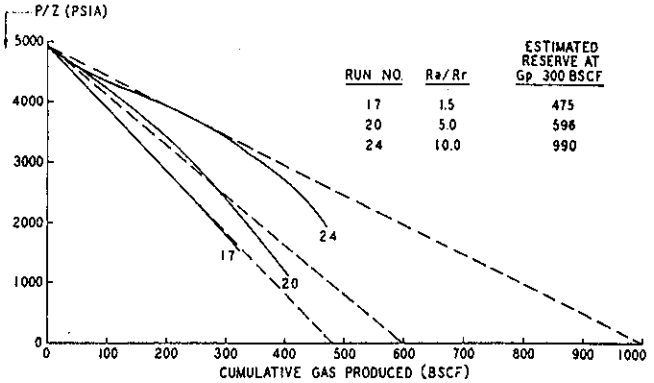

Fig. 10—Comparison of p/z curves for increasing aquifer sizes, van Everdingen-Hurst, radial finite.

APPENDIX A

Derivation of the Basic Equations

The apparent reserves for a gas field are those determined when no water encroachment is assumed, or,

$$V_p = V_{pi} \quad \ldots \quad (A\text{-}1)$$

where V_{pi} is the original pore volume, cu ft.

V_p is the pore volume containing gas at some later time.

$$V_p = (G_a - G_p)B_g \quad \ldots \quad (A\text{-}2)$$

$$V_{pi} = G_a B_{gi} \quad \ldots \quad (A\text{-}3)$$

where G_a = the apparent original gas in place, scf
G_p = cumulative gas produced, scf

B_{gi} and B_g are the gas formation volume factors, cu ft/scf.

$$B_{gi} = \frac{p_{sc} T_i Z_i}{p_i T_{sc}} \quad \ldots \quad (A\text{-}4)$$

$$B_g = \frac{p_{sc} T z}{p T_{sc}} \quad \ldots \quad (A\text{-}5)$$

Substituting Eqs. A-2 and A-3 into Eq. A-1 and solving for G_a gives

$$G_a = G_p\left(\frac{B}{B_g - B_{gi}}\right) \quad \ldots \quad (A\text{-}6)$$

When water encroachment is considered, Eq. A-1 is replaced by

$$V_p = V_{pi} - W_e \quad \ldots \quad (A\text{-}7)$$

to account for the water influx W_e.

Under these conditions, G_a in Eqs. A-2 and A-3 is defined as G_r (real initial in place gas), or,

$$V_p = (G_r - G_p)B_g \quad \ldots \quad (A\text{-}8)$$

and

$$V_{pi} = G_r B_{gi} \quad \ldots \quad (A\text{-}9)$$

Substitution of Eqs. A-8, A-9, and

$$W_e = K_e S(p,t) \quad \ldots \quad (A\text{-}10)$$

into Eq. A-7 gives

$$G_r = \frac{G_p B}{(B_g - B_{gi})} - \frac{K_e S(p,t)}{(B_g - B_{gi})} \quad \ldots \quad (A\text{-}11)$$

where K_e is the water encroachment factor and $S(p,t)$

TABLE 4
Equation B-10—A Constants

R_a/R_r	Middle Range of Δtd_i From	To	A_1	A_2	A_3	A_4	A_5	Stabilized State Values Above the Middle Range
1.5	.1206	0.7	− 0.03255975	−0.02485001	0.03179695	0.007970778	0.6164517	0.6235899
2.0	.418	2.5	0.3852062	−0.09626595	−0.05244533	−0.004754153	1.281475	1.509915
2.5	.815	6.0	0.7919653	0.05396428	−0.06348801	−0.01234595	1.534877	2.634689
3.0	1.33	11.0	1.046089	0.2388103	−0.08575203	−0.008445356	1.574667	3.994681
3.5	1.12	25.0	0.4178854	1.292179	−0.4404957	0.03704949	1.630682	5.650575
4.0	2.05	34.0	− 2.231692	3.177286	−0.8411667	0.06444676	2.779082	7.499222
4.5	2.62	46.0	− 6.108747	5.413047	−1.266439	0.09235701	4.890919	9.619498
5.0	3.06	60.0	− 6.429505	4.822608	−0.8503674	0.03632684	5.599367	11.97866
6.0	5.85	110.0	−24.90336	12.44925	−2.042113	0.1044283	20.58242	17.48006
7.0	8.48	160.0	−43.33130	17.84979	−2.486980	0.1043855	39.95260	23.95055
8.0	9.29	240.0	−51.48727	19.26185	−2.365595	0.08228036	50.46776	31.66351
9.0	9.96	280.0	−31.97360	8.612722	−0.05276312	−0.08174990	38.52328	39.96676
10.0	14.52	360.0	−20.55106	0.6903652	1.759464	−0.2079732	37.02682	49.14654

is a function of pressure and time and describes the unsteady-state water influx.

Subtraction of Eq. A-11 from Eq. A-6 results in the basic equation

$$G_a = G_r + \frac{K_c\, S(p,t)}{(B_a - B_{oi})} \quad . \quad . \quad . \quad . \quad . \quad . \quad . \quad \text{(A-12)}$$

APPENDIX B

Definition of $S(p,t)$

Schilthuis Method

$$S(p,t) = \sum_{i=2}^{n} \Delta p_i\, \Delta t_i \quad . \quad . \quad . \quad . \quad . \quad . \quad . \quad . \quad \text{(B-1)}$$

$$\text{where } \Delta p_i = p_i - \frac{(p_i + p_{i-1})}{2} \quad . \quad . \quad . \quad . \quad . \quad . \quad . \quad \text{(B-2)}$$

$$\text{and } \Delta t_i = t_i - t_{i-1} \quad . \quad . \quad . \quad . \quad . \quad . \quad . \quad . \quad . \quad \text{(B-3)}$$

where n = number of pressure points
t_i = time in years
p = aquifer pressure (inner boundary) psia.

Hurst-Simplified Method

$$S(p,t) = \sum_{i=2}^{n} \frac{\Delta p_i\, \Delta t_i}{\ln(12 t_i)} \quad . \quad . \quad . \quad . \quad . \quad . \quad . \quad . \quad \text{(B-4)}$$

where Δp_i and Δt_i are still defined by Eqs. B-2 and B-3

van Everdingen-Hurst Method

$$S(p,t) = \sum_{i=1}^{n-1} \Delta p_i\, q_{\Delta t_{di}} \quad . \quad . \quad . \quad . \quad . \quad . \quad . \quad . \quad \text{(B-5)}$$

where

$$\Delta p_i = \frac{p_{i+1} - p_i}{2} \quad . \quad . \quad . \quad . \quad . \quad . \quad . \quad . \quad . \quad \text{(B-6)}$$

for $i = 1$, and

$$\Delta p_i = \frac{p_{i+1} - p_{i-1}}{2} \quad . \quad . \quad . \quad . \quad . \quad . \quad . \quad . \quad . \quad \text{(B-7)}$$

for $i = 2$ to $n - 1$.

$q\Delta t_{di}$ is the dimensionless flow rate and is a function of Δt_{di} (the dimensionless time increment) and aquifer geometry.

$$\Delta t_{di} = 2.309 \left(\frac{k \quad \Delta t}{\phi \mu C_w (R_r)^2} \right) \quad . \quad . \quad . \quad . \quad \text{(B-8)}$$

with k in millidarcies, t in years, ϕ a fraction, μ in cp, C_w in 1/psi, R_r in ft.

$q\Delta t_{di}$ is defined under the following conditions. All $\Delta t_{di} < 0.01$, or the linear system

$$q\Delta t_{di} = 2\sqrt{\Delta td_i/\pi} \quad . \quad . \quad . \quad . \quad . \quad . \quad . \quad . \quad \text{(B-9)}$$

Infinite Radial System

$$(0.01 < \Delta t_{di} \leq 10^5)$$

$$q\Delta t_{di} = e^{(A_1 \ln \Delta t_{di} + A_2)\ln \Delta t_{di})^2 + A_3 (\ln \Delta t_{di})^3 + A_4 (\ln \Delta t_{di})^4 + A_5)}$$

where $A_1 = 0.647692$

$A_2 = 0.0177318$

$A_3 = -0.0002737391$

$A_4 = -0.4318125 \times 10^{-5}$

$A_5 = 0.4506432.$

Finite Radial Systems

The finite radial systems are defined by the infinite radial Eq. B-10, where $\Delta t_{di} > 0.01$ and less than the middle range defined in Table 4. In the middle range the dimensionless flow is defined by an equation of the same form as Eq. B-10, but with constants shown in Table 4. Table 4 also gives the steady-state values applicable above the middle range. ★★★

J. R. BRUNS *(left) is a senior mathematical engineer in the Phillips Petroleum Co.'s Computing Dept. For the past seven years he has worked in reservoir engineering computer applications. He has a BS in chemical engineering from the U. of Missouri, an MS in chemical engineering from Illinois Institute of Technology, and a Master of Gas Technology degree from the Institute of Gas Technology.* M. J. FETKOVICH *(right) is a reservoir engineering and gas technology analyst in the Reservoir and Production Project Group of Phillips. He graduated from the U. of Pittsburgh in 1954 with a BS degree in petroleum and natural gas engineering and soon joined Phillips.* V. C. MIETZEN *(center) is a senior electronic computer programmer for Phillips at Bartlesville, Okla. He joined Phillips after receiving his BS degree in petroleum engineering from The U. of Texas in 1960. He worked as a staff engineer in the Pauls Valley, Okla., Area Office before joining the Computer Dept. in 1963.*

Depletion Performance of Layered Reservoirs Without Crossflow

Michael J. Fetkovich, SPE, **Mark D. Bradley,*** SPE, **Adonna M. Works,** SPE, and **Thomas S. Thrasher,** SPE, Phillips Petroleum Co.

Summary. This paper presents a study of the rate/time and pressure/cumulative-production depletion performance of a two-layered gas reservoir producing without crossflow. The gas reservoir has produced for more than 20 years at an effectively constant wellbore pressure, thus giving continuously declining rate/time and pressure/cumulative-production data for analysis. The field data demonstrate that Arps depletion-decline exponents between 0.5 and 1 can be obtained with a no-crossflow, layered reservoir description. Rate-vs.-time and pressure-vs.-cumulative-production predictions were developed from both 2D numerical and simplified tank models of a two-layered, no-crossflow system. These results demonstrate the effects of changes in reservoir layer volumes, permeability, and skin on the depletion performance.

Introduction

Of all the papers about noncommunicating layered reservoirs, only a few have attempted to deal with the subject of depletion and long-term production forecasting. Tempelaar-Lietz[1] originally discussed the effect of the oil production rate from a volumetric reservoir with more than one layer. Lefkovits *et al.*[2] modified the Tempelaar-Lietz constant-rate, two-layer, single-phase-liquid depletion equations to account for two layers of unequal thickness. Fetkovich[3] applied the constant-wellbore-pressure, single-phase-liquid solution to rate/time production data from a layered reservoir to demonstrate that when two noncommunicating layers, each characterized by a single-phase-liquid exponential decline, $b=0$, were produced commingled, the result was that b increased to 0.2.

Hypothetical solution-gas-drive reservoir studies for noncommunicating layers were conducted by Keller *et al.*[4] to investigate the effects of recovery efficiency and GOR behavior and by Gentry and McCray[5] to study the effects of producing noncommunicating layers on the decline-curve exponent, b. Both studies used single-cell models that did not include transient effects. In addition, both used a conventional PI relationship, $q=J(\Delta p)$, to define a rate equation, instead of an inflow-performance-rate relationship that is a function of the difference in pressure squared—i.e., $q=J(\Delta p^2)$. By their nature, more sophisticated multiphase-flow studies would still have difficulty in assigning realistic k_{ro} and k_{rg} relationships for each layer. Further, the difficulty in obtaining the necessary field data, such as individual well measured oil and gas rates, frequent bottomhole shut-in pressures, and a nonlinear $\bar{p}$-vs.-N_p relationship presents a serious verification problem. A similar problem exists for a single-phase-liquid situation because few oil reservoirs are totally, or even highly, undersaturated and produced to abandonment by simple liquid expansion. Those that are highly undersaturated often develop strong waterdrives because of the large reservoir-pressure decline with small production volumes. Such fields often are placed immediately under waterflood. The single-phase-liquid solutions of Tempelaar-Lietz, however, could find application in very-high-pressured gas reservoirs.

To date, we know of no published field-case history that illustrates depletion-performance characteristics [other than repeat-formation-tester (RFT) layer pressures] to identify no-crossflow, layered-reservoir behavior. Single-phase volumetric gas fields and wells offer the best opportunity for detection of layered-reservoir responses because only single-phase flow exists. Furthermore, production data are measured separately for each well, and annual shut-in pressures are normally taken, sometimes with 48- or 72-hour deliverability tests.

For the gas reservoir described in this paper, the simplified rate/time and cumulative-production/time equations of Ref. 3 and the $\bar{p}/z$-vs.-G_p equation provided support that we were dealing with a noncommunicating layered reservoir. The field has produced for more than 20 years at effectively a low constant wellbore pressure, thus giving continuous, declining rate/time data for analysis. The total field and individual wells examined in our study exhibited a rate/time depletion-decline exponent approaching 1.0 with very little early-time transient data evident. A gas well producing from a single homogeneous layer at a flowing wellbore pressure near zero has a maximum depletion-decline exponent of 0.5.[3,6]

Further confirmation and greater flexibility were then obtained with a conventional single-cell, pseudosteady-state, gas-forecasting program that combines gas material balance and a stabilized back-pressure curve for each layer. In addition, a fully implicit radial numerical model consisting of two fifty-cell layers was used to simulate annual 72-hour shut-ins and 48-hour deliverability tests and to verify the results obtained from simplified approaches. Throughout this paper, these approaches will be referred to as the backpressure-curve/material-balance and the radial-model methods, respectively. All basic results and conclusions drawn in this paper, however, can be made with any of the approaches described above. In all figures, the simulated 72-hour shut-in points are strictly the product of the radial model; all other results were consistently obtained by both the backpressure-curve/material-balance and the radial-model approaches. Both constant-wellbore-pressure and constant-rate depletion were investigated. Graphical presentations of rate vs. time and pressure vs. cumulative production clearly demonstrate the effects of changes in the reservoir layer volumes, permeability, k, and skin, s, on the depletion performance of a two-layered system without crossflow.

Field Description

Development drilling began in our field of study in 1961; 212 gas wells had been drilled by early 1966. The reservoir consists of about 350 ft of gross sandstone thickness at 1,800 ft. Initial reservoir pressure was about 428 psia. Other parameters include a reservoir temperature of 80°F, an average porosity of 15%, a water saturation of 51%, and a gas gravity of 0.7. A shale barrier averaging 50 ft thick was clearly identified and correlated across the entire field. Core data indicate a bimodal distribution with a permeability ratio between 10:1 and 20:1.

Wells were generally stimulated upon completion with 500 to 1,000 gal of 15% HCl, followed by a sand fracture, which included 20,000 gal of gel and 40,000 lbm of 20/40 sand. **Table 1** shows stimulation results in terms of skin effect along with other results obtained from initial isochronal tests. In most cases, the exponent of the backpressure curve, n, was 1.0. Of the four tests that did not yield a backpressure exponent of 1.0, one is actually a flow-afterflow test, and the others had not adequately cleaned up after stimulation. All our studies are based on the assumption that non-Darcy flow is not present in the reservoir—i.e., $n=1.0$ for each layer.

The field came on production virtually wide open against an essentially constant wellbore pressure. A type-curve analysis and regression fit of the total field rate/time production data yielded $b=0.89$, practically identical to what we later found from individual well analysis. This b value approaching unity first suggested that we were looking at a no-crossflow, layered reservoir, particularly

*Now at Conoco Inc.

TABLE 1—INITIAL ISOCHRONAL TEST RESULTS

Well	Test Date	Test Wellhead Shut-in Pressure, p_{cs} (psig)	3-Hour Isochronal Tests: CAOF* Mcf/D	3-Hour Isochronal Tests: Exponent n	kh (md-ft)	h (ft)	k (md)	s	k_1 (md)	k_2 (md)
A	Oct. 19, 1960	366.6	16,000	1.00	1,498	64	23.4	−4.6	59	5.9
B	Feb. 20, 1961	326.0	14,600	1.00	1,761	29	60.7	−5.2	152	15.2
C	Jan. 27, 1961	351.6	13,700	1.00	1,332	37	36	−4.8	90	9.0
D	Feb. 27, 1961	385.7	6,200	0.78	1,248	47	26.6	−4.0	66	6.6
E	March 6, 1961	379.9	3,600	1.00	332	74	4.5	−3.8	11	1.1
F	March 13, 1961	407.4	8,800	0.83	984	72	13.7	−4.5	34	3.4
G	Jan. 23, 1963	371.7	3,690	0.69**	565	29	19.5	−4.0	49	4.9
H	Aug. 12, 1963	408.7	5,800	1.00	225	39	5.8	−4.8	14	1.4
I	Oct. 2, 1963	417.9	2,000	0.86	215	23	9.3	−4.0	23	2.3
J	Sept. 9, 1963	405.7	5,900	1.00	397	41	9.7	−4.4	24	2.4
Arithmetic averages		382.1	8,029	0.92	856	46	20.9 18.8†	−4.4	52	5.2

$h_1/h_2 = 1:2$, $k_1/k_2 = 10:1$; $k_1h_1 + k_2h_2 = kh_t$; $h_1 + h_2 = h_t$, $k_1 = 10k_2$, and $h_2 = 2h_1$.
*Calculated absolute open flow.
**Flow-afterflow test.
†$\Sigma kh/\Sigma h$.

because both the field and the individual wells had the same decline exponent.

Well Performance

We present rate/time and pressure/cumulative-production data for two typical wells in the field that cover a range of gas in place. **Fig. 1** presents additional field data in the form of a composite log-rate-vs.-log-time overlay of 10 wells. This technique has also been applied to five California Monterey producing fields.[7]

Fig. 2 is a conventional semilog plot of rate/time data for these two wells. The high initial percentage decline rate, decreasing to a much lower present percentage, is characteristic of wells experiencing hyperbolic decline with high decline exponents. As shown in **Fig. 3**, the log-rate-vs.-log-time plots of these wells indicate little, if any, early transient production; the high b values are the result of differential depletion of a layered reservoir.

The shape of the pressure/cumulative-production data (**Fig. 4**) is typical of most other wells in the field. The rather large displacement between the measured annual 72-hour $\bar{p}/z$ points and the straight line connecting the initial and final points was first misinterpreted as the behavior of a low-permeability reservoir. As Table 1 shows, our analysis of available isochronal test data yielded permeability values much too high to explain this departure. These $\bar{p}/z$ shapes are characteristic of a no-crossflow, layered reservoir with a large contrast in layer permeabilities and volumes.

Basic Equations

Rate/Time Equations. With the assumption of Darcy flow, the depletion rate/time decline equation for a gas well[3] producing from any one layer at a constant wellbore pressure of zero, $p_{wf}=0$, is

$$q_g(t) = (q_{gi})_{max} / \{[(q_{gi})_{max}/G_i]t+1\}^2. \quad \ldots\ldots\ldots\ldots\ldots (1)$$

Note that the exponent 2 is the reciprocal of the Arps[8] exponent $1/b$; i.e., $b=0.50$. Expressed in terms of reservoir variables, $(q_{gi})_{max}$ may be defined as

$$(q_{gi})_{max} = kh(p_i^2) / \{1{,}424(\overline{\mu z})T[\ln(0.472r_e/r_w)+s]\}. \quad \ldots\ldots (2)$$

If a commingled well produces at a constant wellbore pressure, then the flow rate from each layer is independent of the flow rates of all the other layers and the total well production is the sum of all the layers' production. Rate/time decline analysis for a two-layered system is performed with a log-log plot of total flow rate q_{gt} vs. time, where

$$q_{gt}(t) = \frac{(q_{gi})_{max1}}{\{[(q_{gi})_{max1}/G_{i1}]t+1\}^2} + \frac{(q_{gi})_{max2}}{\{[(q_{gi})_{max2}/G_{i2}]t+1\}^2}. \quad \ldots\ldots\ldots\ldots\ldots\ldots\ldots\ldots (3)$$

Only if $(q_{gi})_{max1}/G_{i1} = (q_{gi})_{max2}/G_{i2}$ will the value $b=0.5$ for each layer yield a composite rate/time value of $b=0.5$.

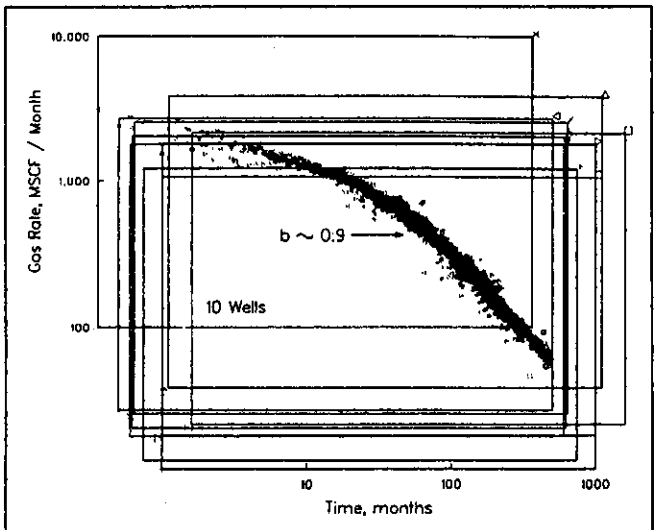

Fig. 1—Overlay of log-rate-vs.-log-time production data of 10 gas wells.

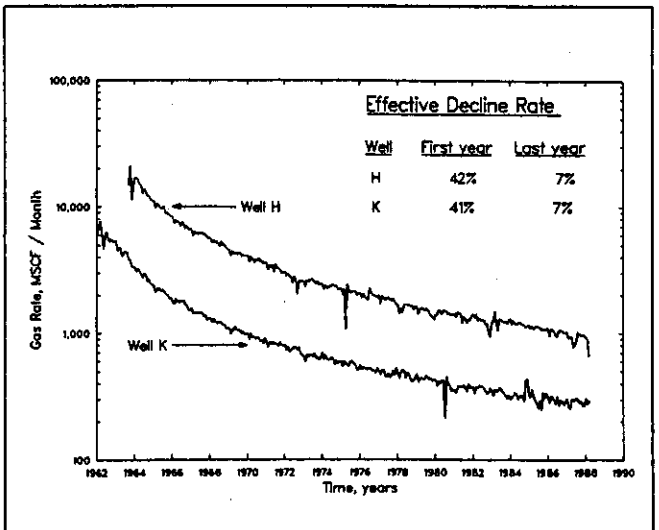

Fig. 2—Semilog plot of rate/time production data.

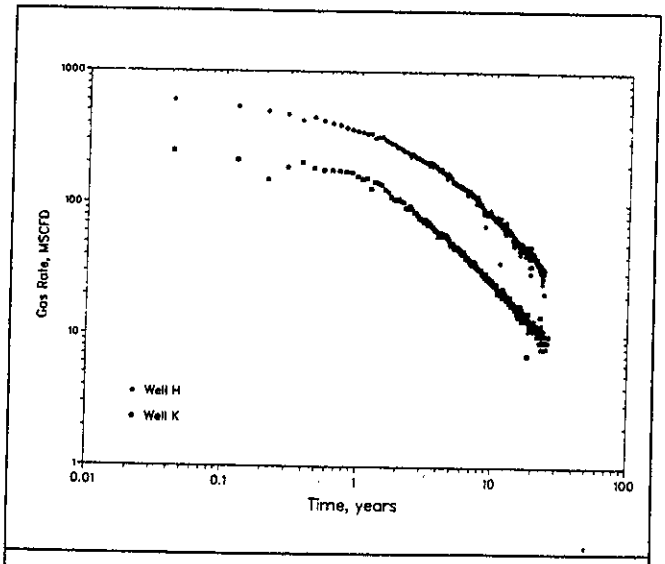

Fig. 3—Log-rate-vs.-log-time production data.

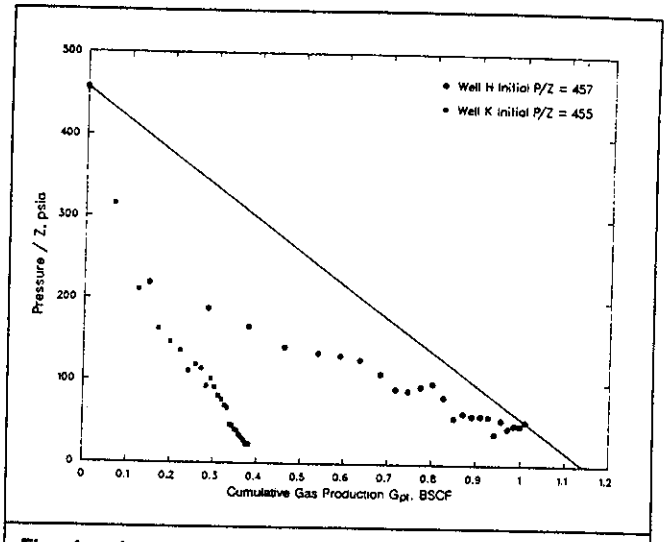

Fig. 4—p/z vs. cumulative production, measured 72-hour shut-ins.

For the limiting case where $(q_{gi})_{max2} \rightarrow 0$ in the low-permeability layer, the total rate/time profile will, of course, be identical to that of the high-permeability layer; each will have a b value of 0.5.

As defined in Ref. 3, the ratio of decline-curve dimensionless time to real time, t_{dD}/t, is equal to $(q_{gi})_{max}/G_i$. Layers having similar values of t_{dD}/t or $(q_{gi})_{max}/G_i$ will deplete at the same rate and could be treated as a single equivalent layer. We will use the ratio

$$[(q_{gi})_{max}/G_i]_R = [(q_{gi})_{max1}/G_{i1}]/[(q_{gi})_{max2}/G_{i2}] \quad \ldots\ldots\ldots (4)$$

as a correlating parameter in our study, along with the layer volume ratio, F_V, defined as G_{i1}/G_{i2}. By convention, Layer 1 is always the more permeable layer.

Assuming that $p_{i1} = p_{i2}$ and $(\mu c_t)_{i1} = (\mu c_t)_{i2}$, and substituting reservoir variables as shown in Ref. 3, we obtain

$$\left[\frac{(q_{gi})_{max}}{G_i}\right]_R = \frac{k_1/\phi_1[\ln(0.472 r_{e2}/r_w)+s_2]}{k_2/\phi_2[\ln(0.472 r_{e1}/r_w)+s_1]} \frac{r_{e2}^2}{r_{e1}^2} \quad \ldots\ldots\ldots (5)$$

Similar ratios were also suggested by Raghavan[9] except for the inclusion of the skin and r_e terms. Note that the assumption of equal initial pressures is not necessary for the constant-wellbore-pressure cases because the layer production rates are independent of each other.

Cumulative-Production/Time Equations. With the assumption of Darcy flow, the cumulative-production/time equation[3] for a gas well producing from any one layer against a constant wellbore pressure of zero is

$$\frac{G_p(t)}{G_i} = 1 - \frac{1}{\{[(q_{gi})_{max}/G_i]t+1\}} \quad \ldots\ldots\ldots (6)$$

Material-Balance Equation. The material-balance equation for any one layer is

$$(\bar{p}/z) = (p_i/z_i)\{1-[G_p(t)/G_i]\}. \quad \ldots\ldots\ldots (7)$$

For a two-layer system with equal initial pressure and fluids, the equation becomes

$$(\bar{p}/z)_t = (p_i/z_i)\{1-[G_{p1}(t)+G_{p2}(t)]/(G_{i1}+G_{i2})\}. \quad \ldots\ldots\ldots (8)$$

Layered-Reservoir Performance Forecasts

To understand the depletion performance of our noncommunicating layered reservoir better, a one-well, two-layered system was designed from reservoir properties of the gas reservoir described previously. The following data were used for both layers: $r_e = 2{,}979$ ft, $r_w = 0.30$ ft, $\phi = 0.15$, $S_w = 0.514$, $\gamma_g = 0.7$, $T = 80°F$, and $p_i = 428$ psia. A total well thickness, h, of 24 ft was used to obtain an average well original gas in place of 1.50 Bscf. All forecasts were made with a minimum bottomhole flowing pressure, p_{wf}, of 42.8 psia, 10% of the initial shut-in pressure. Permeability ratios, F_k, ranging from 1:1 to 1,000:1 were investigated along with layer volume ratios, F_V, of 1:1, 1:2, and 2:1. The low-permeability layer was generally assigned a permeability of 1 md. Various combinations

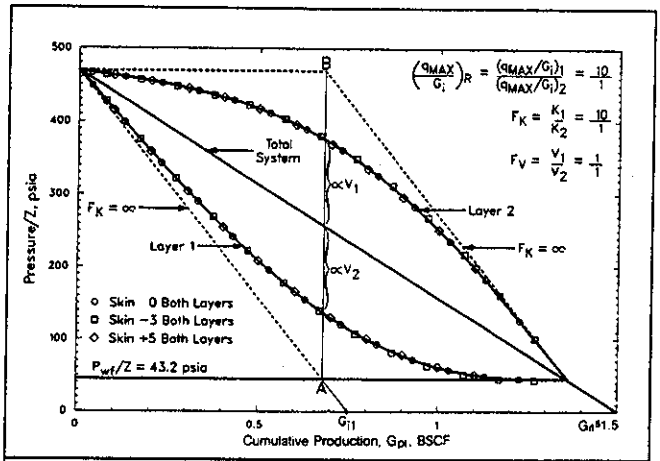

Fig. 5—p/z vs. cumulative production, layer skins equal and $F_V = 1$.

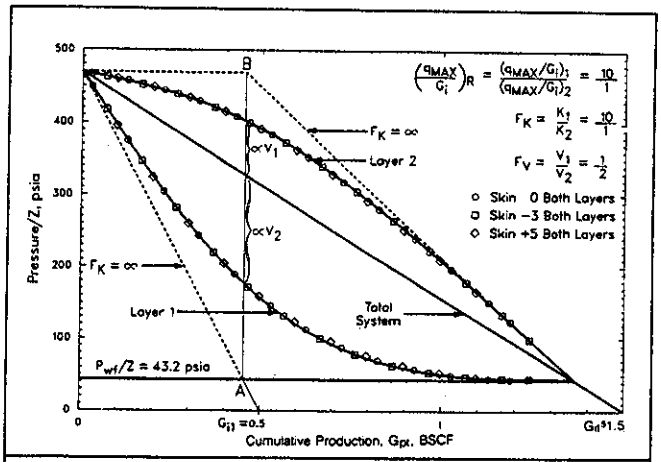

Fig. 6—p/z vs. cumulative production, layer skins equal and $F_V = 1:2$.

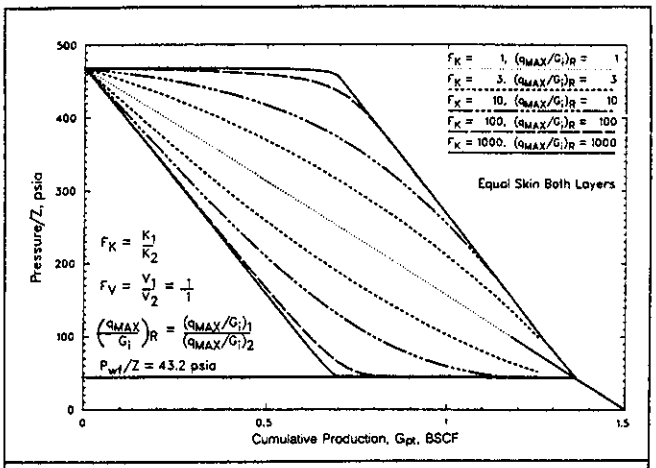

Fig. 7—p/z vs. cumulative production, layer skins equal, $F_V = 1$ and F_k range 1 to 1,000.

of skin, s, of +5, 0, and −3 were also investigated. Realistic constant-rate forecasts were made assuming typical contract rates of take of 1 MMscf/D/8.6 Bscf and 1 MMscf/D/5 Bscf of original gas in place.

Discussion of Results

Pressure/Cumulative-Production Graphs. The pressure/cumulative-production graphs for layered reservoirs are unique because individual layer and total system $\bar{p}/z$ are plotted vs. the total commingled cumulative production from all layers, G_{pt}. This graph can be prepared for any number of layers. **Fig. 5** is such a plot for our two-layered system, assuming $F_V = 1:1$ or 0.750 Bscf/0.750 Bscf. In this case, F_k and $(g_{max}/G_i)_R$ both equal 10 because the skins on both layers are equal (see Eq. 5). Production rates at constant wellbore pressure and two different realistic constant-rate rates of take (1 MMscf/D/8.6 Bscf and 1 MMscf/D/5 Bscf) produced identical results. Note that, for any given F_k, as long as the skins are equal in both layers, differential depletion will be identical for both layers. We also found this to be true for other F_V values. Further, the backpressure-curve/material-balance and radial-model results exactly overlie each other.

Another important observation to be made from Fig. 5 is that with $F_V = 1$, the respective distances between the total system $\bar{p}/z$ and each layer $\bar{p}/z$ are always equal for any value of cumulative production, G_{pt}. Both layer $\bar{p}/z$ values converge at the intersection of the minimum flowing pressure and total system $\bar{p}/z$ lines.

Fig. 5 also demonstrates two limiting conditions: when $F_k = 1$ or $(q_{max}/G_i)_R = 1$, both layers will deplete equally and the $\bar{p}/z$ for each layer will overlie the total system $\bar{p}/z$ curve. At the other extreme, when $F_k \to \infty$, or $(q_{max}/G_i)_R \to \infty$, the maximum differential-depletion envelope is described. The vastly more permeable Layer 1 will totally deplete, while Layer 2 remains at initial pressure; Layer 2 will then deplete after Layer 1 is no longer producing. The envelope can be constructed by first connecting p_i/z_i to G_{i1}. We call the intersection of this line and the horizontal line representing p_{wf}/z Point A. We call the intersection of the vertical line passing through Point A and the horizontal line representing p_i/z_i Point B. Finally, we connect Point B to the point where p_{wf}/z and the total system $\bar{p}/z$ intersect.

TABLE 2—CORRELATION PARAMETER VALUES FOR VARIOUS SKIN COMBINATIONS WHEN $F_k = 10$ and $F_V = 1$

Skin		
Layer 1	Layer 2	$(q_{imax}/G_i)_R$
−3	0	15.5
0	5	15.9
−3	−3	10
0	−3	6.4
5	0	6.3

Observations concerning Fig. 5 also apply to **Fig. 6**. The only difference is that $F_V = 1:2$ in Fig. 6; i.e., Layer 1 contains 0.5 Bscf, while Layer 2 contains 1.00 Bscf. Note that for this F_V, the vertical distance between the total system $\bar{p}/z$ and the Layer 1 $\bar{p}/z$ curve is twice that between the total system $\bar{p}/z$ and the Layer 2 $\bar{p}/z$ curve. By contrast, for $F_V = 2:1$, the distance between the total system and Layer 1 $\bar{p}/z$ curves is half that between the total system and Layer 2 $\bar{p}/z$ curves. In all cases, the vertical distance between the total system $\bar{p}/z$ line and each layer $\bar{p}/z$ curve is inversely proportional to their volume ratios.

A range of F_k from 1 to 1,000 is shown in the pressure/cumulative-production plot of **Fig. 7.** In each case, both layers are assumed to have equal skins and equal volumes. Similar results are obtained for $F_V = 1:2$ and $2:1$. The degree of differential depletion between the two layers increases as $(q_{max}/G_i)_R$ increases and decreases as $(q_{max}/G_i)_R$ decreases. As $(q_{max}/G_i)_R$ approaches unity, the system will behave as a single layer.

Unequal Layer Skins. We have assigned a range of skin values to our individual well studies of +5, 0, and −3 to demonstrate the significance of $(q_{max}/G_i)_R$ as a correlation parameter. **Table 2** gives $(q_{max}/G_i)_R$ values obtained for various skin combinations with $F_k = 10$ and $F_V = 1$.

Fig. 8 shows that, when different layer skins result in the same value of $(q_{imax}/G_i)_R$, $\bar{p}/z$-vs.-G_{pt} curves for each layer exactly overlie each other. Similar results are obtained with regard to the decline exponent, b.

Constant-Rate Cases. To investigate the effect of rate sensitivity on differential depletion, three different constant-rate forecasts were

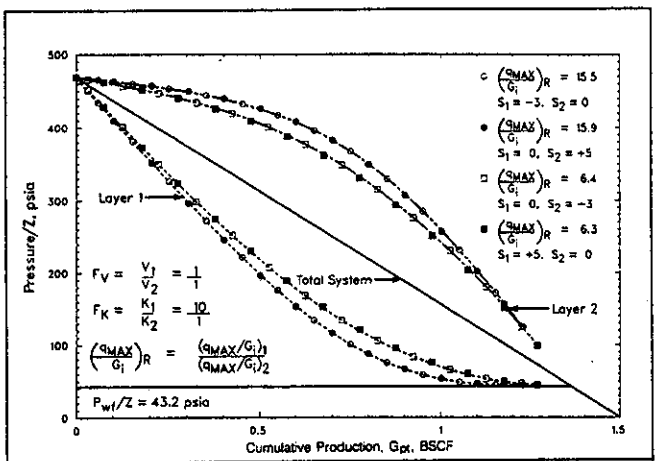

Fig. 8—Effect of different layer skin, s, on p/z-vs.-G_p curves, $F_V = 1$, $F_k = 10$.

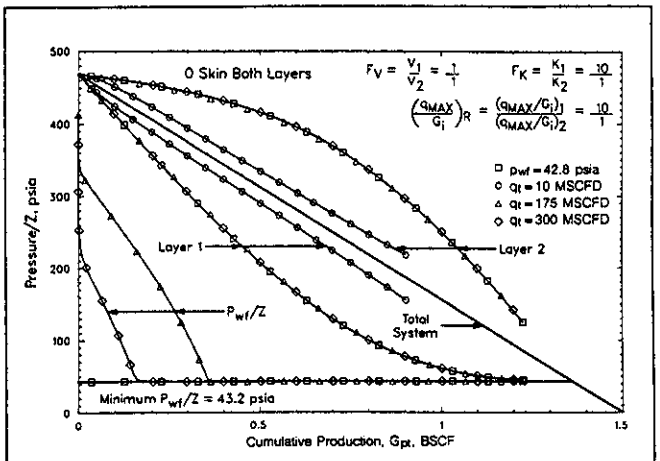

Fig. 9—Effect of rate on differential depletion.

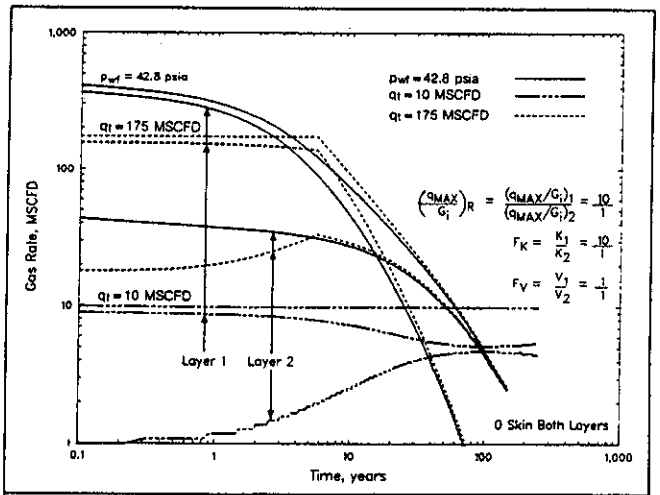

Fig. 10—Layer and composite rates vs. time at constant wellbore pressure and constant rate.

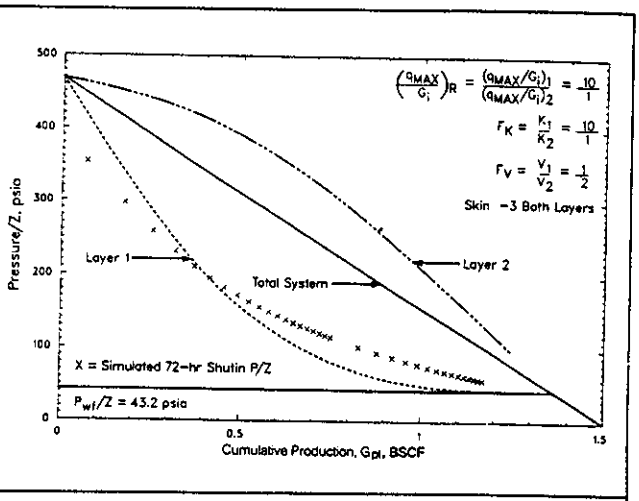

Fig. 11—Simulated 72-hour shut-in p/z compared with layer average pressure p/z, constant-wellbore-pressure case.

made along with a constant-wellbore-pressure case assuming $F_k=10$, $F_V=1$, and equal layer skins. Initial rates of 300 Mscf/D from a 1 MMscf/D/5 Bscf rate of take, 175 Mscf/D from a 1 MMscf/D/8.6 Bscf rate of take, and 10 Mscf/D, representing an economic limit rate, were forecast.

The $\bar{p}/z$-vs.-G_{pt} plot (Fig. 9) demonstrates that differential depletion is not rate-sensitive for our practical rates of interest. This is a result of the gas flow rates being a function of kh and a difference in pressures squared; i.e., $q_g=f(\Delta p^2)$. As p_{wf} approaches initial reservoir shut-in pressure ($\Delta p\rightarrow 0$), as is the case for the 10-Mscf/D forecast, the gas rate becomes a function of a difference in pressures, i.e., $q_g=f(\Delta p)$. Tempelaar-Lietz[1] found that for the single-phase-liquid case, where $q_0=f(\Delta p)$, differential depletion was sensitive to all flow rates and that as the constant-rate $q\rightarrow 0$, both layers deplete equally; i.e., Layer 1, Layer 2, and the total system pressures are all equal. Obviously, very-high-pressure gas wells will behave like the single-phase-liquid case, $q=f(\Delta p)$, and solution-gas-drive reservoirs below the bubblepoint should behave like the low-pressure-gas cases because oilwell inflow performance[10] yields $q_0=f(\Delta p^2)$.

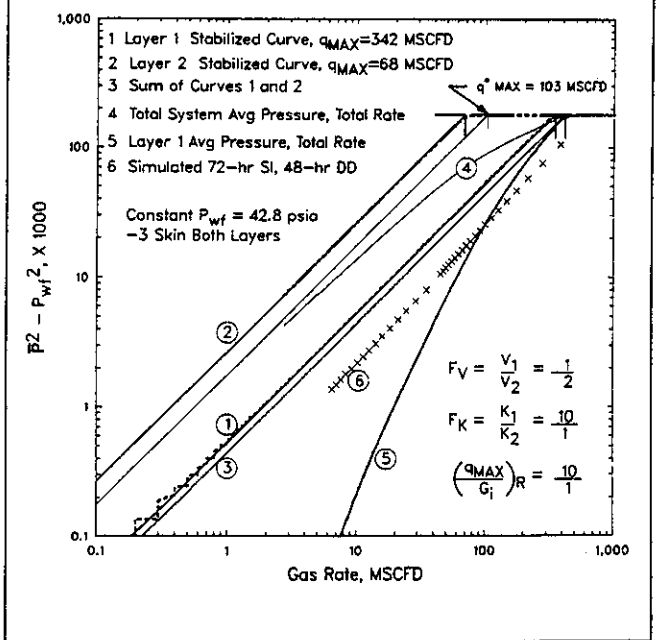

Fig. 12—Layer and composite well backpressure-curve performance, constant wellbore pressure.

Fig. 10 presents individual-layer and composite flow rates for the above cases. Initially, layer rates are a function of kh. When the constant-rate cases go on decline, the rates again become a function of kh. Note that only for the 10-Mscf/D case do the layer rates approach being equal—the constant-rate definition of pseudosteady state for two layers of equal PV. At practical production rates that eventually decline to the economic rate of 10 Mscf/D, pseudosteady state is never achieved. Even for the 10-Mscf/D case, results obtained from both the backpressure-curve/material-balance and radial-model methods were identical.

Field Shut-in Pressures. Routine field data available from layered gas wells consist of monthly commingled production rates, q_t, total system cumulative production, G_{pt}, and commingled shut-in pressures. In our field of study, 72-hour shut-in pressures are taken annually. On the basis of approximate field reservoir parameters ($F_k=10:1$, $F_V=1:2$, and $s_1=s_2=-3$), the radial model was used to simulate annual 72-hour shut-in and 48-hour drawdown-pressure tests. The constant-wellbore-pressure-case results are shown in **Fig. 11.** As expected, the commingled shut-in pressures divided by z basically follow the $\bar{p}/z$ curve of the more permeable layer. Results obtained for a 175-Mscf/D constant-rate case were similar. The 72-hour pressures for the constant-wellbore-pressure case are initially somewhat lower, however, than those for the constant-rate case because the 72-hour shut-in begins from a much lower flowing pressure before shut-in. After about 0.4 Bscf of recovery, the 72-hour pressure begins to exceed the more permeable layer pressure because of interlayer wellbore backflow.

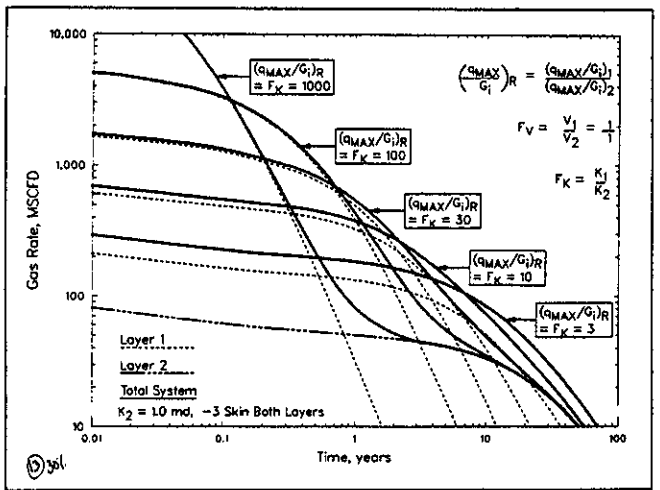

Fig. 13—Effect of changes in $(q_{max}/G_t)_R$ ratio on total system decline for $F_V=1$.

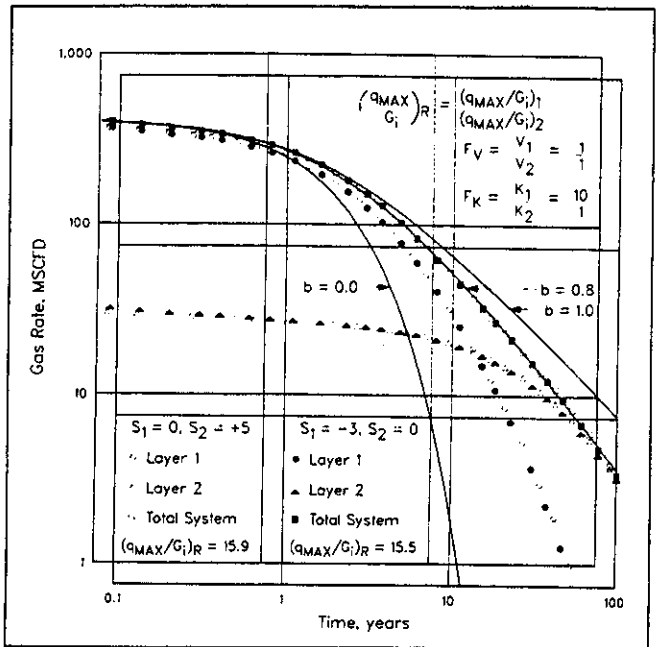

Fig. 14—Effect of layer skins on total system decline exponent *b*, for $F_V = 1$ and $F_k = 10$.

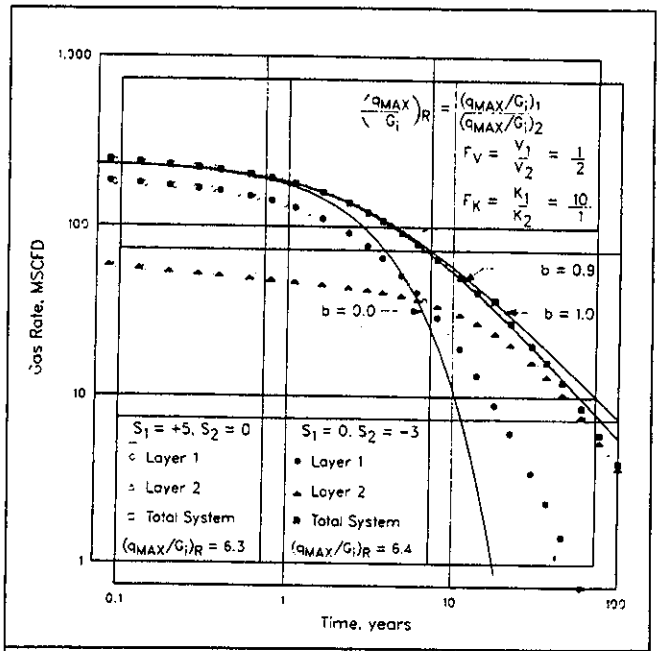

Fig. 15—Effect of layer skins on total system decline exponent *b*, for $F_V = 1:2$ and $F_k = 10$.

TABLE 3—DECLINE EXPONENT *b* AS A FUNCTION OF $[(q)_{max}/G_i]_R$ and F_V

$[(q)_{max}/G_i]_R$	F_V 2:1	1:1	1:2
1	0.4	0.4	0.4
3	0.5	0.55	0.6
5	0.6	0.65	0.7
10	0.65	0.8	1.0
15.5	0.65	0.8	1.0
30*	0.6	0.7	0.8
100*	0.5	0.5	0.5
1,000*	0.4	0.4	0.4

*Double depletion decline *b* is for the first depletion decline.

Backpressure Curves

A stabilized backpressure curve and a material-balance equation are frequently used to prepare long-term production forecasts for single-layer systems. The stabilized backpressure curve is used only during constant-wellbore-pressure production—i.e., the declining production period. A single stabilized backpressure-curve relationship for multilayer systems has never been defined, mainly because previous investigations of multilayered systems are based on constant-rate production—i.e., the rate never experiences decline.

Fig. 12 shows several different backpressure curves developed from a radial-model forecast that assumes $F_V = 1:2$, $F_k = 10:1$, $s_1 = s_2 = -3$, and a constant $p_{wf} = 42.8$ psia. Annual 72-hour shut-ins, each followed by a 48-hour drawdown, were also simulated with the radial model to represent typical official test requirements, test data that would normally be available to construct a 48-hour-depletion backpressure curve. The average reservoir pressure, $\bar{p}$, used to define the backpressure curves in Fig. 12 represents either the simulated 72-hour shut-in pressure or the volumetric average pressure for each layer and the total system.

Curve 1 in Fig. 12 represents the calculated position of the stabilized or pseudosteady-state curve for Layer 1 from the reservoir variables previously defined. The points that overlie the curve were obtained from the radial model. The pressure, $\bar{p}$, and rate, q, are those of Layer 1 only.

Curve 2 represents the stabilized backpressure curve for Layer 2, the low-permeability layer. Curve 3 is simply the sum of Curves 1 and 2. Curve 4 represents the stabilized backpressure curve for the total system, where $\bar{p}$ is the volumetric average pressure of the total system and q is the total flow rate for both layers. Clearly, Curve 4 is not a straight line except at low flow rates. We have therefore avoided the expression "pseudosteady state" when describing it. Curve 4 originates at the q_{max1} of Curve 3 and asymptotically approaches a straight line of unit slope established from the Layer 2 stabilized potential, q_{max2}, and the ratio of layer PV's, such that

$$(q)^*_{max} = (q)_{max2}[(G_{i1} + G_{i2})/G_{i2}]. \quad \ldots\ldots\ldots\ldots\ldots\ldots (9)$$

Because layer flow rates at these low levels become a function only of layer PV's, the position of this straight-line asymptote was independent of layer skins. We were unable to predict the layered-reservoir stabilized-curve limiting position from the constant-rate late-time solution of Ref. 2.

The shape of the total system stabilized curve gives the appearance of a continuous loss in well performance that could be misinterpreted as a changing skin, a loss of reservoir permeability, or an infinite-acting transient decay.

Curve 5 is based on the combined rate from both layers and the volumetric average pressure of the more permeable layer. We expected the commingled shut-in pressure to approach the pressure of the more permeable layer, as in Fig. 11. Curve 6 is a plot of the simulated annual 72-hour shut-in pressure and 48-hour drawdown flow rate obtained while producing against a constant p_{wf} of 42.8 psia. Surprisingly, a straight line with a backpressure-curve exponent of $n = 0.934$ results. (Recall that, for Darcy flow, $n = 1$ is assumed for each layer.) Note that Curve 6, the 48-hour depletion backpressure curve, does not reflect the shape of Curve 4, the layered, stabilized backpressure curve.

Rate/Time Depletion Behavior

Fig. 13 is a comparison of individual layer and total system rate/time responses for various ratios of $(q_{max}/G_i)_R$. Only the contribution of Layer 1, the high-permeability layer, changes from case to case; the permeability of Layer 2 is fixed at 1.0 md in each case. Further, each layer contains a gas in place of 0.75 Bscf, and each has been assigned a skin of −3.

The log-rate-vs.-log-time profile for any single layer can be matched to a depletion *b* stem of 0.4. This result is commensurate with the expected behavior of a dry gas reservoir in the presence of a constant backpressure equal to 10% of the initial reservoir pressure. We have confirmed, however, that a $b = 0.5$ results when $p_{wf} = 0$.

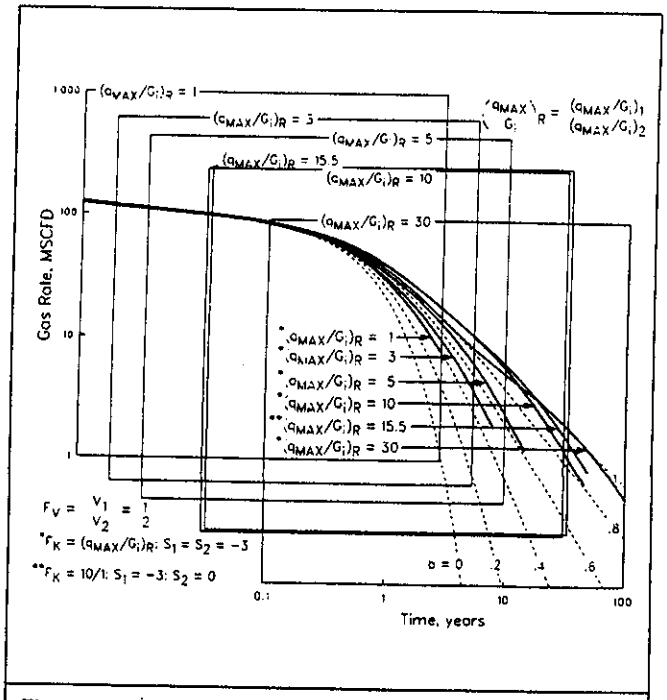

Fig. 16—Composite well declines for $(q_{max}/G_i)_R$ between 1 and 30 and $F_V = 1:2$.

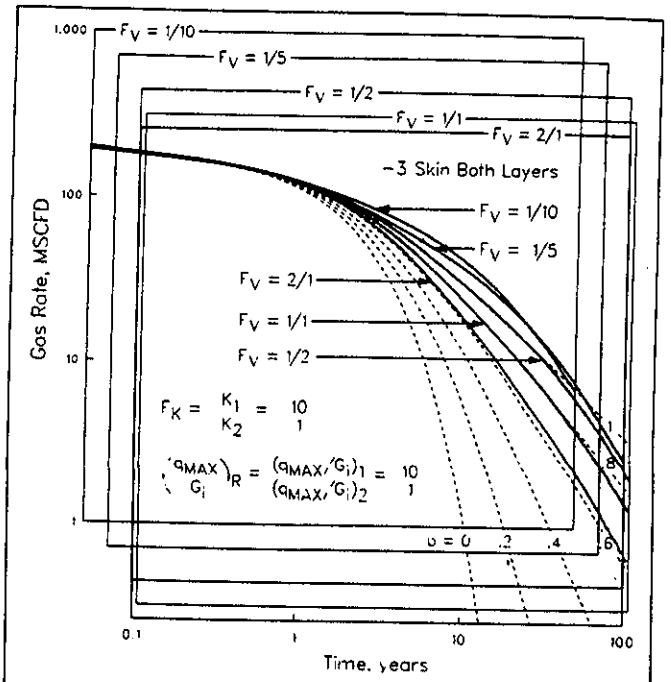

Fig. 17—Composite well declines for F_V between 2:1 through 1:10 and $(q_{max}/G_i)_R = 10$.

When two layers, each characterized by a $b=0.4$, are added together, the composite curve will yield a value of $b>0.4$. Only for the special case in which the ratio of q_{max} to initial gas in place is the same for each layer [$(q_{max}/G_i)_R=1.0$] will the composite curve follow the same depletion stem described by each separate layer. Such cases reduce to a single-layer system.

For a given F_V, the greater the $(q_{max}/G_i)_R$ value, the greater the contrast between early layer producing rates. The low-permeability layer will not contribute a significant fraction of the total rate until the high-permeability layer is depleted. At late time, the total system curve and the low-permeability curve become indistinguishable. For the cases in which $(q_{max}/G_i)_R=F_k=3$ or 10, the composite curve approximates a smooth hyperbolic decline. Differential depletion gives the total rate/time curve the appearance of a single, homogeneous system with a high b value. We know of no other mechanism to explain the occurrence of nearly harmonic decline behavior observed in actual field data.

Note, however, that for cases in which $(q_{max}/G_i)_R > \sim 20$, a double hump appearance is evident in the total rate/time curve. This double-depletion characteristic closely resembles the shape of the type curves developed by Da Prat *et al.*[11] for single-layered naturally fractured reservoirs. The early depletion of the high-permeability layer appears analogous to fracture-volume depletion; the late depletion of the low-permeability layer can be considered analogous to matrix depletion. When attempting to identify a naturally fractured reservoir on the basis of double-depletion rate/time behavior, we must, therefore, consider the possibility of layering with no crossflow. In Monterey reservoirs, for example, the degree of fracturing is highly lithology-dependent and any intralayer fracture/matrix response may be overwhelmed by the layering response among lithologically dissimilar zones of contrasting permeability.

Recall from Fig. 8 that when two separate systems have the same gas in place and share the same F_V and $(q_{max}/G_i)_R$ values, each system will overlie the same $\bar{p}/z$-vs.-G_{pt} curve. **Fig. 14** demonstrates that such systems also will describe similar rate/time curves. In this case, $F_V=1:1$ and $F_k=10:1$ for both systems. For the system shown with open symbols, $s_1=0$ and $s_2=+5$, resulting in $(q_{max}/G_i)_R=15.9$. For the system represented by closed symbols, $s_1=-3$ and $s_2=0$, yielding $(q_{max}/G_i)_R=15.5$. Log-rate-vs.-log-time type curves for these systems exactly match, with a slight shift of both axes resulting from differing layer skins. Note that the total system profiles, shown with square symbols, exactly overlie, each tracing a b stem of 0.8 through 100 years of production.

Fig. 15 shows similar results for two other systems of equal $(q_{max}/G_i)_R$. Both systems assume $F_V=1:2$ and $F_k=10:1$, approximating the values for our field of study. The open symbols refer to the system in which $s_1=+5$ and $s_2=0$, yielding $(q_{max}/G_i)_R=6.3$. The closed symbols identify the system in which $s_1=0$ and $s_2=-3$, resulting in $(q_{max}/G_i)_R=6.4$. Again, composite profiles exactly coincide, this time approximating a b stem of 0.9.

Figs. 14 and 15 reveal that different values of F_V and $(q_{max}/G_i)_R$ produce different b values. **Table 3** shows the complete spectrum of possible Arps b values for various differential-depletion cases. All these results are based on a constant flowing pressure equal to 10% of the initial shut-in pressure. Predictably, for any given F_V, the b value increases as $(q_{max}/G_i)_R$ increases—i.e., as the contrast in layer properties, primarily permeability, becomes more pronounced. For very large values of $(q_{max}/G_i)_R$, however, the double-depletion decline develops and a constant b stem cannot be maintained. At both ends of the $(q_{max}/G_i)_R$ spectrum, therefore, the composite curve collapses to a single-layer profile with $b=0.4$. The highest b values obtained in our study are for $(q_{max}/G_i)_R$ ratios between 10 and 20. Further, for any given $(q_{max}/G_i)_R$, b increases as F_V decreases. Assuming $(q_{max}/G_i)_R=10.0$, for instance, an F_V of 2:1 yields $b=0.65$, an F_V of 1:1 yields $b=0.80$, and an F_V of 1:2 yields $b=1.0$. For very low volume ratios, however, a constant b stem is again impossible to maintain.

Fig. 16 is a type-curve overlay of six $(q_{max}/G_i)_R$ cases, all premising $F_V=1:2$. **Fig. 17** is a similar overlay of five F_V cases, all assuming $(q_{max}/G_i)_R=F_k=10:1$. In both figures, the axes of each individual rate/time plot are shifted so that all cases can be presented on a single Arps depletion type curve. Note that in Fig. 16 the curves generally begin to fall below a fixed b stem at late time. The higher the b stem indicated by the early depletion performance, the earlier in real time this drop-off occurs. For $F_V=1:5$ and 1:10 (Fig. 17), the total system profile briefly exceeds $b=1.0$, only to fall back to a lower b value later in depletion. Eventually, only the low-permeability layer contributes to the total flow rate, and the b value migrates to that of a single layer. Normal wellbore deterioration, liquid loading, etc., experienced even by a single-layer completion, may, in fact, contribute to this migration. With the exception of cases involving low volume ratios, however, our results demonstrate that a fixed b stem will be sufficient for predicting flow rates to a practical economic limit. Nevertheless, caution should be exercised in using a fixed b value to predict

reserves at late time for layered systems. We do not advocate the use of b stems >1.0 for forecasting purposes.

A final point concerns the type-curve-matching procedure used on the curves in Figs. 16 and 17. We were unable to predict analytically exactly where to match each composite rate/time curve with a total system kh. An approximate match could be obtained by first estimating q_{dD} using kh_t and $\overline{\mu B}$, and then shifting the curve from left to right along the time axis. The problem lies in estimating the time to pseudosteady state for a layered system, making the t_{dD} match point difficult to evaluate. Further, the total system PV cannot be estimated exactly from a type-curve match of the total rate profile. If a gas well exhibits $b>0.5$, indicating the presence of a layered system, individual layer volumes may be estimated by graphically desuperposing the total system curve from the high-permeability layer with a trial-and-error procedure.

Discussion

Most reservoirs consist of several layers with reservoir properties varying to some degree between layers. Whether crossflow exists may be of considerable importance in long-term forecasting. If crossflow exists, layers can be combined into a single equivalent layer with the average reservoir properties of the crossflowing layers. Even if crossflow does not exist, layers can still be combined into an equivalent single layer if each has the same diffusivity properties, or q_{max}/G_i. It should also be possible to reduce multilayer systems into equivalent two-layer systems for rate/time analysis or production forecasting. We also found that limited-crossflow cases can behave similarly to no-crossflow cases.

In a no-crossflow layered reservoir, or in a well with commingled reservoir completions, to affect long-term production forecasts significantly, a contrast in layer permeabilities must exist. More specifically, the contrast must be in the correlating parameters $(q_{max}/G_i)_R$ and F_V. Reservoirs most likely to develop these contrasts are naturally fractured reservoirs and very thick reservoirs. The Monterey, Spraberry, Altamount-Bluebell, and Austin Chalk have all exhibited depletion-decline exponents approaching 1, suggesting the presence of layering, with little or no crossflow between some or all layers. The early, rapid rate decline observed in such reservoirs is usually interpreted as fracture-volume depletion instead of the differential depletion of the entire naturally fractured layer or layers. Before this study, the double depletion-rate decline illustrated by Da Prat *et al.*[11] was considered to be one of the identifiable responses of naturally fractured reservoirs. This study shows that a no-crossflow layered reservoir, without natural fracturing, can exhibit the same type of response.

Early recognition of a no-crossflow layered reservoir's precipitous rate and pressure/cumulative-production declines would require early individual-layer tests, coring, and a good geological description. The thick shale break observed in all wells in our field of study should have indicated the need for individual-layer tests, both above and below the potential flow barrier. A vertical-permeability test across the shale may also have been warranted. If high- and low-permeability layers are interbedded, however, it may be difficult to test individual layers; pressure-transient tests may reflect only the kh of the high-permeability layer(s).

Obtaining RFT pressures on later development or replacement wells is another method that can be used for the detection of differential depletion in layered reservoirs. Unfortunately, this is a one-time opportunity for a well. The multilayer testing procedures of Ehlig-Economides and Joseph[12] theoretically offer the opportunity to obtain layer pressures, permeabilities, and skins as frequently as necessary to define the pressure-vs.-cumulative-production curve for each layer.

Conclusions

The following conclusions were derived from results calculated by the backpressure-curve/material-balance and the radial-model methods. We believe that all the conclusions are applicable to the gas reservoir described in this paper. Most would be applicable to any no-crossflow layered reservoir.

1. A two-layered-reservoir description reproduces observed rate/time and pressure/cumulative-production performance that a single-layer description cannot reproduce.
2. For all combinations of properties investigated, the rate/time and pressure/cumulative-production performance is not rate-sensitive at practical production rates.
3. Rate/time and pressure/cumulative-production responses can be correlated with $(q_{max}/G_i)_R$ and F_V. The magnitude of b may provide an indication of the permeability contrast and the volume ratio.
4. Arps depletion-decline exponents between 0.5 and 1 can be obtained with a layered-reservoir description given sufficient contrast in layer properties. A depletion-decline exponent >1.0 could not be maintained for any combination of properties investigated.
5. Except for the special cases in which $(q_{max}/G_i)_R$ approaches unity or infinity, the composite-depletion b value is always greater than that of a single-layer system. Field and well rate/time data that exhibit higher-than-expected b values (between 0.5 and 1.0 for gas reservoirs) suggest a layered reservoir system. Large initial percentage declines, not attributable to infinite-acting transient production, followed later by small percentage declines, are a characteristic of high b values and suggest a layered-reservoir response.
6. During the constant-rate production period, the only performance characteristic that can be used to detect layering is the shape of the pressure/cumulative-production plot. The steeper the initial decline in $\bar{p}/z$, the smaller the F_V, G_{i1}/G_{i2}.
7. Different combinations of layer skins can exhibit similar rate/time and pressure/cumulative-production differential-depletion responses.
8. Shut-in pressures obtained for layered reservoirs will track the pressure of the most permeable layer—more specifically, the layer with the highest value of q_{max}/G_i. Extrapolation of a shut-in $\bar{p}/z$-vs.-G_{pt} curve may possibly underestimate the gas in place, G_{it}, at early times and overestimate it at late times. Similarly, semilog extrapolation of early rate/time data will underestimate recoverable reserves. Continuing to extrapolate late rate/time data along a fixed high b value may overestimate recoverable reserves.
9. The total system stabilized backpressure curve of a layered system is not a straight line.
10. A simplified approach with a stabilized backpressure curve and a material-balance equation for each layer yields the same basic results and conclusions as obtained from a radial model.

Nomenclature

b = reciprocal of decline-curve exponent
B = FVF, res vol/surface vol
c_t = total compressibility, psi^{-1}
F_k = layer permeability ratio
F_V = layer volume ratio
G_i = initial gas in place, Bscf
G_p = cumulative gas production, Bscf
h = thickness, ft
J = productivity index
k = effective permeability, md
n = exponent of backpressure curve
N_p = cumulative oil production, STB
$\bar{p}$ = average reservoir pressure, psia
p_{cs} = wellhead shut-in pressure, psig
p_i = initial reservoir pressure, psia
p_{wf} = wellbore flowing pressure, psia
Δp = pressure drop, psia
q = flow rate, Mscf/D
q_{dD} = decline-curve dimensionless flow rate
$(q_{max}/G_i)_R$ = ratio defined by Eq. 4
$(q_i)_{max}$ = initial surface flow rate from stabilized curve
$(q^*)_{max}$ = defined by Eq. 9
$q(t)$ = surface flow rate at time t
q_t = total constant rate from Layers 1 and 2
r_e = external boundary radius, ft

r_w = wellbore radius, ft
r_{wa} = effective wellbore radius, ft
s = skin factor, dimensionless
S_w = water saturation, fraction
t = time, days
t_{dD} = decline-curve dimensionless time
T = reservoir temperature, °R
V = volume, ft^3
z = gas compressibility factor, dimensionless
γ_g = gas specific gravity
μ = viscosity, cp
ϕ = porosity, fraction of bulk volume

Subscripts

g = gas
i = initial
o = oil
r = relative
t = total of Layers 1 and 2

Acknowledgments

We thank Phillips Petroleum Co. for permission to publish this paper. We also thank L.K. Thomas, U.G. Kiesow, and B.C. Nolen for their contributions to this study. Special thanks to Kay Patton for the excellent typing of this and other papers previously published.

References

1. Tempelaar-Lietz, W.: "Effect of Oil Production Rate on Performance of Wells Producing from More Than One Horizon," *SPEJ* (March 1961) 26–31; *Trans.*, AIME, **222.**
2. Lefkovits, H.C. *et al.*: "A Study of the Behavior of Bounded Reservoirs Composed of Stratified Layers," *SPEJ* (March 1961) 43–58; *Trans.*, AIME, **222.**
3. Fetkovich, M.J.: "Decline Curve Analysis Using Type Curves," *JPT* (June 1980) 1065–77.
4. Keller, W.O., Tracey, G.W., and Roe, R.P.: "Effect of Permeability on Recovery Efficiency by Gas Displacement," paper presented at the 1949 API Meeting, Tulsa, March.
5. Gentry, R.W. and McCray, A.W.: "The Effect of Reservoir and Fluid Properties on Production Decline Curves," *JPT* (Sept. 1978) 1327–41.
6. Carter, R.D.: "Type Curves for Finite Radial and Linear Gas Flow Systems: Constant-Terminal-Pressure Case," *SPEJ* (Oct. 1985) 719–28.
7. Fetkovich, M.J. *et al.*: "Decline Curve Analysis Using Type Curves—Case Histories," *SPEFE* (Dec. 1987) 637–56; *Trans.*, AIME, **283.**
8. Arps, J.J.: "Analysis of Decline Curves," *Trans.*, AIME (1945) **160,** 228–47.
9. Raghavan, R.: "Behavior of Wells Completed in Multiple Producing Zones," *SPEFE* (June 1989) 219–30.
10. Fetkovich, M.J.: "The Isochronal Testing of Oil Wells," paper SPE 4529 presented at the 1973 SPE Annual Meeting, Las Vegas, Sept. 30–Oct. 3.
11. Da Prat, G., Cinco-Ley, H., and Ramey, H.J. Jr.: "Decline Curve Analysis Using Type Curves for Two-Porosity Systems," *SPEJ* (June 1981) 354–62.
12. Ehlig-Economides, C.A. and Joseph, J.: "A New Test for Determination of Individual Layer Properties in a Multilayered Reservoir," *SPEFE* (Sept. 1987) 261–83.

Authors


Fetkovich


Bradley


Works


Thrasher

Michael J. Fetkovich is staff director and senior principal reservoir engineer for the Drilling & Production Div. of Phillips Petroleum Co. in Bartlesville. He holds a BS degree in petroleum and natural gas engineering from the U. of Pittsburgh and a Dr. Ing. degree from the Norwegian Inst. of Technology. Fetkovich was a 1977–78 Distinguished Lecturer discussing Well Testing and Analysis, and he received the 1989 Reservoir Engineering Award. **Mark D. Bradley** is a senior reservoir engineer with Conoco Inc.'s Production Engineering & Research Div. in Houston, specializing in reservoir simulation. Previously at Phillips Petroleum Co., Bradley holds a BS degree in petroleum engineering from the U. of Wyoming. **Adonna M. Works** is a reservoir engineer for the Drilling & Production Div. of Phillips Petroleum Co., studying gas well performance in the Texas panhandle and the Oklahoma Guymon-Hugoton fields. Previously a field engineer, she worked in Oklahoma City and Odessa, TX. Works holds a BS degree in petroleum engineering from the U. of Oklahoma. **Thomas S. Thrasher** is a senior staff reservoir engineering specialist for the Drilling & Production Div. at Phillips Petroleum Co. His primary research interests are advanced decline-curve and pressure-transient analysis. He holds a BS degree in petroleum engineering from the U. of Oklahoma. He currently serves on the SPE Pressure Transient Program Committee and is the Bartlesville Section's membership chairman.

SI Metric Conversion Factors

ft	×	3.048*	E−01	= m
ft^3	×	2.863 640	E−02	= m^3
°F		(°F−32)/1.8		= °C
gal	×	3.785 412	E−03	= m^3
lbm	×	4.535 924	E−01	= kg
md	×	9.869 233	E−04	= μm^2
psi	×	6.894 757	E+00	= kPa

*Conversion factor is exact.

SPEFE

Original SPE manuscript received for review Oct. 2, 1988. Paper accepted for publication April 9, 1990. Revised manuscript received Dec. 20, 1989. Paper (SPE 18266) first presented at the 1988 SPE Annual Technical Conference and Exhibition held in Houston, Oct. 2–5.

Application of a General Material Balance for High-Pressure Gas Reservoirs

Michael J. Fetkovich, SPE, **Dave E. Reese**, SPE, Phillips Petroleum Co., and **C.H. Whitson**, SPE, Norwegian U. of Science and Technology

Summary

This paper presents the derivation of a general gas material balance that has particular application to high-pressure gas reservoirs, [both normal pressured and overpressured (geopressured)]. Its main application is to calculate original gas in place and assist in calculating remaining recoverable reserves from pressure/production data.

The form of the material-balance equation is $(p/z)[1 - \bar{c}_e(p)(p_i - p)] = (p/z)_i(1 - G_p/G)$, which includes a pressure-dependent cumulative effective compressibility term $\bar{c}_e(p)$ that is defined in terms of the following reservoir parameters: pore compressibility, water compressibility, gas solubility, and total water associated with the gas reservoir volume. "Associated" water includes connate water, water within interbedded shales and nonpay reservoir rock, and any limited aquifer volume. $\bar{c}_e$ physically represents the cumulative change in hydrocarbon pore volume (PV) caused by compressibility effects and encroaching water.

High pressure gas reservoirs typically have concave downward p/z vs. G_p plots which may result in serious overestimation of original gas in place and remaining recoverable reserves. The proposed form of the gas material balance equation provides a method to linearize the p/z vs. G_p plot, and thereby predict the true original gas in place. A method is suggested to determine initial gas in place by analyzing the behavior of cumulative effective compressibility backcalculated from pressure/production data. The $\bar{c}_e(p)$ function determined by this procedure, or estimated from logs and geological maps when sufficient production data is not available, is then used to forecast pressure/cumulative behavior. Two field examples are provided showing the application of the material balance equation to high pressure gas reservoirs.

Introduction

High pressure gas reservoirs experiencing depletion drive typically have downward curving p/z vs. G_p behavior. Incorrect extrapolation of early depletion data may result in serious overestimation of original gas in place and remaining reserves.

Bruns *et al.*[1] work in 1965 was a result of a field study conducted on a large moderately overpressured gas reservoir in the Texas Gulf Coast area. Investments were made, and never needed, based on linear extrapolation of the early field p/z vs. G_p performance to an apparent original gas in place that was later found to be overstated by about 200 Bscf. Fig. 5 in Ref. 1 (Run 20) shows the concave downward curvature typical for the pressure response of a limited external aquifer system that simulated the reservoir's response.

This type of "limited" aquifer behavior, where pressure in the reservoir and aquifer are virtually equal, led to the derivation of a general material balance for high pressure gas reservoirs (see Appendix, Ref. 2). The derivation includes pressure-dependent rock and water compressibility (with gas evolving from solution). All water and rock volumes associated with the reservoir and available for expansion, including a limited aquifer volume, were included in a cumulative effective compressibility term $\bar{c}_e(p)$. Rock and water compressibilities were defined to account for cumulative changes in volume to be multiplied by the cumulative pressure drop $(p_i - p)$; instantaneous compressibilities are not used at all. The final form of the material balance is similar to that published by Ramagost and Farshad,[3] except that they considered $\bar{c}_e$ as a constant. The general gas material balance as presented in this paper defines a cumulative effective compressibility $\bar{c}_e(p)$ as a function of pressure.

Original SPE manuscript received for review 11 March 1997. Revised manuscript received 24 November 1997. Paper peer approved 9 December 1997. Paper (SPE 22921) first presented at the 1991 SPE Annual Technical Conference and Exhibition held in Dallas, 6–9 October.

Literature Review

Harville and Hawkins[4] and Hammerlindl[5] attribute the concave downward shape of p/z vs. G_p curves obtained in abnormally pressured gas reservoirs entirely to pore collapse and formation compaction. No definition of pore collapse is given in Ref. 4, but a plot of backcalculated PV change indicated a system compressibility change from 28×10^{-6} psi^{-1} at initial pressure to about 6×10^{-6} psi^{-1} at low pressures. This magnitude of PV change implies associated water volume. The decreasing "system" compressibility is expected for an overpressured reservoir with pressure-dependent PV compressibility, and based on results presented in this paper pore collapse is not a necessary condition for such behavior.

The Anderson "L" reservoir performance presented by Duggan[6] shows curved p/z vs. G_p field behavior which was primarily attributed to shale water influx with no evidence of reservoir pore compaction. The water influx drive mechanism was supported by the fact that several wells watered out. Wallace[7] also concluded that shale water influx is an important drive mechanism in abnormally pressured gas reservoirs. Bass[8] discounts shale water influx, and attributes curved p/z vs. G_p behavior to peripheral water influx from a limited aquifer and formation compaction treated with a constant PV compressibility c_f. For a limited aquifer, Bass defines a term F_p as the ratio of peripheral water PV to the PV of gas-bearing rock.

Roach[9] and Ramagost and Farshad[3] both use the term $p/z[1 - c_e(p_i - p)]$ for geopressured and abnormally pressured gas reservoirs. Both authors consider c_e a constant and they consider the Anderson "L" example.

Bernard[10] does not accept the rock collapse theory as the cause for overpressured p/z vs. G_p behavior, concluding that water influx is the basic drive mechanism. He also uses $p/z[1 - c(p_i - p)]$ where c is a "catch-all" term for treating the effects of rock and water compressibility, a small steady-state acting aquifer, and steady state shale water influx. He further states that the term c is almost impossible to quantify in terms of reservoir properties.

Begland and Whitehead,[11] Prasad and Rogers,[12] and Wang and Teasdale[13] all present studies of overpressured gas reservoirs based on computer models. Refs. 11 and 12 treat c_f and c_w as functions of pressure, including the effect of solution gas in the water. External water sources are also included in Refs. 12 and 13. The differential forms of the material balance used in these references correctly apply instantaneous compressibility in a history-matching approach to determine initial gas in place. A direct plot of $(p/z)[1 - \bar{c}_e(p_i - p)]$ vs. G_p was not made because the $\bar{c}_e$ term had not been defined.

Poston and Chen[14] analyzed several abnormally pressured gas reservoirs, and recognized that calculated values of $c_e > 30 \times 10^{-6}$ psi^{-1} required to linearize the material-balance plot reflected the influence of water influx.

Bourgoyne[15] demonstrates that reasonable values of shale permeability and compressibilities treated as a function of pressure can be used to match abnormal gas reservoir performance behavior. He points out, however, that determining k and c_f of the shale necessary for modeling this behavior is practically impossible.

Ambastha[16] uses Bourgoyne's general material-balance equation to develop a graphical matching technique based on a constant effective compressibility c_e. The example given in that paper shows a lack of uniqueness in determining initial gas in place.

General Material Balance

The general form of the gas material balance is

$$\frac{p}{z}[1 - \bar{c}_e(p)(p_i - p)] = \left(\frac{p}{z}\right)_i - \frac{(p/z)_i}{G}$$

$$\left[G_p - G_{inj} + W_p R_{sw} + \frac{5.615}{B_g}(W_p B_w - W_{inj} B_w - W_e)\right], \quad \ldots\ldots\ldots\ldots\ldots\ldots\ldots\ldots (1)$$

which reduces to

$$\frac{p}{z}[1 - \bar{c}_e(p)(p_i - p)] = \frac{p}{z_i} - \left(\frac{p_i/z_i}{G}\right)G_p \quad \ldots\ldots\ldots\ldots\ldots\ldots (2)$$

when water terms and gas injection are neglected. The cumulative effective compressibility term $\bar{c}_e(p)$ is pressure-dependent, consisting of a cumulative PV compressibility $\bar{c}_f(p)$, cumulative total water compressibility $\bar{c}_{tw}(p)$, and the total pore and water volumes associated (i.e., in pressure communication) with the gas reservoir,

$$\bar{c}_e(p) = \frac{S_{wi}\bar{c}_{tw}(p) + \bar{c}_f(p) + M[\bar{c}_{tw}(p) + \bar{c}_f(p)]}{1 - S_{wi}}. \quad \ldots\ldots\ldots\ldots (3)$$

The formation and total water compressibility terms $\bar{c}_f$ and $\bar{c}_{tw}$ account for cumulative changes in volume from initial pressure to the current pressure.

The interbedded nonpay volume and limited aquifer contributions to pressure support are quantified in terms of the M ratio,

$$M = \frac{V_{pNNP} + V_{pAQ}}{V_{pR}} \quad \ldots\ldots\ldots\ldots\ldots\ldots\ldots\ldots\ldots\ldots (4)$$

An important aspect of the material balance for high-pressure gas reservoirs is that the gas in solution in the connate and associated water provide both pressure support and additional gas available for production. The level of pressure support provided by the evolved solution gas depends on the level of depletion, and it is shown that this support is significant below about 1,500 psia. The solution gas available for production also depends on the level of depletion, i.e., how much of the original solution gas has evolved $[R_{sw}(p_i) - R_{sw}(p)]$ and the quantity of this gas that is mobile.

The term G is used for the initial free gas in place, and it is this quantity that will be determined from the material balance plot given by Eq. 2 when extrapolated to $(p/z)[1 - \bar{c}_e(p_i - p)] = 0$. This condition is reached at a pressure when $1 - \bar{c}_e(p)(p_i - p) = 0$, and not when $p = 0$, i.e., additional gas may be produced after G_p reaches original free gas in place G. At pressures where G_p exceeds G the corrected p/z term $(p/z)[1 - \bar{c}_e(p_i - p)]$ becomes negative. If reservoir pressure could be brought to standard conditions ($p = p_{sc}$) the total gas would be G plus the total solution gas in place G_s, $(G + G_s)$.

The effect of connate water saturation S_{wi} and M are important to the magnitude of $\bar{c}_e$. With typical values of $\bar{c}_f = c_{fi} = 4 \times 10^{-6}$ psi^{-1} and $\bar{c}_{tw} = c_{wi} = 3 \times 10^{-6}$ psi^{-1} for a high-pressured gulf coast sandstone reservoir, the cumulative effective compressibility is initially $\bar{c}_e = 7.5 \times 10^{-6}$ psi^{-1} for $S_{wi} = 35\%$ and $M = 0$; and $\bar{c}_e = 15 \times 10^{-6}$ for $S_{wi} = 35\%$ and $M = 1$. **Fig. 1** shows the percentage of true original free gas in place that would be overestimated by extrapolating early p/z vs. G_p data, indicating that the overestimation is greater for larger initial pressure and higher $\bar{c}_e$ values at initial conditions. For an initial pressure of 10,000 psia and a $\bar{c}_e = 10 \times 10^{-6}$ psi^{-1} the extrapolation of early data gives an estimate of G that is about 25% higher than the true original free gas in place. The sections below discuss the calculation of $\bar{c}_f(p)$ and $\bar{c}_{tw}(p)$ functions.

Cumulative PV Compressibility $\bar{c}_f$. The material balance presented in this paper uses a cumulative PV compressibility $\bar{c}_f$ defined as

$$\bar{c}_f(p) = \frac{1}{V_{pi}}\left[\frac{V_{pi} - V_p(p)}{p_i - p}\right]. \quad \ldots\ldots\ldots\ldots\ldots\ldots\ldots (5)$$

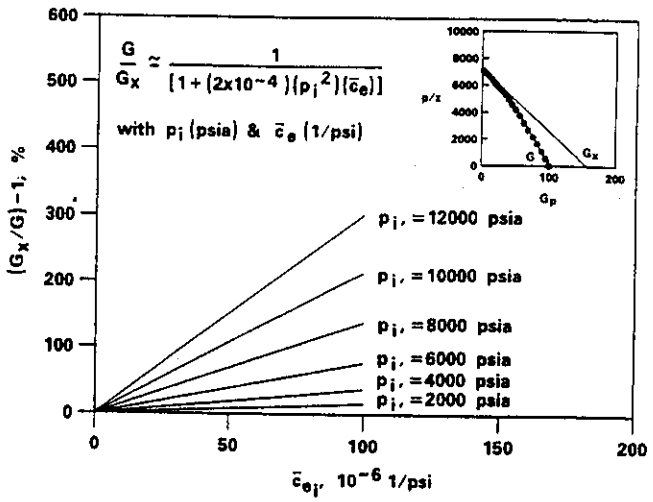

Fig. 1—Effect of p_i and $\bar{c}_e$ on overestimating G.

The term in brackets is the slope of the chord from the initial condition (p_i, V_{pi}) to any lower pressure (p, V_p), as shown in **Fig. 2**. This implies that $\bar{c}_f$ is a function of both pressure and the initial condition. The instantaneous PV compressibility c_f is defined as

$$c_f(p) = \frac{1}{V_p}\frac{\partial V_p}{\partial p} \quad \ldots\ldots\ldots\ldots\ldots\ldots\ldots\ldots\ldots\ldots (6)$$

and is only a function of pressure. At initial pressure the two PV compressibilities are equal: $\bar{c}_f(p_i) = c_f(p_i)$. The instantaneous compressibility function $c_f(p)$ should be used in reservoir simulation and differential forms of the material balance, while the cumulative compressibility function $\bar{c}_f(p)$ must be used with forms of the material balance that apply the cumulative pressure drop $(p_i - p)$, i.e., p/z vs. G_p plots.

The pressure dependence of $\bar{c}_f$ is best determined by special core analysis under appropriate reservoir conditions. **Table 1** summarizes the calculation of $\bar{c}_f$ as a function of pressure using laboratory data for a gulf coast sandstone. **Fig. 3** shows how c_f and $\bar{c}_f$ vary as a function of pressure for this overpressured reservoir rock.

In the absence of pore collapse $\bar{c}_f$ is always greater than or equal to c_f. The cumulative PV compressibility remains higher than the instantaneous compressibility because of an averaging effect that reduces the pressure dependence of $\bar{c}_f$ compared with c_f. An important consequence of this behavior is that a rock exhibiting large PV change because of a high level of overpressure will initially have and maintain a high cumulative compressibility $\bar{c}_f$ as shown in Fig. 3.

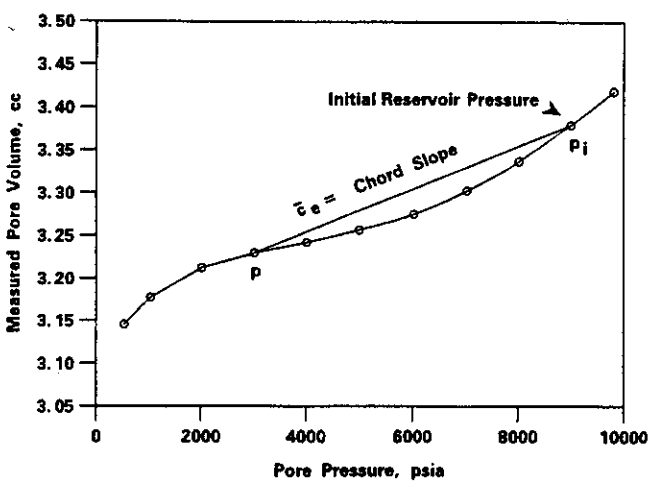

Fig. 2—Cumulative PV compressibility as a chord slope.

TABLE 1—CALCULATION OF PORE VOLUME COMPRESSIBILITY FROM LABORATORY DATA

Reported Laboratory Data					Calculations for p_i = 9,800 psia			
p_o (psia)	V_p (cm³)	V_b (cm³)	ϕ (%)	c_f	p (psia)	$p_i - p$ (psi)	$V_{p_i} - V_p$ (cm³)	$\bar{c}_f$ Eq. 5
200.0	3.420	20.530	16.70	16.50	9,800	0	0.000	16.50
1,000.0	3.379	20.489	16.49	13.70	9,000	800	0.041	14.99
2,000.0	3.337	20.447	16.32	11.40	8,000	1,800	0.083	13.48
3,000.0	3.303	20.413	16.18	9.10	7,000	2,800	0.117	12.22
4,000.0	3.276	20.386	16.07	6.90	6,000	3,800	0.144	11.08
5,000.0	3.257	20.367	15.99	5.00	5,000	4,800	0.163	9.93
6,000.0	3.243	20.353	15.93	3.80	4,000	5,800	0.177	8.92
7,000.0	3.230	20.340	15.88	4.10	3,000	6,800	0.190	8.17
8,000.0	3.213	20.323	15.81	7.30	2,000	7,800	0.207	7.76
9,000.0	3.177	20.287	15.70	16.80	1,000	8,800	0.243	8.07
9,500.0	3.144	20.254	15.50	25.80	500	9,300	0.276	8.68

All compressibilities in 10^{-6} psi^{-1}

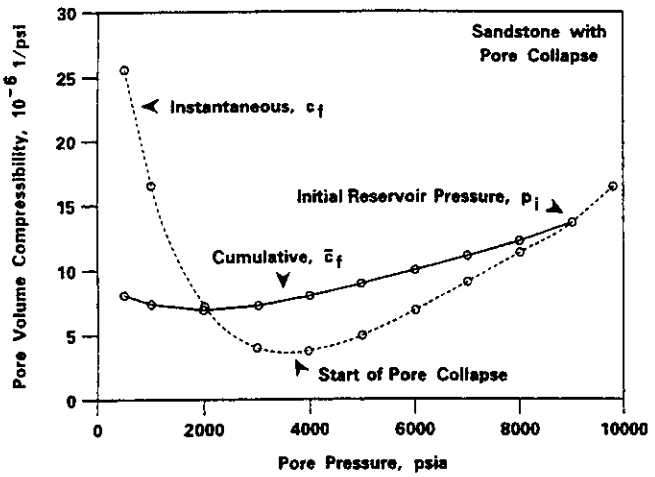

Fig. 3—Cumulative and instantaneous c_f vs. p for a sandstone with pore collapse.

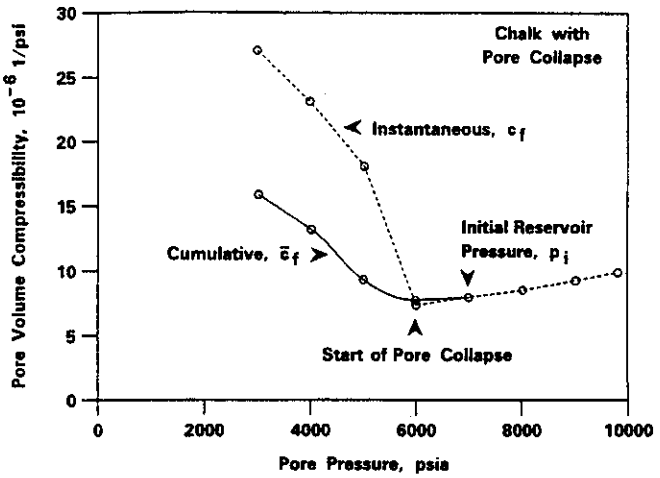

Fig. 4—Cumulative and instantaneous c_f vs. p for a chalk with pore collapse.

Pore collapse is defined as the condition when a rock's instantaneous PV compressibility starts to increase at decreasing reservoir pressure. Pore collapse provides greater pressure support when collapse occurs at a high pressure. However, pore collapse is not reflected by the $\bar{c}_f(p)$ function and will not therefore be seen on the p/z vs. G_p plot at the pressure when pore collapse occurs. In fact, pore collapse may not be identifiable at all on the cumulative compressibility term. For example, the gulf coast sandstone in Fig. 3 exhibits pore collapse at 4,000 psia (about 5,000 psi less than initial pressure p_i). Despite the increase in c_f from 4 to 25 × 10^{-6} psi^{-1} in the pressure range 4,000 to 1,000 psia, the change in $\bar{c}_f$ over the same pressure range is almost insignificant. **Fig. 4** shows a North Sea chalk sample from a reservoir with initial pressure of 7,000 psia exhibiting pore collapse at 6,000 psia. Here the effect pore collapse is greater, causing $\bar{c}_f$ to increase from 6 to 20 × 10^{-6} psi^{-1} in the pressure range from 6,000 to 2,000 psia. In general, however, pore collapse in and of itself does not have a significant effect on the p/z vs. G_p plot.

In the absence of laboratory data, PV compressibilities can be estimated from correlations presented by Hall[17] and by Von Gonten and Choudhary.[18] Hall's correlation (his Fig. 2) gives instantaneous PV compressibility as a function of porosity, i.e., there is no pressure dependence. Von Gonten develops correlations for instantaneous PV compressibility c_f as a function of net overburden pressure (p_o), where p_o equals the overburden gradient times depth minus reservoir pressure.

Cumulative Total Water Compressibility $\bar{c}_{tw}$. The pressure support provided by water is made up of two components. First, the water expansion with decreasing pressure, and second, the release of solution gas and its expansion. The total or composite compressibility effect is expressed as

$$\bar{c}_{tw}(p) = \frac{1}{B_{tw}(p_i)} \frac{B_{tw}(p) - B_{tw}(p_i)}{p_i - p} \quad \ldots\ldots\ldots\ldots\ldots\ldots (7)$$

in terms of the total water formation volume factor B_{tw},

$$B_{tw}(p) = B_w(p) + \frac{[R_{swi} - R_{sw}(p)]B_g(p)}{5.615} \quad \ldots\ldots\ldots\ldots\ldots\ldots (8)$$

Fig. 5 shows typical behavior for B_w and B_{tw} as a function of pressure; the figure also shows the behavior of $\bar{c}_{tw}(p)$ where it is seen that little increase occurs before a pressure of about 1,500 psia, and that, at pressures below 1,000 psia, there is a significant increase in $\bar{c}_{tw}$ with a limiting relationship $\bar{c}_{tw} \propto 1/p$ at low pressures.

$$\bar{c}_{tw}(p \rightarrow 0) \cong \left[\frac{1}{5.615} \frac{Tp_{sc}}{T_{sc}} \frac{R_{swi}}{p_i B_{twi}}\right] \frac{1}{p} \quad \ldots\ldots\ldots\ldots\ldots\ldots (9)$$

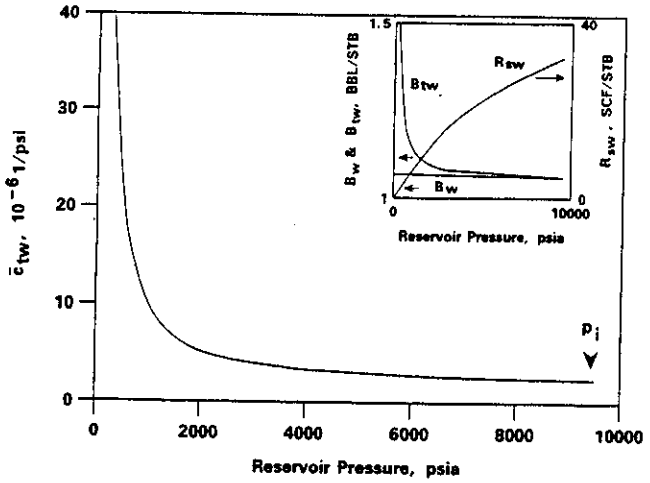

Fig. 5—Cumulative total water compressibility, $\bar{c}_{tw}$, vs. p.

Specifically at standard conditions (p_{sc}), $\bar{c}_{tw}$ is given by

$$\bar{c}_{tw}(p_{sc}) = \left[\frac{1}{5.615}\frac{T}{T_{sc}}\frac{R_{swi}}{p_i B_{wti}} - \frac{1}{p_i}\right]. \quad \ldots\ldots\ldots\ldots\ldots\ldots (10)$$

To calculate $\bar{c}_{tw}$, values of B_w, R_{sw}, and B_g are tabulated with pressure as shown in **Table 2**. These properties can be obtained from correlations at pressures less than about 10,000 psia and 300°F. At more extreme conditions of pressure and temperature, and for gases with high concentrations of nonhydrocarbons CO_2, N_2, and H_2S, we have used the Peng-Robinson[19] equation of state with volume translation and binary interaction coefficients that are dependent on both temperature and salinity.[20]

Another approach for high pressures is simply to extrapolate B_w linearly and R_{sw} with a flattening curvature toward a constant value. Nonhydrocarbons can be treated by evaluating R_{sw} of each component separately at its partial pressure, and summing the values for all soluble components,

$$[R_{sw}(p)]_{TOTAL} = \sum_j [R_{sw}(y_j p)], \quad \ldots\ldots\ldots\ldots\ldots\ldots (11)$$

where y_j is the reservoir gas mole fraction of Component j. Typically the only components with appreciable solubility are methane, CO_2, and H_2S.

TABLE 2—COMPARISON OF c_f FOR NORMAL PRESSURE AND OVERPRESSURED CONDITIONS

Sample	Initial Porosity (%)	Normal Pressure c_{fi} (psi^{-1})	Over-Pressured c_{fi} (psi^{-1})
Gulf coast sandstones			
Sample 1	13	4.8	6.4
Sample 2	20	4.4	16.5
North Sea chalk			
Sample 9 (pore collapse)	32	18.3	7.9
Sample 10 (pore collapse)	30	20.1	7.4
Von Gonten			
Sample 9A	11	3.0	6.0
Sample 4A	22	4.6	9.2
Sample 7A	26	5.9	7.2
Sample 3A	28	8.6	10.6
Sample 6A	25	7.8	8.6

Normal Pressured is 0.5 psi/ft × Depth; Overpressured is 0.8 psi/ft × Depth. Depth Used is 10,000 ft.

Associated Water Volume Ratio M. The total compressibility effect on the gas material balance depends on the magnitudes of rock and total water compressibilities and on the total pore and water volumes in pressure communication with the gas reservoir (including connate water and the PV within the net pay).

Associated water and PVs external to the net pay include nonnet pay (NNP) such as interbedded shales and dirty sands, plus external water volume found in limited aquifers. Including these water volumes in reservoir simulation is referred to as using a "gross" model. In the proposed material balance equations this associated volume is expressed as a ratio relative to the PV of the net pay reservoir,

$$M = M_{NNP} + M_{AQ}, \quad \ldots\ldots\ldots\ldots\ldots\ldots (12)$$

where

$$M_{NNP} = \frac{V_{pNNP}}{V_{pR}} \quad \ldots\ldots\ldots\ldots\ldots\ldots (13)$$

and

$$M_{AQ} = \frac{V_{pAQ}}{V_{pR}}. \quad \ldots\ldots\ldots\ldots\ldots\ldots (14)$$

In the simplest case when $M = 0$, there will be pressure support only from connate water and the net pay PV. This is equivalent in simulation to building a net model. The cumulative effective compressibility term $\bar{c}_e$ will then be expected to have values ranging from 7 to 15 × 10^{-6} psi^{-1} for normal-pressure reservoirs, where the larger values will generally result from high connate water saturation.

Net pay compressibility effects alone can cause noticeable curvature in the p/z vs. G_p plot with potential overestimation of initial free gas in place (G) (see Fig. 1).

M_{NNP}. The nonnet pay water volume ratio M_{NNP} comprises interbedded reservoir PV, including shales and poor quality rock, that are assumed to be completely filled with water. With this definition M_{NNP} can be written in terms of the net to gross ratio R_{NG} defined as

$$R_{NG} = \frac{h_R}{h_R + h_{NNP}} = \frac{h_R}{h_t}. \quad \ldots\ldots\ldots\ldots\ldots\ldots (15)$$

Accounting for different porosities in the net pay and nonnet pay M_{NNP} is given by

$$M_{NNP} = \frac{(\overline{\phi hA})_{NNP}}{(\overline{\phi hA})_R} = \frac{\phi_{NNP}}{\phi_R}\left(\frac{1 - R_{NG}}{R_{NG}}\right). \quad \ldots\ldots\ldots\ldots\ldots\ldots (16)$$

Properties and thicknesses of the net pay and nonnet pay are readily available from log analysis.

M_{AQ}. Aquifers with sufficient permeability and limited areal extent can be treated as part of the total cumulative compressibility term. The water volume ratio of the aquifer M_{AQ} can be determined using geological maps and well control to define areal extent, and electric logs to define the gas/water contact. In general, M_{AQ} is defined as

$$M_{AQ} = \frac{(\overline{\phi hA})_{AQ}}{(\overline{\phi hA})_R}, \quad \ldots\ldots\ldots\ldots\ldots\ldots (17)$$

and for a radial aquifer geometry quantified in terms of the aquifer to reservoir radius r_{AQ}/r_R, the aquifer volume ratio can be expressed

$$M_{AQ} = \frac{(\overline{\phi h})_{AQ}}{(\phi h)_R}\left[\left(\frac{r_{AQ}}{r_R}\right)^2 - 1\right]. \quad \ldots\ldots\ldots\ldots\ldots\ldots (18)$$

Bruns *et al.*[1] show that limited aquifers with r_{AQ}/r_R ratios up to 5 have the same p/z vs. G_p behavior for permeabilities 100 md and higher. This implies that the transient effects in the aquifer have

negligible effect on reservoir performance and the aquifer can be treated as part of the cumulative effective compressibility term. Values of M_{AQ} used in the definition of $\bar{c}_e$ may be as high as 25, [$M_{AQ} \approx (r_{AQ}/r_R)^2 - 1$], in reservoirs with moderate permeability. With higher permeabilities, limited aquifers can include r_{AQ}/r_R ratios greater than 5 and still be treated as part of the cumulative effective compressibility term.

When the aquifer is sufficiently large and requires treatment with either superposition or the Schilthius infinite aquifer model, the $\bar{c}_e$ term should still be used, but it will only contain the effect of net pay and nonnet pay volumes; i.e., $M = M_{NNP}$.

Cumulative Effective Compressibility $\bar{c}_e$. Total cumulative effective compressibility represents all available pressure support from rock and water. The equation for $\bar{c}_e$ is

$$\bar{c}_e(p) = \frac{S_{wi}\bar{c}_{rw}(p) + \bar{c}_f(p) + M[\bar{c}_{rw}(p) + \bar{c}_f(p)]}{1 - S_{wi}} \quad \ldots\ldots\ldots (19)$$

For a specific reservoir a family of $\bar{c}_e(p)$ curves can be generated for several M values. These curves will have specific characteristics depending on the pressure dependence of rock and water compressibilities. The $\bar{c}_{rw}(p)$ curves are relatively constant at high pressure, increasing slightly as pressure decreases, then rising sharply at low pressure around 1,000 psia. Typically, a constant PV compressibility c_f can be assumed and the $\bar{c}_e(p)$ curves will then have the same character as the $\bar{c}_{rw}(p)$ curve. **Fig. 6** illustrates an example of $\bar{c}_e(p)$ curves at various M ratios for a typical gulf coast reservoir with p_i = 9,000 psia, T = 200°F, γ_g = 0.7 (air = 1), and a constant $\bar{c}_f = 3.2 \times 10^{-6}$ psi^{-1}.

For overpressured reservoirs exhibiting a pressure-dependent $\bar{c}_f(p)$, the family of $\bar{c}_e(p)$ curves at high pressures will tend to decrease with depletion. In the absence of pore collapse $\bar{c}_f(p)$ decreases to a constant value at lower pressure and the $\bar{c}_e(p)$ curves at lower pressure are dominated by the increasing $\bar{c}_{rw}(p)$ function. If pore collapse occurs, but not early in depletion, the pore collapse is almost insignificant because the $\bar{c}_f(p)$ function does not start increasing until low pressures because it represents a cumulative PV change, and, when the $\bar{c}_f(p)$ function finally starts to increase it will be masked by the $\bar{c}_{rw}(p)$ function which is increasing as $1/p$. **Fig. 7** illustrates this point for a gulf coast overpressured reservoir with p_i = 9,000 psia, T = 300°F, and γ_g = 0.71 (air = 1). Although pore collapse occurs at approximately 3,500 psia (Fig. 3), $\bar{c}_f$ does not start increasing until 2,000 psia. The increase is insignificant relative to the increase in $\bar{c}_{rw}(p)$ at lower pressures.

The next example is a North Sea chalk (Fig. 4) that shows pore collapse at a pressure only 1,000 psi below initial pressure of 7,000 psia. The $\bar{c}_f(p)$ function increases almost simultaneously with instantaneous c_f, and the effect of $\bar{c}_f(p)$ on $\bar{c}_e(p)$ is shown in **Fig. 8**. Although $\bar{c}_f(p)$ has an impact on $\bar{c}_e(p)$ at moderate and high pressures for this example, the $\bar{c}_{rw}(p)$ function still dominates the behavior of $\bar{c}_e(p)$ at pressures less than 1,500 psia.

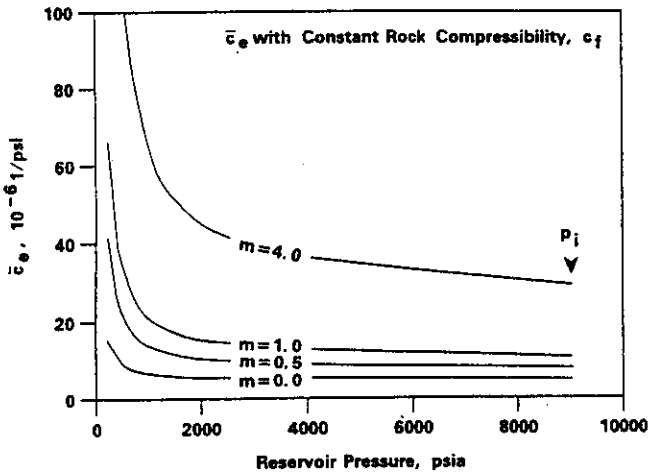

Fig. 6—Cumulative effective compressibility vs. p at various M ratios.

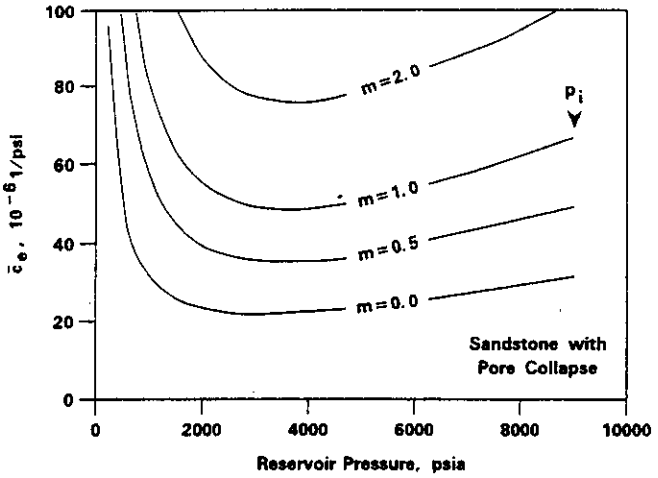

Fig. 7—Cumulative effective compressibility vs. p for a sandstone w/pore collapse.

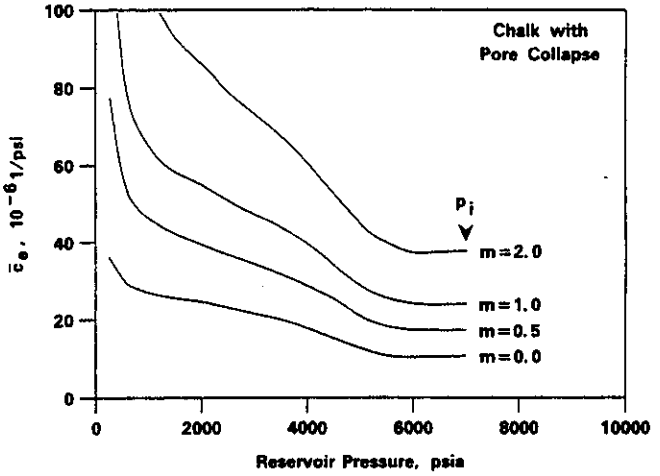

Fig. 8—Cumulative effective compressibility vs. p for a chalk w/pore collapse.

Estimating Gas-in-Place. A method is proposed for estimating the initial (free) gas in place G based on historical pressure/cumulative data. The procedure also determines the water volume ratio M and the $\bar{c}_e(p)$ function. First, a plot of p/z versus cumulative gas production G_p should have the characteristic concave downward shape of a high-pressure reservoir influenced by associated water and PV compressibility.

A range of values for G should then be assumed, with the largest value based on an extrapolation of the early depletion data, and the lowest value being somewhat larger than the current G_p. For an assumed value of G, calculate for each measured p/z and G_p data the $\bar{c}_e$ value from the rearranged material balance, Eq. 2,

$$(\bar{c}_e)_{\text{backcalculated}} = \left[1 - \frac{(p/z)_i}{(p/z)}\left(1 - \frac{G_p}{G}\right)\right]\frac{1}{(p_i - p)} \quad \ldots\ldots\ldots (20)$$

At this point, a plot can be made of backcalculated $\bar{c}_e$ as a function of pressure given the assumed G. Using reservoir rock and water properties, a family of $\bar{c}_e(p)$ curves at various M values can be generated independently to match against the backcalculated $\bar{c}_e$ values. The data should honor the shape and magnitude of one $\bar{c}_e(p)$ curve, where this match yields G, the M value, and a $\bar{c}_e(p)$ function that can be used to forecast future p/z vs. G_p behavior. This procedure gives a sound physical significance to the estimation of G as opposed to a pure statistical best fit that may lead to unrealistic

solutions. The Field Examples section discusses criteria for matching field data, and the expected behavior of $\bar{c}_e(p)$.

Characteristics of p/z vs. G_p Plots for High-Pressure Reservoirs

PV reduction, water expansion, and solution gas evolution, expressed in terms of $\bar{c}_e(p)$ in the general material balance equation, provide pressure support for all reservoirs during depletion. The reservoir does not have to be overpressured or geopressured. The term $\bar{c}_e(p)(p_i - p)$ determines whether the conventional p/z vs. G_p plot yields a straight line. For most low-pressure reservoirs this term is small and is often neglected because a straight-line p/z vs. G_p plot is obtained. Reservoirs undergoing depletion with initial pressure exceeding 5,000 psia are automatically candidates for being treated with the complete material balance equation.

Fig. 9 presents three generated p/z vs. G_p curves for a gulf coast overpressured sandstone reservoir using $M = 0$ (i.e., $\bar{c}_e(p) = [\bar{c}_f(p) + S_{wi}\bar{c}_{rw}(p)]/(1 - S_{wi})$. Curve A accounts for PV reduction, including pore collapse at about 4,000 psia. Curve B uses the same $\bar{c}_f(p)$ function as Curve A down to 4,000 psia (where pore collapse occurs) and thereafter uses a constant instantaneous compressibility of 4×10^{-6} psi^{-1}. Plots of p/z vs. G_p for A and B are almost identical, showing only a slight separation at pressures less than 3,500 psia. This clearly shows the limited effect of pore collapse on the p/z vs. G_p plot when collapse occurs late in depletion. Curve C assumes that the initial PV compressibility of 13×10^{-6} psi^{-1} remains constant throughout depletion. The difference between the two p/z vs. G_p Curves A and C is a result of the actual decrease in PV compressibility. Including an external water volume quantified with $M = 2$ produces more curvature in the p/z vs. G_p plots, but the separation between curves with and without pore collapse is still very small (not shown).

Another example relates to a North Sea chalk reservoir where pore collapse occurs just below initial pressure. **Fig. 10** presents generated p/z vs. G_p plots for $M = 0$ with pore collapse (Curve A) and with no pore collapse (Curve B). The effect of pore collapse is more significant than in the previous example because it occurs at a relatively high pressure.

Field Examples

Ellenburger Gas Reservoir. This field example is for a normal pressured (0.5 psi/ft) 1,600-ft-thick, dry gas reservoir with initial reservoir pressure of 6,675 psia at 200°F. Average porosity is about 5% with connate water saturation in the pay of about 35%. Permeability is high because of an extensive microfracture system that results in a high degree of interwell pressure communication and almost instantaneous pressure buildup to static conditions. Initial CO_2 concentration was about 28 mol%, and a gradual increase in CO_2 concentration to 31 mol% at the present time has been

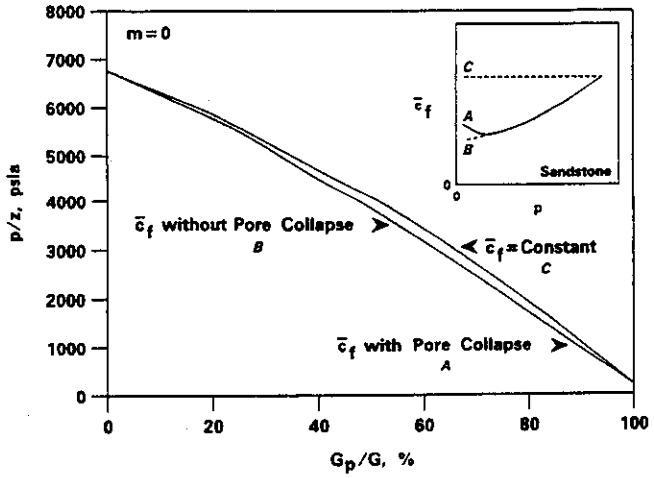

Fig. 9—Effect on p/z vs. G_p with and without pore collapse, sandstone.

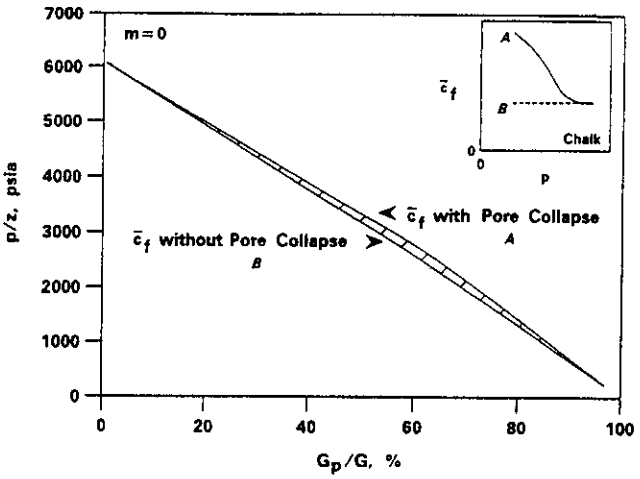

Fig. 10—Effect on p/z vs. G_p with and without pore collapse, chalk.

observed. The reservoir has produced about 3.1 Tscf, and currently has an average fieldwide bottomhole pressure of approximately 1,000 psia. The p/z vs. G_p plot shows a characteristic concave downward behavior, with an initial gas in place estimate of more than 4.4 Tscf using early data (**Fig. 11**). The p/z vs. G_p data at low pressures has started flattening.

The procedure outlined earlier for determining initial free gas in place G was used for this reservoir. **Fig. 12** shows a plot of backcalculated $\bar{c}_e$ vs. pressure for a range of G from 3.0 Tscf to 3.6 Tscf. Another plot of $\bar{c}_e(p)$ was generated independently from rock and fluid properties by use of an equation of state for several values of M with $S_{wi} = 0.35$, $\bar{c}_f = 6.5 \times 10^{-6}$ psi^{-1} (from Hall[17]), and $\bar{c}_{rw}(p)$. **Fig. 13** shows the best-fit of data on the $\bar{c}_e(p)$ curve for $M = 3.3$, corresponding to an initial free gas in place $G = 3.15$ Tscf.

The total water volume including connate and associated waters is given by

$$W = \frac{1}{5.615}\frac{GB_{gi}}{B_{rwi}}\frac{(S_{wi} + M)}{(1 - S_{wi})}, \quad \ldots\ldots\ldots\ldots\ldots\ldots\ldots\ldots\ldots\ldots (21)$$

which yields $8.45(10^9)$ STB. The initial solution gas in place G_s is equal to W times the initial solution gas/water ratio R_{swi},

$$G_s = WR_{swi}. \quad \ldots\ldots\ldots\ldots\ldots\ldots\ldots\ldots\ldots\ldots\ldots\ldots\ldots\ldots (22)$$

Because of the high CO_2 concentration in this reservoir, the solution gas/water ratio ($R_{swi} = 67.5$ scf/STB) is about three times larger than for hydrocarbon gas systems. This yields a solution gas in place of $G_s = 0.55$ Tscf and a total initial gas in place of $G + G_s = 3.70$ Tscf. Fig. 11 shows the p/z vs. G_p forecast using the M value determined from the match to calculate the $\bar{c}_e(p)$ function from S_{wi}, M, $\bar{c}_f$, and $\bar{c}_{rw}(p)$. Also shown on this figure is the plot of $(p/z)[1 -$

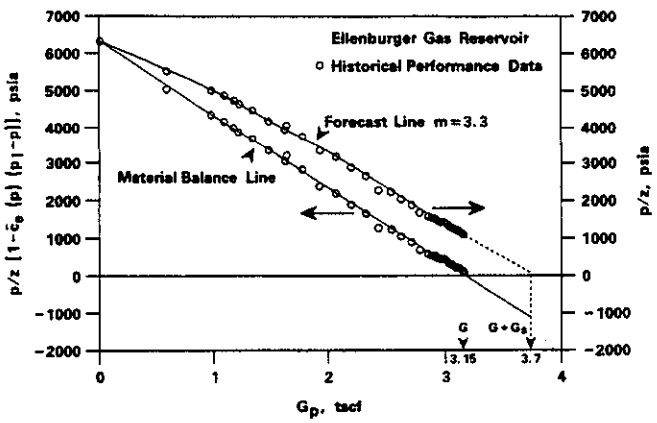

Fig. 11—Pressure vs. cumulative production, Ellenburger gas reservoir.

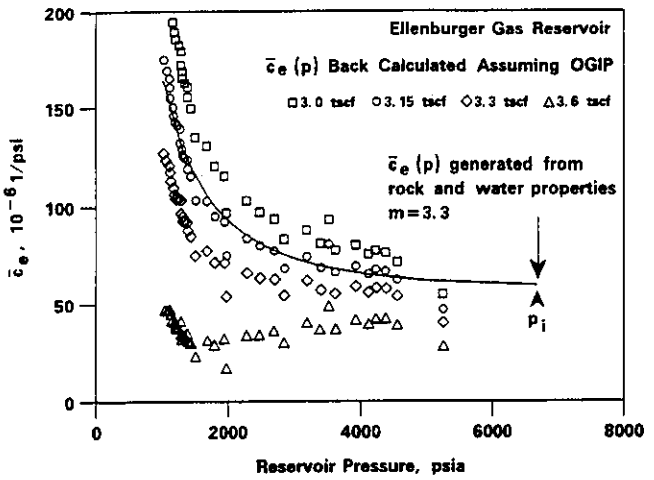

Fig. 12—Backcalculated $\bar{c}_e$ vs. p at various original gas in place (OGIP) values, Ellenburger gas reservoir.

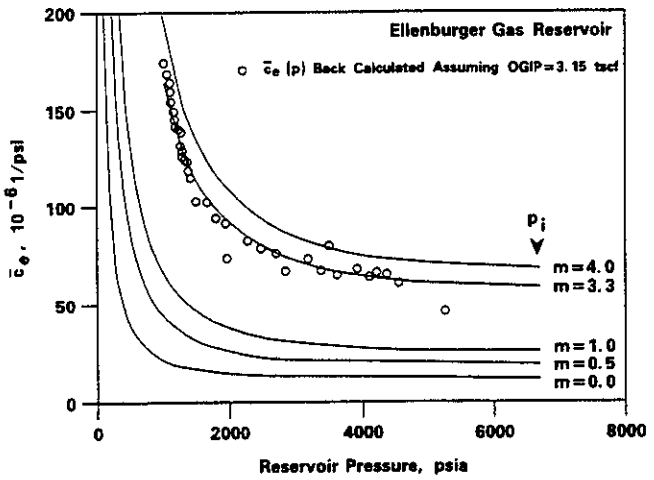

Fig. 13—Matching backcalculated $\bar{c}_e$ to generated $\bar{c}_e$ curves, Ellenburger gas reservoir.

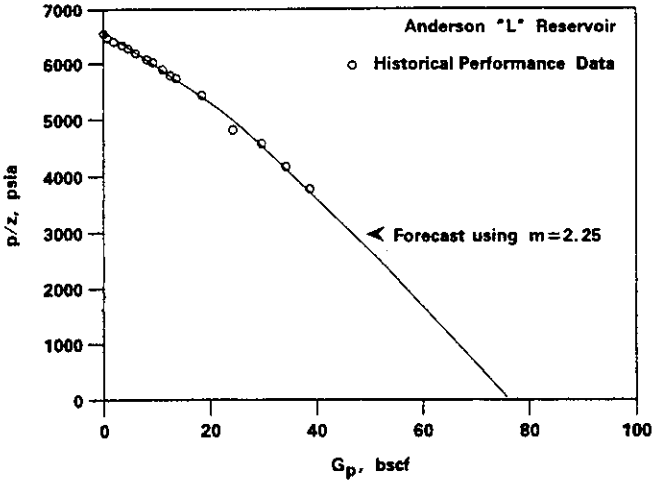

Fig. 14—p/z vs. cumulative production, Anderson "L" reservoir.

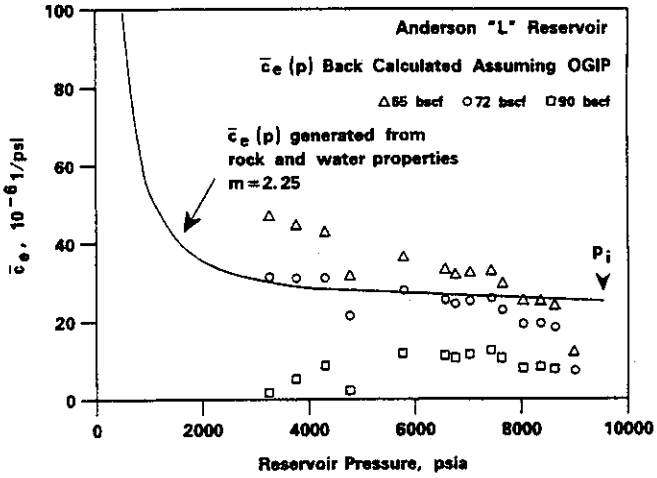

Fig. 15—Backcalculated $\bar{c}_e$ vs. p at various OGIP, Anderson "L" reservoir.

$\bar{c}_e(p)(p_i - p)$] vs. G_p for historical performance data and for the forecast, where it is seen that the current cumulative gas produced equals the original free gas in place.

The associated water volume given by $M = 3.3$ consists of nonnet pay and an external limited aquifer. Log analysis indicates a net-to-gross ratio $R_{NG} = 0.5$, $\phi_R = 0.05$, and $\phi_{NNP} = 0.03$, yielding $M_{NNP} = 0.6$. External water is known to exist but has not been mapped because of lack of well control. The calculated aquifer water volume ratio $M_{AQ} = 2.7$ (3.3 − 0.6), or an equivalent $r_{AQ}/r_R = 1.9$, seems reasonable for a limited aquifer.

Anderson "L". This reservoir has been studied by several authors and it is perhaps the best recognized example of a high-pressure gas reservoir with concave downward $p/z - G_p$ behavior (**Fig. 14**). The reservoir was abandoned after producing 55 Bscf, but pressure tests of public record were discontinued after 40 Bscf had been produced.

Different analyses by other authors have indicated original free gas in place between 65 to 75 Bscf. **Fig. 15** shows backcalculated $\bar{c}_e$ vs. pressure for values of G equal to 65, 72, and 90 Bscf. The 72 Bscf volume is chosen based on a best-fit match with the $\bar{c}_e(p)$ function calculated using $M = 2.25$, $S_{wi} = 0.35$, $\bar{c}_f = 3.2 \times 10^{-6}$ psi^{-1}, and a $\bar{c}_{fw}(p)$ function from equation of state results. Although the first four data do not fall on the slightly increasing $\bar{c}_e(p)$ curve, data at pressures below this value do follow the trend down to the last pressure datum near 3,000 psia.

The 90 Bscf estimate produces unrealistically low $\bar{c}_e$ values, lower than would be calculated using the net reservoir PV and connate water compressibilities. The lowest estimate of 65 Bscf gives a shape for $\bar{c}_e(p)$ that cannot be accounted for using normal $\bar{c}_f(p)$ and $\bar{c}_{fw}(p)$ functions.

The forecasted p/z vs. G_p performance (Fig. 14) is calculated with the match determined above. Total gas in place of is 76 Bscf, which includes 72 Bscf of original free gas plus 4 Bscf of solution gas.

Conclusions

1. A general form of the material balance equation for gas reservoirs has been presented. This equation has particular application to high-pressure reservoirs. A cumulative effective compressibility term $\bar{c}_e(p)$ has been defined in terms of pressure-dependent PV and total water cumulative compressibilities, $\bar{c}_f(p)$ and $\bar{c}_{fw}(p)$, and the total volume of water associated with the net pay reservoir expressed as a ratio M.

2. The general material balance equation applies to all high-pressure reservoirs, both normal pressured and abnormally pressured (overpressured and geopressured).

3. The effect of a limited aquifer can be included as part of the M term for most depletion-type reservoirs. Using the water volume ratio M in the cumulative effective compressibility term, together with normal values of $\bar{c}_f$ and $\bar{c}_{fw}$, explains the "large" $\bar{c}_e$ values commonly reported for high-pressure gas reservoirs when linearizing the material balance equation. In fact, large values of $\bar{c}_e$ backcalculated from field performance data indicate that associated water influx is a dominant drive mechanism.

4. Only cumulative compressibilities ($\bar{c}_f$ and $\bar{c}_{fw}$) can be used in the general gas material balance equation because they are applied

against the cumulative pressure drop $(p_i - p)$ in p/z vs. G_p plots. A method is given for calculating cumulative total water and PV compressibility $\bar{c}_{tw}(p)$ and $\bar{c}_f(p)$.

5. A method is proposed for estimating the original free gas in place from production data. This method uses backcalculated cumulative effective compressibility $\bar{c}_e$ which is plotted against pressure and compared with expected $\bar{c}_e(p)$ behavior calculated solely from rock and water properties for a range of values of the associated water volume ratio M.

6. Pore collapse, in and of itself, does not contribute significantly to pressure support in overpressured gas reservoirs. In fact, pore collapse has little effect unless it occurs early in depletion at a relatively high pressure. The effect of pore collapse, if present, is a positive effect and tends to flatten the p/z vs. G_p curve, not bending the curve downward as has been implied by others.

7. Gas found initially in solution in the connate and associated water is an important component of pressure support late in depletion (below 1500 psia) and may contribute additional producible volumes of gas. Typically, the solution gas in place G_s represents 2 to 10% of the original free gas in place, the value depending primarily on total water volume $(M + S_{wi})/(1 - S_{wi})$ and the initial solution gas/water ratio R_{swi}. Gas reservoirs with high CO_2 concentration (>20 mol%) can have even higher solution gas in place, G_s.

Nomenclature

A = area, ft^2 [m^2]
B = formation volume factor, reservoir per standard volume
c = instantaneous compressibility, 1/psi [1/kPa]
$\bar{c}$ = cumulative compressibility, 1/psi [1/kPa]
G = original free gas-in-place, Bscf [std m^3]
G_p = cumulative gas production, Bscf [std m^3]
G_s = initial solution gas in place, Bscf [std m^3]
G_x = early overestimate of G, Bscf [std m^3]
G_{inj} = cumulative gas injection, Bscf [std^3]
h = thickness, ft [m]
M = volume ratio, dimensionless
R_{NG} = net to gross ratio, dimensionless
p = reservoir pressure, psia [kPa]
p_i = initial reservoir pressure, psia [kPa]
p_o = net overburden pressure, psia [kPa]
r_R = radius of reservoir, ft [m]
r_{AQ} = radius of aquifer, ft [m]
R_{sw} = solution gas water ratio, scf/STB [std m^3/m^3]
S_{wi} = initial water saturation, fraction
T = reservoir temperature, °R [K]
V = volume, ft^3 [m^3]
V_p = PV, cm^3 and ft^3 [m^3]
V_b = bulk volume, cm^3 [m^3]
W = total water in place, bbl [m^3]
W_e = cumulative water influx, bbl [m^3]
W_{inj} = cumulative water injection, bbl [m^3]
W_p = cumulative water production, bbl [m^3]
z = gas compressibility factor, dimensionless
ϕ = porosity, fraction

Subscripts

A = associated water
AQ = limited aquifer
e = effective
f = PV ("formation")
g = gas
t = gross interval thickness
i = initial
inj = injection
NNP = nonnet pay
R = reservoir
sc = standard conditions
tw = total water
w = water

Acknowledgments

We thank the management of Phillips Petroleum Co. for permission to publish this paper. We also acknowledge Fred Kent for work done on the Ellenburger example.

References

1. Bruns, J.R., Fetkovich, M.J., and Meitzen, V.C.: "The Effect of Water Influx on p/z-Cumulative Gas Production Curves," *JPT* (March 1965) 287.
2. Fetkovich, M.J., Reese, D.E., and Whitson, C.H.: "Application of a General Material Balance for High-Pressure Gas Reservoirs," paper SPE 22921 presented at the 1991 SPE Annual Technical Conference and Exhibition, Dallas, 6–9 October.
3. Ramagost, B.P. and Farshad, F.F.: "p/z Abnormal Pressured Gas Reservoirs," paper SPE 10125 presented at the 1981 SPE Annual Technical Conference and Exhibition, San Antonio, Texas, 5–7 October.
4. Harville, D.W. and Hawkins, M.F. Jr.: "Rock Compressibility and Failure as Reservoir Mechanisms in Geopressured Gas Reservoirs," *JPT* (December 1969) 1528.
5. Hammerlindl, D.J.: "Predicting Gas Reserves in Abnormally Pressured Reservoirs," paper SPE 3479 presented at the 1971 SPE Annual Meeting, New Orleans, 3–6 October.
6. Duggan, J.O.: "The Anderson "L'—An Abnormally Pressured Gas Reservoir in South Texas," *JPT* (February 1971) 132.
7. Wallace, W.E.: "Water Production From Abnormally Pressured Gas Reservoirs in Louisiana," *JPT* (August 1968) 969.
8. Bass, D.M.: "Analysis of Abnormally Pressured Gas Reservoirs With Partial Water Influx," paper SPE 3850 presented at the 1972 SPE Abnormal Subsurface Pressure Symposium, Baton Rouge, Louisiana, 15–16 May.
9. Roach, R.H.: "Analyzing Geopressured Reservoirs—A Material Balance Technique," paper SPE 9968 available from SPE, Richardson, Texas (August 1981).
10. Bernard, W.J.: "Gulf Coast Geopressured Gas Reservoirs: Drive Mechanism and Performance Prediction," paper SPE 14362 presented at the 1985 SPE Annual Technical Conference and Exhibition, Las Vegas, Nevada, 22–25 September.
11. Begland, T.F. and Whitehead, W.R.: "Depletion Performance of Volumetric High Pressured Gas Reservoirs," *SPERE* (August 1989) 279; *Trans.*, AIME, **287.**
12. Prasad, R.K. and Rogers, L.A.: "Superpressured Gas Reservoirs: Case Studies and a Generalized Tank Model," paper SPE 16861 presented at the 1987 SPE Annual Technical Conference and Exhibition AIME, Dallas, 27–30 September.
13. Wang, B. and Teasdale, T.S.: "GASWAT-PC: A Microcomputer Program for Gas Material Balance With Water Influx," paper SPE 16484 presented at the 1987 SPE Petroleum Industry Applications of Microcomputers, Del Lago on Lake Conroe, Montgomery Texas, 23–26 June.
14. Poston, S.W. and Chen, H.Y.: "Case History Studies: Abnormal Pressured Gas Reservoirs," paper SPE 18857 presented at the 1989 SPE Productions Operations Symposium, Oklahoma City, Oklahoma, 13–14 March.
15. Bourgoyne, A.T. Jr.: "Shale Water as a Pressure Support Mechanism in Gas Reservoirs Having Abnormal Formation Pressure," *J. Pet. Sci.* (1990) **3**, 305.
16. Ambastha, A.K.: "Analysis of Material Balance Equations for Gas Reservoirs," paper CIM/SPE 90-36 presented at the 1990 CIM/SPE International Technical Meeting, Calgary, Alberta, Canada, 10–13 June.
17. Hall, H.N.: "Compressibility of Reservoir Rocks," *Trans.*, AIME (1953) **198**, 309.
18. Von Gonten, W.D. and Choudhary, B.K.: "The Effect of Pressure and Temperature on Pore-Volume Compressibility," paper SPE 2526 presented at the 1969 SPE Annual Meeting, Denver, Colorado, 28 September–1 October.
19. Peng, D.-Y. and Robinson, D.B.: "A New Two-Constant Equation of State," *Ind. Eng. Chem. Fund.* (1976) No. 1, 59.
20. Soreide, I. and Whitson, C.H.: "Peng-Robinson Predictions for Hydrocarbons, CO_2, and H_2S With Pure Water and NaCl Brine," *Fluid Phase Equilibria* (1992) **77**, 217.

Appendix A—Derivation of General Gas Material Balance

The derivation that follows is based on the following assumptions:

1. Any pressure change caused by production or injection into the reservoir will be felt immediately throughout the total system including (a) *net pay reservoir* (R); (b) *nonnet pay* (NNP), including interbedded shales and poor quality rock assumed to be 100% water-saturated; and (c) *limited aquifer* (AQ), when present, also assumed to be water-saturated. The nonnet pay and aquifer volumes are referred to as "associated" water volumes and both contribute to water influx during depletion.

2. Simple modifications to the material balance equations can be made to generalize for nonnet pay that has an initial free gas saturation.

3. All water in the system is initially saturated with solution gas.

Practically, the assumption of equal pressure throughout the system is reasonable, and any transient effects caused by a large aquifer may be treated by a conventional water influx term (W_e) as shown below.

For the sake of brevity we have chosen to omit explicit reference to pressure dependence—i.e., $\bar{c}_e$, $\bar{c}_f$, and $\bar{c}_{tw}$ should actually read $\bar{c}_e(p)$, $\bar{c}_f(p)$, and $\bar{c}_{tw}(p)$.

Derivation. The volumetric balance at any pressure states that the total PV ($V_{pR} + V_{pA}$) equals the net reservoir PV occupied by gas and water ($V_{gR} + V_{wR}$) plus the associated (nonnet pay and aquifer) PV which also is occupied by gas and water ($V_{gA} + V_{wA}$):

$$(V_{pR} + V_{pA}) = (V_{gR} + V_{wR}) + (V_{gA} + V_{wA}). \quad \ldots\ldots\ldots (A\text{-}1)$$

The net-pay reservoir PV V_{pR} is given by the initial volume V_{pRi} less the change in PV ΔV_{pR},

$$V_{pR} = V_{pRi} - \Delta V_{pR}, \quad \ldots\ldots\ldots (A\text{-}2)$$

$$V_{pRi} = V_{gRi} + V_{wRi}, \quad \ldots\ldots\ldots (A\text{-}3)$$

$$V_{pRi} = GB_{gi} + \frac{GB_{gi}}{1 - S_{wi}} S_{wi},$$

and

$$\Delta V_{pR} = \frac{GB_{gi}}{1 - S_{wi}} \bar{c}_f(p_i - p); \quad \bar{c}_f = (\bar{c}_f)_R, \quad \ldots\ldots\ldots (A\text{-}4)$$

yielding

$$V_{pR} = GB_{gi} + \frac{GB_{gi}}{1 - S_{wi}} S_{wi} - \frac{GB_{gi}}{1 - S_{wi}} \bar{c}_f(p_i - p). \quad \ldots\ldots\ldots (A\text{-}5)$$

PV of the associated rock is given by the initial PV less the change in PV, i.e.,

$$V_{pA} = \frac{GB_{gi}}{1 - S_{wi}} M - \frac{GB_{gi}}{1 - S_{wi}} M\bar{c}_f(p_i - p). \quad \ldots\ldots\ldots (A\text{-}6)$$

The net reservoir gas volume is given by the sum of unproduced free gas, gas released from solution, and any injected gas,

$$V_{gR} = (V_{gR})^{\text{Unproduced}}_{\text{Free Gas}} + (V_{gR})^{\text{Released}}_{\text{From Solution}} + (V_{gR})_{\text{Injected}}, \quad \ldots\ldots (A\text{-}7)$$

resulting in

$$V_{gR} = [G - (G_p - W_pR_{sw})]B_g + \frac{GB_{gi}}{1 - S_{wi}} \frac{S_{wi}}{B_{wi}} (R_{swi} - R_{sw}) \frac{B_g}{5.615} + G_{inj}B_g. \quad \ldots\ldots (A\text{-}8)$$

pressure/volume/temperature properties B_g and R_{sw} are evaluated at current reservoir pressure. Value G_p for a gas condensate is the wet gas volume calculated by adding separator gas to liquid condensate converted to an equivalent surface gas volume. Also, the two-phase Z-factor must be used to calculated B_g for gas condensate reservoirs. Strictly speaking the cumulative water production term W_p represents "free" water production and not the water condensed out of solution from the produced gas wellstream.

The gas volume in the associated PV is a function of the amount of gas that has come out of solution,

$$V_{gA} = \frac{GB_{gi}}{1 - S_{wi}} M \frac{1}{B_{wi}} (R_{swi} - R_{sw}) B_g \frac{1}{5.615}. \quad \ldots\ldots\ldots (A\text{-}9)$$

The water volume in the net-pay reservoir equals the unproduced initial water plus injected water plus water encroachment from an external aquifer,

$$V_{wR} = (V_{wR})_{\text{Unproduced}} + (V_{wR})_{\text{Injected}} + [(V_{wR})_{\text{Encroachment}}], \quad \ldots\ldots\ldots (A\text{-}10)$$

yielding

$$V_{wR} = \left(\frac{GB_{gi}}{1 - S_{wi}} \frac{S_{wi}}{B_{wi}} B_w - \frac{W_pB_w}{5.615}\right) + 5.615W_{inj}B_w + 5.615W_e. \quad \ldots\ldots\ldots (A\text{-}11)$$

The aquifer encroachment term W_e represents any external water volume that is not already included in the M term. Later in the derivation, we show the conditions required so that water encroachment (treated rigorously by the method of superposition) can be included as part of the M term used in the cumulative effective compressibility $\bar{c}_e$.

The water volume in the associated PV is given by simple expansion,

$$V_{wA} = \frac{GB_{gi}}{1 - S_{wi}} M \frac{1}{B_{wi}} B_w \quad \ldots\ldots\ldots (A\text{-}12)$$

Inserting the appropriate equations above in Eq. A-1, rearranging, and grouping terms yields,

$$G(B_g - B_{gi}) + \frac{GB_{gi}}{1 - S_{wi}} \left\{ S_{wi} \left[\frac{(B_w + ((R_{swi} - R_{sw})B_g)/5.615)}{B_{wi}} - \frac{B_{wi}}{B_{wi}} \right] + \bar{c}_f(p_i - p) + M \left[\frac{(B_w + ((R_{swi} - R_{sw})B_g)/5.615)}{B_{wi}} - \frac{B_{wi}}{B_{wi}} \right] + M\bar{c}_f(p_i - p) \right\}$$

$$= (G_p - W_pR_{sw} - G_{inj})B_g + 5.615\left(W_p - W_{inj} - \frac{W_e}{B_w}\right)B_w. \quad \ldots\ldots\ldots (A\text{-}13)$$

Defining the total water/gas formation volume factor B_{tw},

$$B_{tw} \equiv B_w + \frac{(R_{swi} - R_{sw})B_g}{5.615}. \quad \ldots\ldots\ldots (A\text{-}14)$$

Noting that $B_{twi} = B_{wi}$, and defining the cumulative total water/gas compressibility $\bar{c}_{tw}$,

$$\bar{c}_{tw} \equiv \frac{(B_{tw} - B_{twi})}{B_{twi}} \frac{1}{(p_i - p)}. \quad \ldots\ldots\ldots (A\text{-}15)$$

Now, defining a cumulative effective compressibility $\bar{c}_e$,

$$\bar{c}_e \equiv \frac{S_{wi}\bar{c}_{tw} + \bar{c}_f + M(\bar{c}_w + \bar{c}_f)}{1 - S_{wi}} \quad \ldots\ldots\ldots (A\text{-}16)$$

gives

$$G(B_g - B_{gi}) + GB_{gi}[\bar{c}_e(p_i - p)] = B_g\left[G_p - G_{inj} + W_pR_{sw} + \frac{5.615}{B_g}(W_pB_w - W_{inj}B_w - W_e)\right] \quad \text{(A-17)}$$

Dividing through by GB_{gi} and expressing $B_g = (p_{sc}/T_{sc})(zT/p)$ gives the final form of the material balance

$$\frac{p}{z}[1 - \bar{c}_e(p_i - p)] = \left(\frac{p}{z}\right)_i\left\{1 - \frac{1}{G}\left[G_p - G_{inj} + W_pR_{sw} + \frac{5.615}{B_g}(W_pB_w - W_{inj}B_w - W_e)\right]\right\} \quad \text{(A-18)}$$

The p/z vs. cumulative plot, including all terms, would consider $(p/z)[1 - \bar{c}_e(p_i - p)]$ vs. the entire production/injection/encroachment term Q

$$\frac{p}{z}[1 - \bar{c}_e(p_i - p)] = \left(\frac{p}{z}\right)_i - \frac{(p/z)_i}{G}Q, \quad \text{(A-19)}$$

with

$$Q = G_p - G_{inj} + W_pR_{sw} + \frac{5.615}{B_g}(W_pB_w - W_{inj}B_w - W_e), \quad \text{(A-20)}$$

where the intercept is given by $(p/z)_i$ and the slope equals $(p/z)_i/G$. Setting $G_{inj} = W_{inj} = W_p = W_e = 0$ gives the common form of the gas material balance.

$$\frac{p}{z}[1 - \bar{c}_e(p_i - p)] = \left(\frac{p}{z}\right)_i\left(1 - \frac{G_p}{G}\right). \quad \text{(A-21)}$$

Treating Limited Aquifers in $\bar{c}_e$ Term. The material balance thus far has considered any associated water volume expressed in terms of the M parameter. In fact M may include a limited aquifer with up to 25 times the reservoir PV for a system permeability greater than about 100 md, and even larger aquifer volumes for higher permeabilities. The condition that determines when a limited aquifer can be treated as part of the $\bar{c}_e$ term is outlined below. We start with the general material-balance equation including a water encroachment term W_e and a $\bar{c}_e$ term that considers only nonnet pay.

$$\frac{p}{z}[1 - \bar{c}_e(p_i - p)] = \left(\frac{p}{z}\right)_i\left(1 - \frac{G_p}{G} + 5.615\frac{W_e}{GB_g}\right) \quad \text{(A-22)}$$

and

$$\bar{c}_e = \frac{S_{wi}\bar{c}_w + \bar{c}_f + (V_{pNNP}/V_{pR})(\bar{c}_w + \bar{c}_f)}{1 - S_{wi}}. \quad \text{(A-23)}$$

The water encroachment term calculated by superposition is expressed.

$$W_e = B\sum_j Q_D(\Delta t_j)_D\Delta p_j, \quad \text{(A-24)}$$

where $Q_D(t_D)$ is the dimensionless cumulative influx given as a function of dimensionless time t_D and aquifer to reservoir radius $r_D = r_{AQ}/r_R$. Value Δp_j is given by $p_j - p_{j-1}$ (in the limit for small time steps), and $\Delta t_j = t - t_{j-1}$. Assuming that permeability is reasonably high and the ratio r_{AQ}/r_R is not too large, Q_D for the smallest time step will approach the limiting value Q_D^*, and the summation can be closely approximated by

$$\sum_j Q_D(\Delta t_j)_D\Delta p_j \approx Q_D^*(p_i - p), \quad \text{(A-25)}$$

giving a simple expression for W_e that is independent of time and only dependent on reservoir pressure,

$$W_e = BQ_D^*(p_i - p): \quad W_e(\text{bbl}) \quad \text{(A-26)}$$

$$B = \frac{2\pi}{5.615}\phi r_R^2 h(\bar{c}_{tw} + \bar{c}_f),$$

$$Q_D^* = \frac{1}{2}\left[\left(\frac{r_{AQ}}{r_R}\right)^2 - 1\right]. \quad \text{(A-27)}$$

Expressing W_e in terms of aquifer PV V_{pAQ},

$$W_e = \pi(r_{AQ}^2 - r_R^2)\phi h(\bar{c}_{tw} + \bar{c}_f)(p_i - p);$$

and

$$W_e(\text{ft}^3) = V_{pAQ}(\bar{c}_{tw} + \bar{c}_f)(p_i - p). \quad \text{(A-28)}$$

The material-balance equation can then be written

$$\frac{p}{z}[1 - \bar{c}_e(p_i - p)] = \left(\frac{p}{z}\right)_i\left(1 - \frac{G_p}{G}\right) + \left(\frac{p}{z}\right)_i\frac{W_e}{GB_g}5.615 \quad \text{(A-29)}$$

and simplified in a form where the $\bar{c}_e$ term includes the aquifer contribution to pressure support,

$$\left(\frac{p}{z}\right)_i\frac{W_e}{GB_g} = \left(\frac{p}{z}\right)_i\frac{W_e}{G}\frac{T_{sc}}{P_{sc}T}\frac{p}{z} = \frac{p}{z}\frac{W_e}{GB_{gi}};$$

$$GB_{gi} = V_{pR}(1 - S_{wi}) = \frac{p}{z}\frac{V_{pAQ}(\bar{c}_{tw} + \bar{c}_f)(p_i - p)}{V_{pR}(1 - S_{wi})}. \quad \text{(A-30)}$$

Rearranging, we arrive at the general form of the material balance (without water production and gas/water injection terms):

$$\frac{p}{z}[1 - \bar{c}_e(p_i - p)] = \left(\frac{p}{z}\right)_i\left(1 - \frac{G_p}{G}\right), \quad \text{(A-31)}$$

where

$$\bar{c}_e = \frac{S_{wi}\bar{c}_w + \bar{c}_f + ((V_{pNNP}/V_{pR}) + (V_{pAQ}/V_{pR}))(\bar{c}_w + \bar{c}_f)}{1 - S_{wi}} \quad \text{(A-32)}$$

$$M \equiv \frac{V_{pNNP} + V_{pAQ}}{V_{pR}} = \frac{V_{pA}}{V_{pR}}, \quad \text{(A-33)}$$

and

$$\bar{c}_e = \frac{S_{wi}\bar{c}_{tw} + \bar{c}_f + M(\bar{c}_{tw} + \bar{c}_f)}{(1 - S_{wi})} \quad \text{(A-34)}$$

SI Metric Conversion Factors

°F	(°F−32)/1.8	= °C
in.³ × 1.638 706	E+01	= cm³
ft³ × 2.831 685	E−02	= m³
psi × 6.894 757	E+00	= kPa

SPEJ

Michael J. Fetkovich is a Phillips Fellow Emeritus in the Reservoir & Production Technology Branch, Research & Services Div. of Corporate Technology, Phillips Petroleum Co. in Bartlesville, Oklahoma. He holds a BS degree in petroleum and natural gas

engineering from the U. of Pittsburgh and a Dr.Ing. degree from the Norwegian Inst. of Technology. A Distinguished Member, Fetkovich received the 1993 Lester C. Uren Award and the 1989 Reservoir Engineering Award and served as Distinguished Lecturer during 1977–78. **David E. Reese** is a Senior Staff Associate Reservoir Engineer in Phillips' Reservoir & Production Technology Branch, Research & Services Div. of Corporate Technology, working in the areas of gas reservoir engineering, gas and gas-condensate simulation, and decline-curve analysis. He also teaches an industry short course on decline-curve analysis. Reese holds a BS degree in petroleum engineering and an MS degree in petroleum management, both from the U. of Kansas. A 1994–95 Distinguished Lecturer, he is currently serving on the Editorial Review Committee, Gas Reservoir Engineering Reprint Committee, and the Low Permeability Meeting Program Committee. He has served on the Gas Technology Symposium Program Committee, and Annual Meeting Technical committees. **Curtis H. Whitson** is Professor of petroleum engineering at the Norwegian U. of Science and Technology, Trondheim. He also consults, develops software, and teaches industry coursesthrough his own company, Pera A/S. Whitson holds a BS degree in petroleum engineering from Stanford U. and a Dr.techn. degree from Norwegian Inst. of Technology. Coauthor of the book *Well Performance* and of the SPE monograph *Phase Behavior*, he also served on the Editorial Review Committee and on the Reservoir Simulation Symposium Program Committee.

Fetkovich

Reese

Whitson

SPE
Society of Petroleum Engineers

SPE 17707

Using Short-Term Pressure Buildup Tests for Reserves Estimation in Tight Gas Reservoirs

by S.A. Sullivan, S.W. Poston, and L.D. Piper, Texas A&M U.

SPE Members

This paper was prepared for presentation at the SPE Gas Technology Symposium, held in Dallas, TX, June 13–15, 1988.

ABSTRACT

Average reservoir pressure must be known when material balance equations are used to determine gas in place. Most pressure data available for material balance analysis comes from single point tests (static bottom hole pressure tests). Unless the reservoir has been shut-in long enough for the pressure in the reservoir to stabilize there is no direct means of determining the average reservoir pressure.

A method has been developed to estimate gas in place in volumetric gas reservoirs using transient pressure data. The method is similar to the isochronal flow test. Pressure data recorded at a specific shut-in interval is collected during a portion of the producing life of the reservoir. A p/z plot is constructed using this pressure data and the corresponding production data. The p/z curve will plot as a straight line with a slope similar to the stabilized p/z curve. However, this nonstabilized p/z curve will be shifted slightly downward from the stabilized p/z curve. Gas in place can be estimated by drawing a line parallel to the nonstabilized p/z curve through a point on the stabilized p/z curve, such as p_i/z_i. This new line is extrapolated to the point of intersection on the (G_p) x-axis.

This analysis procedure was tested with production data simulated for a single well reservoir model with and without wellbore storage distortion. The procedure was also tested with production data simulated for a hydraulically fractured well model. The results indicate this method can be used to estimate gas in place within a margin of error acceptable for most engineering purposes.

INTRODUCTION

The material balance method can be used to estimate gas in place when pressure-production data for two or more history points are available. The accuracy of this method depends on the accuracy of the pressure-production data and selection of the proper material balance equation.

Regardless of the form of the material balance equation, average reservoir pressure must be known for proper determination of gas in place. Average reservoir pressure is obtained by shutting in the reservoir until pressure stabilizes. In low permeability reservoirs, shutting in the reservoir long enough for pressure to stabilize may not be practical.

Average reservoir pressure can be estimated using transient pressure data if the pressure buildup trend has been recorded beyond wellbore storage. However, when only a single pressure reading is taken there is no direct means of determining average reservoir pressure unless the pressure is stabilized in the reservoir.

The purpose of the following study was to develop a method to estimate gas in place using transient, single point pressure data. The proposed method is based on the same principle as the isochronal flow test.

DISCUSSION

The material balance equation for a gas reservoir where there is no water influx and rock and water expansion are negligible is as follows:

$$\frac{p}{z} = -\frac{p_i G_p}{z_i G} + \frac{p_i}{z_i} \quad \ldots\ldots\ldots\ldots\ldots\ldots \quad (1)$$

References and illustrations at the end of paper.

Equation 1 has the form of an equation of a straight line,

$$y = mx + b \quad \ldots\ldots\ldots\ldots\ldots\ldots\ldots \quad (2)$$

where x is equal to G_p and y is equal to p/z.[1] A plot of p/z versus G_p on cartesion coordinates will yield a straight line with slope, $-p_i/z_iG$, and intercept, p_i/z_i. Extrapolation of the line to the point, p/z = 0, results in an estimate of G, the original gas in place.

The data required to solve the material balance equation are normally acquired during the producing life of the reservoir. As previously mentioned, low permeability reservoirs may require long shut-in times to obtain average reservoir pressure.

There are methods available to determine average reservoir pressure using transient pressure data, if the buildup trend has been recorded.[2,3,4,5,6] However, buildup tests are usually run only after a well has been completed or stimulated. These buildup tests are run to determine the reservoir properties surrounding the well.

Most pressure data comes from single point, bottom hole pressure tests. This type of buildup test is required on an annual basis in most states. The required shut-in time is usually between 24 and 72 hours. This test is sometimes referred to as a static pressure test. Unfortunately, the name implies a static pressure reading has been recorded, this is not always true. The shut-in time required for low permeability reservoirs to reach static reservoir conditions may be longer than 72 hours. If this "static pressure" reading is actually still in a transient state the results of a material balance analysis will provide an erroneous estimate of gas in place.

Isochronal Flow Tests

The isochronal flow test was found to be very useful for obtaining the stabilized deliverability curve with transient pressure data for wells in low permeability reservoirs. Cullender[7] showed a series of flow tests run at different flow rates for the same length of time would yield performance curves having equal slopes. The position of these curves will shift towards the stabilized position as the flow time increases. Figure 1 shows a typical example of this shift. The stabilized deliverability curve can be established by drawing a line with slope equal to the slope of the nonstabilized, fixed-time line through a stabilized point.

The principle behind the isochronal flow test is the radius of investigation depends on dimensionless time and not on flowrate.

Isochronal Buildup Tests

Separate buildup tests conducted for the same length of time will reach the same radius of investigation regardless of the flowrate prior to shut-in. Static conditions will not be attained until the radius of investigation has reached the boundaries of the reservoir or the point of interference with offset wells. However, the shut-in pressure within the radius of investigation will be built up to the same pressure level.

Gas in place in a pressure depleting gas reservoir can be estimated using an analysis procedure analogous to the procedure described above for the ischronal flow test. The proposed analysis procedure uses the same data normally required for material balance analysis for pressure depleting gas reservoirs, except transient shut-in pressures are used instead of average reservoir pressures.

Pressure readings taken during the producing life of the reservoir are recorded at the same shut-in time. The data is plotted on cartesian coordinates as previously described. The slope of this nonstabilized p/z curve is similar to the slope of the stabilized p/z curve. A line parallel to the nonstabilized p/z curve is drawn through the point p_i/z_i. This line is extrapolated to the point, p/z = 0, to determine gas in place (see Fig. 2).

Simulation of an Ideal Reservoir Case

A commericial simulator was used to simulate production data for a single-phase, single-well, radial gas reservoir. The Adaptive Implicit Method (AIM) employed by the simulator permits the simulator to adopt the degree of implicitness required to quarantee stability. Grid spacing and time steps were also chosen to insure stability and accuracy. The data was within 1 percent of the Van Everdingen and Hurst solution.

The reservoir properties for this model are listed in Table 1. Three different cases were run.

The data was generated so that initially gas was withdrawn from the reservoir at a constant rate until the reservoir pressure could no longer sustain that rate. The withdrawal rate was then declined in a stepwise manner.

Periodically, shut-in pressure data was collected at specified time intervals of 0.005 (7.2 minutes), 0.05 (1.2 hours), 0.5 (12.0 hours), 1, 2, 5, and 15 days and at static reservoir conditions. The new analysis procedure was used to estimate gas in place with the pressure-production data collected at each time interval. These estimates were compared with the gas in place estimate at static reservoir conditions.

RESULTS

Pressure-production data was generated for the reservoir models described as Cases 1, (3 md) 2 (0.3 md) and 3 (0.03 md). This data is presented in Figures 3, 4 and 5. The shift of the p/z curve towards the stabilized position as the shut-in time increases can be seen in these figures. In each case the slope of the nonstabilized, fixed-time p/z curve is similar to the slope of the stabilized p/z curve with a few exceptions. These exceptions will be discussed later.

Gas in place was estimated with the data collected at each time interval with the new analysis procedure. These estimates were compared to the estimate of gas in place determined at

static conditions. In Case 1 (3.0 md), all the estimates of gas in place were within 3 percent of the estimate at static conditions. In Case 2 (0.3 md), all the estimates of gas in place were within 6 percent of the estimate at static conditions, except those made with the pressure readings taken at shut-in times of 0.005 and 0.05 days. In Case 3 (0.03 md), all the estimates were within 6 percent of the estimate at static conditions except those made with pressure readings taken at shut-in times of 0.005, 0.05 and 0.5 days.

Pressure data distorted by wellbore storage, (C_D = 100), was generated for the reservoir modeled in Case 2 (0.3 md). This data is presented in Figure 6. Estimates of gas in place made with this data were within 7 percent of the estimate at static conditions except when the shut-in time was 0.005, 0.05 and 0.5 days.

Horner pressure buildup plots for the well were constructed for each of the cases. In each case, significant error in the gas in place estimate occurred when the pressure readings were taken during the early time region of the transient pressure curve. There are two major reasons for this error.

1. The pressure buildup profile for a constant rate case differs from the pressure buildup profile for a constant pressure case. The difference is most significant when the pressure transient has not reached the middle time region.[8] The well in Case 2 was produced at a constant rate during it's early life and later was produced at a constant pressure. The inflection in the p/z curve at the early time intervals caused by changing from constant rate to constant pressure can be seen in Figure 4.

2. Data used for the material balance analysis was recorded before wellbore storage and skin effects had dissipated. The middle time region for the Case 2 (0.3 md) study does not begin until after 1.0 day. Three of the shut-in times used to estimate gas in place, 0.005, 0.05 and 0.5 days, fall in the early time region. In Figure 6, the slopes of the p/z curves constructed at these time intervals are significantly different from the slope of the stabilized p/z curve.

Constant Dimensionless Time

The basic principle supporting the proposed method is the radius of investigation depends on dimensionless time and not on the flowrate prior to shut-in. Dimensionless time is defined as,

$$t_D = \frac{0.0002637kt}{\phi\mu c_t r_w^2} \quad \ldots\ldots\ldots\ldots\ldots\ldots \quad (3)$$

Dimensionless time will vary only with time when the permeability, the porosity, the viscosity, and the total compressiblilty are constant. However, viscosity and compressibility are not constant in gas reservoirs. The value of viscosity and compressibility will vary with pressure as the reservoir is depleted. Therefore, if time is held constant, dimensionless time will vary.

Viscosity and compressibility can be calculated when average reservoir pressure is known. However, this is not normally the case. Case 2 (0.3 md) was used to determine the effects of the variable dimensionless time on the accuracy of the method.

Viscosity and compressibility were calculated at known values of average reservoir pressure. The value of real shut-in time needed for the dimensionless time to be constant during the producing life of the reservoir was calculated for dimensionless times ranging from 5,518 to 827,631 (see Table 2). The times listed in Table 2 were substituted for the shut-in times, 0.1, 0.5, 1.0, 2.0, 5.0 and 15.0 days previously used in Case 2 The case was rerun using the real time intervals listed in Table 2 . The pressure-production data is presented in Figure 7. The improvement in the gas in place estimate was less than one percent at each time interval.

Hydraulically Fractured Reservoir Model

A commercial simulator specifically built to analyze vertically fractured gas wells was used to simulate production data for a vertically fractured single well gas reservoir. The accuracy of the simulator has been verified against numerous analytical solutions of fractured well performance. The grid and time spacings recommended in the users guide were used to insure stability and accuracy.

The reservoir and fracture properties for the model are listed in Table 3. Two different cases were run.

Shut-in pressures were recorded at 0.5, 1.0, 2.0, 3.0, 5.0, 10.0 and 15.0 days and at static conditions. The p/z curves at each of these shut-in times are presented in Figs. 8 and 9 for Cases 5 and 6, respectively. In Case 5 when the relative fracture conductivity was 0.1 the estimates of gas in place were within 10 percent of the estimate of gas in place at static conditions. In Case 6 when the relative fracture conductivity was 10.0 the estimates of gas in place had over 20 percent error.

There are four possible flow regimes for hydraulically fractured wells, fracture linear flow, bilinear flow, formation linear flow and pseudo-radial flow. In a flow test, the flow is considered to be pseudo-radial around a fractured well when the drainage pattern has completed a transformation from rectangular (linear flow) through elliptical (transitional flow) to almost radial. In a pressure buildup test, the physical interpretation is that the pressure has built up to essentially a uniform level first in a narrow rectangle (linear regime) then an ellipse (transitional regime) and finally a near-circle. Pseudo-radial flow occurs with fractures of all conductivities, but the higher the conductivity, the later the drainage pattern can be characterized as essentially radial.[9]

In Case 5 (relative fracture conductivity 0.1) the pressure readings taken at 0.5, 1.0, 2.0, 3.0, 5.0, 10.0 and 15.0 days were taken during the pseudo-radial flow period. In Case 6 (relative fracture conductivity 10.0) the pressure readings taken at these same time intervals were not in the pseudo-radial flow period.

CONCLUSIONS

1. Gas in place can be estimated using transient pressure data if the pressure data is recorded at the same shut-in time for each buildup test.
2. Gas in place can be estimated within a margin of error acceptable for engineering purposes if the pressure data is collected after wellbore storage effects have dissapated.
3. Some buildup tests should be run in order to determine when the end of wellbore storage occurs.
4. Although the isochronal principle states that radius of investigation depends on dimensionless time, constant real time can be used with little additional error in the estimate for low to moderate pressure gas reservoirs.
5. Gas in place can be estimated for hydraulically fractured wells within amargin of error acceptable for engineering purposes if the pressure data is collected after pseudo-radial flow begins.

NOMENCLATURE

b = intercept of straight line equation

c_t = total compressibility, psi^{-1}

G = original gas in place, bscf

G_p = cumulative gas produced, bscf

k = reservoir rock permeability, md

m = slope of straight line equation

p = reservoir pressure, psia

p_i = initial reservoir pressure, psia

r_w = wellbore radius, ft

t = elapsed time, hours

t_D = dimensionless time, $0.000264\ kt/\phi\mu c_t r_w^2$

x = independent variable of straight line equation

y = dependent variable of straight line equation

z = gas compressibility factor

z_i = gas compressibility factor at initial pressure

μ = viscosity, cp

ϕ = porosity, dimensionless

REFERENCES

1. Havlena, D. and Odeh, A. S.: "The Material Balance as an Equation of a Straight Line," J. Pet. Tech. (Aug. 1963) 896-900.
2. Matthews, C. S., Brons, F. and Hazebroek, P.: "A Method for Determination of Average Pressure in a Bounded Reservoir," Trans., AIME (1954) **201**, 182-191.
3. Brons, F. and Miller, W. C.: "A Simple Method for Correcting Spot Pressure Readings," J. Pet. Tech. (Aug. 1961) 803-805.
4. Dietz, D. N.: "Determination of Average Reservoir Pressure from Build-Up Surveys," J. Pet. Tech. (Aug. 1965) 955-959.
5. Odeh, A. S. and Al-Hussainy, R.: "A Method for Determining the Static Pressure of a Well from Buildup Data," J. Pet. Tech. (May 1971) 621-624.
6. Kazemi, H.: "Determining Average Reservoir Pressure from Pressure Buildup Tests," Soc. Pet. Eng. J. (Feb. 1974) 55-62.
7. Cullender, M. H.: "The Isochronal Performance Method of Determining the Flow Characteristics of Gas Wells," Trans., AIME (1955) **204**, 137-142.
8. Uraiet, A. A. and Raghavan, R.: "Pressure Build-up Analysis for a Well Produced at Constant Bottom-Hole Pressure," J. Pet. Tech. (Oct. 1980) 1813-1824.
9. Cinco-Ley, H., Samaniego-V., F. and Dominiquez, N.: "Transient Pressure Behavior for a Well with a Finite Conductivity Vertical Fracture," Soc. Pet. Eng. J. (Aug. 1978) 253-264.

TABLE 1

DESCRIPTION AND PROPERTIES OF AN IDEAL RESERVOIR MODEL

Description:	One well located in the center of a circular reservoir.
Area:	45 acres
Reservoir Thickness:	80 feet
Depth of Midperf:	6250 feet
Reservoir Temperature:	176 °F
Initial Pressure:	2500 psi
Specific Gravity of the Gas:	0.700
Porosity:	0.100
Water Saturation:	0.250
Original Gas in Place:	1.94 bcf
Case 1	
Average Permeability:	3.0 md
Initial Flowrate:	1000 mcf/d
Case 2	
Average Permeability:	0.3 md
Initial Flowrate:	500 mcf/d
Case 3	
Average Permeability:	0.03 md
Inital Flowrate:	500 mcf/d

TABLE 2

VARIATION OF REAL SHUT-IN TIME TO MAINTAIN CONSTANT DIMENSIONLESS TIME (t_D)

t_D / $\bar{p}$	5518	27588	55175	110351	275877	827631
2500	0.100	0.500	1.000	2.000	5.000	15.00
2245	0.110	0.547	1.095	2.190	5.474	16.42
2020	0.120	0.600	1.120	2.399	5.996	17.99
1797	0.132	0.659	1.318	2.635	6.589	19.77
1575	0.193	0.967	1.934	3.869	9.672	29.02
1388	0.213	1.067	2.134	4.267	10.67	32.00
1210	0.236	1.182	2.364	4.728	11.82	35.46

TABLE 3

DESCRIPTION AND PROPERTIES OF A HYDRAULICALLY FRACTURED RESERVOIR MODEL

Description:	One well located at the center of a square reservoir.
Area:	640 acres
Reservoir Thickness:	50 feet
Depth of Midperf:	10075 feet
Reservoir Temperature:	275 °F
Inital Pressure:	6000 psia
Specific Gravity of the Gas:	0.700
Porosity:	0.060
Original Gas in Place:	22.09 bcf
Reservoir Permeability:	0.1 md
Fracture Half Length:	125 feet
Case 5	
Relative Fracture Conductivity:	0.1
Initial Flowrate:	500 mcf/d
Case 6	
Relative Fracture Conductivity:	10.0
Initial Flowrate:	2000 mcf/d

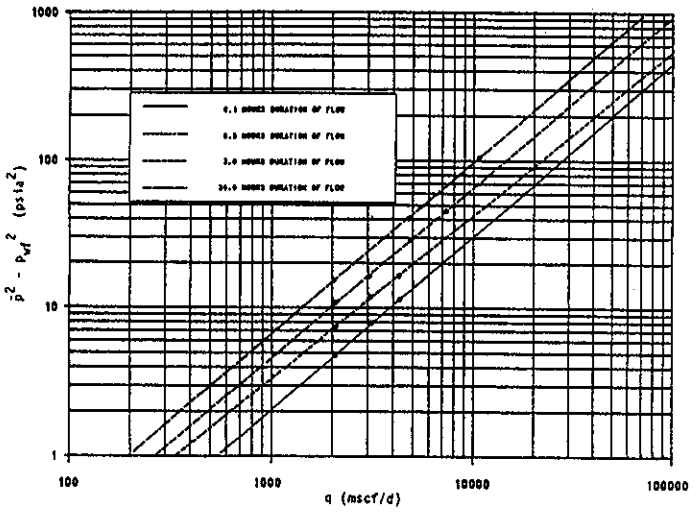

Fig. 1—Isochronal deliverability test for a gas well.

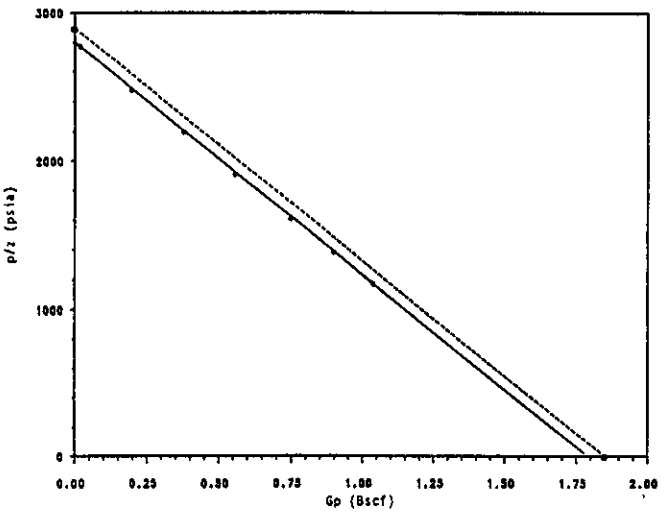

Fig. 2—Illustration of analysis procedure.

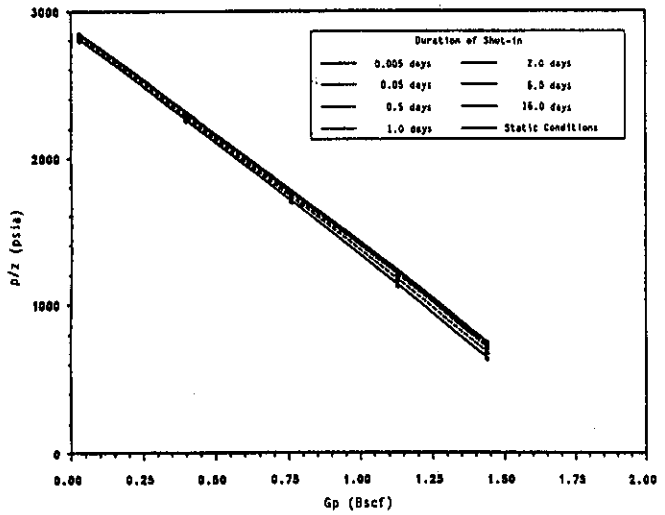

Fig. 3—Isochronal p/z curves for Case 1.

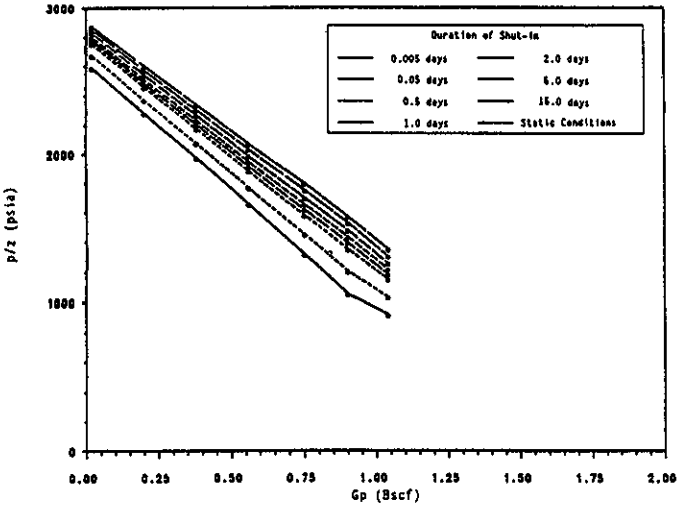

Fig. 4—Isochronal p/z curves for Case 2.

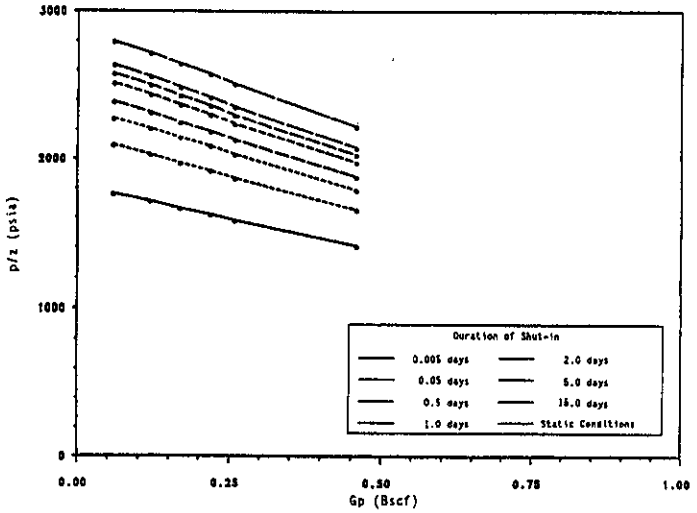

Fig. 5—Isochronal p/z curves for Case 3.

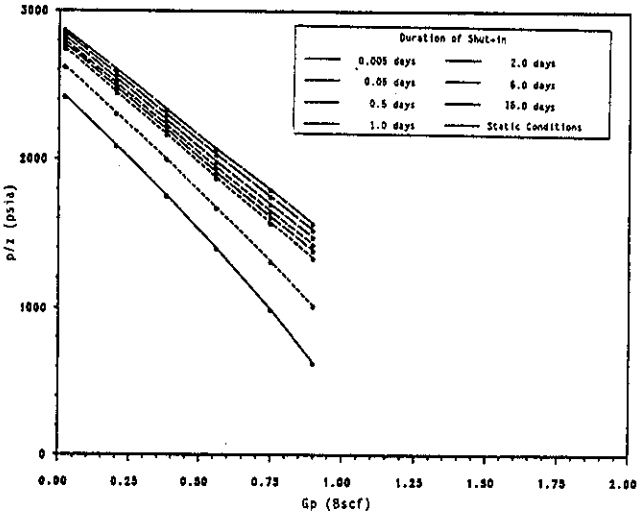

Fig. 6—Isochronal p/z curves for Case 2 with wellbore storage.

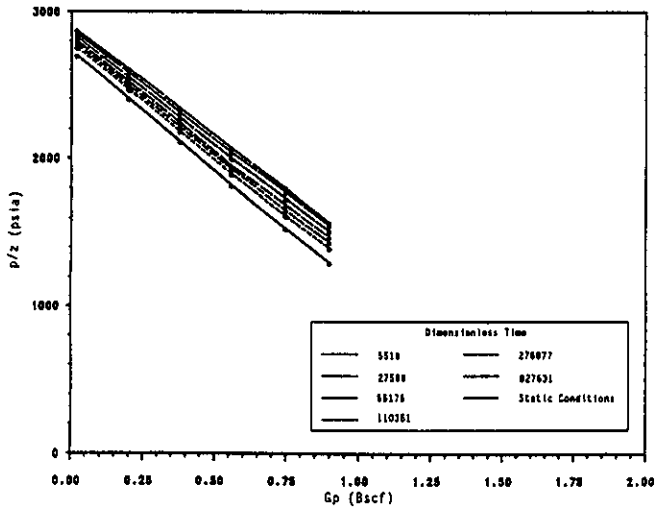

Fig. 7—Isochronal p/z curves for Case 2 for consuant t_D.

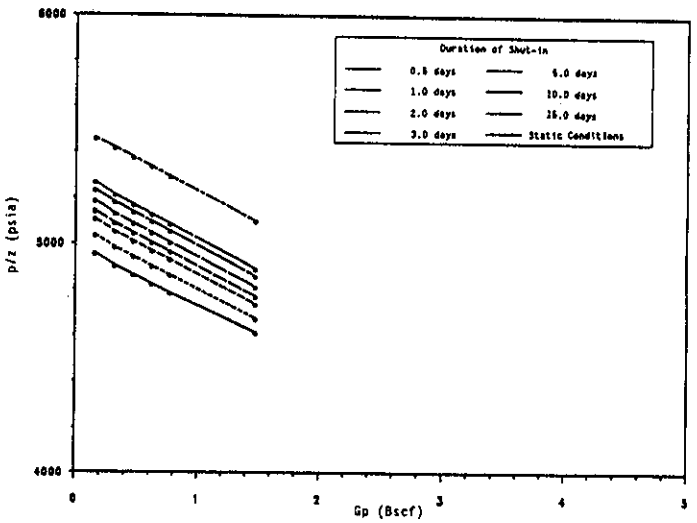

Fig. 8—Isochronal p/z curves for Case 5—hydraulically fractured well $C_r = 0.1$.

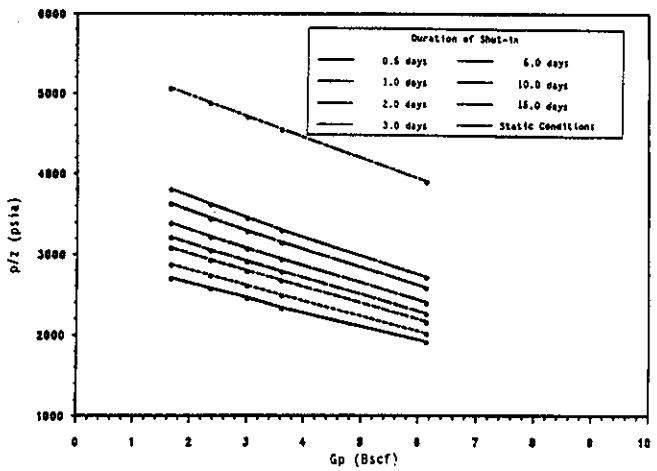

Fig. 9—Isochronal p/z curves for Case 6—hydraulically fractured well $C_r = 10.0$.

SPE 26647

Application of Variable Formation Compressibility for Improved Reservoir Analysis

D.P. Yale, G.W. Nabor,* and J.A. Russell, Mobil R&D Corp., and H.D. Pham** and Mohamed Yousef,† Mobil E&P U.S. Inc.

SPE Members
*Now retired
**Now with Abu Dhabi Natl. Oil Co.
†Now with Saudi Aramco

This paper was prepared for presentation at the 68th Annual Technical Conference and Exhibition of the Society of Petroleum Engineers held in Houston, Texas, 3-6 October 1993.

ABSTRACT

Formation compressibility has long been recognized as an important factor influencing production behavior from overpressured oil and gas reservoirs. However, formation compressibility data are not routinely collected and the use of formation compressibility in reservoir analysis and simulation is often oversimplified.

This paper discusses more accurate methods to determine formation compressibility and introduces a new method for analyzing overpressured oil and gas reservoirs which utilizes the variability of formation compressibility with declining reservoir pressure. The newly developed method departs from earlier proposed methods in the use of variable rather than fixed formation compressibility by employing a "pore volume formation volume factor", B_f, that properly integrates pore volume compressibility effects over the full pressure range of investigation. Using the new concept of B_f, the material balance equation (MBE) can be modified to include the effects of pressure dependent formation compressibility.

We find that the formation compressibility in highly overpressured unconsolidated reservoirs can be the same order of magnitude as gas compressibility and significantly higher than oil compressibility. In some types of reservoirs, an order of magnitude change in formation compressibility can occur during drawdown. We show that in many overpressured and/or unconsolidated reservoirs, proper integration of accurate formation compressibilities is important for reserve estimates, determination of drive energies, and overall reservoir development plans. For example, we find that the use of compressibility values in the MBE which are significantly lower than those which exist in the reservoir could suggest a strong water drive where one does not exist.

1. INTRODUCTION

It is recognized that a decrease in pore volume accompanies a decline in reservoir pressure. The relative change in pore volume per unit of pressure change, i.e., the formation compressibility, depends on the rock type, its degree of competence, and the tectonic setting. Laboratory measurements show a wide range of compressibility levels over the spectrum of rocks from competent carbonates to unconsolidated sands. Compressibility declines, sometimes drastically, as laboratory stress is increased to correspond to reservoir pressure changes from discovery to abandonment.

Formation compressibility is a source of drive energy in addition to that provided by expansion of fluids. Its effect, and also that of water, are often ignored in analyzing reservoir performance since the contribution is minor compared with that of gas or oil plus solution gas. The effects are usually considered, however, when undersaturated oil reservoir performance is analyzed and the contributions of rock and water expansion can easily exceed 10 percent of the total.

The conditions found in abnormally pressured reservoirs also lead to greater significance of formation compressibility as a source of expansion energy, particularly if the formation is poorly consolidated. Abnormal pressure at discovery means a lower effective reservoir stress condition, and a higher formation compressibility. Since pressure level is often high, gas compressibility $[(1/p)-(1/z)(dz/dp)]$ is relatively low, and formation compressibility may in fact be of the same order of magnitude; it will often exceed oil compressibility. Formation compressibility contributions may be further magnified if an aquifer--even a small one--is present since all of the water-bearing rock present will provide formation compressibility drive energy.

References and illustrations at end of paper.

Where reservoir conditions are such that compressibility is expected to be relatively high, and variable with stress level, laboratory measurements are definitely indicated. Use of the data in reservoir analysis is not routine, and approximations are often used. In this paper, we address both the laboratory measurements and also a method for accurately incorporating that data in reservoir performance analysis. The result is one which is quite general and which can be incorporated in existing material balance or reservoir simulation formulations with only minor modifications. Further, methods previously proposed by other investigators prove in fact to be special cases of the general approach developed here.

2. FORMATION COMPRESSIBILITY

Pore compressibility is a laboratory measured rock property which is defined as the relative change in pore volume of a rock sample divided by the change in laboratory stress which caused the change in pore volume:

$$C_p = \frac{\Delta V_p / V_p}{\Delta \sigma_{lab}} \quad \ldots\ldots\ldots\ldots\ldots \quad 1$$

Formation compressibility, however, is defined in most reservoir engineering handbooks as the relative change in pore volume divided by the change in reservoir pressure that caused the change in pore volume:

$$C_f = \frac{\Delta V_p / V_p}{\Delta p} \quad \ldots\ldots\ldots\ldots\ldots \quad 2$$

The difference between pore compressibility and formation compressibility therefore is related to the difference between reservoir pressure and laboratory stress. There are four main stresses which act on any volume of reservoir rock. The overburden stress, σ_z, the horizontal stresses, σ_x, σ_y, and the pore pressure or reservoir pressure, p, which presses out against the overburden and horizontal reservoir stresses. In the laboratory, however, most overburden tests are run using a hydrostatic confining pressure and ambient pore pressure. The reservoir stress state and changes in that stress state must be converted to effective hydrostatic laboratory stress to understand the laboratory data. The following equation has been proposed and derived by many (Geertsma, 1957; Jaeger and Cook, 1976; Teeuw, 1971; Nur and Byerlee, 1971):

$$\sigma_{lab} = K_1 \sigma_z - K_2 p_i + K_3 (p_i - p) \quad \ldots\ldots \quad 3$$

where K_1, K_2, and K_3 are constants dependent on rock type and p_i and p are the reservoir pressure at discovery and at the present time respectively. σ_{lab} is the hydrostatic confining pressure applied to the core sample (minus any pore pressure) to simulate the in-situ stress conditions. Equation 3 is sometimes referred to as the "effective stress" equation. Table 1 gives K_1, K_2, K_3 for various rock types. K_1 and K_2 relate how the three confining stresses in the reservoir and the reservoir pressure interact. K_1 can be defined as:

$$K_1 = (\sigma_x + \sigma_y + \sigma_z) / (3\sigma_z) \quad \ldots\ldots\ldots \quad 3a$$

σ_z can be estimated using an overburden gradient of 1 psi per foot of depth or from integrating a density log. K_2 is equivalent to the Biot "alpha" parameter and is defined by Geertsma (1957) and Nur and Byerlee (1971) as:

$$K_2 = (1 - C_b / C_{gr}) \quad \ldots\ldots\ldots\ldots \quad 3b$$

K_3 relates how the drawdown of the reservoir pressure increases the stress on the formation. It can be defined as:

$$K_3 = K_2 [(1 + v)/(3 - 3v)] \quad \ldots\ldots\ldots \quad 3c$$

Equation 3c is identical to the "uniaxial correction factor" derived by Teeuw (1971) with the exception that he assumes K_2 to be unity.

From Equation 3, we can see that hydrostatic pore compressibility tests, therefore, can be corrected to formation compressibility through the following equation:

$$C_f = K_3 C_p \quad \ldots\ldots\ldots\ldots\ldots\ldots \quad 4$$

TABLE 1

CONSTANTS FOR EFFECTIVE STRESS EQUATION

Rock Type	K_1	K_2	K_3
Consolidated Sandstones*	0.85	0.80	0.45
Friable Sandstones	0.90	0.90	0.60
Unconsolidated Sands	0.95	0.95	0.75
Carbonates*	0.85	0.85	0.55

*These K_2 constants for are valid for many consolidated sandstones and carbonates. For well cemented formations with porosities lower than 15%, the K_2 factor can be between 0.4 and 0.8 due to the formation's low bulk compressibility (see Equation 3b).

2.1 Uniaxial Compaction

As fluids are withdrawn from the reservoir, it is assumed to compact only in the vertical direction (uniaxial compaction) because the vertical extent of the reservoir is so small compared to its lateral extent (Geertsma, 1957; Teeuw, 1971; de Waal, 1986). This leads to a decrease in the horizontal stresses and therefore to a decrease in the average confining stress. This has the effect of

lessening the increase in effective stress as the fluid pressure in the reservoir is decreased. The K_3 constant in equation 4 accounts for the changes in horizontal stresses (see Equation 3c). The variation in Poisson's ratio, v, between consolidated and unconsolidated clastic sediments leads to a variation in K_3 of 0.45 for consolidated sandstones to 0.75 for completely unconsolidated sediments. Therefore, for a consolidated sand, a drawdown of 2000 psi is simulated in the laboratory by an increase in effective stress of only 900 psi.

This uniaxial compaction of the reservoir during drawdown has led some to suggest that the compressibility should be measured uniaxially, mimicking the "no lateral deformation" boundary condition and allowing the sample to deform only in the vertical direction (Lachance and Andersen, 1987; Andersen, 1985; de Waal, 1986). Theoretically, however, (Geertsma, 1957; Jaeger and Cook, 1976) the volumetric change in pore volume is due only to the change in the average volumetric stresses on the sample, therefore properly corrected hydrostatic tests should be equivalent to uniaxial tests.

We argue that the difficulties in maintaining the "no lateral deformation" boundary condition along the entire length of a sample during a triaxial test as well as the cost and difficulty of the tests make uniaxial tests unfavorable. Published data on uniaxial compaction (Lachance and Andersen, 1983; Andersen, 1985) show data which are both significantly less and significantly more than as predicted by theoretically corrected hydrostatic compressibility tests. We suggest, therefore, that formation compressibility be calculated by performing hydrostatic pore compressibility tests and correcting to formation compressibility using Equation 4.

2.2 Laboratory Methods for Pore Compressibility

Laboratory pore compressibility measurements are done by determining the pore volume of a core sample as a function of effective laboratory stress. The pore volume is usually determined either by measuring the total fluid squeezed out of a liquid saturated sample and subtracting it from the pore volume at ambient conditions or by measuring the pore volume directly of a dried sample at each pressure level using the Boyle's law gas expansion technique.

Since pore compressibility is related to the derivative of the pore volume versus stress curve, the accuracy of compressibility data is dependent on the ability of the apparatus to measure very small changes in pore volume. For this reason, liquid squeeze out on samples with more than 10cc pore volume gives better compressibility results than Boyle's law measurements or tests on small samples.

We have found that on samples from friable or unconsolidated formations, sample integrity as well as sample volume is a concern. Pore compressibility is very sensitive to the degree of damage or disturbance of the sample in weak sediments. As shown in Figure 1, full diameter samples from the same unconsolidated formation as a set of plug samples have significantly lower compressibilities. We suggest that core damage during plugging and cleaning disturbed the samples enough to cause this difference. The authors have found that ambient pressure porosities of the plug samples were 2 to 8 porosity units higher than the full diameter core samples.

To maintain sample integrity to insure valid pore compressibility measurements, the authors recommend that unconsolidated core samples be frozen on well site to prevent sample disturbance and desiccation during shipping; that full diameter samples be used to prevent disturbance from plugging and to maximize accuracy; and that the frozen samples be placed in the pressure vessel before cleaning and allowed to thaw under some minimum stress (100 to 300 psi, generally). Brine squeeze-out pore volume testing can be done before any cleaning provided care is taken to fully liquid saturate the sample and that ambient pore volume is measured after the test is complete.

We have also found that the creep associated with the deformation of unconsolidated rocks can cause compressibility tests run at high rates of pressure increase to be invalid. One of the authors and others (de Waal, 1985) have observed creep in unconsolidated core samples to be logarithmic with time. The magnitude of the creep being the most significant in poorly sorted, clay rich unconsolidated core samples. It is unfeasible to run tests at reservoir drawdown rates of 100 psi per month but standard laboratory rates of 1000 to 2000 psi per hour do not allow the creep to occur. We suggest that compressibility tests on core samples run at rates between 50 and 5 psi per hour for unconsolidated samples and 500 to 50 psi per hour for weakly consolidated formations allow a significant portion of the creep to occur thus improving the accuracy of the compressibility data.

2.3 Variability of Formation Compressibility

One of the reasons why formation compressibility has been left out or underestimated in reservoir analysis is that it has been assumed that pore compressibility is fairly constant with stress and of the same order of magnitude as the compressibility of water. Even Hammerlindl (1972) who recognized the importance of compressibility in reservoir analysis, used a constant high formation compressibility value. Figures 3 through 5 show the variability of pore compressibility with pressure and rock type. The figures represent compilations of data for consolidated, friable, and unconsolidated clastic sediments.

Definitions of the degree of consolidation are vague. For the purpose of our compilations the following general guidelines apply. Consolidated sandstones have undergone significant diagenesis and have their grains well cemented and dropping a core sample on the floor does not cause it to disintegrate. In the consolidated

sandstones tested, porosity ranged from less than 1% to 25% with a mean porosity of 15%.

We define "friable" samples as having little or no cement between the grains but holding together even after cleaning and drying. Friable cores, however, will generally break or disintegrate if dropped onto the floor. Porosity of the samples tested ranged between 20% and 33%, with the mean porosity for our data set at 23.1%. We have found that the compressibility of very clean, well sorted unconsolidated sands generally fall into this "friable" category even if they have no cement.

We define "unconsolidated" samples as those which fall apart completely after drying and/or cleaning with porosities between 27% and 40%. They generally have no cement between the grains and are poorly sorted and/or have large clay fractions. Our data set of unconsolidated samples was populated primarily with turbidite-type Gulf Coast sands with a mean porosity of 32.5%.

Figure 2a and 2b show the differences in grain size distributions between a clean, well sorted sand (whose compressibility falls into our "friable" category) and a clay rich, poorly sorted sand (which falls into our "unconsolidated" category). Both sands are unconsolidated from the point of view of having no cement between their grains, but they have widely different formation compressibilities. We have found this strong correlation between degree of sorting and compressibility in a number of unconsolidated formations.

Figure 3 shows formation compressibility versus pressure on a log-log plot for a collection of 121 consolidated sandstones from over 45 formations from around the world reported in the published literature (Chierici et. al. 1967, Dobrynin 1963, Fatt 1958a, 1958b, Wyble 1958, Yale 1984) and measured by the authors. Note the general downward trend versus pressure with an order of magnitude change in compressibility over the pressure range. Note the order of magnitude variation of compressibility within rocks which are all considered "consolidated sandstones".

Figures 4 and 5 show the formation compressibility of friable to unconsolidated rocks which make up a surprisingly large number of reservoirs. These ranges of formation compressibilities are large enough to figure prominently into the total compressibility equation for both oil and gas reservoirs, especially those which are overpressured. The data in Figure 4 are from 140 core samples from 7 reservoirs in the North Sea, Africa, and the U.S. Gulf Coast which we consider "friable". The data in Figure 5 are from 14 full diameter core samples from 4 reservoirs in the Gulf of Mexico and Africa which are unconsolidated and poorly sorted. Note from Figures 4 and 5 that nearly all the samples have compressibilities greater than that of water at stresses up to 10000 psi. Comparing all three figures, we see over 2 orders of magnitude variation in compressibility at any given pressure depending on rock type. Also note that the slopes of the three data sets are different.

These three figures show the importance of including variable formation compressibility in reservoir analysis. Gas compressibility at 8000 to 15000 psi can be in the range of 200 to 20 microsips. In overpressured reservoirs, where the "effective stress" (see Equation 3) can be 3000 to 1000 psi, formation compressibility can be 1 to 50 microsips.

We find that it is the change in gas and formation compressibility with pressure which causes the familiar change in slope of the p/z versus cumulative production plots in overpressured reservoirs. As reservoir pressure decreases, gas compressibility increases and formation compressibility decreases. The change in slope of p/z versus production plots for overpressured reservoirs can be due to a change from a formation compressibility influenced system to a gas compressibility dominated system.

2.4 Type Curves for Formation Compressibility

Pore compressibility measurements are not performed routinely for all reservoirs and data are especially sparse for those formations where it is most important (i.e. friable and unconsolidated formations). Figure 6 and Table 2 give "Type Curves" which can be used to estimate formation compressibility in clastic formations if core data are not available. The three type curves (and the equations given in Table 2) are least square fits through the data compiled in Figures 3, 4, and 5.

TABLE 2

TYPE CURVES-FORMATION COMPRESSIBILITY CLASTIC RESERVOIRS

$$C_f = A(\sigma - B)^C + D$$

The type curves in Figure 6 are defined by the above equation where:

$\sigma = K_1 *$ (overburden stress) $- K_2 * p_i + K_3 * (p_i - p)$ (psi)
and
A, B, C, D are constants depending on rock type as described below.

	Unconsolidated (poorly sorted)	Friable (& well sorted unconsol.)	Consolidated
A	-2.805×10^{-5}	1.054×10^{-4}	-2.399×10^{-5}
B	300	500	300
C	0.1395	-0.2250	0.06230
D	1.183×10^{-4}	-1.103×10^{-5}	4.308×10^{-5}

We caution against the use of type curves unless core data is not available. Many times in unconsolidated or friable reservoirs, very little if any core is available so that estimates from type curves are necessary. We remind

the reader that the "unconsolidated" and "friable" data sets do not cover a wide variety of reservoirs and there will be formations which can be considered "unconsolidated" or "friable" which have compressibilities significantly different from those presented in the type curves. We do believe, however, that the quality of the data in the formations tested is very good due to the measurement procedures followed.

3. THE PORE VOLUME FVF - A NEW CONCEPT

In order to easily incorporate variable formation compressibility into reservoir analysis we define a "pore volume FVF" (formation volume factor) as:

$$B_f = V_p / V_{psc} \quad \ldots\ldots\ldots\ldots\ldots \quad 5$$

It is convenient, though not strictly necessary, to choose one atmosphere and reservoir temperature as the standard or reference condition, where $B_f = 1.0$. The pore volume FVF is easily related to formation compressibility. In differential form the formation compressibility equation (Equation 2) can be written as:

$$C_f\, dp = dV_p / V_p = d\,(\ln V_p) \quad \ldots\ldots\ldots \quad 6$$

which can be integrated between limits p_{sc} and p to give

$$\ln (V_p / V_{psc}) = \int_{p_{sc}}^{p} C_f\, dp = I(p) \quad \ldots\ldots \quad 7$$

or equivalently

$$B_f = e^{I(p)} \quad \ldots\ldots\ldots\ldots\ldots \quad 8$$

The laboratory test from which C_p is determined does, in fact, give a nearly direct determination of B_f. The ratio of sample pore volume at any stress level to pore volume at a stress level corresponding to that reached in the reservoir when pressure declines to standard pressure gives the pore volume formation volume factor; the data needed are an initial pore volume and fluid volume expelled as a function of stress applied to the sample and, of course, a relation such as Equation 3 which ties reservoir pressure to laboratory stress. The laboratory measurement does not even have to be carried to the "standard condition" stress level; it need only cover a stress range which encompasses the expected range of reservoir pressure. This amounts to defining a reference condition tied to the highest stress level reached (i.e., reservoir pressure below the lowest expected operational pressure).

3.1 Modified Fluid Formation Volume Factors

Based on the above formulations we define a modified gas/oil/water FVF as:

$$\tilde{B}_j = B_j / B_f \quad \ldots\ldots\ldots\ldots\ldots \quad 9$$

where j refers to gas, oil, or water. With this definition, we have the advantage of simultaneously considering the changes, with pressure, of both fluid and the pore space associated with that fluid. In material balance work, use of these factors allows us to center attention on fluid volume changes, knowing that pore space changes are being carried along automatically. The result, as we shall see, is a compact form of equation which accurately considers all facets of the formation and fluid expansion processes while retaining an appearance similar to that with which reservoir engineers have long been familiar.

4. MATERIAL BALANCE EQUATION

We will derive the material balance equation (MBE) for a black oil system, using the modified formation volume factors just introduced. The system may be comprised of three zones: gas cap, oil zone, and pot aquifer. Phases present consist of hydrocarbon vapor, hydrocarbon liquid, and brine which are more commonly called free gas, oil, and water. Gas is also looked upon as a component, and may be present either in free form or dissolved in oil and water. Oil and water are not soluble in gas or in each other. A common (average) pressure characterizes all zones and phases.

Since the contribution of water-saturated formation to drive energy may be considerable, the distribution of water in the system is of importance. First, average connate water saturation may be different in the gas cap and oil zone. Second, we allow for the presence of a pot or "steady state" aquifer which is in immediate pressure communication with the hydrocarbon zones. This could be underlying water or simply a small aquifer. In the usual analysis, the energy contribution from a small aquifer might be neglected, but the possibility of high and variable formation compressibility enhances the importance of such a contribution, especially in overpressured systems. Finally, we will allow for water and gas influx from a "transient" aquifer. Precise treatment of such influx requires separate analysis which is beyond the scope of this paper, but the overall effects are easily included in the general formulation.

The analysis begins by relating the pore volumes of the oil, water, and free gas phases to the total pore volume of the system.

$$NB_{oi} + WB_{wi} + G_{Fi} B_{gi} = V_{psc} B_{fi} \quad \ldots\ldots\ldots \quad 10$$

from which

$$V_{psc} = N\tilde{B}_{oi} + W\tilde{B}_{wi} + G_{Fi} \tilde{B}_{gi} \quad \ldots\ldots\ldots \quad 11$$

After some depletion, influx of water and gas, and shrinkage of pore volume, the following will apply:

$$(N - N_p) B_o + (W - W_p + W_e) B_w + (G_{Fi} + G_{si} - G_s - G_p) B_g = V_{psc} B_f \quad \ldots \quad 12$$

The term $(G_{si} - G_s)$ represents the difference in solution gas content between initial and current conditions and can be written after combining like terms as:

$$G_{si} - G_s = N\,(R_{si} - R_s) + N_p\,R_s \quad \ldots\ldots\ldots \quad 13$$

We now go through the algebraic steps of solving Equation 12 for V_{psc}, equating the result to Equation 11, and then gathering all terms dealing with production or influx on the right hand side of the equation while all others are gathered on the left we get:

$$\begin{aligned} &\left(N\left\{\left[\tilde{B}_o + (R_{si} - R_s)\,\tilde{B}_g\right] - \tilde{B}_{oi}\right\}\right) + \\ &\quad W\left\{\tilde{B}_w - \tilde{B}_{wi}\right\} + G_{Fi}\left(\tilde{B}_g - \tilde{B}_{gi}\right) \\ &\qquad = \\ &N_p\left(\tilde{B}_o - R_s\,\tilde{B}_g\right) + \\ &\quad (W_p - W_e)\,\tilde{B}_w + G_p\,\tilde{B}_g \quad \ldots\ldots \end{aligned} \quad 14$$

we can define a modified two-phase formation volume factor by dividing the standard two phase factor by B_t:

$$\tilde{B}_t = \tilde{B}_o + (R_{si} - R_s)\,\tilde{B}_g \quad \ldots\ldots\ldots\ldots \quad 15$$

Note that $\tilde{B}_{ti} = \tilde{B}_{oi}$

A final step to reach the form desired requires relating W and G_{Fi} to N. We define two quantities:

F_{gc} = pore volume ratio, gas cap/oil zone
F_{pa} = pore volume ratio, pot aquifer/oil zone

Then

$$B_{ti}\,V_{psc} = \frac{N\,B_{oi}}{1 - S_{wi}}\left[1 + F_{gc} + F_{pa}\right] \quad \ldots \quad 16$$

and the pore volume of water can be found by multiplying each of the terms within brackets by the appropriate water saturation for each zone:

$$B_{wi}\,W = \frac{N\,B_{oi}}{1 - S_{wi}}\left[S_{wi} + F_{gc}\,S_{wgi} + F_{pa}\right] \ldots \quad 17$$

After division by B_{ti}, substitutions and rearrangement:

$$W = \frac{N\,\tilde{B}_{ti}}{\tilde{B}_{wi}}\left[\frac{S_{wi} + F_{gc}\,S_{wgi} + F_{pa}}{1 - S_{wi}}\right] \ldots\ldots \quad 18$$

For free gas,

$$G_{Fi} = \frac{N\,\tilde{B}_{ti}}{\tilde{B}_{gi}}\left[\frac{F_{gc}(1 - S_{wgi})}{1 - S_{wi}}\right] \quad \ldots\ldots \quad 19$$

When the appropriate substitutions are made in Equation 14, the final result is:

$$N = \frac{N_p\left(\tilde{B}_o - R_s\tilde{B}_g\right) + (W_p - W_e)\tilde{B}_w + G_p\tilde{B}_g}{\tilde{B}_{ti}\left\{\left(\frac{\tilde{B}_t}{\tilde{B}_{ti}} - 1\right) + \left[\frac{S_{wi} + F_{gc}S_{wgi} + F_{pa}}{1 - S_{wi}}\right]\left(\frac{\tilde{B}_w}{\tilde{B}_{wi}} - 1\right) + \left[\frac{F_{gc}(1 - S_{wgi})}{1 - S_{wi}}\right]\left(\frac{\tilde{B}_g}{\tilde{B}_{gi}} - 1\right)\right\}} \quad 20$$

While the preceding equation is a very general form, it does require a calculation of W_e by other means. In addition, using the produced gas-oil ratio:

$$R_p = G_p / N_p \ldots\ldots\ldots\ldots \quad 21$$

we can rearrange terms to yield:

$$N = \frac{N_p\left[\tilde{B}_t + (R_p - R_{si})\,\tilde{B}_g\right] + (W_p - W_e)\,\tilde{B}_w}{\tilde{B}_{ti}\left\{\left(\frac{\tilde{B}_t}{\tilde{B}_{ti}} - 1\right) + \left[\frac{S_{wi} + F_{gc}S_{wgi} + F_{pa}}{1 - S_{wi}}\right]\left(\frac{\tilde{B}_w}{\tilde{B}_{wi}} - 1\right) + \left[\frac{F_{gc}(1 - S_{wgi})}{1 - S_{wi}}\right]\left(\frac{\tilde{B}_g}{\tilde{B}_{gi}} - 1\right)\right\}} \quad 22$$

The numerator is sometimes referred to as the "expanded net-production-plus-excess-gas" formulation.

For gas reservoirs with associated aquifers, the same approach may be used to derive the analog of Eq. 20:

$$G_{Fi} = \frac{G_p\tilde{B}_g + (W_p - W_e)\tilde{B}_w}{\tilde{B}_{gi}\left\{\left(\frac{\tilde{B}_g}{\tilde{B}_{gi}} - 1\right) + \left[\frac{S_{wi} + F_{pa}}{1 - S_{wi}}\right]\left(\frac{\tilde{B}_{wt}}{\tilde{B}_{wti}} - 1\right)\right\}} \quad 23$$

The terms appearing in the denominator of the Equations 20, 22, and 23 are worthy of examination. Each of the terms $\left[\left(\tilde{B}_j / \tilde{B}_{ji}\right) - 1\right]$ represents the expansion of a unit volume of initial fluid, including its dissolved gas, and the contraction of its associated pore space. The factors which multiply $\left[\left(\tilde{B}_j / \tilde{B}_{ji}\right) - 1\right]$ are volume ratios at initial conditions for (water/oil), (free gas/oil) or (water/free gas); the multiplier for the first term is unity of course since the analysis is based on a unit of either oil or of free gas.

The water term is often neglected in material balance formulations, but it should not be. In the general form shown here, its significance becomes more obvious, especially in overpressured reservoirs where formation and gas or oil compressibilities can be comparable in magnitude. The water term may in fact be dominant for quite modest values of F_{pa}.

This can be demonstrated by noting that

$$\ln \tilde{B}_w = \ln B_w - \ln B_t$$

and taking the derivative and rearranging:

$$\left(\tilde{B}_w / \tilde{B}_{wi}\right) = e^{\overline{c_w + c_f}\ (p_i - p)}$$

The exponent is small, since compressibilities are typically 10^{-5} in order of magnitude while pressure changes are 10^{+3} in magnitude, so:

$$\tilde{B}_w / \tilde{B}_{wti} \doteq 1 + \overline{(c_w + c_f)}\ (p_i - p)$$

or

$$\left(\frac{\tilde{B}_w}{\tilde{B}_{wi}} - 1\right) \doteq \overline{(c_w + c_f)}\ (p_i - p) \quad \ldots\ldots \quad 24$$

Similar expressions may be developed for oil and its dissolved gas, and also for free gas, and the pore space associated with each.

Some order-of-magnitude calculations can now be made. If we choose a system at 10,000 psi and 225°F as typical of an overpressured reservoir setting with a weakly consolidated or unconsolidated formation, we can estimate:

c_w	$= 3(10^{-6})$ psi^{-1}	(Osif, 1984)
c_g	$= 37(10^{-6})$ psi^{-1}	(Bradley, 1987)
c_f (frbl)	$= 10(10^{-6})$ psi^{-1}	(friable sand)
c_f (uc)	$= 35(10^{-6})$ psi^{-1}	(unconsolidated sand)

It follows that

$$c_w + c_f \text{ (frbl)} = 13(10^{-6}) \text{ psi}^{-1}$$
$$c_w + c_f \text{ (uc)} = 38(10^{-6}) \text{ psi}^{-1}$$

compared to

$$c_g + c_f \text{(frbl)} = 47(10^{-6}) \text{ psi}^{-1}$$
$$c_g + c_f \text{(uc)} = 72(10^{-6}) \text{ psi}^{-1}$$

Thus, the unit expansibility of water and its pore space is nearly 30 percent of that of gas and its pore space for a weakly consolidated sand and over 50% for an unconsolidated sand. If $S_{wi} = 0.2$, the water term appearing in the denominator of Equation 23, for gas reservoirs, will dominate if $F_{pa} > 2.7$ for a weak sand and for $F_{pa} > 1.3$ for an unconsolidated sand. For oil reservoirs, an estimate of two-phase compressibility will be system-specific, but we can reasonably argue that it will be less than gas compressibility. The water term will then exceed the oil term at even lower values of F_{pa}.

While the preceding development aimed to illustrate the need to account for water-bearing formation in material balance analysis, the key issue is actually the high formation compressibility. In the example, formation compressibility contributes over 20 percent of the expansion energy associated with gas-bearing rock, and over 75 percent of the energy associated with water-bearing rock for weak formations. For unconsolidated formation, formation compressibility contributes nearly 50% of the energy associated with gas-bearing reservoirs. Formation compressibility effects should be included, and water-bearing rock should not be ignored, even though its total volume may appear to be quite modest.

These facts have long been recognized in analyzing performance of overpressured gas reservoirs (Hammerlindl, 1971; Bass, 1972). However, these and other investigators (Ramagost and Farshad, 1981; Bernard, 1987) have suggested only approximations for dealing with the problem. The formulation proposed here explicitly includes the effects of all contributing fluids and their associated pore space, and has the added attraction of allowing variable compressibilities to be included with relative ease.

5. MBE ANALYSIS

The MBE presented in Equations 20 and 23 is more comprehensive than those usually presented, but it has the same format except for the use of the modified formation volume factors $\tilde{B}_{o,w,g}$ in place of the $B_{o,w,g}$. The modified fluid formation volume factors can be calculated independently as a pre-analysis step, and used in place of the usual fluid volume factors in MBE's in current use. It is readily apparent this MBE formulation will reduce to conventional presentations of the MBE (see, for example, Dake, 1978; Bradley, 1987) if appropriate simplifying assumptions are made.

As an example, consider the gas material balance Equation 23. If we divide both numerator and denominator on the right hand side by $\tilde{B}_g$, solve the resulting expression for $\left(1 / \tilde{B}_g\right)$ and then substitute $B_f(p/z) = (\text{constant}) \bullet \left(1 / \tilde{B}_g\right)$, we obtain, after some algebra:

$$\left(\frac{p}{z}\right)\left\{\frac{B_f}{B_{fi}}\left[\frac{F_{pa}+1}{1-S_{wi}}\right] - \frac{B_{wt}}{B_{wti}}\left[\frac{F_{pa}+S_{wi}}{1-S_{wi}}\right]\right\} =$$

$$\left(\frac{p}{z}\right)_i - \left(\frac{1}{G_{Fi}}\right)\left(\frac{p}{z}\right)_i\left\{(G_p) + (W_p - W_e)\left(\frac{B_w}{B_g}\right)\right\} \quad 25$$

If we assume $W_e = 0$, then $G_{Fi} = G$. We also introduce the approximations:

$$B_f = B_{fi}[1 - C_f(p_i - p)]$$
$$B_w = B_{wi}[1 + C_w(p_i - p)]$$

where C_f and C_w are taken to be small and constant. The equation which ultimately results is:

$$\left(\frac{p}{z}\right)\left[1 - \frac{C_w(F_{pa}+S_{wi}) + C_f(F_{pa}+1)}{1-S_{wi}}(p_i - p)\right] = \left(\frac{p}{z}\right)_i - \left(\frac{1}{G}\right)\left(\frac{p}{z}\right)_i\left\{G_p + W_p\frac{B_w}{B_g}\right\} \quad 26$$

The preceding equation is that developed by Bass (1972). If, $F_{pa} = 0$ and $W_p = 0$, then:

$$\left(\frac{p}{z}\right)\left[1-\frac{(C_f + C_w S_{wi})(p_i - p)}{1 - S_{wi}}\right] = \left(\frac{p}{z}\right)_i - \left(\frac{p}{z}\right)_i\left(\frac{G_p}{G}\right) \quad 27$$

which was proposed by Ramagost and Farshad (1981).

Any one of the Equations 25 through 27 can be plotted as "corrected" (p/z) versus "corrected" G_p and the line extrapolated to an intercept to estimate G_{Fi} or G, provided of course that F_{pa} can be estimated with sufficient accuracy to allow an accurate correction to be calculated. Equation 25 has an advantage for cases where influx can reasonably be taken as zero, and the overpressured gas reservoir may well fit this case. Since all variable effects are properly allowed for, F_{pa} may be determined by trial and error as the value which leads to the best straight-line fit of the pressure and production data. Equations 26 and 27 are not really suitable since c_f will in fact change rather rapidly as ($p_i - p$) increases.

6. SIMULATION CONSIDERATIONS

Variable compressibility is easily handled at the partial differential equation level by substituting $\phi_{sc} B_f$ for porosity wherever it appears in the equations. Manipulation of B_f as a pressure-dependent variable should be straightforward. It may be preferable to reformulate the equations in terms of the modified fluid volume factors $\tilde{B}_j$ since these variables can be developed outside the context of the simulation equations, thereby reducing the numerical calculation required. Since B_f is a continuous, slowly changing function of reservoir pressure, there is no reason to anticipate that the $\tilde{B}_j$ functions will be any more difficult to handle numerically than the B_j functions themselves.

7. CASE HISTORIES

Twenty over-pressured gas reservoirs were selected and analyzed with a computer program developed by using the new method and the rock compressibility correlations discussed above. Following are two of the case histories studied.

One factor needed in the analysis is a determination of rock type so the proper s or p relationship can be used. If core data are not available, type curves for formation compressibility can be used although it is always preferable to use laboratory compressibility data from the formation of interest. If type curve compressibility is used yet the degree of consolidation is not certain or available, one should conduct sensitivity studies for all appropriate rock types to determine the best suitable solution. For these case histories, formation compressibility is taken from the type curves presented earlier.

7.1 Case 1

The first selected case history was the Anderson "L" reservoir from the Mobil-David field presented by Duggan (1972). The Anderson "L" is an over-pressured gas reservoir having an initial pressure of 9507 psia at 11,167 feet subsea depth, or a gradient of 0.843 psi/ft. Table 3 provides other pertinent data on this reservoir. In this case, it is assumed that F_{pa}, W_e, G_e and R_{sw} equal zero, and the "L" sand is weakly consolidated.

The pore volume formation volume factors (B_f) are calculated from C_f values by using Equations 7 and 8. Figure 7 shows a graphical presentation of the rock compressibility as a function of reservoir pressure. We can use the B_f concept to "correct" the p/z versus production plot to account for formation and water compressibility. As shown in the braced term on the left side of Equation 25, we can use a factor C :

$$C = \frac{(B_f / B_{fi})^*(F_{pa} + 1) - (B_W / B_{Wi})^*(F_{pa} + S_{Wi})}{(1 - S_{Wi})} \quad 28$$

as a multiplier for p/z. Figure 8 shows the actual and the corrected p/z data plotted against the cumulative wet gas production. The early extrapolation of the actual p/z curve indicates an apparent gas-in-place of 112 Bcf, which is about 61 percent higher than the estimated volumetric gas-in-place of 69.6 Bcf. However, the extrapolation of the corrected p/z curve using linear regression on all data points yields a corrected gas-in-place of 83.6 Bcf. The gas-in-place of 83.6 Bcf was then input into Equation 25 and the estimated gas production at each time step was calculated and plotted in Figure 8. As shown in Figure 8, the calculated gas production shows an excellent match to the actual data.

To determine the degree of confidence in predicting the original gas-in-place early in the productive life of the reservoir when a few data points are available, a sensitivity study was conducted where only the first six data points were considered in the evaluation. In this case, the original gas-in-place determined by linear regression on the first six corrected p/z data points is estimated at 76.0 Bcf. Table 4 shows the regression analysis results for the six and the all-data-point cases. Although the six-data-point case shows a higher standard deviation, both cases give an excellent best fit to the straight line. This seems to imply that the gas-in-place tends to be under-estimated when considering only early data points. To verify this point, we performed additional evaluations based on data groups from a minimum of three to a maximum of sixteen data points. The results from these evaluations and our experience with other case histories indicated that gas-in-place estimates tend to increase when more data points are included and become stable as reservoir pressure drops to about 70 percent of the original reservoir pressure. Currently, we are evaluating the possible causes of these empirical results.

7.2 Case 2

The North Ossun "NS2B" reservoir (Harville and Hawkins, 1969) is an over-pressured gas reservoir having an initial pressure of 8921 psi at 12,500 feet subsea depth, or a gradient of 0.725 psi/ft. Table 5

provides other pertinent data on this reservoir. Furthermore, good geologic data and considerable complex faulting in the area suggest a closed reservoir with a limited water aquifer. In this case, we also assume that W_e, G_e and R_{sw} equal zero.

As in Case 1, B_f is calculated from c_f via Equations 7 and 8 for consolidated and unconsolidated sandstones. Figure 9 shows c_f as a function of pressure. $(p/z)C$ is calculated for the two selected cases:
(a) unconsolidated sandstone with no associated water aquifer ($F_{pa} = 0$), and (b) consolidated sandstone with a water aquifer equal five times the pore volume of the gas reservoir ($F_{pa} = 5$).

Figure 10 shows the actual and the modified p/z data for Case (a) plotted against the cumulative gas production. The early extrapolation of the actual p/z curve indicates an apparent gas-in-place of 210 Bcf. However, the extrapolation of the modified p/z curve $(p/z)C$ yields a corrected gas-in-place of 105 Bcf which is close to the volumetric estimate of 114 Bcf. Also, as shown on Figure 10, the calculated p/z curve, based on the gas-in-place of 105 Bcf, matches very well with the actual data.

To study the contribution of formation compaction and water expansion from a small aquifer to the drive energy, a sensitivity study of this reservoir was conducted using different aquifer sizes (F_{pa}) and rock compressibilities. For each combination of rock type and aquifer size (F_{pa}), the $(p/z)C$ data was calculated and from which a corrected gas-in-place can be determined. Table 6 summarizes the results obtained from twelve different cases analyzed. Comparing the first unconsolidated case ($F_{pa} = 0$) and the last consolidated case ($F_{pa} = 5$), it is seen that both cases give the lowest standard deviations which indicate the correct gas-in-place is within the range of 104 to 108 Bcf. Both cases provide similar calculation results of $(p/z)C$.

7.3 Drive Energy Partitioning and Reserve Estimation

The results from this sensitivity study indicate that a varying combination of rock compaction and water expansion from a small water aquifer could provide the same performance effects to the reservoir system as long as the total energy contribution from these two factors is the same. This observation is consistent with the speculation raised in the MBE Analysis section of this paper. Therefore, it is important to utilize knowledge of the geological setting as well as knowledge of reservoir rock properties to evaluate and confidently predict gas-in-place from pressure performance of over-pressured gas reservoirs. Correct partitioning of drive energies, therefore, is dependent in many cases on accurate measurements or estimates of formation compressibility. Underestimation of formation compressibility may suggest a water drive where one does not exist and vice versa.

Profitable development of overpressured and/or unconsolidated reservoirs is dependent on an accurate understanding of drive mechanisms and total reserves. This is especially true since many if not most of these types of reservoirs are located offshore. Accurate formation compressibility data and application of that data in MBE analysis and reservoir simulation can significantly improve reservoir development in these types of fields.

8. CONCLUSIONS

- Incorporation of variable formation compressibility into reservoir performance analysis is important for overpressured and/or weakly to unconsolidated reservoirs.

- Accurate laboratory measurements of pore compressibility are important and standard methods for measurement of pore compressibility on friable to unconsolidated cores are often inadequate. Tests on full diameter, fresh core samples from unconsolidated formations are preferable to plug samples and slow rate tests are necessary to account for the anelastic nature of these formations.

- Use of the modified Formation Volume Factor as defined in this paper allows variable formation compressibility to be incorporated into the MBE and other reservoir performance analyses easily and effectively.

- Use of variable formation compressibility in material balance analysis for initial reserves leads to more accurate estimates of reserves. Use of accurate laboratory pore compressibility data can allow accurate reserve estimates from early time data in overpressured systems.

- Incorporation of accurate formation compressibility measurements in reservoir performance analysis can allow for the correct partitioning of drive energies and estimates of remaining reserves which can aid in the most efficient development of the reservoir.

9. ACKNOWLEDGMENTS

We would like to thank the managements of Mobil Research and Development Corporation and Mobil Exploration and Producing, U.S. Inc. for permission to publish this paper. We would also like to thank Marty Cohen, Ron Moore, J. Michael Rodriguez, and all the others who helped on this project.

10. NOMENCLATURE

A = constant in Table 2
B = constant in Table 2
B_f = pore volume formation volume factor (FVF), RB/STB
B_{fi} = initial pore volume FVF, RB/STB
B_g = gas FVF, RB/STB
B_{gi} = initial gas FVF, RB/STB
B_o = oil FVF, RB/STB
B_{oi} = initial oil FVF, RB/STB
B_t = two-phase FVF, RB/STB

B_{ti} = initial two-phase FVF, RB/STB
B_w = water FVF, RB/STB
B_{wi} = initial water FVF, RB/STB
$\tilde{B}_g = B_g / B_f$
$\tilde{B}_{gi} = B_{gi} / B_f$
$\tilde{B}_j = B_j / B_f$
$\tilde{B}_o = B_o / B_f$
$\tilde{B}_{oi} = B_{oi} / B_f$
$\tilde{B}_t = B_t / B_f$
$\tilde{B}_w = B_w / B_f$
$\tilde{B}_{wi} = B_{wi} / B_f$
C = constant in Table 2
C = constant in Equation 28 and Figures 8 and 10
C_b = bulk compressibility of the formation, vol/vol/psi
C_f = formation compressibility, vol/vol/psi
C_g = gas compressibility, vol/vol/psi
C_{gr} = grain compressibility of the formation, vol/vol/psi
C_p = pore compressibility, vol/vol/psi
C_{wt} = total water compressibility, vol/vol/psi
D = constant
F_{gc} = pore value ratio, gas cap/oil zone
F_{pa} = pore value ratio, pot aquife/oil zone
G = total initial gas in place, scf
G_{fi} = initial free gas in place, scf
G_p = total gas produced, scf
G_s = solution gas in place, scf
G_{si} = initial solution gas in place, scf
$I(p)$ = integrated formation compressibility
K_1 = constant in Equation 3
K_2 = constant in Equation 3
K_3 = constant in Equation 3
N = oil in place, STB
$\tilde{N} = N / B_f$
v = Poisson's ratio
N_p = total oil produced, STB
$\varnothing_{sc}$ = porosity at standard conditions, fraction
p = reservoir pressue, psi
pi = initial reservoir pressure, psi
R_s = gas in solultion in oil, scf/RB
R_{si} = initial gas in solution in oil, scf/RB
S_{wgi} = initial water saturation, gas cap, fraction
S_{wi} = initial water saturation, oil zone, fraction
σ_i = inital effective laboratory stress, psi
σ_{lab} = effective laboratory stress, psi
$\sigma_{x,y}$ = horizontal stresses, psi
σ_z = overburden stress, psi
V_p = pore volume at reservoir condition, RB
V_{psc} = pore volume at standard condition, STB
W = water in place, STB
W_e = cumulative water influx, STB
W_p = cumulative water produced, STB
z = gas deviation factor

11. REFERENCES

Andersen, M. A.: "Predicting Reservoir Condition Pore-Volume Compressibility from Hydrostatic-Stress Laboratory Data," paper SPE 14213 presented at the 1985 SPE 60th Annual Meeting, Las Vegas, Sept. 22-25.

Bass, D. M.: "Analysis of Abnormally Pressured Gas Reservoirs with Partial Water Influx," paper SPE 3850 presented at the 1972 3rd Symposium on Abnormal Subsurface Pore Pressure, Louisiana State University, May 15-16.

Bernard, W. J.: "Reserves Estimation and Performance Prediction for Geopressured Gas Reservoirs," *J. Pet. Sci. Eng.* (Aug. 1987) **1**, 15-21.

Bradley, H. B. (Editor-in-Chief): *Petroleum Engineering Handbook*, SPE, Richardson, Texas (1987).

Chierici, G.L., Ciucci, G.M., Eva, F., and Long,G. (1967) "Effect of overburden pressure on some petrophysical parameters of reservoir rocks," *Proc. 7th World Petroleum Congress*, **2**, 309.

Dake, L. P.: *Fundamentals of Reservoir Engineering*, Elsevier Scientific Publishing Co., Amsterdam (1978).

de Waal, J. A.: *On Rate Type Compaction Behavior of Sandstone Reservoir Rock*, Ph.D. thesis, Technische Hogeschool Delft, (1986).

Dobrynin, V.M. (1963) "Effect of overburden pressure on some properties of sandstones", *SPEJ*, **2**, 360.

Duggan, J. O.: "The Anderson "L" - An Abnormally Pressured Gas Reservoir in South Texas," *JPT* (February 1972) 132-138.

Fatt, I. (1958a) "Compressibility of sandstones at low to moderate pressures", *Bull. AAPG*, **42**, 1924.

Fatt, I. (1958b) "Pore volume compressibilities of sandstone reservoir rocks", *Trans., AIME*, **213**, 362.

Geertsma, J.: "The Effect of Fluid Pressure Decline on Volumetric Changes of Porous Rocks," *Trans.*, AIME (1957) **210**, 331-340.

Hammerlindl, D. J.: "Predicting Gas Reserves in Abnormally Pressured Reservoirs," paper SPE 3479 presented at the 1971 SPE of AIME 46th Annual Meeting, New Orleans, Oct. 3-6.

Harville, D. W., and Hawkins, M. F.: "Rock Compressibility and Failure as Reservoir Mechanisms in Geopressured Gas Reservoirs," *JPT* (December, 1969) 1528-1530.

Jaeger, J. C., and Cook, N. G. W.: *Fundamentals of Rock Mechanics*, Chapman and Hall, London (1976).

Keelan, D. K. (1985) "Automated core measurement system for enhanced core data at overburden conditions", paper SPE 15185.

Kosar, K. M., Scott, J. D., and Mogenstern, N. R.: "Testing to Determine the Geotechnical Properties of Oil Sands," paper PS/CIM 87-38-59 presented at the 1987 Petroleum Society of CIM 38th Annual Meeting, Calgary.

Lachance, D. P., and Andersen, M. A.: "Comparison of Uniaxial Strain and Hydrostatic Stress Pore-Volume Compressibility in the Nugget Sandstone," paper SPE 11971 presented at the 1983 SPE 58th Annual Meeting, San Francisco, Oct. 5-8.

Nur, A. and Byerlee, J.D. (1971) "An exact effective stress law for elastic deformation of rock with fluids", *Jour. Geophys. Res.*, **76**, 6414-6419.

Osif, T. L.: "The Effects of Salt, Gas, Temperature, and Pressure on the Compressibility of Water," paper SPE 13174 presented at the 1984 SPE 59th Annual Technical Conference and Exhibition, Houston, Texas, Sept. 16-19.

Ramagost, B. P., and Farshad, F. F.: "P/Z Abnormally Pressured Gas Reservoirs," paper SPE 10125 presented at the 1981 SPE of AIME 56th Annual Technical Conference, San Antonio, October 5-7.

Teeuw, D.: "Prediction of Reservoir Compaction from Laboratory Compressibility Data," *SPEJ*, (September, 1971) 263-271.

Teeuw, D.: "Laboratory Measurements of Groningen Reservoir Rock," *Trans.*, Royal Dutch Soc. of Geologists and Mining Eng. (1973) **28**, 19-32.

Wyble, D. O. (1958) "Effect of applied pressure on the conductivity, porosity, and permeability of sandstones," *Trans. AIME*, **213**, 430.

Yale, D.P. (1984) *Network Modelling of Flow, Storage, and Deformation in Porous Rocks*, Ph.D. thesis, Stanford University.

TABLE 3

ANDERSON "L" RESERVOIR DATA

Depth	11167	feet
Initial BHP	9507	psia
Pressure Gradient	0.843	psi/foot
Bottom-hole Temperature	266	°F
Net Gas Pay Thickness	75	ft
Porosity	24	%
Water Saturation	35	%
Volumetric Gas In Place	69.6	Bcf

TABLE 4

ANDERSON "L" ANALYSIS RESULTS

	ALL DATA POINTS	SIX DATA POINTS
Estimated OGIP (Bcf)	83.6	76
Correlation Coefficient	0.9982	0.9922
Standard Deviation (%) of P/Z*C	0.91	6.85

TABLE 5

NORTH OSSUN "NS2B" RESERVOIR DATA

Depth	12500	feet
Initial BHP	8921	psia
Pressure Gradient	0.725	psi/foot
Bottom-hole Temperature	248	°F
Net Gas Pay Thickness	100	ft
Porosity	24	%
Water Saturation	34	%
Volumetric Gas in Place	114	Bcf

TABLE 6

NORTH OSSUN "NS2B" RESERVOIR ANALYSIS RESULTS

[OGIP (Bcf) / correlation coeff./ std.dev.(%)]

	$F_{pa} = 0$	$F_{pa} = 1$	$F_{pa} = 3$	$F_{pa} = 5$
Consolidated	158 / 0.986 / 1.4	143 / 0.991 / 1.4	120 / 0.995 / 1.2	104 / 0.997 / 1.1
Weakly Consol.	149 / 0.990 / 1.4	129 / 0.994 / 1.2	102 / 0.996 / 1.1	84 / 0.994 / 1.7
Unconsolidated	105 / 0.996 / 1.1	74 / 0.992 / 2.3	46 / 0.982 / 13.	32 / 0.975 / 33.

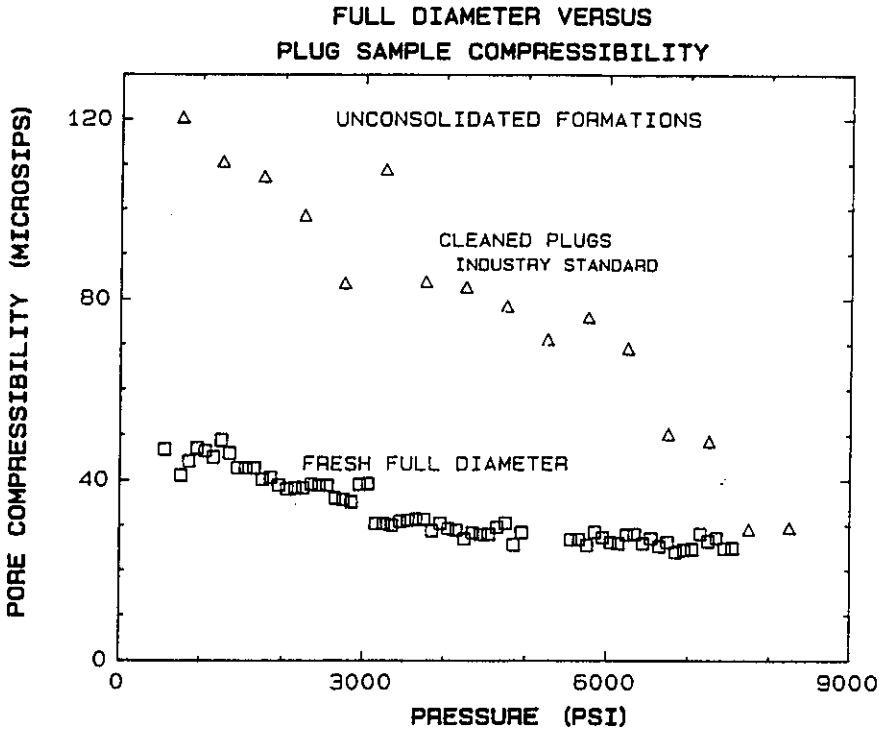

FIGURE 1
Comparison of compressibility from cleaned plugs versus fresh, full diameter cores showing effect of plug damage on pore compressibility

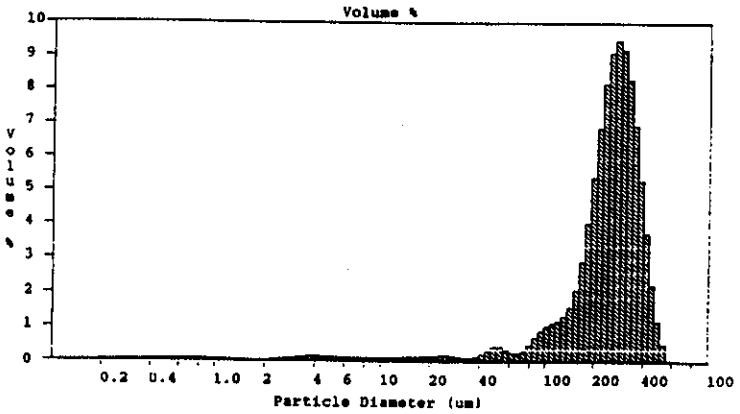

FIGURE 2A
Grain size distribution for clean, well sorted unconsolidated sand

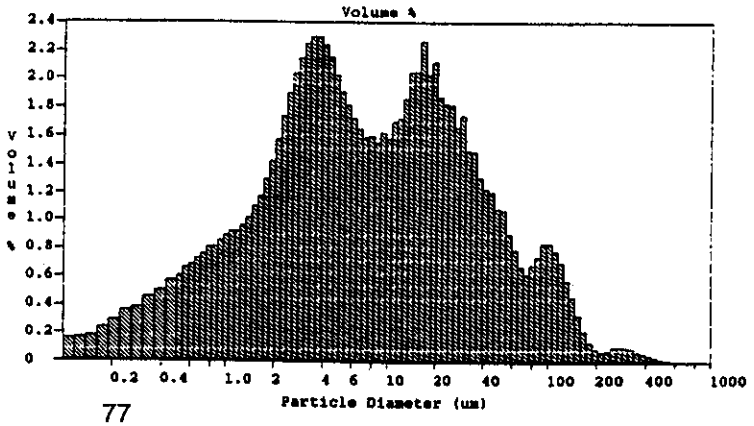

FIGURE 2B
Grain size distribution for clay rich, poorly sorted unconsolidated sand

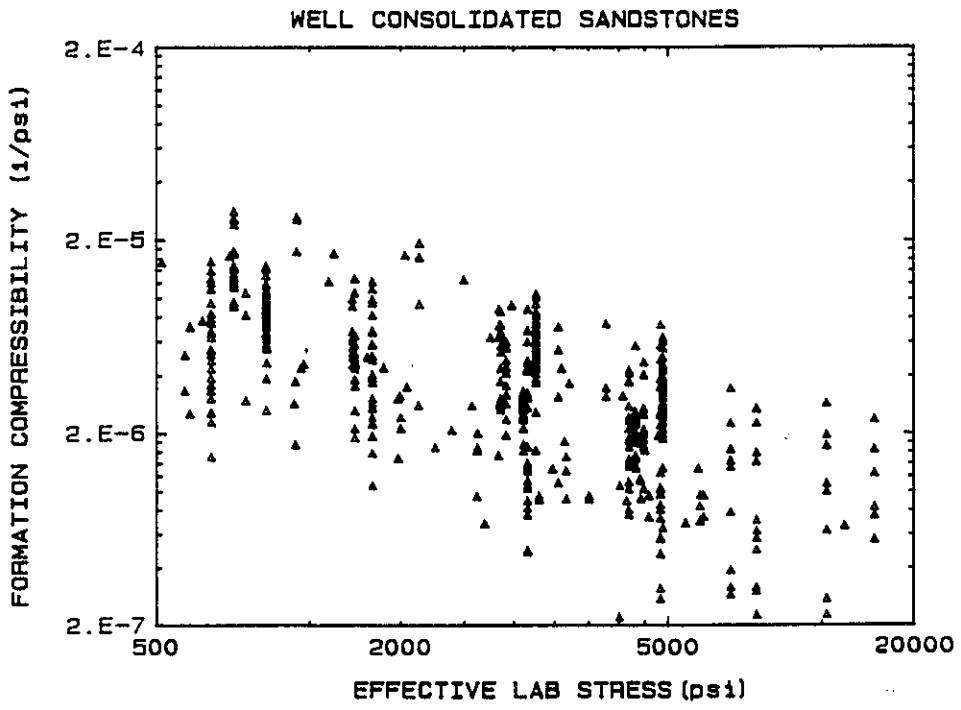

FIGURE 3
Log-log plot of Formation Compressibility versus Effective Laboratory Stress
(121 well consolidated sandstone samples)

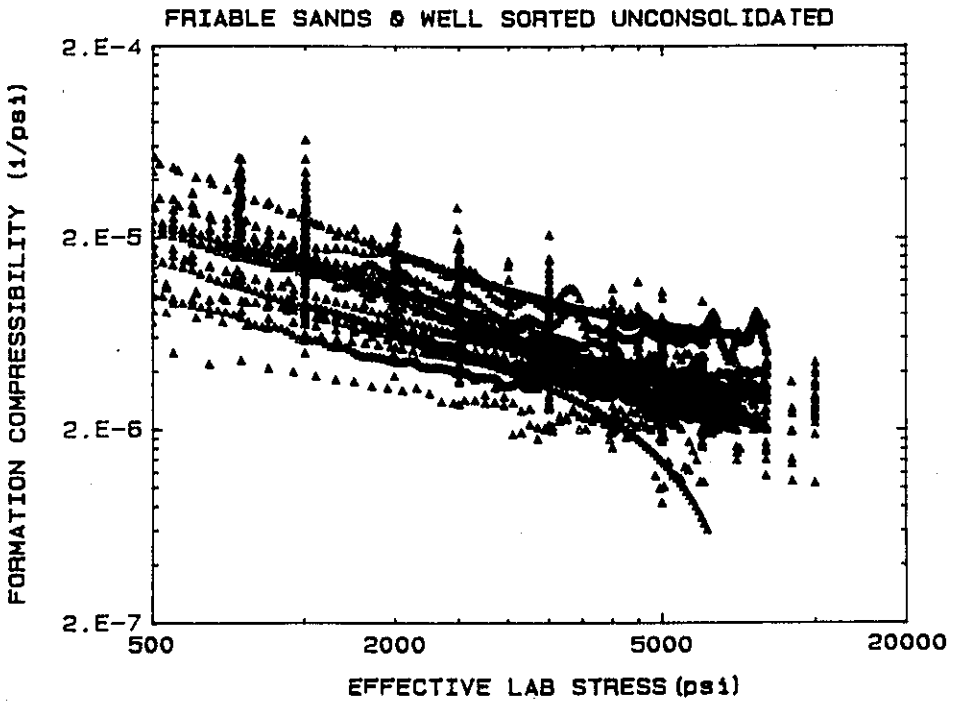

FIGURE 4
Log-log plot of Formation Compressibility versus Effective Laboratory Stress
(140 friable sandstone and well sorted unconsolidated sand samples)

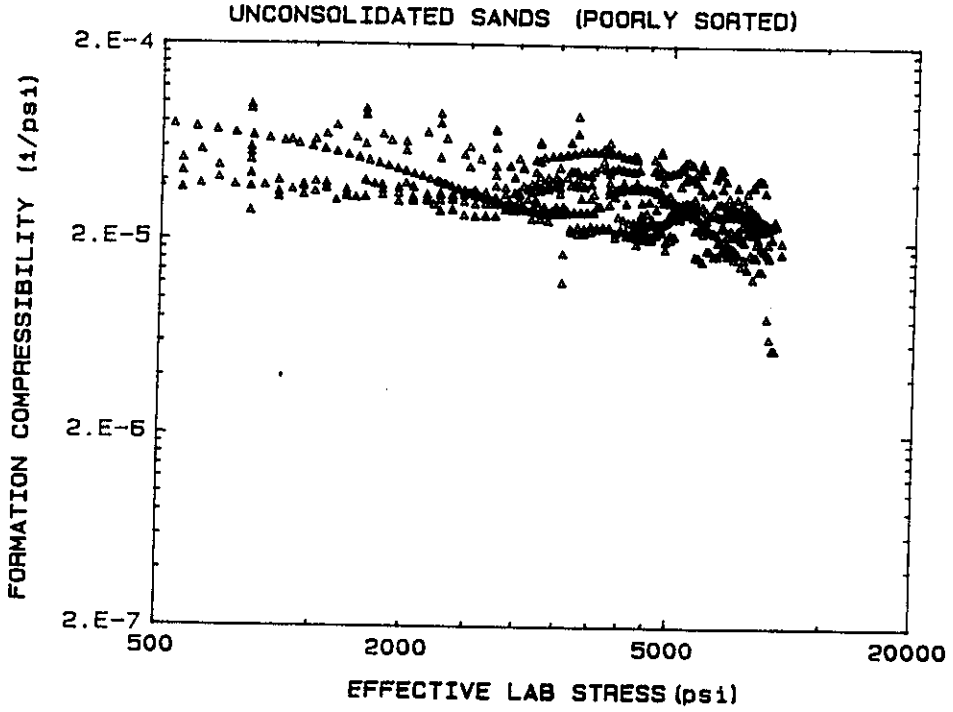

FIGURE 5
Log-log plot of Formation Compressibility versus Effective Laboratory Stress
(14 unconsolidated sand samples)

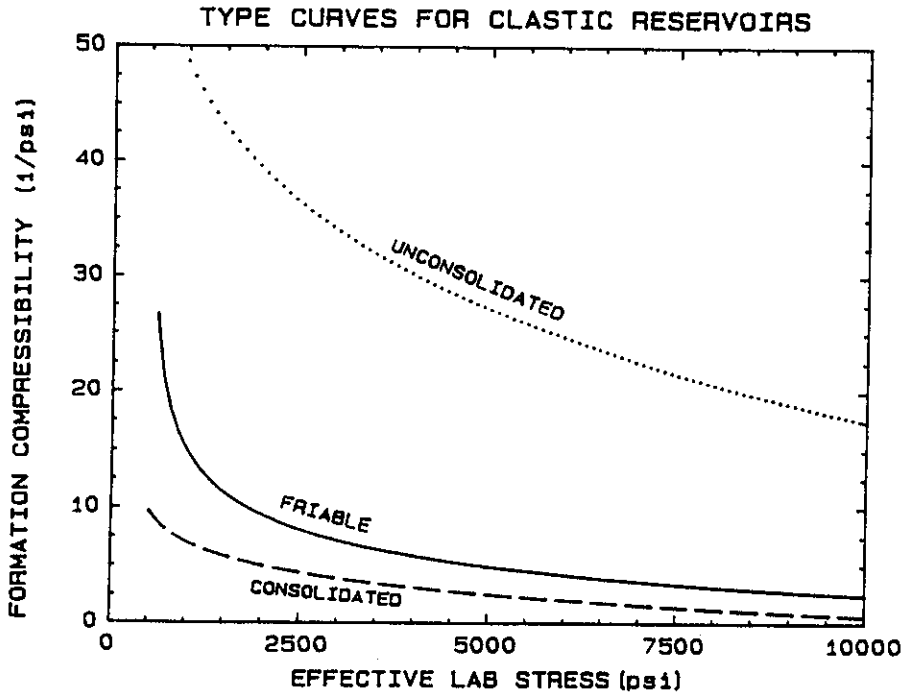

FIGURE 6
Type curves based on non-linear regression of data in Figures 3, 4, and 5

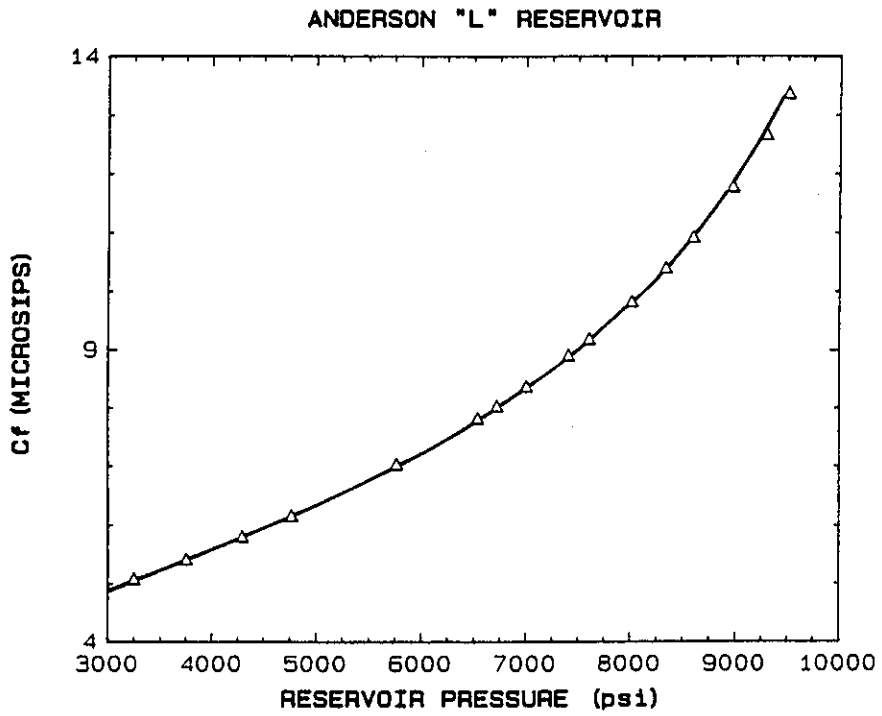

FIGURE 7
Formation compressibility as a function of reservoir pressure for Anderson "L"

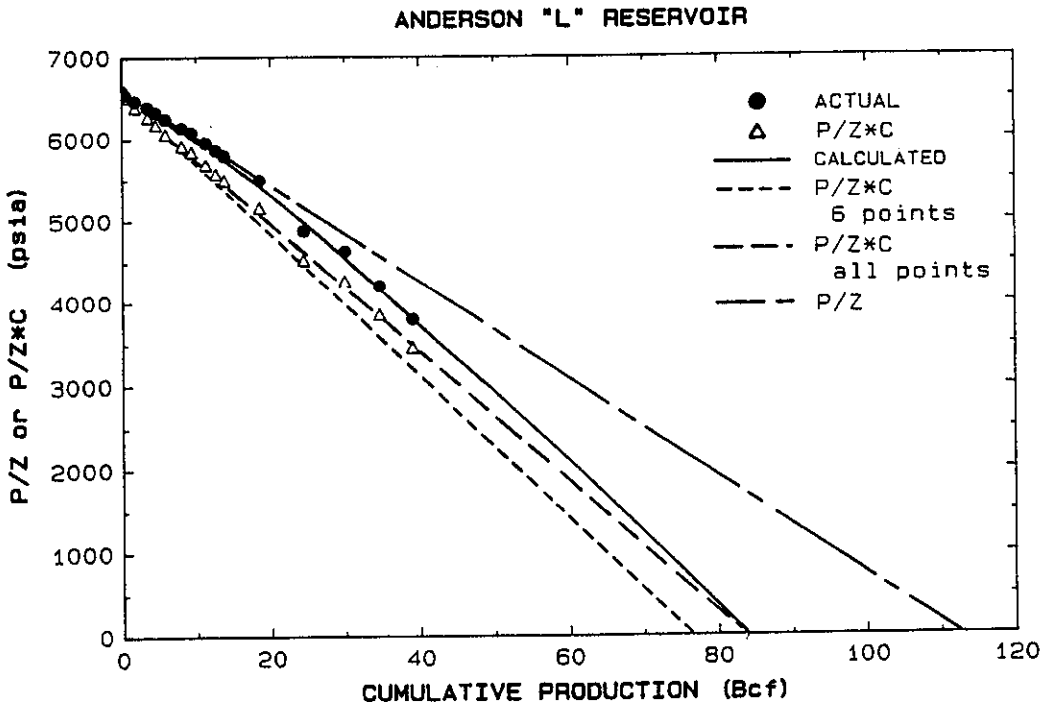

FIGURE 8
P/Z as a function of cumulative gas production
(standard and "variable compressibility" analysis)

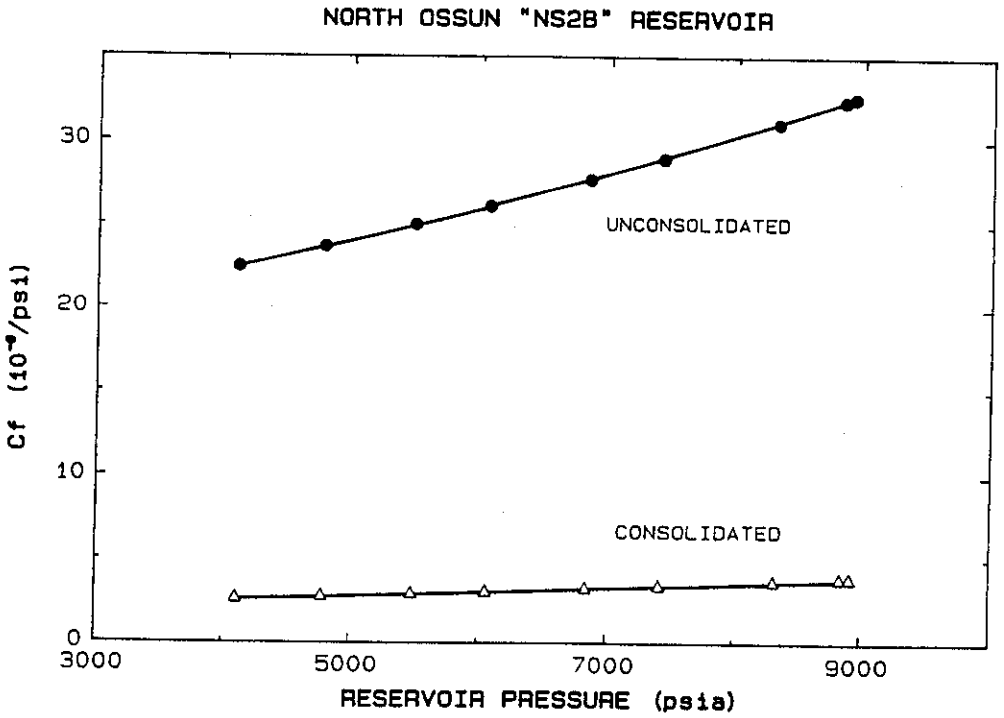

FIGURE 9
Formation compressibility as a function of reservoir pressure for North Ossun (from Type Curves)

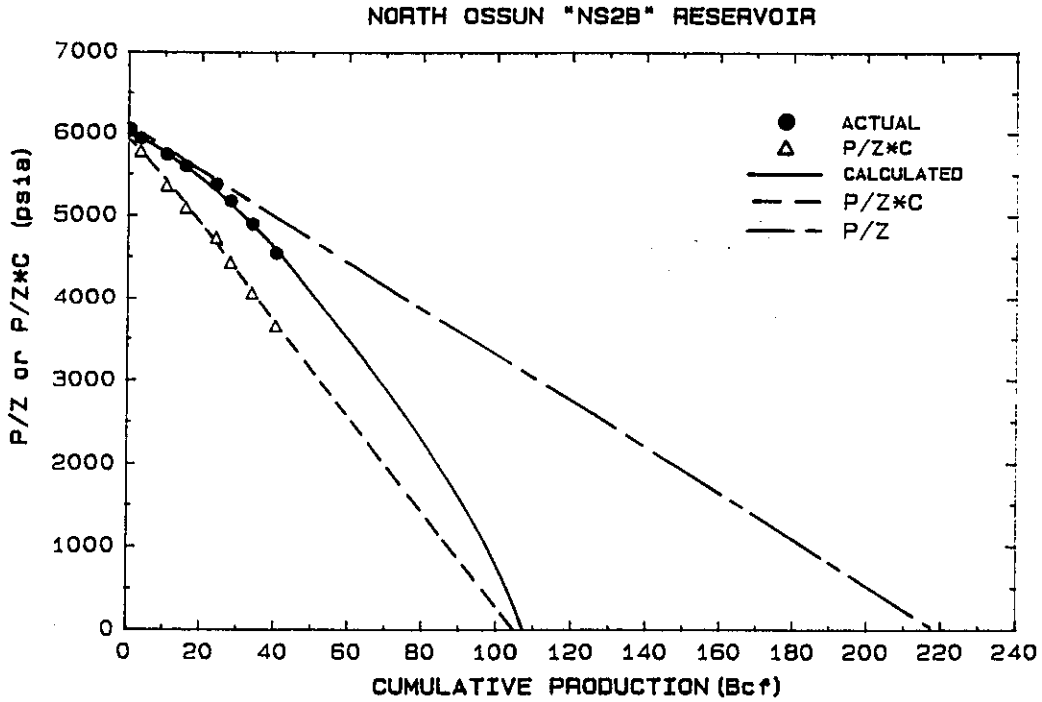

FIGURE 10
P/Z as a function of cumulative gas production (standard and "variable compressibility" analysis)

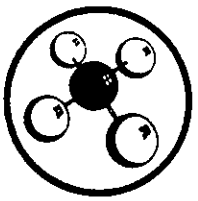

Analysis of Modified Isochronal Tests To Predict The Stabilized Deliverability Potential of Gas Wells Without Using Stabilized Flow Data

G. S. Brar,* SPE-AIME, Alberta Energy Resources Conservation Board
K. Aziz, SPE-AIME, U. of Calgary

Introduction

The most commonly used method to predict the initial stabilized deliverability potential of a gas well is the modified isochronal test that includes an extended flow period to pressure stabilization. Some reservoirs do not attain stabilization even after 100 or more hours of flow and consequently a reliable, extended flow period on such reservoirs can be unreasonably expensive and wasteful. In many instances, new wells are not tied into a pipeline before testing, in which cases gas must be flared during a test. Regulatory agencies such as the Alberta Energy Resources Conservation Board (AERCB) have imposed limitations (20 MMscf) on the amount of gas that can be flared during most gas well tests. To circumvent this problem, the isochronal portion of a test may be conducted while the extended flow period is delayed until the well is tied into a pipeline. Finally, in many cases where complete, modified isochronal tests have been run, extended flow tests simply are not conducted to stabilization and the stabilized deliverability potential must be estimated from just the isochronal flow data.

This paper presents two simple techniques to predict the stabilized deliverability potential, using only the isochronal data from modified isochronal tests. With either of the proposed techniques, which are referred to as "simplified isochronal test (SIT) analyses," it is possible to obtain reasonable values of permeability-thickness (kh), skin factor (s), and inertial-turbulent flow factor (D). These reservoir parameters may be used with other well and reservoir data to predict the stabilized deliverability potential of gas wells.

These techniques are based on existing theory for the analysis of gas well-test data. The quadratic form of the deliverability equation describes the pressure-flow rate relationship. The transient and stabilized flow coefficients in this equation are calculated using SIT methods.

The isochronal-test method described by Cullender[1] and the modified isochronal-test method proposed by Katz *et al.*[2] have been used extensively to develop performance curves for gas wells — particularly the modified isochronal tests. A requirement of such testing procedures is a flow period to pressure stabilization, or stabilized flow. This requirement is not found often, particularly in low-permeability reservoirs. Even in reservoirs with good producing characteristics and fast stabilization, it is undesirable from a conservation standpoint to flare gas needed to establish stabilized flow.

Consequently, the supposedly stabilized deliverability potential reported in tests usually is not representative of the stabilized performance of wells. The methods presented here overcome this deficiency and are valuable in certain situations where it is impossible to conduct a stabilized flow test.

Although it is possible to use the Rawlins and Schellhardt deliverability equation,[3] the more general Forchheimer or Houpert equation (also known as the quadratic form of the deliverability equation) is better suited

*Now with T. Fekete and Assocs. Consultants, Ltd., Calgary, Alta.

0149-2136/78/0002-6134$00.25

*Two new methods (simplified isochronal test [SIT] analyses) to predict the stabilized deliverability potential of gas wells are presented. These techniques use isochronal data from modified isochronal tests and also provide reasonable values of permeability-thickness (*kh*), skin factor (*s*), and inertial-turbulent flow factor (*D*).*

to the proposed methods. This equation also is known as the laminar, inertial-turbulent (LIT) flow equation.[4] In terms of p^2 the equation is

$$\Delta p^2 \equiv \bar{p}_R^{\,2} - p_{wf}^{\,2} = aq + bq^2. \quad \ldots\ldots\ldots\ldots (1)$$

Eq. 1 represents stabilized flow. For transient flow conditions, a is replaced by a_t to give

$$\Delta p^2 \equiv \bar{p}_R^{\,2} - p_{wf}^{\,2} = a_t q + bq^2. \quad \ldots\ldots\ldots\ldots (2)$$

In the AERCB manual,[4] these equations also are presented in terms of p and ψ (pseudo-pressure or real gas potential). To keep the calculations and discussion simple, the p^2 form is used in this paper. The use of p, p^2, or ψ is discussed in a paper by Aziz *et al.*[5]

An assumption inherent in these equations and in the isochronal analysis procedures is that the coefficient b remains constant with time. As will be seen later, this assumption is not correct for actual reservoirs where the formation is heterogeneous and pressure gradients are large. However, for many practical situations it is reasonable to assume that b is constant, and the techniques presented are based on this assumption. Another assumption is that the variation of a_t with time is independent of the flow rate and pressure level.

The next sections illustrate how a and b are computed from the data obtained with modified isochronal tests (excluding data from the extended or stabilized flow periods).

Basic Equations and Proposed Methods

The following equations and the two given above were obtained from Ref. 4. The assumptions and derivations of these equations are described in that reference and are not repeated in this paper.

Transient flow equation:

$$\Delta p^2 = m\left[\log(t/t^*) - 3.23 + 0.869\,s\right] q + 0.869\,m\,D\,q^2, \quad \ldots\ldots\ldots\ldots (3)$$

where

$$\Delta p^2 \equiv \bar{p}_R^{\,2} - p_{wf}^{\,2}$$

$$m = 1{,}632\,\bar{\mu}\bar{Z}\,T/kh$$

$$t^* = \phi\,\bar{\mu}\bar{c}\,r_w^{\,2}/k$$

(t^* is assumed constant for a test).

Pseudosteady state flow equation:

$$\Delta p^2 = 2m\left[\log\left(\frac{0.472\,r_e}{r_w}\right) + \frac{s}{2.303}\right] q + 0.869\,m\,D\,q^2. \quad \ldots\ldots\ldots\ldots (4)$$

Calculation of a_t and b

The least-squares method may be applied to Eq. 2 to give

$$a_t = \frac{\Sigma\,\Delta p^2/q\,\Sigma\,q^2 - \Sigma\,\Delta p^2\,\Sigma\,q}{N\Sigma\,q^2 - \Sigma\,q\,\Sigma\,q}, \quad \ldots\ldots\ldots (5)$$

and

$$b = \frac{N\Sigma\,\Delta p^2 - \Sigma\,\Delta p^2/q\,\Sigma\,q}{N\Sigma\,q^2 - \Sigma\,q\,\Sigma\,q}. \quad \ldots\ldots\ldots (6)$$

Data on the right sides of Eqs. 5 and 6 were obtained from modified isochronal tests. Such data are given for eight different gas well tests in Tables A-1 through A-8 in the Appendix.

Hence, a_t is available as a function of time; b usually is chosen as the value corresponding to the last time increment available on the isochronal drawdowns.

Method 1 To Calculate kh, s, and D

Comparing Eq. 2 with Eq. 3 gives

$$a_t = m\left[\log(t/t^*) - 3.23 + 0.869\,s\right], \quad \ldots\ldots\ldots (7)$$

and

$$b = 0.869\,m\,D. \quad \ldots\ldots\ldots\ldots (8)$$

Hence, a plot of a_t vs $\log t$ should yield a straight line of

$$\text{slope} = m = \frac{1{,}632\,\bar{\mu}\bar{Z}\,T}{kh}, \quad \ldots\ldots\ldots\ldots (9)$$

and

$$\text{intercept} = m\left[\log(1/t^*) - 3.23 + 0.869\,s\right]. \quad \ldots (10)$$

Eqs. 9 and 10 may be solved to give kh and s. Because b is assumed independent of time and pressure level, Eq. 8 may be solved for D.

Method 2 to calculate kh, s, and D

Eqs. 2 and 3 may be rewritten as

$$\Delta p^2 = m\left[\log(t/t^*) - 3.23 + 0.869\,s'\right] q, \quad \ldots\ldots (11)$$

where

$$s' = s + D\,q, \quad \ldots\ldots\ldots\ldots (12)$$

and

$$\Delta p^2 = (a_t + bq)\,q. \quad \ldots\ldots\ldots\ldots (13)$$

Comparing Eq. 11 with Eq. 13 gives

$$(a_t + bq) = m\left[\log(t/t^*) - 3.23 + 0.869\,s'\right]. \quad \ldots (14)$$

Hence, a plot of $(a_t + bq)$ vs $\log t$ should yield a straight line. Assuming four different flow rates are used in a modified isochronal test, the semilog plot should yield four straight lines with

$$\left.\begin{aligned} \text{slopes} = m_1 &= \frac{1{,}632\,(\bar{\mu}\bar{Z})_1 T}{(kh)_1} \\ &\vdots \\ m_4 &= \frac{1{,}632\,(\bar{\mu}\bar{Z})_4 T}{(kh)_4} \end{aligned}\right\}, \quad \ldots\ldots (15)$$

and

$$\left.\begin{aligned} \text{intercepts} = m_1\left[\log(1/t_1^*) - 3.23 + 0.869\,s_1'\right] \\ \vdots \\ m_4\left[\log(1/t_4^*) - 3.23 + 0.869\,s_4'\right] \end{aligned}\right\} \ldots (16)$$

A simplifying assumption that is valid for small drawdowns and creates little error for large drawdowns is made in order to calculate kh, s_1' . . . s_4', s, and D.

Assuming

$$(\bar{\mu}\bar{Z})_1 = (\bar{\mu}\bar{Z})_2 = (\bar{\mu}\bar{Z})_3 = (\bar{\mu}\bar{Z})_4 = \bar{\mu}\bar{Z}$$

and

$$(\bar{\mu}\bar{c})_1 = (\bar{\mu}\bar{c})_2 = (\bar{\mu}\bar{c})_3 = (\bar{\mu}\bar{c})_4 = \bar{\mu}\bar{c},$$

it is simple to solve Eqs. 15 and 16. Then,

$$kh = \frac{(kh)_1 + (kh)_2 + (kh)_3 + (kh)_4}{4}. \quad \ldots\ldots\ldots (17)$$

Because Eq. 12 describes the interrelationship of s', s,

and D and because $s_1' \ldots s_4'$ can be obtained from Eq. 16 corresponding to $q_1 \ldots q_4$, respectively, the least-squares method may be used to give

$$s = \frac{\Sigma s' \Sigma q^2 - \Sigma s' q \Sigma q}{N \Sigma q^2 - \Sigma q \Sigma q}, \quad \ldots\ldots\ldots\ldots (18)$$

and

$$D = \frac{N \Sigma s' q - \Sigma s' \Sigma q}{N \Sigma q^2 - \Sigma q \Sigma q}. \quad \ldots\ldots\ldots\ldots (19)$$

These values of kh, s, and D may be substituted in Eq. 7 to give a_t as a function of t and in Eq. 8 to give b.

Estimation of Stabilized Deliverability

Comparing Eq. 1 with Eq. 4 gives

$$a = 2m \left[\log \left(\frac{0.472 r_e}{r_w} \right) + \frac{s}{2.303} \right], \quad \ldots\ldots (20)$$

and

$$b = 0.869 m D. \quad \ldots\ldots\ldots\ldots\ldots\ldots (21)$$

Because kh, s, and D are calculated as described previously and the other parameters on the right side of Eq. 20 are available, a can be calculated; b is available from Methods 1 or 2.

Estimation of Absolute Open Flow (AOF) Potential

From Eq. 1, with $p_{wf} = 0$, derives

$$\text{AOF} = q = \frac{-a + \sqrt{a^2 + 4b\bar{p}_R^2}}{2b}. \quad \ldots\ldots\ldots (22)$$

This equation represents the "stabilized" AOF potential. In many instances, the extended flow period of a modified isochronal test is not continued to pressure stabilization and the value of AOF reported in the test corresponds to an unstabilized value of a, that is, a_t. In such instances, the AOF is calculated by Eq. 22 with a replaced by a_t.

Estimation of Time to Stabilization

The time to stabilization, or the end of transient flow, may be approximated by[4]

$$t_s \approx \frac{948 \phi \bar{\mu} \bar{c} r_e^2}{k}. \quad \ldots\ldots\ldots\ldots\ldots (23)$$

Field Example — Well 2

A typical calculation procedure is illustrated using the well test data given in Table A-2.

The parameters Δp^2, $\Delta p^2/q$, and q^2 are calculated and tabulated for each time increment; t = 1, 2, 4, 6, and 8 hours in Table 1. For each time increment, a_t and b are calculated using Eqs. 5 and 6, respectively. Ignoring the variation in b and selecting the last value calculated gives

b = 119.07 Mpsia²/MMcf/D² (see Table 3, Col. 3).

Since

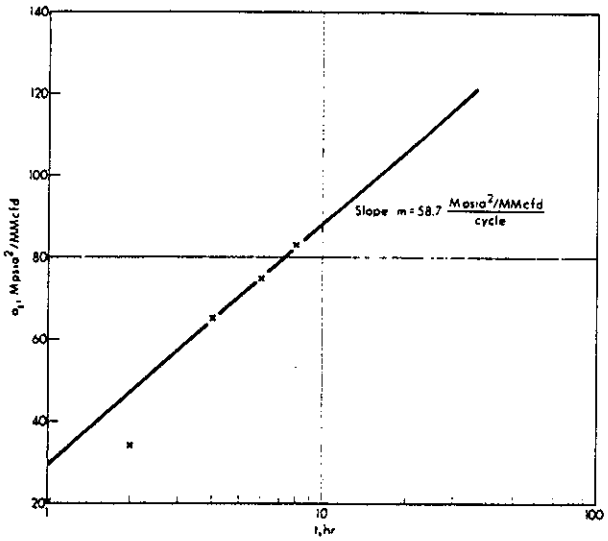

Fig. 1—Plot of a_t vs log t for Gas Well 2.

Δp^2 = 466.42 Mpsia² at 18.5 hours with

q = 1.6052 MMcf/D,

$$a_{18.5} = \frac{\Delta p^2 - b q^2}{q}$$

$$= \frac{466.42 - (119.07)(1.6052)^2}{1.6052}$$

= 99.44 Mpsia²/MMcf/D (see Table 3, Col. 2).

All well tests analyzed in this paper used the Rawlins and Schellhardt deliverability equation.[3] If, however, the LIT flow equation had been used, the test reports would show a stabilized deliverability equation using the above values of $a_{18.5}$ and b, even though the flowing pressure was not stabilized. The time to stabilization (Eq. 23) for one-quarter-section spacing for the well in question is approximately 315 hours (see Table 4, Col. 8). Also, the AOF computed by the LIT flow equation, using the reported extended flow data, is given below from Eq. 22.

AOF = 2.289 MMcf/D (see Table 4, Col. 2).

To estimate reservoir parameters and the actual stabilized deliverability expected for this well, the following procedures are followed.

Method 1

Plot a_t vs log t as shown in Fig. 1. A straight line is drawn through the t = 4-, 6-, and 8-hour points. From this straight line,

slope = m = 58.7 Mpsia²/MMcf/D/cycle

and

intercept = 29.5 Mpsia²/MMcf/D at t = 1 hour.

TABLE 1—CALCULATIONS FOR FIELD EXAMPLE — WELL 2

Flow Rate	q	q^2	t = 1.0 Δp^2	t = 1.0 $\frac{\Delta p^2}{q}$	t = 2.0 Δp^2	t = 2.0 $\frac{\Delta p^2}{q}$	t = 4.0 Δp^2	t = 4.0 $\frac{\Delta p^2}{q}$	t = 6.0 Δp^2	t = 6.0 $\frac{\Delta p^2}{q}$	t = 8.0 Δp^2	t = 8.0 $\frac{\Delta p^2}{q}$
1	0.4746	0.2252	41.01	86.410	46.40	97.767	55.17	116.245	58.91	124.126	62.47	131.627
2	0.8797	0.7739	105.13	119.507	120.75	137.263	156.01	177.345	164.48	186.973	169.11	192.236
3	1.2716	1.6170	207.97	163.550	253.47	199.332	276.34	217.317	309.22	243.174	317.25	249.489
4	1.6589	2.7519	384.61	231.846	403.48	243.221	429.83	259.105	438.51	264.338	445.97	268.835
Σ	4.2848	5.3680	738.72	601.313	824.10	677.583	917.35	770.012	971.12	818.611	994.80	842.187
			a_t = 20.11		a_t = 34.11		a_t = 65.15		a_t = 74.94		a_t = 83.00	
			b = 121.57		b = 126.30		b = 118.89		b = 121.09		b = 119.07	

From Eq. 9,

$kh = 182$ md-ft (see Table 5, Col. 2).

From Eq. 10,

$s = -4.9$ (see Table 5, Col. 3).

From Eq. 8,

$D = 2.32$ MMcf/D^{-1} (see Table 5, Col. 4).

Substituting kh and s in Eq. 20 gives

$$a = 2m\left[\log\left(\frac{0.472 r_e}{r_w}\right) + \frac{(-4.9)}{2.303}\right]$$

Therefore,

$a_{1.320} = 153.96$ (see Table 3, Col. 6)

and

$a_{2.640} = 189.47$ (see Table 3, Col. 7).

Corresponding AOF values can be calculated using Eq. 22:

$\text{AOF}_{1.320} = 2.104$ MMcf/D (see Table 4, Col. 9).

$\text{AOF}_{2.640} = 1.994$ MMcf/D (see Table 4, Col. 12).

These values of AOF are approximately 8 and 15 percent lower than the value of 2.289 MMcf/D computed earlier by using extended flow data reported at 18.5 hours.

Method 2

Calculate $(a_t + bq)$ corresponding to each flow rate and time increment and tabulate as shown in Table 2. Plot $(a_t + bq)$ vs log t as shown in Fig. 2. Four straight lines may be drawn to give

slopes	*intercepts*
$m_1 = 63$ Mpsia^2/MMcf/D/cycle	83
$m_2 = 64$ Mpsia^2/MMcf/D/cycle	130
$m_3 = 65$ Mpsia^2/MMcf/D/cycle	177
$m_4 = 65$ Mpsia^2/MMcf/D/cycle	224.

Therefore,

$$m = \frac{m_1 + m_2 + m_3 + m_4}{4} = 64.$$

From Eq. 15 and 16,

$(kh)_1 = 170$ md-ft and $s_1' = -3.93$,

$(kh)_2 = 167$ md-ft and $s_2' = -3.10$,

$(kh)_3 = 170$ md-ft and $s_3' = -2.21$,

$(kh)_4 = 165$ md-ft and $s_4' = -1.47$.

From Eq. 17,

$$kh = \frac{170 + 167 + 170 + 165}{4} = 167 \text{ md-ft}$$

(see Table 5, Col. 5).

From Eqs. 18 and 19,

$s = -4.9$ (see Table 5, Col. 6)

and

TABLE 2—CALCULATIONS FOR FIELD EXAMPLE — WELL 2

Flow Rate	q	$a_t + bq$				
		$t = 1.0$	$t = 2.0$	$t = 4.0$	$t = 6.0$	$t = 8.0$
1	0.4746	77.81	94.05	121.58	132.41	139.51
2	0.8797	127.06	145.22	169.74	181.46	187.75
3	1.2716	174.70	194.71	216.33	228.92	234.41
4	1.6589	221.78	243.63	262.38	275.82	280.53

$D = 2.10$ MMcf/D^{-1} (see Table 5, Col. 7).

From Eq. 7,

$a_{18.5} = 111.07$ Mpsia^2/MMcf/D (see Table 3, Col. 8).

From Eq. 8,

$b = 116.69$ Mpsia^2/MMcf/D^2 (see Table 3, Col. 9).

Stabilized values of a and AOF can be calculated as shown for Method 1.

Normalized Drawdown

The values of $\Delta p^2/q$ for each flow rate may be plotted vs log t as shown in Fig. 3. Four straight lines may be drawn to give four slopes and intercepts from which kh, s, and D may be calculated by the procedure illustrated above (Method 2). Note that the data scatter observed in Fig. 3 disappears when the data are plotted according to Method 2 (Fig. 2):

$kh = 233$ md-ft (see Table 5, Col. 11),

$s = -5.2$ (see Table 5, Col. 12),

$D = 3.60$ MMcf/D^{-1} (see Table 5, Col. 13).

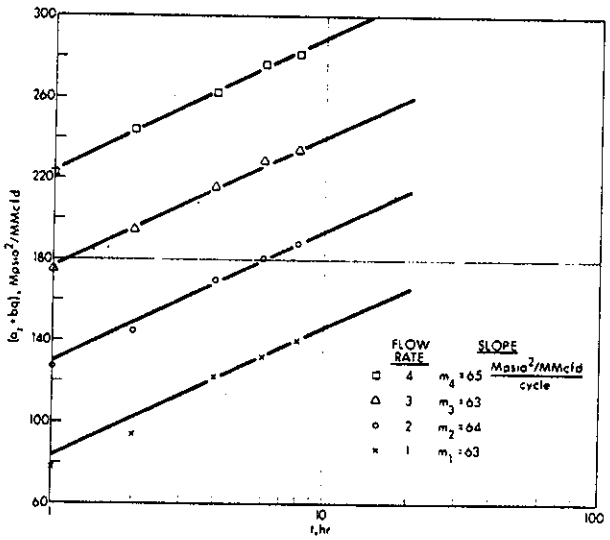

Fig. 2—Plot of $(a_t + bq)$ vs log t for Gas Well 2.

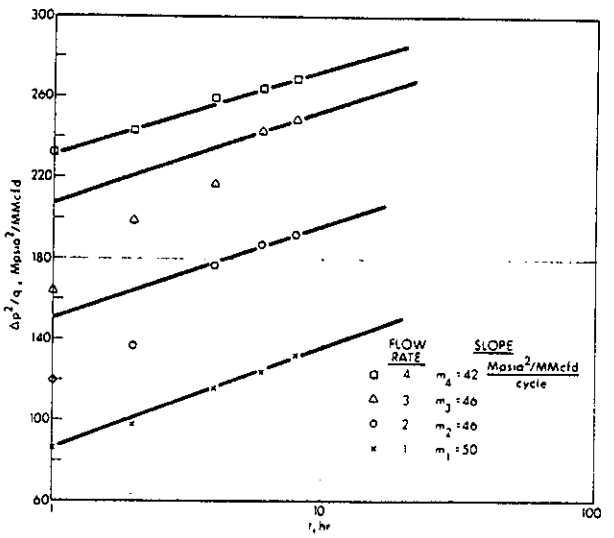

Fig. 3—Plot of $\Delta p^2/q$ vs log t for Gas Well 2.

Application of Proposed Methods to Field Cases

Tables A-1 through A-8 list all the pertinent, modified isochronal test data for eight wells. These tests were selected to cover a fairly wide range of deliverability, AOF, and permeability characteristics. Test selection was limited to tests in which the pressure buildup during the shut-in periods closely approached the initial pressure. Although no rigorous identification of the geological characteristics of each of the reservoirs was attempted, fairly uniform and well behaved sandstone and carbonate reservoirs were selected. Intuitively, it was felt that this simple technique might not predict the behavior of severely faulted, nonuniform, or stratified reservoirs. However, the test-data selection procedure is not considered critical because one primary objective is to predict, with some degree of confidence, the stabilized behavior of reservoirs for which stabilized test data are not available. Simply, this is a practical salvage technique intended to use large amounts of unstabilized data currently available. This does not imply that, within certain limitations, the technique may not be used to design tests that do not require a stabilized flow period.

The example calculation illustrates all procedures necessary to compile Tables 3, 4, and 5.

Table 3 shows the computed values of a_t and b with the usual modified isochronal technique. The value of a_t may or may not represent stabilized flow conditions. The predicted values of a_t for the same extended flow period with Methods 1 and 2 also are shown. This table also indicates the predicted stabilized values of a for quarter- and one-section spacing.

Table 4 lists the values of AOF, calculated by the modified isochronal analysis, Methods 1 and 2. Again, this value corresponds to the duration of the actual extended flow period. The percent of error between the measured and predicted values is shown also. The results of Methods 1 and 2 are used to predict the stabilized AOF for quarter- and one-section spacing.

Table 5 compares the values of kh, s, and D calculated by Methods 1 and 2 (normalized drawdown with buildup analysis). The buildup results were taken directly from the test reports. Although some differences exist between the values obtained with different methods, the predictions with all methods generally are consistent.

Results presented indicate that the SIT analyses predict the stabilized deliverability potential of a well when no data are available for stabilized flow conditions. In many cases, it is important to predict the stabilized deliverability potential of wells in a fully developed reservoir using limited data from a few initial wells in the reservoir,

TABLE 3—COMPARISON OF DELIVERABILITY PARAMETERS OBTAINED BY DIFFERENT METHODS

Well	Modified Isochronal Analysis		Simplified Analysis Method 1				Simplified Analysis Method 2			
	a_t	b	a_t	b	$a_{1,320}$	$a_{2,640}$	a_t	b	$a_{1,320}$	$a_{2,640}$
1	56.69	20.68	66.64	20.68	79.20	91.85	56.98	32.43	65.55	76.25
2	99.44	119.07	104.26	119.07	153.96	189.47	111.07	116.69	167.01	205.53
3	107.07	44.29	108.26	44.29	105.02	109.65	92.24	63.07	89.04	92.83
4	39.15	10.23	43.30	10.23	40.53	45.29	20.69	16.02	24.79	27.79
5	91.94	16.70	96.30	16.70	95.12	101.14	96.19	15.90	93.92	96.44
6	107.72	24.47	103.17	24.47	146.15	182.00	79.20	15.01	145.76	193.00
7	1,158.69	68.79	1,154.55	68.79	971.58	1,158.16	1,220.52	64.50	1,040.36	1,235.77
8	30.15	0.40	24.19	0.40	25.08	31.34	25.46	0.40	26.40	33.51

TABLE 4—COMPARISON OF ABSOLUTE OPEN FLOW POTENTIALS OBTAINED BY DIFFERENT METHODS

Well	Modified Isochronal Analysis		Simplified Analysis				Predicted Stabilized Absolute Open Flow (AOF) Potential					
			Method 1		Method 2		$AOF_{1,320}$			$AOF_{2,640}$		
	AOF,	t	AOF,	Error (percent)	AOF,	Error (percent)	t_t	Method 1	Method 2	t_t	Method 1	Method 2
1	2.128	40.0	1.988	−6.6	1.838	−13.6	420	1.831	1.751	1,680	1.690	1.651
2	2.289	18.5	2.271	−0.8	2.267	− 1.0	315	2.104	2.078	1,260	1.994	1.960
3	2.391	24.0	2.382	−0.4	2.202	− 7.9	24	2.406	2.222	96	2.371	2.119
4	5.340	24.0	5.183	−2.9	4.974	− 6.9	24	5.281	4.862	96	5.115	4.782
5	6.847	7.0	6.755	−1.3	6.874	0.4	10	6.780	6.924	40	6.654	6.869
6	17.296	16.0	17.379	0.5	22.237	28.6	185	16.615	20.351	740	16.007	19.128
7	20.005	120.0	20.026	0.1	20.131	0.6	120	20.992	21.111	480	20.008	20.051
8	184.167	72.0	190.474	3.4	189.109	2.7	85	189.516	188.106	340	182.937	180.719

TABLE 5—COMPARISON OF RESERVOIR PARAMETERS OBTAINED BY DIFFERENT METHODS

Well	Simplified Analysis						Buildup Analysis*			Normalized Drawdown Analysis		
	Method 1			Method 2								
	kh	s	D	kh	s	D	kh	s'	q	kh	s	D
1	482	−3.2	1.13	569	−3.3	1.99	408	−2.4	1.096	550	−3.0	1.54
2	182	−4.9	2.32	167	−4.9	2.10	147	−2.7	1.580	233	−5.2	3.60
3	1,665	7.6	6.62	2,035	8.2	11.53	1,780	13.4	1.326	2,728	14.7	13.50
4	1,623	−2.2	1.49	2,565	−2.4	3.69	2,253	6.1	2.665	2,617	−8.6	6.72
5	1,329	2.4	1.92	3,165	17.2	4.36	1,110	—	—	2,769	−18.9	14.06
6	224	−5.9	0.48	169	−6.6	0.22	—	—	—	169	−6.4	0.18
7	123	−4.5	0.26	118	−4.4	0.23	455	—	—	112	−4.5	0.21
8	2,255	−4.0	0.046	1,990	−5.2	0.039	2,392	−0.71	7.366	1,922	−5.2	0.038

*Results for buildup analysis are in the actual test reports. No attempt has been made to evaluate any buildup data.

which this paper explains.

The SIT analyses work well for most cases considered. No attempt was made to determine the range of applicability of the recommended method. It is obvious that a simple approach has its limitations as will no doubt become apparent. Complete data on eight wells are presented in the Appendix to provide a data base for testing other methods.

Conclusions and Recommendations

The proposed methods, tested with field data included in the paper, provide the following.

1. A prediction of stabilized deliverability potential from data gathered during the isochronal periods (usually 4.0 hours each) of modified isochronal tests.
2. An estimate of permeability-thickness (kh), skin factor (s), and the inertial-turbulent flow factor (D).
3. A reduction in testing time and a saving in cost and flaring of gas in the performance of gas well-deliverability tests.

Method 1 is recommended over Method 2 because it is simpler to use and provides better results in most cases. However, under certain circumstances Method 2 may yield better results. It is recommended also that the proposed methods be tested with actual data on gas wells from other regions.

Nomenclature

a = stabilized deliverability parameter, Mpsia²/MMcf/D
a_t = transient deliverability parameter, Mpsia²/MMcf/D
AOF = absolute open flow potential, MMcf/D
AOF_t = AOF corresponding to extended flow period of t hours' duration
$AOF_{1.320}$ = stabilized AOF for quarter-section spacing
$AOF_{2.640}$ = stabilized AOF for one-section spacing
b = transient and stabilized deliverability parameter, Mpsia²/MMcf/D²
$\bar{c}$ = average compressibility, psia⁻¹
D = inertial-turbulent flow factor, MMcf/D⁻¹
h = pay thickness, ft
k = effective permeability, md
m = slope of semilog straight line
N = number of data points in curve fit
$\bar{p}_R$ = average reservoir pressure, psia
p_{wf} = flowing bottom-hole pressure, psia
q = flow rate, MMcf/D at 14.65 psia, 60°F
r_e = reservoir radius, ft
r_w = well radius, ft
s = skin factor
s' = apparent skin factor
t = flowing time, hours
$t^* = \phi \bar{\mu} \bar{c} r_w^2/k$, hours
t_s = time to stabilization, hours
ϕ = gas-filled porosity
$\bar{\mu}$ = average viscosity, cp

Original manuscript received in Society of Petroleum Engineers office Aug. 2, 1976. Paper accepted for publication April 22, 1977. Revised manuscript received Nov. 21, 1977. Paper (SPE 6134) was presented at the SPE-AIME 51st Annual Fall Technical Conference and Exhibition, held in New Orleans, Oct. 3-6, 1976.

This paper will be included in the 1978 *Transactions* volume.

Acknowledgments

The permission of the Alberta Energy Resources Conservation Board to publish this paper is appreciated sincerely.

References

1. Cullender, M. H.: "The Isochronal Performance Method of Determining the Flow Characteristics of Wells," *Trans.*, AIME (1955) **204**, 137-142.
2. Katz, D. L., Cornell, D., Kobayashi, R., Poettman, F. H., Vary, J. A., Elenbaas, J. R., and Weinaug, C. F.: *Handbook of Natural Gas Engineering*, McGraw-Hill Book Co., Inc., New York (1959) 448.
3. Rawlins, E. L. and Schellhardt, M. A.: *Backpressure Data on Natural Gas Wells and their Application to Production Practices*, U.S. Bureau of Mines, Monograph 7 (1936).
4. *Theory and Practice of the Testing of Gas Wells*, 3rd ed., Alberta Energy Resources Conservation Board, Alberta, Canada (1975).
5. Aziz, K., Mattar, L., Ko, S., and Brar, G.S.: "Use of Pressure, Pressure-Squared or Pseudo-Pressure in the Analysis of Transient Pressure Drawdown Data from Gas Wells," *J. Can. Pet. Tech.* (April-June 1976) No. 2, 15, 58-65.

APPENDIX

Modified Isochronal Test Data for Eight Gas Wells

TABLE A-1—MODIFIED ISOCHRONAL TEST DATA — WELL 1

h = 23 ft
r_w = 0.33 ft
ϕ = 0.17
T = 544°R
$\bar{p}_R$ = 462.9 psia
$\bar{\mu}$ = 0.012 cp
$\bar{Z}$ = 0.95
$\bar{c}$ = 0.00263 psia⁻¹

	p_{ws}			
0	462.9	464.1	461.4	458.5
	p_{wf}			
t	q = 0.248	q = 0.603	q = 0.864	q = 1.135
0.5	456.3	432.6	415.8	392.1
1.0	453.1	429.6	407.3	382.1
2.0	451.6	425.6	401.3	375.0
3.0	450.8	423.4	397.1	371.3
4.0	449.8	422.6	394.7	367.6

Extended flow: p_{wf} = 356.8 psia, t = 40 hours, q = 1.096 MMcf/D

TABLE A-2—MODIFIED ISOCHRONAL TEST DATA — WELL 2

h = 12 ft
r_w = 0.23 ft
ϕ = 0.23
T = 582°R
$\bar{p}_R$ = 922.6 psia
$\bar{\mu}$ = 0.0116 cp
$\bar{Z}$ = 0.972
$\bar{c}$ = 0.00109 psia⁻¹

	p_{ws}			
0	922.6	921.9	919.9	917.6
	p_{wf}			
t	q = 0.4746	q = 0.8797	q = 1.2716	q = 1.6589
1.0	900.1	863.0	798.9	676.3
2.0	897.1	853.9	769.9	662.2
4.0	892.2	833.0	754.9	642.0
6.0	890.1	827.9	732.8	635.2
8.0	888.1	825.1	727.3	629.3

Extended flow: p_{wf} = 620.3 psia, t = 18.5 hours, q = 1.6052 MMcf/D

TABLE A-3—MODIFIED ISOCHRONAL TEST DATA — WELL 3

h = 6.5 ft
r_w = 0.1875 ft
ϕ = 0.172
T = 540°R

$\bar{p}_R$ = 713.5 psia
$\bar{\mu}$ = 0.015 md
$\bar{Z}$ = 0.97
$\bar{c}$ = 0.0014 psia^{-1}

	p_{ws}			
0	713.5	713.5	713.0	712.5
	p_{wf}			
t	q = 0.558	q = 0.750	q = 0.923	q = 1.275
0.5	663.2	642.3	620.5	555.0
1.0	662.7	641.8	615.4	554.4
1.5	662.2	641.5	614.9	553.9
2.0	661.7	641.2	614.4	553.4

Extended flow: p_{wf} = 537.8 psia
t = 24 hours
q = 1.326 MMcf/D

TABLE A-4—MODIFIED ISOCHRONAL TEST DATA — WELL 4

h = 6 ft
r_w = 0.1875 ft
ϕ = 0.19
T = 540°R

$\bar{p}_R$ = 706.6 psia
$\bar{\mu}$ = 0.015 psia
$\bar{Z}$ = 0.97
$\bar{c}$ = 0.0015 psia^{-1}

	p_{ws}			
0	706.6	706.6	703.5	701.2
	p_{wf}			
t	q = 1.520	q = 2.041	q = 2.688	q = 3.122
0.5	655.6	624.5	578.5	541.7
1.0	653.6	620.7	573.9	537.8
1.5	652.1	619.9	572.3	536.3
2.0	651.3	619.1	570.8	534.7

Extended flow: p_{wf} = 567.7 psia
t = 24 hours
q = 2.665 MMcf/D

TABLE A-5—MODIFIED ISOCHRONAL TEST DATA— WELL 5

h = 4 ft
r_w = 0.12 ft
ϕ = 0.19
T = 602°R

$\bar{p}_R$ = 1,188.5 psia
$\bar{\mu}$ = 0.015 cp
$\bar{Z}$ = 0.902
$\bar{c}$ = 0.00088 psia^{-1}

	p_{ws}			
0	1,188.5	1,187.1	1,186.4	1,186.0
	p_{wf}			
t	q = 2.104	q = 3.653	q = 4.026	q = 5.079
0.5	1,072.9	954.0	887.2	721.1
1.0	1,072.6	946.9	883.5	715.5
1.5	1,071.4	944.4	882.5	713.5
2.0	1,070.6	944.2	882.3	713.2

Extended flow: p_{wf} = 738.0 psia
t = 7 hours
q = 4.964 MMcf/D

TABLE A-6—MOFIFIED ISOCHRONAL TEST DATA— WELL 6

h = 56 ft
r_w = 0.10 ft
ϕ = 0.083
T = 642°R

$\bar{p}_R$ = 3,030.4 psia
$\bar{\mu}$ = 0.15 cp
$\bar{Z}$ = 0.845
$\bar{c}$ = 0.00036 psia^{-1}

	p_{ws}			
0	3,030.4	3,030.4	3,030.2	3,027.7
	p_{wf}			
T	q = 4.194	q = 6.444	q = 8.324	q = 9.812
0.5	2,952.1	2,858.9	2,741.8	2,610.3
1.0	2,936.1	2,837.4	2,705.6	2,570.5
2.0	2,922.1	2,808.4	2,644.4	2,525.8
3.0	2,915.0	2,789.6	2,641.2	2,498.8
4.0	2,911.1	2,783.9	2,630.9	2,484.1

Extended flow: p_{wf} = 2,493.0 psia
t = 16 hours
q = 8.063 MMcf/D

TABLE A-7—MODIFIED ISOCHRONAL TEST DATA— WELL 7

h = 35 ft
r_w = 0.1875 ft
ϕ = 0.08
T = 715°R

$\bar{p}_R$ = 7,121.0 psia
$\bar{\mu}$ = 0.0286 cp
$\bar{Z}$ = 1.145
$\bar{c}$ = 0.000074 psia^{-1}

	p_{ws}		
0	7,121.0	7,101.0	7,085.0
	p_{wf}		
t	q = 8.584	q = 9.879	q = 12.867
1.0	6,612.0	6,291.0	5,939.0
2.0	6,447.0	6,158.0	5,658.0
3.0	6,339.0	6,095.0	5,535.0
4.0	6,296.0	6,057.0	5,468.0
5.0	6,270.0	6,026.0	5,420.0
6.0	6,250.0	6,006.0	5,388.0
7.0	6,238.0	5,989.0	5,360.0
8.0	6,226.0	5,975.0	5,338.0
9.0	6,216.0	5,965.0	5,319.0

Extended flow: p_{wf} = 5,845.0 psia
t = 120 hours
q = 9.225 MMcf/D

TABLE A-8—MODIFIED ISOCHRONAL TEST DATA— WELL 8

h = 454 ft
r_w = 0.2615 ft
ϕ = 0.675
T = 718°R

$\bar{p}_R$ = 4,372.6 psia
$\bar{\mu}$ = 0.023 cp
$\bar{Z}$ = 0.87
$\bar{c}$ = 0.000169 psia^{-1}

	p_{ws}			
0	4,372.6	4,356.0	4,344.3	4,343.6
	p_{wf}			
t	q = 31.612	q = 44.313	q = 56.287	q = 70.265
1.0	4,296.6	4,239.2	4,143.6	4,053.5
2.0	4,283.0	4,220.1	4,113.9	4,011.7
3.0	4,274.1	4,206.5	4,111.8	3,994.6
4.0	4,266.8	4,199.3	4,103.3	3,973.3
5.0	4,262.5	4,192.0	4,097.0	3,959.6
6.0	4,258.3	4,190.4	4,093.5	3,951.9

Extended flow, p_{wf} = 3,794.0 psia
t = 72 hours
q = 77.346 MMcf/D

TABLE A-9—BUILDUP TEST DATA — WELLS 1 THROUGH 4

Well 1		Well 2		Well 3		Well 4	
t = 78 hours		t = 158 hours		t = 72.25 hours		t = 44.5 hours	
q = 1.096 MMcf/D		q = 1.58 MMcf/D		q = 1.325 MMcf/D		q = 2.665 MMcf/D	
t	p_{ws}	t	p_{ws}	t	p_{ws}	t	p_{ws}
0.5	418.8	0.5	847.0	0.7	697.2	0.5	686.0
1.0	431.1	1.0	863.9*	2.0	702.2	1.0	688.3
1.5	436.7	1.5	876.0	4.0	704.8	1.5	690.6
2.0	441.3	2.0	884.8	8.0	706.4	2.0	691.4
3.0	447.3	2.5	891.9	12.0	707.9	2.5	692.1
4.0	450.1	3.5	901.0*	16.0	708.9	4.5	694.4
8.0	458.0*	4.5	905.2	20.0	709.4	6.5	696.7
14.0	461.7	6.5	909.0	24.0	709.7	8.5	697.5
22.0	464.2	8.5	914.0	28.0	709.9	20.5	701.3
30.0	465.0	10.5	916.5	40.0	710.4*	32.5	702.1*
38.0	465.6	14.5	918.1	52.0	710.9	56.5	703.6
46.0	466.0	18.5	919.6	64.0	711.2	80.5	704.4
54.0	466.2	22.5	920.7	76.0	711.5	94.5	704.4*
62.0	466.2	26.5	920.7	96.2	712.0*		
70.0	466.4	30.5	920.8				
82.0	466.4	34.5	920.8				
89.0	466.4*	42.5	921.0				
		50.5	921.0				
		58.5	921.2				
		66.5	921.2				
		74.5	921.2				
		82.5	921.2				
		90.5	921.2				

Data points between * *included as the straight-line portion on a semilog buildup plot.

TABLE A-10—BUILDUP TEST DATA — WELLS 5 THROUGH 8

Well 5		Well 6		Well 7		Well 8	
t = 72.0 hours		t = 20.0 hours		t = 120.0 hours		t = 18,763.5 hours	
q = 4.920 MMcf/D		q = 7.650 MMcf/D		q = 9.38 MMcf/D		q = 77.346 MMcf/D	
t	p_{ws}	t	p_{ws}	t	p_{ws}	t	p_{ws}
0.5	1,133.0	0.5	2,873.7	1.0	6,541.0	1.0	4,179.7
1.0	1,148.0	1.0	2,915.4	2.0	6,704.0	2.0	4,224.1
1.5	1,153.2	2.0	2,975.9	4.0	6,828.0	3.0	4,248.2
2.0	1,155.4	3.0	3,002.2	8.0	6,938.0	5.0	4,280.5
3.0	1,158.1	4.0	3,014.3	12.0	6,990.0	7.0	4,299.4*
5.0	1,161.0	6.0	3,018.9	16.0	7,019.0	9.0	4,308.9
7.0	1,162.8	8.0	3,020.5	20.0	7,039.0	11.0	4,317.9
11.0	1,165.2	12.0	3,022.6	24.0	7,052.0	15.0	4,329.5*
15.0	1,166.9	16.0	3,023.0	35.0	7,076.0	19.0	4,334.7
23.0	1,169.4	20.0	3,023.5	41.0	7,081.0	23.0	4,339.0
31.0	1,171.0*	32.0	3,024.4	44.0	7,085.0	27.0	4,342.9
43.0	1,173.2	44.0	3,025.3	72.0	7,092.0	33.0	4,345.9
55.0	1,174.8	56.0	3,026.2	84.0	7,092.9	37.3	4,346.8
67.0	1,175.8	68.0	3,026.9	96.0	7,094.2		
74.0	1,178.2	80.0	3,027.4	108.0	7,097.7		
79.0	1,178.2	104.0	3,028.5	120.0	7,103.7*		
103.0	1,180.2	110.5	3,028.8	132.0	7,106.3		
127.0	1,181.1*	117.5	3,028.8	144.0	7,107.2		
151.0	1,183.2			156.0	7,108.1		
175.0	1,184.0			168.0	7,110.7		
199.0	1,184.8			192.0	7,110.7		
223.0	1,186.7			216.0	6,110.7		
244.0	1,188.0			240.0	7,111.5*		

Data points between* *included as the straight-line portion on a semilog buildup plot.

JPT

Discussion of Analysis of Modified Isochronal Tests To Predict the Stabilized Deliverability Potential of Gas Wells Without Using Stabilized Flow Data

Fred H. Poettmann, SPE, Colorado School of Mines

The graduate course taught at the Colorado School of Mines, "Natural Gas Engineering," is a comprehensive applied problem course. The subjects include natural gas and hydrate phase behavior, flow and metering of gas, both single and multiphase flow, reservoir behavior (including reserve calculations and gas well testing), and gas storage (including LNG and underground storage of gas). The subjects are illustrated with problems that either define a principle or demonstrate a comprehensive design calculation procedure. The literature is used extensively. Classic papers and contemporary literature are reviewed and studied in detail for the information they contain and for testing and calculation procedures they offer. The literature is researched for actual field data used in the problems.

One such paper, G.S. Brar and K. Aziz's "Analysis of Modified Isochronal Tests To Predict the Stabilized Deliverability Potential of Gas Wells Without Using Stabilized Flow Data" (Feb. 1978 *JPT*, Pages 297–304),[1] is studied in detail.

The use of isochronal or modified isochronal testing procedures for slow-stabilizing (low-permeability) gas wells is a well-established practice in the gas industry. In slowly stabilizing gas wells, the determination of the stabilized flow behavior by field testing can be extremely time-consuming and wasteful of gas. Consequently, much has been published in the literature on the calculation of the stabilized flow behavior of gas wells from transient test data and from the isochronal testing of a gas well.[1-5]

We discuss a method that offers some distinct advantages and is a shorter procedure than Brar and Aziz's[1] Method 1. (Both methods produce identical answers.) It is a method for rapidly estimating the stabilized deliverability behavior of a gas well from isochronal test data. It does not depend on the calculation of the skin factor, s, or non-Darcy flow constant, D, and does not require the use of the wellbore radius, r_w, to predict the stabilized flow behavior of the well.

The deliverability of a gas well can be described by Rawlins and Schellhardt's well-known backpressure equation, which is still widely used by the gas industry in the U.S., or by the more general quadratic form of the deliverability equation known as the Forchheimer equation.[2,6] The quadratic equation can be expressed in terms of pressure, pressure squared, or real-gas pseudopressure.[2] For illustration and comparison with data available in the literature, the pressure-squared form of the quadratic equation will be used, although the procedure applies equally well to all forms [i.e., p, $m(p)$, where $m(p)$ is the real gas pseudopressure] of the equation.

The equation is

$$\bar{p}_R^{\,2}-p_{wf}^2=aq+bq^2. \quad \text{(D-1)}$$

The coefficient b is assumed to remain constant with time for both the transient or isochronal and pseudosteady-state conditions. The coefficient a is a linear function of the logarithm of time during the transient or isochronal flow period and becomes constant once stabilized or pseudosteady-state flow conditions prevail. Thus, by establishing the relationship of a as a function of the log of time from short-time isochronal tests and then determining the time to stabilization or end of transient flow, one can calculate the stabilized value of a.

The coefficients a and b can be expressed as follows. For transient flow,

$$a=\frac{1{,}422\bar{\mu}\bar{Z}T}{k_g h}\left[\ln\left(\frac{kt}{1{,}688\phi\bar{\mu}\bar{c}_t r_w^2}\right)^{1/2}+s\right]. \quad \text{(D-2)}$$

For pseudosteady-state flow,

$$a=\frac{1{,}422\bar{\mu}\bar{Z}T}{k_g h}\left(\ln\frac{0.472r_e}{r_w}+s\right). \quad \text{(D-3)}$$

For both pseudosteady-state and transient flow conditions,

$$b=\frac{1{,}422\bar{\mu}\bar{Z}TD}{hk_g}, \quad \text{(D-4)}$$

where $\bar{Z}$ is the compressibility factor.

A number of procedures are described in the literature for calculating the stabilized value of a.[1-3] They all involve the determination of the permeability-thickness product, kh, Darcy skin, s, and the non-Darcy flow constant, D, from transient test data. These parameters, along with the appropriate physical properties of the reservoir rock and gas and other well data, are substituted into the expressions for the stabilized value of a and b (Eqs. D-3 and D-4, respectively) to determine the equation for the stabilized flow behavior of the well.

Because of the determination of the many variables involved, the resulting expression for stabilized flow could be in considerable error. It is not uncommon for kh, s, and D to vary dramatically depending on the method of calculation and assumptions made.[1]

This procedure minimizes the chances for error because it involves the determination of a as a function of log t directly from modified isochronal test data.

By equating Eqs. D-2 and D-3 and solving for t, one obtains an expression for the time at which the values of a of Eqs. D-2 and D-3 become the same. We will refer to this time as "pseudostabilization" time, t_{ps}. Thus

$$t_{ps} = \frac{376\phi\bar{\mu}\bar{c}_t r_e^2}{k_g}. \quad \ldots\ldots\ldots\ldots\ldots\ldots\ldots\ldots (D\text{-}5)$$

This is the time that is used to establish the stabilized value of a obtained from the modified isochronal test data. It should be used only for this calculation procedure and should not be confused with the well-known relationship for calculating stabilization time:

$$t_s = \frac{948\phi\bar{\mu}\bar{c}_t r_e^2}{k_g}. \quad \ldots\ldots\ldots\ldots\ldots\ldots\ldots\ldots (D\text{-}6)$$

Calculation Procedure

1. At least three or four isochronal or modified isochronal tests should be conducted.
2. Plot $(\bar{p}_R^2 - p_{wf}^2)/q$ vs. q on coordinate paper for each time period. By the least-squares method applied to Eq. D-1, determine a and b for each time period.
3. Plot a vs. log t. Determine by least-squares fit the intercept and slope for the straight-line equation of a as a function of log t.

TABLE D-1—BRAR AND AZIZ WELL 2 CALCULATED VALUES OF a AND b[1]

Time (hours)	a	b
4	65.15	118.89
6	74.94	121.09
8	83.00	119.07

Average value of b = 119.68.

TABLE D-2—WELL TEST DATA

r_e, ft	
160-acre spacing	1,320
640-acre spacing	2,640
ϕ	0.23
$\bar{T}$, °R	582
$\bar{\mu}$, cp	0.0116
$\bar{c}_t$, psia^{-1}	0.00109
h, ft	12
k_g,* md	15.17*
$\bar{Z}$	0.972
t_{ps160}, hours	125.62
t_{ps640}, hours	502.47

*The value of k_g can be estimated either from core analysis using a weighted-average value while taking into account water saturation effects or, preferably, from transient test data. The value of k_g in this example was calculated from isochronal test data in Ref. 2.

TABLE D-3—BRAR AND AZIZ CALCULATED a VALUES[1]

Spacing (acres)	Method 1	Method 2	This Paper
160	154	167	153
640	189	206	189

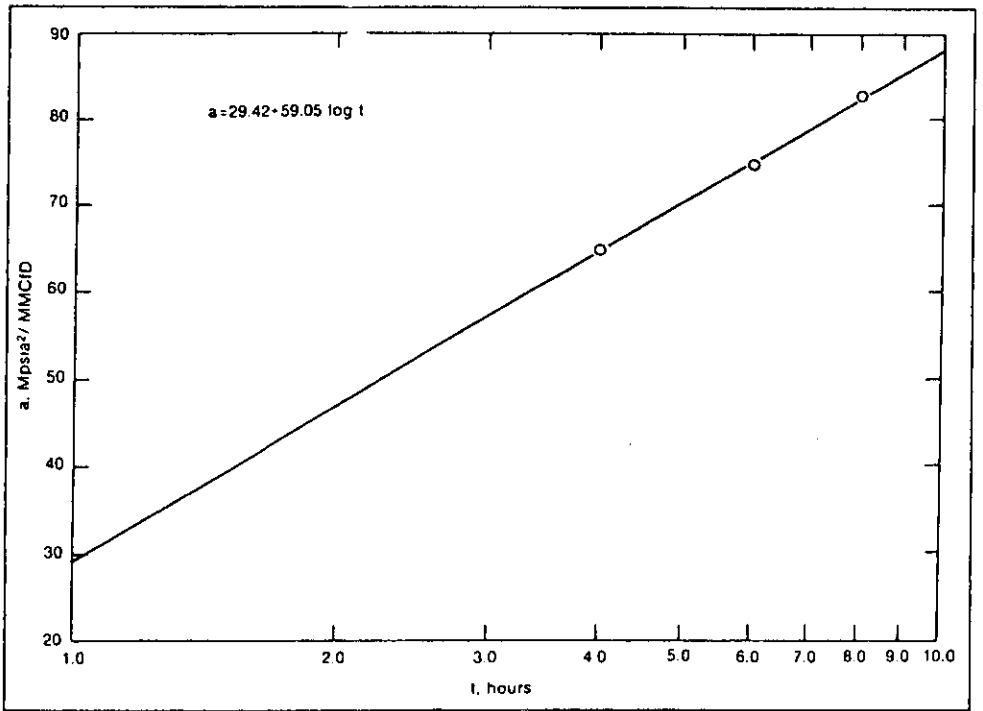

Fig. D-1—Plot of a vs. log t.

4. Calculate pseudostabilization time from Eq. D-5.

5. From the pseudostabilization time calculated in Step 4, determine the value of a from the relationship established in Step 3. This is the stabilized value of a.

Example Calculation. This calculation uses well test data from Brar and Aziz's paper. Values of a and b calculated by Brar and Aziz for Well 2 are listed in Table D-1.

Plot a vs. log t (Fig. D-1) and determine the slope and intercept using least-squares fit. The coefficient of determination is 0.99825, the intercept is 29.42, and the slope is 59.05.

The equation of a as a function of log t is

$$a=29.42+59.05 \log t. \quad \ldots\ldots\ldots\ldots\ldots\ldots (D\text{-}7)$$

Determine the stabilized value of a for 160- and 640-acre [648×10^3- and 2.6×10^6-m^2] spacing by substituting pseudostabilization time, calculated from Eq. D-5, into Eq. D-7. Well data for this calculation are listed in Table D-2.

By substituting these values into Eq. D-7, we obtain the stabilized values of a: $a_{160}=153.37$ and $a_{640}=188.92$. The stabilized deliverability equations for 160- and 640-acre [648×10^3- and 2.6×10^6-m^2] spacing, respectively, are

$$\bar{p}_R^2-p_{wf}^2=153.37q+119.68q^2 \quad \ldots\ldots\ldots\ldots (D\text{-}8)$$

and

$$\bar{p}_R^2-p_{wf}^2=188.92q+119.68q^2. \quad \ldots\ldots\ldots\ldots (D\text{-}9)$$

Brar and Aziz[1] calculated values of a for the same well using two methods for calculating kh, s, and D and the well and reservoir data in Table D-2. Comparison of the results is shown in Table D-3.

Method 1 of Brar and Aziz should give identical results with the method presented above because both methods use the linear expression of a vs. log t for transient flow to determine the stabilized value of a. Brar and Aziz use the slope and intercept of Eq. D-2 to calculate reservoir parameters that are then substituted into the stabilized equation for a (Eq. D-3). The method presented in this paper states that at the end of the transient flow and the start of pseudosteady-state flow, the transient value of a and stabilized value of a become equal. Thus, by equating Eqs. D-2 and D-3, one can calculate a pseudostabilization time that can be substituted into the linear equation of a vs. log t to give the stabilized value of a.

Conclusions

A shorter method than that published by Brar and Aziz[1] is described for rapid estimation of the stabilized deliverability behavior of a gas well from isochronal test data. The method is potentially more accurate than other calculation procedures because it relies primarily on the test data to determine the stabilized performance behavior. It does not depend on calculation of skin factor, s, or non-Darcy flow constant, D, and minimizes the use of other well and reservoir parameters, such as r_w, to predict the stabilized flow behavior.

Acknowledgment

We thank Hossein Kazemi for his advice and review of this procedure.

References

1. Brar, G.S. and Aziz, K.: "Analysis of Modified Isochronal Tests To Predict the Stabilized Deliverability Potential of Gas Wells Without Using Stabilized Flow Data," *JPT* (Feb. 1978) 297–304; *Trans.*, AIME, **265**.
2. *Theory and Practice of the Testing of Gas Wells*, third edition, Alberta Energy Resources Conservation Board, Calgary (1975).
3. Odeh, A.S., Moreland, E.E., and Schueler, S.: "Characterization of a Gas Well From One Flow Test Sequence," *JPT* (Dec. 1975) 1500–04; *Trans.*, AIME, **259**.
4. Ramey, H.J. Jr.: "Non-Darcy Flow and Wellbore Storage Effects in Pressure Buildup and Drawdown of Gas Wells," *JPT* (Feb. 1965) 223–33; *Trans.*, AIME, **234**.
5. Poettmann, F.H. and Schilson, R.E.: "Calculations of the Stabilized Performance Coefficient of Low Permeability Natural Gas Wells," *JPT* (Sept. 1959) 240–46; *Trans.*, AIME, **216**.
6. Rawlins, E.L. and Schellhardt, M.A.: *Backpressure Data on Natural Gas Wells and Their Application to Production Practices*, Monograph 7, U.S. Bureau of Mines, Washington, DC (1936).

SI Metric Conversion Factors

acre	×	4.046 873	E+03	= m^2
cp	×	1.0*	E−03	= Pa·s
ft	×	3.048*	E−01	= m
psi^{-1}	×	1.450 377	E−01	= kPa^{-1}
°R		°R/1.8		= K

*Conversion factor is exact.

JPT

(SPE 12933)

Authors' Reply to Discussion of The Analysis of Modified Isochronal Tests To Predict the Stabilized Deliverability Potential of Gas Wells Without Using Stabilized Flow

G.S. Brar, SPE, T. Fekete and Assocs. Consultants Ltd.
L. Mattar, SPE, T. Fekete and Assocs. Consultants Ltd.

In his discussion of the Brar and Aziz paper,[1] Poettmann[2] introduces a simple idea for calculating the stabilized flow potential of a gas well from isochronal data. He introduces the concept of a time to "pseudostabilization, t_{ps}," which is different from the time to stabilization known as t_s or t_{pss} (time to pseudosteady state).[4] Poettmann's method of calculation is straightforward, simple, and apparently correct. When viewed from the perspective of the time to stabilization (as traditionally defined), however, this method appeared to be contradictory and confusing, and yet hard to refute. After considerable analysis and comparison of the various definitions of stabilization, we wish to present a reply to Poettmann's discussion. We shall first address some specific ideas discussed by Poettmann and then expound on his main idea.

Poettmann's method does not involve the direct calculation of permeability, k, or skin effect, s. In fact, in his example and footnote, he used the value of k from Brar and Aziz's paper.[1] In reality, both k and s could have been obtained from his Fig. 1. From his Eq. 2, it is obvious that the slope of the line of the a vs. log t plot (his Fig. 1) can be used to calculate k and the intercept used to calculate s. Thus

$$k=\frac{1{,}422\mu ZT}{h}\times\frac{1}{m}\times\frac{2.303}{2}=15.16$$

and

$$s=\frac{\Delta p^2 \text{ (at } t=1 \text{ hour)}}{m/1.151}-\ln\left(\frac{k}{1{,}688\phi\mu c r_w{}^2}\right)^{1/2}$$

$$=-4.9.$$

Though the values of k and s are not needed directly for Poettmann's method, they do represent useful well and completion characteristics and are thus definitely worth evaluating. In fact, most pressure-transient interpretation is directed toward defining kh and s.

In reality, there is little difference between Brar and Aziz's and Poettmann's methods in terms of analysis of the transient data. The difference is in the extrapolation of the results obtained from the transient analysis into the stabilized flow prediction. Brar and Aziz use the pseudosteady-state equation,

$$\Delta p^2=2\times 1{,}632\times\frac{\mu ZT}{kh}\left[\log\left(0.472\frac{r_e}{r_w}\right)+\frac{s}{2.303}\right]\times q+bq^2, \quad \text{.....(R-1)}$$

whereas Poettmann uses the transient equation,

$$\Delta p^2=1{,}632\times\frac{\mu ZT}{kh}\left[\log\left(\frac{kt}{\phi\mu c r_w{}^2}\right)+0.869s\right]\times q+bq^2, \quad \text{.....(R-2)}$$

where

$$t=t_{ps}=376\frac{\phi\mu c r_e{}^2}{k}. \quad \text{.....(R-3)}$$

As Poettmann pointed out, Eqs. R-1 and R-2 will give the same answer. This is not surprising, because t_{ps} was obtained by making Eqs. R-1 and R-2 equal to each other. But this is where the confusion begins. In traditional reservoir engineering theory, Eq. R-2, the transient-flow equation, holds true until time to stabilization, given by

$$t_s=948\frac{\phi\mu c r_e{}^2}{k}, \quad \text{.....(R-4)}$$

after which the pseudosteady-state equation, Eq. R-1, is valid. Poettmann admonishes us not to confuse the two. In spite of his advice, we were thoroughly confused and believe a great many other people will be also. This is the situation as it will appear to most readers:

We have a transient-flow equation and a pseudosteady-state-flow equation upon which everybody agrees. Traditionally, we thought the changeover point from one to the other was given by Eq. R-4 (see Refs. 3 and 4), yet here we have a very sound paper[2] that shows that the changeover point is given by Eq. R-3. There is a factor of 2.5 between these two calculations, an apparently substantial difference. How do we resolve this dilemma?

We were confused until we realized that the problem lies in certain approximations and assumptions we make, without realizing that we are making them or forgetting

that we did. We are referring to p_i and $\bar{p}_R$. Therein lies the root of the problem, for which further clarification follows.

We shall start with some definitions of p_i and $\bar{p}_R$, develop the correct equations, show the incorrect or the unclear ones, and finally extend the process to all shapes and sizes of reservoirs.

Before flow begins, the pressure throughout the reservoir is constant. This pressure is called the initial pressure, p_i, and is best defined by

$$p=p_i \text{ for } t\leqq 0,\ r\leqq r_e.$$

Before flow begins from the reservoir, the average pressure in the reservoir, $\bar{p}_R$, also equals p_i. Once flow from the reservoir has started, however, a pressure profile will exist in the reservoir. This profile changes continuously with time throughout the reservoir will exist. At any time, the average pressure in the drainage area, $\bar{p}_R$, can be obtained by material balance calculation, by volumetric averaging of the pressure profile in the reservoir, or by a pressure buildup to a stabilized pressure. Mathematically,

$$\text{for } t\leqq 0,\ \bar{p}_R=p_i;$$

$$\text{for } t>0,\ \bar{p}_R=p_i-\text{pressure loss caused by production}$$

$$=p_i-\frac{qBt}{\pi r_e{}^2 h\phi c}. \quad \ldots\ldots\ldots\ldots \text{(R-5)}$$

It is clear, then, that for a finite reservoir that has produced some fluid, $\bar{p}_R<p_i$. If the production has been small, then $\bar{p}_R$ may be close to p_i and may be assumed to equal p_i for practical purposes. Until the value of $p_i-\bar{p}_R$ has been quantified and is known to be negligible, however, $\bar{p}_R$ must be accepted as being less than p_i. This point may seem trivial, but it is at the heart of the dilemma. The problem is that, when we are changing from Eq. R-1 to R-2, we are also changing (without a full evaluation of its implication) our definition of Δp^2. In Eq. R-2, Δp^2 is defined by

$$\Delta p^2=p_i{}^2-p_{wf}{}^2, \quad \ldots\ldots\ldots\ldots\ldots\ldots \text{(R-6)}$$

whereas in Eq. R-1, Δp^2 is defined by

$$\Delta p^2=\bar{p}_R{}^2-p_{wf}{}^2. \quad \ldots\ldots\ldots\ldots\ldots\ldots \text{(R-7)}$$

In this respect, Poettmann's Eq. D-1 is misleading because the same definition of Δp^2 is used for both the transient and the pseudosteady-state equations. Strictly speaking, his definition of a for transient flow is correct only if $p_i{}^2$ is used rather than $\bar{p}_R{}^2$. His transition from transient to pseudosteady state occurs at t_{ps} rather than at t_s because he is using $\bar{p}_R$ rather than p_i. Admittedly, $\bar{p}_R$ is initially close to p_i, and during the isochronal flow period the difference is negligible. As flow progresses into pseudosteady state, however, $\bar{p}_R$ may become appreciably less than p_i, depending on the rate and duration of production.

There are several alternative ways of expressing the pseudosteady-state-flow condition. If proper track is kept of p_i and $\bar{p}_R$ and the appropriate material balance relationship is honored, the following equations result for pseudosteady-state flow. Note in every case whether p_i or $\bar{p}_R$ is being used.

Alternative 1.

$$\text{For } t=\frac{948\phi\mu c r_e{}^2}{k},$$

which is traditionally defined as the time to stabilization,

$$p_i{}^2-p_{wf}{}^2=1{,}632\ \frac{\mu ZT}{kh}\left[\log\left(\frac{kt}{\phi\mu c r_w{}^2}\right)-3.23+0.869s\right]q+bq^2. \quad \ldots\ldots\ldots\ldots\ldots\ldots \text{(R-8)}$$

This is the transient-flow equation and is applicable up to and including the time to stabilization, t_s.

Alternative 2.

$$\text{For } t>\frac{948\phi\mu c r_e{}^2}{k},$$

$$p_i{}^2-p_{wf}{}^2=1{,}422\frac{\mu ZT}{kh}\left(\frac{2\times 2.637\times 10^{-4}kt}{\phi\mu c r_e{}^2}\right)q+2\times 1{,}632\frac{\mu ZT}{kh}\left[\log\left(0.472\frac{r_e}{r_w}\right)+\frac{s}{2.303}\right]q+bq^2. \quad \ldots\ldots\ldots\ldots\ldots\ldots \text{(R-9)}$$

This is the true pseudosteady-state equation based on p_i and producing time, t.

Alternative 3. If it is noted that the first term on the right side of Eq. R-9 is the depletion term and that when subtracted from $p_i{}^2$ it gives $\bar{p}_R{}^2$, the following equation results:

$$\bar{p}_R{}^2-p_{wf}{}^2=2\times 1{,}632\frac{\mu ZT}{kh}\left[\log\left(0.472\frac{r_e}{r_w}\right)+\frac{s}{2.303}\right]q+bq^2. \quad \ldots\ldots\ldots\ldots\ldots\ldots \text{(R-10)}$$

This is the form of the pseudosteady-state equation used most frequently. It appears to be independent of time, but this is only an illusion because $\bar{p}_R$ is dependent on the duration of production. This form of the equation is very useful because the cumulative production when $t=0$ need not be known as was the case for Eq. 9. It is also the form used in absolute open-flow test interpretation.

Eqs. R-9 and R-10 are equivalent and will give the same results, provided p_i or $\bar{p}_R$ is used as appropriate. Note that $\bar{p}_R$ is the average pressure in the reservoir at the time that the stabilized flow is being evaluated. It is *not* equal to p_i. However, it is often assumed that during short flow

tests, $\bar{p}_R = p_i$. This is reasonable, but it is incorrect to extrapolate this assumption to the time to stabilization, by which time there may be an appreciable difference between $\bar{p}_R$ and p_i.

Sometimes p_i is used in place of $\bar{p}_R$ in Eq. R-10, because $\bar{p}_R$ at the time of stabilization is not known. Whereas this approximation may be acceptable in some instances, it will give the wrong value of stabilized flow rate when compared to calculations using Eq. R-8 or R-9.

For the same reasons, it is wrong to assume that the right sides of Eqs. R-8 and R-10 will give the same answers when it is evident that the left sides of these equations are not the same.

Alternative 4. Poettmann has asked, in effect, "If p_i in Eq. R-8 were replaced by $\bar{p}_R$, what would be the corresponding value of t for the equation to give the same results as Alternatives 1 through 3?" The resultant t was his t_{ps}, given by

$$t_{ps} = \frac{376\phi\mu c r_e^{\,2}}{k},$$

and his stabilized flow equation is

$$\text{for } t = \frac{376\phi\mu c r_e^{\,2}}{k},$$

$$\bar{p}_R^{\,2} - p_{wf}^{\,2} = 1{,}632\frac{\mu ZT}{kh}\left[\log\left(\frac{kt}{\phi\mu c r_w^{\,2}}\right) - 3.23 + 0.869s\right]q + bq^2. \quad \text{.....(R-11)}$$

Note the similarity in form between Eqs. R-11 and R-8. Note also that p_i is replaced by $\bar{p}_R$ and that t used in Eq. R-11 is less than t used in Eq. R-8 for the very good reason that $\bar{p}_R$ is less than p_i.

It is confusing to call t_{ps} the pseudostabilization time. The process by which t_{ps} was arrived at is parallel to the concept used in obtaining the effective drainage radius idea.[3] In both cases, a transient equation is being expressed as an equivalent steady state. t_{ps} is more properly thought of as the time required to be used in the transient equation, which will result in the form of the steady-state equation. By analogy with the effective drainage radius, r_d, we propose that it be called effective drainage time, t_d (not to be confused with dimensionless time, t_D).

Brar and Aziz[1] and Poettmann[2] used the transient-flow equation,

$$p_i^{\,2} - p_{wf}^{\,2} = a_t q + bq^2, \quad \text{.....(R-12)}$$

where a_t is a function of time given by

$$a_t = 1{,}632\frac{\mu ZT}{kh}\left[\log t + \log\left(\frac{k}{\phi\mu c r_w^{\,2}}\right) - 3.23 + 0.869s\right], \quad \text{.....(R-13)}$$

to develop a plot of a_t vs. log t for the transient-flow data.

The process of extrapolating the graph of a_t vs. log t to a value of t introduced by Poettmann and given by

$$t_d = \frac{376\phi\mu c r_e^{\,2}}{k} \quad \text{.....(R-14)}$$

is valid, provided it is used in conjunction with Eq. R-11, which is rewritten as

$$\bar{p}_R^{\,2} - p_{wf}^{\,2} = aq + bq^2, \quad \text{.....(R-15)}$$

where a is the value of a_t for $t = t_d$.

Other Reservoir Shapes

The previous discussions were directed (for simplicity) at circular reservoirs. The principles involved apply equally well to other reservoir shapes. The equations of Alternatives 1 through 4 are restated below to apply to any reservoir shape (except where noted).

Alternative 1a. This alternative is usable *only* for a well centrally located in its drainage area. (If a well is off center, there is a significant difference between the end of the infinite-acting period and the onset of pseudosteady state.)

$$\text{For } t = \frac{\phi\mu cA}{2.637\times10^{-4}k}\times t_{DApss},$$

$$p_i^{\,2} - p_{wf}^{\,2} = 1{,}632\frac{\mu ZT}{kh}\left[\log\left(\frac{kt}{\phi\mu c r_w^{\,2}}\right) - 3.23 + 0.869s\right]q + bq^2 \quad \text{.....(R-8a)}$$

Note that Eq. R-8a is the same as Eq. R-8. t_{DApss} is the dimensionless time for the beginning of pseudosteady state. $t_{DApss} = 0.1$ for a well in the center of a square or a circle. For other shapes, t_{DApss} is given in Refs. 3 and 4.

Alternative 2a.

$$\text{For } t \geqq \frac{\phi\mu cA}{2.637\times10^{-4}k}t_{DApss},$$

$$p_i^{\,2} - p_{wf}^{\,2} = 1{,}422\frac{\mu ZT}{kh}\left(\frac{2.637\times10^{-4}kt}{\phi\mu cA}2\pi\right)q + 1{,}632\frac{\mu ZT}{kh}\left[\log\left(\frac{2.246A}{r_w^{\,2}C_A}\right) + 0.869s\right]q + bq^2. \quad \text{.....(R-9a)}$$

C_A is a shape factor that depends on the well/reservoir configuration; values for it can be found in the same places as t_{DApss}.

Alternative 3a.

$$\bar{p}_R{}^2 - p_{wf}{}^2 = 1{,}632\frac{\mu ZT}{kh}\left[\log\left(\frac{2.246A}{r_w{}^2 C_A}\right) + 0.869s\right]q + bq^2. \quad \text{(R-10a)}$$

Alternative 4a. Poettmann's method can be extended to any reservoir shape by extrapolating the graph of a_t vs. log t to a value of time

$$t_d = 3{,}814\frac{\phi\mu cA}{kC_A}. \quad \text{(R-14a)}$$

This is equivalent to calculating a_t from Eq. R-13 for a value of $t = t_d$ as obtained from Eq. R-14a.

This value of a_t is then substituted for a in the stabilized-flow equation:

$$\bar{p}_R{}^2 - p_{wf}{}^2 = aq + bq^2. \quad \text{(R-15a)}$$

Conclusions

1. The method proposed by Poettmann[2] is a valid extension of the Brar and Aziz[1] method.
2. The term t_d is suggested as being preferable to Poettmann's t_{ps} in that it is less confusing.
3. Four alternative stabilized-flow equations are given.
4. It is important to use the appropriate value of p_i or $\bar{p}_R$ in these alternative equations. Indiscriminate use of these pressures will lead to the wrong answer, particularly for low-permeability reservoirs.
5. Poettmann's method has been extended to a well/reservoir configuration of any shape by deriving $t_d = 3{,}814\ \phi\mu cA/kC_A$.

Nomenclature

a = coefficient in stabilized deliverability equation
a_t = coefficient in transient deliverability equation
A = drainage area, ft^2
b = coefficient in deliverability equation
B = FVF, ft^3/Mcf
c = compressibility, psia^{-1}
C_A = shape factor
h = net pay, ft
k = permeability, md
m = slope
Δp^2 = $(p_i{}^2 - p_{wf}{}^2)$ or $(\bar{p}_R{}^2 - p_{wf}{}^2)$
p = sandface pressure, psia
p_i = initial pressure, psi
$\bar{p}_R$ = average reservoir pressure, psia
p_{wf} = bottomhole flowing pressure, psia
q = flow rate, Mcf/D
r_d = effective drainage radius, ft
r_e = external radius, ft
r_w = wellbore radius, ft
s = skin effect
t = time, hours
t_d = effective drainage time, hours
t_D = dimensionless time
t_{DApss} = dimensionless time to pseudosteady state (based on area)
t_{ps} = time to pseudostabilization (defined by Poettmann), hours
t_{pss} = time to stabilization, also known as pseudosteady state, hours
t_s = time to stabilization, also known as time to pseudosteady state, hours
T = temperature, °F
Z = compressibility factor
μ = viscosity, cp
ϕ = gas-filled porosity

References

1. Brar, G.S. and Aziz, K.: "The Analysis of Modified Isochronal Tests to Predict the Stabilized Deliverability of Gas Wells Without Using Stabilized Flow Data," *JPT* (Feb. 1978) 297–304; *Trans.*, AIME, 265.
2. Poettmann, F.H.: "Discussion of Analysis of Modified Isochronal Tests to Predict the Stabilized Deliverability of Gas Wells Without Using Stabilized Flow Data," *JPT* (Oct. 1986) 1122–24.
3. "Theory and Practice of the Testing of Gas Wells," third edition, Alberta Energy Resources Conservation Board, Alberta, Canada (1975).
4. Earlougher, R.C. Jr.: *Advances in Well Test Analysis*, Monograph Series, SPE, Richardson, TX (1977) 5.

(SPE 16320)

Further Discussion of The Analysis of Modified Isochronal Tests To Predict the Stabilized Deliverability of Gas Wells Without Using Stabilized Flow Data

S.B. Hinchman, SPE, Marathon Oil Co.
H. Kazemi, SPE, Marathon Oil Co.
F.H. Poettmann, SPE, Colorado School of Mines

Brar and Mattar conclude that Poettmann's extension of Brar and Aziz's analysis of a modified isochronal test (Oct. 1986 *JPT*, Pages 1122–24) is correct, is shorter, and has other advantages.[1,2] For instance, Poettmann's method does *not* depend on calculation of skin factor, s, non-Darcy flow coefficient, D, and wellbore radius, r_w. Brar and Mattar, however, propose the extension of Poettmann's method to noncircular drainage geometrics by replacing the calculation of pseudostabilization time, t_{ps}, given by the original Eq. D-5 with a more general form given below:

$$t_{ps}=3{,}814\frac{\phi\bar{\mu}\bar{c}_t A}{k_g C_A}, \quad \ldots\ldots\ldots\ldots\ldots\ldots\ldots\ldots \text{(D-1)}$$

where A is the drainage area in square feet and C_A is the shape factor, which is 31.62 for a circular drainage area. We agree with this extension and recognize that t_{ps}, calculated from this Eq. D-1, will be used in a least-squares plot of a vs. log t to obtain the stabilized value of a for use in the original Eq. D-1, reprinted below:

$$\bar{p}_R^2-p_{wf}^2=aq+bq^2.$$

Furthermore, Brar and Mattar's discussion has been thought-provoking. For instance, we agree that the original Eq. D-1 is *not* exactly correct during the transient-flow period, and it should be written as

$$p_i^2-p_{wf}^2=aq+bq^2. \quad \ldots\ldots\ldots\ldots\ldots\ldots\ldots \text{(D-2)}$$

However, because during the transient period $\bar{p}_R \simeq p_i$, it is generally acceptable to use the original Eq. D-1 instead of Eq. D-2 in practice. This is why the original Eq. D-1 has been used in the past. On the other hand, we believe that during the pseudosteady-state flow, the first Eq. D-1 must be used for deliverability calculations.

Finally, the following simple argument could replace much of the discussion by Brar and Mattar. We restrict this discussion to circular drainage areas only. From pseudosteady-state flow considerations, one obtains

$$\bar{p}_R^2(t_s)-p_{wf}^2(t_s)$$

$$=1{,}422\frac{\bar{\mu}\bar{z}T}{k_g h}\left(\ln\frac{0.472r_e}{r_w}+s\right)q+bq^2. \quad \ldots\ldots \text{(D-3)}$$

From material balance, we obtain

$$p_i^2-\bar{p}_R^2(t_s)=1{,}422\frac{\bar{\mu}\bar{z}T}{k_g h}(0.5). \quad \ldots\ldots\ldots\ldots \text{(D-4)}$$

The derivation of Eq. D-4 is given in the Appendix.

Adding Eqs. D-3 and D-4, we get

$$p_i^2-p_{wf}^2(t_s)$$

$$=1.422\frac{\bar{\mu}\bar{z}T}{k_g h}\left(0.5+\ln\frac{0.472r_e}{r_w}+s\right)q+bq^2$$

$$=1.422\frac{\bar{\mu}\bar{z}T}{k_g h}\left[\ln\left(\frac{k_g t_s}{1{,}688\phi\bar{\mu}\bar{c}_t r_w^2}\right)^{1/2}+s\right]q+bq^2. \quad \ldots\ldots\ldots\ldots\ldots\ldots\ldots\ldots \text{(D-5)}$$

Eq. D-5 simply states that if t_s (given by the original Eq. D-6) is used to calculate the stabilized value of a, the deliverability equation has the form

$$p_i^2-p_{wf}^2=a(t_s)q+bq^2, \quad \ldots\ldots\ldots\ldots\ldots\ldots \text{(D-6)}$$

while the correct form is

$$\bar{p}_R^2-p_{wf}^2=a(t_{ps})q+bq^2. \quad \ldots\ldots\ldots\ldots\ldots\ldots \text{(D-7)}$$

Eq. D-7 was the intent of Poettmann's method.

The deliverability of a gas well can also be expressed by the well-known backpressure equation of Rawlins and Schellhardt:

$$q=C(\bar{p}_R^2-p_{wf}^2)^n. \quad \ldots\ldots\ldots\ldots\ldots\ldots \text{(D-8)}$$

This equation is still widely used in the U.S. One reason for its wide use is that all state regulatory agencies in the U.S. require gas well test data to be reported in this form.

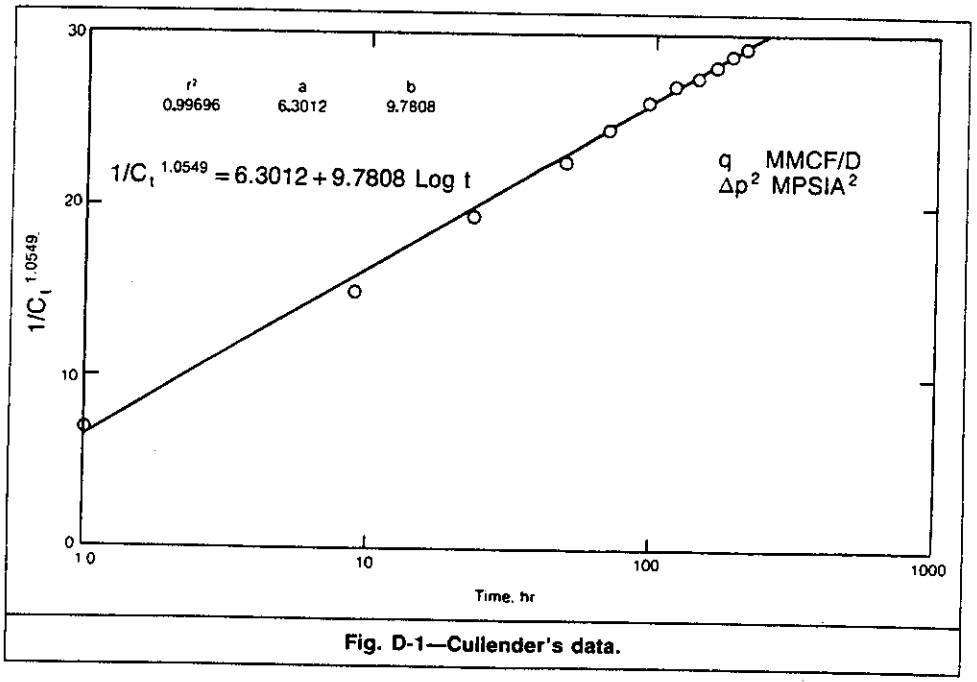

Fig. D-1—Cullender's data.

A procedure similar to that discussed by Poettmann for the Forchheimer equation can also be used to calculate the transient-performance coefficient, C_t, as a function of the logarithm of time for the Rawlins and Schellhardt equation. Consider the transient Forchheimer equation as follows:

$$p_i^2-p_{wf}^2=\frac{1{,}632\bar{\mu}\bar{z}T}{k_g h}q\left(\log\frac{k_g t}{1{,}688\bar{\mu}\bar{c}_t r_w^2}+0.869s\right)+bq^2. \quad \ldots\ldots\ldots\ldots\ldots\ldots \text{(D-9)}$$

This equation states that for a transient condition of flow when Δp^2 is plotted vs. log t for a constant flow rate, a straight line results with slope m where

$$m=\frac{1{,}632\bar{\mu}\bar{z}T}{k_g h}q. \quad \ldots\ldots\ldots\ldots\ldots\ldots \text{(D-10)}$$

Now consider the transient Rawlins and Schellhardt equation:

$$q=C_t(p_i^2-p_{wf}^2)^n, \quad \ldots\ldots\ldots\ldots\ldots\ldots \text{(D-11)}$$

rearranging

$$p_i^2-p_{wf}^2=\frac{1}{C_t^{1/n}}q^{1/n}, \quad \ldots\ldots\ldots\ldots\ldots\ldots \text{(D-12)}$$

and for a flow rate of $q=1$

$$p_i^2-p_{wf}^2=\frac{1}{C_t^{1/n}}. \quad \ldots\ldots\ldots\ldots\ldots\ldots \text{(D-13)}$$

(C_t will vary depending on how Δp^2 and q are expressed. In this discussion, Δp^2 is expressed in Mpsia^2 and q is expressed in MMcf/D.)

Therefore, plotting $1/C_t^{1/n}$ as a function of log t will result in a straight line of slope m' where $1/C_t^{1/n}$ is Δp^2 for a constant flow rate of 1 MMcf/D [28 320 m^3/d].

$$m'=\frac{1{,}632\ \bar{\mu}\bar{z}T}{k_g h}. \quad \ldots\ldots\ldots\ldots\ldots\ldots \text{(D-14)}$$

We now have a method for arriving at the stabilized value of the performance coefficient C, to be used in the Rawlins and Schellhardt Eq. D-8. This is analogous to the procedure used for the Forchheimer equation.

Also, one can calculate the permeability k_g from the slope m' of the $1/C_t^{1/n}$ plot vs. log t and use this value of k_g to calculate pseudostabilization time, t_{ps}. One might argue that this is not valid because the Forchheimer equation, when plotted as log Δp^2 vs. log q, is not a straight line. However, practical flow rates in deliverability testing generally vary over only one order of magnitude—i.e., one log cycle—whereas it takes a change of several orders of magnitude in the flow rate to observe the nonlinear behavior of the Forchheimer equation. In other words, short segments of the Forchheimer plot can be represented as straight lines on a plot of log Δp^2 vs. log q, as is the case in deliverability testing.

A number of isochronal and modified isochronal test data were plotted in this manner, and in all cases the plots resulted in straight lines for $1/C_t^{1/n}$ vs. log t. In addition, the procedure was verified by simulation of isochronal gas well tests with the Forchheimer equation. The Forchheimer equation was used to generate pressures to be analyzed with the Rawlins and Schellhardt backpressure expression. Large variations in flow rate, flow time, and reservoir properties were studied. In all instances, a plot of $1/C_t^{1/n}$ vs. log t resulted in a straight line. The slope of the line was able to reproduce the reservoir properties input if calculated for a constant rate of 1 MMcf/D

[28 320 m^3/d] (Eq. D-14). Fig. D-1 shows a plot of $1/C_t^{1/n}$ vs. log t for a long-term flow test from Cullender's paper,[3] Gas Well 3. The following is an example problem.

A modified isochronal test of 0.5, 1.0, 2.0, and 3.0 hours was taken. The test results were plotted on log-log paper based on the Rawlins and Schellhardt Eq. D-8, and a least-squares fit of the test data for each time period was made. The n values for the four time periods were averaged and equaled 0.887. The isochronal values of C_t are given in Table D-1. The C_t values were then converted to $1/C_t^{1/n}$ and plotted as a function of the log of time, as shown in Fig. D-2. A least-squares fit of the data resulted in the following equation:

$$\frac{1}{C_t^{1.1274}} = 1{,}708.46 + 1{,}393.03 \log t, \quad \ldots\ldots (D\text{-}15)$$

where 1,393.03 is the slope m'. The permeability k_g was then calculated from this slope using Eq. D-14,

$$k_g = \frac{1{,}632(0.028)(1.06)(656)}{(1{,}393)(20)} = 1.14 \text{ md},$$

where

$\phi = 0.102$,
$h = 20$ ft [6.096 m],
$\bar{\mu} = 0.028$ cp [0.028 mPa·s],
$\bar{z} = 1.06$,
$T = 196°F$ [91°C], and
$\bar{c}_t = 8.28 \times 10^{-5}$ psia^{-1} [0.0012×10^{-5} kPa^{-1}].

This value of k_g compared very favorably with the average of three buildup tests of 1.132 md.

Using the calculated value of k_g and reservoir gas properties as listed, one can calculate the pseudostabilization time for any spacing desired and can substitute it into Eq. D-15 to obtain the stabilized value of C.

TABLE D-1—ISOCHRONAL VALUES OF C_t

Time (hours)	C_t
0.5	1.754×10^{-3}
1.0	1.345×10^{-3}
2.0	1.120×10^{-3}
3.0	1.015×10^{-3}

In 1959, Poettmann and Schilson published a paper in which they derived an equation for C_t as a function of the log of time.[4]

$$C_t = \frac{C_1 \left(\ln \frac{\alpha}{a} t_1^{1/2}\right)^n}{\left(\ln \frac{\alpha}{a} t^{1/2}\right)^n} \quad \ldots\ldots\ldots\ldots (D\text{-}16)$$

This equation can be rearranged as follows:

$$\frac{1}{C_t^{1/n}} = \frac{2 \ln \frac{\alpha}{a}}{C_1 \ln \frac{\alpha}{a} t_1} + \frac{1}{C_1 \ln \frac{\alpha}{a} t_1} \ln t. \quad \ldots\ldots (D\text{-}17)$$

Both the intercept and slope of Eq. D-17 were obtained from the isochronal test data by a circuitous route. It is thus equivalent to Eq. D-15. Eqs. D-16 and D-15 result in the same values of C_t. It is just a little embarrassing to realize that 27 years ago a complicated procedure for calculating the transient value of C_t was published that is equivalent to the much more simplified and direct procedure discussed above.

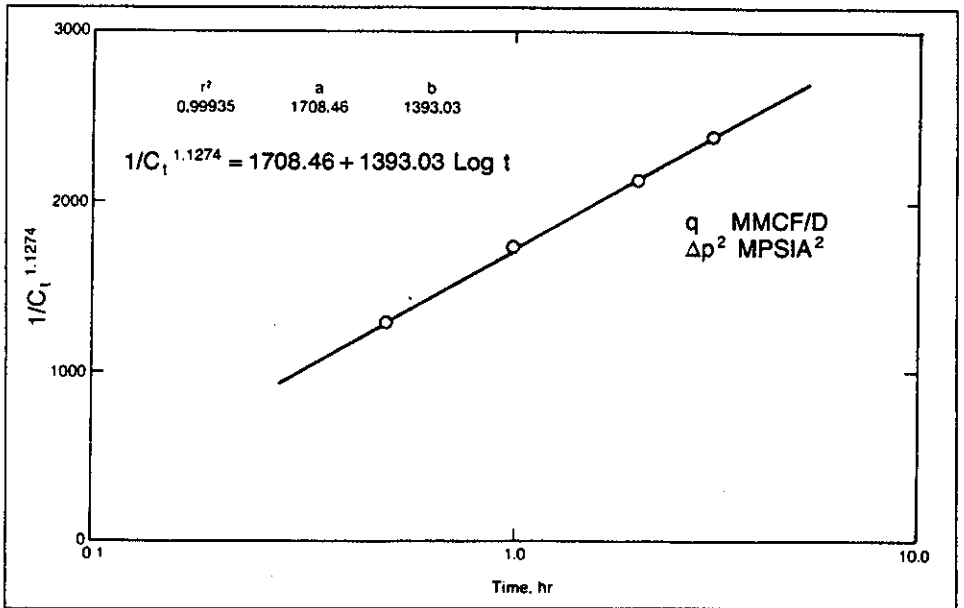

Fig. D-2—Data from a modified isochronal test.

Conclusions

We agree with Brar and Mattar that Poettmann's* extension of Brar and Aziz's analysis is correct. In addition, an analogous procedure can be used to calculate the stabilized performance coefficient, C, for the Rawlins and Schellhardt backpressure equation.

Acknowledgment

The material for the discussion on the transient-performance coefficient, C_t, was taken from material submitted by Steven B. Hinchman to fulfill requirements for the MS degree at the Colorado School of Mines.

References

1. Brar, G.S. and Aziz, K.: "Analysis of Modified Isochronal Tests To Predict the Stabilized Deliverability Potential of Gas Wells Without Using Stabilized Flow Data," *JPT* (Feb. 1978) 297-304; *Trans.*, AIME, **265**.
2. Poettmann, F.H.: "Discussion of Analysis of Modified Isochronal Tests To Predict the Stabilized Deliverability Potential of Gas Wells Without Using Stabilized Flow Data," *JPT* (Oct. 1986) 1122-24.
3. Cullender, M.H.: "The Isochronal Performance Method of Determining the Flow Characteristics of Gas Wells," *Trans.*, AIME (1955) **204**, 137.
4. Poettmann, F.H. and Schilson, R.E.: "Calculation of Stabilized Performance Coefficient of Low Permeability Natural Gas Wells," *JPT* (Sept. 1959) 240–46; *Trans.*, AIME, **216**.

*During the publication process, the nomenclature to Poettmann's discussion of the Brar and Aziz paper was inadvertently omitted. It has been added in the 1986 *Transactions* volume. Please refer to Brar and Mattar's nomenclature for symbols used in this discussion.

Appendix—Derivation of Eq. D-4

$$p_i^2-\bar{p}_R^2=(p_i+\bar{p}_R)(p_i-\bar{p}_R)\simeq 2\bar{p}_R(p_i-\bar{p}_R), \quad \text{(A-1)}$$

where

$$2\bar{p}_R(p_i-\bar{p}_R)=2\bar{p}_R\frac{(10^3q)B_gt_s}{\pi r_e{}^2h\phi\bar{c}_t}$$

$$=2\bar{p}_R\frac{(10^3q)(0.02827\ T\bar{z}/\bar{p}_R)\left(\dfrac{948\phi\bar{\mu}\bar{c}_tr_e{}^2}{24k_g}\right)}{\pi r_e^2h\phi\bar{c}_t}$$

$$=711\frac{\bar{\mu}\bar{z}T}{k_gh}q. \quad \text{(A-2)}$$

Thus

$$p_i^2-\bar{p}_R^2=1{,}422\frac{\bar{\mu}\bar{z}T}{k_gh}q(0.5), \quad \text{(A-3)}$$

which is the same as Eq. D-4.

SI Metric Conversion Factors

ft^3	× 2.831 685	E−02	=	m^3
psi	× 6.894 757	E+00	=	kPa

(SPE 16391)

SPE 20283

Applying Gas-Well Load-Up Technology

Steve B. Coleman, SPE, consultant; **Hartley B. Clay,** SPE, and **David G. McCurdy,** SPE, Exxon Co. U.S.A.; and **H. Lee Norris III,** SPE, Exxon Production Research Co.

Summary. This paper incorporates critical-rate and blowdown-limit technology into system-network-analysis (SNA) techniques to predict abandonment pressures for depletion-drive reservoirs and demonstrates that SNA by itself tends to underestimate the abandonment pressure. A number of practical operational considerations pertaining to the use of this technology are also outlined.

Introduction

At the outset of this series,[1-3] we said that the technology of low-pressure gas-well load-up would be presented to enhance the understanding of gas-well load-up problems and to establish more consistent and accurate analytical methods for evaluating the economic abandonment of depletion-drive gas reservoirs. The first three parts of the series presented the technology for determining a well's critical rate, for predicting wellbore hydraulics during load-up, and for calculating a new producing limit known as the gas-well blowdown limit. This final part presents practical methods for using this technology to predict abandonment pressures, to evaluate production alternatives, and to perform a reservoir depletion analysis. This paper also summarizes considerations for operating low-pressure gas wells and fields.

Methods for Predicting Abandonment Pressures

In the past, the most common method for predicting the abandonment pressure of a depletion-drive gas reservoir was comparison to a similar reservoir's past performance. Because of recent advances in computing technology and two-phase-flow calculation methods, an increasing number of engineers are using a more rigorous SNA[4] to predict reservoir abandonment pressures. This process involves integrating the reservoir flow performance (inflow) and the wellbore/ system flow performance (outflow) for various flow rates and static reservoir pressures. The results of the integration can then be plotted and analyzed. **Fig. 1** is an example of such a plot.

The abandonment pressure for each well/ system configuration is typically interpreted as the static reservoir pressure where the wellbore/system performance becomes unproducible—i.e., where the inflow and outflow performance curves no longer intersect. Two-phase-flow correlations indicate that at this point the wellbore will load up and the well will die.

Using the Liquid-Droplet-Model Critical Rate To Predict Abandonment Pressures

If we compare this load-up point to the critical-rate calculation presented in Part 1 of this series,[1] we can construct a comparison plot like that in **Fig. 2.** As this figure shows, as the static reservoir pressure declines, the tangency point diverges from the critical rate. Thus, the previous analysis with the tangency point as the load-up point yielded a lower abandonment pressure than is indicated by liquid-droplet-model critical-rate technology. The data presented in Part 1 showed that the liquid-droplet-model critical rate accurately predicts the load-up threshold for low pressures. We can conclude that the two-phase-flow correlation does not correctly interpret this same point of wellbore instability.

Although examination of the causes of this difference is beyond the scope of this paper, it is worthy of a few comments. As a general rule, most two-phase-flow correlations use an interpretation of vertical flow regime to predict where the transition from mist to slug flow begins. This transition point is generally considered the point where the wellbore becomes unstable. The correlations, however, cannot determine the point where liquid droplets begin to be held up in the wellbore. This difference in load-up-point interpretations could explain the divergence between the two methods.

Using the Blowdown-Limit Model To Predict Abandonment Pressures

A comparison of the abandonment pressures predicted with liquid-droplet technology combined with SNA to historical data for various reservoirs showed that the critical-rate abandonment pressure is still not the correct ultimate abandonment pressure of most depletion-drive reservoirs. In fact, many reservoirs are depleted below the pressure predicted with this method. To understand the reason behind this, it is helpful to examine the technology of the blowdown-limit model[3] and its application to the same SNA analysis.

If we take the example in Fig. 2 and add the calculated blowdown limit to the analy-

sis, we can create the plot in **Fig. 3.** Notice that the abandonment pressure predicted by the blowdown limit is lower than the critical-rate abandonment pressure. As we know from the supporting data,[3] this pressure probably is more closely aligned with the reservoir's true abandonment pressure.

It is important to note here that, although plotting the blowdown limit on the SNA graph is useful in enhancing our understanding of the comparison to the SNA method, the actual position of the blowdown-limit point on the plot is somewhat discretionary. The reason is that the SNA method is an analysis of a steady-state system, and the blowdown-limit model is an unsteady-state analysis. This leads us to the next section, which examines the well/reservoir deliverability during this unsteady-state period between the critical rate and the blowdown limit.

Post-Critical-Rate Deliverability

Experience tells us that if a reservoir is depleted to the blowdown limit, actual well deliverability decays considerably during the post-critical-rate production period. For example, once a well reaches its critical rate, loads up, and dies, the operator generally must take action to bring the well back to production (i.e., blow the well down, swab the well, etc.). We know[3] that the success of well unloading depends on many variables. During this period when the operator is attempting to unload the well, the well obviously is not producing at its optimum deliverability. Also, once the well is brought back to production, unless action is taken to prevent the well from reaching its critical rate again, the well will again load up and die. Each time this cycle repeats itself, the operator experiences increasing difficulty in bringing the well back to production. **Figs. 4 and 5** are production plots for typical wells producing with this behavior.

Obviously, this cyclic production behavior no longer follows the steady-state predictive method used in SNA analysis. Instead, the well's actual deliverability is only a percentage of that predicted with SNA. Therefore, our previous SNA analysis plot should be redrawn as shown in **Fig. 6.** The steady-state performance curve connecting the critical-rate point with the blowdown limit is now shown as dashed to represent the unsteady-state nature of this production period.

Table 1 summarizes the production data collected for numerous low-pressure wells producing in this post-critical-rate production period. The actual deliverability is significantly less (43%) than the potential deliverability. Because of many physical and human variables that affect this deliverability ratio, sorting the data to determine an empirical predictive relationship was considered impractical. The data, however, represent typical production behavior of wells in the post-critical-rate period.

Evaluating Production Alternatives

A variety of alternatives are available for producing and optimizing the recovery of

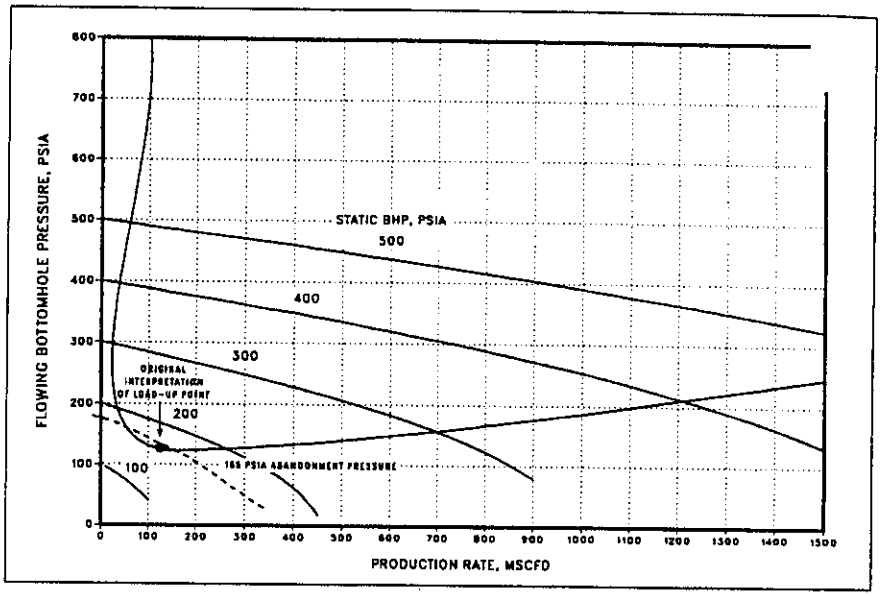

Fig. 1—Well-performance curve, SNA: 2⅞-in. tubing, 115-psia WHFP.

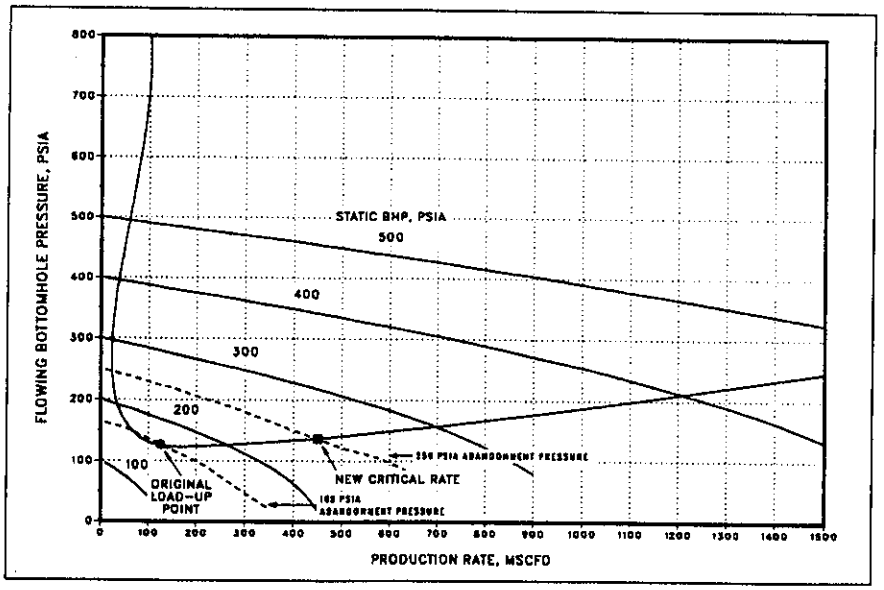

Fig. 2—Well-performance curve with critical rate shown.

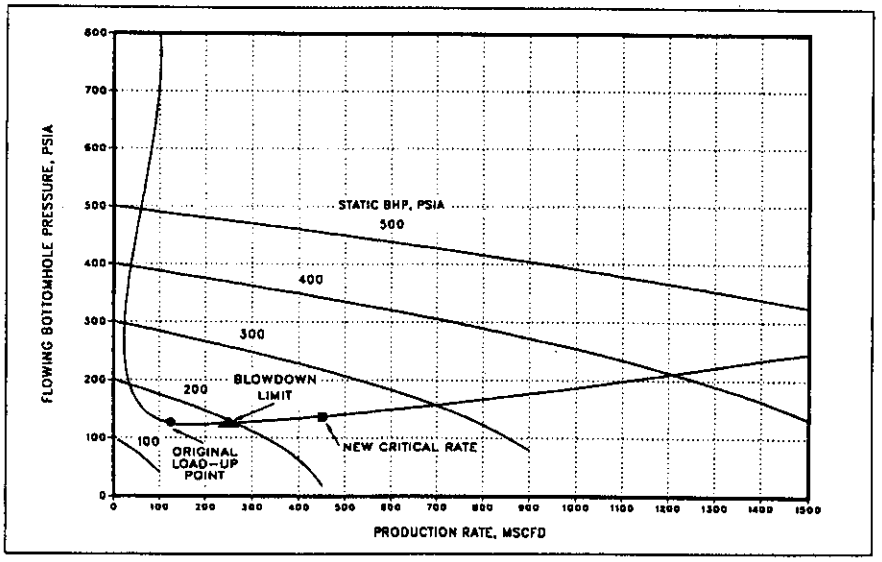

Fig. 3—Well-performance curve with critical rate and blowdown limit shown.

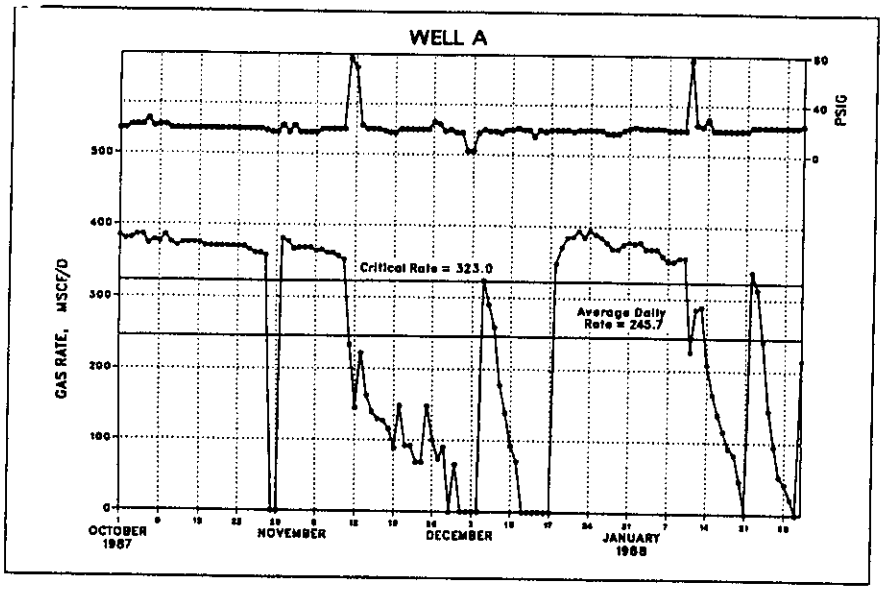

Fig. 4—Well A production profile.

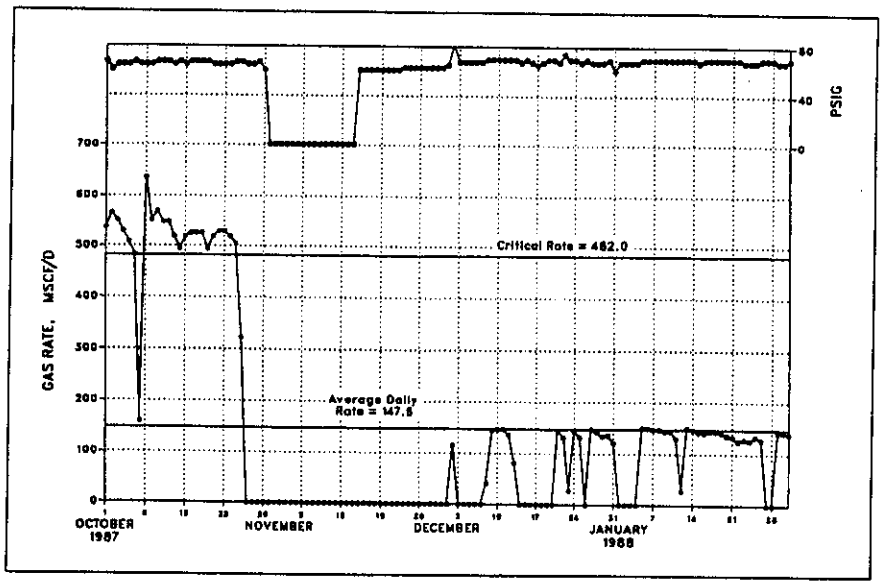

Fig. 5—Well B production profile.

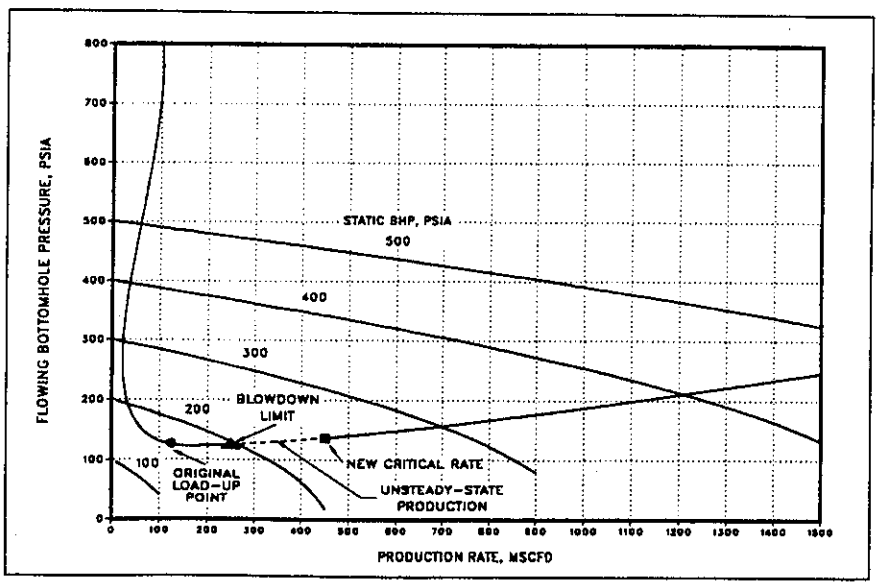

Fig. 6—Well-performance curve with critical rate and blowdown limit shown.

reserves from depletion-drive reservoirs. **Table 2** lists the most common alternatives. The choices are grouped broadly by the static reservoir pressure in which they are most likely applicable. To determine the economic feasibility of any one of these alternatives, both the deliverability and ultimate recovery resulting from the alternative must be determined.

SNA techniques, combined with the gas-well load-up technology, can be used to compare these performance differences. For example, **Fig. 7** is an SNA plot for a typical gas well depicting the impact of installing a siphon string on flow performance and abandonment pressure. **Fig. 8** is a similar SNA plot that examines the impact of reducing the wellhead flowing pressure (WHFP) by installing compression. In each case, the combined analysis is very useful in evaluating the relative performance and abandonment pressure for each alternative.

Reservoir Depletion Analysis

Obviously, use of the SNA techniques is manageable only on a well-by-well basis. When a depletion plan is developed for a reservoir that has many wells, the SNA can become very cumbersome, particularly if many alternatives are evaluated. Also, the SNA method does not readily yield a rate-vs.-time flow stream, which is essential in evaluating the economics of investing in any alternative.

The engineer has two options to handle this more complicated scenario. First, a single SNA that represents a "typical" well/reservoir system can be conducted and analyzed. The results from this single analysis can then be extrapolated over the remainder of the wells. Second, if a more rigorous examination is desired, then a computer simulation of the entire multiwell reservoir is required. In either case, it is worthwhile to examine the impact of the gas-well load-up concepts presented here. In the logic diagram of **Fig. 9**, the decision flow path for performing a depletion analysis is outlined. The impact of gas-well load-up technology is denoted by the items in ellipses. The three primary points of impact are the critical rate, the post-critical-rate deliverability, and the blowdown limit.

Fig. 10 further illustrates the effect of gas-well load-up technology. In this rate-vs.-time plot for a typical multiwell depletion-drive gas reservoir, the decline is particularly dramatic when the wells reach their blowdown/economic limit. This behavior is typical of actual production trends for these types of reservoirs.

Gas-well load-up technology, combined with this type of analysis, can yield the flow streams necessary to evaluate the economics of most alternatives. It can also provide information valuable for planning.

Operational Considerations

One of the results of this work was an enhanced awareness that operating a low-

TABLE 1—LOW PRESSURE GAS-DEPLETION STUDY—DELIVERABILITY STATISTICS SUMMARY

Well	Days $q > q_c$	Percentage (%)	Days $q > q_c$	Percentage (%)	Days $q = 0$	Percentage (%)	Days	Load-Up Frequency	Average Load-Up (days)	Average Dead Time (days)	q Potential (Mscf/D)	q Average (Mscf/D)	Δq (Mscf/D)	Difference (%)	Bottomhole Static Pressure (psig)
1	67	44.1	33	21.7	52	34.2	152	3	50.7	17.3	600.0	293.8	306.2	51.0	778
2	64	42.1	10	6.6	78	51.3	152	4	38.0	19.5	850.0	320.1	529.9	62.3	640
3	112	73.7	37	24.3	3	2.0	152	11	13.8	0.3	700.0	470.5	229.5	32.8	558
4	100	65.8	36	23.7	16	10.5	152	6	25.3	2.7	900.0	515.9	384.1	42.7	477
5	38	30.9	50	40.7	35	28.5	123	3	41.0	11.7	850.0	504.3	345.7	40.7	663
6	9	6.2	34	23.4	102	70.3	145	2	72.5	51.0	900.0	71.2	828.8	92.1	459
7	49	39.8	17	13.8	57	46.3	123	8	15.4	7.1	415.0	188.9	226.1	54.5	121
8	103	83.7	7	5.7	13	10.6	123	5	24.6	2.6	400.0	234.0	166.0	41.5	153
9	113	91.9	6	4.9	4	3.3	123	5	24.6	0.8	550.0	464.7	85.3	15.5	169
10	60	48.8	7	5.7	56	45.5	123	5	24.6	11.2	500.0	147.6	352.4	70.5	179
11	66	52.8	43	35.0	15	12.2	123	5	24.6	3.0	370.0	245.7	124.3	33.6	182
12	107	87.0	14	11.4	2	1.6	123	8	15.4	0.3	450.0	393.8	56.2	12.5	197
13	27	22.0	83	67.5	13	10.6	123	3	41.0	4.3	350.0	198.1	151.9	43.4	200
14	94	76.4	11	8.9	18	14.6	123	6	20.5	3	515.0	411.7	103.3	20.1	212
15	0	0.0	107	87.0	16	13.0	123	8	15.4	2	150.0	90.1	59.9	39.9	216
16	32	26.0	13	10.6	78	63.4	123	7	17.6	11.1	500.0	133.1	366.9	73.4	240
17	49	39.8	45	36.6	29	23.6	123	21	5.9	1.4	300.0	242.7	57.3	19.1	244
18	5	4.1	17	13.8	101	82.1	123	5	24.6	20.2	150.0	51.1	98.9	65.9	260
19	59	48.0	58	47.2	6	4.9	123	1	123.0	6	300.0	235.7	64.3	21.4	304
20	113	91.9	4	3.3	6	4.9	123	2	61.5	3	370.0	318.3	51.7	14.0	349
21	36	30.0	20	16.7	64	53.3	120	1	120.0	64.0	300.0	150.0	150.0	50.0	398
22	0	0.0	121	79.6	31	20.4	152	4	38.0	7.8	200.0	55.7	144.3	72.2	401
23	5	4.1	39	31.7	79	64.2	123	5	24.6	15.8	200.0	70.8	129.2	64.6	494
24	5	4.1	112	91.1	6	4.9	123	6	20.5	1.0	200.0	166.1	33.9	17.0	537
25	1	0.8	79	64.2	43	35.0	123	6	20.5	7.2	325.0	183.9	141.1	43.4	568
26	45	37.2	69	57.0	7	5.8	121	5	24.2	1.4	800.0	443.0	357.0	44.6	670
27	0	0.0	118	95.9	5	4.1	123	8	15.4	0.6	200.0	132.2	67.8	33.9	702
28	49	39.8	45	36.6	29	23.6	123	8	15.4	3.6	500.0	257.5	242.5	48.5	256
29	86	69.9	29	23.6	8	6.5	123	8	15.4	1.0	550.0	439.5	110.5	20.1	296
30	63	51.2	28	22.8	32	26.0	123	13	9.5	2.5	450.0	373.1	76.9	17.1	230
31	70	56.9	53	43.1	0	0.0	123	2	61.5	0.0	440.0	397.3	42.7	9.7	408
32	0	0.0	71	57.7	52	42.3	123	7	17.6	7.4	355.0	166.0	189.0	53.2	482
33	0	0.0	92	100.0	0	0.0	92	66	1.4	0.0	200.0	171.9	28.1	14.0	188
34	17	13.8	37	30.1	69	56.1	123	5	24.6	13.8	350.0	131.4	218.6	62.5	333
35	32	21.1	115	75.7	5	3.3	152	6	25.3	0.8	300.0	161.5	138.5	46.2	719
36	0	0.0	54	43.9	69	56.1	123	2	61.5	34.5	200.0	32.0	168.0	84.0	316
37	29	19.1	87	57.2	36	23.7	152	69	2.2	0.5	600.0	311.1	288.9	48.2	298
38	39	25.7	97	63.8	16	10.5	152	10	15.2	1.6	600.0	347.5	252.5	42.1	507
39	50	54.3	36	39.1	6	6.5	92	6	15.3	1.0	900.0	527.1	372.9	41.4	899
40	83	54.6	23	15.1	46	30.3	152	4	38.0	11.5	900.0	310.5	589.5	65.5	685
Total	1,876		1,957		1,303		5,136	359	1,246.0	354.0	1,869.0	10,359.4	8,330.6		
Average	46.9	36.4	48.9	38.4	32.6	25.1	128.4	9.0	31.1	8.9	467.3	259.0	208.3	43.1	399.2
Standard Deviation	36.8	0.3	35.0	0.3	29.2	0.2	14.9	13.9	26.4	13.4	229.6	141.9	167.6	20.9	201.2

pressure gas well or field that is at or near its apparent abandonment can be affected dramatically by a number of very simple operational factors. As we stated in the beginning of this series, many millions of cubic feet of natural gas are abandoned every year. In some cases, a simple operational change may have postponed the abandonment and resulted in the recovery of additional reserves.

Several factors should be considered for operating a depleting gas well or field.

1. As we know from Part 1 of this series, the critical rate for a well is affected significantly by the WHFP. If a well's WHFP is allowed to rise periodically, causing the well to produce below its critical rate, then the well will load up and die.

An example is a well that produces to a compressor. In many cases, when the compressor goes down, the piping is configured in such a manner as to allow the well to spill over to the next-higher pressure system to continue production. During this period of higher flowing pressure, the well is still producing but is also accumulating load fluids and may die. If it does die, the operator may not be able to get the well unloaded and returned to production.

On the other hand, if the well had been shut in during this period of compressor downtime, the operator probably would have very little trouble bringing the well back to its original production rate. The risk of the well dying during compressor downtime can be assessed with the transient load-up hydraulics presented in Part 2 of this series.[2]

2. Another lesson to be learned from the critical-rate and blowdown-limit technology is that the operator will have a much greater chance of success of blowing down a well if the well is not allowed to die completely. If a rate decline is observed on a well's L-10 chart as a result of some event that caused the well to reach its critical rate, then it is

TABLE 2—ALTERNATIVE DEPLETION METHODS

Typical Bottomhole Static Pressure Range (psi)	Alternative
>1,500	Natural flow
500 to 1,500	Medium-pressure systems
200 to 500	Low-pressure systems
	Swabbing
	Pit blowdowns
	Surfactants
	Reservoir flooding
150 to 200	Lower-pressure systems
	Siphon strings
	Intermittent gas lift
	Intermittent rod pump
	Plunger lift
	Jet pump
	Swabbing
	Pit blowdowns
	Surfactants
	Reservoir flooding
<150	Ultralow-pressure systems
	Sipon strings
	Intermittent gas lift
	Jet pump
	Swabbing
	Surfactants
	Reservoir flooding

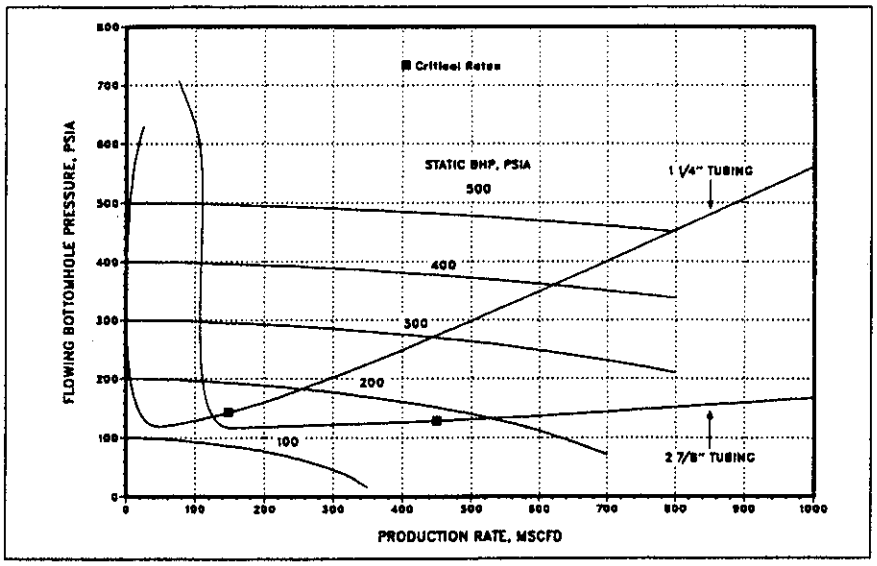

Fig. 7—Well-performance curve comparing effect of tubing size.

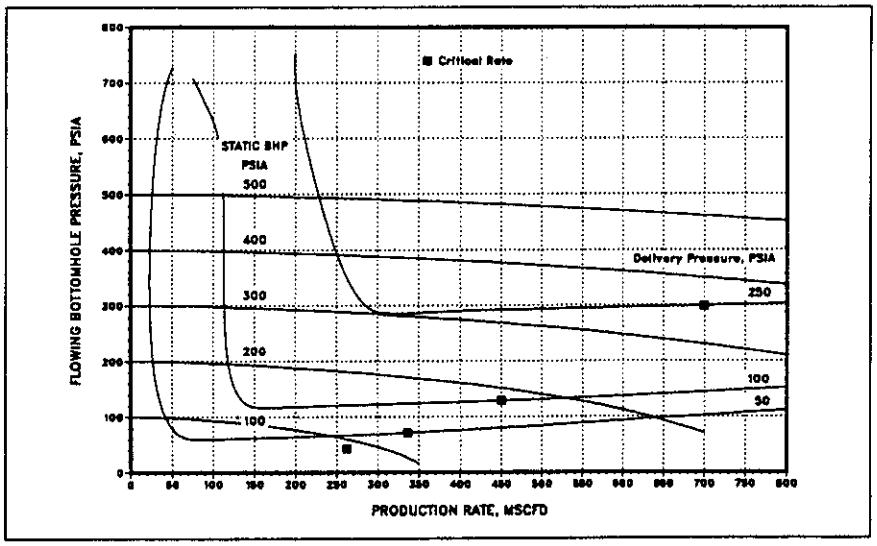

Fig. 8—Well-performance curve comparing effect of wellhead pressure.

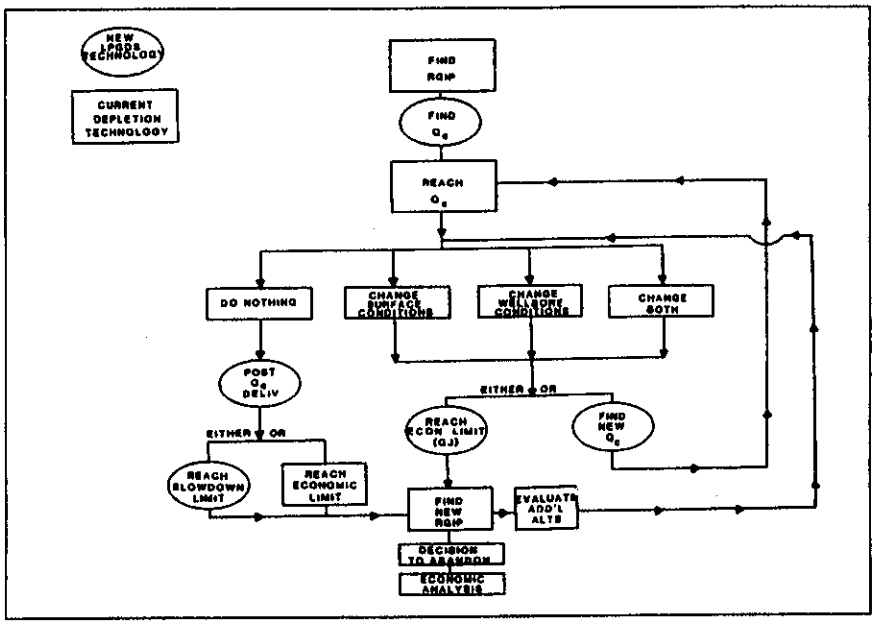

Fig. 9—Depletion logic flow diagram.

best to attempt to unload the accumulated fluids before the well dies completely.

3. The blowdown-limit technology also gives some clues about the operational techniques of blowdown. For instance, if an operator is having difficulty keeping a well on production after a blowdown, it may be because he or she is not successfully removing all the load fluid. Some fluid comes to the surface, but the rest falls back as a result of slippage. An adequate blowdown period must be provided to clear the wellbore of load fluid. Multiple successive blowdowns, each followed by a short shut-in period, increase the chance of total fluid removal and therefore the likelihood of a successful blowdown. This may be especially true for deeper wells.

4. Swabbing techniques also warrant consideration. Some operator guidelines set a minimum distance above the perforations that the swabber must maintain to prevent the swab tools from getting caught in the perforations. If the distance is significant, then the load fluid remaining above the perforations may impair the well's deliverability so that it will not be able to remain unloaded. Consideration should be given to these swabbing guidelines to avoid such occurrences.

5. As we discussed in Part 1, tubing size plays a significant role in determining the minimum flow rate required to keep a well above its critical rate. In conventional wellbores, a tubing packer is set in the casing some distance above the perforations. While the well is flowing above its critical rate, the tubing ID and wellhead conditions dictate when load-up will occur. As discussed in this paper, however, after an operational upset or some other occurrence that causes the well to go into load-up, the casing ID will determine the minimum gas velocity required to unload the well and restore it to normal production. To maximize ultimate recovery and minimize loading problems, the tubing packer should be placed as close to the perforations as possible.

Conclusions

1. The combined technology of gas-well load-up/blowdown and SNA provides a practical method for determining the ultimate abandonment pressure for many alternative depletion techniques for depletion-drive gas reservoirs.

2. Used by itself, SNA may estimate lower abandonment pressures than actually achievable because of gas-well load-up from critical-rate considerations. This is particularly true for lower pressures. However, depending on the operation of the well, abandonment pressure may be reduced below that indicated by critical-rate considerations to a point known as the blowdown limit.

3. Once a well reaches its critical rate and begins to have loading problems, if corrective measures are not taken to keep the well unloaded, then the well's deliverability will be reduced significantly. Typical post-critical-rate deliverability is about 43% of a well's potential deliverability.

4. Gas-well load-up technology can significantly affect a reservoir depletion analysis. The primary areas of impact are the critical rate, post-critical-rate deliverability, and blowdown limit. The effect of these items can play an important role in determining the economics and timing of any chosen depletion plan.

5. A number of operational lessons can be learned from gas-well load-up and blowdown technology that can enhance the ultimate recovery of gas from a depletion-drive reservoir.

Acknowledgments

We express our appreciation to the management of Exxon Co. U.S.A. and Exxon Production Research Co. for the support and encouragement given while we conducted this study. Special thanks go to the Operations personnel and the Production/Reservoir Technology support staff of Exxon's South Texas Div., who provided invaluable cooperation and assistance in gathering and manipulating data and in preparing the necessary technical review packages.

References

1. Coleman, S.B. *et al.*: "A New Look at Predicting Gas-Well Load-Up," *JPT* (March 1991) 329–33.
2. Coleman, S.B. *et al.*: "Understanding Gas-Well Load-Up Behavior," *JPT* (March 1991) 334–38.

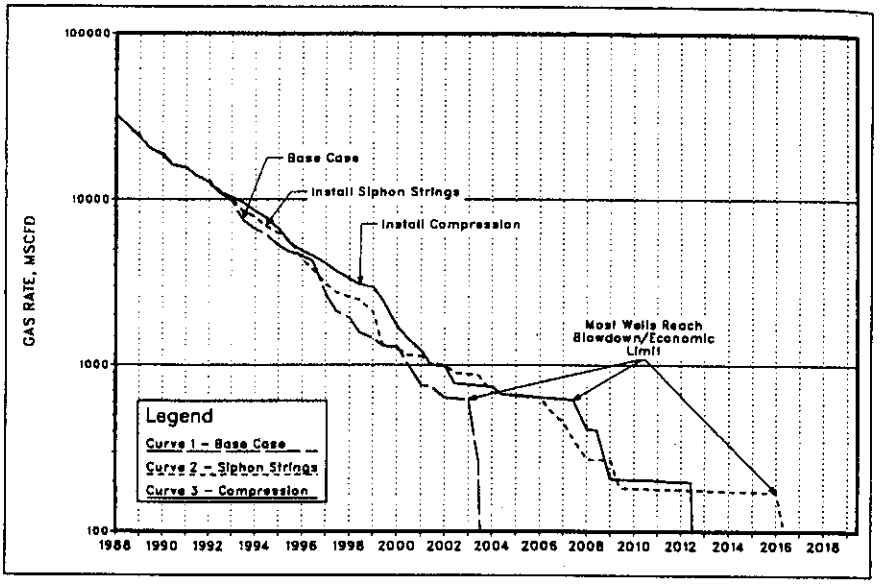

Fig. 10—Typical depletion-drive reservoir, rate vs. time.

3. Coleman, S.B. *et al.*: "The Blowdown-Limit Model," *JPT* (March 1991) 339–43.
4. Brown, K.E. and Leah, J.F.: "Nodal Systems Analysis of Oil and Gas Wells," *JPT* (Oct. 1985) 1751–63.

SI Metric Conversion Factors

ft^3	× 2.831 685	E−02	= m^3
in.	× 2.54*	E+00	= cm
psi	× 6.894 757	E+00	= kPa

*Conversion factor is exact.

Provenance

Original SPE manuscript, **Optimizing Recovery of Natural Gas From Depletion-Drive Reservoirs: Part 4—Application of Gas-Well Load-Up Technology,** received for review Nov. 16, 1989. Paper (SPE 20283) accepted for publication Feb. 9, 1990. Revised manuscript received Dec. 21, 1990.

JPT

Characterization of Tight Reservoirs

W. J. Lee, SPE, Texas A&M U., and C.W. Hopkins, SPE, S.A. Holditch & Assocs. Inc.

Summary

This paper gives methods to characterize tight gas reservoirs in sufficient detail to allow an engineer to make accurate long-range production forecasts. These forecasts are the basis for sound engineering and business decisions. Because of the complexity and variability of tight gas reservoirs, we can present only general procedures for developing reservoir descriptions. Accordingly, we illustrate a reservoir characterization method with three examples of successful tight gas reservoir studies. The procedures in these examples can be modified as needed for other specific formations or areas.

Introduction

Production rates from many tight reservoirs are marginal, but these reservoirs account for a large percentage of the long-term gas supply. Because of the marginal economics, efficiency is the key to drilling and producing these tight reservoirs. To optimize production, we must have a good understanding of the reservoir, but often the economics cannot support collecting the data necessary to describe the reservoir properly. A reservoir engineering study for tight reservoirs requires us to balance data collection costs with the level of detail necessary to describe the reservoir accurately. One must determine what level of reservoir characterization is needed to optimize production from tight reservoirs efficiently. Unfortunately, because of the diverse nature of tight reservoirs, there is no single answer. The question must be answered on a case-by-case basis.

Reservoir studies of tight reservoirs are performed to meet many different objectives. Because tight wells require hydraulic fracturing, fracture treatment optimization studies are quite common. A reservoir study is sometimes performed in conjunction with a detailed geologic study to help identify key well characteristics or field trends to be used as exploration tools and to predict reserves. A reservoir study can identify infill-well potential and the potential for increased productivity and reserves as the result of the installation of compression or liquid lift equipment. Finally, reservoir studies can resolve conflicting data or determine why some wells are not producing as expected.

Unfortunately, analysis of tight reservoirs is one of the most difficult problems facing a reservoir engineer. Many tight formations are extremely complex, producing from multiple layers with permeabilities that often are enhanced by natural fracturing. Unfortunately, low productivity and marginal economics often prevent expenditures of money and time to collect the data needed for a detailed reservoir study. Because the permeability of these formations is low, many standard formation evaluation techniques do not provide adequate results. Standard log-based correlations for permeability or other productivity indicators often fail in tight reservoirs, so correlations must be developed on an area-specific basis. Many tight shale reservoirs have productive gross intervals exceeding 300 ft, making it difficult to determine where the gas is produced, thus complicating completion decisions. Even in tight gas sands made up of interbedded sands and shales, layering can have a pronounced effect on well production. Natural fractures often occur in these tight formations, making wells that appear similar on logs perform quite differently.

When we do not describe the reservoir in sufficient detail, the production forecasts we generate are frequently wrong.[1,2] Unless we can predict postfracture well performance accurately, we cannot optimize the fracturing process.[3] Sound business decisions regarding compressor installation, infill drilling, or remediation treatments are not possible. Unfortunately, for layered reservoirs, oversimplified reservoir descriptions frequently result in an overestimated well productivity.

Fig. 1 shows predicted 20-year performance for a Devonian shale well for three different reservoir descriptions: "lumped" one-layer, 3-layer, and 10-layer reservoirs. All three predictions are based on the same gas in place and the same total permeability-thickness product, kh. Note that the lumped one-layer model overpredicts the gas recovery by a factor of two. The four-layer model prediction is closer to actual but is still high by about 17%. Any business decisions based on the single-layer prediction would be seriously in error.

Background

Development of tight gas reservoirs has been increasing substantially over the last decade. Because of this trend, the Gas Research Inst. (GRI) and the U.S. DOE have been funding detailed research in tight gas sands and shales throughout the U.S. This research has led to significant advances in hydraulic fracturing and a better understanding of the complexity of the tight reservoirs.

The importance of describing a layered reservoir has been discussed in the literature for several decades. Much of this discussion has centered on pressure-transient analysis of layered reservoirs (with and without crossflow) and descriptions of the nonideal build-up test pressure responses often observed in the field. Lefkovits *et al.*[4] presented analytical solutions for flow in layered reservoirs and identified several characteristic features of reservoirs with discrete, noncommunicating layers. Other investigators[5–15] presented numerous solutions describing pressure and flow rate that include the effects of interlayer crossflow, stimulation, or unsteady- (transient) or pseudo-steady-state (boundary-dominated) flow. Comprehensive analytical reservoir models have been developed specifically to model the pressure or flow rate response from layered reservoirs.[15]

Although much theory has been presented in the literature, case studies documenting layered reservoir analyses are not as common.[1,2,16–19] Much has been presented on fracture treatment optimization in tight reservoirs, but generally the impact of layering is not discussed.[3,19–25] The majority of layered reservoir analyses involve history matching data by use of reservoir simulators, although the recent availability of comprehensive analytical models should make layered analyses easier and more cost-effective.

Even with sophisticated computer programs for analysis of layered reservoirs, this analysis is still not straightforward. Cost-effective data collection methods for describing layered reservoirs are not developed easily because of the diverse nature of tight reservoirs and widely varying production volumes. Well-testing techniques

This paper is SPE 29091. **Distinguished Author Series** articles are general, descriptive representations that summarize the state of the art in an area of technology by describing recent developments for readers who are not specialists in the topics discussed. Written by individuals recognized as experts in the area, these articles provide key references to more definitive work and present specific details only to illustrate the technology. **Purpose:** to inform the general readership of recent advances in various areas of petroleum engineering. A softbound anthology, *SPE Distinguished Author Series: Dec. 1981-Dec. 1983*, is available from SPE's Book Order Dept.

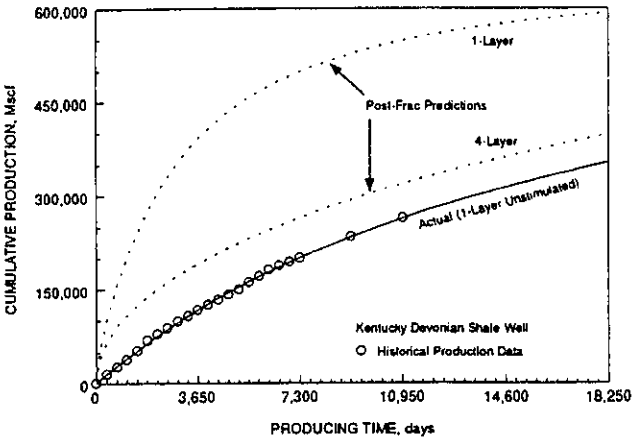

Fig. 1—Effect of oversimplified reservoir description on post-fracture performance predictions.

have been presented for estimating permeability in multiple layers in a single wellbore, but these techniques are often expensive to apply to every well. Log-based correlations are cost-effective but often must be calibrated for a specific formation in a specific area. The most cost-effective method for analyzing tight reservoirs usually involves detailed study of a few select wells so that the results can be used to streamline a procedure for analyzing other wells.

This paper presents three examples of reservoir studies performed on tight formations. The methods presented can be used as a guide to tailor reservoir studies to meet specific objectives in other fields or areas.

Field Examples

The three studies were performed on tight formations to provide examples of data collection and analysis. Two examples are from tight sands; one is for a productive gas shale. The first example describes a stimulation optimization study performed on the Elk sands of central Pennsylvania. The study is fairly straightforward because a layered reservoir model was not needed to describe the pre- and post-fracture production from the wells for stimulation optimization. The second example describes the integration of production and pressure-transient data to describe the Medina sand as a layered reservoir. This study was performed to determine why some wells did not perform as expected.

The last example illustrates a reservoir study performed on the Devonian shale in the Appalachian basin. Naturally fractured shale formations are among the most difficult reservoirs to characterize because of reservoir complexities and low profit margins. The GRI and DOE have been studying the shale for more than a decade; early results suggested that the shale was best described as a layered, naturally fractured reservoir. This example illustrates the detailed or "advanced" method used to construct and validate the reservoir description. Also presented is a more cost-effective "intermediate" method used to provide an adequate production forecast. An economic analysis indicated the cost-effectiveness of the methods.

Fracture Treatment Optimization Study

One common objective for studying tight reservoirs is to optimize the performance of hydraulic fracture treatments. Almost all tight reservoirs must be fracture stimulated to be economical. But fracturing costs can account for more than 50% of total well costs in some cases. To optimize a fracture treatment, a reservoir analysis must be performed in conjunction with a fracture treatment design analysis. Reservoir data (permeability, gas in place, natural fracturing, etc.) must be known, along with fracture treatment design data (rock mechanical properties, bounding layer stresses, fracturing-fluid viscosities, formation/fracturing-fluid interactions, etc.).

It is not uncommon to obtain three vastly different fracture treatment designs when three different service companies are asked to determine the optimal fracture treatment for a particular well or field. Because of the complexity of the problem, the data requirements for an optimization study are often uneconomical to obtain. Thus, the optimal treatment will vary considerably based on the assumptions in the analysis. A successful fracture treatment optimization is one that optimizes the production with minimal data collection costs. This process lends itself best to detailed study of a few wells, the results from which can be applied to many other wells. Sharing data and costs by operators benefits everyone in these studies.

This first example is a fracture treatment optimization study performed in the Elk sands of central Pennsylvania.[3] A systematic method for optimizing fracture treatments by integrating reservoir information with a fracture design model is outlined. In this particular case, a single-layer reservoir model was sufficient for describing the reservoir and predicting well performance. This example is important because it illustrates how data from several test wells can be used to simplify and streamline the optimization process for future wells—an essential feature of most fracture treatment optimization studies.

The Elk sands in the Council Run field are completed at depths from 4,000 to 4,700 ft and have small net pay thicknesses ranging from 5 to 10 ft. The wells are normally pressured, with reservoir pressures ranging from 1,700 to 2,000 psia; gas porosities range from 5% to 15%. Historically, wells in the Council Run field were stimulated with 40,000 lbm of 20/40-mesh sand and 25,000 gal of 10 lbm/ 1,000 gal linear gel fluid. Maximum sand concentrations pumped were generally <3 lbm/gal.

Wells usually were not tested before stimulation for evaluating reservoir quality. Eastern States Exploration (ESE) broke down an Elk sand well with acid to test the well's ability to flow before fracturing. After breakdown, the well flowed at a rate comparable to that of a hydraulically fractured well. This suggested that the historical treatments may not have been effective and that modifications to the fracture treatments might increase production.

On the basis of the results of the breakdown treatment, ESE initiated a fracture treatment optimization study on the Elk sand formation in the Council Run field by integrating results from prestimulation well-test and production data analysis, fracture treatment design models, and poststimulation well-test and production data analysis. After several treatment and procedure modifications, an inexpensive and cost-effective method was developed to optimize stimulation results.

During the first part of the study, existing data were collected and reviewed to evaluate the potential for improved stimulation results. Initial open-flow test data[24] and postfracture production data were analyzed on 10 wells with single-point flow analysis[24] techniques and production data analysis[25] techniques. The 10 wells were selected to provide a sample set including good, average, and poor wells.

Without an independent estimate of permeability from prefracture well-test or other data, it is difficult to obtain unique estimates of permeability and stimulation effectiveness from production data analysis alone.[25] Therefore, a range of permeabilities and qualitative estimates for stimulation effectiveness were determined from the production data. Of the 10 wells, 5 appeared to be moderately stimulated; the others were not stimulated at all. Production forecasts based on these analyses indicated that substantial increases in production were attainable and that further study was justified.

The historical fracture treatments pumped were reviewed with a fracture design simulator. At the time, the general consensus in the field was that the fracture treatments were relatively contained with fracture heights at the wellbore of ≈ 150 to 200 ft. With a pseudo-3D fracture design model,[26] the historical treatments were simulated to estimate effective fracture half-lengths. Because of the low viscosity of the fracturing fluid (≈ 16 cp), severe sand settling was predicted; the majority of the sand settled to the bottom of the fracture, resulting in effective fracture half-lengths of ≈ 10 to 30 ft.[27] The fracturing model showed that, with increases in fracturing-fluid viscosity and the maximum sand concentration to 6+ lbm/gal, effective fracture half-lengths of 500 to 1,000 ft could be expected.

The modified treatments were pumped on five test wells, and detailed treating pressure data were collected on each well. Before stimulation, each well was broken down and flow tested for several

weeks to estimate formation permeability. With the permeability estimated from the prefracture production data, the postfracture production data were analyzed to estimate effective fracture half-lengths created by the modified stimulation treatments.

All the fracture treatments resulted in an increase in production from prefracture rates, as **Table 1** shows. However, the effective fracture half-lengths estimated from the production data were still shorter than those predicted with the fracture design model. Unless we can predict postfracture performance accurately using fracture design and reservoir models, we cannot design the optimal treatment. Therefore, a third phase in the study was initiated to reconcile the differences between the half-lengths predicted from performance data and the designed fracture half-lengths.

A review of the detailed treating pressure records from the five wells suggested that uncontained fracture height growth occurred because of a decreasing net fracture pressure.[28] Each fracture treatment was then resimulated with the fracture design model, assuming uncontained, radial fracture height growth.[29] As Table 1 shows, the predicted effective fracture half-lengths from the radial growth model more closely matched the fracture half-lengths determined from well performance.

For the third phase of the study, four wells were broken down, flow tested for 2 weeks, and shut in for 2-week pressure-buildup tests. Analysis of the pressure data yielded permeabilities of 0.0064 to 0.11 md. Three of the four tests exhibited a characteristic dual-porosity test response, possibly as a result of natural fractures.[30,31] Optimal fracture treatments were designed for each well by predicting performance with the assumption that different effective fracture half-lengths (150 to 450 ft) could be created in each well. The fracture design simulator with uncontained fracture growth was used to predict treatment sizes and costs for creating each fracture half-length assumed in the forecasts. The optimal fracture treatment size was chosen as the one that maximized the ratio of fracture net present value[18] to fracture treatment cost (**Fig. 2**). Fracture net present value is calculated from the difference between forecasted production with and without a hydraulic fracture. A risk factor was also included in the analysis to account for the lower success rates associated with pumping larger treatments in this area.

After each "optimized" treatment was pumped and cleaned up, postfracture flow and pressure-buildup tests were conducted to evaluate treatment effectiveness. In three of the four wells, the fracture half-lengths designed and achieved compared favorably (**Table 2**). **Fig. 3** compares the predicted postfracture flow rates with the actual postfracture flow rates for one test well. These forecasts were found to be valid even after several years of production. Because we can predict postfracture flow rates, we can now design optimal fracture treatments for the Council Run field.

To streamline the optimization method so that it can be applied efficiently to every new well, numerous simulation runs were made using the reservoir model and the fracture design simulator. An empirical fracture design optimization curve was developed for wells in the Council Run field (**Fig. 4**). New wells in the field are drilled with air, and after penetrating the Elk sand, a flow test is conducted and used to estimate permeability. Treatment optimization is performed by using this value of permeability with Fig. 4 to determine the optimal fracture half-length and job size on a well-by-well basis.

Fig. 4 illustrates some key results about the optimal fracture half-lengths in the Council Run field. First, as permeability decreases, the optimal fracture half-length increases. However, when the permeability is too small, hydraulic fracturing is uneconomical because the expected increase in production is insufficient to justify the fracturing costs. Finally, two curves are shown for a 5- and a 10-ft net pay thickness, typical in the Council Run field. For the thicker sands, the optimal half-length is longer because the expected incremental production is larger.

This example was fairly simple in scope but clearly identified the benefits of the optimization process and how the process can be streamlined for increased efficiency. The many other potential complications in tight reservoir analysis were not addressed in this example. Layered reservoir effects, unimportant in this example because of the thin pay, can be very important in other applications.[1,15,32] The remaining two examples focus on different aspects of layered reservoir analysis. Other potential fracture treatment optimization complexities include simultaneous optimization of drainage area,[20,33] directional permeability anisotropy and its effect on production,[20] and more complex two-phase analyses.[16]

Evaluation of Low-Productivity Wells

The Medina sand is a common completion target throughout Ohio and western Pennsylvania and usually must be fracture stimulated to be productive. In unpublished results, an operator completing wells in western Pennsylvania performed an in-depth study of the producing characteristics of the Medina, which is classified as a tight gas sand in many areas. Some wells that were completed in the late 1980's were not performing as expected.

In western Pennsylvania, the Medina sandstone is typically completed at depths from 4,000 to 6,000 ft. The Medina consists of 60 to 100 ft of gross sandstone interspersed with shale beds. Typical productive pay ranges from 50 to 70 ft; porosities range from 5% to 10%; and initial pressures range from 1,500 to 2,000 psig.

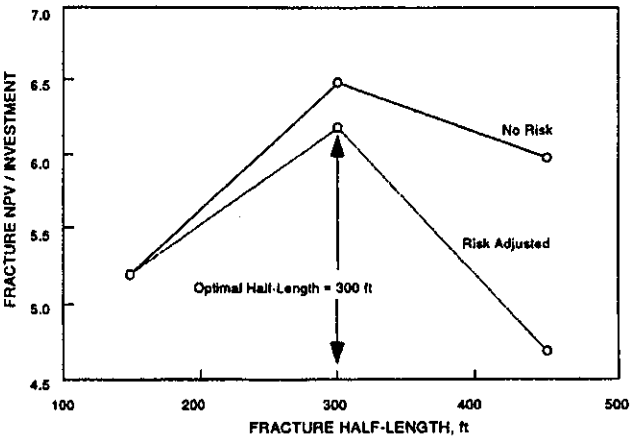

Fig. 2—Fracture optimization plot for typical well with and without adjustments for risks.

TABLE 1—COMPARISON OF FRACTURE HALF-LENGTH PREDICTED BY DESIGN MODEL AND CALCULATED FROM PERFORMANCE DATA

	Calculated Fracture Half-Length (ft)				
Well	Production Data Analysis	Radial Fracture Height Growth Model	Contained Fracture Height Growth Model	Prefracture Flow Rate (Mscf/D)	Postfracture Flow Rate (Mscf/D)
CR-8	180	300	625	24	125
CR-10	500	240	450	22	80
CR-11	300	320	680	50	350
CR-12	100	360	1,400	38	240
CR-13	34	260	500	29	60

TABLE 2—STIMULATION RESULTS FOR FINAL FOUR ELK STUDY WELLS				
Well	Design Fracture Half-Length (ft)	Achieved Fracture Half-Length (ft)	Prefracture Flow Rate (Mscf/D)	Postfracture Flow Rate (Mscf/D)
CR-14	150	120	110	350
CR-15	300	230	100	450
CR-16	450	450	25	100
CR-17	200	34	60	100

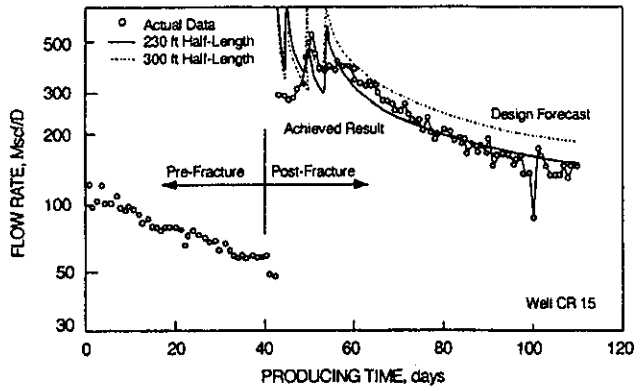

Fig. 3—Comparison of predicted-to-achieved, post-fracture performance for well CR-15.

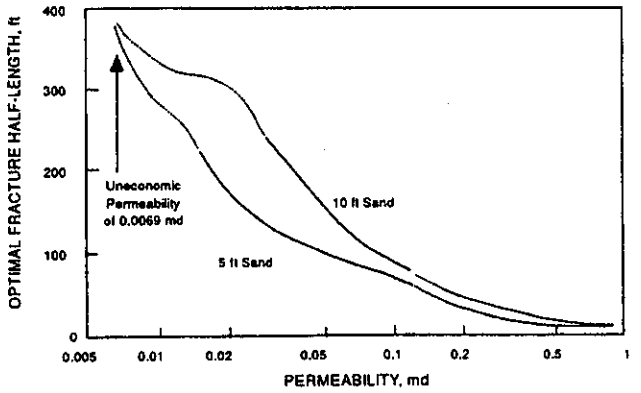

Fig. 4—Optimal fracture design half-length as a function of permeability for 5- and 10-ft Elk sands in the Council Run field.

Five wells, chosen to represent typical wells, were selected for further study. On the basis of a correlation between productive net pay thickness and estimated ultimate recovery, one well was producing better than expected, two wells as expected, and two wells below expectations. It was hypothesized that the observed production decline on several wells was the result of a loss in fracture conductivity over time. To evaluate the hydraulic fracture in each well, 4-week pressure-buildup tests were conducted on each well after the well produced for ≈2 to 4 years. Recoveries were between 82 and 369 MMscf in 2 years, a typical range for Medina wells. Each well had been fracture stimulated with 90,000 lbm of sand and 75%-quality foam (5-lbm/gal maximum sand concentration) during initial completion operations.

The initial phase of the study consisted of analyzing the historical production data[25] to estimate ranges for permeability and stimulation effectiveness. This analysis was performed to obtain a general idea of the productive characteristics of the wells with a "simple" reservoir description. Generally, it is best to start with simple models and progress to more complex models only as needed to describe a reservoir adequately.

Our analysis indicated that all wells were still infinite-acting—i.e., boundary effects were not yet important. Permeability-thicknesses ranged from 0.05 to 1.4 md-ft based on a range of assumed fracture half-lengths. We were unable, however, to match the production data assuming no stimulation, which suggested that all five wells were at least slightly stimulated.

The 4-week pressure-buildup tests were analyzed with conventional type-curve analysis techniques. All five buildup test plots had shapes characteristic of stimulated wells (**Fig. 5**). Both the pressure change and pressure derivative graphs are parallel, indicating that, without an estimate for permeability, a unique estimate for fracture half-length is not possible with conventional techniques. Because all five tests were still exhibiting linear flow from the formation to the fracture (half-slope on a log-log plot), we could estimate minimum fracture half-lengths ranging from 238 to 527 ft for the five wells.

Because unique estimates for permeability and fracture half-length were not possible from either conventional production or buildup test analysis, a finite-difference reservoir simulator was used to history match both the production and buildup data, a process that often results in less ambiguous results because the same reservoir description must model both long-term production and short-term pressure-buildup behavior. Because more data must be matched, a less ambiguous result can be obtained.

We first tried to match the production and pressure buildup data using a single-layer reservoir model.[25] Only one well could be matched with this model. For the other four wells, an adequate match of the production data resulted in a poor match of the buildup data (**Fig. 6**). The measured bottomhole pressures (BHP's) after 4 weeks of shut-in ranged from 330 to 559 psia, substantially lower than the initial pressures of 1,500 to 1,700 psia. Therefore, the simulated BHP's during the buildup tests would increase too rapidly to match the measured data, regardless of the combinations of permeability and fracture half-length used.

To determine why only one well could be matched with the single layer model, a detailed review of the available log and core data was performed. A log resistivity-to-permeability correlation developed for the area was used to rank net pay thickness based on above-average, average, and below-average permeabilities. The well that could be matched with a single-layer model lacked high-permeability pay; other wells had high-permeability pay ranging from 15% to 40% of the total pay.

Using the permeability correlation to distribute the net pay and porosity into high-permeability and low-permeability layers, the production and buildup data were rematched with a two-layer model.[35]

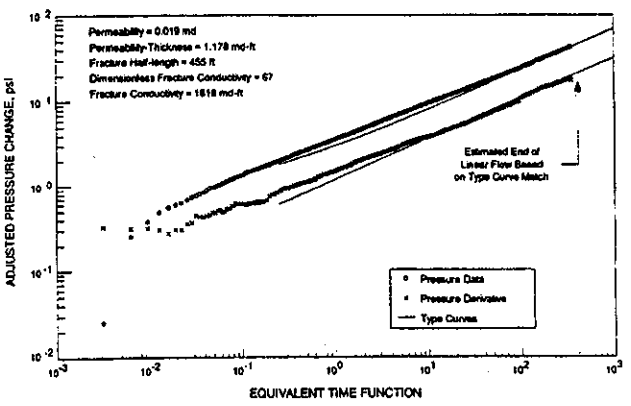

Fig. 5—Type curve match of the Medina well pressure-buildup data on the Cinco type curve for finite-conductivity fractures.

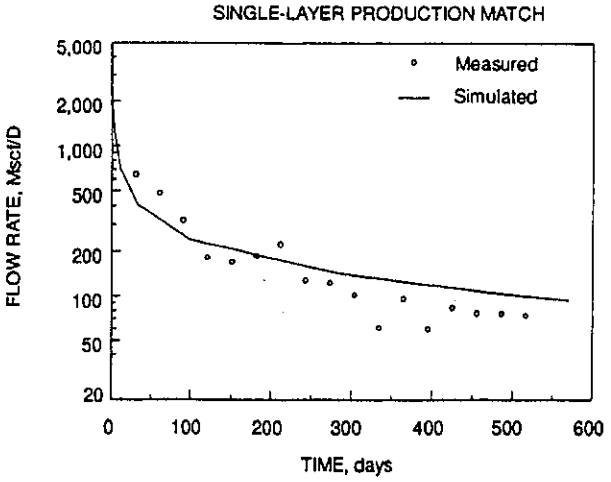

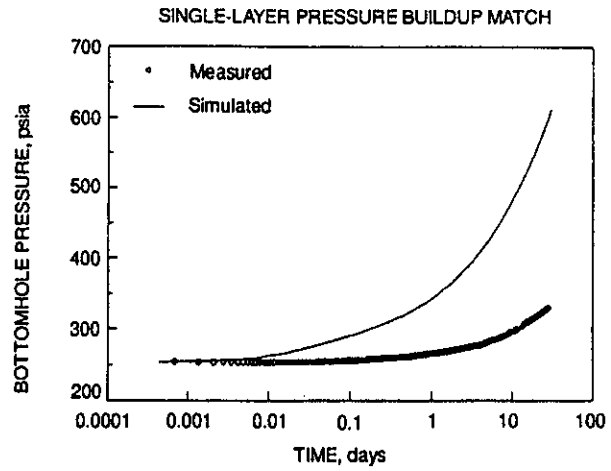

Fig. 6—History match of production and pressure-buildup data from the Medina well with single-layer reservoir model.

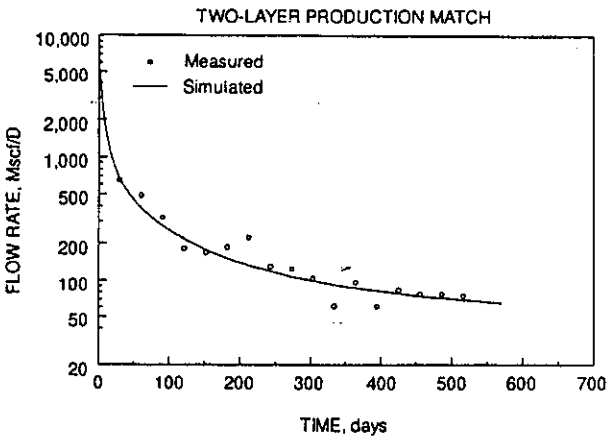

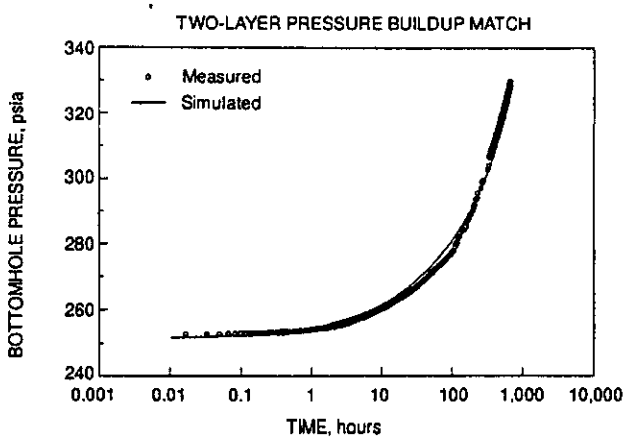

Fig. 7—History match of production and pressure-buildup data from the Medina well with two-layer reservoir model.

Much better matches of both the production and pressure buildup data were obtained for all four wells (**Fig. 7 and Table 3**).

All four reservoir descriptions were similar in that they consisted of a high-permeability layer of finite area and an infinite-acting lower-permeability layer, both in contact with a long hydraulic fracture. A 70-acre drainage area was used to simulate the lower-permeability layer to honor current well spacing.

The results in Table 3 may not be unique because changes in our assumptions of layer properties will change our match results. However, this exercise did illustrate that a two-layer model with one layer having the majority of the permeability and the other having the majority of the gas in place is needed to match all the data. During the buildup test, crossflow in the fracture and wellbore from the low-permeability to the high-permeability layer resulted in the low final buildup test pressures. Essentially, the low-permeability layer is recharging the high-permeability layer. The inverse of this behavior is the cause of the decline in production in these wells. It is also responsible for the high flush production that is typical after these wells have been shut in.

The reservoir study of the Medina wells was beneficial for several reasons. First, the results indicate that the initial declines of these wells are the result of an effectively stimulated high-permeability layer depleting rapidly. After partial depletion of this layer, long-term performance is controlled by the low-permeability layer. Refracturing, which was considered for increasing productivity, would probably not increase the production from these wells. In fact, several poorly producing wells were refractured without any appreciable increase in production. Finally, the results were used to modify the correlation of productive net pay and ultimate recovery by including the permeability-resistivity correlation. This resulted in a better indicator of well potential.

Analysis of Naturally Fractured Shale Reservoir

A shale reservoir is probably one of the most complex types of formations that we develop. Typically, shale reservoirs are thick (100 + ft) with large amounts of gas in place. However, because of extremely low matrix permeabilities, natural fracturing is usually required for wells to be economical. Our last example illustrates a complex reservoir characterization of the Devonian shale.[1] This example illustrates the development of two reservoir descriptions for the shale. One description was based on a detailed or "advanced" data set. The second was based on a less detailed, "intermediate" data set.

Devonian Shale. The GRI and DOE have been funding research in the Devonian shale of the Appalachian basin for over a decade; the shale constitutes a large potential gas resource. Much of this research has focused on advancing hydraulic fracturing technology as a means to increase the deliverability from these generally low-productivity wells.[35] However, early results indicated that wells never performed as well as expected after stimulation, suggesting that more detailed reservoir characterization was needed. The "simple" single-layer forecasts generally overstated the production potential of the shale, both before and after stimulation (Fig 1).[1,35] GRI undertook a field-based research program in 1992 to understand the production potential of shale wells and to reconcile the discrepancies between actual and predicted post-stimulation production potential.

TABLE 3—TWO-LAYER HISTORY MATCH RESULTS FOR MEDINA SAND WELLS

Well	Layer 1 Permeability-Thickness Product (md-ft)	Layer 1 Original Gas In Place (MMscf)	Layer 2 Permeability-Thickness Product (md-ft)	Layer 2 Original* Gas in Place (MMscf)	Fracture Half-Length (ft)
A	—	—	0.07	1,060	520
B	0.616	226	0.10	725	600
C	1.05	254	0.42	861	680
D	5.07	82	0.305	687	470
E	0.132	94	0.008	726	680

*Based on 70-acre drainage area, Layer 2 still infinite-acting.

During 1992 and 1993, two Devonian shale wells [the COOP 1 and Experimental Development (ED)] were drilled and evaluated in Pike County, KY, in cooperation with Ashland Exploration. Both wells, located ≈ 1 mile apart, were completed in the Devonian shale and fracture stimulated with variable-quality nitrogen foam and sand treatments. Extensive log, whole-core, and pre- and post-stimulation pressure-transient data collected on both wells were used to develop detailed naturally fractured and layered reservoir descriptions. These reservoir descriptions were used to predict accurately both pre- and post-stimulation production performance from both wells.[2]

In Pike County, the Devonian shale consists of organic-rich black shales interbedded with organic-poor gray shales. The primary completion interval consists of the Transition zone and Lower Huron members of the Ohio shale. The Transition zone, generally 100 to 150 ft thick, lies above the Lower Huron shale. It consists of interbedded gray and black shales and represents a transition from the gray shales of the overlying Chagrin shale to the black shales of the underlying Lower Huron. The Lower Huron consists of 200 to 275 ft of predominantly black shales with moderate amounts of gray shales and some siltstones.

As part of this projcet, a methodology was developed for describing the shale as a layered, naturally fractured reservoir. Detailed data were collected solely to support this reservoir characterization effort. The method consisted of three main steps: (1) identify layers; (2) estimate the amount of gas in each layer; and, (3) estimate the permeability (matrix and bulk) in each layer.

From a review of whole core, natural fracture identification logs, and borehole camera data, natural fractures observed ranged from 1 to 10+ ft in vertical extent. These fractures were found to terminate at lithologic changes within the core and/or zones with large stress contrasts. On the basis of this observation, a combination of stress profile, lithology, fracture identification, and porosity logs was used to select layer boundaries.

Selection of initial layer boundaries was based on lithology changes that were further refined by use of a stress profile log computed from a full-waveform sonic log and calibrated to cased-hole stress tests. Computed porosity and fracture identification logs were reviewed to ensure that a selected layer boundary did not intersect identified natural fractures or high-porosity intervals. For the shale intervals in the two wells, we selected 11 layers (Layers A through K) that correlated between the two wells.

For each layer, free gas and net pay thickness were estimated with a shale-specific log interpretation model.[36] Adsorption isotherms, measured in the laboratory on whole-core samples, indicated that approximately one-half the gas in place is adsorbed to the organic material or dissolved in the liquids in the two wells.[1]

Finally, the third and most difficult step was to estimate both matrix and bulk permeabilities for each layer. Previous attempts to estimate Devonian shale matrix permeabilities were unsuccessful owing to coring-induced microcracks and the inability of most existing permeameters to measure permeabilities below about 10^{-5} md. New grain cup and pulse permeameter techniques were developed to measure matrix permeabilities of 10^{-7} to 10^{-9} md.[37]

If matrix permeability is sufficiently low, the bulk permeability of each layer will be dominated by the permeability of the natural fracture system in the layer. Natural fracture and bulk permeabilities were estimated from individual-layer nitrogen slug tests and conventional well tests in combination with natural fracture information from whole core, natural fracture logs, and borehole camera logs.

Nitrogen slug tests[38] are similar to water slug tests often performed on coalbed methane wells but are shorter (about 2 hours) and less damaging to the low-pressure Devonian shales. The test consists of isolating a layer in the open or cased hole, injecting a "slug" of nitrogen into the wellbore to a pressure above reservoir pressure but below fracturing pressure, and monitoring the pressure falloff. From analysis of the data, estimates of individual-layer bulk permeabilities, skin factors, and reservoir pressures were obtained. In fact, these tests verified the layered reservoir description. We identified variable reservoir pressure profiles in both wells, which indicated that the layers were not in vertical communication and therefore should be treated as individual reservoirs.[38]

The natural fracture identification tools were used to quantify the natural fractures (strike, frequency, and location) in each layer.[39] For simplicity of modeling, the natural fractures were grouped into two sets, east/west-trending fractures (primary) and all other striking fractures (intersecting). The east/west-trending fractures were chosen as the primary fractures because they tended to be more continuous vertically, had wider apertures, and tended to intersect a created northeast/southwest-trending hydraulic fracture. With this fracture information, bulk permeabilities in the primary direction, k_x, and intersecting direction, k_y, could be calculated.

Fig. 8 summarizes the key components of the reservoir descriptions for the six primary layers in both wells. These reservoir descriptions were used to predict pre- and post-stimulation performance for both wells using a 3D, single-phase reservoir simulator that includes adsorbed and free gas, explicit modeling of the natural fractures, and unsteady-state gas flow in the matrix. **Fig. 9** is an example of the excellent comparison between predicted and actual flow rates, both before and after stimulation, for the COOP 1 well.

A comparison between the reservoir descriptions developed for the two wells suggested that natural fractures, distributed discretely into lithologic layers, were the best indicator of well productivity. The importance of natural fracturing was not surprising. However, we found it necessary to describe the fractures quantitatively (frequency, strike, and location) because lumped fracture properties were insufficient for describing the production potential from individual layers and the total well potential. The most productive layers had numerous natural fractures with different striking directions, resulting in a well-connected natural fracture system.

Detailed data were collected at great cost on these two shale wells specifically for describing the shales as layered, naturally fractured reservoirs. Unfortunately, because of the rigid economics for shale and other tight wells, it is not cost-effective to collect this type of information routinely. Therefore, the available data were reviewed to determine whether a more cost-effective method could be used with similar results.

Using a smaller and less expensive or intermediate data set, a five-layer reservoir description was developed for the ED well, which contrasts with the 11-layer model developed with the full or advanced data set. A sensitivity analysis indicated that the most important parameters for predicting well performance accurately were the

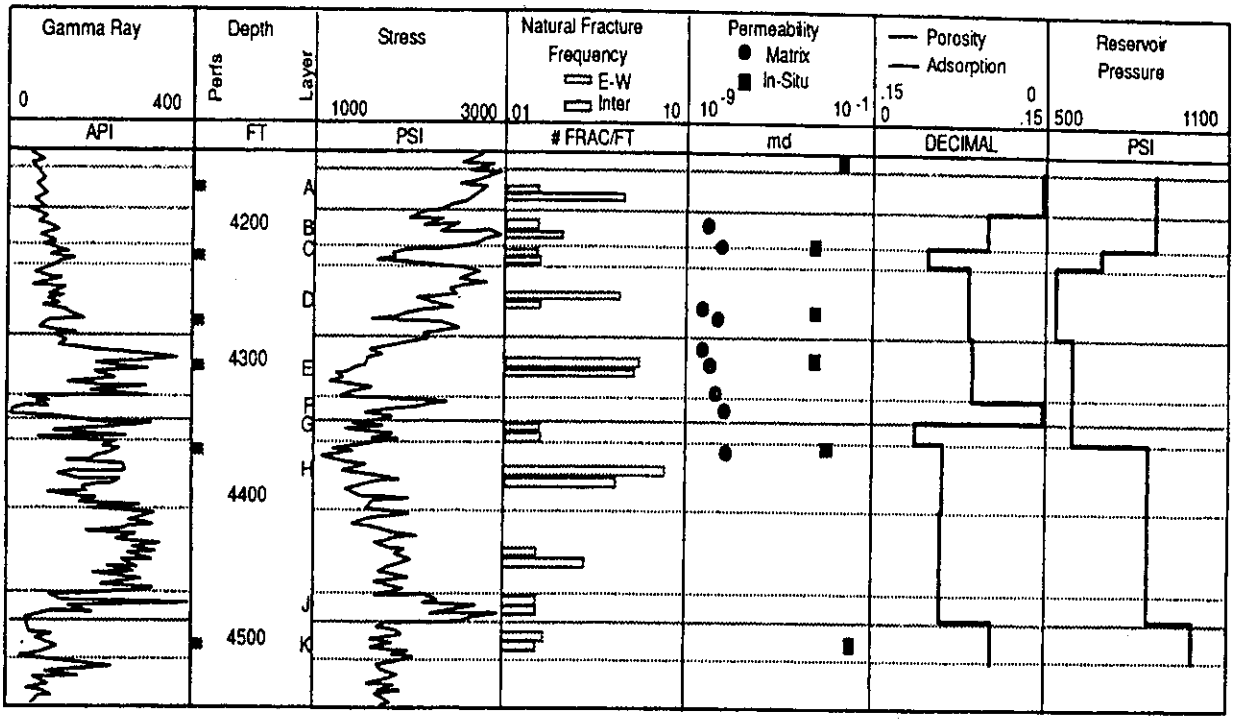

Fig. 8—Devonian shale well reservoir description.

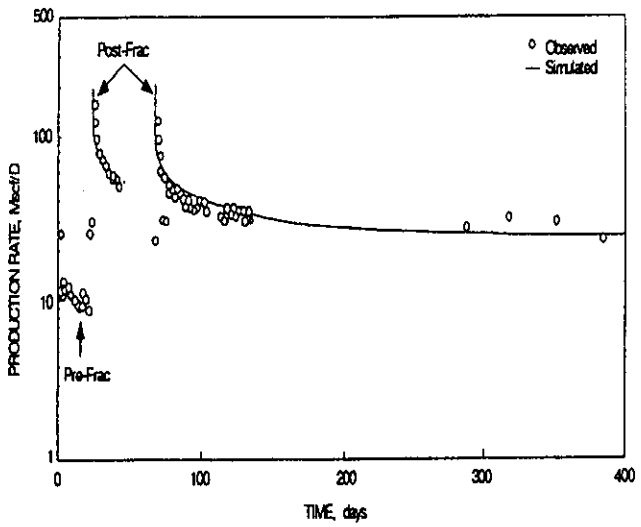

Fig. 9—Simulation of pre- and postfracture production from Coop 1 shales with 11-layer model.

layer permeabilities and fracture spacing.[40] For the intermediate data set, fracture spacings were estimated from borehole camera data, and layer permeabilities were estimated from fracture spacing information or one-point data and calibrated to the total-well pressure-buildup test. Average values for matrix permeability and gas adsorption were assumed on the basis of lithology correlations, and stress profiles were calculated from calibrated cased-hole sonic logs.

This less expensive data set provided a reasonable representation of the layered reservoir (**Fig. 10**). The intermediate data set resulted in a 30-year predicted recovery within 10% of the more detailed 11-layer model. The single-layer model predicts a recovery of more than twice the 11-layer model at 30 years.

Even though we identified an intermediate data set that provided reasonable results, the cost effectiveness of the approach was still in question. To evaluate the relative benefits of acquiring the different data sets, a statistical study was performed using a low-, intermediate-, and high-cost data set.[40] The study suggested that collecting data in sufficient detail to describe the shales as a layered reservoir was generally cost-effective, with the intermediate data set providing the optimal results.

By adequately describing the shales, the realistic potential of hydraulic fracturing for increasing production can be evaluated and optimized. That is, the treatment size can be adjusted on the basis of a well's natural productivity to maximize the economic benefit of the treatments. Results showed that these characterization efforts were economical, especially if hydraulic fracture growth is at least confined mainly to the completion interval because of a favorable stress profile.

This example illustrates one of the more detailed attempts to describe a low-permeability reservoir with a layered, naturally fractured model. It clearly shows that, if the reservoir is described correctly, both pre- and post-stimulation production can be predicted accurately for sound engineering decisions. The level of detail in this example usually is impractical on a routine basis. But the example does illustrate how detailed data can be collected and analyzed for one or two wells to help understand the reservoir in a particular area. This understanding can then be used to develop a more cost-ef-

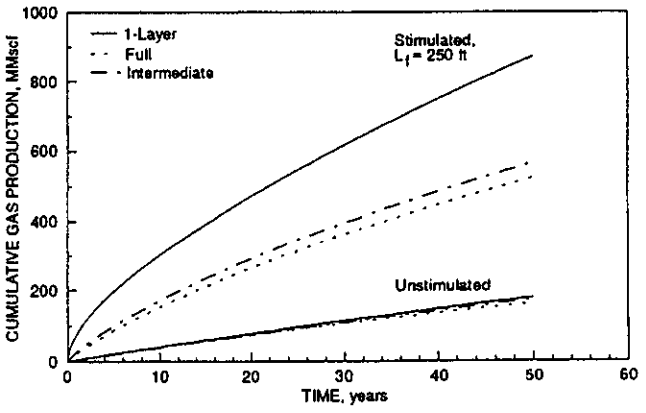

Fig. 10—Well performance estimates using full and intermediate data sets.

fective "intermediate" data collection method (natural fracture logs, core, and borehole camera) method for application to future wells.

Concluding Remarks

Simplistic reservoir descriptions for complex reservoirs can lead to optimistic production forecasts. A reservoir description should be developed in sufficient detail to allow realistic production forecasts whenever the data collection costs are justified. In formations with marginal economics, simplified correlations or procedures should be developed to construct reservoir descriptions and to forecast production.

Many tight gas sands and shales are naturally fractured and/or layered. Simple reservoir descriptions might seem adequate for modeling either short-term transient behavior or long-term boundary-dominated reservoir behavior, but the correct reservoir description must model both. We presented two examples of layered reservoirs in which the reservoir description leads to a match of both short- and long-term behavior. These examples illustrated data requirements for both shale and sand reservoirs.

A third example illustrated a fracture optimization study. Fracture treatment design models and reservoir models for predicting performance must be used together during optimization. If one model is incorrect, the fracture design and implementation process cannot be optimized. Therefore, the optimization process may require several iterations (prefracture design, implementation, postfracture evaluation) until the results from the two models agree.

References

1. Jochen, J.E. and Lancaster, D.E.: "Reservoir Characterization of an Eastern Kentucky Devonian Shales Well Using a Naturally Fractured, Layered Description," paper SPE 26192 presented at the 1993 SPE Rocky Mountain Regional/Low Permeability Reservoirs Symposium, Denver, April 26–28.
2. Frantz, J.H., Gatens, J.M. III, and Hopkins, C.W.: "Using a Multilayer Reservoir Model To Describe a Hydraulically Fractured, Low-Permeability Shale Reservoir," paper SPE 24885 presented at the 1992 SPE Annual Technical Conference and Exhibition, Washington, DC, Oct. 4–7.
3. Hopkins, C.W. *et al.*: "Stimulation Optimization in a Low-Permeability, Upper Devonian Sandstone Reservoir: A Case History," paper SPE 21499 presented at the 1991 SPE Gas Technology Symposium, Houston, Jan. 23–25.
4. Lefcovits, H.C. *et al.*: "A Study of the Behavior of Bounded Reservoirs Composed of Stratified Layers," *SPEJ* (March 1961) 43; *Trans.*, AIME, **222.**
5. Russell, D.G. and Prats, M.: "Performance of Layered Reservoirs With Crossflow—Single-Compressible-Fluid Case," *SPEJ* (March 1962) 53; *Trans.*, AIME, **225.**
6. Bennett, C.O. *et al.*: "Approximate Solutions for Fractured Wells in Layered Reservoirs," *SPEJ* (Oct. 1985) 729.
7. Bennett, C.O. *et al.*:"Analysis of Finite-Conductivity Fractures Intercepting Multilayer Reservoirs," *SPEFE* (June 1986) 259; *Trans.*, AIME, **281.**
8. Kuchuk, F.J. and Wilkinson, D.J.: "Transient Pressure Behavior of Commingled Reservoirs," *SPEFE* (March 1991) 111.
9. Fetkovich, M.J. *et al.*: "Depletion Performance of Layered Reservoirs Without Crossflow," *SPEFE* (Sept. 1990) 310; *Trans.*, AIME, **289.**
10. Cobb, W.M. *et al.*: "Well-Test Analysis for Wells Producing Commingled Zones," *JPT* (Jan. 1972) 27; *Trans.*, AIME, **253.**
11. Raghavan, R. *et al.*: "Well-Test Analysis for Wells Producing From Two Commingled Zones of Unequal Thickness," *JPT* (Sept. 1974) 1035; *Trans.*, AIME, **257.**
12. Larsen, L.: "Determination of Skin Factors and Flow Capacities of Individual Layers in Two-Layered Reservoirs," paper SPE 11138 presented at the 1982 SPE Annual Technical Conference and Exhibition, New Orleans, Sept. 26–29.
13. Kuchuk, F. *et al.*: "Well Testing and Analysis Techniques for Layered Reservoirs," *SPEFE* (Aug. 1986) 342.
14. Raghavan, R.: "Behavior of Wells Completed in Multiple Producing Zones," *SPEFE* (June 1989) 219.
15. Johnston, J.L. and Lee, W.J.: "Identification of Productive Layers in Low-Permeability Gas Wells," *JPT* (Nov. 1992) 240.
16. Holditch, S.A., Robinson, B.M., and Whitehead, W.S.: "The Analysis of Complex Travis Peak Reservoirs in East Texas," paper SPE 16427 presented at the 1987 SPE/DOE Low Permeability Reservoirs Symposium, Denver, May 18–19.
17. Lancaster, D.E., *et al.*: "Reservoir Evaluation, Completion Techniques and Recent Results from Barrett Shale Development in the Fort Worth Basin," paper SPE 24884 presented at the 1992 Annual Technical Conference and Exhibition, Washington, Oct. 4–7.
18. Meng, H.Z. and Brown, K.E.: "Coupling of Production Forecasting, Fracture Geometry Requirements and Treatment Scheduling in the Optimum Hydraulic Fracture Design," paper SPE 16435 presented at the 1987 SPE Low Permeability Reservoirs Symposium, Denver, May 18–19..
19. Rodgers, J.D.: "Optimization of Hydraulic Fracturing Treatments Applying Post-Fracture Pressure Analysis for the Upper Clearfork Formation," paper SPE 18822 presented at the 1989 SPE Production Operations Symposium, Oklahoma City, March 13–14.
20. Meehan, D.N.: "Optimization of Fracture Length and Well Spacing in Heterogeneous Reservoirs," paper SPE 21717 presented at the 1991 Produetion Operations Symposium, Oklahoma City, April 7–9.
21. Anderson, R.W. and Phillips, A.M.: "Use of Single-Well Simulators and Economic Performance Criteria To Optimize Fracturing Treatment Design," *SPEPE* (Feb. 1990) 27.
22. Aminian, K. *et al.*: "The Evaluation and Optimization of Hydraulic Fracturing Treatments for the Big Injun Formation in West Virginia," paper SPE 18540 presented at the 1986 SPE Eastern Regional Meeting, Charleston, Nov. 1–4.
23. Ahmed, U. *et al.*: "Optimizing Hydraulic Fracture Designs in Formations With Poor Containment," paper SPE 13375 presented at the 1984 Eastern Regional Meeting, Charleston, Oct. 31–Nov. 2.
24. Lee, W.J. *et al.*: "Estimating Formation Permeability from Single-Point Flow Data," paper SPE 12847 presented at the 1984 SPE/DOE/GRI Unconventional Gas Recovery Symposium, Pittsburgh, May 13–15.
25. Murtha, J.A. *et al.*: "Practical Analysis Methods for Well Test and Production Data," S.A. Holditch & Assocs. Inc. topical report to the GRI, GRI Contract No. 5084-213-0980, Oct. 1987.
26. Palmer, I.D. and Luiskufty, C.T.: "A Model of the Hydraulic Fracture Process and Comparison of Results With Other Models," paper SPE 1364 presented at the 1985 SPE/DOE Symposium on Low Permeability Gas Reservoirs, Denver, May 19–22.
27. Prats, M.: "Effect of Vertical fractures on Reservoir Behavior-Incompressible Fluid Case," *SPEJ* (June 1961) 105; *Trans.*, AIME, **222.**
28. Nolte, K.G. and Smith, M.B.: "Interpretation of Fracturing Pressures," paper 8297 presented at the 1979 SPE Annual Technical Conference and Exhibition, Las Vegas, Sept. 23–26.
29. Geertsma, J. and de Klerk, F.: "A Rapid Method of Predicting Width and Extent of Vertical, Hydraulically Induced Fractures," *JPT* (Dec. 1969) 1571; *Trans.*, AIME, **246.**
30. Warren, J.E. and Root, P.S.: "The Behavior of Naturally Fractured Reservoirs," *SPEJ* (Sept. 1963) 245; *Trans.*, AIME, **249.**
31. Bourdet, D. *et al.*: "Interpreting Well Tests in Fractured Reservoirs," *World Oil* (April 1984) 111.
32. Frantz, J.H. Jr. *et al.*: "Reservoir and Stimulation Evaluation of the Berea Sandstone Formation in Pike County, Kentucky," paper SPE 25896 presented at the 1993 SPE Rocky Mountain Regional/Low Permeability Reservoirs Symposium, Denver, April 12–14.
33. Holditch, S.A., Jennings, J.W., and Neuse, S.H.: "The Optimization of Well Spacing and Fracture Length in Low Permeability Gas Reservoirs," paper SPE 7496 presented at the 1978 SPE Annual Technical Conference and Exhibition, Houston, Oct. 1–3.
34. *SHALEGAS, A Simulator for Fractured Gas Reservoirs*, S.A. Holditch & Assocs. Inc., College Station, TX (Jan. 1993) version 4.1.
35. McBane, R.A.: "Building on the CSW Program: A Plan to Characterize the Ohio Shale," *Devonian Gas Shales Technology Review* (March 1992) **7**, 3–5.
36. Truman, R.B. and Campbell, R.L. Jr.: "Devonian Shale Well Log Interpretation," ResTech Houston final report to the GRI, GRI Contract No. 5083-213-1390, GRI87/00092, April 1987.
37. Ning, X. *et al.*: "The Measurement of Matrix and Fracture Properties in Naturally Fractured Cores," paper SPE 25898 presented at the 1993 SPE Rocky Mountain Regional/Low Permeability Reservoirs Symposium, Denver, April 26–28.
38. Jochen, J.E., Hopkins, C.W., and Frantz J.H. Jr.: "Quantifying Layered Reservoir Properties With a Novel Permeability Test," paper SPE 25864 presented at the 1993 SPE Rocky Mountain Regional/Low Permeability Reservoir Symposium in Denver, April 26–28.
39. Kubik, W. and Lowry P.: "Fracture Identification and Characterization Using Cores, FMS, CAST, and Borehole Camera: Devonian Shale, Pike County, Kentucky," paper SPE 25897 presented at the 1993 SPE Rocky Mountain Regional/Low Permeability Reservoirs Symposium, Denver, April 26–28.
40. Voneiff, G.W. and Gatens, J.M. III: "The Benefits of Applying Technology to Devonian Shale Wells," paper SPE 26890 presented at the 1993 SPE Eastern Regional Meeting, Pittsburgh, Nov. 2–4.

SI Metric Conversion Factors

acre × 4.046 873	E − 01 = ka
cp × 1.0*	E + 00 = mPa · s
ft × 3.048*	E − 01 = m
ft^3 × 2.831 685	E − 02 = m^3
gal × 3.785 412	E − 03 = m^3
mile × 1.609 344*	E + 00 = km
psi × 6.894 757	E + 00 = kPa

*Conversion factor is exact.

W. John Lee holds the Samuel Roberts Nobel Chair in Petroleum Engineering at Texas A&M U. and works with S.A. Holditch & Assocs. Inc. in College Station. An SPE Distinguished Member since 1987, Lee is the author of *Well Testing* and contributed to *Advances in Hydraulic Fracturing.* He is currently writing two new SPE books. Lee has served on numerous committees and has received many awards, including the 1982 Distinguished Achievement Award for Petroleum Engineering Faculty, and 1986 Reservoir Engineering Award, and a 1987 Regional Service Award. **C.W. Hopkins** is senior petroleum engineer for S.A. Holditch & Assocs. Inc. He also is a member of the Well Completions Committee.

Lee

Hopkins

SPE/DOE/GRI 12847

Estimating Formation Permeability From Single-Point Flow Data

by W.J. Lee, T.B. Kuo, and S.A. Holditch, *Texas A&M U.*; and D.A. McVay, *S.A. Holditch & Assocs. Inc.*

Members SPE-AIME

This paper was presented at the 1984 SPE/DOE/GRI Unconventional Gas Recovery Symposium held in Pittsburgh, PA, May 13-15, 1984. The material is subject to correction by the author. Permission to copy is restricted to an abstract of not more than 300 words. Write SPE, 6200 North Central Expressway, P.O. Box 64706, Dallas, Texas 75206 USA. Telex 730989 SPEDAL.

ABSTRACT

Many operators do not routinely run pre-stimulation pressure buildup tests in low permeability gas reservoirs. Frequently, all that is available is a single-rate flow test. To obtain permeability estimates for FERC filings and to evaluate the reservoir, a new method has been developed for analyzing typical pre-fracture production data.

Permeability estimates obtained from this method have been used as a major source of data in numerous successful tight gas determinations, including the Cotton Valley, Wilcox Lobo, and Canyon formations in Texas.

The paper shows that this simple method can be quite reliable. This conclusion is based on a comparison of permeabilities estimated with this technique and with more rigorous determinations from pressure buildup tests.

INTRODUCTION

Accurate reservoir description is necessary to develop tight gas reservoirs economically. A critical formation property is in-situ permeability. An accurate estimate of formation permeability is needed for fracture design calculations and for predicting future production as a function of time. Permeability estimates are also needed to determine if a reservoir qualifies for FERC's "tight gas formation" classification.

In many cases, operators do not run pressure buildup tests on low permeability gas wells prior to hydraulic fracture stimulation. Frequently a well is perforated, broken down and produced for only a few days prior to performing a massive hydraulic fracture treatment. Chokes are changed frequently in this testing program, and there are often shut-in periods of varying lengths between flow periods. This pre-fracture flow data cannot be analyzed using conventional pressure transient analysis techniques; therefore, pre-stimulation permeability estimates are not available. To compound the problem, post-fracture pressure buildup tests leading to unambiguous interpretations are often prohibitively time consuming. Thus, an alternate method to estimate formation permeability, even if it is less accurate than the buildup tests, is needed to evaluate tight gas reservoirs using available pre-fracture flow data.

This paper presents an approximate method (ONEPT) for determining formation permeability from single-point flow data. This new method uses conventional transient flow equations in situations where only the initial formation pressure, the final flowing pressure, the cumulative gas production, and the final flow rate are known. The ONEPT method is appealing because, in contrast to pressure buildup data, which are often not available, single-point flow data are nearly always available on gas wells. This paper describes the ONEPT method and documents its validity in two field studies in which it is compared to the results of pressure buildup tests. In addition, the paper shows the effect on permeability estimates of wellbore storage, variable rate history (including shut-in periods), and uncertainties in skin factor. These effects were determined using finite-difference reservoir simulation.

THEORETICAL BACKGROUND

For a well producing gas from a homogeneous reservoir of uniform thickness, with uniform initial pressure, and with no flow across the outer boundary, the diffusivity

References & illustrations at end of paper.

equation and boundary conditions for radial flow can be expressed as follows:

$$\frac{1}{r}\frac{\partial}{\partial r}\left(r\frac{\partial \psi}{\partial r}\right) = \frac{\phi c_t \mu}{0.000264\ k}\frac{\partial \psi}{\partial t} \quad (1)$$

$$\psi = \psi_i \qquad \text{at all } r, \text{ for } t = 0 \quad (2)$$

$$\frac{\partial \psi}{\partial r} = \frac{q_{sc} P_{sc} T}{1.987\times10^{-5} kh\ T_{sc} r_w}$$

$$\text{at } r = r_w \text{ for } t > 0 \quad (3)$$

$$\frac{\partial \psi}{\partial r} = 0 \qquad \text{at } r = r_e \text{ for } t > 0 \quad (4)$$

where ψ is the pseudopressure of gas[1], defined as:

$$\psi(p) = 2\int_{p_0}^{p} \frac{p}{\mu z}\,dp \quad (5)$$

The pseudosteady-state solution to equations 1-4 is

$$\frac{kh}{1422\ q_g T}(\psi_i - \psi_{wf}) = \ln\left(\frac{r_e}{r_w}\right) - 0.75 + s' \quad (6)$$

when standard conditions are P_{sc} = 14.65 psia and T_{sc} = 60°F.

The term s' is the apparent skin factor which includes the true skin, s, and a term to quantify the extra pressure drop due to non-Darcy flow.

$$s' = s + Dq_g \quad (7)$$

The transient radius of drainage concept is employed in the development of the ONEPT method. The transient radius of drainage, r_d, is the effective drainage radius of a moving transient at any time. It is similar to the radius of investigation, and is given by the following equation:

$$r_d = \left(\frac{kt}{376\ \phi\ \mu\ c_t}\right)^{1/2} \quad (8)$$

At any time before the transient reaches the external drainage radius, r_d can be substituted for r_e in the pseudosteady-state flow equation:

$$\frac{kh}{1422\ q_g T}(\psi_i - \psi_{wf}) = \ln\left(\frac{r_d}{r_w}\right) - 0.75 + s' \quad (9)$$

Equation 9 implies that a well can always be considered to be flowing at pseudosteady-state conditions with a drainage radius that is continually moving outward.

DESCRIPTION OF THE ONEPT METHOD

The proposed ONEPT method is simply an iterative solution of equations 8 and 9. If a well is produced at a constant rate for a length of time such that boundary effects have not yet been felt at the wellbore, then equation 9 will describe the relationship between the pressure drop and the flow rate. Most single-point flow tests in tight gas reservoirs are not run long enough to see boundary effects; therefore, the flow rate and bottomhole pressure at the end of a test should behave as predicted by Equation 9. Since both equations 8 and 9 contain permeability, they will not be satisifed simultaneously unless the correct value of permeability is used.

Using flowing bottomhole pressure and flow rate values measured at the end of a single-point flow test, the permeability can be determined using the following procedure:

1) Assume an arbitrary value of permeability, k_1. For a tight gas reservoir, the assumed value can be 0.1 millidarcy.

2) Use the value of k_1 to calculate the transient radius of drainage, r_d, from Eq. 8. The gas viscosity and total compressibility, c_t, are evaluated at the initial pressure of the reservoir.

3) Using r_d from step 2, Eq. 9 is used to solve for a new estimate of permeability, k_2.

4) The calculated permeability, k_2, is then be compared to the assumed permeability, k_1. If the difference between the two values is negligible, the calculation technique has converged. Otherwise, let k_2 become the assumed value, k_1, and repeat steps 2-4 until convergence is achieved.

5) The final calculated permeability is denoted as k_c.

A gas well flowing at a constant bottomhole pressure can also be analyzed by the same technique, although Equation 6 was derived for a drawdown with constant flow rate. Winestock and Colpitts[2] showed that, in general, Equation 6 is valid for smoothly changing flow rates in radial flow.

The data required for the ONEPT technique includes flowing bottomhole pressure, flow rate, cumulative production and producing time at the end of the single-point flow test. The flowing bottomhole pressure can be estimated from the flowing tubing pressure using various methods. Other data required include formation properties such as porosity, net gas pay, reservoir temperature, and gas fluid properties, primarily viscosity and compressibility.

Note that the technique requires an estimate of apparent skin factor, s', which is usually not known. This requirement is the biggest limitation to this method, and usually the main source of error. However, if a reasonable estimate for skin is available, then an adequate estimate of permeability can be calculated. The effect of uncertainties in skin factor on calculated permeability has been investigated and is discussed in this paper.

Although the skin factor requirement appears disheartening at first, it must be emphasized that this method is applied only when pressure buildup data are not available. Pressure buildup test analysis is more accurate and should be used when buildup data are available.

The ONEPT technique is particularly useful in analyzing a large number of wells in a field where only a few of the wells have had pressure buildup tests performed prior to stimulation. It has been our experience that a pre-stimulation flow rate can be obtained on almost every well. Therefore, if the existing pre-stimulation pressure buildup data can be analyzed to determine a typical value of skin factor for the completion practices used in the field, then this value can be used to analyze the single-rate flow test data for the remaining wells. For example, many tight gas wells will have skin factors of +2 to +3 due to drilling operations but then will have skin factors of -1 to -2 after a ballout treatment. If one develops the expected range of skin factors under certain conditions in certain formations, the ONEPT technique can be used with confidence.

VALIDATION OF THE ONEPT TECHNIQUE

The accuracy of the ONEPT method was investigated by using a finite-difference reservoir model to simulate the performance of a gas well producing from a homogeneous reservoir of uniform thickness with one-dimensional radial gas flow. The simulated pressure data were then analyzed using the ONEPT technique. The permeabilities investigated ranged from 0.01 to 1 millidarcy and the wellbore storage coefficient, C_D, was varied from 0 to 10,000. Skin factors in the range of -5 to +6 were included in the study.

Both constant rate and constant bottomhole pressure flow tests were investigated. The effects of wellbore storage and assumed skin factor on calculated permeabilities is discussed. Sequences of changing flow rates, with and without intervening shut-in periods, were also investigated. The ONEPT technique was also applied to a single-point flow test in a fractured gas well. For each case, the permeability, k_c, calculated from the ONEPT method was compared to the formation permeability, k_a, provided to the simulator and the ratio, k_c/k_a, was displayed graphically. To display the results in a general way, the permeability ratio was graphed as a function of dimensionless producing time.

$$t_D = \frac{0.0002637\ k\ t}{\phi\ c_t\ \mu\ r_w^2} \qquad (10)$$

rather than real producing time.

Effect of Wellbore Storage

The results of using the ONEPT method to determine the formation permeability for single-rate drawdown tests in the presence of wellbore storage are presented in Figures 1 and 2. Figure 1 shows that when the skin factor is +5, the calculated permeability tends to be higher than the actual permeability at early times, and it approaches the actual permeability at later times. As illustrated in Figure 1, wellbore storage effects, which are not accounted for in the pseudo steady-state flow equation, can be extremely important. However, after wellbore storage effects have ceased, the error is less than 5% for all cases.

Figure 2 shows k_c/k_a versus t_D for a well with a negative skin factor, -3. For large wellbore storage coefficients (C_D > 1,000), the ratio k_c/k_a tends to be high at earliest times, but it falls in the 1.0 - 1.2 range at t_D/C_D greater than or equal to 10. For cases with smaller wellbore storage coefficients (C_D < 1,000), k_c/k_a tends to be less than 1.0 at t_D less than 2000. However, at later times, k_c/k_a is in the range 1.0 - 1.2.

Effect of Assumed Skin Factor

The effect of uncertainties in the assumed value of apparent skin factor on calculated permeabilities is investigated here. The apparent skin factor, s', is a critical parameter. This is unfortunate, since it is usually known with less accuracy than any other formation property needed for the ONEPT analysis. However, the results illustrate that if a reasonable value of s' is entered, then an adequate estimate of permeability is possible.

Figure 3 is a graph of k_c/k_a versus t_D for several different values of assumed skin factor. A value of s' equal to zero was used in the simulator-generated constant rate flow test. Wellbore storage effects were not simulated in this test. The values of assumed skin factor used in the ONEPT analysis ranged from -5 to +6. The error is greatest at early times. As dimensionless time increases, the k_c/k_a ratios approach unity. Assuming a negative skin resulted in negative permeabilities for certain ranges of t_D, as shown by the two lower curves.

Figure 3 can be used as a guide to the possible error associated with apparent skin

factor uncertainties. Although it is apparent that significant errors in assumed skin factor will result in significant errors in calculated permeability, for most cases the error involved will not be prohibitive. At worst, the calculated permeability can be considered an order-of-magnitude estimate. It is reemphasized that this technique is used when pressure buildup data is not available. In the absence of pressure buildup data, an order-of-magnitude estimate of permeability is of considerably more practical value than no estimate at all. When using the ONEPT technique for tight-gas determinations, the analyst has an ethical obligation to use an upper bound on skin factor so that an upper bound on estimated permeabilities is provided to regulatory authorities.

Constant Pressure Drawdown

A low permeability gas well is more likely to be produced with a constant back-pressure than with a constant flow rate. This constant back-pressure can be approximated reasonably as constant bottom-hole pressure after earliest times. In such a constant pressure drawdown test, the formation permeability can also be calculated by the iterative method proposed. Since the drawdown is conducted with constant wellbore pressure, the gas flow rate is a function of flowing time. Normally, the flow rate and the cumulative gas production at the end of a flow test can be obtained without difficulty. For constant pressure test data, it was found most accurate to use pseudo-producing time instead of actual test time in the analysis. Pseudo-producing time is calculated by dividing the cumulative production by the final flowing rate.

$$t_p = \frac{\text{cumulative production}}{\text{final production rate}} \qquad (11)$$

The pseudo-producing time is then used in place of producing time in equation 8.

$$r_d = \left(\frac{k\, t_p}{376\, \phi\, \mu\, c_t}\right)^{1/2} \qquad (12)$$

Figure 4 shows the results of applying the ONEPT method to a constant pressure flow test. The skin factor for this simulated well was +3. The k_c/k_a ratios are graphed versus dimensionless pseudo-producing time

$$t_{D_p} = \frac{0.0002637\, k\, t_p}{\phi\, c_t\, \mu\, r_w^2} \qquad (13)$$

Figure 4 shows that the calculated permeabilities deviate significantly from the actual permeabilities only in the earliest time range ($t_D < 1000$). After this time, calculated permeabilities never differ by more than 5% from the actual permeability. For all values of dimensionless wellbore storage coefficient, the calculated permeability is higher than the actual permeability.

Variable Rate Tests

In practice, many wells are tested with a sequence of different chokes and, thus, different rates, with no shut-in periods between the different rates. This common testing procedure was simulated using flow rates in both ascending and descending order, and the ONEPT technique was applied to calculate permeability at the end of these flow sequences. The flow rates had the following relationships:

$$q_2 = 2q_1,\ q_3 = 3q_1,\ q_4 = 4q_1$$

for an increasing rate sequence, and

$$q_2 = 0.75q_1,\ q_3 = 0.5q_1,\ q_4 = 0.25q_1$$

for a decreasing rate sequence.

Best results were obtained when we used pseudo-producing time in the ONEPT procedure. In this case

$$t_p = \frac{\text{cumulative production}}{q_4}$$

The results of applying the ONEPT method to analyze these flow sequences are presented in Figures 5 and 6. The ratio k_c/k_a is plotted versus t_D for different values of C_D. Figure 5 presents the results for an increasing rate sequence. After the effects of wellbore storage have ceased, the calculated permeabilities are higher than the actual values by less than 5%. The results for a decreasing rate sequence are presented in Figure 6. The error is slightly greater here than for the increasing rate sequence. The calculated permeability is 5 to 10% lower than the actual permeability after wellbore storage effects have ceased. These results indicate that even when there are large differences in rate from start to finish of a testing program, the ONEPT method (using pseudo-producing time) can lead to results of acceptable accuracy.

We also simulated flow tests with the same increasing and decreasing rate sequences as indicated above, but with intervening shut-in periods between the flow periods. We found that the permeability estimated from ONEPT by treating the last flow period as a single-rate test (and using the pressure at the start of the last flow period as the original reservoir pressure) led to acceptable permeability estimates. Figure 7 presents the ONEPT analysis results for these tests. Permeability ratio is plotted versus dimensionless time for both increasing and decreasing rate sequences. In all cases the calculated permeability is higher than the actual. Calculated permeabilities

for the increasing rate sequence are slightly more accurate than for the decreasing rate sequence.

Flow Tests in Hydraulically Fractured Wells

Since some wells cannot be tested until after they have been hydraulically fractured, it is of interest to determine the error resulting from application of the ONEPT technique to a situation with some contribution from linear flow.

The results of using the ONEPT method to estimate formation permeability of fractured wells are presented in Figures 8 and 9. Figure 8 shows the ratio of calculated permeability to actual permeability versus dimensionless time for a well with a short fracture. The well simulated has a wellbore radius of 0.33 feet and a fracture extending 50 feet from the well. Gringarten et al.[3] presented an equation to estimate the "equivalent skin" for a fractured well:

$$s = -\ln\left(\frac{L_f}{2\,r_w}\right) = -\ln\left(\frac{50}{2 \times 0.33}\right) = -4.3 \quad (14)$$

The lower curve in Fig. 8 represents the results of using the "equivalent skin", -4.3, in calculating the formation permeability. It shows that the permeability determined can be negative, or meaningless, for $t_D < 2 \times 10^4$, if the equivalent skin is used in the radial flow equation. At greater times, the calculated permeability becomes positive and approaches the actual permeability. At $t_D = 2 \times 10^4$, the flow pattern in the reservoir is changing from linear to pseudo-radial. This can occur only after the transient radius of drainage, r_d, exceeds the fracture half-length, L_f. If the flow regime in the reservoir becomes pseudo-radial, then the formation permeabilities determined from the data obtained in this time range are reliable. When $r_d < L_f$, linear flow dominates the well's performance, and this results in meaningless or inaccurate permeability estimates using the ONEPT method.

The middle and upper curves reveal that the use of incorrectly assumed higher skin factors of -3 and -1 lead to overestimates of permeability.

The curves in Figure 9 show the relationship between k_c/k_a and t_D for a well with a long fracture (L_f = 500 ft). The assumed skin factors are the parameters of interest. The lower curve in Figure 9 is the result of using the correct "equivalent skin" in the ONEPT method. The "equivalent skin" is -6.6 for a well with wellbore radius of 0.33 feet and a 500 ft fracture.

The lower curve has no quantitative meaning since the calculated permeabilities are negative, but it again illustrates the inaccuracy resulting from using the radial flow equation and equivalent skin to analyze the pressure data measured during the linear flow regime of a fractured well. The middle curve results from using a higher skin factor, -5. In the early time region, $t_D < 8 \times 10^3$, the calculated permeability is not reliable, as it varies substantially with t_D and even becomes negative. In the late region the calculated permeability stabilizes, but it is significantly higher than the actual value. The upper curve is the result of using an even higher assumed skin, -3, in the analysis. It shows that the ONEPT method yields permeabilities as high as 5 times the actual value, even at $t_D = 10^6$. At this time, flow from the well is just changing from linear-flow domination to pseudo-radial flow. Note that the calculated permeability is approaching the actual permeability as t_D increases.

FIELD EXAMPLES

The section presents the results of application of the ONEPT method to the analysis of single-rate flow tests in a large gas field, Field A. Fourteen wells in this field were analyzed using both pressure buildup test analysis and the ONEPT method. In addition to the flow test data, log data, including net pay thickness, total porosity, and water saturation, were also available. Table 1 lists the single rate flow test data and log data for the fourteen completions. The well data was not complete, however, so it was necessary to assume "typical" values of certain input parameters, particularly initial pressure and producing time. Table 2 lists average properties for a "typical" completion in Field A. These properties were used whenever good estimates were not available.

Table 3 presents a comparison of pressure buildup test results with ONEPT analysis results for the fourteen completions. The skin factor calculated from buildup test analysis was input as the apparent skin factor, s', in the ONEPT analysis. In all cases, calculated permeabilities are of the same order of magnitude as the buildup analysis values. Several are within 15% of the buildup values. Considering the quality of the input data, we feel the results are in excellent agreement, and, therefore, verify the application of the ONEPT technique.

Since several input parameters were assumed in the ONEPT analysis, it was of interest to determine the sensitivity of the analysis to these parameters. We studied the effect of certain input parameters on the results of ONEPT analysis by varying each important parameter and comparing the perturbed results to those of a base case. Parameters which were varied include producing time, net pay thickness, gas porosity, initial reservoir pressure, and true skin factor. Other parameters, such as gas gravity, condensate gravity, etc., probably

do not vary significantly from well to well and were not included in the sensitivity analysis.

Table 4 presents the results of the base case analysis, the values of the perturbed input parameters, and the perturbed results. Inspection of Table 4 reveals that, within the range of variance which we investigated, the assumed values of initial reservoir pressure, P_i, and skin factor, s, most influence the results. Skin factor is therefore the most critical parameter, since less is known about it than any other parameter in the absence of pressure buildup test data. As seen from Table 4, if the assumed skin factor is larger than the true value, the permeability is too high; if it is lower than the true value, permeability is too low.

Variance of other input parameters has little effect on the calculated permeabilities. Only when several of these parameters are in error at the same time should the calculated permeabilities be significantly in error.

The second example presents results from a successful tight gas determination in the Wilcox Lobo formation in south Texas. The results of pressure buildup test analysis and single-point flow test analysis were used in qualifying several areas in the Wilcox Lobo for FERC's "tight gas formation" classification. Some typical properties of the Wilcox Lobo are listed in Table 5. Additional formation properties and a comparison of calculated permeabilities from pressure buildup and ONEPT analyses are included in Table 6. As in the previous example, the skin factor calculated from pressure buildup test analysis was input as the apparent skin factor, s', in the ONEPT analysis. With the exception of one well, the calculated permeabilities are within 10% of each other. This again verifies the application of the ONEPT technique, provided reasonable estimates of skin factor are input.

CONCLUSIONS

This study led to the following conclusions:

1) The formation permeability can be estimated from the pressure and flow rate measurement taken at the end of a short flow test. This method makes it possible to determine the formation permeability for a well where no other drawdown or buildup data exists.

2) Wellbore storage effects and incorrectly assumed apparent skin factors can significantly affect the accuracy of the ONEPT technique. Reasonable estimates of skin factor must be available for the ONEPT method to provide acceptable results.

3) Permeability estimates based on flow tests in which rates were changed, with or without intervening shut-in periods, can be reasonably accurate.

4) If an upper bound for skin factor is used, the formation permeability determined from single-rate flow test data tends to be higher than the actual permeability for most cases. This is important in FERC tight gas hearings, where it can be of benefit to show that the maximum permeability for a well falls below the "tight gas" criterion.

5) Attempts to use the ONEPT technique to analyze the drawdown data obtained from a fractured well before the pseudo-radial flow regime is reached may result in meaningless negative permeabilities or in calculated values substantially in error.

6) Comparisons of permeabilities estimated from the ONEPT technique and pressure buildup tests show good agreement.

NOMENCLATURE

C_D	=	Dimensionless wellbore storage coefficient
D	=	Non-Darcy flow coefficient
c_t	=	Total compressibility, psi^{-1}
h	=	Net pay thickness,ft
k	=	Formation permeability, md
k_a	=	Actual formation permeability, md
k_c	=	Calculated formation permeability, md
L_f	=	Fracture half-length, ft
P_w	=	Pressure at wellbore, psi
P_{wf}	=	Flowing wellbore pressure, psi
P_{ws}	=	Shut-in wellbore pressure, psi
q_g	=	Gas flow rate, Mscf/D
q_{sc}	=	Gas flow rate at standard condition, MCF/D
r_d	=	Transient radius of drainage, ft
r_e	=	External radius of reservoir, ft
r_w	=	Wellbore radius, ft
s	=	Skin factor
s'	=	Apparent skin factor
t	=	Flow time, hours
t_p	=	Pseudo-producing time, hours

t_D	=	Dimensionless time
T	=	Reservoir temperature, °R
T_{sc}	=	Standard condition temperature, °R
z	=	Gas-law deviation factor, dimensionless
ψ	=	Pseudopressure, psi^2/cp
ϕ	=	Porosity, fraction
μ	=	Gas viscosity, cp

Subscripts

D	=	Dimensionless variables
i	=	Initial condition
wb	=	Wellbore condition

REFERENCES

1) Al-Hussainy, R. and Ramey, H.J., Jr.: "Application of Real Gas Flow Theory to Well Testing and Deliverability Forecasting," Trans., AIME (1966) 237.

2) Winestock, A. G. and Colpitts, G.P.: "Advances in Estimating Gas Well Deliverability," J. Can. Pet. Tech., 4 (3), 1965, 111-119.

3) Gringarten, A. C. , Ramey, H. J., Jr. and Raghavan, R.: "Unsteady-State Pressure Distributions Created by a Well with a Single Infinite-Conductivity Vertical Fracture," Soc. Pet. Eng. J. (Aug. 1974) 347-360; Trans., AIME, 257.

TABLE 1 - ONE-POINT TEST AND LOG DATA - FIELD A

Well Number	Flow Test Rate (Mcf/d)	Flowing Wellhead Pressure (psi)	Total Porosity (fraction)	Water Saturation (fraction)	Net Pay (feet)
1	11,800	3,150	0.163	0.33	26
2	7,800	1,450	0.135	0.16	49
3	5,400	760	0.145	0.33	64
4	9,400	230	0.107	0.55	17
5	9,000	450	0.158	0.43	7
6	11,700	1,550	0.145	0.27	25
7	10,100	200	0.138	0.27	52
8	800	780	0.113	0.53	18
9	9,600	1,230	0.117	0.44	54
10	2,500	1,250	0.130	0.40	18
11	9,300	2,000	0.126	0.39	21
12	13,000	1,500	-	-	-
13	6,100	740	0.143	0.38	28
14	5,400	160	0.125	0.31	20

TABLE 2 - "TYPICAL" PROPERTIES - FIELD A

Depth to formation (feet)	13,500
Net pay thickness (feet)	50
Gas porosity (fraction)	0.10
Initial reservoir pressure (psia)	6,000
Bottom-hole temperature (°F)	270
True skin factor (s)	15
Drainage area (acres)	320
Dry gas gravity (air = 1.0)	0.75
Gas-Condensate ratio (SCF/STB)	1,000
Condensate gravity (°API)	80
Producing time (hours)	24
Flowing wellhead temperature (°F)	90
Wellbore radius (feet)	0.354
Effective tubing I.D. (inches)	2.5784
Expected flowing tubing pressure (psi)	1,000

TABLE 3 - COMPARISON OF PERMEABILITIES - FIELD A

Well Number	Pressure Buildup Test Results		Permeability From ONEPT Method
	Permeability (md)	Apparent Skin Factor, s'	Permeability (md)
1	86.5	50.0	73.9
2	13.3	151.5	23.9
3	4.9	16.7	1.5
4	2.0	3.8	4.1
5	20.7	3.7	13.8
6	6.6	7.18	7.0
7	25.8	82.6	12.1
8	0.89	14.3	0.66
9	7.3	51.0	8.4
10	1.1	4.0	1.3
11	9.0	13.7	9.7
12	7.0	9.6	4.2
13	2.4	6.9	2.2
14	5.4	40.8	7.9

TABLE 4 - SENSITIVITY ANALYSIS RESULTS - FIELD A

Case	Permeability-Thickness (md-ft)	Permeability (md)
Base	132	2.63
t_p = 12 hours	130	2.59
t_p = 48 hours	134	2.68
h = 25 feet	136	5.45
h = 100 feet	128	1.28
ϕ_g = 0.05	135	2.72
ϕ_g = 0.20	128	2.56
P_i = 4,000 psi	327	6.54
P_i = 8,000 psi	82	1.64
s = 5	72	1.44
s = 50	338	6.76

Base Case Parameters

t_p	= 24 hours
h	= 50 feet
ϕ_g	= 0.10
P_i	= 6000 psi
s	= 15

TABLE 5 - "TYPICAL" PROPERTIES - WILCOX LOBO

Depth to formation (ft)	9,500
Bottom-hole temperature (°F)	270
Dry gas gravity (air = 1.0)	0.62
Gas-condensate ratio (SCF/STB)	1,300,000
Condensate gravity (°API)	60

TABLE 6 - COMPARISON OF PERMEABILITIES - WILCOX LOBO

Well Number	Initial Reservoir Pressure (psi)	Gas Porosity (fraction)	Net Gas Pay (ft)	Flow Test Rate (Mcf/d)	Flowing Bottomhole Pressure (psi)	Producing Time (hrs)	Buildup Test Analysis		
							Perm. (md)	Apparent Skin Factor	ONEPT Perm. (md)
1	6850	0.086	20	16	138	496	0.00482	9.3	0.00534
2	7400	0.06	20	81	344	18.3	0.00217	-2.63	0.00132
3	6550	0.081	50	1,407	1,915	14.9	0.0643	-1.67	0.0709
4	7760	0.115	86	2,483	5,715	18	0.331	2.94	0.339
5	6340	0.103	81	2,556	3,892	58.8	0.182	-0.07	0.194
6	5810	0.093	37	351	1,556	312	0.0384	0.28	0.0394
7	5850	0.074	18	169	2,360	547.9	0.0449	-0.03	0.0460

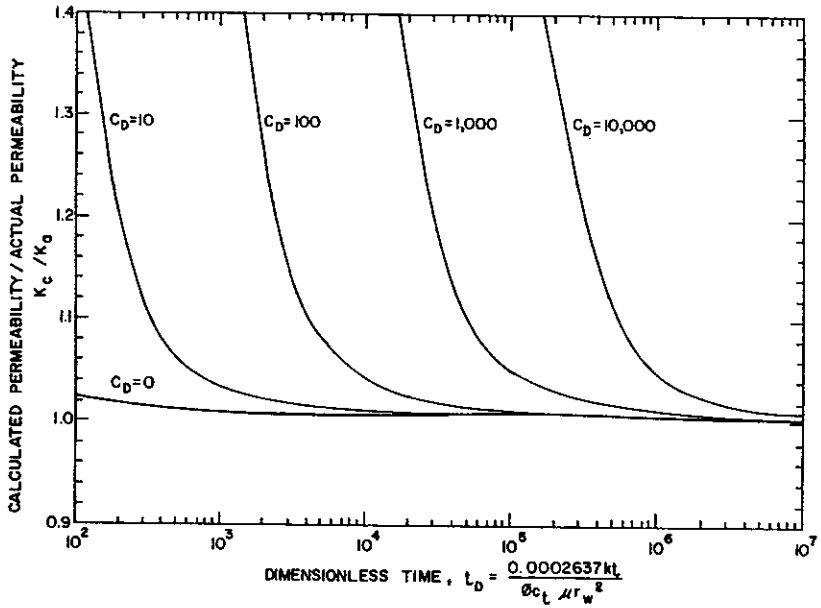

Fig. 1—Permeability ratios for a single-rate flow test, skin factor = +5.

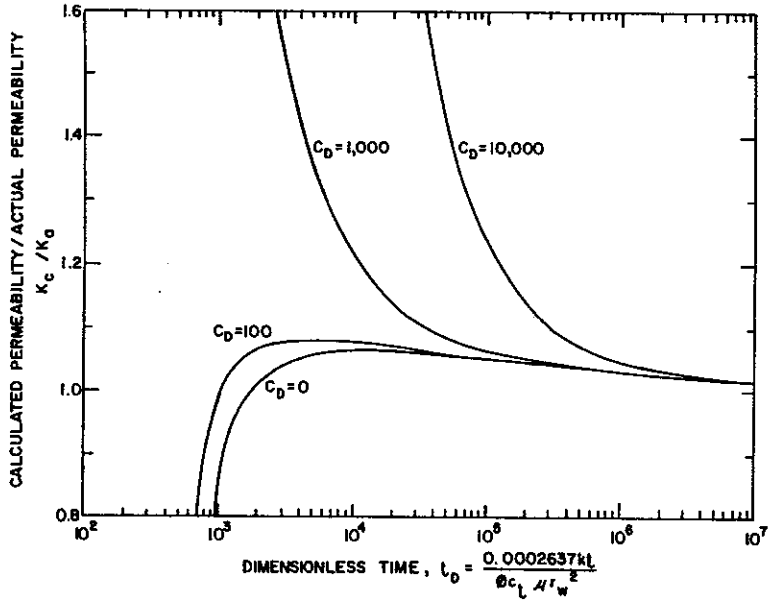

Fig. 2—Permeability ratios for a single-rate flow test, skin factor = −3.

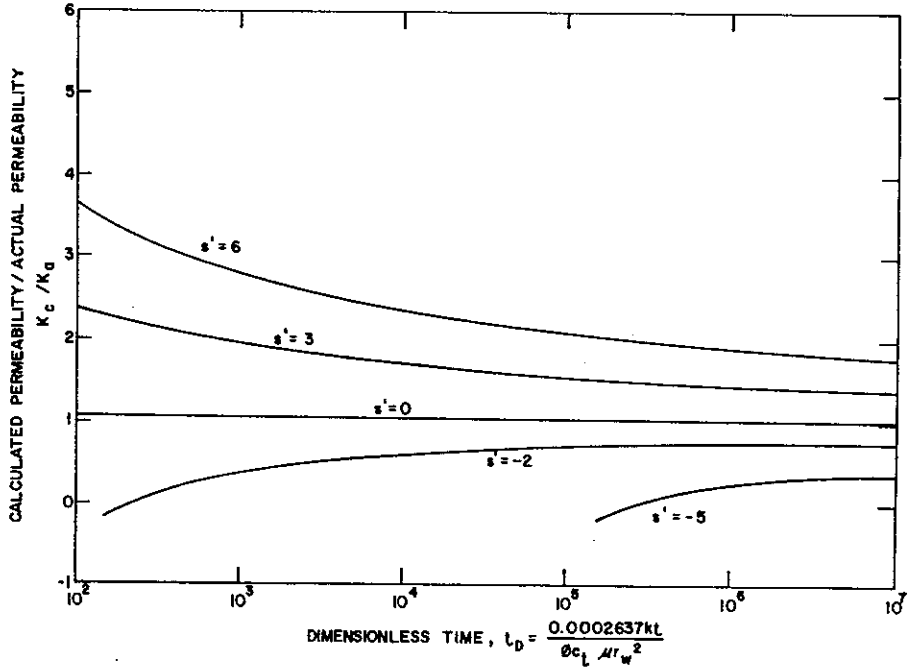

Fig. 3—Permeability ratios for various assumed skin factors. The actual skin factor is 0.

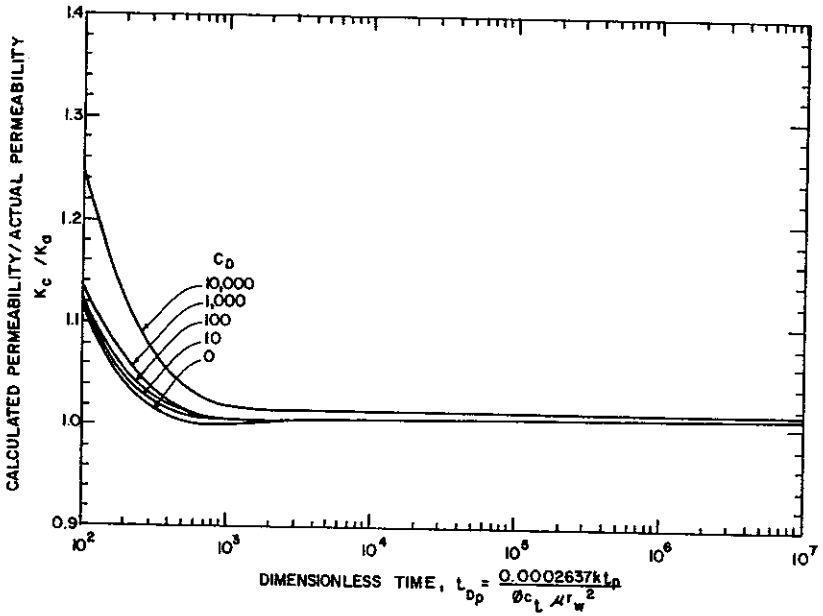

Fig. 4—Permeability ratios for a constant pressure flow test.

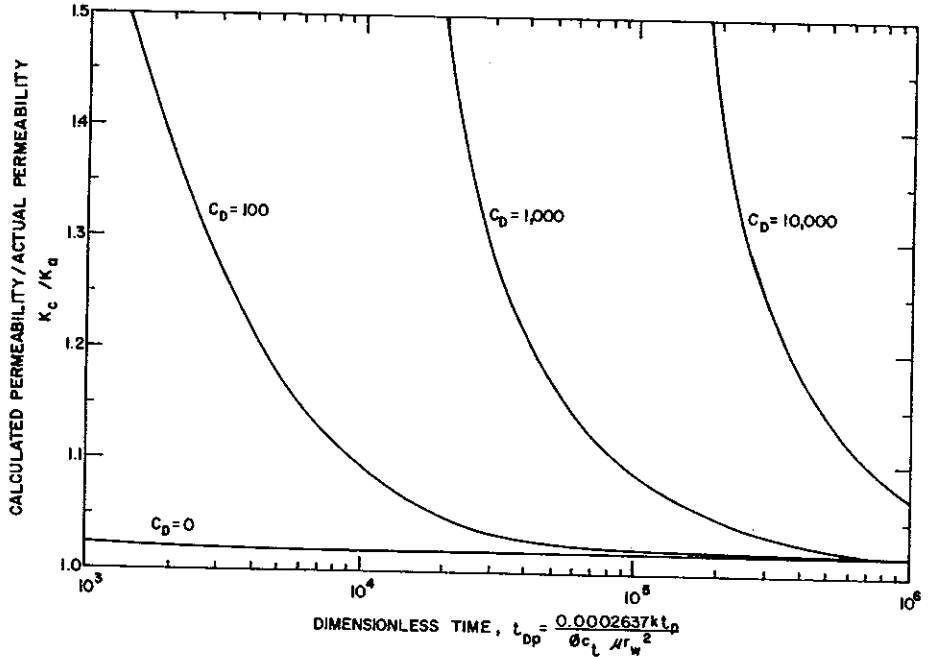

Fig. 5—Permeability ratios for a variable-rate flow test with an increasing rate sequence.

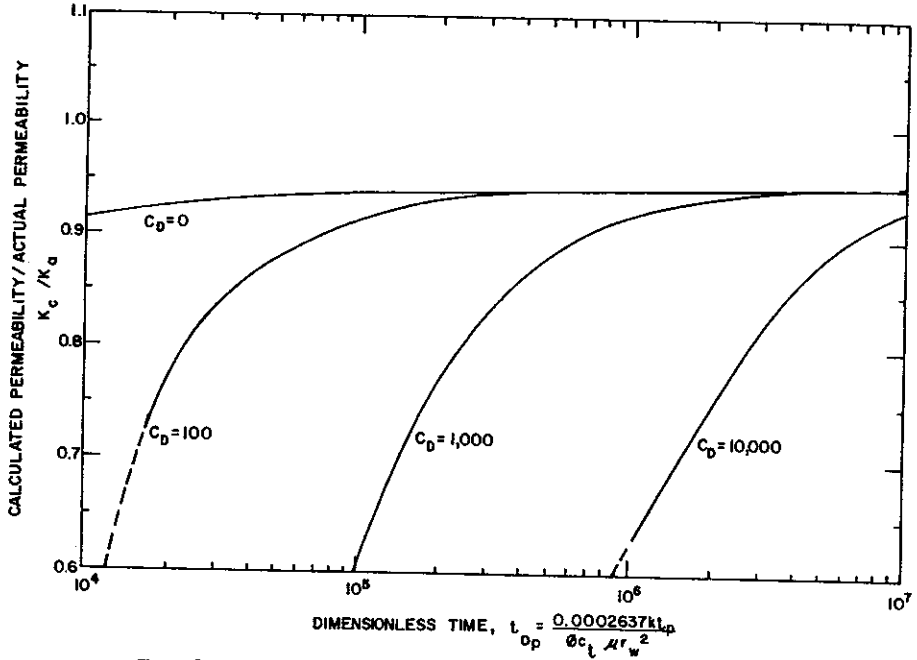

Fig. 6—Permeability ratios for a variable-rate flow test with a decreasing rate sequence.

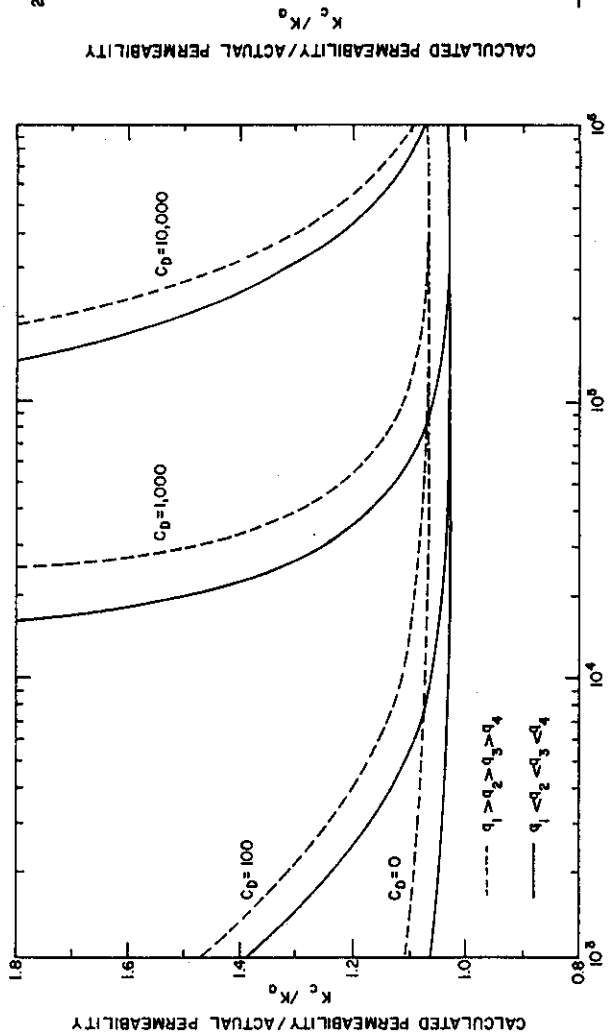

Fig. 7—Permeability ratios for a variable-rate flow test with intervening shut-in periods.

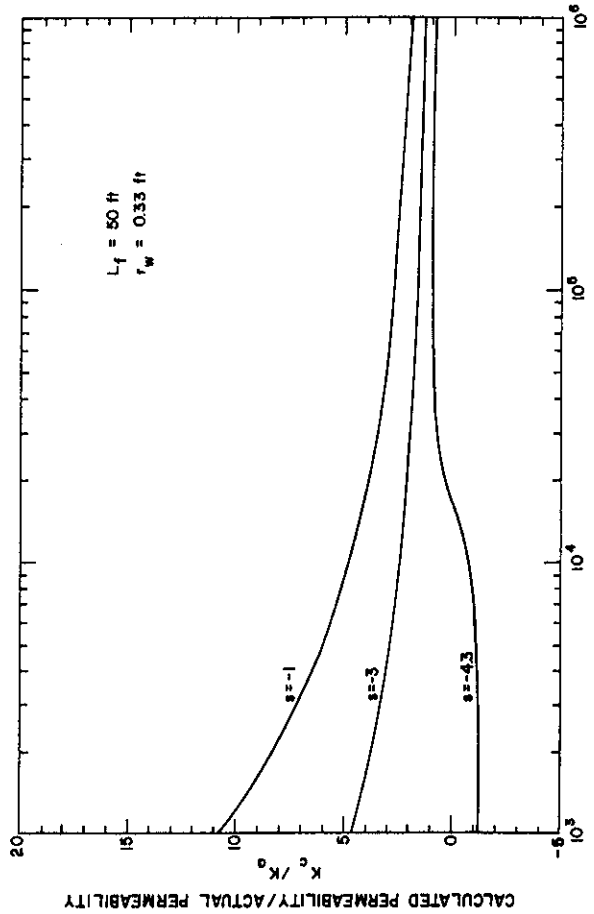

Fig. 8—Permeability ratios for a flow test in a well with a short hydraulic fracture.

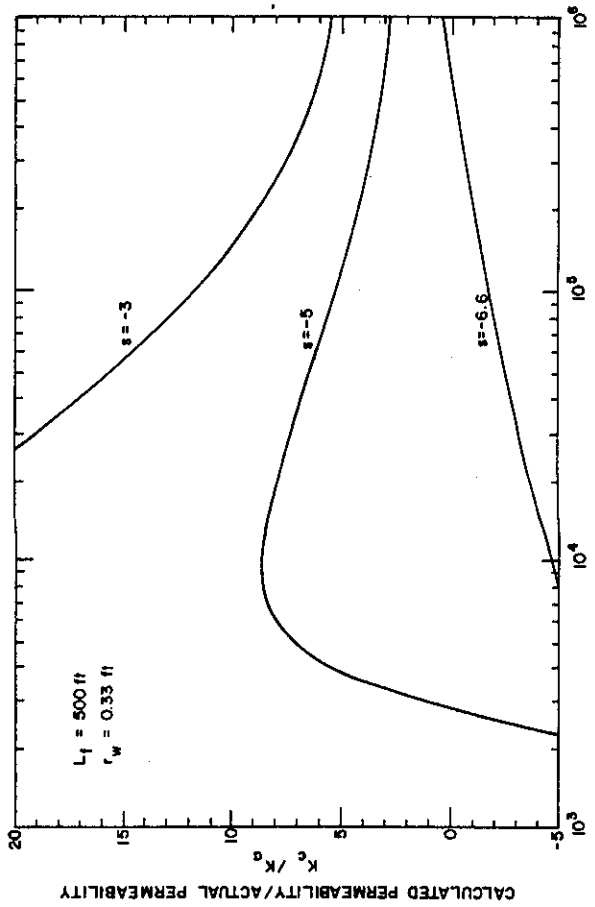

Fig. 9—Permeability ratios for a flow test in a well with a long hydraulic fracture.

Evaluation and Performance Prediction of Low-Permeability Gas Wells Stimulated by Massive Hydraulic Fracturing

R. G. Agarwal, SPE-AIME, Amoco Production Co.
R. D. Carter, SPE-AIME, Amoco Production Co.
C. B. Pollock, SPE-AIME, Amoco Production Co.

Introduction

Because of the deteriorating gas supply situation in the U.S. and the increasing demand for energy, the current trend is to consider seriously the exploitation and development of low-permeability gas reservoirs. This has been possible because of changes in the economic climate and advances in well stimulation techniques, such as massive hydraulic fracturing (MHF). It now appears that MHF is a proven technique for developing commercial wells in low-permeability or "tight" gas formations. As the name implies, MHF is a hydraulic fracturing treatment applied on a massive scale, which may involve the use of at least 50,000 to 500,000 gal treating fluid and 100,000 to 1 million lb proppant. The purpose of MHF is to expose a large surface area of the low-permeability formation to flow into the wellbore. A low-permeability formation is defined here as one having an in-situ permeability of 0.1 md or less.

Methods for evaluating a conventional (small-volume) fracturing treatment are available,[1-16] but the evaluation of an MHF treatment has been a challenge for engineers. To evaluate the success of any type of fracture stimulation, prefracturing rates commonly are compared with postfracturing production rates. These comparisons are valid qualitatively if both pre- and postfracturing rates are measured under similar conditions (that is, equal production time, same choke sizes, minimal wellbore effects, etc.). Unfortunately, to evaluate the success of different kinds of fracturing treatments, pre- and postfracturing production rates often are measured and compared using not only the same well tested under dissimilar conditions, but also the same kind of comparisons between different wells that may even have different formation permeabilities. Thus, results often are invalid and may cause misleading conclusions. Moreover, such comparisons do not help predict long-term performance. To predict long-term performance for MHF wells, reliable estimates of fracture length, fracture flow capacity,* and formation permeability are needed.

Pressure transient methods for analyzing wells with small-volume fracturing treatments are based on the concept of infinite or high fracture flow capacity and are used to determine the effectiveness of a stimulation by estimating the fracture length. Our experience indicates that these methods are not adequate for analyzing wells with finite flow-capacity fractures. Such methods provide unrealistically short fracture lengths for MHF wells with finite flow-capacity fractures. Furthermore, fracture flow capacities cannot be determined.

This paper presents (1) a discussion of the limitations of the conventional analysis methods and alternative techniques for determining fracture length and fracture flow capacity on MHF wells; (2) a set of constant well-rate and constant well-pressure *type curves* for analyzing MHF wells; (3) a discussion of the type-curve matching technique; (4) actual application of the new type curves when analyzing the performance of MHF

0149-2136/79/0003-6838$00.25

*The term "fracture flow capacity" used here also is referred to as "fracture conductivity" in certain publications and is defined by Eq. 1.

This paper discusses how to analyze past performance and predict future performance of tight gas wells stimulated by massive hydraulic fracturing (MHF) using finite fracture flow-capacity type curves. The limitations of conventional pressure transient analysis and other methods of evaluating MHF treatment are discussed. A set of constant well-rate and wellbore-pressure type curves is presented.

wells; and (5) performance prediction of MHF wells.

The concept of finite flow-capacity fractures is not new in the literature;[17-22] however, a technique for analyzing MHF wells still is being developed. Cinco-L. *et al.*[23] pointed out the need to consider finite flow capacity in the fracture and proposed a possible solution. This is thought to be the first step in developing the technology for the evaluation of MHF wells.

Authors who have presented results of pressure transient behavior for wells with finite flow-capacity fractures include Cinco-L. *et al.*,[23] who used a semianalytical approach involving the numerical solution of a Fredholm integral equation. This technique can be applied only to the case of small, constant compressibility or to a system with a constant fluid viscosity-compressibility product. Also, Sawyer *et al.*[21] presented results for specific cases from a finite-difference simulator, but their finite-difference formulation required the use of small time steps. Crafton and Harris[22] presented a locally one-dimensional, finite-difference formulation that has time-step limitations. Holditch and Morse[39] also describe a simulator for MHF gas well prediction.

A computer program (called the MHF simulator) was used to generate the type curves presented here. This program is a two-dimensional, single-phase (darcy), finite-difference model that simulates nonideal gas flow. Fig. 1 is a schematic diagram of the finite-difference grid system and quadrant symmetry. Additional information about the simulator is provided in Appendix A.

Conventional Methods and Their Limitations

Conventional methods (both square-root time graph and type curve) for computing fracture length are based on the concept of linear flow into a high or infinite flow-capacity fracture. In a vertically fractured well, the fracture flow capacity or fracture conductivity is defined as[20]

$$\text{Fracture flow capacity} = k_f w, \text{ md-ft} \quad \ldots\ldots\ldots \quad (1)$$

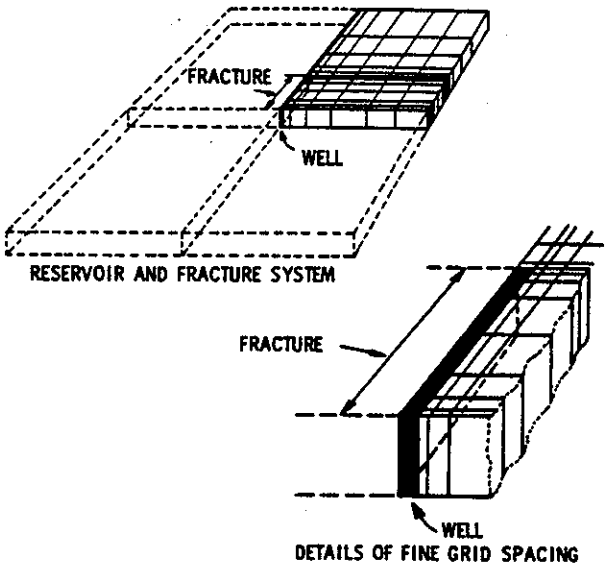

Fig. 1—Schematic of MHF simulator grid system showing quadrant symmetry.

This definition for fracture flow capacity implies that fracture height is equal to formation thickness.

A fracture is said to have an *infinite flow capacity* when there is little or no pressure drop along the axis of the fracture. The fracture is said to have a *finite flow capacity* when there is a significant pressure drop along its axis. Since the distinction between the definitions of fracture flow capacity and formation flow capacity is often confusing, it may be worthwhile to restate the definition of the formation flow capacity.

$$\text{Formation flow capacity} = kh, \text{ md-ft} \quad \ldots\ldots\ldots \quad (2)$$

Square-Root Time Graph Method

This method for calculating fracture length is based on an expression derived for a linear system. Although not shown here, the linear flow equation indicates that pressure or Δp is directly proportional to $\sqrt{\text{time}}$. In a fractured well, where fracture flow capacity is high and wellbore storage and damage effects are minimal, early-time flow from the formation into the fracture should be linear, and early-time pressure data plotted as a function of $\sqrt{\text{time}}$ should fall on a straight line. The slope of the line is related to the fracture length by the following equations.[10,41,42]

Oil Well[11,41]

$$x_f = \frac{4.064\ qB}{m_{v_f}} \sqrt{\frac{\mu}{k\phi c_t}} \quad \ldots\ldots\ldots\ldots \quad (3)$$

Gas Well[10]

$$x_f = \frac{40.925\ qzT}{m_{v_f}} \sqrt{\frac{\mu}{k\phi c_t}}. \quad \ldots\ldots\ldots\ldots \quad (4)$$

To investigate the applicability of Eqs. 3 and 4 to MHF wells, computer runs were made using the MHF simulator to study the effect of finite flow capacity in the fracture on pressure drawdown. Fig. 2 shows $\Delta(p^2)$ plotted as a function of $\sqrt{\text{time}}$. Fracture flow capacity was varied from 1 to 500 md-ft. Early-time pressure data for higher fracture flow capacities fall on a straight line as expected. The slope of the line, m_{v_f}, is inversely proportional to the fracture length. However, the early-time pressure data for finite flow capacity fractures display a curved portion before straightening to a line of proper slope. The duration of this curved portion depends on the fracture flow capacity. The lower the fracture flow capacity, the longer the duration of the curved portion. For low flow-capacity fractures, it may be almost impossible to determine the correct straight-line slope. In other cases, the time necessary for the correct straight line may be so long that conducting the test is impractical. In any case, if the early-time slope is used in the fracture length equation, the slope, m_{v_f}, will be erroneously high, the computed fracture length will be unrealistically small, and no quantitative information will be obtained regarding flow capacity in the fracture.

When using the fracture length equation, one must know the formation permeability, k. Normally, the formation permeability is estimated from a semilog plot of late-time postfracturing buildup data. For an MHF well, where the fracture is long and/or the formation permeability is small, testing times usually will not be long enough to provide the correct semilog straight-line slope. Cinco-L. *et al.* observed that this should occur for

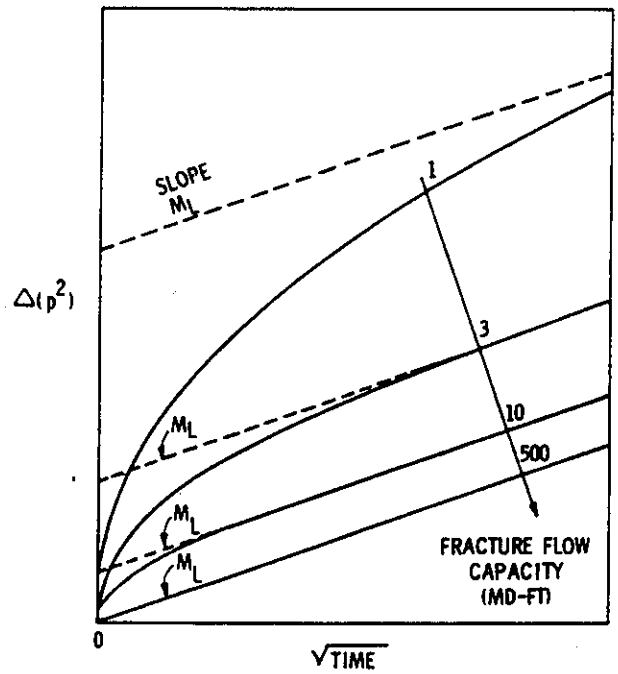

Fig. 2—$\Delta(p^2)$ vs time for finite flow-capacity vertical fracture.

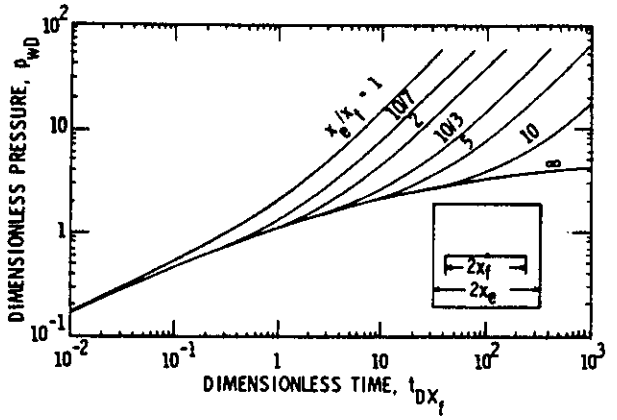

Fig. 3—Constant-rate type curves for infinite flow-capacity vertical fracture (after Gringarten *et al.*[15]).

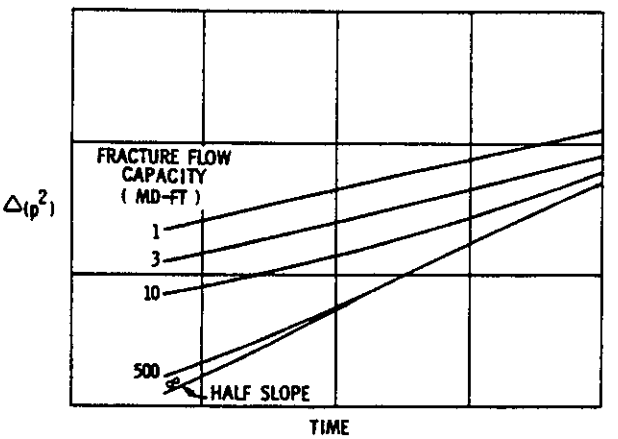

Fig. 4—Log-log graph of $\Delta(p^2)$ vs time for finite flow-capacity vertical fractures.

$t_{DX_f} > 2.5$. Before this, if an erroneous value of the slope is used, usually an optimistic value of formation permeability will be computed. In the fracture length equation, the effect is to provide an even shorter estimated fracture length, which suggests that the formation permeability should be determined from a prefracturing drawdown or buildup test. Possibly, the *kh* value that controls postfracturing behavior could be different from the value determined from a prefracturing pressure transient test because of local reservoir heterogeneity. Analysis methods discussed here assume a homogeneous reservoir.

Type Curve Method

The type curve method for calculating fracture length using the type curve for a vertically fractured well, such as presented by Gringarten *et al.*[15] and shown in Fig. 3, also is based on the concept of infinite flow capacity in the fracture. Fig. 3 (see $x_e/x_f = \infty$) reveals that the early portion of the type curve has a straight-line slope of one-half on a log-log graph. This corresponds to a straight line on the graph of pressure difference vs $\sqrt{\text{time}}$ (Fig. 2). The deviation from the half-slope line represents elliptical flow or the transition from linear to radial flow response at the well.

Part of the computer data generated for finite flow-capacity fractures shown in Fig. 2 was replotted on log-log paper (Fig. 4). Note that early $\Delta(p^2)$ vs time data for finite flow-capacity fractures do not display the characteristic half-slope line, but indicate a line of much flatter slope.

Furthermore, if data are plotted as shown in Fig. 3, instead of obtaining a single curve, a family of curves will be obtained that depends on fracture flow capacity, formation permeability, and fracture length. However, for infinite fracture flow capacity and a given formation permeability, a unique curve exists for each value of x_e/x_f. Therefore, data from wells with finite flow-capacity fractures generally cannot be analyzed using the type curves developed for infinite flow-capacity fractures.

Vertically Fractured Wells With Finite Flow-Capacity Fractures

It should be evident from the preceding discussion that both the square-root time graph and the type curve methods based on the concept of infinite flow-capacity fracture do not apply when analyzing wells with finite flow-capacity fractures. Moreover, no finite flow-capacity type curves were available in the literature until recently. Cinco-L. *et al.* presented constant-rate type curves for finite flow-capacity fractures in a slightly compressible system. Their type curves provide the first step for evaluating the finite flow-capacity fractures. For MHF well applications, the time range of Cinco-L. *et al.*'s type curves should be extended to earlier times. Testing times on low-permeability gas wells seldom will be long enough for the test data to be on the radial flow portion of the type curves. Moreover, since low-permeability MHF gas wells normally produce at a constant well pressure, rather than a constant rate, it may be useful to generate constant well-pressure type curves, especially if the rate vs time performance data are to be analyzed. However, if the producing rate is constant, or

nearly constant, or if the rate declines smoothly with bottom-hole flowing pressure $\Delta(p^2)/q$ vs time should be plotted, and the constant-rate type curve should be used. The MHF simulator previously described was used to generate the constant-rate and constant well-pressure type curves for a time range sufficient to estimate fracture length and fracture flow capacity. The type curves presented here assume (1) constant compressibility-viscosity product in the system, (2) uniform fracture flow capacity, (3) no wellbore storage or damage, (4) no wellbore cleanup effects, (5) no confining pressure and turbulence effects, and (6) insignificant drainage boundary effects for the duration of the test.

The implications of Assumption 1 are discussed next. We found that real gas flow behavior for the fracture system is in good (but not perfect) agreement with constant viscosity-compressibility product (liquid flow) solutions for drawdown conditions, if the behavior is not affected by drainage boundaries. For a number of gas reservoirs with relatively dry gas (<0.65 gravity) and ranging in pressure up to 5,000 psia, these type curves may be used *if the real gas pseudopressure is used and* μc_t *for the gas is evaluated at the initial reservoir pressure.*

Since solutions for the liquid case (Eq. B-3) are "universal" and do not depend on the pressure behavior of a particular gas, these solutions are presented as type curves here. If one questions the applicability of these curves for a particular reservoir (e.g., because of unusual gas properties or reservoir pressure), then type curves can be generated by obtaining solutions for gas flow (Eq. B-2) using a μc_g function, temperature, and pressure specific to the reservoir in question.

Constant-Rate Finite Flow-Capacity Type Curves

Fig. 5 presents constant-rate type curves for finite flow-capacity fractures. Dimensionless pressure drop, p_{wD}, has been plotted as a function of dimensionless time, t_{Dx_f}, on log-log paper with the dimensionless fracture flow capacity, F_{CD}, as a parameter. Dimensionless variables shown in Fig. 5 are in field units and are defined as follows.

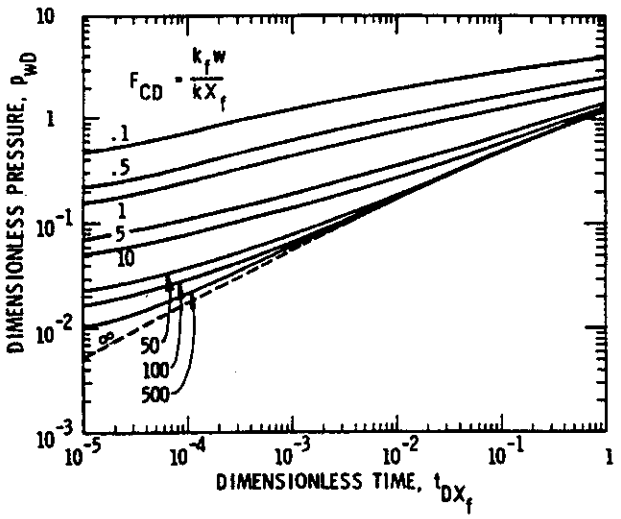

Fig. 5—Constant-rate log-log type curves for finite flow-capacity vertical fractures.

Dimensionless Pressure Drop, p_{wD}

For an *oil well,*

$$p_{wD} = \frac{kh\Delta p}{141.2\ q\mu B}, \quad \ldots\ldots\ldots\ldots\ldots\ldots\ldots\ldots\ (5)$$

where Δp = pressure difference, psi,
= (initial pressure) − (flowing pressure) for drawdown,
= (shut-in pressure) − (last flowing pressure) for buildup.

Dimensionless pressure for a *gas well* expressed in terms of pressure squared and real gas pseudopressures of Al-Hussainy and Ramey[24] are shown by Eqs. 6 and 7, respectively.

$$p_{wD} = \frac{kh\ \Delta(p^2)}{1{,}424\ q\mu z T}, \quad \ldots\ldots\ldots\ldots\ldots\ldots\ (6)$$

$$p_{wD} = \frac{kh\ \Delta[m(p)]}{1{,}424\ qT} \quad \ldots\ldots\ldots\ldots\ldots\ldots\ (7)$$

Also note that, for Eqs. 6 and 7 to be consistent, μ and z must be chosen so that $\Delta[m(p)] = \Delta(p^2)/\mu z$.

The question often arises of whether to make a graph of $\Delta(p^2)$, p, or $\Delta[m(p)]$ to analyze gas wells. This aspect[41,42] has been investigated recently and will not be discussed here.

Dimensionless Time, t_{Dx_f}

Based on the fracture half-length,

$$t_{Dx_f} = \frac{2.634 \times 10^{-4}\ kt}{\phi\ (\mu c_t)_i x_f^2} \quad \ldots\ldots\ldots\ldots\ldots\ (8)$$

The definitions of dimensionless pressure, p_{wD}, and dimensionless time, t_{Dx_f}, are the same as those used by Gringarten *et al.*[15] and Cinco-L. *et al.*[23]

Dimensionless Fracture Flow Capacity, F_{CD}

Here, F_{CD} is defined as

$$F_{CD} = \frac{k_f w}{k x_f}, \quad \ldots\ldots\ldots\ldots\ldots\ldots\ (9)$$

This definition of the dimensionless fracture flow capacity is slightly different from that used by earlier investigators, but appears more convenient.

Prats'[20] definition in our terms is

$$\alpha = \frac{\pi}{2F_{CD}} \quad \ldots\ldots\ldots\ldots\ldots\ldots\ (10)$$

Cinco-L. *et al.*'s[23] definition is

$$C_r = \frac{F_{CD}}{\pi} \quad \ldots\ldots\ldots\ldots\ldots\ (11)$$

In Fig. 5, dimensionless fracture flow capacity, F_{CD}, ranges from 0.1 to 500. Note that the higher values of F_{CD} normally correspond to higher fracture flow capacities. However, higher values of F_{CD} also may be caused by lower formation permeability or short fracture length. Gringarten *et al.*'s[15] infinite flow-capacity fracture solution is shown in Fig. 5 by the dotted line. A curve for F_{CD} values of 500 or greater should represent an infinite flow-capacity fracture approximately. This accounts for the utility of the infinite flow-capacity type curves of Gringarten *et al.* for the analysis of wells

stimulated with conventional fractures. In such wells the short fracture lengths yield high F_{CD} values, even though the fracture flow capacity may be no higher than that in MHF wells. At lower values of t_{Dx_f}, there appears to be a wide separation among different F_{CD} curves. However, this separation diminishes as the value of t_{Dx_f} increases. Dimensionless time, t_{Dx_f}, ranges from 10^{-5} to 1. For greater values of t_{Dx_f}, Cinco-L. *et al.* type curves may be used. For t_{Dx_f} values smaller than 10^{-5}, type curves are influenced by porosity and compressibility in the fracture. This phenomenon also was observed by Cinco-L. *et al.*

Although the type curves presented here were generated using pressure drawdown data, they may be used to analyze buildup data, if producing time before shut in, t_p, is significantly large compared with the shut-in time, Δt. That is, $t_p + \Delta t \simeq t_p$. The effect of small producing time ($t_p + \Delta t >> t_p$) on buildup data is to give an appearance of a lower fracture flow capacity. The same also appears true for the turbulence effect, which has not been included in these type curves. Certain other limitations of these type curves are stated in the assumptions. Since finite flow-capacity type curves for different F_{CD} values do not have distinct shapes, extreme caution and diligence should be exercised in their use.

To check the validity of both Cinco-L. *et al.*'s analytical model and our numerical model, three sets of computer runs were made using the MHF simulator for C_r values of 0.2, 1, and 100. Fig. 6 shows excellent agreement between the two sets of results. Note that Cinco-L. *et al.* carried their results up to $t_{Dx_f} = 100$ and observed that, depending on the C_r value, these solutions will approach the radial flow semilog straight line of slope 1.151/log cycle for $t_{Dx_f} > 2.5$. In low-permeability MHF wells, testing times may be prohibitively long to reach the radial flow regime; hence, this aspect has not been included here.

Constant-Pressure, Finite Flow-Capacity Type Curves

Fig. 7 presents constant wellbore-pressure type curves for finite flow-capacity fractures. These type curves are especially useful when analyzing performance data (production rate vs time) for MHF gas wells that generally are produced at a constant well pressure, rather than a constant rate. The reciprocal of the dimensionless rate, $1/q_D$, was plotted as a function of dimensionless time, t_{Dx_f}, on log-log paper with dimensionless fracture flow capacity, F_{CD}, as a parameter. Definitions of t_{Dx_f} and F_{CD} remain the same as defined earlier for Fig. 5. $1/q_D$ is defined as follows.

Reciprocal Dimensionless Rate, $1/q_D$

For an *oil well*,

$$\frac{1}{q_D} = \frac{kh\Delta p}{141.2\, q\mu B} \quad \ldots\ldots\ldots\ldots\ldots\ldots \quad (12)$$

Eq. 12 is similar to Eq. 5. The basic difference between the two equations is that in the case of dimensionless pressure drop, the rate is constant and Δp varies with time, whereas in the case of dimensionless rate, the well pressure remains constant and the flow rate varies with time. Thus, equations for the reciprocal dimensionless rate for a *gas well* will be similar to Eqs. 6 and 7 with this distinction.

These type curves have the same t_{Dx_f} and F_{CD} ranges and are similar in shape to the previously described constant-rate type curves shown in Fig. 5. However, $1/q_D$ values as a function of t_{Dx_f} are greater than p_{wD} values, as expected. To our knowledge, these constant-pressure type curves for finite flow-capacity fractures are being presented here for the first time. Earlier, Prats[20] and Locke and Sawyer[25] discussed constant-pressure solutions for infinite flow-capacity fractures. Morse and Von Gonten[40] presented constant-pressure and constant-rate results to demonstrate the effects of fracturing on unstabilized well productivity.

Application of constant-pressure type curves (similar to those shown in Fig. 7) using field examples will be illustrated later.

Semilog and Square-Root Dimensionless Time Graphs

Dimensionless variables presented so far were plotted on

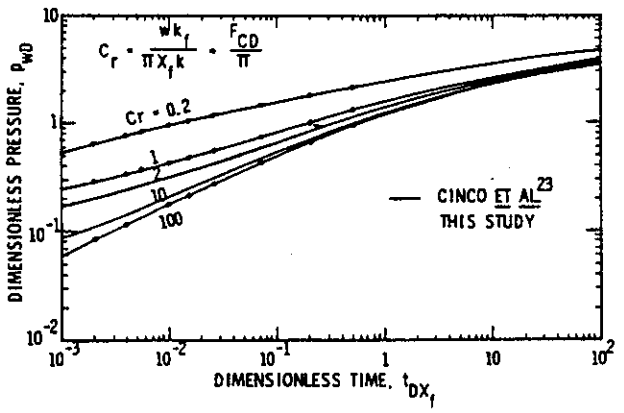

Fig. 6—Comparison of constant-rate type curves for finite flow-capacity vertical fractures.

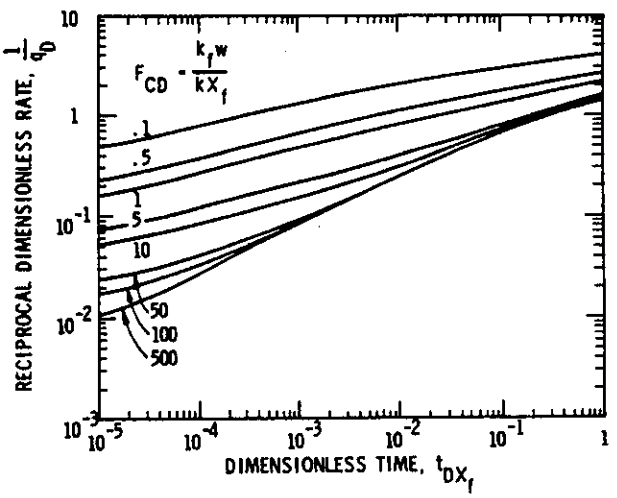

Fig. 7—Constant-pressure log-log type curves for finite flow-capacity vertical fractures.

log-log graph paper (Figs. 5 and 7). Although a separate type curve is obtained for each F_{CD} value, the individual curves do not exhibit distinct shapes of their own. For this reason, it may be useful to plot the dimensionless variables in other ways that could be used to verify the analysis performed on log-log type curves.

Fig. 8 presents constant-rate, finite flow-capacity type curves on semilog graph paper, where p_{wD} is plotted on the Cartesian scale and t_{Dx_f} is plotted on the logarithmic scale. The slope of 1.151 per log cycle, reflecting transient radial flow, also is shown.[15] Since all these type curves show a slope much less than 1.151 in the time range for which most testing will be performed, radial flow response will not occur. If postfracturing buildup data are plotted on semilog graph paper to determine formation permeability, there is a danger of calculating an optimistic value. This results from selecting a portion of the curve that is not a true straight line. If the formation permeability is known from a prefracturing buildup test, Fig. 8 can be used to determine fracture length and fracture flow capacity by type-curve matching

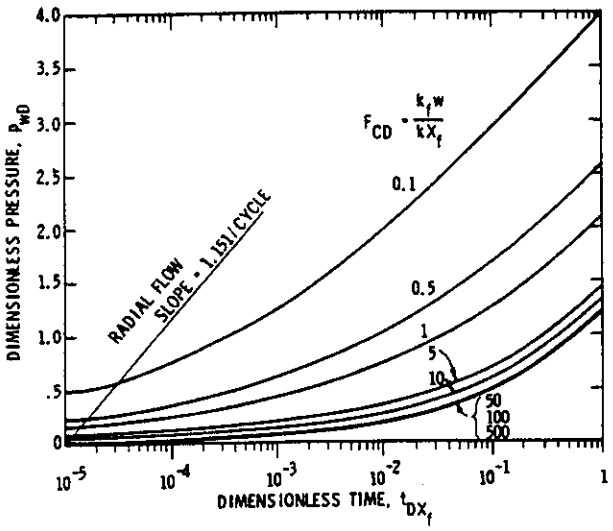

Fig. 8—Constant-rate type curves for finite flow-capacity vertical fractures (semilog graph).

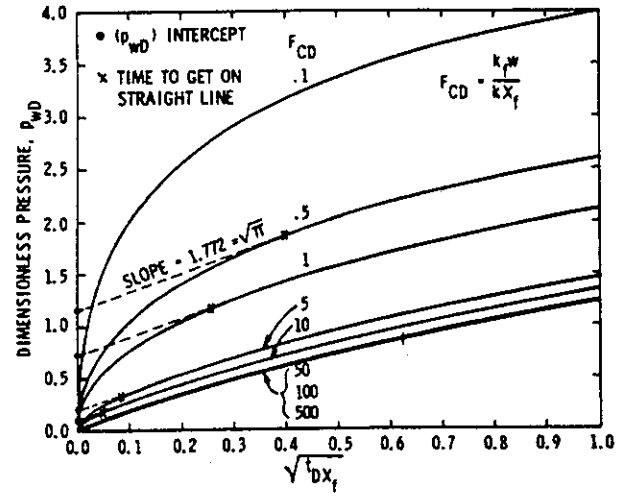

Fig. 9—Constant-rate type curves for finite flow-capacity vertical fractures ($\sqrt{t_{DX_f}}$ graph).

techniques. However, in regard to the shape of the semilog curves, note that they have the same shortcomings as the log-log type curves. Although not shown, a graph similar to Fig. 8 may be prepared for constant-pressure type curves.

Fig. 9 presents constant-rate type curves plotted on Cartesian paper, where p_{wD} is plotted as a function of $\sqrt{t_{Dx_f}}$. A similar graph may be prepared for constant-pressure type curves. As expected, the general characteristics of these curves are similar to those shown in Fig. 2. Early-time data for infinite fracture flow capacity fall on a straight line, with a slope of $\sqrt{\pi}$ or 1.772 that passes through the origin. As the dimensionless fracture flow capacity, F_{CD}, decreases, straight lines of the same slope are seen. These intersect the y axis at increasing values of p_{wD}. (Fig. 9). Also, the length of the straight-line segment of the curve decreases with decreasing F_{CD} values and appears to vanish for $F_{CD}<0.1$. The time required for a curve to reach its straight-line segment also is shown in Fig. 9. Approximate equations for estimating this time for $F_{CD} > 0.5$ are

$$t_{Dx_f} \approx 0.06\,(F_{CD})^{-1.39}, \quad \ldots\ldots\ldots\ldots\ldots\ldots \quad (13)$$

$$t \approx 227.8\,\frac{\phi\mu_i c_t x_f^2}{k}\left(\frac{k_f w}{k x_f}\right)^{-1.39} \text{ hours.} \quad \ldots \quad (14)$$

Eq. 14 can be used to estimate when conventional analysis (pressure vs $\sqrt{\text{time}}$) may or may not be applied. In spite of the inherent problem with the shape of the curves shown in Fig. 9, if used with care, they may be used to verify the log-log analysis and also for matching.

Fig. 10 shows a graph of $(p_{wD})_{\text{intercept}}$ as a function of F_{CD}. Values of $(p_{wD})_{\text{intercept}}$ are read from Fig. 9 and are discussed above. Fig. 10 may be used to estimate, at least qualitatively, the flow capacity of the fracture.

Type-Curve Matching Technique

The type-curve method is a graphical technique for solving transient flow problems by curve matching. This technique is not new (it was used by Theis[26] as early as 1935 for hydrology problems), but has been used widely in the petroleum industry only since 1970.[27,28] Before attempting to apply this technique to MHF wells, a set of appropriate type curves is needed. Sometimes such a set is already available, or it may have to be generated for the specific field or application, using a mathematical

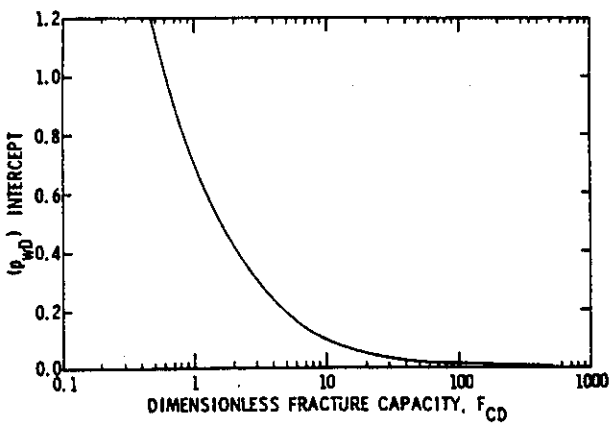

Fig. 10—$(p_{wD})_{\text{intercept}}$ vs F_{CD} for finite flow-capacity vertical fractures.

model (for example, the MHF simulator described in Appendix A) and plotted on a log-log graph (Figs. 5 and 7).

To use type curves for MHF wells, field data (pressure and/or rate) should be plotted on tracing paper as a function of time using the same (logarithmic) graphical scale as that of the type curves. Principal axes should be drawn on the tracing paper in both x and y directions. The tracing paper should be shifted both horizontally and vertically (i.e., parallel to the x and y axes) until a suitable match is obtained. Once a match is obtained between the field data and a type curve, any point on the tracing paper may be chosen as the match point. Both real and dimensionless values of the match point should be read and recorded, along with the appropriate F_{CD} value.

The pressure and/or rate match should give the value of formation permeability, k. The time match gives the value of fracture half-length, x_f. Using the F_{CD} value, the fracture flow capacity is calculated as

$$k_f w = (F_{CD})\, k x_f, \text{ md-ft.} \quad \ldots\ldots\ldots\ldots\ldots\ldots \quad (15)$$

If the formation flow capacity, kh, is known from a prefracturing buildup test, the matching procedure is simpler and much more reliable. In this case, a value of dimensionless pressure, p_{wD} or $1/q_D$, may be computed corresponding to a real value of pressure drop and/or rate using Eqs. 5 through 7 or Eq. 12. By doing this, the position of real pressure drop on the y axis of the tracing paper is fixed in relation to the p_{wD} value on the y axis of the type-curve graph. Once this is done, the tracing paper needs to be moved in only one direction — along the x axis. The procedure for obtaining a match, selecting a match point, and computing fracture parameters is similar to that discussed earlier.

Application of Type-Curve Method Using Field Examples

MHF Well A

To illustrate the application of the finite flow-capacity type curves, a low-permeability MHF gas well will be considered. Before the MHF treatment, a pressure buildup test was conducted on this well to obtain the initial pressure and formation permeability. The well had been on production for about 1 year. No postfracturing buildup test was performed on this well. The objectives are (1) to compute the fracture length and fracture flow capacity, and (2) to predict the future performance.

Data required for the type-curve analysis are presented in Table 1. Actual rate data are shown in Fig. 11, and smooth rate data are given in Table 1. Since the variations in bottomhole flowing pressure were small, the well could be assumed to produce at a constant well pressure. Type curves, similar to those shown in Fig. 7, were generated for the specific gas field and were used. The type curves generated for this application are only slightly different from those shown in Fig. 7. This is due to initial reservoir pressure and drawdown conditions for the subject well.

TABLE 1—DATA FOR TYPE-CURVE ANALYSIS
(MHF Gas Well A)

Reservoir Data	
Reservoir pressure, p_i, psi	2,394
Reservoir temperature, T, °R	720
Formation thickness, h, ft	32
Formation permeability, k^*, md	0.0081
Formation porosity, ϕ, fraction PV	0.107
Total system compressibility, c_t, psi^{-1}	2.34×10^{-4}
Initial gas viscosity, μ_i, cp	0.0176
Difference between the initial and flowing real gas pseudopressures, $[\Delta m(p)]$, psi^2/cp	396×10^6

Performance Data		
Time (Days)	q^{**}(Mcf/D)	$1/q$ (Mcf/D)$^{-1}$
20	625	1.6×10^{-3}
35	476	2.1×10^{-3}
50	408	2.45×10^{-3}
100	308	3.25×10^{-3}
150	250	4.00×10^{-3}
250	208	4.81×10^{-3}
300	192	5.21×10^{-3}

*From prefracturing buildup test.
**Smoothed rate data.

Steps Used in Type-Curve Matching

Step 1. $1/q$ vs time data (Table 1) are plotted on tracing paper using the log-log scale of the type curves. Main x and y axes also are drawn on the tracing paper. Such a plot is shown in Fig. 12.

Step 2. Since formation flow capacity, kh, is known

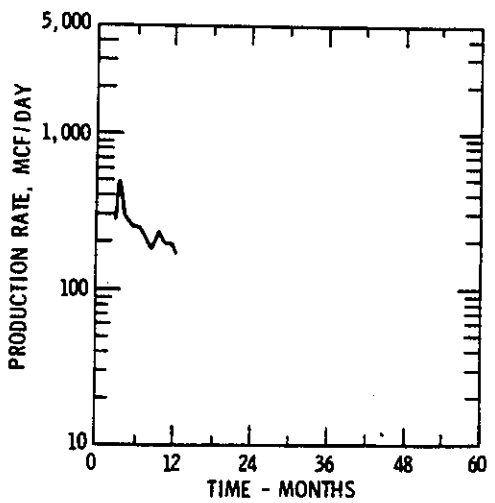

Fig. 11—Actual performance (rate vs time) data for MHF Well A.

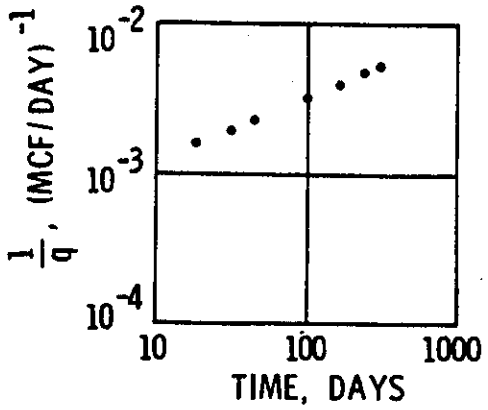

Fig. 12—Reciprocal smooth rate vs time for MHF Well A.

from the prefracturing test, for a value of $1/q = 10^{-3}$, the corresponding value of $1/q_D = 0.1$ is computed:

$$\frac{1}{q_D} = \frac{kh\ \Delta[m(p)]}{1{,}424\ qT} = \frac{(0.0081)(32)(396 \times 10^6)}{(1{,}424)(720)\ q} =$$

$$\frac{100}{q} = (100)(10^{-3}) = 0.1.$$

Thus, the position of $1/q = 10^{-3}$ on the y axis of the tracing paper is fixed in relation to $1/q_D = 0.1$ on the y axis of the type-curve graph paper.

Step 3. The tracing paper is moved horizontally along the x axis until a match is obtained. Such a match is shown in Fig. 13.

Step 4. A match point (Fig. 13) is chosen:

$$t = 100 \text{ days} = 2{,}400 \text{ hours}$$

$$t_{Dx_f} = 2.2 \times 10^{-2}$$

$$F_{CD} = 50.$$

Step 5. Fracture half-length, x_f, is computed using Eq. 8 as follows:

$$x_f^2 = \frac{(2.634 \times 10^{-4})kt}{\phi\mu_i c_t\ t_{Dx_f}} =$$

$$\frac{(2.634 \times 10^{-4})(0.0081)(2{,}400)}{(0.107)(0.0176)(2.34 \times 10^{-4})(2.2 \times 10^{-2})}$$

$$= 528{,}174,$$

$$x_f = 727 \text{ ft.}$$

Thus, the total fracture length $2x_f = 1{,}454$ ft.

Step 6. Fracture flow capacity is computed using Eq. 15:

$$(k_f w) = F_{CD}(kx_f) = (50)(0.0081)(727)$$

$$= 294 \text{ md-ft.}$$

If the prefracturing buildup test data were not available, matching would require shifting the tracing paper along both the x and y axes, which could be difficult. This emphasizes the need for determining kh from a prefracturing test.

Performance Prediction

To predict the future performance of an MHF well, the fracture characteristics determined from the type-curve analysis, together with reservoir and fluid properties and drainage area geometry, are entered in the MHF simulator. Fig. 14 shows the match of the past performance and prediction for the future performance of MHF Well A. It appears that an acceptable match has been obtained. A similar type-curve analysis was performed for MHF Well B. Although details of the analysis are not included here, Fig. 15 shows the predicted performance for MHF Well B. Once again, a fairly good match was obtained. Several wells were analyzed using the same technique and performance was predicted. Note that later performance matched better than early performance. This is not surprising because a cleanup period exists immediately after a well is put on production following a fracturing treatment. This cleanup period can last for some time. Since the MHF simulator does not consider this effect, the type-curve matching relied more on late-time performance than on early-time performance. In some cases where limited performance data are available, the use of the MHF simulator in conjunction with the fracture characteristics determined from the type-curve analysis may not provide a satisfactory match of performance readily. In these cases, a trial-and-error procedure may be required to improve the match.

Discussion of Results

Fracture characteristics determined by type-curve analysis together with reservoir and fluid properties, when entered in the MHF simulator, gave reasonably good matches of past performance and provided confidence in future predictions. However, we do not imply that type-curve analysis provides unique values of fracture length and capacity. There are many factors[29-39] (such as wellbore storage, fracture face damage due to liquid invasion, relative permeability effects, gas compressibility, confining pressure, turbulence, varying fracture capacity, and lateral and vertical reservoir heterogeneities) that may complicate the analysis.

Finite flow-capacity type curves for different values of F_{CD} look alike and do not possess distinct shapes. This is a definite disadvantage when using these type curves. Extreme caution and diligence are required. This also points out the need for determining formation permeability from the prefracturing buildup test.

As for future performance predictions, it should be noted that because of the slow response of pressure transients in tight gas formations, long-term performance data will be needed before the lateral extent of the drainage area of the well can be estimated reasonably.

Concluding Remarks

This study concerning evaluation and prediction of performance of low-permeability wells stimulated by massive hydraulic fracturing warrants the following statements.

1. Conventional pressure transient methods (both square-root time graph and type curve), based on the concept of infinite flow-capacity fracture, are not adequate for evaluating MHF wells with finite flow-capacity fractures.

2. Finite flow-capacity type curves appear suitable for analyzing MHF wells. Since low-permeability MHF gas

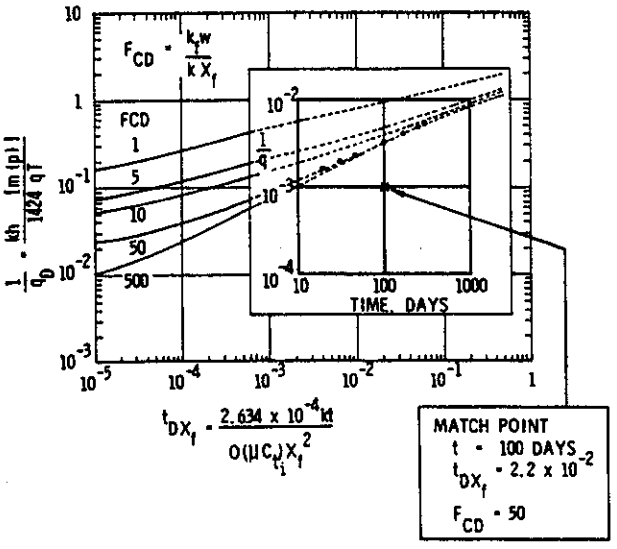

Fig. 13—Type-curve matching for MHF Well A.

wells generally produce at a constant bottomhole pressure rather than at a constant rate, the constant well-pressure type curves appear more appropriate for analyzing the performance data. However, where production rates are reasonably constant or vary smoothly with bottomhole pressure, constant-rate type curves should be used. In the last case, for the type-curve analysis, $\Delta(p^2)/q$ should be plotted as a function of time.

3. Finite flow-capacity type curves presented here for both the constant-rate and constant-pressure type curves are intended for use with drawdown data. However, they may be used to analyze pressure buildup data if producing time before shut in is sufficiently long ($t_p + \Delta t \approx t_p$) so that the buildup data are least affected.

4. Comparison of constant-rate type curves generated by Cinco-L. *et al.*'s[23] analytical model with the MHF simulator of this study appears excellent. The time range of Cinco-L. *et al.*'s data needs to be extended to earlier times for MHF applications.

5. In low-permeability MHF wells, testing times may not be long enough because of practical limitations to permit semilog pressure analysis for determining formation permeability.

6. For an MHF well, the testing program must be carefully planned and should include (1) prefracturing pressure buildup, (2) postfracturing pressure buildup, and (3) collection of long-term pressure and flow-rate performance data.

7. Since finite flow-capacity type curves do not have distinct shapes, extreme caution and diligence should be exercised in their use. Knowledge of formation permeability from a prefracturing test may simplify matching. Use of semilog and square-root graphs with log-log type curves should be helpful.

8. There are many factors, such as wellbore storage, liquid invasion, wellbore cleanup, confining pressure, turbulence, and reservoir heterogeneity, that complicate the analysis. These factors have not been considered here and deserve further investigation.

9. The use of a mathematical model, such as the MHF simulator, with type-curve analysis can provide a good prediction of well performance.

Nomenclature

A = drainage area of MHF well
B = formation volume factor, RB/STB
c_t = total system compressibility, 1/psi
C_r = relative fracture flow capacity defined by Cinco-L. *et al.*,[23] dimensionless
F_{CD} = dimensionless fracture flow capacity (see Eq. 9)
h = formation thickness, ft
k = formation permeability, md
$k(x,y)$ = permeability as a function of x and y coordinates
k_f = fracture permeability, md
$m(p)$ = real gas pseudopressure, psi^2/cp
$\Delta[m(p)]$ = difference in real gas pseudopressures, psi^2/cp
m_{v_f} = slope in psi/$\sqrt{\text{hour}}$ or psi^2/$\sqrt{\text{hour}}$
p = pressure, psi
p_i = initial pressure, psi
p_{wD} = dimensionless pressure or pressure drop
Δp = pressure drop, psi
$\Delta(p^2)$ = difference in squares of pressures, psi^2
q = flow rate, STB/D or Mcf/D
q_D = dimensionless flow rate
S = saturation, fraction
t = flowing time, hours
t_{Dx_f} = dimensionless time based on x_f
Δt = shut-in time, hours
T = reservoir temperature, °R
w = fracture width, ft
x_e = distance from well to the reservoir boundary, ft
x_f = fracture half-length, ft
z = real gas deviation factor
α = relative capacity defined by Prats,[20] dimensionless
μ = viscosity, cp
$(\mu c_t)i$ = viscosity-compressibility product at initial condition, cp
ϕ = formation porosity, fraction
ϕ_f = fracture porosity, fraction

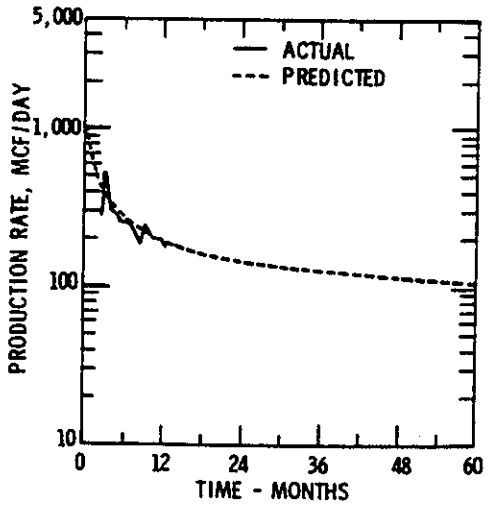

Fig. 14—Match and performance prediction for MHF Well A.

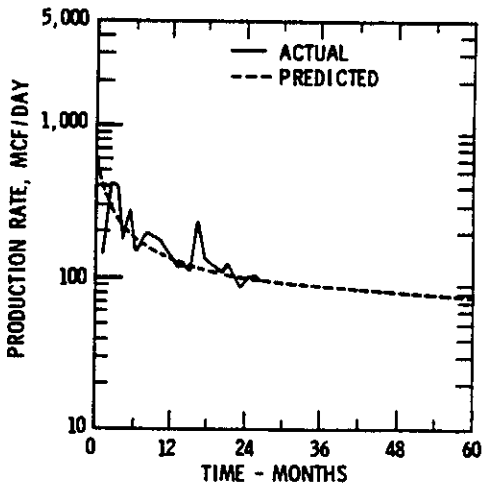

Fig. 15—Match and performance prediction for MHF Well B.

Subscripts

CD = dimensionless flow capacity
D = dimensionless
Dx_f = dimensionless, based on x_f
e = external boundary
f = fracture
i = initial
p = producing
w = wellbore

References

1. Churchill, R. V.: *Operational Mathematics*, 2nd ed., McGraw-Hill Book Co., Inc., New York City (1958) 130-132.
2. Carslaw, H. S. and Jaeger, J. C.: *Conduction of Heat in Solids*, 2nd ed., Clarendon Press, Oxford (1959) 275.
3. Prats, M., Hazebroek, P., and Strickler, W. R.: "Effect of Vertical Fractures on Reservoir Behavior — Compressible-Fluid Case," *Soc. Pet. Eng. J.* (June 1962) 87-94; *Trans.*, AIME, **225.**
4. Miller, F. G.: "Theory of Unsteady-State Influx of Water in Linear Reservoirs," *J. Inst. Pet.* (Nov. 1962) **48,** 365.
5. Scott, J. O.: "The Effect of Vertical Fractures on Transient Pressure Behavior of Wells," *J. Pet. Tech.* (Dec. 1963) 1365-1369; *Trans.*, AIME, **228.**
6. Nabor, G. W. and Barham, R. H.: "Linear Aquifer Behavior," *J. Pet. Tech.* (May 1964) 561-563; *Trans.*, AIME, **231.**
7. Russell, D. G. and Truitt, N. E.: "Transient Pressure Behavior in Vertically Fractured Reservoirs," *J. Pet. Tech.* (Oct. 1964) 1159-1170; *Trans.*, AIME, **231.**
8. Lee, W. J. Jr.: "Analysis of Hydraulically Fractured Wells With Pressure Buildup Test," paper SPE 1820 presented at the SPE-AIME 42nd Annual Fall Meeting, Houston, Oct. 1-4, 1967.
9. Matthews, C. S. and Russell, D. G.: *Pressure Buildup and Flow Tests in Wells*, Monograph Series, Society of Petroleum Engineers of AIME, Dallas (1967) **1,** 102.
10. Millheim, K. K. and Cichowicz, L.: "Testing and Analyzing Low-Permeability Fractured Gas Wells," *J. Pet. Tech.* (Feb. 1968) 193-198; *Trans.*, AIME, **243.**
11. Clark, K. K.: "Transient Pressure Testing on Fractured Water Injection Wells," *J. Pet. Tech.* (June 1968) 639-643; *Trans.*, AIME, **243.**
12. Wattenbarger, R. A. and Ramey, H. J. Jr.: "Well Test Interpretation of Vertically Fractured Gas Wells," *J. Pet. Tech.* (May 1969) 625-632; *Trans.*, AIME, **246.**
13. van Everdingen, A. F. and Meyer, L. J.: "Analysis of Buildup Curves Obtained After Well Treatment," *J. Pet. Tech.* (April 1971) 513-524; *Trans.*, AIME, **251.**
14. Raghavan, R., Cady, G. V., and Ramey, H. J. Jr.: "Well-Test Analysis for Vertically Fractured Wells," *J. Pet. Tech.* (Aug. 1972) 1014-1020; *Trans.*, AIME, **253.**
15. Gringarten, A. C., Ramey, H. J. Jr., and Raghavan, R.: "Unsteady-State Pressure Distributions Created By a Well With a Single Infinite-Conductivity Vertical Fracture," *Soc. Pet. Eng. J.* (Aug. 1974) 347-360; *Trans.*, AIME, **257.**
16. Gringarten, A. C., Ramey, H. J. Jr., and Raghavan, R.: "Applied Pressure Analysis for Fractured Wells," *J. Pet. Tech.* (July 1975) 887-892; *Trans.*, AIME, **259.**
17. Dyes, A. B., Kemp, C. E., and Caudle, B. H.: "Effect of Fractures on Sweep-Out Pattern," *Trans.*, AIME (1958) **213,** 245-249.
18. van Poollen, H. K., Tinsley, J. M., and Saunders, C. D.: "Hydraulic Fracturing — Fracture Flow Capacity vs Well Productivity," *Trans.*, AIME (1958) **213,** 91.
19. McGuire, W. J. and Sikora, V. J.: "The Effect of Vertical Fractures on Well Productivity," *Trans.*, AIME (1960) **219,** 401-403.
20. Prats, M.: "Effect of Vertical Fractures on Reservoir Behavior — Incompressible Fluid Case," *Soc. Pet. Eng. J.* (June 1961) 105-118; *Trans.*, AIME, **222.**
21. Sawyer, W. K., Locke, C. D., and Overbey, W. K. Jr.: "Simulation of Finite-Capacity Vertical Fracture in a Gas Reservoir," paper SPE 4593 presented at the SPE-AIME 48th Annual Fall Meeting, Las Vegas, Sept. 30-Oct. 3, 1974.
22. Crafton, J. W. and Harris, C. D.: "A Direct Finite-Difference Simulation of a Gas Well with a Finite Capacity Vertical Fracture," paper SPE 5736 presented at the SPE-AIME Fourth Symposium on Numerical Simulation of Reservoir Performance, Los Angeles, Feb. 19-20, 1976.
23. Cinco-L., H., Samaniego-V., F., and Dominguez-A., N.: "Transient Pressure Behavior for a Well With a Finite-Conductivity Vertical Fracture," *Soc. Pet. Eng. J.* (Aug. 1978) 253-264.
24. Al-Hussainy, R. and Ramey, H. J. Jr.: "Application of Real Gas Flow Theory to Well Testing and Deliverability Forecasting," *J. Pet. Tech.* (May 1966) 637-642; *Trans.*, AIME, **237.**
25. Locke, C. D. and Sawyer, W. K.: "Constant Pressure Injection Test in a Fractured Reservoir — History Match Using Numerical Simulation and Type Curve Analysis," paper SPE 5594 presented at the SPE-AIME 50th Annual Fall Technical Conference and Exhibition, Dallas, Sept. 28-Oct. 1, 1975.
26. Theis, C. V.: "The Relation Between the Lowering of the Piezometric Surface and the Rate and Duration of Discharge of a Well Using Ground Water Storage," *Trans.*, AGU (1935) 519-524.
27. Agarwal, R., Al-Hussainy, R., and Ramey, H. J. Jr.: "An Investigation of Wellbore Storage and Skin Effect in Unsteady Liquid Flow: 1. Analytical Treatment," *Soc. Pet. Eng. J.* (Sept. 1970) 279-290; *Trans.*, AIME, **249.**
28. Ramey, H. J. Jr.: "Short-Time Well Test Data Interpretation in the Presence of Skin Effect and Wellbore Storage," *J. Pet. Tech.* (Jan. 1970) 97-104; *Trans.*, AIME, **249.**
29. Tannich, J. D.: "Liquid Removal From Hydraulically Fractured Gas Wells," *J. Pet Tech.* (Nov. 1975) 1309-1317.
30. van Poollen, H. K.: "Productivity vs Permeability Damage in Hydraulically Produced Fractures," *Drill. and Prod. Prac.*, API (1957) 103.
31. Raymond, L. R. and Binder, G. G. Jr.: "Productivity of Wells in Vertically Fractured Formations," *J. Pet. Tech.* (Jan. 1967) 120-130; *Trans.*, AIME, **240.**
32. Howard, G. C. and Fast, C. R.: *Hydraulic Fracturing*, Monograph Series, Society of Petroleum Engineers of AIME, Dallas (1970) **2.**
33. Cooke, C. E. Jr.: "Effect of Fracturing Fluids on Fracture Conductivity," *J. Pet. Tech.* (Oct. 1975) 1273-1282; *Trans.*, AIME, **259.**
34. Ramey, H. J. Jr. and Gringarten, A. C.: "Effect of High Volume Vertical Fractures on Geothermal Steam Well Behavior," paper presented at the Second United Nations Symposium on the Use and Development of Geothermal Energy, San Francisco, May 20-29, 1975.
35. Vairogs, Juris, Hearn, C. L., Dareing, Donald W., and Rhoades, V. W.: "Effect of Rock Stress on Gas Production from Low-Permeability Reservoirs," *J. Pet. Tech.* (Sept. 1971) 1161-1167; *Trans.*, AIME, **251.**
36. Vairogs, Juris and Rhoades, Vaughan W.: "Pressure Transient Tests in Formations Having Stress-Sensitive Permeability," *J. Pet. Tech.* (Aug. 1973) 965-970; *Trans.*, AIME, **255.**
37. Geertsma, J.: "Estimating the Coefficient of Inertial Resistance in Fluid Flow Through Porous Media," *Soc. Pet. Eng. J.* (Oct. 1974) 445-450.
38. Cooke, C. E. Jr.: "Conductivity of Fracture Proppants in Multiple Layers," *J. Pet. Tech.* (Sept. 1973) 1101-1107; *Trans.*, AIME, **255.**
39. Holditch, S. A. and Morse, R. A.: "The Effects of Non-Darcy Flow on the Behavior of Hydraulically Fractured Gas Wells," *J. Pet. Tech.* (Oct. 1976) 1169-1179.
40. Morse, R. A. and Von Gonten, W. D.: "Productivity of Vertically Fractured Wells Prior to Stabilized Flow," *J. Pet. Tech.* (July 1972) 807-811.
41. Earlougher, R. C. Jr.: *Advances in Well Test Analysis*, Monograph Series, Society of Petroleum Engineers of AIME, Dallas (1977) **5,** 151.
42. *Theory and Practice of the Testing of Gas Wells*, 3rd ed., Energy Resources Conservation Board, Calgary, Alta., Canada (1975).

APPENDIX A — MHF Simulator

Description of MHF Simulator

The two-dimensional simulator used here is based on a conventional, implicit five-point, backward difference equation that approximates Eq. B-1 or Eq. B-2. If the pressure-dependent coefficient of the time derivative is

computed predictively, the set of linear equations is solved either by direct or iterative methods. If the coefficient is evaluated using the chord method, it is incorporated into the iterative method. Use of the chord method improves the material balance slightly. However, in either case, the material balance is well within acceptable bounds. The fracture is portrayed as a row of grid blocks having a narrow width, high permeability, and porosity representative of fracturing proppant. Fine-grid spacing is used at the well and fracture tip and also near the fracture in a direction normal to the fracture. The simulator has no time-step limitations except those arising from truncation error considerations. The simulator can be applied to both real gas and constant compressibility problems and uses the real gas pseudopressure. Fig. 1 illustrates the grid-block distribution of the reservoir-fracture system and the assumed quadrant symmetry. Details of fine grid spacing used at the well and fracture tip also are shown. For generating type curves, drainage boundaries were chosen far enough from the well-fracture system so that pressure behavior would be unaffected by their presence during the time of interest.

The initial condition is one of constant pressure. The boundary condition at the well is either one of constant rate or one of constant bottomhole flowing pressure. The fracture has a constant width and permeability. Although they can be accounted for in the simulator, turbulence, wellbore storage, and confining pressure effects were neglected in the results presented here. The simulator does not account for gravitational effects.

Input Data for MHF Simulator

Data entered in the MHF simulator consists of reservoir data, fracture data, and fluid properties data. Reservoir data normally include formation permeability, k; formation thickness, h; formation porosity, ϕ; fluid saturation, S; reservoir temperature, T; initial pressure, p_i; and dimensions of drainage area, A. Fracture data should include fracture half-length, x_f; fracture width, w; fracture permeability, k_f; and fracture porosity, ϕ_f. Fluid properties such as viscosity and formation volume factors are provided as a function of pressure. For an MHF gas well, gas viscosity and z factors are provided as a function of pressure.

Operating conditions such as a constant well pressure, constant well rate, or a combination of both drawdown and buildup conditions may be specified.

Original manuscript received in Society of Petroleum Engineers office Sept. 15, 1977. Paper accepted for publication April 21, 1978. Revised manuscript received Sept. 8, 1978. Paper (SPE 6838) first presented at the SPE-AIME 52nd Annual Fall Technical Conference and Exhibition, held in Denver, Oct. 9-12, 1977.

This paper will be included in the 1979 *Transactions* volume.

APPENDIX B
Gas Flow and Liquid Flow Equations

If turbulence can be neglected and porosity, gas saturation, and permeability do not vary with time, gas flow through an isotropic porous medium is described by

$$\nabla \cdot \left[\frac{k}{k_{fm}} \nabla m(p)\right] = \frac{\phi \mu c_t}{k_{fm}} \frac{\partial m(p)}{\partial t} \quad \ldots\ldots \text{(B-1)}$$

Eq. B-1 also can be written as

$$\nabla \cdot \left[\frac{k}{k_{fm}} \nabla m(p)\right] = \frac{(\mu c_t)}{(\mu c)_i} \frac{\partial m(p)}{\partial t'}, \quad \ldots\ldots \text{(B-2)}$$

where $t' = k_{fm}t/\phi(\mu c_t)_i$, the subscript i refers to initial pressure conditions, k is permeability to gas (function of position), k_{fm} is permeability to gas in the unfractured formation (constant), and $m(p)$ is the gas flow potential or real gas pseudopressure, defined as

$$m(p) = 2 \int_{p_i}^{p} \frac{p}{\mu(p) z(p)} dp.$$

All other symbols are standard SPE letter symbols. Units are centimeters, seconds, atmospheres, and centipoise.

For drawdown conditions, for the fracture problem geometry, and provided that the behavior is unaffected by drainage boundaries, we have found that solutions to

$$\nabla \cdot \left[\frac{k}{k_{fm}} \nabla m(p)\right] = \frac{\partial m(p)}{\partial t'} \quad \ldots\ldots\ldots\ldots \text{(B-3)}$$

are good approximations for Eq. B-2. We obtained and compared solutions to Eqs. B-2 and B-3 for several actual μc_t functions for reservoir pressures up to 5,000 psia and found that the solutions were in good, but not perfect, agreement.

Type curves generated as solutions to Eq. B-3 are universal and do not depend on properties of specific reservoir/gas systems. More accurate type curves, specific to a given reservoir/gas system, can be obtained as solutions to Eq. B-2.

SI Metric Conversion Factors

B/D	× 1.589 873	E − 01	= m^3/d
cp	× 1.00	E − 03	= Pa·s
ft	× 3.048	E − 01	= m
gal (U.S.)	× 3.785 412	E − 03	= m^3
lbf	× 4.448 222	E + 00	= N
md-ft	× 3.008 142	E + 02	= $\mu m^2 \cdot m$
MMscf/D	× 2.831 685	E + 04	= standard m^3/d
psi, psia	× 6.894 757	E + 00	= kPa

JPT

Type Curves for Evaluation and Performance Prediction of Low-Permeability Gas Wells Stimulated by Massive Hydraulic Fracturing

R. G. Agarwal, SPE-AIME, Amoco Production Co.
R. D. Carter, SPE-AIME, Amoco Production Co.
C. B. Pollock, SPE-AIME, Amoco Production Co.

0149-2136/79/0005-8145$00.25

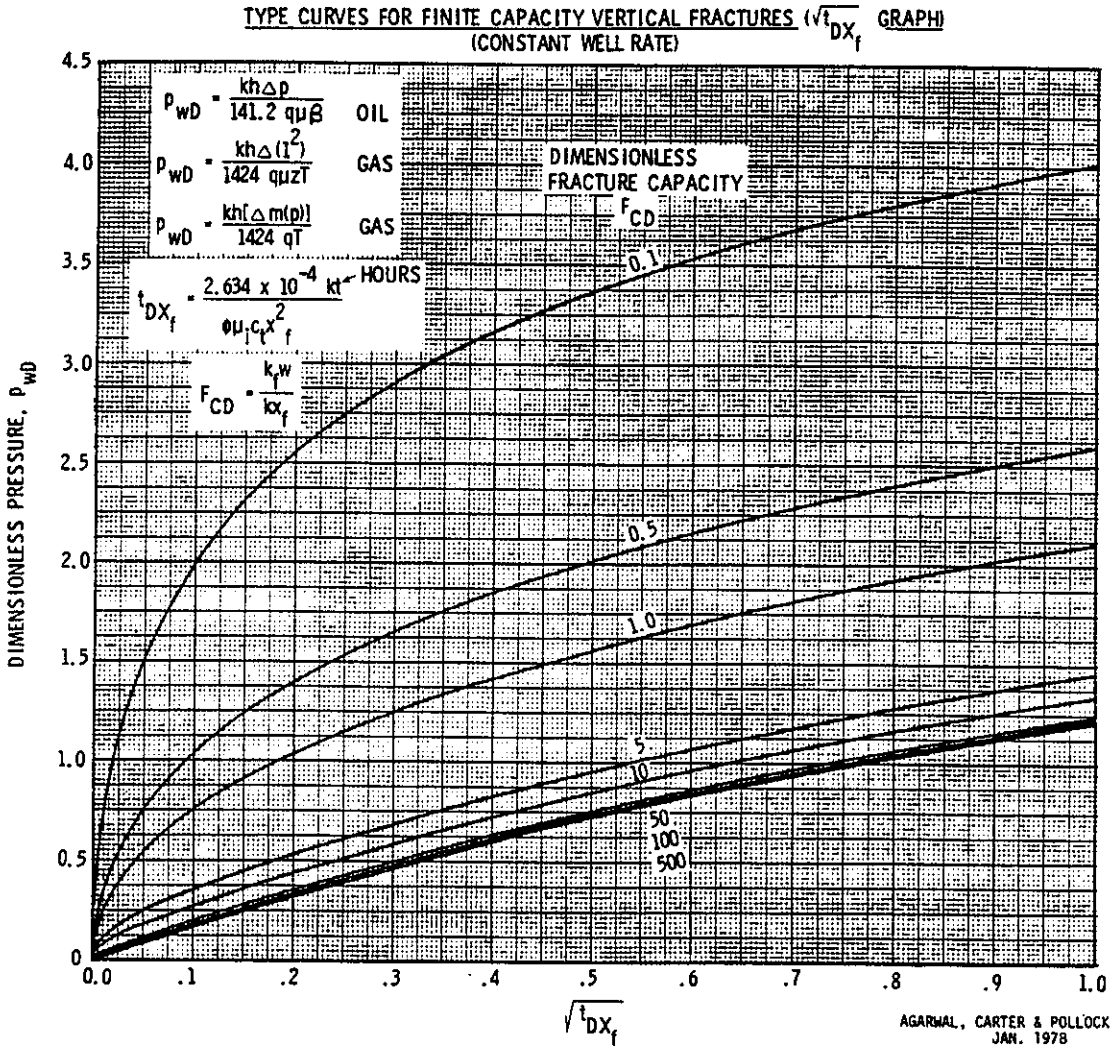

These type curves accompany SPE 6838, which was published in March JPT, *Pages 362-372. This paper (SPE 8145) will be included with SPE 6838 in the 1979* Transactions *volume.*

Errata

The authors have noted the corrections for the following equations that appeared on Page 363 in the March *JPT*.

Oil Well[11, 41]

$$x_f = \frac{4.064\ qB}{m_{v_f} h} \sqrt{\frac{\mu}{k\phi c_t}} \quad \ldots\ldots\ldots\ldots\ldots\ldots \quad (3)$$

Gas Well[10]

$$x_f = \frac{40.925\ qzT}{m_{v_f} h} \sqrt{\frac{\mu}{k\phi c_t}} \quad \ldots\ldots\ldots\ldots\ldots\ldots \quad (4)$$

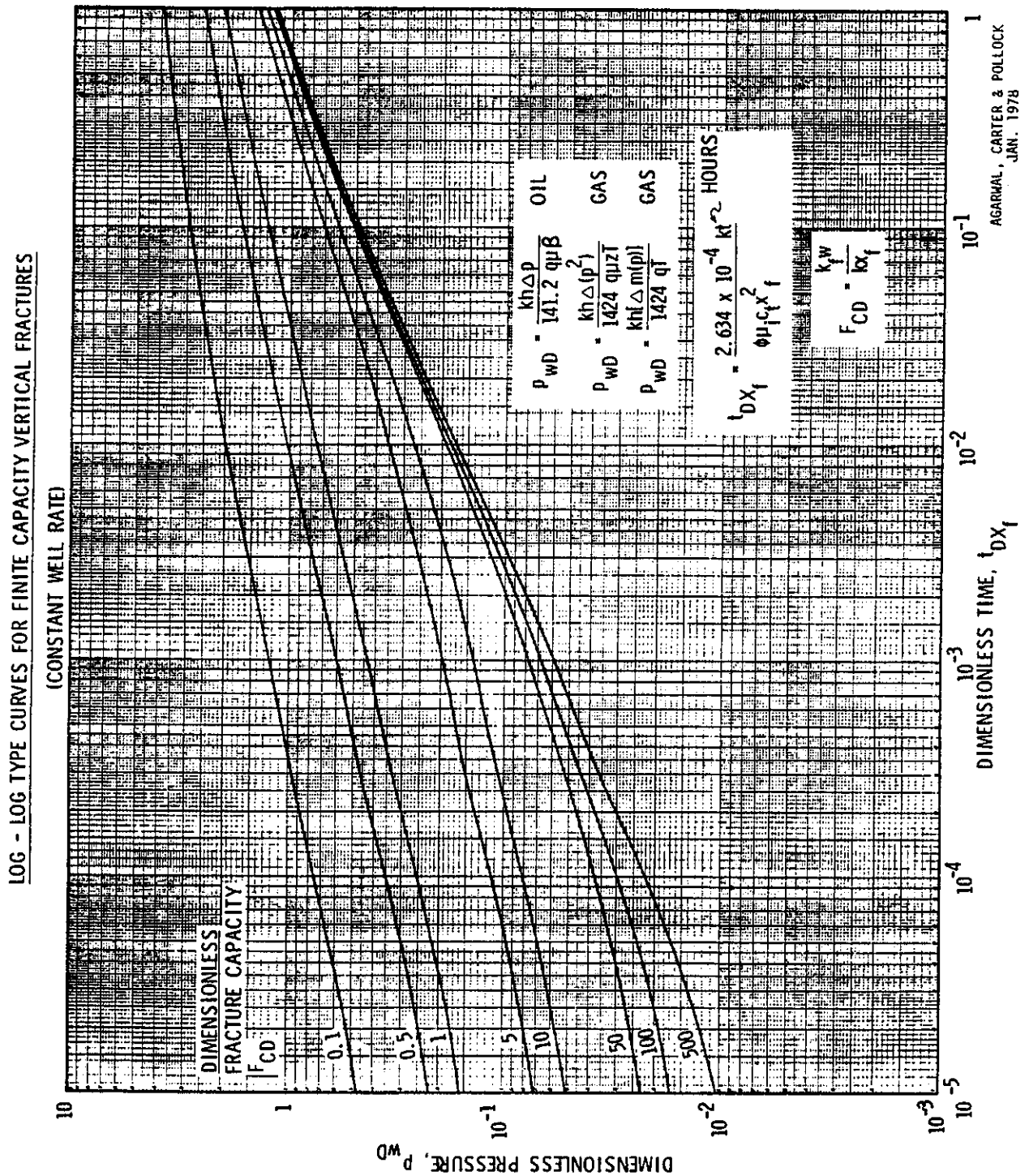

SEMI-LOG TYPE CURVES FOR FINITE CAPACITY VERTICAL FRACTURES
(CONSTANT WELL RATE)

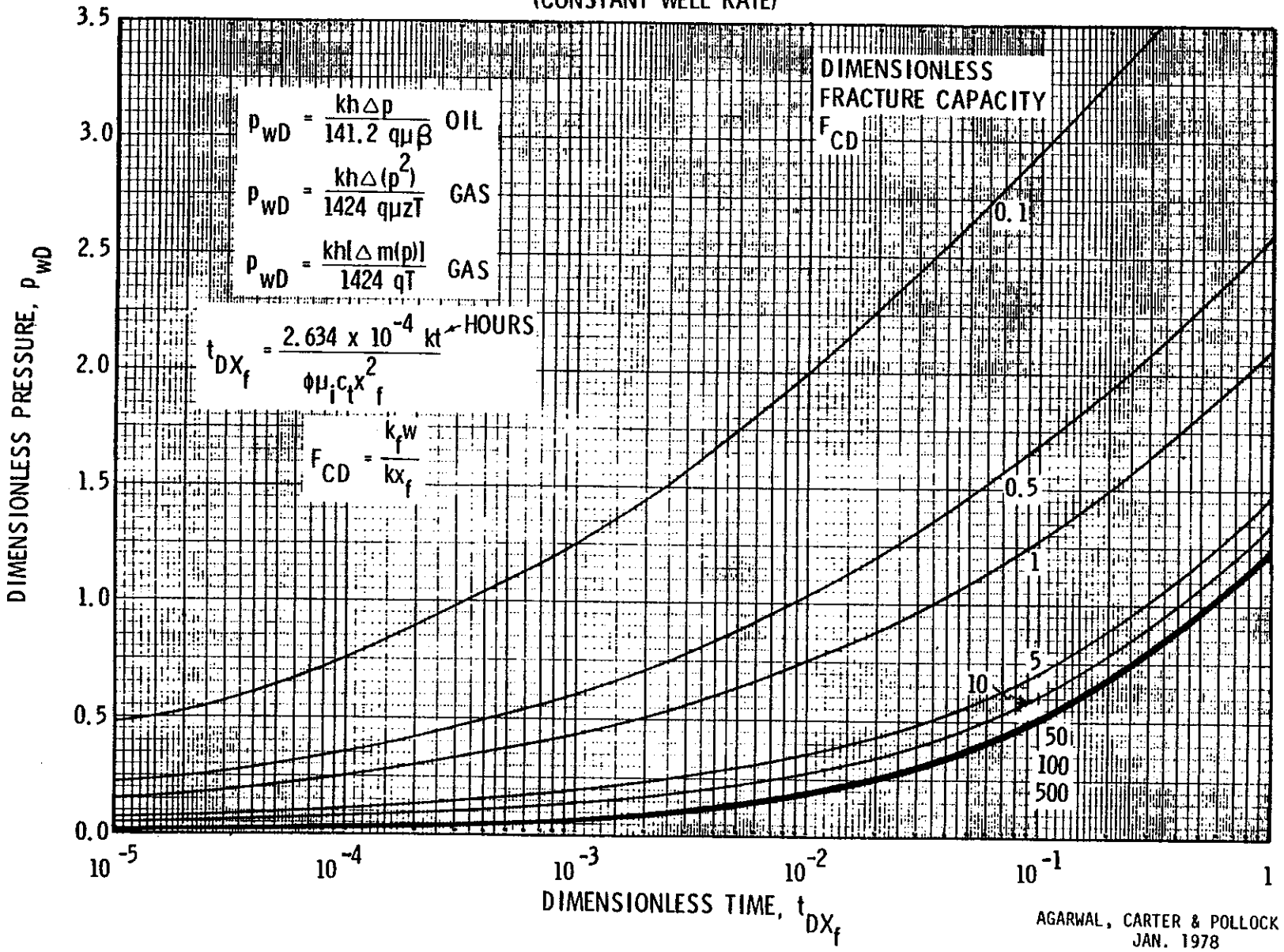

AGARWAL, CARTER & POLLOCK
JAN. 1978

LOG - LOG TYPE CURVES FOR FINITE CAPACITY VERTICAL FRACTURES

(CONSTANT WELLBORE PRESSURE)

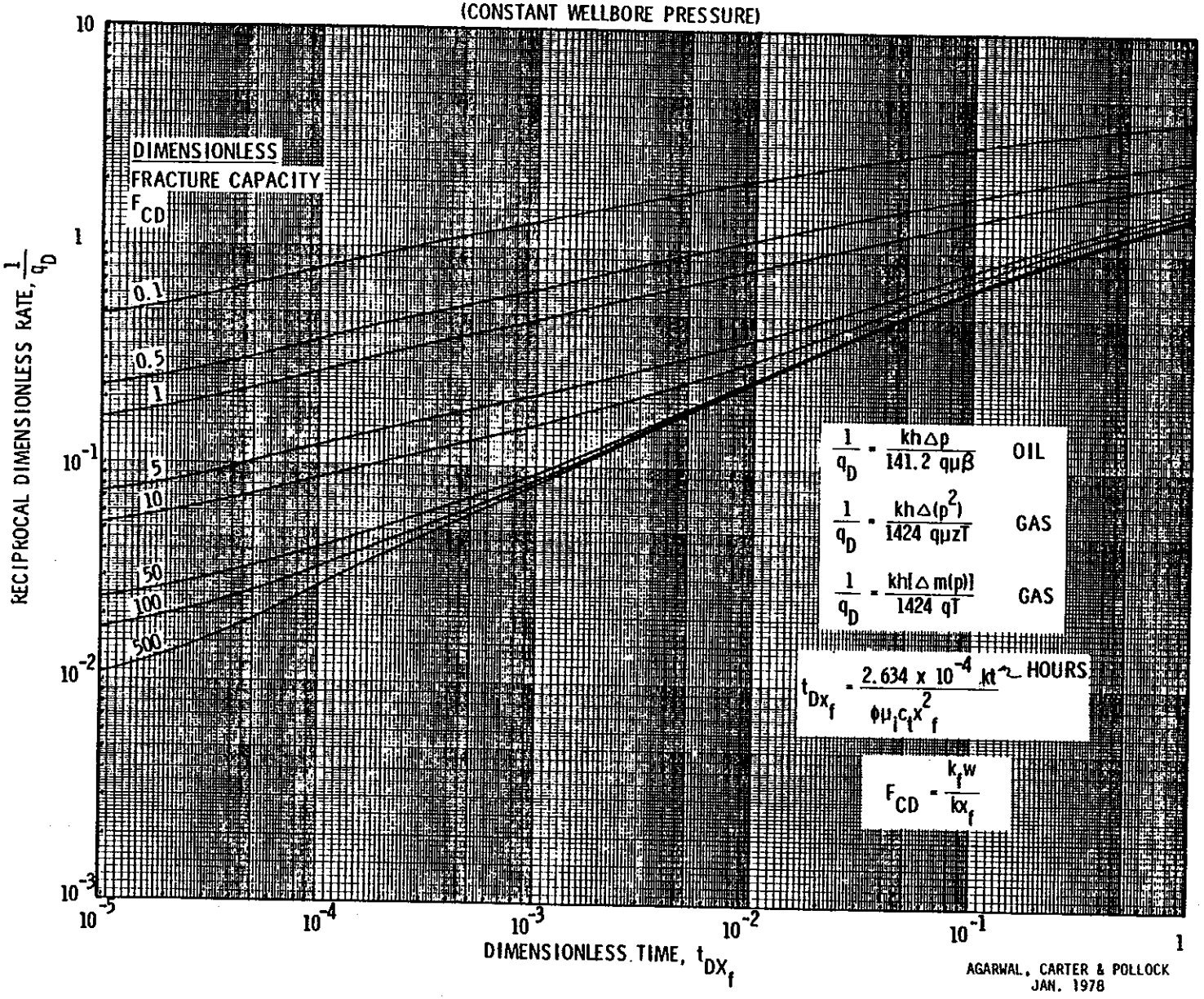

JPT

Type Curves for Finite Radial and Linear Gas-Flow Systems: Constant-Terminal-Pressure Case

Robert D. Carter, SPE, Amoco Production Co.

Abstract

This paper presents gas-production-rate results in type curve form for finite radial and linear flow systems produced at a constant terminal (bottomhole) pressure. These results can be used in the analysis of actual gas and oil rate/time data to estimate reservoir size and to infer reservoir shape. The type curves are based on dimensionless variables that are a generalized form of those presented previously.[1,2] In addition, an approximate drawdown parameter is presented. Example applications that demonstrate the applicability of the type curves to a variety of reservoir configurations are given. The Appendix contains derivations of the dimensionless variables and the drawdown parameter.

Introduction

The gas-bearing rock in some low-permeability gas fields consists of sandstone lenses of uncertain but limited size. In such fields, the reservoir area and volume drained by individual wells cannot be inferred from well spacing. Moreover, good reserve estimates using plots of p/z vs. cumulative production are often not possible because of the difficulty of obtaining reservoir pressure from buildup tests. Therefore, reserve estimation techniques that use performance data, such as production rate as a function of time, are needed.

Although this problem has been recognized, the techniques proposed in the past for application to gas reservoirs have been mostly empirical. The present work offers a method that is consistent with the basic theory of gas flow in porous media for analyzing production data to estimate reserves. This method will also provide some inference about reservoir shape.

Type Curves

Basic Assumptions. Six basic assumptions are made in generating the type curves.

1. The flow geometry is radial; therefore, the reservoir either is circular and is produced by a concentrically located well of finite radius or is a sector of a circle produced by the corresponding sector of the well (Fig. 1). In the limit as $(r_e/r_w)=R\rightarrow 1$, the flow regime becomes a linear one.
2. Permeability, porosity, and thickness are constant throughout the reservoir.
3. The pressure at the well radius (usually corresponding to the bottomhole flowing pressure [BHFP]) is held constant.

4. The initial reservoir pressure is constant (independent of position).
5. Non-Darcy flow is neglected.
6. The flowing fluid is either a gas with viscosity and compressibility that vary with pressure or an oil with a constant viscosity/compressibility product.

Definitions. The type curves are based on specially defined dimensionless time (t_D), dimensionless rate (q_D), a flow geometry parameter (η), and a drawdown parameter (λ). These variables are defined by the following equations, which are derived in the Appendix.

$$q_D=\frac{1424qT(1/B_1)}{\sigma kh[m(p_i)-m(p_{wf})]}. \quad \ldots\ldots\ldots\ldots\ldots\ldots (1)$$

$$t_D=\frac{2.634\times 10^{-4}\times 24kt}{\phi\mu(p_i)c_g(p_i)r_w^2}\alpha_1^2. \quad \ldots\ldots\ldots\ldots\ldots\ldots (2)$$

$$\eta=\frac{(R^2-1)}{2}\left(\frac{\alpha_1^2}{B_1}\right). \quad \ldots\ldots\ldots\ldots\ldots\ldots (3)$$

$$\lambda=\frac{\mu(p_i)c_g(p_i)}{2}\times\frac{[m(p_i)-m(p_{wf})]}{\left[\left(\frac{p}{z}\right)_i-\left(\frac{p}{z}\right)_{wf}\right]}. \quad \ldots\ldots (4)$$

Results. The type curves for rate as a function of time are presented in Fig. 2. A finite-difference radial-gas-flow simulator was used to generate the data for constructing the type curves.

Two flow periods can be identified. The infinite-acting (or transient) period is that period before which the curves become concave downward. The transient period ends at t_D values ranging from about 0.15 to about 1.0, depending on the value of η that characterizes the curve. The curves are concave downward during the late-time or depletion period. Notice that the primary characterizing parameter during the infinite-acting period is η, and λ is the characterizing parameter for late-time behavior ($t_D>1$). The curves for $\eta=1.234$ (linear flow) are straight lines with a negative half-slope during the infinite-acting period.

As indicated in the Appendix, the expressions for q_D and t_D when used in conjunction with the parameter η

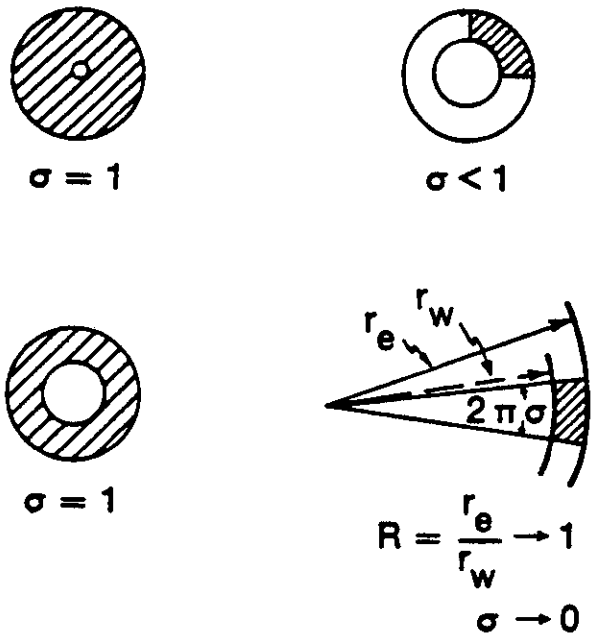

Fig. 1—Flow system basis for type curves.

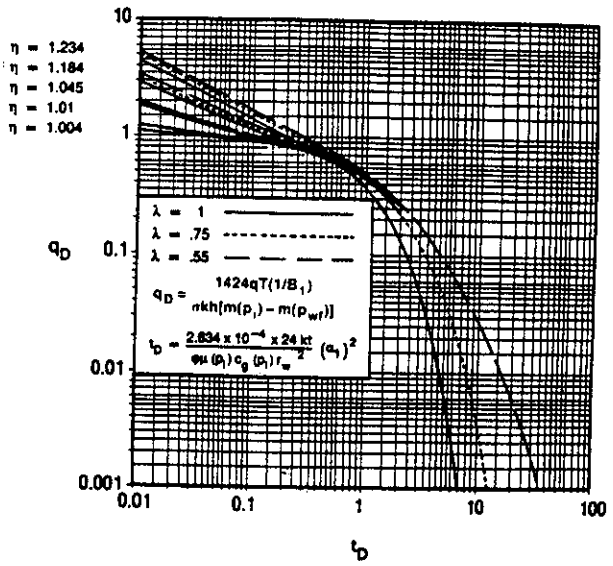

Fig. 2—Radial-linear gas-reservoir type curves.

are a generalized form of the definitions presented earlier.[1,2] Also, the Appendix shows that the two sets of definitions tend to coincide as R increases. Each value of η corresponds to a value of R. Fig. 3 is a plot of η as a function of R. As R increases, η approaches a value of 1. For values of R greater than 30, $\eta = 1$.

In an earlier study,[2] constant-terminal-pressure results for liquid flow are extended to a variety of well/reservoir configurations for the late-time period during which the rate follows an exponential decline. The connection between this earlier work and the results presented in the present paper is discussed in the Appendix.

The approximate correlating parameter (λ) accounts for the changing value of μc_g during depletion. A λ-value of unity corresponds to liquid flow (viscosity/compressibility product is constant); a λ-value of around 0.5 corresponds to maximum gas-reservoir drawdown. A derivation and discussion of λ appears in the Appendix.

The rate/time data appearing as a log-log plot in Fig. 2 is shown as a semilog plot in Fig. 4. These curves show that only when $\lambda = 1$ is the behavior consistent with exponential decline (straight line on Fig. 4 coordinates). For values of $\lambda < 1$, the curves are concave upward, with the most pronounced curvature at the lowest value of λ. Thus, in cases in which $\lambda < 1$, a straight-line extrapolation of semilog rate/time data may yield performance predictions that are too conservative.

In the strictest sense, the type curves apply only to radial flow in a circular reservoir toward a concentric well (or in a sector of a circular reservoir spanning $2\pi\sigma$ radians). Nevertheless, they may be used with good approximation to match late-time data for many well/reservoir systems of nonradial shape. Tests of the type curves using simulator-generated data for a variety of well/fracture/

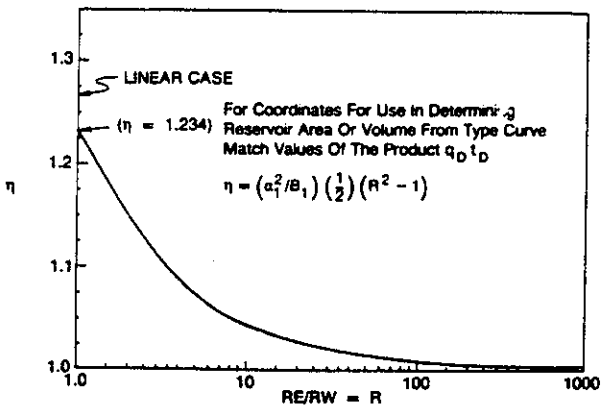

Fig. 3—Type curve parameter $\eta(R)$.

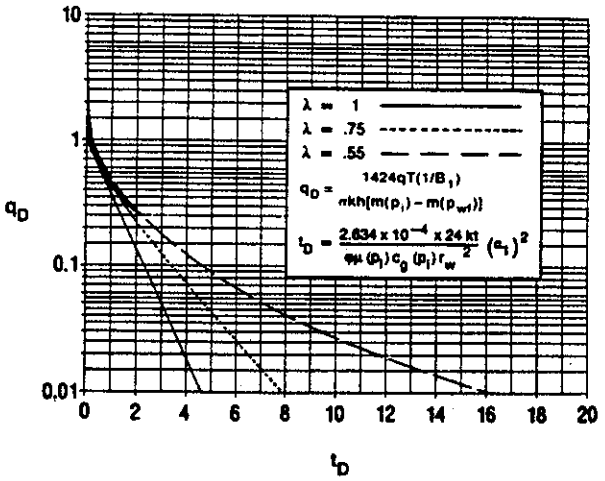

Fig. 4—Semilog radial-linear gas-reservoir type curves.

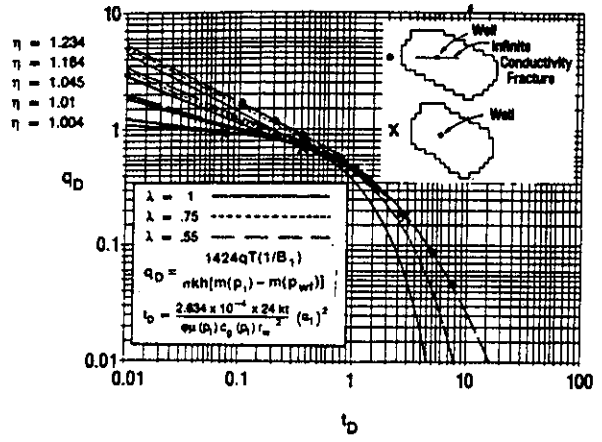

Fig. 5—Rate behavior of fractured and unfractured wells.

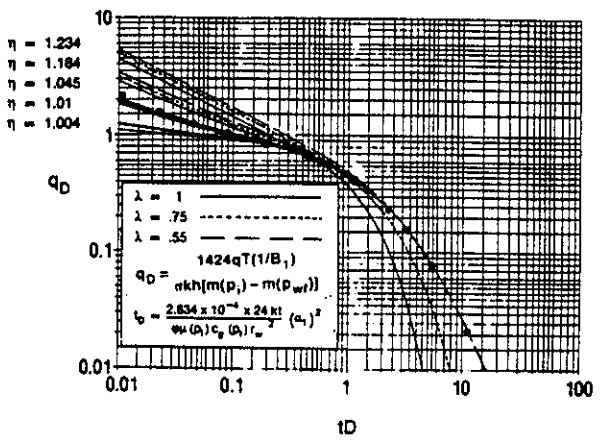

Fig. 6—Example 1 type-curve match.

reservoir configurations have confirmed the usefulness of these curves. Fig. 5 shows the type-curve matches for fractured and unfractured wells in small, irregularly shaped reservoirs, illustrating the difference in characteristic behavior caused by the fracture. In this case, the fracture causes the rate/time behavior to approach that of a linear flow system ($R \rightarrow 1$ and $\eta = 1.234$); the unfractured case is matched by the type curve for $\eta = 1.004$ (large R). In these cases, the irregular external boundary apparently does not cause the rate/time behavior to differ significantly from that of the type-curve system.

The type curves cannot be used directly to analyze the behavior of wells connected to two or more independently acting reservoir segments of differing size, shape, and/or (k/ϕ). In such cases, the curves can be used in decomposition or trial-and-error history-matching procedures, which are beyond the scope of this paper. For multiple reservoir-segment cases, the early rate data plotted on the type curve graph can fall above and have a steeper slope than the curve for linear flow ($\eta = 1.234$).

The type curves can be applied to constant-terminal-pressure-rate data from a single-phase liquid system, such as an oil reservoir above the bubblepoint. This can be a useful addition to other pressure-transient results because the reservoir size of a slightly compressible liquid reservoir often can be estimated from the production of a relatively small fraction of the original fluid in place.

Use of the Type Curves to Estimate Gas or Oil Content

Matching Procedure for Gas Wells. To analyze gas well data, use the following type-curve-matching procedure.

1. Using Eq. 4, compute λ for the system and data set of interest. This computation requires information that is normally available. Data items needed to determine λ are initial reservoir pressure, p_i; BHFP, p_{wf}; and curves or tables of viscosity, z-factor, and $m(p)$ as functions of pressure covering the pressure interval from p_{wf} to p_i. Although in principle it is possible to determine λ from the type-curve match itself, this is not recommended. This parameter should be determined before type-curve matching is done, and the type-curve match should honor the calculated value of λ. For undersaturated oil reservoirs, $\lambda = 1$.

2. Plot rate q (Mscf/D or MMscf/D) as a function of time (t) in days using the same log-log scale as the type curves. (Although q_D is expressed in Mscf/D, either Mscf/D or MMscf/D may be used in this plot.) "Smooth" rate data should be used. If actual rate values are erratic or fluctuate, it may be best to obtain averaged values of rate by obtaining the slope of straight lines drawn through adjacent points spaced at regular intervals on the plot of cumulative production vs. time. This plot should be made on tracing paper or on a transparency so that it can be laid over the type curves for matching.

3. If the computed value of λ for the data to be matched is not the same as one of the values for which a type curve is shown, the needed curve can be obtained by interpolation and graphical construction. Graphical quadratic interpolation is recommended.

4. Match the rate data to a type curve corresponding to the computed value of λ. The type-curve-matching process is described by Earlougher.[3] From this match, values of q_D and t_D corresponding to specific values for q and t are obtained. Also, a value for η should be obtained from the match. It is strongly emphasized that late-time data points are to be matched in preference to early-time data points because matching some early rate data often will be impossible.

5. An estimate for the gas that would be recoverable by reducing the average reservoir pressure from its original value to p_{wf} is then given by

$$\Delta G = G(p_i) - G(p_{wf}) = \frac{qt\eta}{\lambda q_D t_D}, \quad \ldots\ldots\ldots\ldots\ldots\ldots (5)$$

where the units for gas quantity (Mscf or MMscf) are determined from the units for gas production rate (Mscf/D or MMscf/D).

Original gas content can be determined as

$$G(p_i) = \Delta G \frac{\left(\frac{p}{z}\right)_i}{\left(\frac{p}{z}\right)_i - \left(\frac{p}{z}\right)_{wf}}. \quad \ldots\ldots\ldots\ldots\ldots\ldots (6)$$

TABLE 1—DATA FOR EXAMPLE PROBLEM 1*

Pressure (psia)	Viscosity (cp)	z-Factor
1	0.0143	1.0
601	0.0149	0.9641
1,201	0.0157	0.9378
1,801	0.0170	0.9231
2,401	0.0188	0.9207
3,001	0.0208	0.9298
3,601	0.0230	0.9486
4,201	0.0252	0.9747
4,801	0.0275	1.0063
5,401	0.0296	1.0418

Time (days)	Production Rate (MMscf/D)
1.27	8.30
10.2	3.40
20.5	2.63
40.9	2.09
81.9	1.70
163.8	1.41
400	1.07
800	0.791
1,600	0.493
2,000	0.402
3,000	0.258
5,000	0.127
10,000	0.036

*For this problem, p_i = 5,400 psia; p_{wf} = 500 psia; T = 726°R; h = 50 ft; ϕ = 0.035; s_w = 0.5, λ = 0.55

Matching Procedure for Oil Wells. The type curves for $\lambda=1$ can be applied to oil reservoirs above the bubble-point. The procedure is similar to that described for gas wells. Production rate in STB/D is plotted vs. time (in days) on the same log-log scale as the type curves. After a match is obtained on one of the curves for $\lambda=1$, original oil in place may be computed with[4]

$$N(p_i)=\left(\frac{qt\eta}{q_D t_D}\right)\left[\frac{1+c_0(p_i-p_{wf})}{(p_i-p_{wf})(c_e)}\right]. \quad \ldots\ldots\ldots (7)$$

It is clear from Eqs. 5 and 7 that determining reservoir gas or oil content does not require knowledge of the values of parameters appearing in the equations defining q_D and t_D. Such values would be needed only if estimations of permeability, reservoir areal extent, or shape were to be attempted.

Applications of the Type Curves

Example Calculation 1. This example performance data set was obtained from a simulator run in which a fractured well and its drainage area were matched. The geometry was nonradial. Input data and resulting output are given in Table 1. The calculated value of λ for this problem is 0.55; therefore, the type curves for a λ value of 0.55 can be used directly from Fig. 2. The early portion of the rate/time data before about 20 days cannot be used with the type curves of Fig. 2. This reinforces the statement that the late-time data points are always to be matched in preference to early-time data. Fig. 6 shows the type-curve match of the data. (The rate scale in MMscf/D and the time scale are not shown.) Match points are q=1 MMscf/D [28.636×10^3 std m^3/d], q_D=0.605, η=1.045, t=1,000 days, and t_D=1.1. With Eq. 5,

$$G(p_i)-G(p_{wf})=\Delta G=\frac{qt\eta}{\lambda q_D t_D}$$

$$=\frac{1\times1{,}000\times1.045}{0.55\times0.604\times1.1}=2{,}860 \text{ MMscf.}$$

With Eq. 6,

$$G(p_i)=\Delta G\left[\frac{\left(\frac{p}{z}\right)_i}{\left(\frac{p}{z}\right)_i-\left(\frac{p}{z}\right)_{wf}}\right]$$

$$=2{,}860\left[\frac{\frac{5{,}400}{1.0418}}{\left(\frac{5{,}400}{1.0418}\right)-\left(\frac{500}{0.970}\right)}\right]$$

$$=3{,}176 \text{ MMscf.}$$

From simulator results, the correct value for $G(p_i)$ is 3,087 MMscf [88.4×10^6 std m^3]. Therefore, the error in the type curve determination is

$$\text{Error}(\%)=\frac{3{,}176-3{,}087}{3{,}087}\times100=2.9\%.$$

To obtain a definitive match, it is necessary to have some data extending into the portion of the type curves that are concave downward ($t_D \geqq 0.7$ to $t_D \geqq 2$, depending on the value of η).

The drainage area, S, for the well can be estimated with the following equation:

$$S=\frac{G(p_i)}{h\phi\left(\frac{p_i}{z_i}\right)\frac{520\times10^{-6}}{14.7T}}. \quad \ldots\ldots\ldots\ldots\ldots (8)$$

Substituting values from Table 1 and type-curve-match results where applicable yields

$$S=\frac{3{,}176}{(50)[(0.07)(1-0.5)]\left(\frac{5{,}400}{1.0418}\right)\left(\frac{520\times10^{-6}}{14.7\times726}\right)},$$

or

$S\cong7.19\times10^6$ sq ft, or $S\cong165$ acres.

Input data for the drainage area dimensions are for a drainage area of 160 acres [64.75 ha].

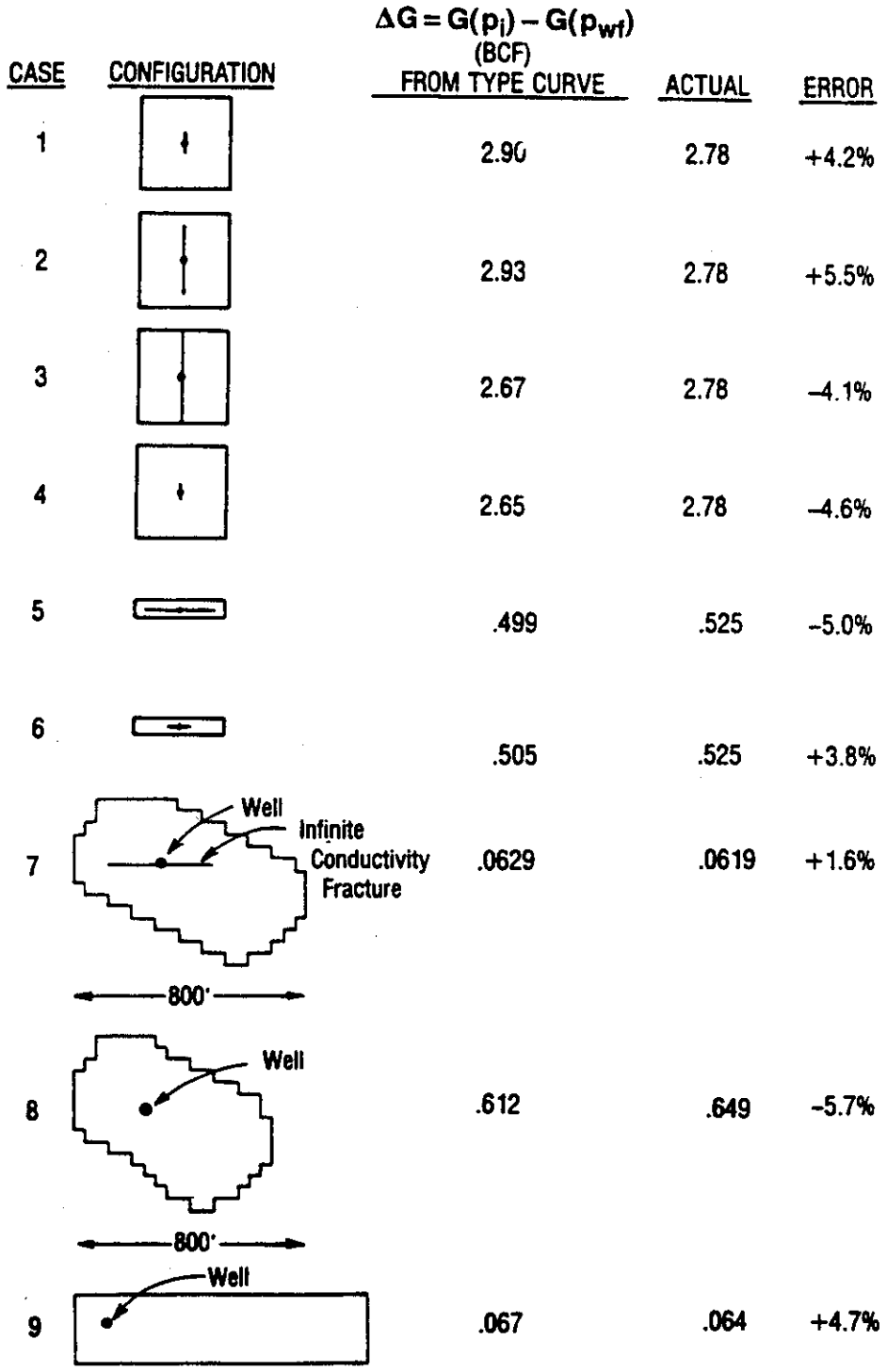

Fig. 7—Test application result summary.

Once a type-curve match is obtained, a prediction of future performance is generated by simply converting $q_D - t_D$ rate/time pairs along the matched type curve.

Example Calculation 2. A well has been on production for 300 days. All the rate data fall on a negative half-slope line. The current producing rate is 20 Mscf/D [0.57×10^3 std m^3/d]. The computed value for λ is 0.55.

A definitive type-curve match cannot be made for this well because no data correspond to the concave downward portion of the type curve. However, a lower bound estimate for $G(p_i) - G(p_{wf})$ can be made.

All the data will fall on the early portion of the type curve for $\eta = 1.234$ and $\lambda = 0.55$. If the last data point is assumed to be matched at the end of the negative half-slope straight line on this curve, the following match

points are obtained: $q=20$ Mscf/D [0.57×10^3 std m^3/d] $q_D=0.68$, $\eta=1.234$, $t=300$ days, $t_D=0.6$, and $\lambda=0.55$; therefore, a lower bound value for

$$G(p_i)-G(p_{wf})=\frac{20\times300\times1.234}{0.55\times0.68\times0.6}$$

$$=32{,}995 \text{ Mscf.}$$

Because the well has produced 12 MMscf [343.6×10^3 std m^3], gas remaining to be produced (to reduce the average reservoir pressure to p_{wf}) is *at least* $32.995-12=20.995$ MMscf [$944.8\times10^3-343.6\times10^3=601.2\times10^3$ std m^3].

Additional Simulator Tests of the Type Curves

Fig. 7 presents a summary of nine tests of the type curves in which the performance data for each test were generated with a gas reservoir simulator. Of these, six well/reservoir systems were symmetrical, and three were asymmetrical. The predicted well performances were type-curve matched to obtain estimates of ΔG. Fig. 7 presents a comparison of the computed and actual values of $G(p_i)-G(p_{wf})$. They are in good agreement. These results suggest that the type curves should be applicable to a wide variety of well/reservoir configurations.

Summary

1. Log-log type curves have been developed for production rate as a function of time for flow in bounded radial and linear gas and liquid systems having constant pressure at the outflow face. The type curves are based on definitions of dimensionless rate, q_D, and time, t_D, that are generalizations of those presented earlier. The new, generalized, dimensionless quantities permit representation of solutions for R approaching unity. Hence, flow in linear systems may also be represented.
2. The type curves are also based on a drawdown parameter, λ, that permits good approximate representation of real gas flow with a single set of curves.
3. When the type curves are plotted in semilog form (log q_D vs. t_D on a linear scale), all the curves are concave upward except for the liquid flow case ($\lambda=1$). Thus it has been shown that straight-line semilog extrapolations of gas-well rate data may predict rates and recovery that are too low.
4. The type curves may be used with good approximation to describe the late-time behavior of many gas-well/reservoir systems that are neither radial nor linear and in fact may be asymmetrical.
5. For many well/reservoir systems, the rate/time data can be used in a *simple* type-curve matching and calculation procedure to estimate original gas in place. However, data are required over that portion of the producing history corresponding to a t_D value of at least 0.7 to 2 for reliable estimates. If only data corresponding to values of t_D less than this range are available, it may be possible to obtain only a lower-bound estimate of gas in place.

Nomenclature

A = area of flow system in the plane normal to the direction of flow, sq ft [m^2]
B_j = coefficient of the jth term in Eq. A-15 as defined by Eq. A-16
c_e = effective compressibility, psi^{-1} [kPa^{-1}] (as defined in Ref. 5)
$c_g(p)$ = gas compressibility, defined by Eq. A-4, psi^{-1} [kPa^{-1}]
c_o = compressibility of oil, psi^{-1} [kPa^{-1}]
G_{DR}, G_{DL} = dimensionless cumulative production expressed as a fraction of the gas that would be recovered by reducing the average reservoir pressure from p_i to p_{wf}
$G(p)$ = reservoir gas content corresponding to average reservoir pressure p, Mscf or MMscf [std m^3]
h = pay thickness, ft [m]
J_n = Bessel function of first kind of order n
k = effective permeability, md
L = length of linear system parallel to the direction of flow, ft [m]
$m(p)$ = real gas pseudopressure or real gas flow potential, defined by Eq. A-2, psi^2/cp [$(kPa)^2/(Pa\cdot s)$]
p = pressure, psia [kPa]
p_i = initial reservoir pressure, psia [kPa]
p_{wf} = bottomhole flowing pressure, psia [kPa]
p' = pressure variable of integration, psia [kPa]
q_g = gas production rate, Mscf/D [std m^3/d]
q_D = dimensionless rate used in the type curves, defined by Eq. A-18
q_{DR} = dimensionless time defined by Eq. A-10
q_o = oil production rate, STB/D [stock-tank m^3/d]
r_e = external radius of type curve reservoir region, ft [m]
r_w = internal radius of type curve reservoir region, ft [m]
R = radius ratio r_e/r_w
s_w = water saturation, fraction
S = well drainage area, acres [ha]
t = time, days [d]
t_D = dimensionless time used in the type curves, defined by Eq. 2
t_{DL} = dimensionless time as defined by Eq. A-12
t_{DR} = dimensionless time defined by Eq. A-9
T = reservoir temperature, °R [K]
Y_n = Bessel function of second kind of order n
$z(p)$ = gas deviation (or supercompressibility) factor, dimensionless
α_j = time coefficient in the jth term in Eq. A-15 as defined by Eq. A-17
η = type curve parameter characterizing effect of radius ratio R, dimensionless, defined by Eq. 3

λ = type curve parameter used to characterize gas well drawdown, dimensionless, defined by Eq. 4

μ = gas viscosity, cp [Pa·s]

$\overline{\mu c_g}$ = mean value of viscosity/compressibility product over the pressure interval p_i to p_{wf}, cp/psi [Pa·s/kPa], defined by Eq. A-5 or A-6

σ = fraction of 2π radians defining the concentric ring sector constituting the type curve approximation to the reservoir shape, dimensionless

ϕ = hydrocarbon porosity (for a gas reservoir, usually porosity times $[1-s_w]$), fraction

References

1. Fetkovich, M.J.: "Decline Curve Analysis Using Type Curves," *J. Pet. Tech.* (June 1980) 1065–77.
2. Ehlig-Economides, C.A. and Ramey, H.J. Jr.: "Pressure Buildup for Wells Produced at Constant Pressure," *Soc. Pet. Eng. J.* (Feb. 1981) 105–14.
3. Earlougher, Robert C. Jr.: *Advances in Well Test Analysis*, Monograph Series, SPE, Richardson, TX (1977) 5, 264.
4. Craft, B.C. and Hawkins, M.F.: *Applied Petroleum Reservoir Engineering*, Prentice-Hall Publishers, Inc., Englewood Cliffs, NJ (1959) 437.
5. Al-Hussainy, R., Ramey, H.J. Jr., and Crawford, P.B.: "The Flow of Real Gases Through Porous Media," *J. Pet. Tech.* (May 1966) 624–42.
6. van Everdingen, A.F. and Hurst, W.: "The Application of the Laplace Transformation to Flow Problems in Reservoirs," *Trans.*, AIME (1949) 186, 305–24.
7. Kidder, R.E.: "Unsteady Flow of Gas Through a Semi-Infinite Porous Medium," *J. Applied Mechanics* (Sept. 1957) 329–32.

APPENDIX

Derivation of Type Curve Variables and Parameters and Validation of the Type Curves

The type curves were generated from numerical solutions of unsteady-state radial gas-flow and exact liquid flow solutions. The definitions for q_D, t_D, and η were derived by use of exact liquid flow solutions. These variable definitions, therefore, are rigorously correct for liquid flow ($\lambda=1$). From the numerical gas flow solutions, it was found that they were also valid for gas flow ($\lambda<1$). The following provides derivations of λ, q_D, t_D, and η. The basic assumptions are given in the text.

Derivation of λ.

A parameter λ that approximately correlates the drawdown behavior of different constant-terminal-pressure gas flow systems is derived. This parameter makes possible the concept and creation of generalized type curves that can be used (with good approximation) with any natural gas composition, initial reservoir pressure, and outflow face (BHFP) pressure. By appropriately modifying the viscosity and z factor (as functions of pressure), it is also possible to determine values of λ that account for confining-pressure effects on permeability and porosity, assuming that confining pressure is a function only of local reservoir pressure.

First, recall that the time rate of change of gas content at a point in a gas reservoir (for isothermal flow) is proportional to $\partial(p/z)/\partial t$. If Darcy's equation holds, the partial differential equation describing the flow of gas through a porous medium is $L[k,m(p)]=\nu\partial(p/z)/\partial t$. The specific form of the operator L depends on the coordinate system used and other considerations.

By use of the chain rule, it can be shown that

$$\frac{\partial\left(\frac{p}{z}\right)}{\partial t}=\frac{\mathrm{d}\left(\frac{p}{z}\right)}{\mathrm{d}m}\frac{\partial m}{\partial t}, \quad \text{(A-1)}$$

where

$$m(p)=2\int_{p_c}^{p}\frac{p'\mathrm{d}p'}{\mu(p')z(p')}. \quad \text{(A-2)}$$

It also can be shown that

$$\frac{\mathrm{d}\left(\frac{p}{z}\right)}{\mathrm{d}m}=\frac{1}{2}[\mu(p)c_g(p)], \quad \text{(A-3)}$$

where

$$c_g=\frac{1}{p}\left(1-\frac{p}{z}\frac{\mathrm{d}z}{\mathrm{d}p}\right). \quad \text{(A-4)}$$

A result equivalent to Eq. A-3 was given by Al-Hussainy *et al.*[5]

Now determine a mean value for the product $\mu(p)c(p)$ over the interval (p_i, p_{wf}). Replacing the derivative on the left side of Eq. A-3 with a finite-difference quotient and solving for the viscosity/compressibility product, one obtains

$$\overline{\mu c_g}=2\frac{\left[\left(\frac{p}{z}\right)_i-\left(\frac{p}{z}\right)_{wf}\right]}{[m(p_i)-m(p_{wf})]}, \quad \text{(A-5)}$$

or

$$\overline{\mu c_g}=\frac{\left[\left(\frac{p}{z}\right)_i-\left(\frac{p}{z}\right)_{wf}\right]}{\int_{p_{wf}}^{p_i}\frac{p'\mathrm{d}p'}{\mu(p')z(p')}}. \quad \text{(A-6)}$$

Eq. A-6 is almost the same as Eq. 34 of Al-Hussainy *et al.*[5] The distinction is that Eq. A-6 is in terms of fixed pressure values p_i and p_{wf}, whereas Al-Hussainy *et al.* were concerned with an average pressure $\bar{p}$, which is a function of time.

Finally, define a parameter (λ) as

$$\lambda=\frac{\mu(p_i)c_g(p_i)}{\overline{\mu c_g}}, \quad \text{(A-7)}$$

TABLE A-1—REAL GAS PROPERTIES USED TO TEST THE λ CONCEPT

Pressure (psia)	Viscosity (cp)	z-Factor	$m(p)$ (psi²/cp)	$c_g(p)$ (psi⁻¹)
14.7	0.0112	0.9981	0	0.068
500	0.0117	0.9374	0.2273×10^{8}	0.213×10^{-2}
1,000	0.0125	0.8813	0.9124×10^{8}	0.112×10^{-2}
1,500	0.0140	0.8372	2.012×10^{8}	0.754×10^{-3}
2,000	0.0160	0.8104	3.432×10^{8}	0.541×10^{-3}
2,500	0.0185	0.8030	5.052×10^{8}	0.396×10^{-3}
3,000	0.0212	0.8124	6.765×10^{8}	0.293×10^{-3}
3,500	0.0238	0.8340	8.520×10^{8}	0.223×10^{-3}
4,000	0.0263	0.8637	10.28×10^{8}	0.175×10^{-3}
4,500	0.0286	0.8986	12.04×10^{8}	0.141×10^{-3}
5,000	0.0308	0.9368	13.78×10^{8}	0.115×10^{-3}
5,500	0.0328	0.9772	15.51×10^{8}	0.982×10^{-4}
6,000	0.0348	1.0198	17.21×10^{8}	0.833×10^{-4}

TABLE A-2—PRESSURE TRAVERSES USED TO TEST THE λ CONCEPT

Case	p_i (psia)	p_{wf} (psia)	λ
1	6,000	1,636	0.55
2	6,000	3,547	0.75
3	6,000	5,910	0.99
4	4,000	365	0.55
5	4,000	2,173	0.75
6	2,000	656	0.75

or, substituting Eq. A-5 into Eq. A-7,

$$\lambda=\frac{\mu(p_i)c_g(p_i)}{2}\frac{[m(p_i)-m(p_{wf})]}{\left[\left(\frac{p}{z}\right)_i-\left(\frac{p}{z}\right)_{wf}\right]}, \quad \ldots\ldots (A\text{-}8)$$

which is Eq. 4 of the text.

A value for λ of unity corresponds to liquid flow (or gas flow in the case where $(p_i-p_{wf})/p_i \ll 1$).

For an ideal gas, taken herein as one with constant viscosity and z factor, Eq. A-8 reduces to

$$\lambda=\frac{p_i+p_{wf}}{2p_i}.$$

For a *producing* well, $0<p_{wf}<p_i$. Therefore, with substitution of the limiting values zero and p_i for p_{wf} into the above expression, it is found that $0.5<\lambda<1.0$ for an ideal gas.

Some Properties of λ

If dimensionless time for the radial flow system is given as

$$t_{DR}=\frac{2.634\times10^{-4}\times24kt}{\phi\mu(p_i)c_g(p_i)r_w^2}, \quad \ldots\ldots (A\text{-}9)$$

and dimensionless rate is given as

$$q_{DR}=\frac{1{,}424qT}{\sigma kh[m(p_i)-m(p_{wf})]}, \quad \ldots\ldots (A\text{-}10)$$

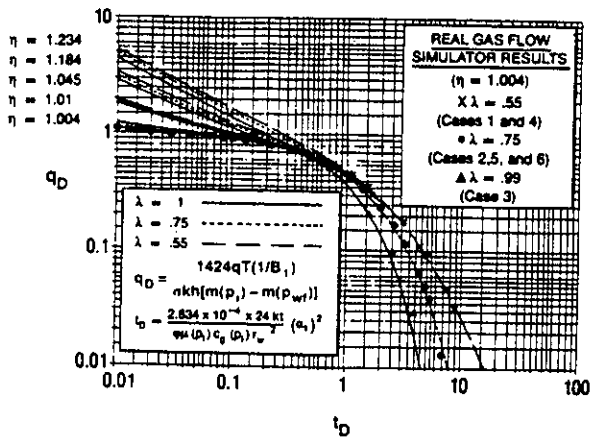

Fig. A-1—Results validating the λ concept.

then dimensionless cumulative production is expressed as

$$G_{DR}=2\lambda\frac{r_w^2}{(r_e^2-r_w^2)}\int_0^{t_{DR}} q_{DR}\,dt'_{DR} \quad \ldots\ldots (A\text{-}11)$$

and is the gas produced to time t expressed as a fraction of the gas recoverable by reducing the average reservoir pressure from p_i to p_{wf}.

If dimensionless time and rate, respectively, are defined for the linear system by

$$t_{DL}=\frac{2.634\times10^{-4}\times24kt}{\phi\mu(p_i)c_g(p_i)L^2} \quad \ldots\ldots (A\text{-}12)$$

and

$$q_{DL}=\frac{(2\pi)(1{,}424)LT_q}{Ak[m(p_i)-m(p_{wf})]}, \quad \ldots\ldots (A\text{-}13)$$

then

$$G_{DL}=\lambda\int_0^{t_{DL}} q_{DL}\,dt'_{DL}, \quad \ldots\ldots (A\text{-}14)$$

where G_{DL} is the gas recovered at time t expressed as a fraction of the amount recoverable by reducing the average pressure from p_i to p_{wf}. Thus λ is a factor that relates dimensionless gas recovery to the integral over dimensionless time of dimensionless rate.

Consider two flow systems that have the same flow geometry but different gas compositions. If the pressure traverses (p_i, p_{wf}) for the two systems are selected so that each system has the same value of λ (the pressure traverses will not be the same in general), then the rate/time curves expressed in dimensionless form will be in very close (but not exact) agreement. Thus it is possible to construct rate/time depletion type curves for gas-flow systems based on one gas composition that can be applied with acceptable accuracy to systems having different gas compositions.

The greatest disagreement between two systems will usually occur at later times when prediction accuracy is less important.

At very late times when the average reservoir pressure is approaching p_{wf}, the final rate/time behavior should approach an exponential decay curve determined by $\mu(p_{wf})c_g(p_{wf})$. This time portion of the rate behavior may be of less interest because often it will occur near the point of abandonment. Two systems with different gas compositions will not usually have the same value for $\mu(p_{wf})c_g(p_{wf})$ even though they have a common value of λ.

For convenience, the type curves were generated with an ideal gas system and then compared and tested with simulator results for a real gas system whose properties are given in Table A-1. Several comparison cases were run in which specified values of λ were obtained by the use of different pressure traverses with the real gas system of Table A-1. The pressure traverses and corresponding values of λ are in Table A-2. Values for λ were computed using Eq. A-8. Notice that more than one pressure traverse can yield a given value for λ. The real gas simulator results are shown plotted as points on the type curves in Fig. A-1. These results are for $r_e/r_w=R=1{,}000$, but similar agreement was obtained also for flow in a linear system.

Derivation of the Dimensionless Type-Curve Variables q_D, t_D, and η

The type curves are based upon radial-linear flow systems.

The exact liquid ($\lambda=1$) flow solution for cumulative production as a function of time for radial systems is given by Eq. VII-10 of Ref. 6. The exact solution for production rate as a function of time can be obtained by the use of the first derivative with respect to time of this equation. The result is

$$q_{DR}(t_{DR})=\sum_{j=1}^{\infty} B_j e^{-\alpha_j^2 t_{DR}}, \quad \ldots\ldots\ldots\ldots \text{(A-15)}$$

where

$$B_j=\frac{2J_1^2(\alpha_j R)}{[J_0^2(\alpha_j)-J_1^2(\alpha_j R)]} \quad \ldots\ldots\ldots\ldots\ldots \text{(A-16)}$$

and

$$R=r_e/r_w,$$

and α_j is the jth root of

$$J_1(\alpha_j R)Y_0(\alpha_j)-Y_1(\alpha_j R)J_0(\alpha_j)=0. \quad \ldots\ldots \text{(A-17)}$$

The values of α_j are real and distinct. Also, $\alpha_1<\alpha_2<\alpha_3\ldots$.

For the sake of compactness, it is desirable to develop a coordinate system for areal-extent (reservoir limit) type curves that bring the curves together at large values of time. In view of the foregoing equations, it is clear that at late times the first term on the right side of Eq. A-15 will predominate. Therefore, the needed system of dimensionless variables can be obtained by normalizing on the basis of the first-term coefficients B_1 and α_1. Thus

$$q_D=\frac{q_{DR}}{B_1}, \quad t_D=\alpha_1^2 t_{DR}.$$

Notice that B_1 and α_1 in this case are obtained for radial geometry with Eqs. A-16 and A-17. It is also possible to use the exact solution for linear liquid flow to define a q_D and a t_D in terms of B_1 and α_1 for linear flow; $q_D(t_D)$ for radial flow and $q_D(t_D)$ for linear flow will coincide for large t_D.

In fact, it can be shown that

$$\lim_{R\to 1} q_D(t_D)$$

based on radial flow is equal to $q_D(t_D)$ based on linear flow.

In terms of q_D and t_D, Eq. A-15 becomes

$$q_D=e^{-t_D}+\sum_{j=2}^{\infty}\frac{B_j}{B_1}e^{-(\alpha_j^2/\alpha_1^2)t_D}. \quad \ldots\ldots\ldots \text{(A-18)}$$

At large values of t_D, the terms under the summation sign will become small relative to e^{-t_D}. Therefore, all the type curves for different specific values of R will tend to coincide for large values of t_D.

The parameter η is a function of R and is used to compute drainage area gas content. It is obtained by noting that

$$G(p_i)-G(p_{wf})=\Delta G=\left(\frac{1}{9}\right)\left(\frac{1}{\lambda}\right)\left(\frac{R^2-1}{2}\right)$$

$$\times\frac{\sigma h\phi r_w^2\mu(p_i)c_g(p_i)[m(p_i)-m(p_{wf})]}{T}, \quad \ldots \text{(A-19)}$$

or, by use of the definitions of q_D and t_D,

$$\Delta G=\frac{qt}{q_D t_D}\left(\frac{1}{\lambda}\right)\frac{(R^2-1)}{2}\frac{\alpha_1^2}{B_1}. \quad \ldots\ldots\ldots \text{(A-20)}$$

Thus, η is defined by

$$\eta=\frac{(R^2-1)}{2}\left(\frac{\alpha_1^2}{B_1}\right), \quad \ldots\ldots\ldots\ldots\ldots \text{(A-21)}$$

and Eq. A-20 may be written as

$$\Delta G=\frac{qt\eta}{q_D t_D\lambda}. \quad \ldots\ldots\ldots\ldots\ldots\ldots\ldots \text{(A-22)}$$

Original gas in place is given by

$$G(p_i)=\frac{qt\eta}{q_D t_D\lambda}\frac{\left(\frac{p}{z}\right)_i}{\left(\frac{p}{z}\right)_i-\left(\frac{p}{z}\right)_{wf}}. \quad \ldots\ldots\ldots \text{(A-23)}$$

The parameter η is shown as a function of R in Fig. 3. Notice that $\eta \to 1$ as R increases.

Fetkovich[1] and Ehlig-Economides and Ramey[2] have shown in effect that, when R is large (i.e., greater than 30),

$$\alpha_1^2 \cong \left(\frac{2}{R^2-1}\right) \div \left(\ln R - \frac{3}{4}\right) \quad \ldots\ldots\ldots\ldots (A\text{-}24)$$

and

$$B_1 \cong 1 \div \left(\ln R - \frac{3}{4}\right). \quad \ldots\ldots\ldots\ldots\ldots\ldots (A\text{-}25)$$

Therefore, for $R > 30$,

$$\eta \cong \left(\frac{R^2-1}{2}\right)\frac{\alpha_1^2}{B_1} \cong 1.$$

Validation of the $q_D - t_D - \eta$ System for $\lambda < 1$

Numerical solutions were obtained for constant-terminal-pressure radial ideal gas flow for values of λ of 1, 0.75, and 0.55. When these results were plotted in terms of q_D and t_D, they formed distinct curves at late times determined by λ-values only. At early times, the curves tend to be defined by η (or equivalently by R). As η approaches its limiting value as R approaches unity, early-time separation of the curves for different λ values is manifested. The validity of the early-time behavior of the curves as R approaches unity (linear flow) was confirmed by a study utilizing Kidder's expression of the semi-infinite gas flow problem with constant terminal pressure.[7]

All of these characteristics can be observed in the basic log-log type curves shown in Fig. 2.

Gas Flow Behavior as R Approaches Unity (Linear Flow)

As $R \to 1$, it can be shown that

$$\lim_{R\to 1} \eta_{(\text{radial})} = \lim_{R\to 1} \left(\frac{R^2-1}{2}\right)\frac{\alpha_{1_{\text{radial}}}^2}{B_{1_{\text{radial}}}} = \frac{\alpha_{1_{\text{linear}}}^2}{B_{1_{\text{linear}}}}.$$

Thus a limiting value for η as $R \to 1$ is available. Because

$$\alpha_{1_{\text{linear}}} = \frac{\pi}{2} \text{ and } B_{1_{\text{linear}}} = 2,$$

then

$$\eta_{\text{linear}} = \lim_{R\to 1} \eta_{\text{radial}} = \frac{\left(\frac{\pi}{2}\right)^2}{2} = 1.234.$$

This value is shown for $\eta(R=1)$ in Fig. 3. This value permits a smooth continuation to $R=1$ of the function $\eta(R)$.

Relation Between the Type Curves and the Results of Ehlig-Economides and Ramey

Ehlig-Economides and Ramey[2] show that late-time rate behavior for liquid flow in a variety of reservoir shapes can be expressed by an equation involving an exponential in time. This equation includes a shape factor to account for flow geometry. When this equation is normalized with the same procedure as described in this Appendix for these type curves, the result is equivalent to that obtained with the late-time portion of the Fig. 2 type curves with a value of η of unity.

The exponential equation result of Ref. 2 relies on the assumption that the Laplace transform of a specific late-time approximation to the pressure solution for constant rate can be used in Eq. VI-32 of Ref. 6. This will not always be possible for every configuration.

SI Metric Conversion Factors

ft	×	3.048*	E−01	= m
psi^{-1}	×	1.450 377	E−04	= Pa^{-1}
psi	×	6.894 757	E+00	= kPa
°R	×	5/9		= K
scf	×	2.863 640	E−02	= std m^3

*Conversion factor is exact.

SPEJ

Original manuscript received in the Society of Petroleum Engineers office May 24, 1984. Paper accepted for publication Feb. 26, 1985. Revised manuscript received Feb. 18, 1985. Paper (SPE 12917) first presented at the 1984 SPE Rocky Mountain Regional Meeting held in Casper May 21–23.

SPE 28628

Useful Concepts for Decline Curve Forecasting, Reserve Estimation, and Analysis

M.J. Fetkovich, E.J. Fetkovich, and M.D. Fetkovich, Phillips Petroleum Co.

SPE Members

This paper was prepared for presentation at the SPE 69th Annual Technical Conference and Exhibition held in New Orleans, LA, U.S.A., 25-28 September 1994.

Abstract

The fundamental bases for the rate-time and rate-cumulative production equations are given in this paper. The paper defines the decline curve variables, b, D_i, and q_i, in terms of simple reservoir engineering concepts and reservoir drive or recovery mechanisms. Guidelines are given as to what decline exponent, b, should be used for various types of gas and oil reservoirs. Reasonable values of D_i and q_i can also be estimated, even when very little or no production data are available.

Other topics covered are when and how rate-time data should be normalized using flowing pressures or number of wells; when and how rate-time data should be reinitialized for log-log type curve analysis, smoothing production data; and how to treat changes in skin due to stimulation or restimulation. The evaluation and limitation of calculated reservoir variables are discussed along with the effect of tubing restricted flow on rate-time decline data.

Guidelines and fundamental concepts are depicted on a few simple charts that the reservoir engineer can use to help make more accurate forecasts and reserve determinations using rate-time decline curve approaches. (Full size figures are available on request.)

Introduction

Decline Curve Analysis, based on the Arps[1] equations, has always been considered to be purely empirical with no basis on physical laws governing the flow of oil and gas through the formation. The works of Fetkovich[2-11] and others[12-30] have attempted to place decline curve analysis on a sound, fundamental basis utilizing the constant wellbore pressure analytical solution and simple combinations of material balance equations and pseudosteady-state rate equations to derive rate-time decline equations for oil and gas wells. The derivations illustrate under what circumstances specific values of the hyperbolic decline exponent, b, should result. It is from these derivations that the variables in Arps' equations can be expressed in terms of reservoir variables and reservoir engineering concepts. Decline curve analysis, or more specifically rate-time analysis, is not simply an art based on applying a purely empirical equation to be analyzed with statistical approaches. Reliance on a statistical analysis, void of reservoir engineering concepts, often leads to unrealistic and unreliable forecasts and reserve estimates.

The purpose of this paper is to give the engineer that is responsible for making forecasts and determining reserves for numerous operated or non-operated wells some guidelines and fundamental concepts to make them quickly and more accurately. This paper is an attempt to assemble, in one place, the more important concepts and observations disseminated in previously published and unpublished papers.

Arps' Equations

Conventional decline curve analysis is based on the empirical equations of Arps.[1] The general rate-time equation, hyperbolic is

$$q(t) = \frac{q_i}{[1 + b D_i t]^{\frac{1}{b}}} \quad (1)$$

For b = 0, the decline is exponential

$$q(t) = \frac{q_i}{e^{D_i t}}, \quad (2)$$

and for b = 1, harmonic

$$q(t) = \frac{q_i}{(1 + D_i t)}. \quad (3)$$

Equations 1 and 2 rearranged to calculate the time, t, it would take to reach a future rate q(t) - normally some abandonment rate, q_a, is for hyperbolic and harmonic

References and illustrations at end of paper.

$$t = \frac{[q_i/q(t)]^b - 1}{bD_i}, \quad (4)$$

and for exponential, b = 0

$$t = \frac{\ln [q_i/q(t)]}{D_i}. \quad (5)$$

Cumulative Production Equations

The hyperbolic cumulative production-time equation is

$$Q_p = \frac{q_i}{(1-b)D_i}\left[1 - (1 + bD_i t)^{\frac{b-1}{b}}\right], \quad (6)$$

where Q_p is being used to represent either oil or gas cumulative production, N_p or G_p. For b = 1, harmonic decline

$$Q_p = \frac{q_i}{D_i}[\ln(1 + D_i t)], \quad (7)$$

and exponential, b = 0

$$Q_p = \frac{q_i}{D_i}(1 - e^{-D_i t}). \quad (8)$$

The rate-cumulative production equations are for the hyperbolic form

$$Q_p = \frac{q_i^b}{(1-b)D_i}\left[q_i^{1-b} - q(t)^{1-b}\right]. \quad (9)$$

At q(t) = 0, the equation reduces to and defines D_i

$$D_i = \frac{1}{(1-b)}\left(\frac{q_i}{Q_{puo}}\right), \quad (10)$$

where Q_{puo} is the ultimate recoverable reserves to q(t) = 0 flowing against some constant wellbore flowing pressure, p_{wf}.

The exponential form, b = 0, is

$$Q_p = \frac{q_i - q(t)}{D_i}, \quad (11)$$

which for q(t) = 0 reduces to and defines the exponential decline D_i

$$D_i = \frac{q_i}{Q_{puo}}. \quad (12)$$

The harmonic form, b = 1, is

$$Q_p = \frac{q_i}{D_i}\ln\left(\frac{q_i}{q(t)}\right), \quad (13)$$

where when q(t) = 0, Q_p is infinite and D_i is not definable.

$$D_i = \left(\frac{q_i}{N_{po}}\right)\ln\left(\frac{q_i}{q(t)}\right). \quad (14)$$

As will be pointed out later, the pure harmonic form is not derivable for any realistic reservoir systems. The use of the harmonic equation to forecast production and remaining recoverable reserves is not recommended.

An analysis of some 149 oil fields' production data, assembled by Cutler - 1924 and analyzed by Arps -1945, for the distribution of b found that the range of the exponent, b, was between 0 and 0.7 with 90 percent having b less than 0.5. No harmonic declines were found and less than 15 percent had a b value less than 0.1. The rapid development and virtual wide-open production of many of these oil fields resulted in the ideal situation for constant wellbore pressure production over their entire life.

Although the original Arps exponential and hyperbolic equations were developed empirically on the basis of oil production data, Arps' forms of equations can be rigorously derived for volumetric dry gas systems that permit a physical basis to be placed on each of the variables, q_i, q(t), b, and D_i.

Exponential Decline (Derived)

The single phase liquid, exponential decline equation, valid for undersaturated oil or water flow, has been derived in Refs. 2 and 3. The derivation is based on a simple material balance equation and pseudosteady-state or stabilized backpressure curve equation. Both equations are depicted graphically in Fig. 1. The use of this approach has also been used in Ref 3 to derive the Arps form of equations for single phase gas and solution gas drive volumetric systems.

The complete form of the derived exponential equation for constant wellbore pressure production is

$$q(t) = \frac{q_i}{e^{\left[\frac{D_i}{\left(1 - \frac{p_{wf}}{\bar{p}_R}\right)}\right]t}}, \quad (15)$$

where

$$D_i(p_{wf}) = \frac{q_i/N_{puo}}{\left[1 - \frac{p_{wf}}{\bar{p}_R}\right]}. \quad (16)$$

Both q_i and N_{puo} are a function of the constant pressure, p_{wf}. For $p_{wf} = 0$

$$D_i = \frac{q_{i\,max}}{N_{puo,o}}, \quad (17)$$

where $N_{puo,o}$ is the ultimate recoverable to q(t) = 0 and $p_{wf} = 0$.

Note that different levels of constant wellbore pressures, p_{wf}, always result in an exponential decline and D_i is the same for all levels of backpressure. (This is not the case for derived forms of the hyperbolic equation.) The goal of any prudent operator to maximize production and recoverable reserves and to minimize drainage of reserves to offset wells is to maintain the flowing pressure, p_{wf}, as close to 0 as is economically possible. Therefore, $p_{wf} \approx 0$ was the basis for deriving hyperbolic forms of decline equations which turn out to be very useful for understanding some important concepts of decline curve analysis.

Some Basic Concepts

Figure 1 depicts in a graphical form the ($\bar{p}_R$-p_{wf}), pseudosteady-state rate equation, and the $\bar{p}_R$-N_p, material balance equation, from which the exponential decline equation was derived. The drawdown backpressure curve is also a depletion curve in that all flow rates q(t), including q_i, will trace down the curve as the reservoir pressure, $\bar{p}_R$, declines as a result of production. The backpressure curve is fixed, J_o is constant, for all stages of pressure depletion providing there are no skin changes or the drainage radius, r_e, does not change. In equation form, the pseudosteady-state backpressure equation is

$$q(t) = \frac{kh\,(\bar{p}_R(t) - p_{wf})}{141.2\,\mu B\left[\ln\left(\frac{r_e}{r_w}\right) - \frac{3}{4} + s\right]}, \quad (18)$$

or in its simplest form

$$q(t) = J_o(\bar{p}_{R(t)} - p_{wf})^{1.0}. \quad (19)$$

For a total field or lease backpressure curve, we would have

$$q_T(t) = W\,J_{oavg}\,(\bar{p}_R - p_{wf}), \quad (20)$$

where W is the total number of wells and J_{oavg} represents our average well PI. Or we could sum the individual wells to obtain a total field or lease composite backpressure curve.

$$q_T(t) = \sum_{j=1}^{W} J_{oj}\,(\bar{p}_R - p_{wf}). \quad (21)$$

The material balance equation, graphically depicted in Fig. 1, relates the cumulative production, N_p, to the reservoir pressure, $\bar{p}_R$, is

$$\bar{p}_R = -\left(\frac{\bar{p}_{Ri}}{N_{puo}}\right)N_p + \bar{p}_{Ri}. \quad (22)$$

A basic assumption again is that r_e does not change, i.e., the well (or lease) is neither draining nor being drained by offset wells. For a total field, the reservoir volume, or r_e, always remains fixed.

An important reservoir engineering concept useful for interpreting decline performance and understanding and applying decline curve analysis is that each well in a common reservoir undergoing pseudosteady state depletion drains a volume in proportion to its producing rate. From this we can point out a couple of important concepts that result.

- The decline rate, D_i or q_i/N_{puo}, theoretically should be the same for all wells in the common reservoir. Wells that have a noticeably different D_i are not in communication.
- When a new well(s) is added (drilled) or an old well(s) is restimulated in a common reservoir, the decline rate, D_i, will increase for each well. The depletion of the total field will be essentially accelerated. All other wells will lose some of their remaining reserves.

Gas Well Decline Equations (Derived)

Most of the fundamental reservoir engineering concepts and definitions of the terms in the Arps equations, q_i, q(t), b, and D_i can be made from the derivation of the single phase gas equations.

Derivation of the gas well decline equations is completely analogous to that previously used to derive the single phase liquid exponential decline. The rate decline q(t) with time for a single phase, single layer, gas flow system, as in the single phase liquid solution, is based entirely on reservoir pressure depletion of a closed finite system. For single phase gas, we use the pseudosteady state or stabilized backpressure equation and material balance equation, as depicted graphically in Fig. 1. The derived rate-time equation for a gas well producing against a constant pressure, p_{wf}, is for all backpressure curve exponents $n > 0.5$ a hyperbolic

$$q(t) = \frac{q_i}{\left[1 + (2n-1)\left(\frac{q_i}{G}\right)t\right]^{\frac{2n}{2n-1}}}, \quad (23)$$

and an exponential for the backpressure curve exponent $n = 0.5$.

$$q(t) = \frac{q_i}{e^{\left(\frac{q_i}{G}\right)t}}. \quad (24)$$

With the derivations based on $p_{wf} = 0$, $q_i = q_{imax}$, and $G = G_i$, where q_{imax} is the stabilized absolute open-flow potential and G_i is the original gas-in-place. At backpressures other than $p_{wf} = 0$, q_i is a rate from the stabilized backpressure curve at the specified flowing pressure, p_{wf}. G is the recoverable gas to an abandonment pressure equal to p_{wf}, where G is equal to the original gas-in-place times a recovery factor.

$$G = G_i\,(R.F.), \quad (25)$$

where

$$R.F. = \left(1 - \frac{p_{wf}}{\bar{p}_R}\right). \quad (26)$$

These same type definitions involving in-place volume and recovery factor are also used for single phase and multi-phase oil systems, i.e., q_i and N_{puo}.

Note that the basic form of the gas well decline equations, 23 and 24, are identical to that of the Arps form of equations, Eqs. 1 and 2. They exactly reproduce or overlay the Arps type curve over its entire length. D_i expressed in more familiar and readily available reservoir engineering terms is for both the hyperbolic and exponential forms

$$D_i = 2n\left(\frac{q_i}{G}\right). \quad (27)$$

All the terms in Eq. 27 can be calculated or estimated from initial multipoint, pressure transient analysis results and geological data before any rate decline data is even available. Or in the case of a replacement well or offset location to be drilled, values from offset wells can be used.

With regard to q_i, q_i is a rate from the stabilized wellhead or the bottomhole backpressure curve. If tubular friction is not significant, the bottomhole and wellhead curves will be essentially the same except for a hydrostatic head term. q_i is not simply a producing rate at early time – q_i is very specifically a pseudosteady-state rate at the surface. It can be substantially less than actual early time transient flow rates as would be produced from low permeability wells with large negative skins.

The Arps decline exponent, b, can be expressed in terms of the backpressure curve exponent, n, for wells producing at very low flowing pressure

$$b = \frac{2n-1}{2n}. \quad (28)$$

The exponent n from a gas well backpressure performance curve can therefore be used to calculate or estimate b and D_i. Using Eq. 28, we can determine the physical limits of b over the accepted theoretical range of the backpressure curve exponent, n, which is between 0.5 and 1 for a single layer homogeneous system.

Backpressure Exponent n	Decline Exponent b
.50 High k	0
.56	.1
.62	.2
.71	.3
.83	.4
1.0 Low k	.5

:e harmonic decline exponent, b = 1, cannot be obtained. In fact, no other /estigators have been able to derive an exponent b greater than 0.5 for any isonable single-layer, homogeneous reservoir system or drive mechanism. ps' study of the range of the exponent b for 149 oil fields also tends to pport the 0.5 value as a physical upper limit of b. He found that 90% of : oil fields studied had b values less than 0.5.

: will be discussed later, a layered no-crossflow reservoir system, or its uivalent, can result in decline exponents that cover the range of b between ; and 1 − values of b greater than 0.5 can be used to identify layered no-ossflow reservoirs. In Arps' distribution study he found no value of b :ater than 0.7. It should also be pointed out that attempting to fit all or me of the "transient" production rate data of a well with the Arps eudosteady- state equation will result in an "apparent" b value higher than really is. In some cases, it will even be greater than 1.

imulative Production Equations

ie cumulative production-time equation is for n > 0.5, the hyperbolic form

$$\frac{G_p}{G} = 1 - \left[1 + (2n-1)\left(\frac{q_i}{G}\right)t\right]^{\frac{1}{(1-2n)}}, \quad (29)$$

d for n = 0.5, the exponential form

$$\frac{G_p}{G} = 1 - e^{-\left(\frac{q_i}{G}\right)t}, \quad (30)$$

th of which can be readily reduced to the cumulative production-time uations 6 and 8 and then the rate-cumulative production equations 9 and

ite-Cumulative Production Equations (Derived)

ie rate-cumulative production equations for single phase liquid and gas can directly derived from the backpressure curve and material balance uations (see Fig. 1). From the backpressure curve equation at $\bar{p}_{Ri}$ and $\bar{p}_{R(t)}$ iere

$$C_{gi} = C_g(t) = \frac{q}{(\bar{p}_R^2)^n}, \quad (31)$$

:n

$$\frac{q(t)}{q_i} = \left[\frac{\bar{p}_{R(t)}}{\bar{p}_{Ri}}\right]^{2n}. \quad (32)$$

om the material balance equation slope

$$\frac{\bar{p}_{Ri}}{G_i} = \frac{\bar{p}_{R(t)}}{G_i - G_{p(t)}}, \quad (33)$$

$$\frac{\bar{p}_{R(t)}}{\bar{p}_{Ri}} = \frac{G_i - G_{p(t)}}{G_i}. \quad (34)$$

bstituting 34 into 32 and simplifying, we get

$$\frac{q(t)}{q_i} = \left[1 - \frac{G_{p(t)}}{G_i}\right]^{2n}. \quad (35)$$

r n = 0.5 or exponential decline, b = 0

$$q(t) = q_i - \left(\frac{q_i}{G_i}\right)G_{p(t)}. \quad (36)$$

The Arps hyperbolic rate-cumulative production equation 9 converted to our nomenclature with q(t) = 0 is

$$G_p = \frac{q_i^b}{(1-b)D_i}\left[q_i^{(1-b)}\right]. \quad (37)$$

Using the gas relationship $b = \frac{2n-1}{2n}$ and $D_i = 2n\left(\frac{q_i}{G}\right)$ Equation 37 reduces to

$$\frac{q(t)}{q_i} = \left[1 - \frac{G_{p(t)}}{G}\right]^{2n}, \quad (38)$$

which is identical to Equation 35. A similar approach was used for the single phase liquid and solution gas drive decline equations with similar results.

Since both the rate-time and rate-cumulative equations are derived using the same backpressure and material balance equations, both methods of analyzing production data should get identical results.

Backpressure Curve Exponent (n)

Because gas and oil are sold at the wellhead, we must consider the affect that the tubing string has on production for flowing gas and oil wells. It is the exponent, n, of the wellhead backpressure curve that affects the decline exponent, b. Examination of field performance backpressure curves[7] indicates that low permeability gas wells yield bottomhole backpressure curves with n values more nearly approaching 1.0 while high permeability gas wells yield n values approaching 0.5.

The Forchheimer form of the backpressure equation is

$$\bar{p}_R^2 - p_{wf}^2 = Aq + Bq^2, \quad (39)$$

where A is a laminar flow pressure drop term and B is a turbulent flow pressure drop term. When kh is large, the Aq term becomes small and we have

$$q = \frac{1}{\sqrt{B}}(\bar{p}_R^2 - p_{wf}^2)^{0.5}. \quad (40)$$

Similarly, when kh is small Aq becomes large with the Bq^2 term becoming negligible when compared to the laminar pressure drop term. We would then have

$$q = \frac{1}{A}(\bar{p}_R^2 - p_{wf}^2)^{1.0}. \quad (41)$$

Expressing the flow equation at a surface or wellhead datum and including a pressure drop term for the tubing or flow string, we have

$$p_c^2 - p_t^2 = A_{WH}q + (B_{WH} + T_{WH})q^2, \quad (42)$$

where T_{WH} represents a friction pressure drop term for flow through the tubing and is indistinguishable from the reservoir turbulent pressure drop component (B_{WH}) at the surface datum. Equation 42 is more useful for performance monitoring when expressed as the wellhead backpressure curve

$$q = C_{WH}(p_c^2 - p_t^2)^n, \quad (43)$$

where the range of n is between 0.5 and 1.

It should be recognized that a storm choke, flowline, and other surface equipment can be included in Eqs. 42 and 43, even further driving the value of n to 0.5 in high capacity flowing gas and oil wells. Note that as a limiting

condition in Eq. 42 if T_{WH} is large compared to A_{WH} and B_{WH}, a very large bottomhole deliverability well with a relatively small diameter tubing string, Equation 42 reduces to

$$q = T_{WH}(p_c^2 - p_t^2)^{0.5}. \quad (44)$$

When the exponent (n) of the wellhead backpressure curve approaches 0.5, the well is considered to be "tubing limited" and will always exhibit exponential rate-time decline. Once tubing limited "always tubing limited" - the backpressure performance curve does not shift to the right as reservoir pressure, $\bar{p}_R$ declines. The wellhead backpressure curve based on 25+ years of performance data presented in Fig. 2 has an exponent n = 0.55. The effect of a tubing changeout, $2\frac{7}{8}$" to 3½", is shown both on the backpressure curve and the semi-log production plot. A 50% increase in production was achieved by simply increasing the tubing diameter. Yet the well is still "tubing limited". (Well depth and casing programs often dictate a maximum tubing size.) Note that the log-log production plot initialized after the tubing changeout to a larger diameter fits a decline exponent, b = 0.1, stem of the type curve. The decline exponent is exactly what would be predicted by using Eq. 28 and simply knowing that the backpressure curve exponent is 0.55.

This example illustrates that the wellhead deliverability curve and exponent n could, in some instances, be totally described by the pressure drop through the tubing string. We could use Eq. 44 to establish for a given tubing size a maximum position for a wellhead curve, its wellhead potential q_{imax} or q_i, exponent n = 0.5 and it will exhibit exponential decline, b = 0. For any other diameter flow string, one need only ratio ($D^{2.612}$new/$D^{2.612}$present) x T_{WH} to draw in its new wellhead deliverability curve. Using 3.476 and 2.992 inches ID for the tubing sizes in Fig. 2 we get a curve shift 1.5 x T_{wh} that reproduces the actual results obtained, i.e., a 50% increase in production.

When a well is tubing limited, n → 0.5, it should be recognized that a significant deterioration in the bottomhole performance curve will not be reflected in any change in the wellhead backpressure performance curve. Conversely, any improvement in the bottomhole performance curve, such as a stimulation or restimulation, will not result in any increase in surface production, i.e., there will be no change in the wellhead deliverability curve and no increase in production. Clearly, one will not be able to calculate reservoir variables from rate-time analysis on tubing limited gas or oil wells since most of the pressure drop in the well is tubing friction pressure drop.

Backpressure Effects on b

The level of backpressure, p_{wf}, does not affect b for single phase liquid flow, it's always exponential, i.e., b = 0. The effect of backpressure on a gas well is demonstrated for a backpressure curve exponent n = 1 in Fig. 9 given in Ref. 3. Backpressure is expressed as a ratio of $p_{wf}/\bar{p}_{Ri}$, where p_{wf} is the constant pressure against which the rate declines with time and can also be considered as an abandonment pressure, p_{wfa}. The rate-time type curve for a backpressure ratio, $p_{wf}/\bar{p}_{Ri}$ = 0 has a decline exponent b value of 0.5 and would yield a recovery factor $[1-p_{wf}/\bar{p}_{Ri}]$ of 100%. At a backpressure ratio of $p_{wf}/\bar{p}_{Ri}$ = 0.9, where $p_{wf} \rightarrow \bar{p}_{Ri}$, the rate-time type curve exhibits exponential decline, b = 0, and would yield a recovery factor $[1-p_{wf}/\bar{p}_{Ri}]$ of only 10%. Backpressure ratios shown on the figure yielding 20% and 50% recoveries will not trace any of the Arps type curve stems over its entirety – they cut across several of the b stems. From a practical standpoint, no operator would produce a well that is on decline at such high backpressure to abandonment. A more realistic ultimate backpressure ratio limit, $p_{wf}/\bar{p}_{Ri}$, for volumetric gas wells in particular, would be 0.1. This would yield a maximum recovery factor of 90% and result in a decline exponent b = 0.4. The b value of 0.4 should be considered as a good limiting value for gas wells when not clearly defined by actual production data.

Solution Gas Decline Equations (Derived)

As presented and discussed in Ref. 3, the material balance and rate equations used to derive rate-time equations for solution gas drive oil wells are

$$\bar{p}_R^2 = -\left(\frac{\bar{p}_{Ri}^2}{N_{puo}}\right) N_p + \bar{p}_{Ri}^2, \quad (45)$$

and

$$q_o = J'_{oi}\left(\frac{\bar{p}_R}{\bar{p}_{Ri}}\right)(\bar{p}_r^2 - p_{wf}^2)^n. \quad (46)$$

The ratio $(\bar{p}_R/\bar{p}_{Ri})$ is used in the rate equation to approximate the decrease in relative permeability, k_{ro}, with pressure depletion. The reader is referred to Ref. 6, Table 9 and Fig. 25 where the work of Levine and Pratts and Vogel were used to justify the pressure ratio approximation to the k_{ro} change in equation 46.

The derived rate-time equation for an oil well producing against a constant pressure, p_{wf}, is for all backpressure curve exponents n > 0.5, hyperbolic.

$$q(t) = \frac{q_i}{\left[1 + \frac{(2n-1)}{2}\left(\frac{q_i}{N_{puo}}\right)t\right]^{\frac{2n+1}{2n-1}}}, \quad (47)$$

and exponential for n = 0.5

$$q(t) = \frac{q_i}{e^{-\left(\frac{q_i}{N_{puo}}\right)t}}. \quad (48)$$

High capacity, flowing oil wells that are "tubing limited", friction pressure drop dominated will tend to exhibit exponential decline, as is the case for tubing limited gas wells.

With the derivations based on p_{wf} = 0, $q_i = q_{i\,max}$. At backpressures other than p_{wf} = 0, q_i is a rate from the stabilized backpressure curve at the specified flowing pressure, p_{wf}. N_{puo} is equal to the original oil-in-place times a recovery factor

$$N_{puo} = N \times R.F. \quad (49)$$

where the recovery factor may be obtained from correlations, historical performance, or Tarner type material balance forecasts at some selected gas-oil relative permeability curve.

D_i, in terms of reservoir engineering terms, is for both the hyperbolic and exponential forms

$$D_i = \frac{2n+1}{2}\left(\frac{q_i}{N_{puo}}\right). \quad (50)$$

The Arps decline exponent, b, can be expressed by the backpressure curve exponent, n, for wells producing at very low flowing pressures

$$b = \frac{2n-1}{2n+1}. \quad (51)$$

For n = 1, the value that one would assume in the absence of an actual multipoint test having been run on any well in the field, b would be equal to 0.33. A slope n = 1 should be considered as being typical for most solution gas drive reservoirs and also would be equivalent to assuming the Vogel IPR relationship. With n = 1,

$$D_i = 3/2\,(q_i/N_{puo}). \quad (52)$$

In the absence of a clearly defined decline exponent from field data, a value of b = 0.3 should be assumed for a solution gas drive reservoir, i.e., n = 1 in Eq. 51. However, indication of an unfavorable relative permeability, k_g/k_o, relationship would dictate a decline exponent approaching exponential decline, b = 0, because of the anticipated lower recovery factor (see Fig. 3).

Recovery or Drive Mechanisms and "b"

In many instances, rate-time data existing in the depletion period is of such poor quality or limited extent that a unique value of b cannot be determined. Reliance on a statistical analysis, void of reservoir engineering concepts, to determine the decline exponent often leads to unrealistic or illogical values of b and unreliable or indefensible forecasts and reserves estimates.

From basic reservoir engineering principles, several of the expected values of b have been derived for different reservoir drive or recovery mechanisms. These values should be used when production data is poor, insufficient, or totally lacking. They can also be used to support or confirm clearly defined values of b determined from good quality production data.

Following is a tabulation of the values of b that should be expected for homogeneous single layer or layered crossflow systems (see Fig. 4). The range of the expected b values for these systems is from 0 to 0.5.

b = undeterminable

- Constant rate or increasing rate production period.
- Flow rates are all in the transient or infinite-acting period with no supplemental engineering or geological information.

b = 0, exponential

- Single phase liquid (highly undersaturated oil wells).
- High pressure gas.
- Low pressure gas with wellhead backpressure curve exponent n = 0.5 (tubing limited wells, both gas and oil flowing wells).
- Depletion or solution gas drive with unfavorable k_g/k_o.
- Poor waterflood performance.
- Wells with a high backpressure, $p_{wf}/\bar{p}_R \rightarrow 1$. Gas wells undergoing liquid loading.
- Gravity drainage with no free surface (Derived value).

b = 0.3

Typical for solution gas drive (a Derived value).

b = 0.4 to 0.5

Typical for gas wells (Derived values).
b = 0.5 for $p_{wf} = 0$; b = 0.4 for $p_{wf} = 0.1\ \bar{p}_{Ri}$.

b = 0.5

- Gravity drainage with a free surface (Derived value).
- Full water drive in oil reservoirs (field data observations).

An unpublished study conducted several years ago on West Texas fields being waterflooded found values of b ranging from exponential, b = 0, to b = 0.9 or nearly harmonic. The decline exponent, b, was essentially the same for different leases within a given "field" but different fields had different values of b.

Figure 3 is an attempt to illustrate the concept that the decline exponent "b" is a reflection of recovery efficiency or drive mechanism. The pressure-percent recovery figure, after Cole,[31] depicts typical values of percentage recoveries (recovery efficiency) for various reservoir drive mechanisms from the least efficient, totally undersaturated reservoir with a b = 0, to a much more efficient gravity drainage or water drive recovery mechanism with a b = 0.5. Different drive mechanisms and typical recoveries are also depicted in between.

Also shown on this figure is a corresponding rate-time decline type curve consisting of a transient period followed by depletion stems ranging from b = 0 to 0.5. Note that as b increases, the percent recovery increases. (These same recovery values are also depicted on the Cole pressure - % recovery plot.) With the transient or infinite-acting production period fixed, it requires a larger value of b, or better recovery efficiency mechanism, to get a larger area under the rate-time curve to achieve higher fraction recoveries. Before the outermost boundary is encountered, the transient period would be the same regardless of what later drive mechanism is established once a depletion process begins.

Layered, No-Crossflow Decline Behavior

Most reservoirs consist of several layers with reservoir properties varying between layers. The fact that no-crossflow reservoirs are perhaps the most prevalent and important, reservoir heterogeneity is of considerable significance in long-term forecasting and reserve estimates. If crossflow exists in a layered reservoir, adjacent layers can simply be combined into a single equivalent layer using the average reservoir properties of the crossflowing layers. It will then perform as an equivalent homogeneous single layer system. For a homogeneous single layer system, the maximum value of b is 0.5. Decline curve exponents, b, ranging between 0.5 and 1 are a predicted response for layered, no-crossflow reservoirs[10] and can therefore be used to identify them. We have found that layered, no-crossflow reservoirs have the greatest potential for increasing current production and recoverable reserves.

Low permeability, stimulated wells' production performance can appear similar to layered, no-crossflow reservoir responses on a semi-log production curve. However, a log-log type curve plot can be used to distinguish between the two. Further confirmation of no-crossflow can be made by measuring layer pressures and having some idea of the well's permeability level.

For two or more layers producing against a common flowing pressure, p_{wf}, the commingled production rate, q_T, is simply the sum of separate producing rates or forecasts from each of the individual layers. Producing at a constant wellbore pressure, production from each layer is independent of all the other layers present.

$$q_{TOTAL} = q_1 + q_2 + \cdots + q_n. \tag{53}$$

For a two layered system, or its equivalent (most multi-layered systems can be reduced to an equivalent of two layers by combining layers with similar (q/G) or (q/N_{puo} values), we can write

$$q_T = \frac{q_{i1}}{[1+b_1 D_{i1} t]^{1/b_1}} + \frac{q_{i2}}{[1+b_2 D_{i2} t]^{1/b_2}}, \tag{54}$$

or

$$q_T = \frac{q_{i1}}{e^{D_{i1} t}} + \frac{q_{i2}}{e^{D_{i2} t}}, \tag{55}$$

or even

$$q_T = \frac{q_{i1}}{[1+b_1 D_{i1} t]^{1/b_1}} + \frac{q_{i2}}{e^{D_{i2} t}}, \tag{56}$$

where D_i is defined by Eqs. 10 and 12 and layer 1 normally represents the higher deliverability layer.

The sum of two or more separate forecasts usually results in a forecast with the decline exponent, b, greater than that of each individual layer. We have, for a commingled system using single phase gas variables, for example

$$q_{TOTAL} = \frac{q_{iT}}{\left[1 + \frac{b_T}{(1-b_T)}\left(\frac{q_{iT}}{G_T}\right)t\right]^{1/b_T}}. \quad (57)$$

where q_{iT} is the sum of each layer's flow rates, q_i, and G_T is the total ultimate recoverable gas in each layer. The exponent b_T is the single value of b that results in the best match, or fit, of the commingled production rates, excluding late-time commingled production rates when necessary. Very late time production rates will ultimately result in the b value of layer 2 producing by itself. Use of the early to middle time production data permits reasonable calculated values of q_{iT} and G_T from actual production performance data.

Table 1 contains predicted values of the decline exponent, b, for a two-layer system as a function of (q_i/G) ratio vs. volume ratio, V_R or G_R, for single phase gas and (q_i/N_{puo}) ratio versus volume ratio, V_R or $[N_{puo}]_R$, for single phase liquid. The high deliverability layer is normally the numerator in both ratios. It is important to recognize that the q_i for the high deliverability layer is not just a reflection of layer permeability, k, but also of layer skin, s, and layer shut-in pressure, $\bar{p}_R$. With regard to layer volume, V or (G or N_{puo}), the pore volume ratio, V_R, will essentially remain constant for all producing times, whereas the gas-in-place ratio, G_R or $[N_{puo}]_R$, changes with time due to differential pressure depletion. This becomes significant when we consider a constant rate production period followed by a declining production rate period, i.e., the volume ratio, G_R, will be different at the beginning and end of the constant rate period.

From Table 1, we see that the highest b values listed are for (q_i/G or q_i/N_{puo}) ratios between 10 and 15.5 (see Ref. 10 for the results of larger ratios). Further, for any given (q_i/G or q_i/N_{puo}) ratio, b increases as the volume ratio decreases.

The $(q_i/G)_R$ ratio is written as

$$(q_i/G)_R = \frac{q_{i1}/G_1}{q_{i2}/G_2}, \quad (58)$$

where layer 1 is generally the higher deliverability layer. Assuming, for simplicity, that $p_{i1} = p_{i2}$ and (μc_i) are equal for both layers and substituting reservoir variables, we have

$$(q_i/G)_R = \frac{k_1/\phi_1}{k_2/\phi_2} \frac{\left[\ln\left(\frac{.472\, r_{e2}}{r_w}\right) + s_2\right]}{\left[\ln\left(\frac{.472\, r_{e1}}{r_w}\right) + s_1\right]} \cdot \frac{r_{e2}^2}{r_{e1}^2}. \quad (59)$$

With a (q_i/G) ratio of 10, one normally assumes that this would represent a layered, no-crossflow system with a 10 to 1 contrast in permeability. From Eq. 59, this would be true if $\phi_1 = \phi_2$, $r_{e1} = r_{e2}$, and $s_1 = s_2$. Note that thickness, h, has cancelled from the equation. However, if layer k_s, ϕ_s, and r_{es} are all equal, we would still have a (q_i/G) ratio of 10 for the following skin conditions on each layer.

s_1	s_2
-7	0
0	+72
-7.6	- 4
-2.2	+50

Some small contrast in permeability would lead to even more reasonable values of skin on each layer to still maintain the 10 ratio and the resulting high decline exponents, b, reflected in the table. For all reservoir variables of each layer being equal, including skins, s, an r_{e1} = 630 ft and r_{e2} = 2000 ft would also result in a ratio = 10. One need not have a high contrast in permeability to have significant layered, no-crossflow reservoir production performance behavior that exhibits high values of the decline exponent, b.

In a layered, no-crossflow system, the maximum recoverable reserves from the low deliverability layer will occur as $(q_i/G)_R$ approaches 1. We, therefore, must have as large a negative skin, s_2, on the low permeability layer(s) as possible and as early in the production life as possible. On commingled wellbore systems, even with attempts at diversion, the stimulation seems to preferentially occur in the higher permeability layer(s). This preferential stimulation of the high permeability layer(s) will most likely occur in open hole completions that have been acidized commingled. By restimulating wells with the objective of targeting the low permeability layers, substantial increases in production and recoverable reserves can be achieved. This potential can normally be identified through high decline exponents, b. Note from Table 1 that the higher the b value, the more volume in the low permeability layer and therefore the more potential for increased production and recoverable reserves. With a single layered system, exhibiting a low b value, restimulation generally results in accelerated production. With a layered, no-crossflow system exhibiting a high b value restimulation can result in substantial increased recoverable reserves, depending on the volume of the low permeability layer(s). The (hydraulically) fractured well example given in Ref. 3 had a b of between 0.6 and 1 to fit both the before and after stimulation data. The rather successful treatment reflected in both the increase in production and additional recoverable reserves is an example of what one could expect from a proper restimulation of a layered, no-crossflow well.

Following is a list of some of the more important characteristics of layered, no-crossflow behavior:

- High value of the decline exponent, b; b > 0.5.
  This is reflected as an early rapid decline in rate followed by an extended period of a low percentage decline.
- Reservoir has an indicated unusually long producing life.
- Unusually rapid decline in reservoir shut-in pressure. Later, a nearly constant measured shut-in pressure with cumulative production. (This is because the pressures usually represent the most permeable layer, but production is coming from the low permeability layer(s).)
- Large discrepancy between pressure performance oil or gas-in-place and volumetrics. (Indicated low recovery factor.)
- Thick reservoirs have a very high likelihood of exhibiting layered, no-crossflow behavior. (There appears to be a strong correlation of increasing b with thickness.)
  Thin reservoirs don't automatically mean they will behave as a single layer. (We have measured differential depletion in a nine-foot sand.)
- Naturally fractured reservoirs permit a contrast in $(q_i/G)_R$ required for layered, no-crossflow behavior, i.e., high b values as seen in the Monterey formation.
- Layer pressures indicating differential depletion.
- Production logs indicating wellbore backflow during shut-ins or rate reductions. Lack of backflow does not mean lack of layered, no-crossflow behavior.

The reader is referred to Ref. 10 for additional material on layered, no-crossflow reservoir behavior.

We recognize the similarity of rate-time and pressure cumulative production and a few of the other listed characteristics are similar to that of a composite reservoir model; however, we find it to be an unrealistic model on an individual well basis. It is a possible model on a fault block or a field-wide basis. The question of which it may be is readily resolved by the taking of layer pressures and comparing pressure data on an areal basis.

Production Data Treatments

Production data from a commercial data base is usually available on a monthly production basis, with the production sometimes being erratic and difficult to analyze. We have found that 6-month or 12-month averaging, with the average rate $q_{avg}(t)$ plotted at the midpoint of the time period, works very satisfactorily (see Ref. 4, Figs. 20 and 21 for examples). No material is either created or destroyed this way, as can be done with purely mathematical smoothing approaches. Further, this averaging is nearly equivalent to cumulative production-time plots that are often made to make the same erratic rate-time data "look" better. A derivative at the mid-point of the year would result then in rate-time data for a rate-time plot. It is much easier to relate rate-time data to one's experience, particularly transient behavior, than it is cumulative production time plots.

Transient production data, however, result in the opposite recommendation. Average monthly production on low permeability, highly stimulated wells or fields will not reveal some useful data (see Ref. 4, Figs. 32 and 33). We have had extremely good success utilizing daily production from meter charts on individual wells in the Carthage Cotton Valley field. Figure 5 is an example of daily production rates, taken exclusively from meter charts, on a Cotton Valley well. No special testing was involved. The well was produced at a fixed choke setting. The small dots on the figure are daily production rates, and the large, open circles are average monthly production rates reported by a commercial data base. The daily rate data are an order of magnitude more revealing than the monthly production data. Some observations that can be made are:

- After a year's production, the well is still in transient flow.
- The upward transient spikes after shut ins, flush production, reveal that the well is low permeability and successfully stimulated. The downward spikes are real and are a result of an increase in backpressure.
- All four transient spikes reinitialized in time can be used to confirm the location on the log-log plot of the initial transient flow data for type curve analysis (see Ref. 4, Fig. 34).
- None of the data should be analyzed using Arps' equations. If Arps' equation was used, a $b > 1$ will be obtained, resulting in invalid forecasts and reserve estimates.
- kh, skin, s, F_{CD} and radius of investigation, $r_e(t)$, can be calculated from type curve matching this data. Pore volume or gas-in-place cannot be determined since no depletion data are evident.

Normalization

Another important technique we use in rate-time analysis for low permeability stimulated wells is rate normalization, i.e., $q(t)/(p_i-p_{wf}(t))$. Often, during transient production, both the rate q(t) and flowing pressure, $p_{wf}(t)$ are both declining smoothly and monotonically. Normalizing the rate by dividing by $(p_i-p_{wf}(t))$, is identically equivalent to rigorous superposition and will permit the normalized data to overlay the q_D-t_D type curves. Extrapolation of the fit into the future by tracing along the type curve results in a rate-time forecast as if the well were being produced at the last value of p_{wf}. Production rates at a different backpressure, p_{wf}, would then require a superposition calculation.

Abrupt changes in flowing pressure, p_{wf}, normally a reduction in p_{wf} to increase production and recoverable reserves, is adequately discussed in References 3, 5, and 29 (Table 2 and Fig. 14), (Table 9 and 9A, and Fig. 9) and pages 438-441, respectively.

Figure 6 illustrates graphically the principal of superposition applied to a single reduction in flowing pressure to p_{wf2}. The same principal applies to an increase in p_{wf2} as would be applicable in attempting to handle the gas bubble curtailment period of the mid-1980's. Instead of the rates in Fig. 6 being additive, one would subtract q_2 and obtain the pressure reduction rate results also seen in Fig. 5. In Fig. 5, the reduced rate effect is even exaggerated for a p_{wf} increase because of the log scale. Note also from Fig. 6 that, at long times, the effect of a p_{wf} change is relatively small compared to the rate from the original flowing pressure extrapolated into the future based on the superposition principal. This should be kept in mind when worrying about the effects of production upsets on long-term forecasting. (See also Figs. 34 and 35 of Ref. 4 for the negligible effect of numerous field shut-ins on the overall total field production.)

One additional normalization procedure that we have used is well count normalization when the well count is increasing smoothly and monotonically as a result of continuous drilling in a field or lease. One of the more noticeable effects we have seen was in the Sooner Trend field between 1970 and 1982. The total field production data matched a decline exponent $b = 1$ during this period of continuous drilling. Normalized by well count to an average well basis, the decline exponent was found to be $b = 0.23$ instead of, $b = 1$ unnormalized.

Reinitialization of Data

There are several obvious situations where rate-time data must be reinitialized because the drive or production mechanism has changed. The most obvious situation is production above and below the bubble point pressure. Above the bubble point production will follow exponential decline, $b = 0$. Further, the calculation of reservoir variables, kh, s, and original oil-in-place, N, will be the period where the calculations will be most accurate. Below the bubble point pressure, the values of the decline exponent, b, and N_{puo}, would change and the value of b will be greater than exponential decline depending on the k_g/k_o relationship. Pressure-cumulative production and gas-oil-ratio performance often help indicate when the reinitialization should be done. Some other conditions where the production data might be reinitialized are:

- Primary, secondary, and tertiary recovery periods would all be reinitialized. The decline exponent, b, however should be similar for each period.
- An abrupt change in the number of wells on a lease or in a field. An infill well on a one-well section, for example, will result in a change in q_{iT}, $(q_{i1} + q_{i2})/G$ as compared to q_{i1}/G before the infill well.
- Restimulation of an original well would be similar, $q_{i\ new}/G$, as compared to $q_{i\ old}/G$.
- Also similar would be a tubing change-out to a larger diameter where the well was tubing limited. Not only would q_i change afterwards, but the decline exponent, b, could also change due to the increase in wellhead backpressure slope, n (see Fig. 2 and Eq. 28).

Finally, anytime during the depletion period, one can reinitialize the problem and get the same resulting forecast. However, there becomes a point where there is not sufficient rate-time data to uniquely match or define the decline exponent, b. Using a different value of b would result in a different forecast and reserve estimate. One of the problems with reinitializing is obtaining a new $\bar{p}_R$ to utilize in attempting to calculate reservoir variables.

Stimulation and Restimulation (Depletion)

The effects of a stimulation or a restimulation, providing a well is not tubing or equipment limited, result in a change in deliverability, q_i, and possibly the remaining recoverable gas or oil, G or N_{puo}. The decline exponent, b, normally can be assumed to remain the same.

For an individual layer, a convenient "rule-of-thumb" equation[29] to approximate an increase in rate due to a stimulation or restimulation is

$$q_{i\,new} = q(t)_{old}\left(\frac{7 + s_{old}}{7 + s_{new}}\right), \qquad (60)$$

where $q(t)_{old}$ is the producing rate just prior to stimulation, and $q_{i\ new}$ is the new q_i for the reinitialized forecast. We would then have

$$q(t)_{new} = \frac{q_{i\,new}}{[1 + b\,D_{i\,new}\,t]^{1/b}}, \quad (61)$$

where b is assumed to be the same for before and after stimulation and

$$D_{i\,new} = \frac{1}{(1-b)}\left(\frac{q_{i\,new}}{G \text{ or } N_{puo\,remaining}}\right). \quad (62)$$

G or N_{puo}, if assumed to be the same as that obtained prior to stimulation, would be simply acceleration, which would be the case if all offsets were stimulated or restimulated at the same time. If offsets were not restimulated, then the remaining reserves would increase in direct proportion to the increase in producing rate as a result of a radius of drainage readjustment, i.e., drainage of offset wells would occur.

For layered, no-crossflow systems, we would assume that the low deliverability layer was not stimulated originally and calculate its increase due to restimulation to q_{i2} with the high deliverability layer, $q_1(t)$, remaining the same. In this case, the increase in reserves would be a result of reducing the amount of differential depletion between layers.

Calculating Reservoir Variables

There are two periods of rate decline, transient decline, then followed by depletion decline. These two periods, and their production response, are illustrated on the log-log type curve of Fig. 7.

Transient Decline

Production data existing during the transient decline period can be matched to a constant wellbore pressure type curve to calculate both kh and skin, s, from the following equations

$$kh = 141.2\mu B\left\{\frac{[q/(p_i - p_{wf})]}{q_D}\right\}_{match}, \quad (63)$$

and

$$r_{wa} = \sqrt{\frac{0.00634\,kh}{(\mu c_t)_i\,\phi h}\left(\frac{t}{t_D}\right)_{match}}, \quad (64)$$

where

$$r_{wa} = r_w e^{-s}, \quad (65)$$

or in terms of skin

$$s = -\ln(r_{wa}/r_w). \quad (66)$$

Equation 63 is written to emphasize the need to normalize the rates q by using flowing pressure, p_{wf}, when necessary. To calculate kh and s from transient data, we also prefer to use the more general radial flow constant wellbore pressure solution type curve in terms of q_D-t_D, Fig. 2-A of Ref.3, with the effective wellbore radius, r_{wa}. This type curve covers a much broader range of q_D-$t_D(r_{wa})$ that applies to most of the very low permeability, successfully stimulated wells. Wells with large, positive skins of any permeability level lose uniqueness in that the rate-time data would be in the region where q(t) appears to be nearly constant because of large $t_D(r_{wa})$ values. Equation 64 is written in terms of kh and ϕh to emphasize the point that when we pick h we are assigning an oil or gas-in-place – not simply determining k. The significance is now apparent in that we are making production forecasts. It's one thing to reduce the k by a half by assigning a range of thickness, h, and quite different to cut the oil or gas-in-place by half. Generally, people who do pressure transient analysis seldom apply the results to production forecasting. In general, we have found very good agreement between kh and skins calculated using rate-time analysis and the constant wellbore pressure solutions compared to pressure transient build-up analysis using constant rate solutions when the data are available and properly taken. See Refs. 3, 4, and 5 for some good field examples.

Depletion Decline

Rapidly declining transient production data in tabular form, or even on a semilog plot, often is misinterpreted to be depletion. The primary use of the composite type curve (Fig. 7) is to be able to distinguish between transient and depletion production decline by making a log-log plot of the production data, matching it, and then forecasting future production by extending the match down the appropriate depletion stem. If production data exists only in depletion, we can calculate oil or gas-in-place and a combined kh and r_{wa} or skin and productivity index, J.

In its simplest form, using the Arps equation and match points from a type curve match on the depletion stem, b, calculate

$$q_i = \left(\frac{q(t)}{q_{Dd}}\right)_{match}, \quad (67)$$

and

$$D_i = \left(\frac{t_{Dd}}{t}\right)_{match}, \quad (68)$$

where

$$\frac{kh}{\left[\ln\left(\frac{.473\,r_e}{r_{wa}}\right)\right]} = \frac{141.2\,\mu B}{(\bar{p}_R - p_{wf})} \cdot q_i. \quad (69)$$

By assuming some value of skin, or r_{wa}, we can calculate a value of kh.

Calculate the pseudosteady-state productivity index for the rate equation

$$J = \frac{q_i}{\bar{p}_R - p_{wf}}. \quad (70)$$

Using Eq. 10 for hyperbolic decline (Eq. 12 would be used for exponential), we can calculate the recoverable reserves

$$G \text{ or } N_{puo} = \frac{1}{(1-b)}\left(\frac{q_i}{D_i}\right). \quad (71)$$

Then, gas or oil-in-place at the start of decline is

$$G_i \text{ or } N = \frac{G \text{ or } N_{puo}}{R.F.}. \quad (72)$$

In terms of reservoir variables, we could solve for pore volume, V_p, and/or r_e from the following equations

$$G_i \text{ or } N = V_p(1-s_w)B, \quad (73)$$

where

$$V_p = \pi r_e^2 \phi h. \quad (74)$$

Calculated numbers using the above equations should be reasonable and consistent with values calculated for offsets. They should never be accepted blindly, i.e., a calculated r_e much less than spacing does not imply infill drilling.

Conclusions

Rate-time analysis (decline curve analysis), has been placed on a sound, fundamental basis utilizing the constant wellbore pressure analytical solutions. Derivations combining the material balance and pseudosteady-state rate equations result in rate-time decline equations for oil and gas wells. It is from these derivations that the variables in Arps' equations can be expressed in terms of reservoir variables. Using these solutions with sound reservoir engineering concepts, it becomes possible to provide more accurate production forecasts and better oil and gas reserves for both wells and/or individual fields.

Nomenclature

b	=	decline exponent
B	=	formation volume factor, res vol/surface vol
C_g	=	gas-well productivity index (backpressure curve coefficient) Mscf/D/(psi)^{2n}
c_t	=	total compressibility, psi^{-1}
D_i	=	initial decline rate, t^{-1}
e	=	natural logarithm base 2.71828
G	=	gas-in-place, surface-measured
G_p	=	cumulative gas produced, surface-measured
h	=	thickness, ft.
J_o	=	productivity index, STB/D/psi
J_o'	=	productivity index (backpressure curve coefficient) STB/D/(psi)^{2n}
k	=	effective permeability, md
n	=	exponent of backpressure curve
N_p	=	cumulative production, STB
N_{puo}	=	ultimate recoverable oil @ q(t) = 0, STB
$N_{puo,o}$	=	ultimate recoverable oil @ q(t) = 0 and p_{wf} = 0, STB
N	=	oil-in-place, STB
p_c	=	wellhead shut-in-pressure, psia
p_R	=	average reservoir pressure, psia
p_t	=	flowing wellhead tubing pressure, psia
p_w	=	flowing wellhead annulus pressure, psia
p_{wf}	=	bottomhole flowing pressure, psia
q_i	=	initial surface rate of flow from stabilized curve
$q_{i(max)}$	=	initial surface rate of flow from stabilized curve at p_{wf} or p_t = 0
$q(t)$	=	surface rate of flow at time t
q_D	=	dimensionless rate
q_{Dd}	=	decline curve dimensionless rate
Q_p	=	oil or gas cumulative production, N_p or G_p, surface measure
r_e	=	external boundary radius, ft.
r_w	=	wellbore radius, ft.
r_{wa}	=	effective wellbore radius, ft.
R. F.	=	recovery factor, fraction
s	=	skin
S_w	=	water saturation, fraction
t	=	time, days
t_D	=	dimensionless time
t_{Dd}	=	decline curve dimensionless time
T	=	reservoir temperature, °R
V_R	=	layer volume ratio, pore volumes
V_p	=	reservoir pore volume, ft^3 or BBl
W	=	number of wells
Z	=	gas compressibility factor, dimensionless
μ	=	viscosity, cp
ϕ	=	porosity, fraction of bulk volume

Subscripts

a	=	at abandonment
g	=	gas
i	=	initial
o	=	oil
R	=	ratio
T	=	total of each layers productions
u	=	ultimate

Acknowledgements

We wish to thank Phillips Petroleum Company for permission to publish this paper. Special thanks to Kay Patton for the excellent typing of this paper and the several drafts that preceded it.

References

1. Arps, J. J.: "Analysis of Decline Curves," *Trans.*, AIME (1945) 160, 228-47.
2. Fetkovich, M. J.: "A Simplified Approach to Water Influx Calculations - Finite Aquifer Systems," *JPT* (July 1971) 814-828.
3. Fetkovich, M. J.: "Decline Curve Analysis Using Type Curves," *JPT* (June 1980) 1065-77.
4. Fetkovich, M. J., Vienot, M. E., Bradley, M. D., and Kiesow, U. G.: "Decline Curve Analysis Using Type Curves - Case Histories," *SPE Formation Evaluation* (Dec. 1987) 637-656.
5. Fetkovich, M. J., Vienot, M. E., Johnson, R. D., and Bowman, B. A.: "Case Study of a Low-Permeability Volatile Oil Field Using Individual-Well Advanced Decline Curve Analysis," paper SPE 14237 presented at the SPE 60th Annual Technical Conference and Exhibition, Las Vegas, NV, (Sept. 22-25, 1985).
6. Fetkovich, M. J.: "The Isochronal Testing of Oil Wells," paper SPE 4529, presented at the 48th Annual Fall Meeting, Las Vegas, NV, (Sept. 30 - Oct. 3, 1973).
7. Fetkovich, M. J.: "Multipoint Testing of Gas Wells," SPE Mid-Continent Section, Continuing Education Course, Tulsa, (March 17, 1975).
8. Fetkovich, M. D., Guerrero, E. T., Fetkovich, M. J., and Thomas, L. K.: "Oil and Gas Relative Permeabilities Determined From Rate-Time Performance Data," paper SPE 15431 presented at the 61st Annual Technical Conference and Exhibition of SPE, New Orleans, LA, (October 5-8, 1986).
9. Fetkovich, M. J.: *Advances in Well Deliverability and Production Forecasting*, Ph.D. Dissertation, The University of Trondheim (1988).
10. Fetkovich, M. J., Bradley, M. D., Works, A. M., and Thrasher, T. S.: "Depletion Performance of Layered Reservoirs Without Crossflow," *SPE Formation Evaluation*, (September 1990).
11. Fetkovich, M. J., Needham, R. B., and McCoy, T. F.: "Analysis of Kansas Hugoton Infill Drilling, Part II: Twelve Year Performance History of Five Replacement Wells," paper SPE 20779 presented at the 65th SPE Annual Technical Conference and Exhibition, New Orleans, LA, (Sept. 23-26, 1990).
12. Gentry, R. W. and McCray, A. W.: "The Effect of Reservoir and Fluid Properties on Production Decline Curves," *JPT*, (Sept. 1978), 1327-41.
13. Matthews, C. S. and Lefkovits, H. C.: "Gravity-Drainage Performance of Depletion-Type Reservoirs," *Trans.* AIME 207, (1956) 265.
14. Lefkovits, H. C. and Matthews, C. S.: "Application of Decline Curves to Gravity-Drainage Reservoirs in Stripper Stage," *Petroleum Transactions*, AIME, Vol. 213, (1958), 275.
15. Stewart, P. R.: "Low Permeability Gas Well Performance at Constant Pressure," *JPT*, (Sept. 1970), 1149-1156.
16. Locke, C. D. and Sawyer, W. K.: "Constant Pressure Injection Test in a Fractured Reservoir – History Match Using Numerical Simulation and Type curve Analysis," paper SPE 5594 presented at

the 1975 SPE Annual Technical Conference and Exhibition, Dallas, (Sept. 28 - Oct. 1).

17. Uraiet, A. A. and Raghavan, R.: "Unsteady Flow to a Well Producing at a Constant Pressure" and "Pressure Buildup Analysis for a Well Produced at Constant Bottomhole Pressure," *JPT, Trans.* AIME, 269, (Oct. 1980), 1803-1824.
18. Smith, R. V.: *Practical Natural Gas Engineering*, PenWell Books, Tulsa (1980).
19. Ehlig-Economides, C. A. and Ramey, H. J. Jr.: "Transient Rate Decline Analysis for Wells Produced at Constant Pressure," *SPEJ* (Feb. 1981) 98-104.
20. Carter, R. D.: "Characteristic Behavior of Finite Radial and Linear Gas Flow Systems – Constant Terminal Pressure Case," paper SPE 9887 presented at the 1981 SPE/DOE Symposium on Low Permeability Gas Reservoirs, Denver, (May 27-19).
21. Da Prat, G., Cinco-Ley, H. and Ramey, H. J. Jr.: "Decline Curve Analysis Using Type Curves for Two-Porosity Systems," *SPEJ* (June 1981) 354-62.
22. Carter, R. D.: "Type Curves for Finite Radial and Linear Gas-Flow Systems: Constant-Terminal-Pressure Case," *SPEJ* (Oct. 1985) 719-28.
23. Fraim, M. L. and Wattenbarger, R. A.: "Gas Reservoir Decline Curve Analysis Using Type Curves with Real Gas Pseudo-Pressure and Pseudo-Time," paper SPE 14238, presented at the SPE Annual Technical Conference and Exhibition, Las Vegas, NV, (Sept. 1985).
24. Schmidt, S. H., Caudle, B. H., and Miller, M. A.: "Gas Well Decline Analysis Incorporating Real Gas Behavior and non-Darcy Flow," paper SPE 15521 presented at the SPE Annual Technical Conference and Exhibition, New Orleans, (Oct. 5-8, 1986).
25. Fraim, M. L. and Lee, W. J.: "Determination of Formation Properties From Long-Term Gas Well Production Affected by non-Darcy Flow," paper SPE 16934 presented at the SPE Annual Technical Conference and Exhibition, Dallas (Sept. 27-30, 1987).
26. Aminian, K., Ameri, S., Stark, J. J., and Yost, A. B.: "Gas-Well Production Decline in Multiwell Reservoirs," *JPT*, (Dec. 1990) 1573-1579.
27. Blasingame, T. A., McCray, T. C., and Lee, W. J.: "Decline Curve Analysis for Variable Pressure Drop/Variable Flowrate System," paper SPE 21513 presented at the SPE Gas Technology Symposium, Houston (June 23-24, 1991).
28. Vega, J. P., Samaniego, V., Berumen, S. C.: "A Method for Gas Well Decline Analysis Under Constant Pressure Conditions and High-Velocity Flow," paper SPE 22926 presented at the SPE 66th Annual Technical Conference and Exhibition, Dallas (Oct. 6-9, 1991).
29. Golan, M. and Whitson, C. H.: *Well Performance*, Prentice Hall, Englewood Cliffs, NJ, Second Edition (1991), 669.
30. Palacio, J. C. and Blasingame, T. A.: "Decline-Curve Analysis Using Type Curves - Analysis of Gas Well Production Data," paper SPE 25909 presented at the Joint Rocky Mountain Regional and Low Permeability Reservoir Symposium, Denver, CO, (April 26-28, 1993).
31. Cole, F.W.: *Reservoir Engineering Manual*, Gulf Publishing Company, Houston, TX (1969) 48.

TABLE 1

Decline Exponent "b" as a Function of $\left[\frac{q_i}{G \text{ or } N_{puo}}\right]_R$ and Volume Ratio, V_R

	Single Phase Gas V_R or G_R				Single Phase Liquid V_R or $[N_{puo}]_R$				
$\left[\frac{q_i}{G}\right]_{Ratio}$	$\frac{2}{1}$	$\frac{1}{1}$	$\frac{1}{2}$	$\frac{1}{5}$	$\left[\frac{q_i}{N_{puo}}\right]_{Ratio}$	$\frac{2}{1}$	$\frac{1}{1}$	$\frac{1}{2}$	$\frac{1}{5}$
1	.4	.4	.4	.4	1	0	0	0	0
3	.45	.5	.5	.5	3	.1	.2	.25	.2
5	.5	.55	.6	.65	5	.2	.3	.4	.45
10	.6	.65	.7	.8	10	.3	.4	.5	.65
15.5	.6	.7	.75	.8	15.5	.35	.45	.6	.7

$q_{total} = q_1 + q_2$; individual layer b = 0.4 for gas and b = 0 for single phase liquid.

$$\text{Gas: } q_{Total} = \frac{q_{iT}}{\left[1+b_T\left(\frac{1}{1-b_T}\right)\left(\frac{q_{iT}}{G_T}\right)t\right]^{1/b_T}} = \frac{q_{i1}}{\left[1+0.4\left(\frac{1}{1-0.4}\right)\left(\frac{q_{i1}}{G_1}\right)t\right]^{1/0.4}} + \frac{q_{i2}}{\left[1+0.4\left(\frac{1}{1-0.4}\right)\left(\frac{q_{i2}}{G_2}\right)t\right]^{1/0.4}}$$

$$\text{Liquid: } q_{Total} = \frac{q_{iT}}{\left[1+b_T\left(\frac{1}{1-b_T}\right)\left(\frac{q_{iT}}{N_{puoT}}\right)t\right]^{1/b_T}} = \frac{q_{i1}}{e^{\left(\frac{q_{i1}}{N_{puo1}}\right)t}} + \frac{q_{i2}}{e^{\left(\frac{q_{i2}}{N_{puo2}}\right)t}}$$

STABILIZED CURVE RATE EQUATIONS

(n = EXPONENT OF BACK-PRESSURE CURVE)

$$q_g = C_g (\bar{P}_r^2 - P_{wf}^2)^n$$

$$q_o = J'_o \left(\frac{\bar{P}_r}{\bar{P}_{ri}}\right)(\bar{P}_r^2 - P_{wf}^2)^n$$

$$q_o = J_o (\bar{P}_r - P_{wf})$$

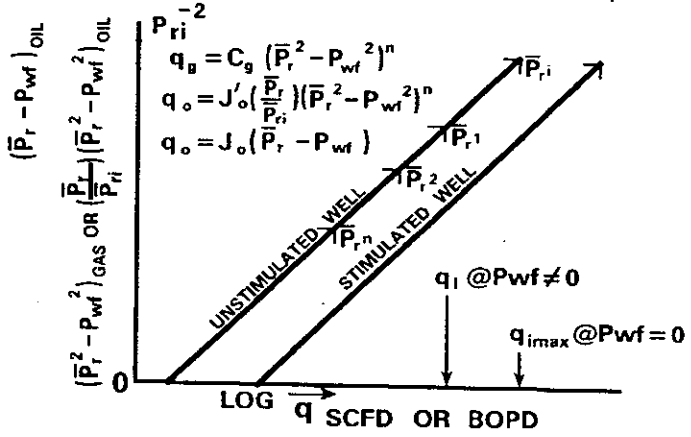

MATERIAL BALANCE EQUATIONS

$$\bar{P}_r = -\left(\frac{\bar{P}_{ri}}{G_i}\right) G_p + \bar{P}_{ri}$$

$$\bar{P}_r^2 = -\left(\frac{\bar{P}_{ri}^2}{N_{puo}}\right) N_p + \bar{P}_{ri}^2$$

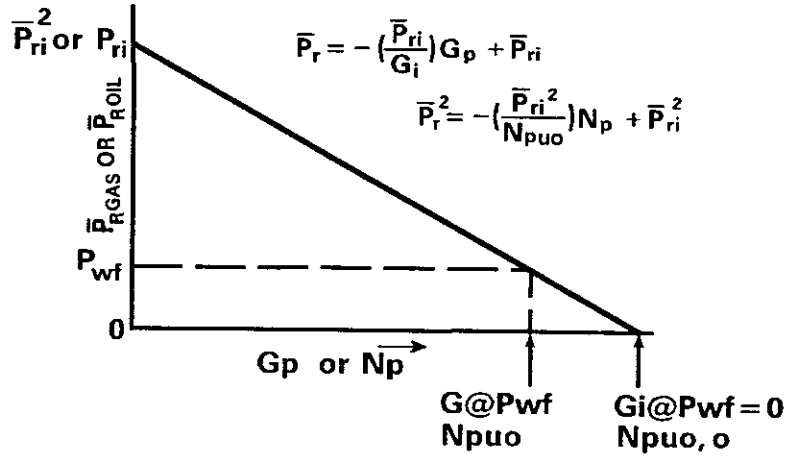

RESULTING RATE TIME EQUATIONS (Pwf ≅ 0)

GAS	OIL
EXPONENTIAL, n = 0.5	
$q_{g(t)} = \frac{q_{gi}}{e^{\frac{q_{gi}}{G}t}}$	$q_{o(t)} = \frac{q_{oi}}{e^{(\frac{q_{oi}}{N_{puo}})t}}$
$D_i = \frac{q_{gi}}{G}$ OR $2n(\frac{q_{gi}}{G})$	$D_i = \frac{q_{oi}}{N_{puo}}$ OR $\frac{2n+1}{2}(\frac{q_{oi}}{N_{puo}})$
HYPERBOLIC, n > 0.5	
$q_{g(t)} = \frac{q_{gi}}{[1+(2n-1)(\frac{q_{gi}}{G})t]^{\frac{2n}{2n-1}}}$	$q_{o(t)} = \frac{q_{oi}}{[1+\frac{2n-1}{2}(\frac{q_{oi}}{N_{puo}})t]^{\frac{2n+1}{2n-1}}}$
$D_i = 2n(\frac{q_{gi}}{G})$	$D_i = \frac{2n+1}{2}(\frac{q_{oi}}{N_{puo}})$
$\frac{1}{b} = \frac{2n}{2n-1}$ OR $b = \frac{2n-1}{2n}$;	$\frac{1}{b} = \frac{2n+1}{2n-1}$ OR $b = \frac{2n-1}{2n+1}$
FOR n = 1	
$D_i = 2(\frac{q_{gi}}{G})$	$D_i = \frac{3}{2}(\frac{q_{oi}}{N_{puo}})$
$b = \frac{1}{2} = 0.5$	$b = \frac{1}{3} = 0.33$

EXPONENT b IN TERMS OF BACK PRESSURE CURVES

WELLHEAD SLOPE n		DECLINE b_{GAS}	DECLINE b_{OIL}
.5	HIGH K AND TUBING LIMITED	0	0
.6		.17	.1
.7		.29	.17
.8		.38	.23
.9		.44	.29
1.0	LOW K AND RESERVOIR LIMITED	.50	.33

$G = OGIP \times R.F. = Gi \times R.F.$ WHERE $R.F. \cong (1 - \frac{Pwf}{Pri})$

$Npuo = OOIP \times R.F. = N \times R.F.$ WHERE R.F. = f(Kg/Ko) SOLUTION GAS DRIVE

Fig. 1 Rate and Material Balance Equations Used to Derive Rate-Time Decline Equations for Gas and Oil Wells

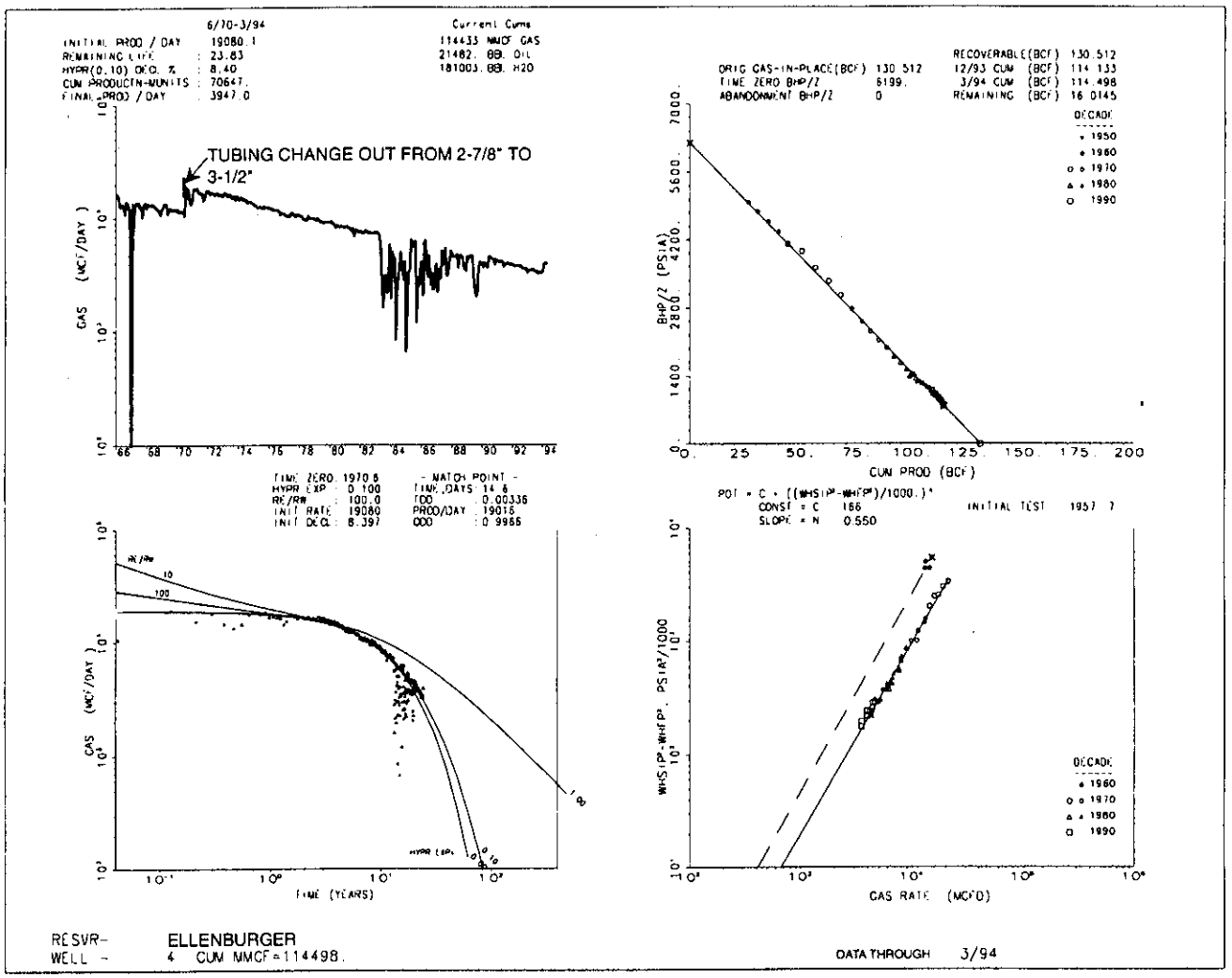

Fig. 2 Well Performance Plots of Material Balance, Backpressure Curve and Rate-Time, Semi-Log and Log-Log Graphs

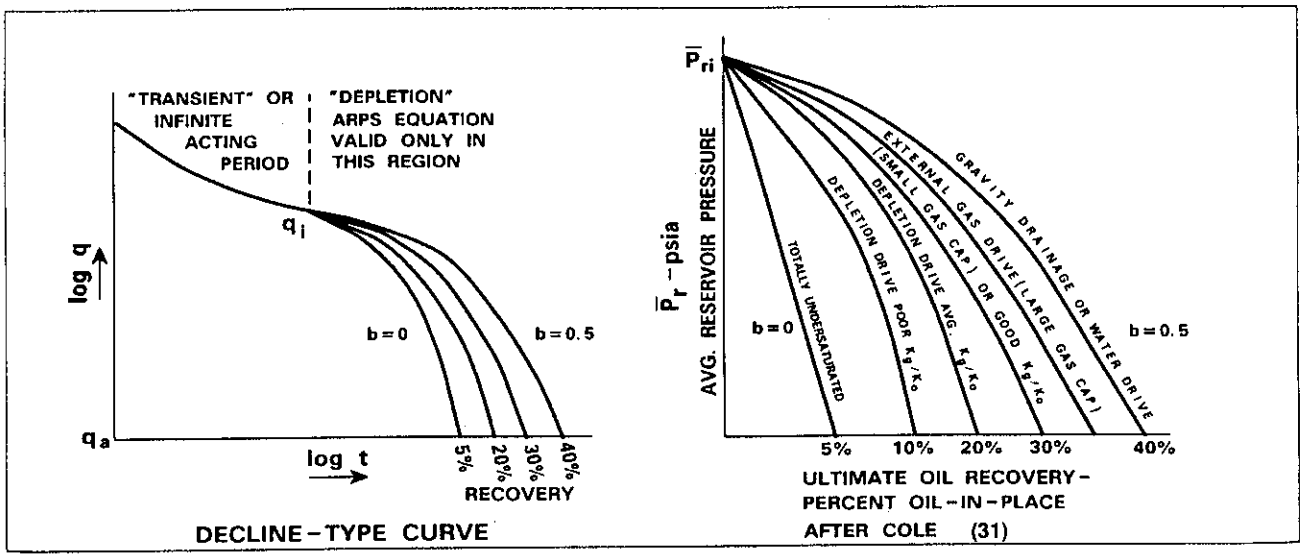

Fig. 3 Decline Exponent "b" as a Reflection of Recovery Efficiency or Drive Mechanism

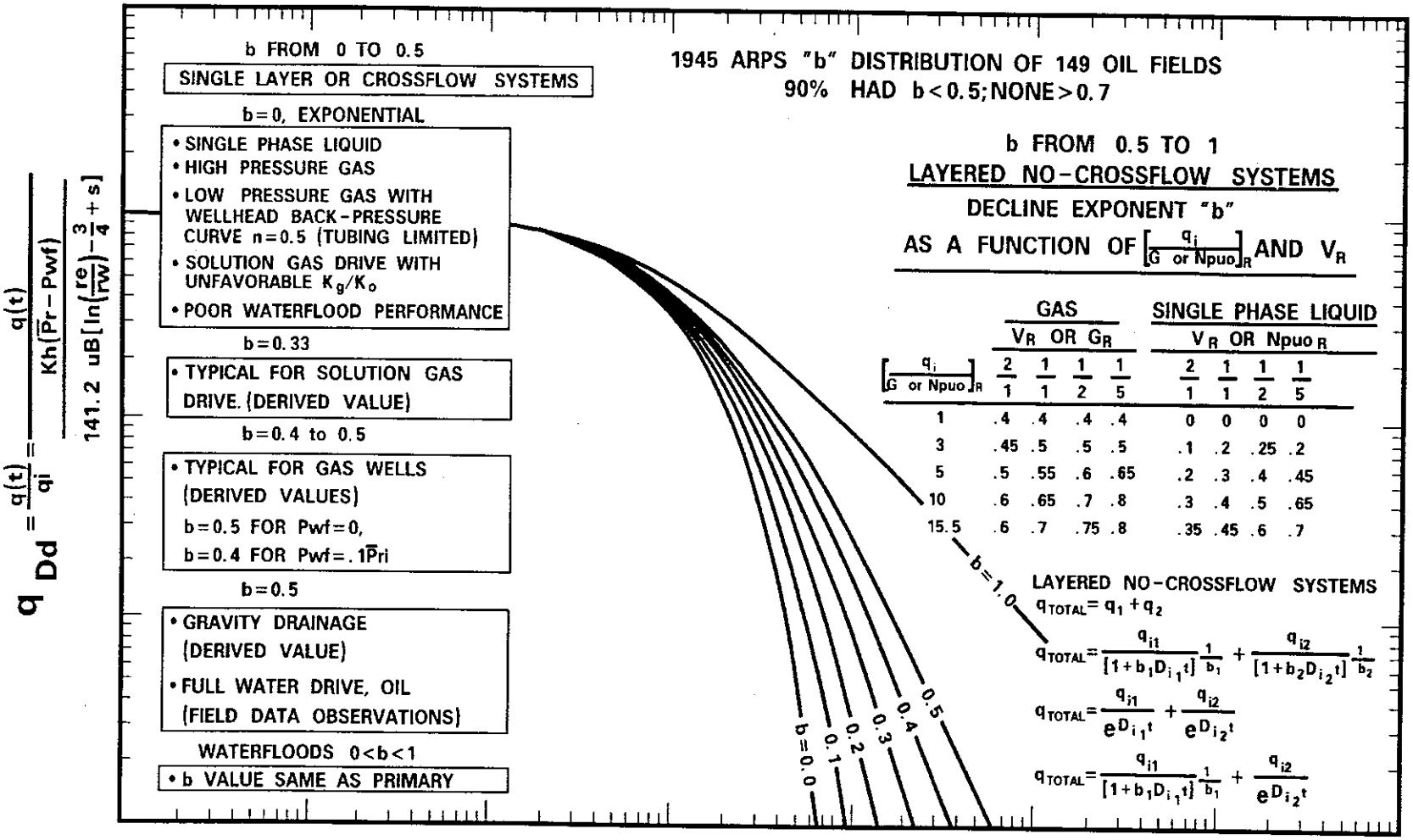

$$q_{Dd} = \frac{q(t)}{qi} = \frac{q(t)}{\frac{Kh(\bar{P}r - Pwf)}{141.2\ uB\left[\ln\left(\frac{re}{rw}\right) - \frac{3}{4} + s\right]}}$$

$$t_{Dd} = D_i t = \begin{cases} \text{GAS} = \dfrac{1}{(1-b)}\dfrac{qi}{G}\,t = 2n\left(\dfrac{qi}{G}\right)t \\ \text{OIL} = \dfrac{1}{(1-b)}\dfrac{qi}{Npuo}\,t = \dfrac{2n+1}{2}\left(\dfrac{qi}{Npuo}\right)t \end{cases}$$

Fig. 4 Decline Exponents "b" for Various Reservoir Drive Mechanisms

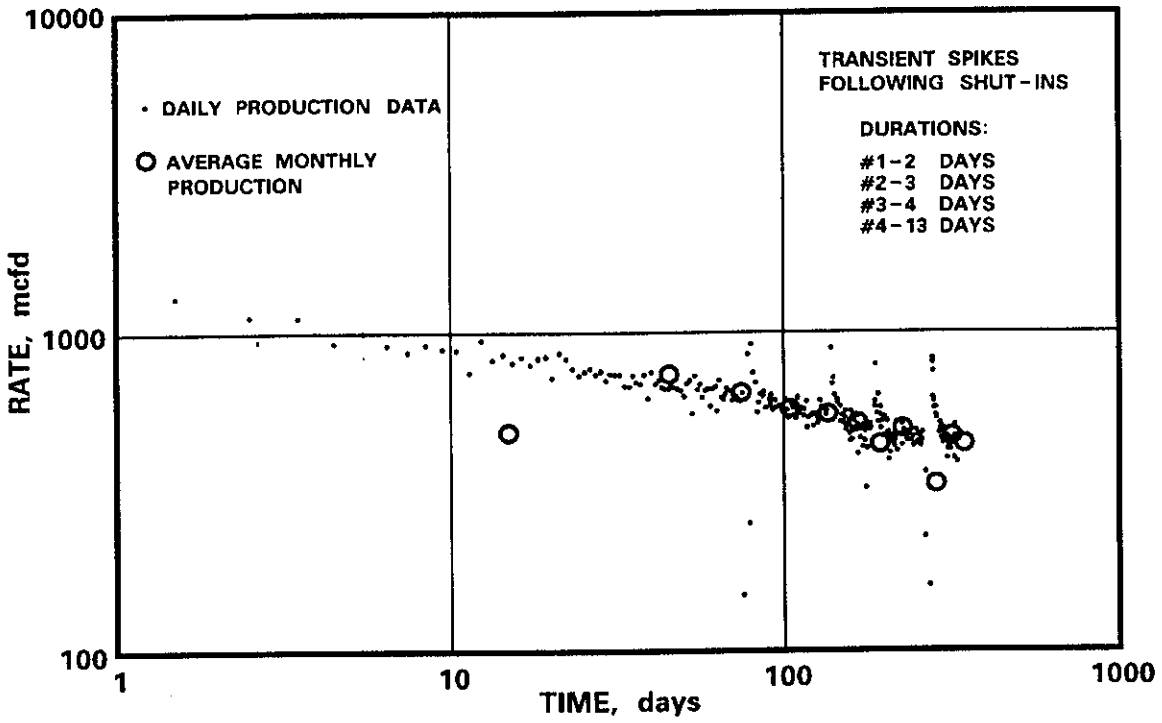

Fig. 5 Daily Production Data Compared to Average Monthly Production Carthage Cotton Valley Field

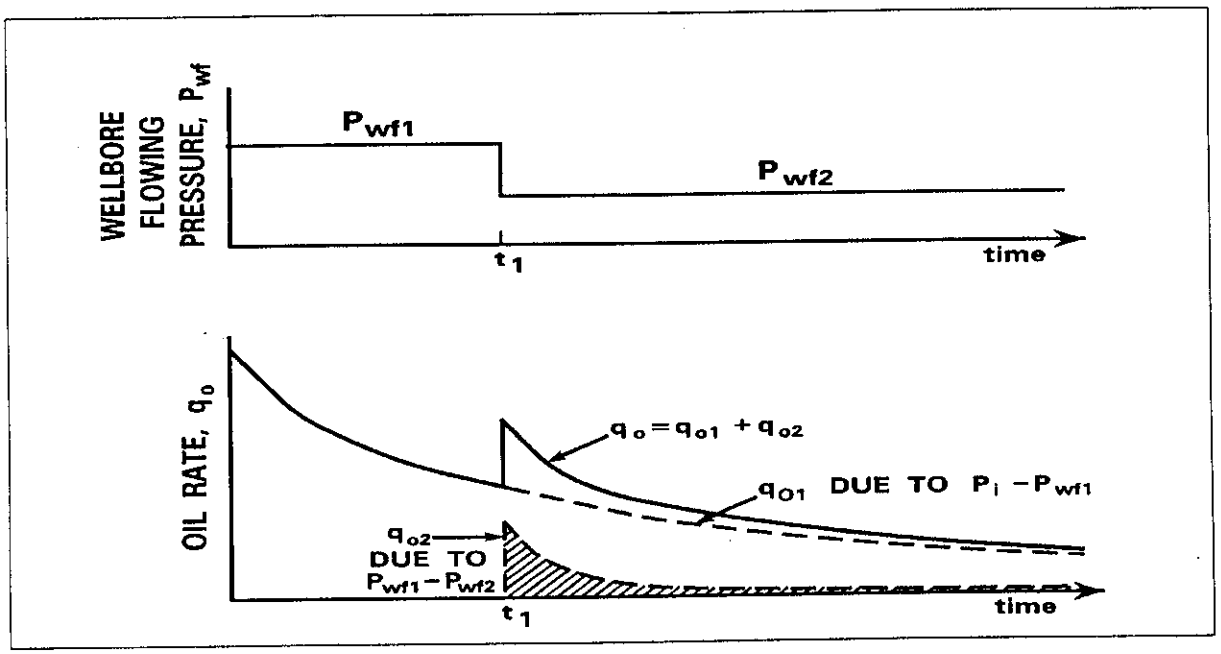

Fig. 6 Superposition Applied to Constant-Pressure Production Experiencing a Change in Backpressure

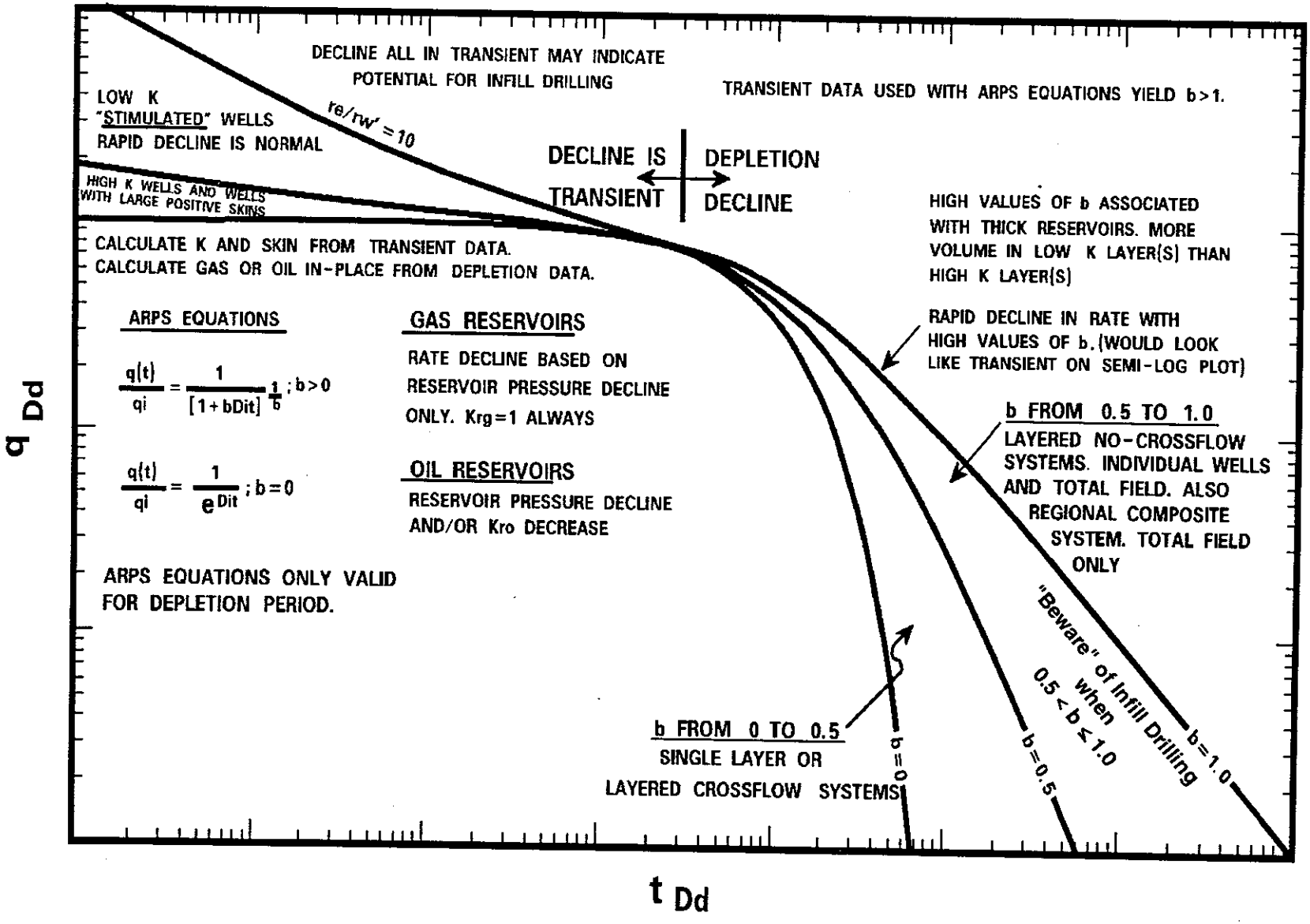

Fig. 7 Composite of Analytical and Emperical Type Curves with Comments

Gas Reservoir Decline-Curve Analysis Using Type Curves With Real Gas Pseudopressure and Normalized Time

M.L. Fraim, SPE, Texas A&M U.
R.A. Wattenbarger, SPE, Texas A&M U.

Summary. A normalized time has been developed that linearizes the rate decline vs. normalized time for a gas reservoir producing against constant wellbore pressure during (external) boundary-dominated flow. This allows type-curve matching of the exponential decline curve for a reservoir with any shape. Values of G, $k_g h$, and k_g/ϕ can be determined from this type-curve match. It was determined that gas reservoir depletion plotted vs. actual time does not match exponential, harmonic, or hyperbolic decline curves, and future performance can lead to overestimates of reserves and future rate.

Introduction

Fetkovich[1,2] introduced the idea of applying log-log type-curve analysis to single-well analysis for both transient- and boundary-dominated flow periods. Boundary-dominated flow for constant-pressure production is similar to pseudosteady-state flow for constant-rate production. His type-curve analysis was intended to be a rapid way to estimate performance when a well is producing against a constant bottomhole pressure (BHP). From his type curves, future performance can be forecast along with estimates of oil in place and ultimate recovery (Fig. 1).

For boundary-dominated flow, Fetkovich showed the Arps[3] family of curves with b as a parameter. The $b=0$ case is for exponential decline of a liquid reservoir. Fetkovich used the curves with values of b between 0 and 1 (hyperbolic and harmonic decline) for matching solution-gas-drive depletion and gas reservoir depletion. Matching and extrapolating these curves is equivalent to using the harmonic and hyperbolic declines with the usual semilog decline curves. He showed cases where these curves were useful.

Carter[4] developed another set of decline curves for boundary-dominated flow that used a parameter, λ, to represent variations in the decline curves from real gas properties:

$$\lambda=\frac{(\mu c_g)_i(p_{pi}-p_{pwf})}{2[(p/z)_i-(p/z)_{wf}]}. \quad \ldots\ldots\ldots\ldots\ldots\ldots\ldots\ldots\ldots\ldots (1)$$

where

$$p_p=2\int_0^p \frac{p}{z(p)\mu(p)}\,dp,$$

which can also be expressed as

$$p_p=2\int_0^p \frac{1}{\mu(p)c_g(p)}\,d[\bar{p}/z(p)]. \quad \ldots\ldots\ldots\ldots\ldots\ldots\ldots\ldots\ldots\ldots (2)$$

A value of $\lambda=1.0$ represents the liquid case, and values of $\lambda<1.0$ represent the degree of gas property variation as a result of the severity of the drawdown.

Agarwal[5] and Lee and Holditch[6] used a pseudotime to linearize the transient analysis of gas wells with massive hydraulic fractures. Their pseudotime was defined as

$$t_a=\int_0^t \frac{1}{\mu(p_{wf})c_t(p_{wf})}\,dt. \quad \ldots\ldots\ldots\ldots\ldots\ldots\ldots\ldots\ldots\ldots (3)$$

The viscosity and compressibility values in their integrated time function are taken at the bottomhole flowing pressure (BHFP), which is varying with time.

This paper is concerned with the longer-term boundary-dominated flow of real gases in closed reservoirs. The objective is to improve the use of Fetkovich's type curves for gas well analysis. A normalized time is introduced that applies to the viscosity and compressibility at the average reservoir pressure rather than the wellbore pressure. This normalized time is used for boundary-dominated flow analysis, as well as for transient analysis. Only Darcy flow is considered.

Real Gas Normalized Time

We will now show that the depletion of a closed real gas reservoir can be expressed as an exponential decline ($b=0$) if a normalized time is used. The normalized time is defined as

$$t_n=\int_0^t \frac{(\mu c_t)_i}{\mu(\bar{p})c_t(\bar{p})}\,dt. \quad \ldots\ldots\ldots\ldots\ldots\ldots\ldots\ldots\ldots\ldots (4)$$

We will first develop the expression for exponential decline with the assumption that rock compressibility and water compressibility equal 0, for simplicity. We will then generalize to the total-compressibility, c_t, case in the Appendix.

The basis of our derivation is a material-balance equation for a real gas expansion in a closed reservoir:

$$(\bar{p}/z)=(\bar{p}/z)_i(1-G_p/G). \quad \ldots\ldots\ldots\ldots\ldots\ldots\ldots\ldots\ldots\ldots (5)$$

This is the equation for the straight line p/z plot. We also use the pseudosteady-state equation for a real gas in terms of p_p expressed in the form of a productivity index equation as[7,8]

$$q_g=J_g(p_p-p_{pwf}). \quad \ldots\ldots\ldots\ldots\ldots\ldots\ldots\ldots\ldots\ldots (6)$$

The expression for J_g is

$$J_g=\frac{1.987\times10^{-5}k_g h}{\tfrac{1}{2}\ln\left(\frac{2.2458A}{C_A r_w^2}\right)}\frac{T_{sc}}{p_{sc}T}. \quad \ldots\ldots\ldots\ldots\ldots\ldots\ldots\ldots\ldots\ldots (7)$$

Eqs. 5 through 7 are the basis for our derivation. First, we differentiate Eq. 5 to represent the pressure depletion with time:

$$d(\bar{p}/z)=\frac{-q_g(\bar{p}/z)_i}{G}dt. \quad \ldots\ldots\ldots\ldots\ldots\ldots\ldots\ldots\ldots\ldots (8)$$

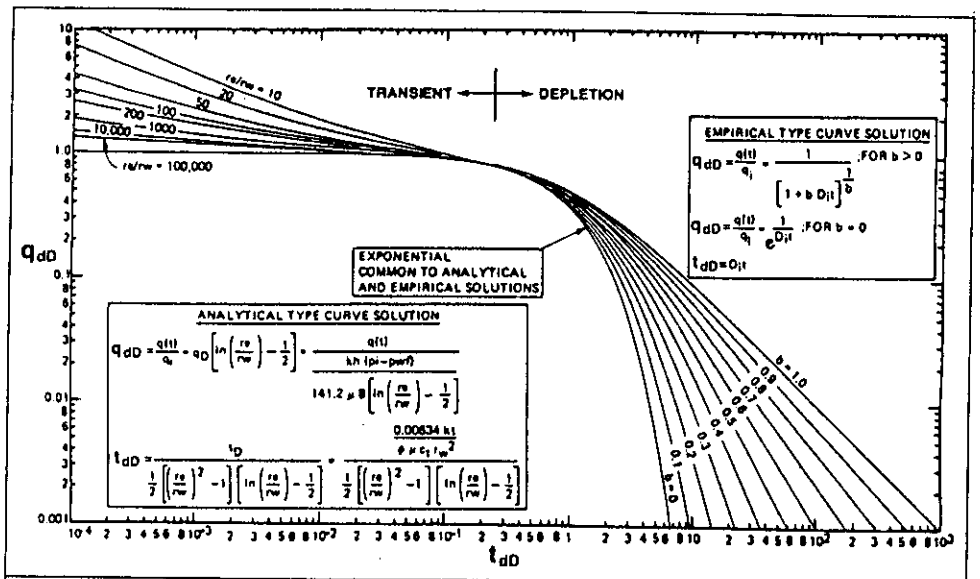

Fig. 1—Composite of analytic and empirical type curves (after Fetkovich[1]).

Then, we differentiate Eq. 6 to show how the rate changes with depletion:

$$dq_g = J_g dp_p = \frac{2J_g}{\mu(\bar{p})c_g(\bar{p})} d(\bar{p}/z). \quad \ldots\ldots\ldots\ldots\ldots\ldots (9)$$

Eqs. 8 and 9 can be combined to form the following expression of rate change with time:

$$dq_g = \frac{-2J_g}{\mu(\bar{p})c_g(\bar{p})} \frac{(\bar{p}/z)_i q_g}{G} dt. \quad \ldots\ldots\ldots\ldots\ldots\ldots (10)$$

Eq. 10 applies to boundary-dominated flow. To follow the development of Fetkovich's type curve, it is useful to extend Eq. 6 and thus Eq. 10 to $t=0$. The rate obtained from Eq. 5 at $t=0$ is defined as q_i, an extrapolated "initial" rate. With this extrapolation of Eq. 6 to $t=0$, we can integrate Eq. 10 from $t=0$ to any later time, t, that has a flow rate, q_g, and an average reservoir pressure, $\bar{p}$. Thus,

$$\int_{q_i}^{q} \frac{dq_g}{q_g} = \int_0^t \frac{-2J_g}{\mu(\bar{p})c_g(\bar{p})} \frac{(\bar{p}/z)_i}{G} dt, \quad \ldots\ldots\ldots\ldots\ldots\ldots (11)$$

which then becomes

$$\ln(q/q_i) = \frac{-2J_g(\bar{p}/z)_i}{G(\mu c_g)_i} \int_0^t \frac{(\mu c_g)_i}{\mu(\bar{p})c_g(\bar{p})} dt. \quad \ldots\ldots\ldots\ldots\ldots\ldots (12)$$

The integral expression in Eq. 12 becomes our basis for defining normalized time, t_n, in Eq. 4:

$$\ln(q/q_i) = \frac{-2J_g(\bar{p}/z)_i}{G(\mu c_g)_i} t_n. \quad \ldots\ldots\ldots\ldots\ldots\ldots (13)$$

Eq. 13 is in the form of an exponential decline. Notice that Eq. 13 has a constant coefficient when the t_n variable is used.

If we express normalized time in terms of the usual dimensionless time,

$$t_D = \frac{0.00633 k_g t_n}{(\phi\mu c_g)_i r_w^2}, \quad \ldots\ldots\ldots\ldots\ldots\ldots (14)$$

and substitute our expression for J, then our exponential decline can be written as

$$\ln(q/q_i) = \frac{t_D}{\tfrac{1}{2}\left(\frac{A}{\pi r_w^2} - 1\right) \tfrac{1}{2} \ln\left(\frac{2.2485A}{C_A r_w^2}\right)}. \quad \ldots\ldots\ldots\ldots\ldots\ldots (15)$$

The significance of Eqs. 13 and 15 is that we can express real gas depletion exactly in terms of exponential decline when the normalized time is used. Thus, all closed gas reservoirs with constant BHP fit the Fetkovich $b=0$ type curve for boundary-dominated flow.

These results can be generalized to include formation and liquid compressibility by replacing c_g with c_t. Because saturations are included in c_t, S_g must be accounted for. Note that t_n should be modified if formation compressibility is important. If the value of $(p_i - \bar{p})(c_f + S_w c_w)$ is significant compared to 1.0 at any stage of depletion, then the definition of t_n should be changed from Eq. 3 to Eq. A-16. A development of this correction is shown in the Appendix.

The assumption that Eq. 6 applies at $t=0$ leads to an assumption that $\mu(p_i)$ and $c_t(p_i)$ can be evaluated at initial conditions, even though the gas properties corresponding to q_i are based on a slightly lower initial pressure. We have found that errors occurring from this assumption occur only during the transient time and are not significant if transient cumulative production is used in the material-balance equation. Thus, gas rate vs. normalized time will trace the log-log type curve in both the transient- and boundary-dominated flow regimes.

Type Curve Variables

Fetkovich's decline-curve dimensionless variables have been modified to include normalized time and the area of a general reservoir shape. These variables use a value of 19.1785 for C_A (see Refs. 9 and 10) rather than 31.62 to conform with Fetkovich's type curve construction. Thus,

$$q_{dD} = \frac{q_g p_{sc} T \tfrac{1}{2} \ln\left(\frac{2.2485A}{19.1785 r_w^2}\right)}{1.987\times10^{-5} T_{sc} k_g h (p_{pi} - p_{pwf})} \quad \ldots\ldots\ldots\ldots\ldots\ldots (16)$$

and

$$t_{dD} = \frac{\frac{0.00633 k_g t_n}{(\phi\mu c_t)_i r_w^2}}{\tfrac{1}{2}\left(\frac{A}{\pi r_w^2} - 1\right) \tfrac{1}{2} \ln\left(\frac{2.2485A}{C_A r_w^2}\right)}. \quad \ldots\ldots\ldots\ldots\ldots\ldots (17)$$

TABLE 1—RESERVOIR DATA FOR ALL CASES

Shape	Case 1	Case 2	Case 3	Case 4
h, md	200	200	200	200
k, md	10	10	10	10
T, °F	200	200	200	200
ϕ, fraction	0.30	0.30	0.30	0.30
c_t, 1/psi	3.0×10^{-6}	3.0×10^{-6}	3.0×10^{-6}	3.0×10^{-6}
c_w, 1/psi	3.0×10^{-6}	3.0×10^{-6}	3.0×10^{-6}	3.0×10^{-6}
S_{gi}, %	0.99	0.99	0.99	0.99
r_w, ft	0.25	0.25	0.25	0.25
s	0	0	0	0
A, ft^2	3.848×10^{7}	3.848×10^{7}	3.848×10^{7}	3.848×10^{7}
p_i, psia	5,000	5,000	3,000	8,000
p_{wf}, psia	3,000	3,000	500	1,000
G, Bscf	61.51	61.51	40.52	81.63
Gas gravity	0.601	0.601	0.601	0.601
λ	0.721	0.721	0.564	0.428

Note that in the transient time for a nonradial shape ($C_A<20$), the decline curve will not trace the equivalent (r_e/r_w) transient stem on the Fetkovich curves. For shapes with $C_A<4$, the rate will have to decline to 40% of the "initial" boundary-dominated rate, q_i, before a reasonable match can be obtained on a radial type curve.

To obtain normalized time, we must assume a value for original gas in place, G. The first guess is found by matching the curve of actual time vs. rate decline and calculating a value for G. This value of G is then used to calculate normalized time and to match this curve with the base fit b curve closest to the exponential curve. A new value of G is calculated. This process is repeated until convergence is obtained for the exponential decline curve. From our experience, it usually takes three tries for a closed-boundary reservoir.

The following properties can be determined from the match point (MP):

$$G=\left(\frac{q_g}{q_{dD}}\right)_{MP}\left(\frac{t_n}{t_{dD}}\right)_{MP}\frac{2(\bar{p}/z)_i S_{gi}}{(\mu c_t)_i(p_{pi}-p_{pwf})}. \quad \ldots\ldots\ldots\ldots (18)$$

$$(G_p)_{ult}=\left(\frac{q_g}{q_{dD}}\right)_{MP}\left(\frac{t_n}{t_{dD}}\right)_{MP}\frac{S_{gi}}{\lambda}. \quad \ldots\ldots\ldots\ldots\ldots\ldots (19)$$

$$k_g h=\left(\frac{q_g}{q_{dD}}\right)_{MP}\frac{p_{sc}T\,\tfrac{1}{2}\ln\left(\frac{2.2485A}{19.1785r_w^2}\right)}{1.987\times10^{-5}T_{sc}(p_{pi}-p_{pwf})}. \quad \ldots\ldots\ldots (20)$$

and

$$k_g/\phi=\left(\frac{t_{dD}}{t_n}\right)_{MP}\frac{\left(\frac{A}{\pi}-r_w^2\right)\ln\left(\frac{2.2485A}{19.1785r_w^2}\right)}{\frac{0.00633}{4(\mu c_t)_i}}. \quad \ldots\ldots\ldots (21)$$

Reservoir Simulation Runs

Numerical results were generated to test the validity of the normalized-time transformation. A three-dimensional (3D), three-phase, general-purpose simulator was used to simulate the real gas reservoirs. After each run was made, the results were processed to transform the time from actual time to normalized time. The results of both actual- and normalized-time plots were then compared.

The runs reported in this section were either two-dimensional (x,y) coordinates or one-dimensional radial coordinates. Some 3D runs were made for analyzing layered reservoirs. They are reported in another section.

Cases 1 through 4 were chosen to illustrate the use of the normalized time. The data for these four cases are presented in Table 1. The reservoir and gas properties were held constant for all four cases. The only properties that were varied for the four cases were the initial reservoir pressure, the constant BHFP, and the reservoir size and shape.

The simulated results for these four cases are shown in Figs. 2 through 5. Each of these plots shows production rate vs. time. Each figure shows three curves. The solid line represents the analytic solution for the exponential decline case ($b=0$) after boundary effects, and a value of $r_e/r_w=14{,}000$ for the earlier (flat) part of the

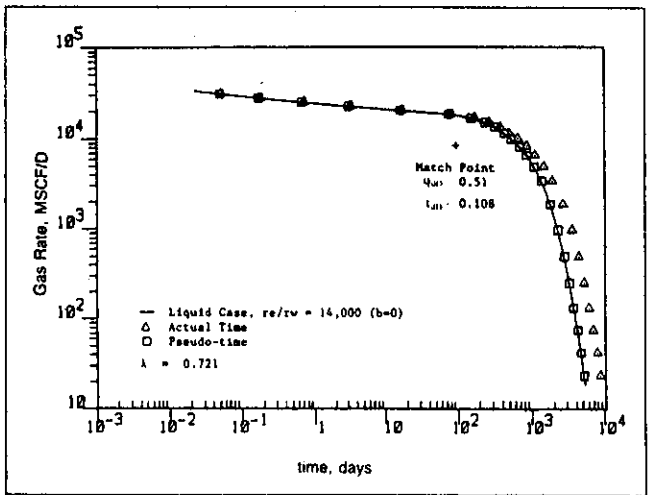

Fig. 2—Case 1—Actual time and pseudotime compared with liquid exponential decline case.

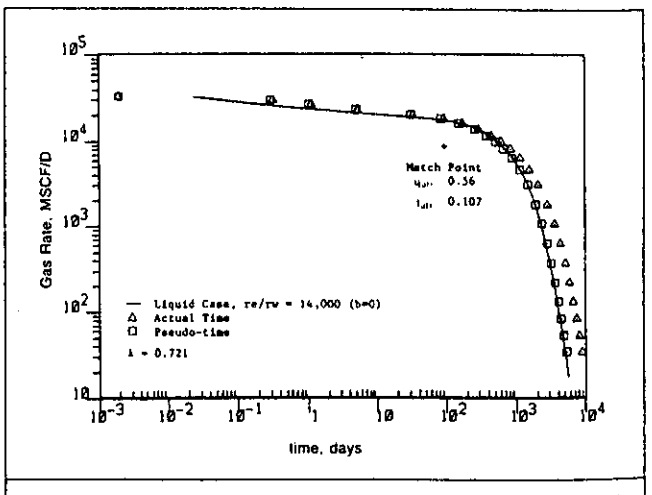

Fig. 3—Case 2—Actual time and pseudotime compared with liquid exponential decline case.

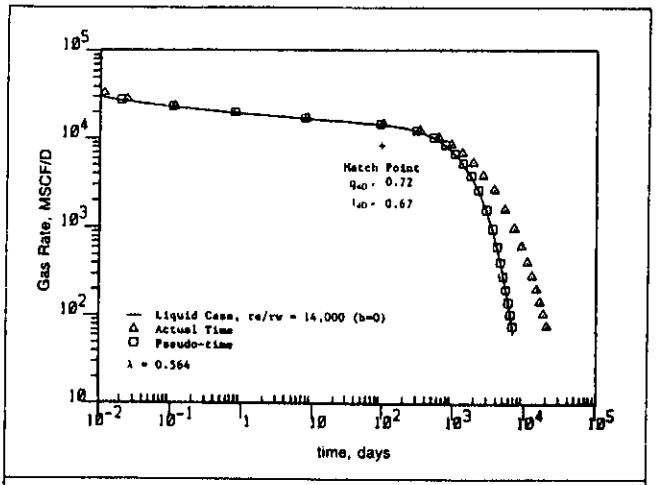

Fig. 4—Case 3—Actual time and pseudotime compared with liquid exponential decline case.

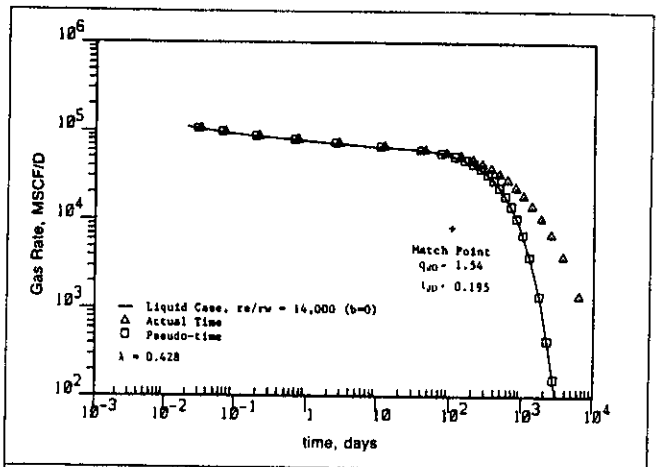

Fig. 5—Case 4—Actual time and pseudotime compared with liquid exponential decline case.

curve, which represents transient behavior. The second curve in Figs. 2 through 5 is shown by triangles that represent the simulated results plotted as actual time in days. The third curve in Figs. 2 through 5 is shown by squares that represent the time scale transformed to normalized time.

Figs. 2 through 5 show that the normalized-time transformation brings the boundary-dominated flow region exactly on the analytic solutions. This confirms that the normalized-time cases can be analyzed with liquid solutions given by Fetkovich's type curve for $b=0$.

The simulated results plotted as actual time (triangles) do not follow the Fetkovich type curves for any value of b. This means that a closed gas reservoir does not follow an exponential, harmonic, or hyperbolic decline curve. If only early-time data are available for a field case, the early boundary-dominated flow behavior might appear to follow one of the b curves. The analysis based on that curve will lead to incorrect results.

Note also in Figs. 2 through 5, as expected, that the normalized time transformation does not affect the transient solutions. This is true because the average reservoir pressure does not decline significantly during transient flow.

The spread between the two curves (the extent of the correction from actual time to normalized time) varies for the four cases shown. The degree of deviation between the two curves is related to the pressure drawdown as compared with the initial pressure. The higher this fractional drawdown, the greater the deviation between the two curves. The λ parameter (Eq. 1) is an index of the fractional drawdown. For values of λ approaching 1.0, there is little drawdown, and little deviation from gas properties between the two curves would be expected. As λ decreases, the fractional drawdown is greater and a greater deviation is observed as shown, for example, in Figs. 4 and 5.

Case 2, shown in Fig. 3, shows the results for a rectangular reservoir with an aspect ratio of 2 : 1 with the well located in the middle of one end. The early transient data do not match the analytic solution for a radial case, but the data will match the analytic solution for a rectangular shape. Because average reservoir pressure is independent of reservoir shape, the time transformation is valid for any reservoir shape.

Now let us turn our attention to the type-curve analysis of the curves shown in Figs. 2 through 5 for the actual-time curves and the normalized-time curves.

Procedure for Calculation of Normalized Time for a Gas Reservoir

Step 1. Make an evenly spaced table of (p/z) vs. $\bar{p}_p$. The $\bar{p}_p$ function should not vary more than 3% in a pressure interval. The fine spacing ensures that the finite-difference slopes evaluated from this table are accurate. Then,

$$p_p = 2\int_0^p \frac{\mathrm{d}(\bar{p}/z)}{\mu_g c_t}, \quad \ldots\ldots\ldots\ldots\ldots\ldots\ldots\ldots\ldots\ldots (22)$$

where

$$c_t = S_g c_g + S_w c_w + c_f. \quad \ldots\ldots\ldots\ldots\ldots\ldots\ldots\ldots\ldots\ldots (23)$$

Step 2. Find the $(\bar{p}/z)_j$ for each cumulative production point, G_{pj}, using the Ramagost and Farshad material-balance equation[13]:

$$(\bar{p}/z)_j \left[1 - \frac{(p_i - \bar{p})(S_{wi}c_w + c_f)}{S_{gi}}\right] = (p/z)_i (1 - G_{pj}/G). \quad \ldots\ldots\ldots\ldots\ldots\ldots\ldots\ldots\ldots\ldots (24)$$

Step 3. Evaluate $\bar{p}_p$ from the evenly spaced table.

Step 4. Calculate Δt_n from

$$(\mu c_t)_{\bar{p}_j} = 2\left\{\frac{(\bar{p}/z)_{j-1} - (\bar{p}/z)_j}{(\bar{p}_{pj-1} - \bar{p}_{pj})}\right\} \quad \ldots\ldots\ldots\ldots\ldots\ldots\ldots\ldots\ldots\ldots (25)$$

and

$$\Delta t_{nj} = \frac{(\mu c_t)_i}{(\mu c_t)_p} \Delta t_j. \quad \ldots\ldots\ldots\ldots\ldots\ldots\ldots\ldots\ldots\ldots (26)$$

where $(\mu c_t)_p$ is the correct pressure-average value of (μc_t) over each time interval.

Step 5. Evaluate t_{ni} from

$$t_{ni} = \sum_{j=1}^{i} \Delta t_{nj}. \quad \ldots\ldots\ldots\ldots\ldots\ldots\ldots\ldots\ldots\ldots (27)$$

Step 6. Plot q_{gi} vs. t_{ni}, find the match point, and calculate G. If it is significantly different from the assumed G, then repeat the procedure starting with Step 2.

This procedure will assume radial flow into the well over the net pay thickness if the Fetkovich curve is used. This is a good assumption for long-term rate performance of hydraulically fractured wells. We assumed that rock and water properties are constant over the pressure range and that gravity forces and Darcy flow around the wellbore were negligible. For slowly changing rates, we have found that plotting $q_g/(p_i - p_{wf})$ vs. normalized time gives excellent results. For drastic changes in p_{wf}, we recommend the superposition principle.

If any of the reservoir properties vary, then the engineer will calculate average reservoir properties for that drainage area. We have found that we can use average volumetric compressibilities for water and gas for volumetric aquifers with PV's less than four times the gas reservoir PV.

TABLE 2—PVT PROPERTIES (abridged)

Pressure (psi)	Viscosity (cp)	Compressibility Factor	Gas Compressibility (10^{-3} psi^{-1})	Real Gas Pseudopressure (10^9 psi^2/cp)	Storage Pseudopressure (10^9 psi^2/cp)
500	0.1272	0.9693	2.2870	0.01965	0.01969
1,000	0.1373	0.9388	1.0500	0.07487	0.07673
1,500	0.1479	0.9184	0.6734	0.16380	0.17820
2,000	0.1570	0.9102	0.5299	0.28220	0.28780
2,500	0.1676	0.9105	0.3890	0.42550	0.43270
3,000	0.1786	0.9198	0.3046	0.58880	0.59730
3,500	0.1899	0.9364	0.2433	0.76770	0.77660
4,000	0.2018	0.9590	0.1978	0.95790	0.96630
4,500	0.2136	0.9861	0.1635	1.1560	1.1630
5,000	0.2258	1.0165	0.1372	1.3590	1.3630

Example 1

Simulation Case 1—Circular Reservoir. In this example, we show how the rate vs. normalized time matches the type curve for a perfect case. An abridged fluid property table is shown in Table 2. The actual (p/z) increment was 12 psi [83 kPa]. If data storage is a problem, slice the table into partitions such that each partition is accurately approximated with a quadratic or cubic polynomial.

The rate-vs.-time data are shown in Table 3. The plot of the rate vs. real time is shown in Fig. 2. The real-time match point is shown, but the b used is not shown. Notice that the plot of the rates parallels the exponential decline curve late in life. This phenomenon is caused by the fluid properties' becoming constant as the average reservoir pressure approaches wellbore pressure.

Now we will discuss the iteration procedure for this gas well.

Initial Match (Actual Time). For the initial time match, the rate is plotted vs. time and match on the type curve. When matching the actual time decline curve, use the $b>0$ curves for the best accuracy.

For the match point (see Fig. 2),
$q_{dD}=0.52$, $t_{dD}=1.08$, $q=10{,}000$, $t=1{,}000$,

$$G=\frac{q_g}{q_{dD}}\frac{t_n}{t_{dD}}\frac{2(p/z)_i S_{gi}}{(\mu c_t)_i(p_{pi}-p_{pwf})} \quad \ldots\ldots\ldots\ldots\ldots\ldots (18)$$

$$=\left(\frac{10{,}000}{0.55}\right)\left(\frac{1{,}000}{1.08}\right)$$

$$\times\left[\frac{(2)(4{,}918.5)(0.99)}{(3.099\times10^{-6})(1.359\times10^{9}-5.888\times10^{8})}\right]$$

$=70.6$ Bscf [2×10^9 std m^3].

Iteration 1 (Normalized Time). For the match point, $t_{dD}=1.24$, $q_{dD}=0.511$, $G=64.3$ Bscf [1.82×10^9 std m^3], $t=1{,}000$, and $q=10{,}000$.

Iteration 2 (Normalized Time). For the match point, $t_{dD}=1.29$, $q_{dD}=0.51$, $G=62.0$ Bscf [1.76×10^9 std m^3], $t=1{,}000$, and $q=10{,}000$.

Iteration 3 (Normalized Time). For the match point, $t_{dD}=1.30$, $q_{dD}=0.51$, $G=61.50$ Bscf [1.74×10^9 std m^3], $t=1{,}000$, and $q=10{,}000$.

The third iteration decline curve traces the $b=0$ type curve. The engineer can now calculate the reservoir properties with a high level of confidence:

$$k_g h=\frac{q_g}{q_{dD}}\frac{p_{sc}T\,\tfrac{1}{2}\ln\left(\frac{2.2485A}{19.1785r_w^2}\right)}{1.987\times10^{-5}T_{sc}(p_{pi}-p_{pwf})} \quad \ldots\ldots\ldots\ldots\ldots\ldots (20)$$

$$=\frac{10{,}000}{0.55}\frac{14.7(660)\ln\left[\frac{(2.2485)(3.848\times10^7)}{(19.1785)(0.25^2)}\right]}{(2)(1.985\times10^{-5})(520)}$$

$$\times\frac{1}{(1.3593\times10^{9}-5.888\times10^{8})}$$

$=199.7$ md-ft [61 md·m],

TABLE 3—CASE 1 DATA

Production Rate (Mscf/D)	Actual Time (days)	Third Iteration Pseudotime (days)
30,400	0.052	0.050
27,300	0.180	0.168
24,600	0.729	0.676
22,200	3.38	3.13
20,100	17.7	16.3
18,100	83.2	75.3
16,400	174	154
14,700	276	239
13,000	389	330
11,300	520	431
9,650	668	540
7,990	880	690
6,330	1,150	872
4,750	1,490	1,090
3,250	1,950	1,370
1,800	2,690	1,800
921	3,550	2,280
472	4,410	2,750

TABLE 4—RESULTS OF MANUAL TYPE-CURVE MATCH

Data from Match Points	Case 1	Case 2	Case 3	Case 4
t_{dD} at $t_n=1{,}000$	1.30	1.18	0.75	2.22
q_{dD} at $g(t)_n=10{,}000$	0.51	0.55	0.70	1.54
t_{dD} at $t=10{,}000$	1.08	1.07	0.67	1.95
q_{dD} at $q(t)=1{,}000$	0.52	0.56	0.72	1.54
Arps factor, b				
t_n	0	0	0	0
t	0.3	0.3	0.4	0.7
G, Bscf				
t_n	61.49	61.41	40.2	81.3
t	73.30	70.00	52.9	91.5
Model	61.51	61.51	40.5	81.6
kh, md-ft				
t_n	200	200	198	201
t	187	197	191	202
Model	200	200	200	200
k/ϕ, md				
t_n	32.5	32.4	32.9	31.9
t	27.0	28.9	29.4	27.8
Model	32.8	32.8	33.0	32.5

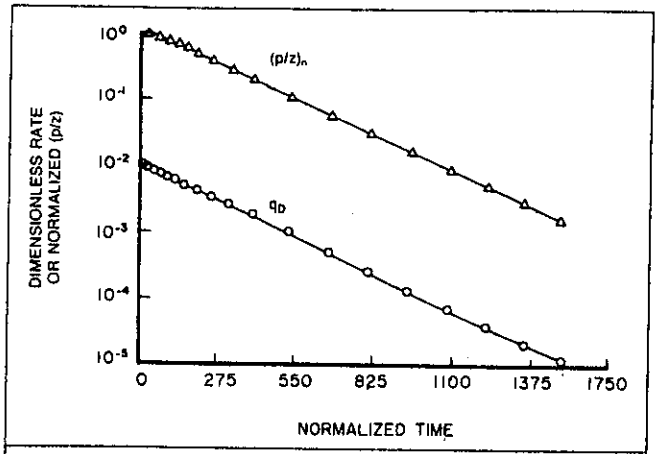

Fig. 6—Case 1—normalized (p/z) compared to dimensionless rate.

TABLE 6—CALCULATED FLUID PROPERTIES, WELL A

Pressure (psia)	p/z (psi)	$1/\mu c_g$ (psi/cp)	Pseudopressure (psia²/cp)
14.65	14.67	1,114	0.22324×10^{4}
208.75	212.19	15,508	0.33256×10^{7}
417.50	431.12	30,166	0.13372×10^{8}
626.25	656.41	43,964	0.30111×10^{8}
835.00	887.47	56,955	0.53457×10^{8}
1,043.75	1,123.47	69,238	0.83255×10^{8}
1,252.50	1,363.33	80,943	0.11928×10^{9}
1,461.25	1,605.76	92,219	0.16126×10^{9}
1,670.00	1,849.27	103,221	0.20885×10^{9}
1,878.75	2,092.29	114,101	0.26166×10^{9}
2,087.50	2,333.22	124,992	0.31929×10^{9}
2,296.25	2,570.54	136,004	0.38130×10^{9}
2,505.00	2,802.90	147,216	0.44725×10^{9}
2,713.75	3,029.18	158,682	0.51672×10^{9}
2,922.50	3,248.48	170,430	0.58929×10^{9}
3,131.25	3,460.18	182,468	0.66457×10^{9}
3,340.00	3,663.88	194,794	0.74221×10^{9}
3,548.75	3,859.39	207,399	0.82188×10^{9}
3,757.50	4,046.66	220,266	0.90329×10^{9}
3,966.25	4,225.80	233,383	0.98618×10^{9}
4,175.00	4,396.99	246,733	0.10703×10^{10}
4,383.75	4,560.49	260,301	0.11555×10^{10}

and

$$k_g/\phi=\frac{t_{dD}}{t_n}\frac{\left(\frac{A}{\pi}-r_w^2\right)\ln\left(\frac{2.2845A}{19.1785r_w^2}\right)}{\frac{0.00633}{4(\mu c_t)_i}} \quad \ldots\ldots\ldots\ldots (21)$$

$$=\frac{1.20}{1{,}000}\frac{\left(\frac{3.848\times10^{7}}{\pi}-0.25^2\right)}{\frac{0.00633}{43.099\times10^{-6}}}$$

$$\times\frac{\ln\left[\frac{(2.2485)(3.848\times10^{7})}{(19.1785)(0.25^2)}\right]}{1}$$

$$=32.5 \text{ md vol/vol.}$$

The results for the other cases are shown in Table 4. The average percentage error was less than 1% for Case 1 with a manual type-curve match. We have found errors around 1% when we used superposition to match the slowly changing or stair-step BHP cases.

TABLE 5—FIELD EXAMPLE—WEST VIRGINIA; WELL A RESERVOIR AND FLUID PROPERTIES

Gas specific gravity	0.57 (air = 1.00)
ϕ, %	6.0
S_w, %	35.0
p_i, psi	4,175
h, ft	70
T, °F	160
r_w, ft	0.354
p, psi	500

TABLE 7—GAS RATE vs. TIME, WELL A

Time (days)	Gas Rate (Mscf/D)
9.36	2,382.8
31.57	2,339.8
58.12	1,755.3
89.97	1,832.2
119.02	1,542.6
148.51	1,580.6
167.35	1,555.7
206.37	1,676.5
230.26	1,386.0
260.95	1,364.2
287.52	1,297.9
315.07	1,207.3
349.02	1,194.8
375.68	1,229.6
406.99	1,156.6
428.66	1,057.5
466.85	1,040.5
502.28	1,132.8
554.18	915.6
635.06	927.0
689.14	712.1
728.47	834.0
759.19	692.9
789.24	775.7
865.26	682.1
969.14	702.2
1,049.65	679.3
1,056.52	614.0
1,144.50	580.8
1,276.13	519.4
1,367.30	469.7
1,453.01	575.4
1,559.88	410.8
1,662.55	353.1
1,799.91	359.4
1,892.29	409.2
2,110.90	346.0
2,152.70	254.0
2,331.22	249.9
2,465.40	276.6
2,498.23	220.9
2,583.15	239.1
2,692.33	196.4
2,818.95	184.7
2,930.14	210.3
3,104.16	189.1

Normalized (p/z) vs. Normalized Time

Plotting normalized average reservoir pressure vs. normalized time is a better method to converge on G when the rate data are unstable. The method is based on the cumulative production vs. time. First, Eq. 15 is integrated to find

$$\ln[1-G_p/(G_p)_{ult}]=\frac{t_D}{\frac{1}{2}\left(\frac{A}{\pi r_w^2}-1\right)\frac{1}{2}\ln\left(\frac{2.2485A}{C_A r_w^2}\right)} \quad \ldots (28)$$

TABLE 8—NORMALIZED (p/z) vs. NORMALIZED TIME, WELL A

Time (days)	Normalized Time (days)	Normalized (p/z) (days)	$(\mu c_g)_i/(\mu c_g)_p$
0.00000	0.00000	1.000000	1.000000
9.36030	9.31159	0.991142	0.994796
31.5730	31.0261	0.970311	0.977573
58.1210	56.9002	0.948723	0.974616
89.9798	87.1038	0.926027	0.948045
119.029	113.930	0.906559	0.923474
148.520	140.533	0.888269	0.902071
167.359	157.214	0.876536	0.885434
206.378	190.987	0.851493	0.865557
230.263	211.162	0.836967	0.844663
260.951	236.588	0.820209	0.828557
287.527	258.195	0.806160	0.813015
315.075	280.214	0.792455	0.799289
349.027	306.859	0.776260	0.784784
375.688	327.414	0.763425	0.770962
406.994	351.145	0.748591	0.758035
428.662	367.327	0.739064	0.746834
466.853	395.410	0.723153	0.735336
502.280	420.970	0.707863	0.721470
554.185	457.596	0.686750	0.705635
635.069	512.933	0.657155	0.684154
689.146	548.877	0.639553	0.664683
728.472	574.545	0.627479	0.652711
759.190	594.334	0.618164	0.644205
789.248	613.484	0.609398	0.637091
865.269	661.008	0.587391	0.625149
969.145	723.947	0.558837	0.605910
1,049.66	771.214	0.536749	0.587074
1,056.52	775.186	0.534985	0.578340
1,144.51	825.351	0.514110	0.570152
1,276.14	898.066	0.485351	0.552436
1,367.31	946.937	0.467443	0.536045
1,453.02	991.824	0.449654	0.523677
1,559.88	1,046.37	0.428724	0.510403
1,662.56	1,097.50	0.413146	0.497996
1,799.92	1,164.28	0.393709	0.486187
1,892.29	1,208.15	0.379610	0.474938
2,110.90	1,308.56	0.346825	0.459298
2,152.71	1,327.24	0.341845	0.446736
2,331.22	1,405.63	0.323982	0.439150
2,465.40	1,463.13	0.309952	0.428560
2,498.23	1,477.02	0.306708	0.422821
2,583.16	1,512.61	0.298949	0.419164
2,692.34	1,557.75	0.289506	0.413440
2,818.95	1,609.30	0.279921	0.407100
2,930.15	1,653.89	0.271197	0.400988
3,104.16	1,722.35	0.257395	0.393448

From the material-balance equation, Eq. 24, we can derive the relation for $[1-G_p/(G_p)_{ult}]$:

$$1-G_p/(G_p)_{ult}=\frac{(\bar{p}/z)_j C_{av}-(\bar{p}/z)_{wf}C_{wf}}{(\bar{p}/z)_i-(\bar{p}/z)_{wf}C_{wf}}, \quad \ldots\ldots\ldots\ldots (29)$$

where

$$C_{av}=1-(p_i-\bar{p})(S_{wi}c_w+c_f)/S_{gi}$$

and

$$C_{wf}=1-(p_i-p_{wf})(S_{wi}c_w+c_f)/S_{gi}.$$

The right side of Eq. 29 is called normalized and will be denoted $(p/z)_n$. If the pressure drawdown is not too large, then C_{wf} and C_{av} can be approximated by setting them equal to 1.

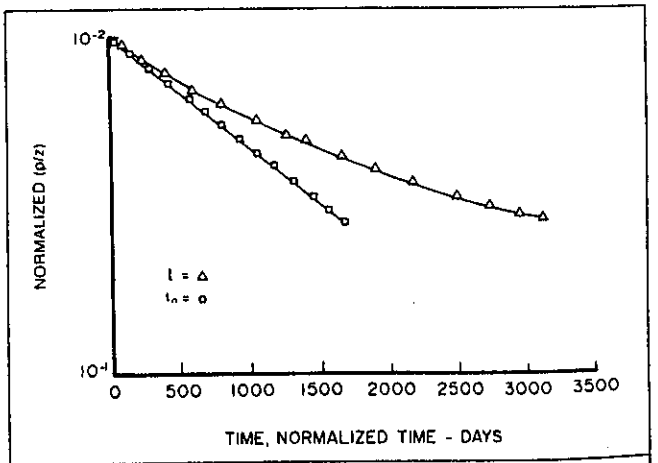

Fig. 7—Field case—sixth iteration $(\bar{p}/z)_n$ for actual and normalized time.

TABLE 9—NORMALIZED TIME vs. t_D, q_g, q_D, Q_D, Well A				
Normalized Time (days)	t_D	q_g	q_D	Q_D
9.31159	228,652.0	2,382.857	0.342112	78,790.0
31.0261	761,867.0	2,339.839	0.335936	264,077.0
56.9002	0.139722×10^7	1,755.315	0.252015	456,101.0
87.1038	0.213889×10^7	1,832.293	0.263066	657,978.0
113.930	0.279764×10^7	1,542.693	0.221488	831,145.0
140.533	0.345087×10^7	1,580.630	0.226935	993,829.0
157.214	0.386049×10^7	1,555.702	0.223356	0.109819×10^7
190.987	0.468981×10^7	1,676.541	0.240705	0.132095×10^7
211.162	0.518522×10^7	1,386.024	0.198995	0.145015×10^7
236.588	0.580958×10^7	1,364.227	0.195865	0.159922×10^7
258.195	0.634015×10^7	1,297.929	0.186347	0.172418×10^7
280.214	0.688083×10^7	1,207.334	0.173340	0.184608×10^7
306.859	0.753512×10^7	1,194.827	0.171544	0.199013×10^7
327.414	0.803986×10^7	1,229.633	0.176541	0.210430×10^7
351.145	0.862259×10^7	1,156.633	0.166061	0.223625×10^7
367.327	0.901996×10^7	1,057.562	0.151837	0.232099×10^7
395.410	0.970956×10^7	1,040.594	0.149401	0.246252×10^7
420.970	0.103372×10^8	1,132.847	0.162645	0.259852×10^7
457.596	0.112366×10^8	915.629	0.131459	0.278632×10^7
512.933	0.125954×10^8	927.012	0.133093	0.304956×10^7
548.877	0.134780×10^8	712.191	0.102251	0.320613×10^7
574.545	0.141083×10^8	834.010	0.119741	0.331353×10^7
594.334	0.145943×10^8	692.993	0.994946×10^{-1}	0.339638×10^7
613.484	0.150645×10^8	775.724	0.111373	0.347435×10^7
661.008	0.162315×10^8	682.126	0.979345×10^{-1}	0.367010×10^7
723.947	0.177770×10^8	702.224	0.100820	0.392409×10^7
771.214	0.189377×10^8	679.369	0.975386×10^{-1}	0.412056×10^7
775.186	0.190352×10^8	614.004	0.881540×10^{-1}	0.413624×10^7
825.351	0.202670×10^8	580.809	0.833881×10^{-1}	0.432192×10^7
898.066	0.220526×10^8	519.489	0.745843×10^{-1}	0.457773×10^7
946.937	0.232527×10^8	469.746	0.674425×10^{-1}	0.473702×10^7
991.824	0.243549×10^8	575.430	0.826159×10^{-1}	0.489525×10^7
1,046.37	0.256942×10^8	410.884	0.589916×10^{-1}	0.508142×10^7
1,097.50	0.269498×10^8	353.190	0.507083×10^{-1}	0.521998×10^7
1,164.28	0.285897×10^8	359.430	0.516043×10^{-1}	0.539287×10^7
1,208.15	0.296670×10^8	409.223	0.587531×10^{-1}	0.551828×10^7
1,308.56	0.321326×10^8	346.006	0.496769×10^{-1}	0.580990×10^7
1,327.24	0.325912×10^8	254.003	0.364678×10^{-1}	0.585420×10^7
1,405.63	0.345162×10^8	249.916	0.358811×10^{-1}	0.601308×10^7
1,463.13	0.359282×10^8	276.662	0.397210×10^{-1}	0.613788×10^7
1,477.02	0.362691×10^8	220.960	0.317237×10^{-1}	0.616674×10^7
1,512.61	0.371432×10^8	239.122	0.343314×10^{-1}	0.623575×10^7
1,557.75	0.382516×10^8	196.469	0.282075×10^{-1}	0.631975×10^7
1,609.30	0.395174×10^8	184.754	0.265256×10^{-1}	0.640500×10^7
1,653.89	0.406123×10^8	210.328	0.301974×10^{-1}	0.648260×10^7
1,722.35	0.422935×10^8	189.105	0.271502×10^{-1}	0.660537×10^7

Substituting Eq. 29 into Eq. 28, we find

$$\ln\left[\frac{(\bar{p}/z)_j C_{av} - (\bar{p}/z)_{wf} C_{wf}}{(\bar{p}/z)_i - (\bar{p}/z)_{wf} C_{wf}}\right] = \frac{t_{nD}}{\frac{1}{2}\left(\frac{A}{\pi r_w^2} - 1\right) \frac{1}{2} \ln\left(\frac{2.2485A}{C_A r_w^2}\right)},$$

which can also be expressed as

$$\ln[(\bar{p}/z)_n] = t_{dD}. \qquad (30)$$

Thus, we can plot normalized (p/z) vs. normalized time and get a semilog straight line with an intercept approximately equal to 1. For most of the field cases we matched, the intercept ranged from 1.02 to 0.95. We used Case 1 data to test the method, except we added a random 5% of the current average reservoir pressure drop to the BHP to represent fluid loading in the gas well. The plot of the dimensionless rate and normalized (p/z) vs. normalized time is shown in Fig. 6. Note that the normalized (p/z) is almost a straight line, and a unique match can be made on G and lifetime average BHP. The least-squares best-fit straight line of the normalized (p/z) data had slope error of less than 2% and an intercept of 1.015.

Calculated Results

Table 4 shows four basic closed-boundary reservoir cases that vary in shape and pressure. In each case, the normalized-time correction improves the accuracy of the type curves. Cases 1 and 3 are radial cases where the pressure was varied. Cases 1 and 2 have a very accurate match because the well's decline curve can be matched in the transient region and in the decline region. Case 4 is a square with a very high drawdown. The square also behaves like the radial case. Therefore, both regions were used to match the decline curve. Case 2 is a 2 : 1 rectangle, and its transient region cannot be used in the decline-curve match because only circular shapes are given. For shapes with $C_A < 4$, the rate has to decline to 40% of the "initial" boundary-dominated flow rate, q_i, before a good match can be obtained with the radial-flow type curve.

Example 2

Field Case—Low-Permeability Fractured Gas Well. The data for this well come from Ref. 2. The reservoir data are shown in Table 5, the calculated fluid properties are shown in Table 6, and the digitized raw rate-time data are shown in Table 7. This well was chosen because we wanted an independent actual time match of the data.

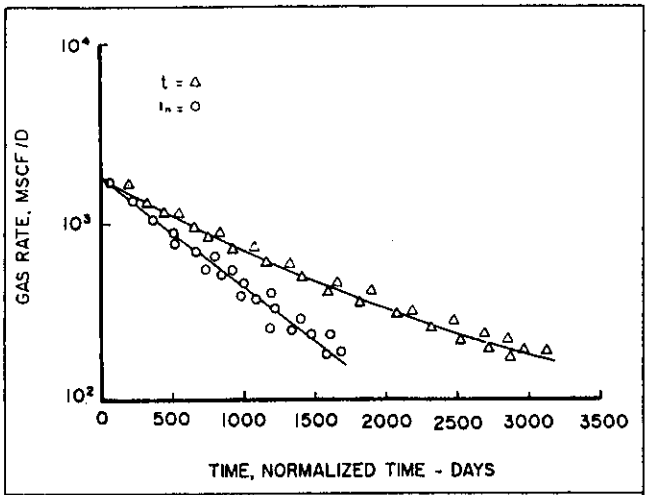

Fig. 8—Field case—gas rate for actual and normalized time.

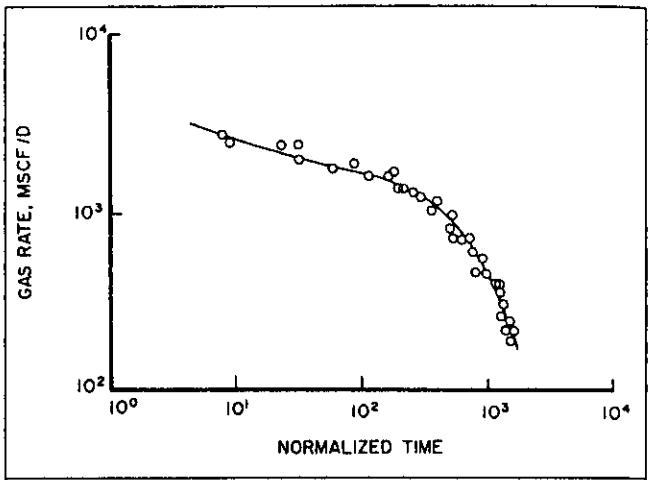

Fig. 9—Field case—final match of gas rate, $r_e/r_w = 24$.

This is a hydraulically fractured gas well completed in the Onondaga chert in West Virginia. The well was initially produced for 200 days and then shut in for a 106-day buildup in an attempt to determine average reservoir pressure. With this average reservoir pressure, they estimated G to be 3.36 Bscf [0.09×10^9 std m^3] using the material-balance equation. The well also has a problem of water loading up the wellbore. The time, normalized time, normalized (p/z) and pressure-average $(\mu c_t)/(\mu c_t)_p$ data are shown in Table 8. It took six iterations to converge on G using the normalized (p/z) plot because we had to increase the line pressure from 500 to 710 psi [3.4 to 4.9 MPa] to represent the lifetime average BHP. With the 710-psi [4.9-MPa] BHP, we almost had a perfect straight line on the normalized (p/z) vs. normalized-time plot, as shown in Fig. 7.

In the next step, we plot rate vs. the normalized time that was generated during the (p/z) match. Normalized time, dimensionless time, gas rate, dimensionless rate, and dimensionless cumulative production are shown in Table 9. In Fig. 8, we see a large range of scatter for the rate data that is caused by the liquid loading, occasional shut-ins, and blows to the atmosphere. Note that two to three data points were skipped between each plotted data point. With this much scatter in the data, it is easy to get a small range of reasonable fits to the type curve. Thus, we calculate a small range of gas in place for the reservoir and we see a small range of r_e/r_w ratios that could be used in the skin calculation. But if we use the normalized time from the (p/z) match, we fix the time axis and vary the rate axis for the best fit that gives a more unique and accurate match. The gas in place calculated from the rate-time match should agree with the (p/z) match; if they do not agree, the rate-time curve is moved up or down. For large differences, the wellbore pressure should be changed and the process should be repeated. For manual type-curve matching, we found an r_e/r_w stem equal to 20. For a computer-generated type curve, we found an r_e/r_w stem equal to 25. Finally, we used a linear optimization program that chose an r_e/r_w stem equal to 24, which is shown in Fig. 9.

After a match is obtained, the best-fit r_e/r_w stem is recorded and the permeability and porosity are calculated. With the porosity, saturations, and original gas in place, the external radius can be calculated. Finally, with the external radius and the r_e/r_w ratio, the effective wellbore radius can be calculated. These results are shown in Table 10 and are compared with the best-fit results of Refs. 1 and 2. Note that they used the gas in place from the buildup test to help estimate the r_e/r_w stem. The main advantage of this method is that we are very confident in the future performance prediction of the Fetkovich curve using normalized time. With the actual-time method, you must pick the best-fit b curve to extrapolate the future production, which Fetkovich and we have shown to be inaccurate.

In an effort to determine the effect of two-phase flow in the fracture and the effect of liquid loading the wellbore, we compared the declines of the normalized (p/z) and dimensionless rate, as shown in Fig. 10. From our experience, the (p/z) plot is a good approximation of the rate decline of a well at perfect conditions. From Table 10 we see that the dimensionless-rate plot declines about 1.75 times faster than the (p/z) plot. Thus, we have an approximate method of calculating reserves for a well at completely unloaded conditions and at current conditions. With these incremental reserves we can determine whether it is profitable to install equipment or to replace tubing to keep the wellbore unloaded.

TABLE 10—RESULTS OF NORMALIZED TIME MATCH AND ACTUAL TIME MATCH, WELL A

	Normalized Time	Actual Time
Normalized (p/z)		
Slope of $\ln(\bar{p}/z)_n$ vs. t_n	-0.343743×10^{-3}	
Y-intercept	0.989647	
Estimated G, Mscf	0.303451×10^7	
Produced G, Mscf	0.251800×10^7	
p_i, psi	4,175	4,175
p_{wf}, psi	710	500
Residual	0.999833	
Gas Rate		
Effective r_e/r_w	24	20
Estimated G, Mscf	0.303451×10^7	0.360×10^7
s	−5.07873	−5.17
k, md	0.07678	0.070
Slope of ln(rate) vs. t_n	-0.601474×10^{-3}	
Residual	0.983423	
r_e, ft	1,128.5	1,242
r_w, ft	47.2	62.1

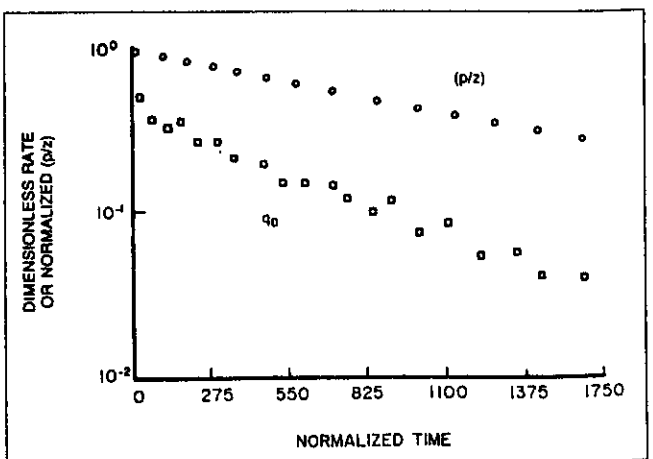

Fig. 10—Field case—decline comparison of (p/z) and dimensionless rate.

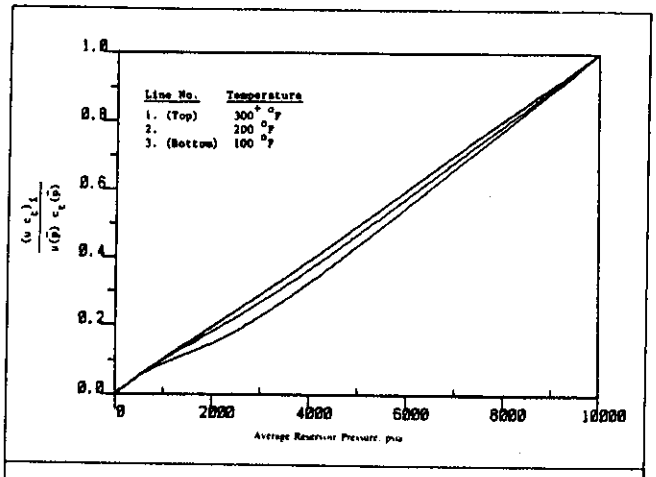

Fig. 11—Variation of the t_n integrand with reservoir temperature; gas gravity = 0.6, p_i = 10,000 psia.

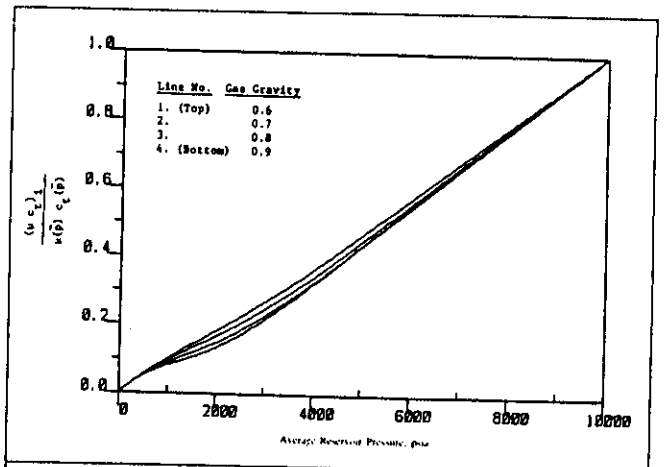

Fig. 12—Variation of the t_n integrand with gas gravity; reservoir temperature = 200°F, p_i = 10,000 psia.

Other Cases

Crossflow and layered-reservoir cases were investigated, and we found that gas behaves like a liquid with normalized time. We came to the same conclusion as Russell[11] in that a reservoir with crossflow can behave like a homogeneous reservoir. We also came to the same conclusion as Fetkovich[1] that for a layered reservoir, the decline for the reservoir is the summation of the decline curves for each layer. Each layer has its own normalized time. Wellbore pressure changes were also investigated. Normalized time is reset back to zero for each pressure change,[1] and the material-balance equation still uses total cumulative production.

Discussion

A time transformation is introduced to account for the variation of fluid properties as the average reservoir pressure depletes. This normalized time is different from the pseudotime used by Agarwal[5] and Lee and Holditch[6] because the fluid properties, μ and c_t, are evaluated at average reservoir pressure in the time integration rather than at the wellbore pressure. We have also chosen to use a μc_t ratio as the integrand so that the normalized time has the dimensions of time (days).

We have shown that the transformation of simulation results seems to linearize the pseudosteady-state results exactly without affecting the transient results. Through this linearization, all the simulated results fit the liquid-acting exponential decline case ($b=0$). None of the simulated results, plotted as actual time or normalized time, fit any of the harmonic or hyperbolic decline curves ($b>0$).

By use of the normalized-time plots, it is possible to determine G, kh, and k/ϕ from type-curve analysis.

The method has the disadvantage of requiring an estimate of G before the normalized time can be calculated. However, we have found that two or three iterations are all that is required in estimating G and then calculating the same G from the type-curve match. Figs. 11 and 12 show how $(\mu c_g)_i/(\mu c_g)_p$ varies with pressure for various gas gravities and reservoir temperatures. The curves are almost linear, making the integration of normalized time fairly easy and accurate.

Conclusions

1. None of the cases of a gas reservoir producing at constant flowing pressure matches any of Fetkovitch's exponential, harmonic, or hyperbolic decline curves when actual time is used.
2. When transformed to normalized time, the boundary-dominated-flow curves match the type curve for liquid exponential depletion exactly.
3. The normalized-time transformation does not have any significant effect on transient behavior.
4. Correct values of G, kh, and k/ϕ can be determined accurately with normalized time type-curve analysis. This applies for any reservoir shape if sufficient boundary-dominated flow data are available.
5. If formation compressibility is important, Eq. A-16 should be used to evaluate normalized time rather than Eq. 3.

Nomenclature

A = area, ft^2 [m^2]
b = decline-curve parameter
c_f = rock compressibility, 1/psi [1/kPa]
c_g = gas compressibility, 1/psi [1/kPa]
c_t = total compressibility, 1/psi [1/kPa]
c_w = water compressibility, 1/psi [1/kPa]
C_A = Deitz shape factor
G = original gas in place, Mscf [std m^3]
G_p = cumulative gas production, Mscf [std m^3]
$(G_p)_{ult}$ = ultimate cumulative gas production at p_{wf}, Mscf [std m^3]
h = formation thickness, ft [m]
J = oil productivity index, scf/D-psi [std m^3/d·kPa]
J_g = gas productivity index, Mscf/D-psi^2-cp [std m^3/d·kPa^2·Pa·s]
k = formation permeability, md
N = oil in place, STB [stock-tank m^3]
p = pressure, psia [kPa]
$\bar{p}$ = average reservoir pressure, psia [kPa]
p_i = initial reservoir pressure, psia [kPa]
p_p = real gas pseudopressure, psi^2/cp [kPa^2/Pa·s]
$\bar{p}_p$ = storage pseudopressure, psi^2/cp [kPa^2/Pa·s]
p_{sc} = pressure at standard conditions, psia [kPa]
p_{wf} = wellbore flowing pressure, psia [kPa]
Δp = $p_i - \bar{p}$
$(p/z)_n$ = normalized p/z (Eq. 30)
q_{dD} = decline-curve dimensionless rate (Eq. 16)
q_D = dimensionless rate = 795,746 $q_g/[kh(p_{pi}-p_{pwf})]$
q_g = surface flow rate, Mscf/D [std m^3/d]
q_i = initial rate, applying Eq. 5 at $t=0$
Q_D = dimensionless cumulative production = 5,015.8$G_p/[h(\phi\mu c_t)_i r_w^2(p_{pi}-p_{pwf})]$
r_e = equivalent outer-boundary radius, ft [m]
r_w = wellbore radius, ft [m]
r_w' = effective wellbore radius, $r_w e^{-s}$, ft [m]
s = skin
S = saturation
t = time, days
t_{dD} = decline-curve dimensionless time (Eq. 17)
t_D = dimensionless time (Eq. 14)
t_n = normalized time, days
T = reservoir temperature, °R [K]
T_{sc} = temperature at standard conditions, °F [°C]

V_p = reservoir PV, Mcf [m³]
λ = defined by Eq. 1
μ = gas viscosity, cp [Pa·s]
ϕ = porosity, fraction

Subscripts

dD = dimensionless decline
D = dimensionless
g = gas
i = initial conditions
j = counter
o = oil
sc = standard conditions
t = total
w = water
wf = wellbore flowing conditions

Acknowledgments

We acknowledge the helpful suggestions made by W.J. Lee and T.A. Blasingame during this work.

References

1. Fetkovich, M.J.: "Decline Curve Analysis Using Type Curves," *JPT* (June 1980) 1065-77.
2. Fetkovich, M.J.: "Decline-Curve Analysis Using Type Curves—Case Histories," *SPEFE* (Dec. 1987) 637-56.
3. Arps, J.J.: "Analysis of Decline Curves," *Trans.*, AIME (1945) **160**, 228-47.
4. Carter, R.D.: "Type Curves for Finite Radial and Linear Gas-Flow Systems: Constant-Terminal-Pressure Case," *SPEJ* (Oct. 1985) 719-28.
5. Agarwal, R.G.: "Real Gas Pseudo-Time—A New Function for Pressure Buildup Analysis of MHF Gas Wells," paper SPE 8279 presented at the 1979 SPE Annual Technical Conference and Exhibition, Las Vegas, Sept. 23-26.
6. Lee, W.J. and Holditch, S.A.: "Application of Pseudotime to Buildup Test Analysis of Low-Permeability Gas Wells With Long-Duration Wellbore Storage Distortion," *JPT* (Dec. 1982) 2877-87.
7. Al-Hussainy, R., Ramey, H.J. Jr., and Crawford, P.B.: "The Flow of Real Gases Through Porous Media," *JPT* (May 1966) 624-36; *Trans.*, AIME, **237**.
8. Russell, D.G. and Prats, M.: "The Practical Aspects of Interlayer Crossflow," *JPT* (June 1962) 589-94.
9. Ehlig-Economides, C.A. and Ramey, H.J. Jr.: "Transient Rate Decline Analysis for Wells Produced at a Constant Pressure," *SPEJ* (Feb. 1981) 98-104.
10. Lee, W.J.: *Well Testing*, Textbook Series, SPE, Richardson, TX (1982) 1, 9-11, 76-88.
11. Earlougher, R.C. Jr.: *Advances in Well Test Analysis*, Henry L. Doherty Series, SPE, Richardson, TX (1977) 5.
12. Wattenbarger, R.A. and Ramey, H.J. Jr.: "Gas Well Testing With Turbulence, Damage and Wellbore Storage," *JPT* (Aug. 1968) 99-107; *Trans.* AIME, **243**.
13. Ramagost, B.P. and Farshad, F.F.: "P/Z Abnormally Pressured Gas Reservoirs," paper SPE 10125 presented at the 1981 SPE Annual Technical Conference and Exhibition, San Antonio, Oct. 5-7.

Appendix

The exponential decline case assumes that the exponent is constant, or that q vs. t is exactly a straight line when plotted on semilog graph paper. The following investigates when this is true and when it is an approximation.

Exponential decline seems to apply to the liquid case when c is constant. At initial conditions (the beginning of pseudosteady state), the initial rate is given by

$$q_{oi}=J_o(p_i-p_{wf}). \quad \text{(A-1)}$$

At later times the production rate is given by

$$q_o=J_o(B_{oi}/B_o)(\bar{p}-p_{wf}). \quad \text{(A-2)}$$

Differentiating Eq. A-2 gives

$$dq_o=J_o(B_{oi}/B_o)(1+c_o)d\bar{p}. \quad \text{(A-3)}$$

If c_o is ignored in Eq. A-3, then we have

$$dq_o=J_o(B_{oi}/B_o)d\bar{p}. \quad \text{(A-4)}$$

Now, with any fluid flowing, we have the general expression for dp:

$$d\bar{p}=\frac{-q_oB_o}{V_pc_t}dt. \quad \text{(A-5)}$$

When Eq. A-5 is substituted into Eq. A-4, then

$$dq_o=-J_o(B_{oi}/B_o)\frac{q_oB_o}{V_pc_t}dt. \quad \text{(A-6)}$$

For this case, when $c_t=c_o$, $c_f=0$, and $S_{oi}=1.0$, then we can express the final result in terms of oil in place, N.

$$\int_{q_i}^{q}\frac{dq_o}{q_o}=\frac{-J_o}{Nc_o}\int_{t_{pss}}^{t}dt. \quad \text{(A-7)}$$

This is then integrated to give

$$\ln(q_o/q_{oi})=\frac{-J_o}{Nc_o}t_2, \quad \text{(A-8)}$$

which is in the form of exponential decline because the coefficient of t is constant.

When c_f and c_w are considered and c_o is not constant, this derivation proceeds in the same manner except for the last step when V_p is expressed in terms of N. This modification gives the following result:

$$\ln(q/q_i)=\frac{-J_oS_{oi}}{N}\int_0^t\frac{1}{c_t(1-\Delta pc_f)}dt. \quad \text{(A-9)}$$

Eq. A-9 shows that an integral time transformation is required (even for the liquid case) to get an exponential decline if the oil compressibility changes significantly.

Now, let's go to the gas case. Eq. A-2 is replaced by

$$q_g=J_g(\bar{p}_p-p_{pwf}), \quad \text{(A-10)}$$

which is differentiated to give

$$dq_g=\frac{2J_gp}{z\mu}dp. \quad \text{(A-11)}$$

Because Eq. A-5 applies to gas production as well as liquid production, it is substituted into Eq. A-11 to give

$$dq_g=\frac{-2J_gp}{z\mu}\frac{q_g}{V_pc_t}\left(\frac{z}{p}\right)\left(\frac{p_{sc}T}{T_{sc}}\right)dt, \quad \text{(A-12)}$$

which simplifies to

$$\frac{dq_g}{q_g}=\frac{-2J_g}{V_p\mu c_t}\left(\frac{p_{sc}T}{T_{sc}}\right)dt. \quad \text{(A-13)}$$

When V_p is expressed in terms of G, then we get the following form, where $\Delta p = p_i - \bar{p}$:

$$\frac{dq_g}{q_g} = \left[\frac{-2J_g S_{gi}(\bar{p}/z)_i}{G}\right]\left[\frac{dt}{\mu(\bar{p})c_t(\bar{p})(1-\Delta pc_f)}\right], \qquad \text{(A-14)}$$

which can then be integrated into the final form

$$\ln(q_g/q_{gi}) = \frac{-2J_q S_{gi}(\bar{p}/z)_i}{G(\mu c_t)_i}\int_0^t \frac{(\mu c_t)_i dt}{\mu(\bar{p})c_t(\bar{p})(1-\Delta pc_f)}. \qquad \text{(A-15)}$$

From Eq. A-15, it can be seen that the formation and water compressibility terms enter the integral transformation. Thus, a more general expression for pseudotime is

$$t_n = \int_0^t \frac{(\mu c_t)_i dt}{\mu(\bar{p})c(\bar{p})(1-\Delta pc_f)}, \qquad \text{(A-16)}$$

which simplifies to Eq. 4 when formation and water compressibility or drawdown are small.

The pseudotime expressed by Eq. A-16 seems to be general and could be applied to any type curve that has been developed for exponential decline.

Procedure for Calculating General Pseudotime for a Gas Reservoir.

Step 1. Make an evenly spaced table of $(\bar{p}/z)$ vs. $\bar{p}_p$, where

$$\bar{p}_p = \int_0^p \frac{2d(\bar{p}/z)}{\mu_g c_t(1-\Delta pc_f)} \qquad \text{(A-17)}$$

and

$$c_t = S_g c_g + S_w c_w + c_f. \qquad \text{(A-18)}$$

Note that this relation assumes that gas is the only mobile phase and that the relative permeability for gas is constant.

Step 2. Find the (p/z) for each cumulative production point, G_p, using Ramagost's material-balance equation:

$$\int_0^p \frac{c_t(1-\Delta pc_f)}{S_{gi}c_g} d(\bar{p}/z) = (\bar{p}/z)_i(G_p/G). \qquad \text{(A-19)}$$

Step 3. Evaluate $\bar{p}_p$ from the evenly spaced table.

Step 4. Calculate Δt_n from

$$(\mu c_t)_{av} = 2\left[\frac{(\bar{p}/z)_{j-1} - (\bar{p}/z)_j}{\bar{p}_{p_{j-1}} - \bar{p}_{pj}}\right] \qquad \text{(A-20)}$$

and

$$\Delta t_{nj} = \frac{(\mu c_t)_i}{(\mu c_t)_{av_j}}\Delta t_j. \qquad \text{(A-21)}$$

where $(\mu c_t)_{av}$ is the pressure-averaged $(\mu_g c_t)(1-\Delta pc_f)$ over each time interval.

Step 5. Evaluate t_{n_i} from

$$t_{n_i} = \sum_{j=1}^{i} \Delta t_{nj}.$$

Step 6. Plot q_{g_i} vs. t_{n_i}.

SI Metric Conversion Factors

cp	× 1.0*	E−03	=	Pa·s
ft	× 3.048*	E−01	=	m
ft^2	× 9.290 304*	E−02	=	m^2
ft^3	× 2.831 685	E−02	=	m^3
°F	(°F−32)/1.8		=	°C
psi	× 6.894 757	E+00	=	kPa

*Conversion factor is exact.

SPEFE

Original SPE manuscript received for review Sept. 22, 1985. Paper accepted for publication March 19, 1987. Revised manuscript received March 11, 1987. Paper (SPE 14238) first presented at the 1985 SPE Annual Technical Conference and Exhibition held in Las Vegas, Sept. 22-25.

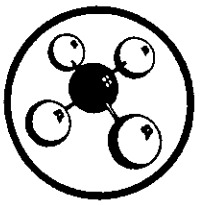

Accelerated Blowdown of a Strong Water-Drive Gas Reservoir

J. L. Lutes,* SPE-AIME, Exxon Co., U.S.A.
C. P. Chiang, SPE-AIME, Exxon Co., U.S.A.
R. H. Rossen, SPE-AIME, Exxon Co., U.S.A.
M. M. Brady, Exxon Co., U.S.A.

Introduction

The added recovery benefits attributable to accelerated blowdown of strong water-drive gas reservoirs are well known.[1,2] The planning for effective blowdown of such reservoirs requires the accurate prediction of reservoir pressure and production performance. Deliverability maintenance investments must be scheduled well in advance and economic incentives depend on accurate forecasts of gas recovery.

Beginning in late 1969, a strong water-drive gas reservoir in the Katy field was blown down at a reserves/production ratio (R/P) of less than 2. Although gas recovery during blowdown was more than 30 percent greater than that obtained at a low production rate equivalent to an R/P of 15, reservoir pressure/production performance varied considerably from predictions made using a conventional van Everdingen-Hurst[3] unsteady-state material balance. Reservoir pressures declined more rapidly than predicted, and gas recovery was less than expected. Performance of the reservoir suggested the presence of a substantial pressure gradient in the water-invaded region, and the conventional material balance used was not capable of modeling it.

To obtain accurate predictions, the van Everdingen-Hurst unsteady-state material balance equations were modified to account for higher pressures in the water-invaded region. Using the modified equations, it was possible to match accurately the pressure/production performance for the Katy reservoir.

*Now deceased.

Katy V-C Reservoir Description and History

The Katy V-C reservoir is a uniformly developed sand in the Yequa formation, approximately 40 ft thick, having an original productive area of 7,300 acres. Structurally, the reservoir is an elongate, north-south trending, unfaulted anticline with 105 ft of structural closure above the original gas-water contact at −7,240 ft. Dip on the flanks is a fairly uniform 180 ft/mile.

Original gas in place was 330 Bcf. Reservoir rock and fluid data developed from laboratory analysis are shown in Table 1.

Early development of the reservoir was designed to supply gas for a small sale and as make-up for fuel and shrinkage incurred in cycling other zones. Fig. 1 shows the completion history.

Cycling of the V-C reservoir began in 1950. The cycle program included overinjection during the early years. This contributed to a substantial repressuring. The cycle pattern was end-to-end with injection confined to Well 4302, completed below the original gas-water contact. A bottom-hole pressure measured in this well, outside the original productive limits and before injection, was 270 psi above the pressure in the uninvaded gas zone as measured uniformly in three wells active at the time.

After cycling was completed, limited gas production was resumed until Sept. 1969 when accelerated blowdown was started. Before blowdown, the production rate had declined below 15 MMcf/D as water influx began repressuring the reservoir (Fig. 2). Cumulative production to Sept. 1969 was 151 Bcf while the reservoir pressure was 2,830 psi.

The final blowdown of a Gulf Coast water-drive gas reservoir at a reserves/production ratio of less than 2 provided an increase in gas recovery. Pressure/production performance did not conform to conventional tank-type material balance predictions because of a large pressure gradient in the water-invaded region. The material balance equation was altered to account for the pressure behind the front and was adapted to an economic optimizer program.

TABLE 1—RESERVOIR ROCK AND FLUID DATA

Original pressure, psig	3,303
Temperature, °F	212
Original formation volume factor, RB/Mscf	0.9248
Compressibility factor (at p_o)	0.9100
Porosity, percent	25.6
Permeability, md	600
Water saturation, percent	31.0
Residual gas saturation, percent	28.7

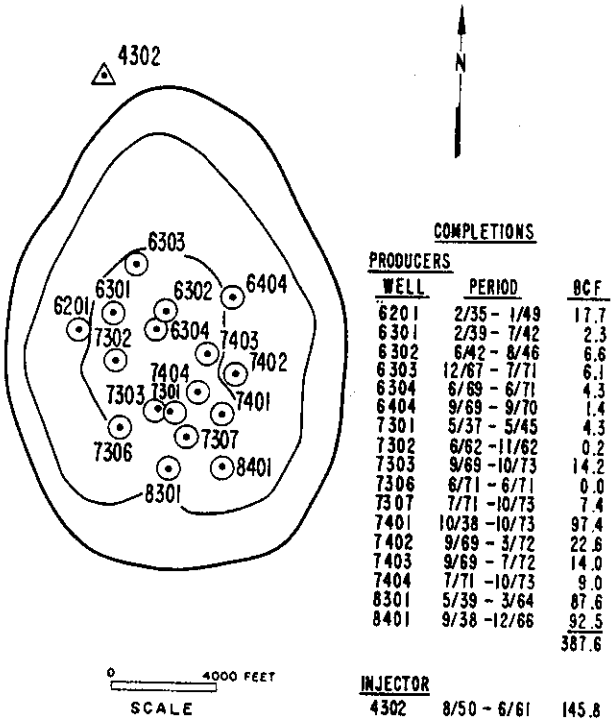

COMPLETIONS

PRODUCERS

WELL	PERIOD	BCF
6201	2/35 - 1/49	17.7
6301	2/39 - 7/42	2.3
6302	6/42 - 8/46	6.6
6303	12/67 - 7/71	6.1
6304	6/69 - 6/71	4.3
6404	9/69 - 9/70	1.4
7301	5/37 - 5/45	4.3
7302	6/62 - 11/62	0.2
7303	9/69 - 10/73	14.2
7306	6/71 - 6/71	0.0
7307	7/71 - 10/73	7.4
7401	10/38 - 10/73	97.4
7402	9/69 - 3/72	22.6
7403	9/69 - 7/72	14.0
7404	7/71 - 10/73	9.0
8301	5/39 - 3/64	87.6
8401	9/38 - 12/66	92.5
		387.6

INJECTOR

4302	8/50 - 6/61	145.8

Fig. 1—Structure and completion history.

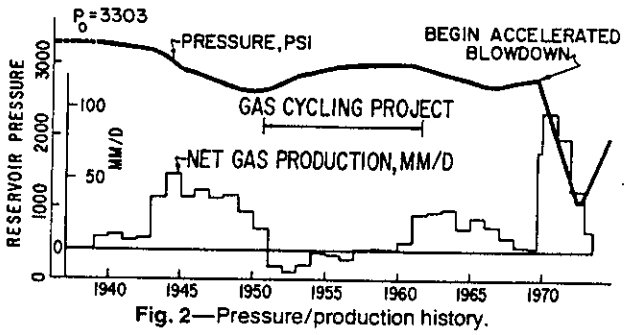

Fig. 2—Pressure/production history.

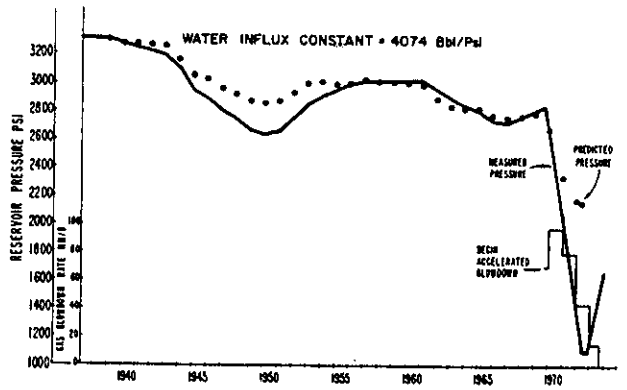

Fig. 3—Predicted pressure performance in conventional unsteady-state material balance.

Accelerated Blowdown

The V-C gas reservoir was placed on accelerated blowdown in Sept. 1969 as part of a fieldwide selective reservoir depletion plan.[4] The plan involved the sequential depletion of 12 overlying gas zones with varying water drives and reserves at rates designed to achieve maximum recovery.

Accelerated production averaged 69 MMcf/D during late 1969. By the end of the year, developed capacity was 78 MMcf/D, which represented an R/P of 2.9. Production buildup continued and by the end of 1970 the R/P was reduced to 1.5. Average production in 1970 was 97 MMcf/D.

Although reservoir pressure declined sharply at about 2 psi/D, water influx from the structural flanks continued to water out producing wells. Reasonably uniform water advance along bedding planes with a near vertical front was indicated when producing wells ceased to flow within 1 to 3 months after initial water production.

A 700-psi gathering system with compression was placed in operation in Nov. 1971 to maintain high-rate withdrawals and continue pressure decline. By May 1972, reservoir pressure had stabilized at 1,100 psi. For 4 months, reservoir pressure in the final 120-acre uninvaded region remained at 1,100 psi as 5.0 Bcf was recovered. Then, reservoir pressure began increasing rapidly. By mid-1973, all wells were invaded by water and production ceased. At the end of 1973, reservoir pressure in four remaining inactive wells had increased 440 psi (Fig. 2).

Reservoir Performance During Blowdown

Fig. 3 shows actual vs predicted reservoir pressure performance, using the conventional van Everdingen-Hurst unsteady-state material balance equations. Actual reservoir pressure was as much as 1,000 psi lower than predicted. To account for the discrepancy between observed and predicted performance, a review of the V-C reservoir behavior was undertaken.

The p/Z vs cumulative production plot had an uncharacteristic appearance for a strong water-drive gas reservoir during the accelerated blowdown period. As shown in Fig. 4, the slope of the plot became steeper with each survey period. This may be interpreted to show the effect of water advance acting as a moving boundary, progressively reducing the volume of uninvaded gas in which pressure/production performance is acting near volumetric levels. Finally, as complete invasion neared, the plot was almost vertical. An inference can be made that pressures in the reservoir behind the advancing water could be substantially above pressures in the uninvaded zone that are shown on the plot.

The rapid repressuring at the crest further suggested that pressures in the water-invaded region were higher than those ahead of the advancing water. In Aug. 1974, a bottom-hole pressure was measured in Well 8203, located approximately 1,800 ft inside the original reservoir boundary but 6,000 ft from the final productive area. That pressure was 750 psi higher than the pressure at the crest, which had increased to 1,950 psi.

On the basis of that measurement, it was estimated that average pressure in the water-invaded region was as much as 600 psi greater than pressure at the front in Aug. 1974. It was also probable that the difference between

invaded and uninvaded zone pressures was even greater when the reservoir pressure was first reduced to 1,100 psi in 1972.

Gas recovery during the final blowdown phase was 91 Bcf — an estimated 28 Bcf more than would have been expected if production had continued at an R/P of 15. Over-all recovery was 242 Bcf or 73.3 percent of the original gas in place. While cumulative gas production clearly indicated additional recovery of gas from behind the invading waterfront, calculations show that recovery would have been approximately 40 Bcf more if pressure behind the front also had been reduced to 1,100 psi.

The substantial pressure gradient in the water-invaded region indicated by the above conditions (because of relative permeability effects) increased the amount of trapped gas and thus reduced the volume of recoverable gas that might percolate forward. In addition, the pressure gradient across the reservoir during blowdown resulted in a much lower pressure in the uninvaded zone than at the original gas-water contact, causing gas zone pressures to decline more rapidly than predicted.

Gas balance calculations were made to determine the amount of trapped gas and to quantify the probable magnitude of pressure behind the water front.

Residual gas saturation (S_{gr}) was based on laboratory imbibition and waterflood data for V-C zone core samples (Table 1). A single-field in-situ residual gas measurement using a tracer technique was obtained in 1974 that indicated an S_{gr} of 25.4 percent. The higher value (28.7 percent) indicated by the laboratory data was used in the calculations. A conformance factor (combined vertical and areal sweep efficiency) was estimated at 95 percent, based on log data from wells drilled behind the advancing water front.

Gas compressibility factors were adjusted to account for cycling effects. Six time steps were selected that coincide with periods of uniform pressure performance (Fig. 5). Water-invaded reservoir volumes at the end of each time step were determined from well production data and logs of wells drilled through the reservoir. Corresponding gas-water contacts are shown in Fig. 6.

The gas balance calculations compared the sum of trapped gas, uninvaded gas, and produced gas with the volume of original gas in place. The results of those calculations are shown in Table 2. Table 3 describes pressure and volumetric data used in the calculations.

The approach taken in calculating the balances involved the following. (1) Trapped gas during each time period was calculated, based on the average of pressures at the beginning and end of each step. (2) The sum of gas volumes trapped, uninvaded, and produced was then compared with the original gas in place. (3) If the sum exceeded the original gas in place, the difference was considered to have percolated forward and been produced. (4) The volume of gas trapped was adjusted accordingly. Assuming that the residual gas saturation remained constant as pressures declined (that is, 100-percent percolation), the average pressure in the water-invaded region was calculated to be consistent with the adjusted trapped gas volumes.

Percolation was minimal until the accelerated blowdown period. The balance calculation shows that 13.0 Bcf percolated during the main blowdown period and an additional 8.8 Bcf percolated before final invasion. Pressure performance consistent with the resulting trapped gas volumes would require an average water-invaded zone pressure of 2,200 psi at the time the uninvaded zone

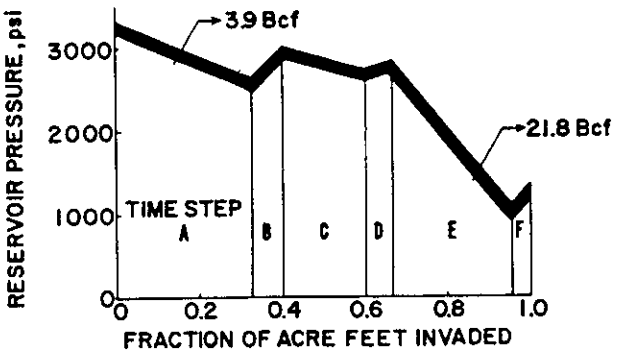

Fig. 5—Time steps for gas balance calculations showing percolation volumes.

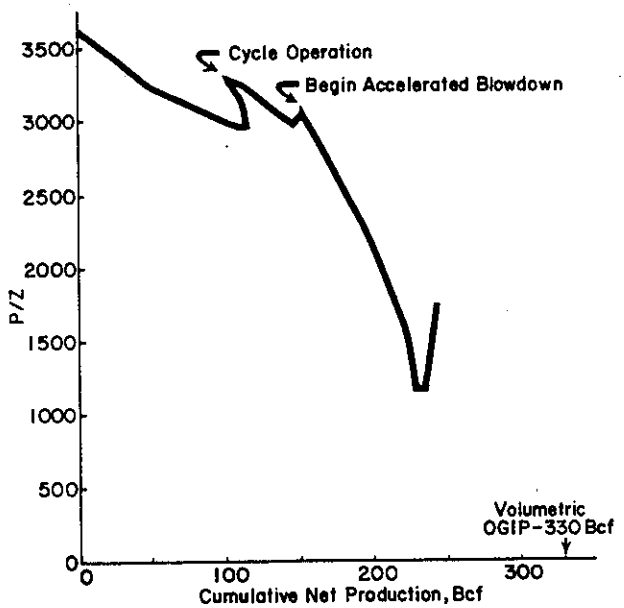

Fig. 4—p/Z vs cumulative production.

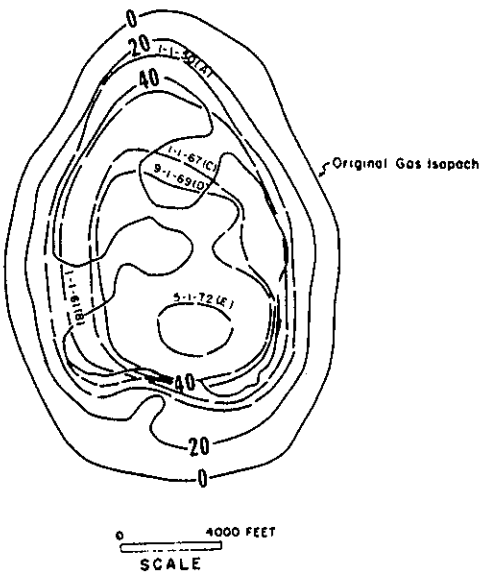

Fig. 6—Gas-water contacts for gas balance time steps.

TABLE 2—GAS BALANCE CALCULATIONS TO SHOW AMOUNT OF PERCOLATION AND PRESSURE IN WATER-INVADED REGION

Period	Gas Trapped (Bcf) During Period	Gas Trapped (Bcf) Cumulative	Gas Trapped (Bcf) Cumulative Adjusted for Percolation	Remaining Uninvaded (Bcf)	Cumulative Production (Bcf)	Gas Balance (Bcf) No Percolation	Gas Balance (Bcf) With Percolation	Percolation From Gas Balance (Bcf)	Invaded Zone Pressure Required for Adjusted Trapped Gas
A	43.6	43.6	39.7	181.8	108.6	334.0	330.1	3.9	
B	9.2	52.8	48.9	178.6	100.2	331.6	327.7	0	
C	25.3	78.1	74.2	108.8	146.7	333.6	329.7	0	
D	7.8	85.9	82.0	95.0	151.2	332.1	328.2	0	
E	25.8	111.7	94.8	4.5	230.8	347.0	330.1	13.0	2,200
F	2.3	114.0	88.3	0	241.8	355.8	330.1	8.8	2,000
								25.7	

TABLE 3—GAS BALANCE CALCULATIONS — PRESSURE AND VOLUME FACTORS

Period	Fraction of Gas Acre-Feet Invaded	Reservoir Pressure (psig) Beginning of Period	Reservoir Pressure (psig) End of Period	Reservoir Pressure (psig) Average	Formation Volume Factors (RB/Mscf) $B_{g\,beg}$	Formation Volume Factors (RB/Mscf) $B_{g\,end}$	Formation Volume Factors (RB/Mscf) $B_{g\,avg}$
A	0.33	3,303	2,640	2,972	0.9248	1.1313	1.0162
B	0.40	2,640	3,000	2,820	1.1313	1.0257	1.0860
C	0.60	3,000	2,720	2,860	1.0257	1.1226	1.0720
D	0.66	2,720	2,830	2,775	1.1226	1.0824	1.1016
E	0.96	2,830	1,100	1,965	1.0824	2.8313	1.5525
F	1.00	1,100	1,360	1,230	2.8313	2.2703	2.5202

pressure first reached 1,100 psi (at the end of Period E). During the final time step, F, while the reservoir pressure ahead of the front was increasing to 1,360 psi as the remaining wells watered out, the average pressure in the water-invaded region required to account for the reduction in trapped gas would have declined to less than 2,000 psi. This pressure decline behind the front as water advance continued would provide for the added 8.8 Bcf that apparently percolated during the final time step — even though pressure at the wells was increasing. While no field pressure measurements were made behind the front at the end of blowdown, the difference of 640 psi (2,000 − 1,360 psi) between invaded and uninvaded zone pressures derived from the gas balance calculations is consistent with the 600-psi difference estimated from the field pressure measurement made 1 year later in Aug. 1974. Fig. 7 shows possible reservoir pressure profiles during the final stages of blowdown.

The existence of the invaded zone pressure gradient was confirmed by subsequent one-dimensional numerical simulations based on the solution of partial differential equations that describe the reservoir using finite difference techniques. The one-dimensional simulations showed that pressure/production performance could be matched easily, and that average reservoir pressure in the water-invaded region at the end of the blowdown was 640 psi higher than pressures ahead of the front.

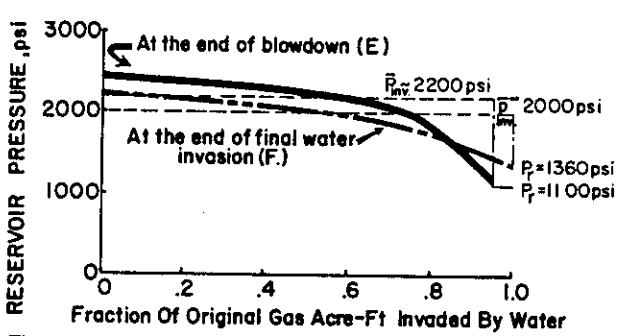

Fig. 7—Schematic of pressure profiles in water-invaded region at the end of blowdown.

Modified Material Balance

Although performance of the Katy V-C reservoir during blowdown was simulated successfully using a one-dimensional numerical model, it is better to use simpler tank-type models. Such models are easier to use and require only a fraction of the computer time that one-dimensional methods require. A rapid tank-type model also could be linked with an economic program to determine optimum investment and production schedules for reservoirs.[5] Accordingly, the conventional van Everdingen-Hurst unsteady-state material balance equations were modified to predict pressure performance for strong water-drive gas reservoirs.

Based on results described before, the presence of a pressure gradient and trapped gas within the water-invaded region must be accounted for; therefore, the conventional material balance equation,

$$G B_{gi} = (G - G_p) B_g + W_e, \quad \ldots\ldots\ldots\ldots\ldots\ldots (1a)$$

was modified to include the following trapped-gas term

$$G B_{gi} = (G - G_p - G_t) B_g + G_t B_{gt} + W_e, \quad \ldots\ldots\ldots (1b)$$

where

G = original gas in place, Mscf
G_p = cumulative gas production at time t, Mscf
G_t = volume of gas in invaded region at time t, Mscf

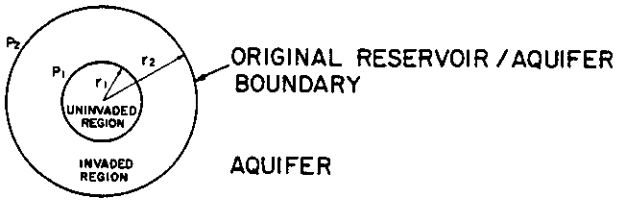

Fig. 8—Reservoir model of modified material balance where r_2 equals distance from center of reservoir to original gas-water contact, ft; r_1 equals distance from center of reservoir to gas-water contact at some elapsed time t, ft; p_2 equals pressure at r_2 at time t; and p_1 equals pressure at r_1 at time t.

B_{gi} = original gas volume factor, RB/Mscf
B_g = gas volume factor for uninvaded region at time t, RB/Mscf
B_{gt} = gas volume factor of trapped gas at time t, RB/Mscf
W_e = cumulative water influx at time t, res bbl.

The reservoir model corresponding to Eq. 1b and the uninvaded and invaded regions referred to are illustrated in Fig. 8.

The water influx term, W_e, is described by the van Everdingen-Hurst unsteady-state water influx equation for a radial aquifer.[3]

$$W_e = C \sum_{j=1}^{n} \Delta p_j \, \partial \left[t_D(n) - t_D(j-1) \right]. \quad \ldots\ldots\ldots (2)$$

See Nomenclature for definition of terms involved in Eq. 2.

The procedure for predicting reservoir pressure and water influx based on Eqs. 1b and 2 for any given time step is summarized below.

1. Compute the original reservoir radius

$$r_2 = \left[(G B_g \times 5.615)/(\pi h (1 - S_{wi}) \phi \right]^{1/2}, \quad \ldots\ldots\ldots (3)$$

where

h = reservoir net thickness, ft
S_{wi} = connate water saturation, fraction
ϕ = average porosity of the formation, fraction

2. Estimate the pressure, p_2, at the original reservoir boundary.
3. Solve for water influx, W_e, from Eq. 2.
4. Calculate the radius of the uninvaded zone,

$$r_1 = \left[r_2^2 - \frac{W_e \times 5.615}{(1 - S_{gr} - S_{wi}) \phi \pi h} \right]^{1/2}, \quad \ldots\ldots\ldots (4)$$

where S_{gr} is the residual gas saturation.

5. Calculate the pressure, p_1, at the invading water front assuming radial flow,

$$p_1 = p_2 - \frac{q \mu_w \ln \left(\frac{r_2}{r_1} \right)}{0.00708 \, k_w h}, \quad \ldots\ldots\ldots (5)$$

where

$q = \Delta W_e / \Delta t$, RB/D
ΔW_e = net water influx for time step Δt, res bbl
Δt = time step duration, day

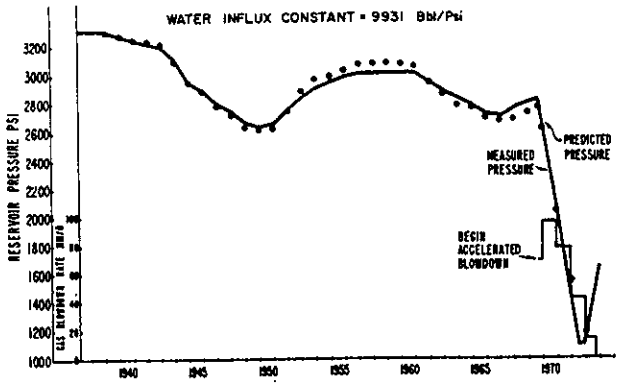

Fig. 9—Performance match with modified material balance.

k_w = effective permeability to water within reservoir limits, md.

6. Calculate the average pressure, $\bar{p}$, in the water-invaded region from the following equation.

$$\bar{p} = p_2 - \frac{2 q \mu_w}{0.00708 \, k_w h} \left[\frac{1}{4} = \frac{r_1^2 \ln \left(\frac{r_2}{r_1} \right)}{2 (r_2^2 - r_1^2)} \right] \ldots\ldots (6)$$

Eq. 6 is derived in the Appendix.

7. Calculate the trapped gas volume, G_t, from

$$G_t = \int_{r_1}^{r_2} \frac{\phi S_{gr} \, 2 \pi r h}{B_{gt} \, 5.615} \, dr$$

$$= \frac{A}{2} \left(p_2 - \frac{B}{2} \right) (r_2^2 - r_1^2) + AB \, \frac{r_1^2}{2} \ln \left(\frac{r_2}{r_1} \right), \quad \ldots\ldots\ldots (7)$$

where

$$A = \frac{2 \pi h S_{gr} \phi}{(5.615)(0.00502) ZT}$$

$$B = \frac{q \mu_w}{0.00708 \, k_w h}$$

$$B_{gt} = 0.00502 \, \frac{ZT}{\bar{p}}$$

T = absolute temperature, °R
Z = compressibility, fraction.

8. Solve Eq. 1b for W_e.
9. Compare W_e calculated from Step 3 with that calculated from Step 8. If the W_e's are not within a specified tolerance, go to Step 2, estimate another p_2, and repeat the procedure.

The above procedure assumes that the gas reservoir behaves like a tank and that (1) pressure is uniform throughout the uninvaded region of the reservoir; (2) the van Everdingen-Hurst unsteady-state water influx equation satisfactorily describes aquifer behavior; (3) residual gas saturation is constant throughout the water-invaded region; and (4) the radial flow equation can be used to describe the pressure distribution in the water invaded region.

Fig. 9 shows a performance match obtained by using the modified material balance equations. This match has been used in similar situations with equal success. Additionally, the model has been attached successfully to an economics optimizer and used to schedule investments and production to achieve optimum results for a single- or multi-reservoir gas field.

Conclusions

1. The conventional material balance assumption of uniform pressures throughout the original reservoir limits is not adequate for the proper blowdown scheduling of strong water-drive gas reservoirs. A large pressure gradient is seen to exist in the water-invaded region mainly resulting from relative permeability effects in the presence of trapped gas.

2. The effect of this gradient is twofold: (1) the lower pressures ahead of the front affect deliverability maintenance and (2) the higher pressures behind the front affect recovery by limiting the amount of gas that may percolate forward to be recovered.

3. A modified tank-type aquifer model has been developed that accounts for the pressure gradient as a function of the relative permeability effect. It has matched the pressure/production performance of a number of water-drive gas reservoirs produced at varying rates. The model has been used with an economics optimizer program for effective blowdown planning.

Nomenclature

c_{f+w} = rock plus water compressibility, psi^{-1}
$C = 1.12\, h\, \phi_a\, c_{f+w}\, r_R^2\, f_R$, bbl/psi
f_R = fraction of reservoir periphery in contact with aquifer
h = net thickness of formation, ft
k_w = water permeability in aquifer, md
$Q_{tD} = Q_{tD}(t_D, r_D)$ = dimensionless water influx function
$r_D = r_a/r_R$ = ratio of aquifer to reservoir radius
r_R = effective reservoir radius, ft

$$t_{D(j)} = \frac{0.00633 k_w t_j}{\phi_a\, \mu_w\, c_{f+w}\, r_R^2}$$

t_j = time at end of jth time interval, day

$$W_e = C \sum_{j=1}^{n} \Delta p_j\, Q\left[t_{D(n)} - t_{D(j-1)}\right]$$

$$\Delta p_j = \begin{Bmatrix} (p_{j-2} - p_j)/2 & j > 1 \\ (p_o - p_j)/2 & j = 1 \end{Bmatrix} = \text{reservoir pressure change for the } j\text{th time step, psi}$$

μ_w = water viscosity, cp
ϕ_a = aquifer porosity, fraction

Acknowledgments

The authors thank Exxon Co., U.S.A., and Exxon Production Research Co. for permission to publish this paper. They also thank D. W. Berry and M. E. Swick for their assistance in developing the computer program.

References

1. Agarwal, R. G., Al-Hussainy, R., and Ramey, H. J., Jr.: "The Importance of Water Influx in Gas Reservoirs," *J. Pet. Tech.* (Nov. 1965) 1336-1342; *Trans.*, AIME, **234.**
2. Matthes, G., Jackson, R. F., Schuler, S., and Marudiak, O. P.: "Reservoir Evaluation and Deliverability Study, Bierwang Field, West Germany," *J. Pet. Tech.* (Jan. 1973) 23-30.
3. van Everdingen, A. F. and Hurst, W.: "The Application of the Laplace Transformation to Flow Problems in Reservoirs," *Trans.*, AIME (1949) **186,** 305-322.
4. Finch, M. P. and Marek, J. A.: "The Long-Range Planning Function as Related to Katy Field Gas Sales," *J. Pet. Tech.* (Feb. 1972) 145-148.
5. Huppler, J. D.: "Scheduling Gas Field Production for Maximum Profit," *Soc. Pet. Eng. J.* (June 1974) 279-294; *Trans.*, AIME, **257.**

APPENDIX

The volumetric average pressure for a radial system for the water-invaded region may be expressed by the integral

$$\bar{p} = \frac{\int dn}{V/ZRT} = \frac{\int p/ZRT\, d_v}{V/ZRT} = \frac{\int p\, d_v}{V} = \frac{\int_{r_1}^{r_2} p \cdot 2\pi rh\phi\, dr}{\pi (r_2^2 - r_1^2) h \phi} = \frac{2\int_{r_1}^{r_2} prdr}{(r_2^2 - r_1^2)} \quad \text{..... (A-1)}$$

The incompressible fluid pressure at any radius given by the radial flow equation is

$$p = p_2 - \frac{q\mu_w \ln\left(\frac{r_2}{r}\right)}{0.00708\, k_w h} \quad \text{..... (A-2)}$$

Substituting Eq. A-2 for p in Eq. A-1 gives

$$\bar{p} = \frac{2\int_{r_1}^{r_2} \left[p_2 - \frac{q\mu_w \ln\left(\frac{r_2}{r}\right)}{0.00708\, k_w h}\right] r\, dr}{r_2^2 - r_1^2}, \quad \text{... (A-3)}$$

$$\bar{p} = p_2 - \frac{2q\mu_w}{0.00708\, k_w h}\left[\frac{1}{4} - \frac{r_1^2 \ln\left(\frac{r_2}{r_1}\right)}{2(r_2^2 - r_1^2)}\right]. \quad \text{..... (A-4)}$$

JPT

Original manuscript received in Society of Petroleum Engineers office Aug. 2, 1976. Paper accepted for publication Feb. 28, 1977. Revised manuscript received July 26, 1977. Paper (SPE 6166) was presented at the SPE-AIME 51st Annual Fall Technical Conference and Exhibition, held in New Orleans, Oct. 3-6, 1976.

SPE 26141

A Tight Gas Field Study: Carthage (Cotton Valley) Field

W.D. McCain and G.W. Voneiff, S.A. Holditch & Assocs. Inc.; E.R. Hunt, Ercill Hunt & Assocs. Inc.; and M.E. Semmelbeck, S.A. Holditch & Assocs. Inc.

SPE Members

This paper was prepared for presentation at the SPE Gas Technology Symposium held in Calgary, Alberta, Canada, 28-30 June 1993.

INTRODUCTION

Evaluation of the need for infill drilling in complex, low-permeability, gas reservoirs requires the application of advanced technology. Use of typical engineering tools such as conventional decline curve analysis, conventional pressure transient analysis, and single layer reservoir descriptions often create inaccurate results and misleading conclusions. Despite the accuracy of advanced analysis techniques, these techniques are typically not performed on a well-by-well basis in field-wide studies because the cost cannot be justified. As a result, accurate conclusions, valid for all areas of a field, are not obtained.

In this paper we present a practical means of applying advanced analysis techniques to an entire field. We describe a powerful statistical method for dividing the reservoir into areas of like productive behavior. This method provides an unbiased means of comparing well performance, selecting areas for advanced analysis, and defining the areal locations where specific conclusions apply. Emphasis is placed on incorporating a sound geological and petrophysical description, and evaluating the consistency of reservoir descriptions developed through independent geological and reservoir engineering techniques.

This analysis technique was used to evaluate the infill drilling potential of the Carthage (Cotton Valley) field in east Texas. The Carthage field, discovered in 1968, is a thick, layered, low-permeability gas reservoir underlying 250,000 acres in Panola County, Texas. See Fig. 1. At the time of this study, there were approximately 900 wells producing 400 million cubic feet and 300 barrels of condensate per day. The Carthage Cotton Valley sand has been classified as "tight gas" by the FERC. Prior to this study, there were three periods of intense drilling activity corresponding to authorizations of 640-, 320-, and 160-acre drilling densities. Carthage is currently experiencing a fourth active drilling period, in which numerous wells are being drilled on 80-acre spacing in selected areas of the field.

GEOLOGY

The geological study provided a basis for the understanding of field and well performance. Because the objective of this study was to evaluate current well performance and extrapolate our analysis to infill locations, it was critical to understand the internal structure of the reservoir and those factors which control thickness, permeability, porosity and continuity within the reservoir. The geologic study concluded that the depositional environment and subsequent diagenesis resulted in extensive compartmentalization throughout the field. While some intervals could be expected to be more continuous than others, permeability barriers and baffles exist throughout the reservoir. Sand packages which can be correlated across significant distances within the field are comprised of thin sand/shale sequences and very fine laminations which are impossible to detect on conventional logs. Severe heterogeneity is apparent both vertically and laterally.

References and illustrations at end of paper.

Carthage Field is located on a gentle anticlinal dome at 8000 feet subsea beneath the city of Carthage. Sandstones of the Jurassic Cotton Valley Group were deposited in a strandplain-barrier bar system resulting in a relatively continuous progradational sandstone-shale sequence.[1] This depositional environment is similar to the present day Galveston Island area. This environment is characterized by barrier bar deposition, storm cuts, lagoonal muds and organic burrowing. Variation in mean sea level and stream deposition result in highly variable thicknesses and areal extent of continuous sand bodies. .

Examination of slabed cores shows intrinsive lamination deposits throughout the section. Thickness of most laminations are on the order of a few inches or less. These are impossible to detect by conventional logs. Shale laminations deposited in crossbedded sands result in lateral as well as vertical flow barriers. Lithology changes occur throughout the section results in highly stratified reservoir facies.

Thin section analysis shows extensive deposition of authigenic minerals in pores and pore throats. Growth of clays in pores and pore throats is evident in photomicrographs. Reservoir facies which had well sorted, high permeability sands at the time of deposition were particularly susceptible to invasion by mineral-rich waters. In fact, many of the most permeable flow units in the reservoir at present are those which initially had lower permeabilities or were isolated from ground water flow by encapsulating clay or silt deposits.

Fig. 2 is a schematic cross section showing the nomenclature of sand/shale packages as they will be referred to in this paper. At the bottom of the section lies the thick, marine Bossier Shale. The Taylor Sand, where present, is up to 200 ft thick and is one of the most prolific zones in the field. It underlies the northern half of the field as shown in Fig. 3.

The Taylor is separated from the Upper Cotton Valley (UCV) by a thick silty shale which is between 150 and 350 feet thick. The UCV is a sequence of alternating shale and low-permeability sandstones about 1000 feet thick. The A-Sand occurs within the limestone at the top of the Cotton Valley, and, where present, is up to 70 feet thick and is of relatively high quality. It occurs in an east-west band across the center of the field.

PRESSURE MEASUREMENTS

Typically, pressure transient or "static" pressure tests are analyzed to validate conclusions of pressure interference or depletion. Lower initial reservoir pressures at infill locations indicate some depletion. In Carthage, initial "static" shut-in pressures after brief flow periods are measured on many new wells. These "static" pressures are assumed to be the average reservoir pressures, however, the pressures are usually still building slowly at the end of the shut-in period. An in-depth analysis of many of these pressures revealed that the typical shut-in time of 1-3 days was insufficient for the pressures to build reasonably close to the average reservoir pressure due to layering effects and differential depletion between layers.

Valid initial pressure measurements were made by attaching a pressure device to the perforating gun and perforating slightly underbalanced while measuring the pressure. This procedure minimizes the amount of pre-buildup production and also reduces the volume of wellbore storage. Thus, the pressure can equalize rapidly to the initial reservoir pressure.

Since most wells were perforated and fractured in stages, this procedure permitted pressure measurements in various zones of interest (and reduced the problem of layer dominated pressure response). Figs. 4 and 5 show initial pressures that are considered valid due to their measurement technique and/or extended shut-in period. There appears to be very little interference between wells in the Upper Cotton Valley. However, some wells recently completed in the Taylor Sand have encountered partial depletion. There were not enough measurements in the A-Sand to present graphically, however, the A-Sand is probably also showing partial depletion at this time. The apparent compartmentalization in the Upper Cotton Valley is consistent with the geological description of the formation.

PRODUCTION DATA ANALYSIS

One method of determining the appropriate well density for a field is comparison of estimated ultimate recovery (EUR) for older wells and infill wells. If infill wells are found to have a consistently lower EUR, then it is probable that the infill locations have been partially depleted by the older offsets, and further infill drilling may not be warranted. A typical technique applied to determine EUR is conventional decline curve analysis. Conventional decline curve analysis provides a sound basis for determining EUR for homogeneous, single layer reservoirs with reasonable permeability. However, at Carthage, the technique cannot be applied because the low-permeability, layered, heterogeneous, and anisotropic nature of the Cotton Valley does not fit the simple reservoir description on which the conventional analysis is based.

Specifically, conventional decline curve analysis employs the use of Arp's equations, which are only valid for production data from single layer, homogeneous reservoirs obtained after boundary dominated flow begins.[2, 3] When these equations are used to estimate EUR from transient production data (before boundary dominated flow), results are often inconsistent and/or incorrect. Fig. 6 illustrates that it takes several years of production to reach boundary dominated flow in a single-layer reservoir with 0.01 md permeability (typical permeability for Cotton Valley). The existence of layers, as at Carthage, will further delay the onset of boundary dominated flow. In such a situation, the best that one can hope for from a conventional analysis is a consistent evaluation from well to well.

The proper determination of EUR in complex reservoirs requires either the use of advanced type curve methods[4] or reservoir simulation. These techniques allow for the proper analysis of both transient and boundary dominated flow data, usually identifying the existence of boundaries earlier in the life of a well than possible with conventional decline curve analysis. However, despite these benefits, advanced techniques cannot usually be justified on all wells in a field because of the high cost of applying these techniques.

To bridge the gap between low-cost, low-accuracy methods and high-cost accurate techniques, we developed a statistical production analysis method that allows the use of a small number of localized advanced evaluations, and provides areal locations where conclusions from the localized studies can be applied. This method gives accurate conclusions across the entire field without the expense of advanced analysis on all wells in the field. The statistical analysis is inexpensive to perform, and the advanced analysis is limited to a few small areas, keeping costs to a reasonable level.

The statistical technique evaluates the performance of each well with surrounding wells to determine if infill wells are performing similarly or differently than older offsets. The statistical analysis is performed by constructing and evaluating graphs of well performance plotted against the date of first production. To minimize bias, we characterize well performance by using a performance indicator that does not rely on input that could be subjective (such as decline curve extrapolations) and is available for all wells in the field. Since this technique was new, we performed the evaluation with three performance indicators to determine if one indicator was best. The three productivity indicators selected were: 1) maximum monthly production rate, 2) average monthly production rate for the most productive twelve month period, and 3) monthly production rate (five-month average) at the time a cumulative production of 250 MMscf was reached.

Fig. 7 shows "indicator plots" for each of the three indicators for nine wells in a 1280 acre area. The indicators are plotted against date of first production and a statistically fit (least-squares) straight line is shown through each set of data. With this plot, the question, "Are the new wells performing differently than the older wells?", can be converted into the statistical hypothesis, "Is the slope of the indicator plot line significantly different than zero?". Slopes of zero mean that the new wells are performing identically to the older wells, indicating no interference or depletion at infill well locations. Negative slopes indicate some interference between wells. The hypothesis was answered with the Student's t-test.[5] If there appears to be a positive or negative slope, the Student's t-test determines if the slope is significant considering the amount of scatter in the data. None of the three lines on Fig. 7 were found to have a slope different than zero, thus, in this area of the field, infill wells are finding virgin, not depleted, conditions.

This statistical technique was applied field-wide. The entire field was divided into equal sized study units of approximately 3300 acres. Each study unit contained between 10 and 20 wells. The analysis showed that the Carthage field has two areas where infill wells are inferior to older wells, suggesting interference and depletion. These two areas comprise about one-third of the field as shown in Fig. 8. Note the correlation between these areas and the locations of the sands with more continuity, the Taylor and the A-sand. In the remaining two-thirds of the field, the productive behavior of wells indicates that there is no interference between wells, possibly due to separate reservoir compartments as suggested by the geological description and by the pressure measurements.

The "Best Year" indicator can be used to provide a rough estimate of the per well gas recovery that could be expected in compartmentalized regions. Fig. 9 shows the relationship between the "Best Year" performance indicator and the actual gas recovery after 10 years of production. The ten year recovery can be analyzed economically using a production profile based on the reservoir simulation results for a particular area. For example, if a well must produce 1.5 BCF in 10 years to be profitable, then Fig. 9 indicates that a well will be profitable if it averages 30,000 Mcf/M during its first year. Thus, those areas of the field in which the most recent wells average

30,000 Mcf/M as shown are potential candidates for further infill drilling.

The use of the "Best Year" production rate for this purpose is an easy and inexpensive method for gauging the infill drilling potential of the field. This technique is recommended only for analysis of large areas (>3000 acres) where reservoir compartmentalization has been found, and is not meant to gauge the expected profitability of a single well, but rather the expected profitability of the average well in a group of wells. This technique indicates that approximately 1/2 of the *compartmentalized* area of Carthage (1/3 of the *total* Carthage area) should result in profitable infill wells. This indicates that there are about 400 infill potential drilling locations in the field

STATE-OF-THE-ART LOG ANALYSIS IN TIGHT, LAYERED FORMATIONS

To assure accuracy of net effective pay calculations, diligence beyond that of traditional methods was employed in pre-interpretation activities such as log quality assurance, log to log depth alignments, borehole environmental corrections, and repair of data in intervals where logs are invalid because of stress induced borehole breakouts. Gamma ray logs, neutron logs and SP logs were used to determine shaliness. Shaliness along with density and neutron logs were used to arrive at porosity. Porosity, shaliness, and electrical parameters (accurately determined from "Pickett Plots") were used in a dual water model to calculate water saturations.[6,7] Log calculated porosity values were compared to core derived porosity values.

The combined effect of all the above data base work was that valid data was used to calculate net pay. This led to accurate net pay calculations.

Errors in gas-in-place calculations that can be expected from the log analyst who has by-passed or improperly applied the pre-interpretation effort are tabulated in Table 1. The log analyst may by-pass this intense effort by his own lack of experience or because of unreasonable time and money constraints.

Logs from thirteen wells were analyzed in preparation for the simulation study. Two other organizations independently analyzed those same logs. One, using pre-interpretation diligence similar to that described above, got results within 5 percent of our results. The other, with pre-interpretation time severely limited by the client, obtained net pay about 2.5 times too high.

Table 1

Effect of Not Properly Applying Pre-Interpretation Activities

Pre-Interpretation Log Analysis Work	Potential Range of Impact on Net Pay Calculations If Only Normal Diligence is Applied
1. Log to Log Depth Alignment	±25%
2. Borehole Size, Salinity, and Invasion Effects	±15%
3. Enlarged Borehole & Mud Weight Effects	±25%
4. Neutron Environmental Effects	±5%
5. Borehole curvature	±0.5%
6. Borehole Rugosity	0% to + 200%
7. Log Normalization	-10% to +15%
8. Combined Effects	+120%

DETERMINING CUTOFFS FOR NET PAY ANALYSIS

The logical first step for determining net pay is to determine net sand footage. That is, separate the shales which are not productive from the sands which are potentially productive. Rather than use a subjective cutoff value for shaliness, an objective value was determined statistically from the data base of 26,839 data levels for the thirteen wells analyzed. Fig. 10 is a plot of the total data levels remaining after a shale cutoff was applied. The point where the shale cutoff deviated from the straight line was taken to represent amount of shale where the data changes classification from a sandstone to a shale. In this study, when shale fraction exceeded 30%, the interval was considered to be shale and therefore not a potential producing level. After applying this cutoff, 8,573 potential producing levels remained, each 1/2 foot thick.

Water saturation was the second cutoff. The same statistical approach that was used on the shaliness cutoff was applied to find an objective water saturation cutoff. Fig. 11 is a plot that begins with the 8,573 potential producing sandstone levels when no cut is made (S_w=100%) and decreases to zero potential producing sandstone levels when a cutoff of S_w = 0% is applied. The appropriate cutoff value is found when the plot shows a deviation from a straight line. In this case, at a water saturation of 50%. This value was confirmed by field experience which showed that

intervals that have calculated water saturations greater than 50% produce some gas with a high water cut. Conversely, intervals that have calculated water saturations less than 50% produce gas with a low water cut. Thus, the statistical method appears valid. After applying the shaliness cutoff and the water saturation cutoff, 3,689 potential gas producing levels remained.

The third cutoff was based on porosity. The porosity cutoff is used to determine which of the remaining 3,689 potential gas producing levels are likely to give up the gas. These potential gas producing levels were subjected to porosity cutoff values ranging from 0% to 10% and the results plotted in Fig. 12. Again, the first deviation from the straight line is taken as an objective porosity cutoff. (In this case, 4%.) This cutoff value of porosity was confirmed by core analysis in the relatively small data base available. A 4% porosity cutoff is equivalent to an in-situ gas permeability cutoff of 0.0005 md. 3,432 gas producing levels (net effective pay) remained in the data base after this final cut.

EVALUATION OF HYDRAULIC FRACTURE STIMULATION

Massive hydraulic fracture treatments with multiple stages are usually performed on Cotton Valley wells in the Carthage Field. Two to four stages are typically pumped in Upper Cotton Valley zones and one stage is pumped in the Taylor when it is present. The effectiveness of these fracture treatments plays an important role in the performance of wells in the field. The problem lies in how to evaluate the effect of fracturing on well performance. This information is necessary to obtain an accurate estimation of fracture properties for use in reservoir simulation.

Reservoir permeability and fracture properties can be determined using pre- and post-fracture pressure buildup tests. Few wells in Carthage have been tested in this way. First, the test times required to obtain data that can be analyzed are excessively long. Second, such data are extremely difficult to analyze with any degree of confidence due to the effects of multiple layers. And, third, effective net pay in the stage is different after fracturing due to fracture height growth into additional productive layers.

Fracture properties were calculated directly with a hydraulic fracture treatment model. The analysis accounted for factors such as varying fracture fluid properties and proppant concentrations as well as multiple reservoir layers with different fracture gradients, leakoff coefficients, and other formation properties.

The data required for calculating fracture properties with this model are the types and amounts of proppant and fracturing fluids pumped during the treatment and the mechanical properties of the various layers of the formation being stimulated. The treatment data are available from standard service company field reports. The mechanical properties of the formation were estimated from logs and correlations with mechanical property data obtained from a well in the Cotton Valley Formation.[8] The well is located in a different field in East Texas, however, we assumed that the mechanical properties of the formation were similar and could be used for our purposes. Ideally, stress test data from the field under study should be used to obtain correlations between wireline log data and the formation mechanical properties.

Young's modulus, Poisson's ratio, and fracture gradient data were correlated to gamma ray deflection and used to estimate these properties in Carthage Field wells. The entire Cotton Valley was divided into as many as 20 intervals and mechanical properties were calculated from the gamma ray within each interval. This level of detail in formation characterization is necessary to properly calculate fracture growth in this formation.

Fig. 13 shows the formation stress computed from the gamma ray log correlations for a typical Carthage well. Also shown on this figure are locations of perforations for each the five fracture treatment stages. Few, if any, of the shale layers in the UCV are "clean" and thick enough to stop fracture height growth. The only certainty is that fracture height growth will be limited by the thick, competent zones above the UCV and below the Taylor Sand. The shale between the Taylor and UCV is generally about 150 feet thick and in some wells may limit upward growth from the Taylor fracture stage and downward growth from the UCV fracture stages.

Fig. 14 shows the propped fracture dimensions calculated by the fracture model for the five-stage fracture treatment in the well discussed above. The lower most stage is in the Taylor zone. In this portion of the field the shale above the Taylor is over 300 feet thick (the thickest observed in the field). The shale provided a good barrier to fracture height growth in the Taylor as is evident by the long contained fracture achieved in this zone. The fracture stages in the Upper Cotton Valley, however, had computed fracture heights of 250 to 600 feet. Height growth is generally upward in the Upper Cotton Valley except for the

upper most stage which grows primarily downward due to the competent zone at the top.

The same analysis was made for all the wells in the simulation study areas. The results were incorporated in the simulation studies.

The main conclusion from hydraulic fracture modeling is that the staged fracture treatments which have been used on Carthage wells are connecting all of the porous and permeable zones within the Upper Cotton Valley. It appears, in fact, that the volume and/or number of stages could be reduced and still provide adequate stimulation.

RESERVOIR SIMULATION

In order to determine if an additional infill drilling would be profitable in the field, we evaluated the drainage efficiency of the current 160 acre well density and predicted future performance for 80 acre well density in four 640 acre units.

A detailed simulation study of the entire Carthage Field was not possible within any reasonable time or budget constraints. Also, one or more small scale simulations performed on arbitrary regions of the field run the risk of not being representative of the field as a whole. The analysis of performance indicators showed, however, that there are large regions of the field in which wells perform similarly. This evidence showed that detailed reservoir simulation should be performed on representative areas of the field and that the conclusions from these areas could be extrapolated to areas of like well performance. This approach results in an optimal solution to the problem of characterizing well and reservoir performance and determining recovery efficiency as a function of well density.

The four simulation study areas are representative of: 1) The area of good continuous Taylor sand development in the northern part of the field, 2) The area of good continuous A-sand development in the middle of the field, 3) The central area of the field between the good Taylor and A-sand regions, and 4) The southern fringe of the field where well performance had been marginal to poor.

The first step in the simulation study was to history match the first few years of production history for each individual well. In general, the observed gas production rates were fixed and the flowing pressures were matched until the wells reached line pressure at which time the match was in observed gas flow rates. Flow meter surveys and bottomhole pressure measurements on the study wells and nearby wells were also matched, thereby increasing confidence in the simulation results.

The hydraulic fracture properties from the fracture simulations were found to be consistent with observed well performance. Initial estimates of permeability were obtained. The effects of non-Darcy flow in the fractures and fracture closure during periods of high drawdown were also investigated. It was found that the effects of non-Darcy flow and fracture closure were negligible due to the large contrast between fracture conductivity and formation permeability. However, formation permeability reduction with pressure depletion was incorporated in all simulations.

Next the 4-well 640-acre study areas were history matched. The height growth of the hydraulic fractures indicated that the reservoir could be modeled with two layers, one representing the high productivity zone (Taylor or A-sand, where present) and the other representing the remaining reservoir layers which are connected by the hydraulic fractures (UCV).

A limit had to be placed on gas pore volume in order to match the older wells in each unit. Simply reducing permeability was not sufficient to achieve a match of production history, boundaries had to be placed around the wells in the layer representing the UCV zone. These boundary effects were evident in the history match of the first wells in the units even before the 320 acre density wells were drilled.

Preliminary work on the study area in the southern fringe area indicated that the most likely reason for the poor performance of wells in this area is extremely low permeability. Future projections of wells in this area indicated that, while additional recovery was likely from increased well density, these new wells would be uneconomical to drill. However, if current wells in fringe areas like this one are profitable, infill wells should perform as well as the older wells.

The simulation results revealed that the Taylor Sand and A-Sand, where present, are reasonably continuous across the field. However, the very thick UCV, which contributes a substantial amount of the total gas production, is highly compartmentalized. These compartments are less than 100 acres in areal extent and could be as small as 40 acres in size.

Once an acceptable match of all available data was obtained, 15 year projections were made based on current 160 acre well density and based on 80 acre well density. All existing wells for which compartment size could not be determined and all new wells were assigned the minimum compartment size of those determined by history matching. This provided

the most conservative estimate of reserves for the new wells. The results of these performance predictions confirmed the results of the production data analysis and study of initial well pressures.

SUMMARY

A. field study of the 800+ well Carthage (Cotton Valley) Field has been completed. The study included (1 geological description of the Cotton Valley formation, 2) critical evaluation of all available pressure measurements, 3) statistical comparisons of production data for all wells in the field, 4) careful and tedious log pre-interpretation activities and analysis, 5) objective selection of cutoffs for determination of net pay, 6) evaluation by simulation of each hydraulic fracturing stage of each well of four study areas, and 7) simulation of four 640-acre study areas.

CONCLUSIONS

1. The Upper Cotton Valley Sandstones in the Carthage (Cotton Valley) Field are severely compartmented with compartments generally smaller than 100 acres.

2. The Taylor Sand and the A-Sand in the Carthage (Cotton Valley) reservoir are reasonably continuous where they exist.

3. There are as many as 400 economically viable infill drilling locations in the Carthage (Cotton Valley) Field.

4. The massive hydraulic fracture treatments used in the Carthage (Cotton Valley) Field generally do not achieve design half-lengths because there are no strong barriers to height growth in the Cotton Valley Sandstone formation.

5. A statistical analysis of production data was developed to evaluate wells when conventional decline curve analysis is not appropriate.

6. A field tested procedure for measuring initial reservoir pressure during staged hydraulic fracture treatments is described. This is the best method for use in low-permeability layered reservoirs.

7. Techniques for identification and repair of faulty log data prior to interpretation are described. These are particularly useful in interpreting logs from hard, layered reservoirs.

8. A new method of determining values of shale volume, water saturation, and porosity for use as cutoffs in calculating net pay was developed, compared with field data, and used in this study.

9. A procedure for correlating formation mechanical properties to well log data for use in designing and evaluating hydraulic fracture treatments was used to study the staged hydraulic fracture treatments in the Carthage (Cotton Valley) Field.

ACKNOWLEDGMENTS

The bulk of the data used in this study was provided by many of the operators in the field. Some of the operators provided substantial financial support. The authors are grateful for both. Appreciation is also due to S. A. Holditch & Associates for supporting the preparation of the paper.

REFERENCES

1. "SFE No. 3, Application of Advanced Technologies in Tight Gas Sandstones - Travis Peak and Cotton Valley Formations, Waskom Field, Harrison County, Texas," CER Corporation and S. A. Holditch & Associates, Inc., Topical Report to the Gas Research Institute, GRI Contract 5090-211-1940, GRI-91/0048, Feb. 1991.

2. Fetkovich, M. J.: "Decline Curve Analysis Using Type Curves," *JPT* (June, 1980) 1065-1077.

3. Fetkovich, M. J., Vienot, M. E., Bradley, M. D., and Kiesow, U. G.: "Decline-Curve Analysis Using Type Curves - Case Histories," *SPEFE* (Dec., 1987) 637-656.

4. Spivey, J. P., Gatens, M. E., and Lee, W. J.: "Integral Type Curves for Advanced Decline Curve Analysis," paper SPE 24301 presented at the SPE Mid-Continent Gas Symposium, Amarillo, April 13-14, 1992.

5. Milton, J. S. and Arnold, J. C.: *Introduction to Probability and Statistics: Principles and Applications for Engineering and the Computing Sciences*, 2nd ed., McGraw-Hill, New York (1990) 362-365.

6. Howard, W.E. and Hunt, E.R.: "Travis Peak and Integrated Approach to Formation Evaluation," paper SPE 15208 presented at the Unconventional Gas Technology Symposium, Louisville, KY, May 18-21, 1986.

7. Pickett, G.R.: "Acoustic Character Log and Their Application in Formation Evaluation," *JPT* (June 1963) 659-667; Trans., AIME, 228.

8. Robinson, B.M., Holditch, S.A., Whitehead, W.S., and Peterson, R.E.: "Hydraulic Fracturing Research in East Texas: Third GRI Staged Field Experiment," *JPT* (Jan. 1992) 78-87.

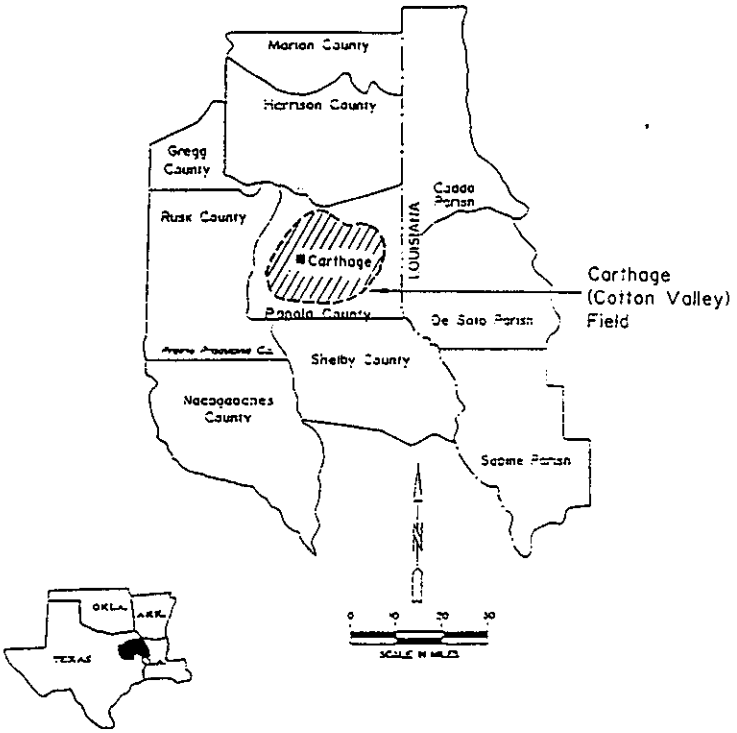

Fig. 1 - Carthage (Cotton Valley) Field location.

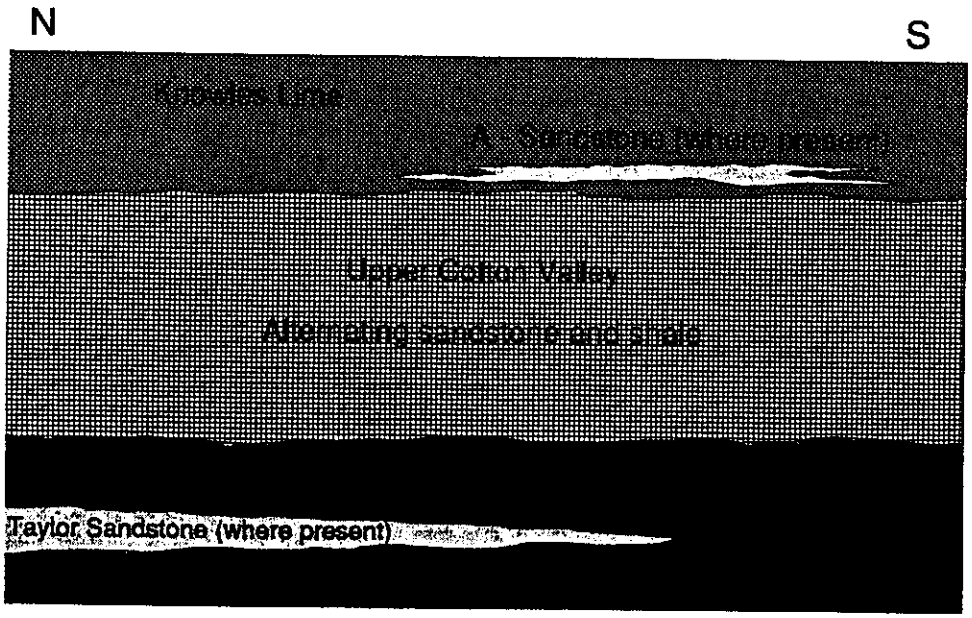

Fig. 2- Schematic N-S cross section for Carthage (Cotton Valley) Field.

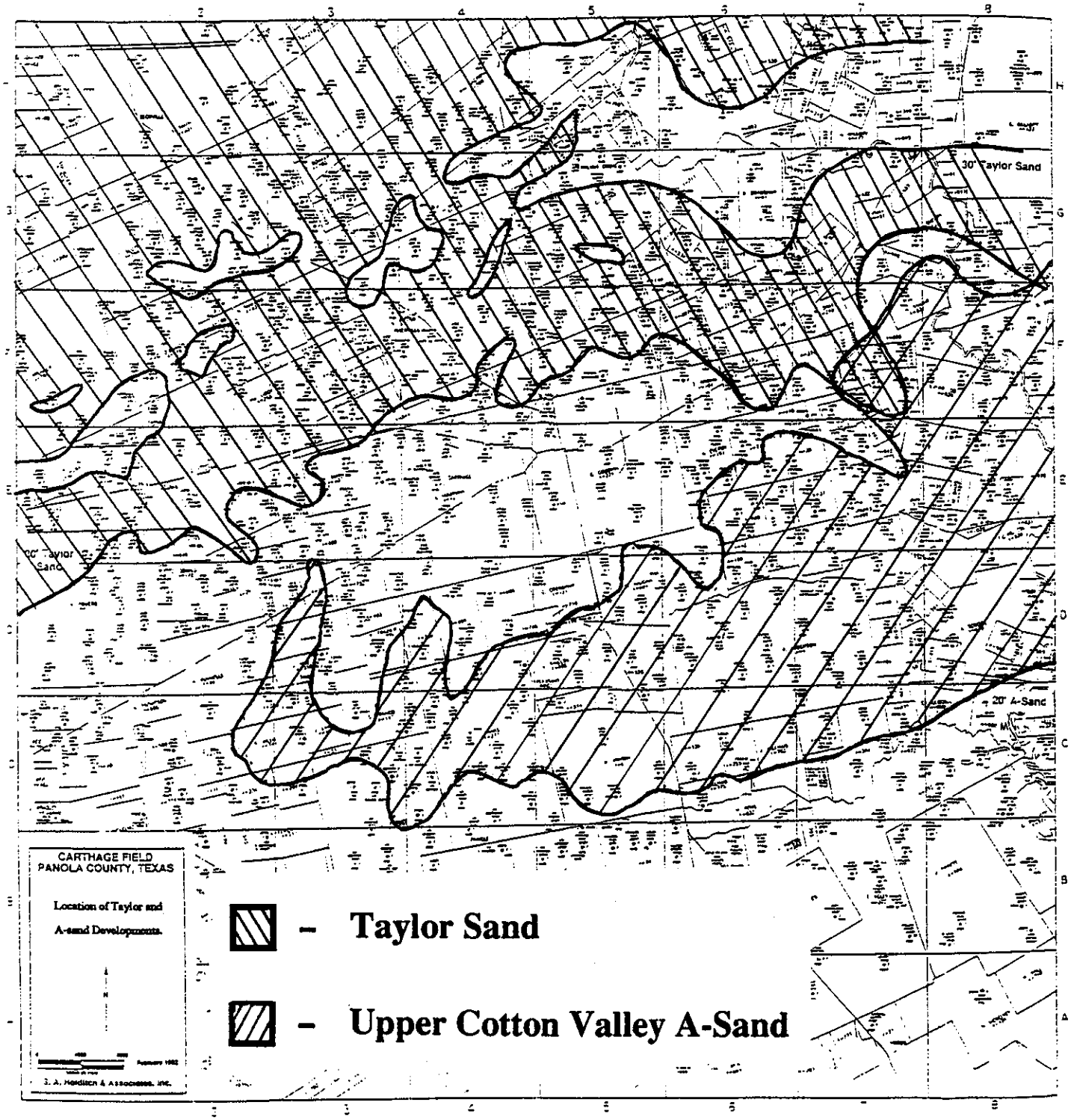

Fig. 3 - Base map of Carthage (Cotton Valley) Field showing locations of Taylor and A Sandstone. This map is centered on the field and contains all but a few fringe wells.

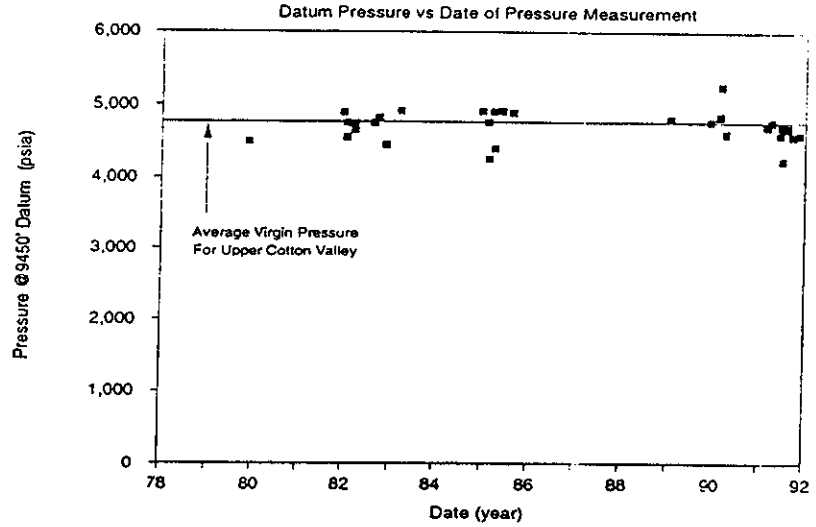

Fig. 4 - All available valid initial pressures for wells completed in the Upper Cotton Valley sand/shale sequence in the Carthage (Cotton Valley) Field.

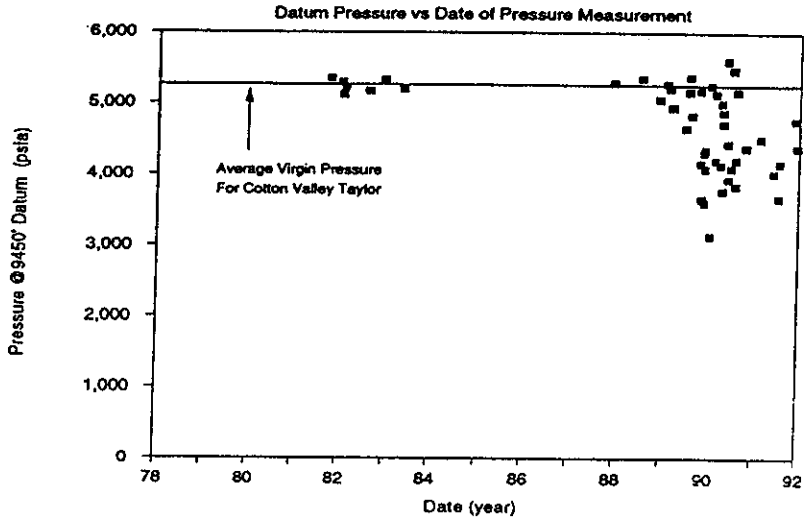

Fig. 5 - All available valid initial pressures for wells completed in the Taylor Sandstone in the Carthage (Cotton Valley) Field.

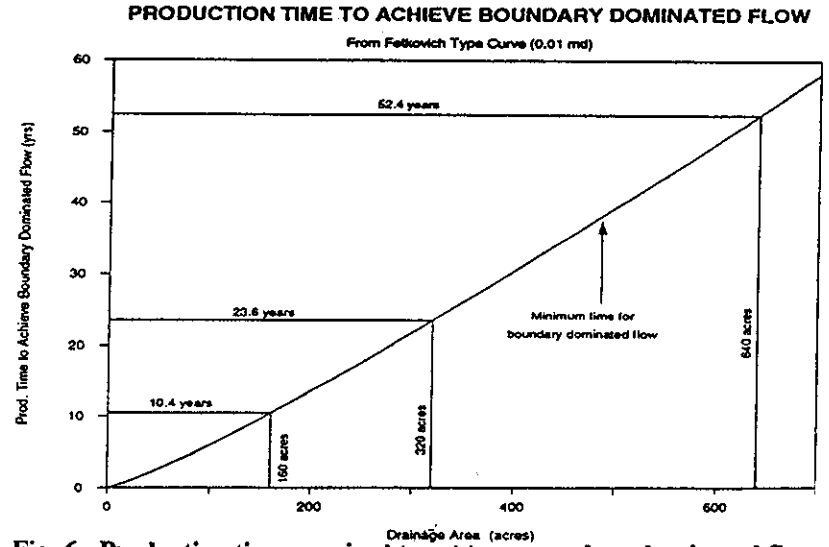

Fig. 6 - Production time required to achieve boundary dominated flow (from Fetkovich type curve[2] at 0.01 md).

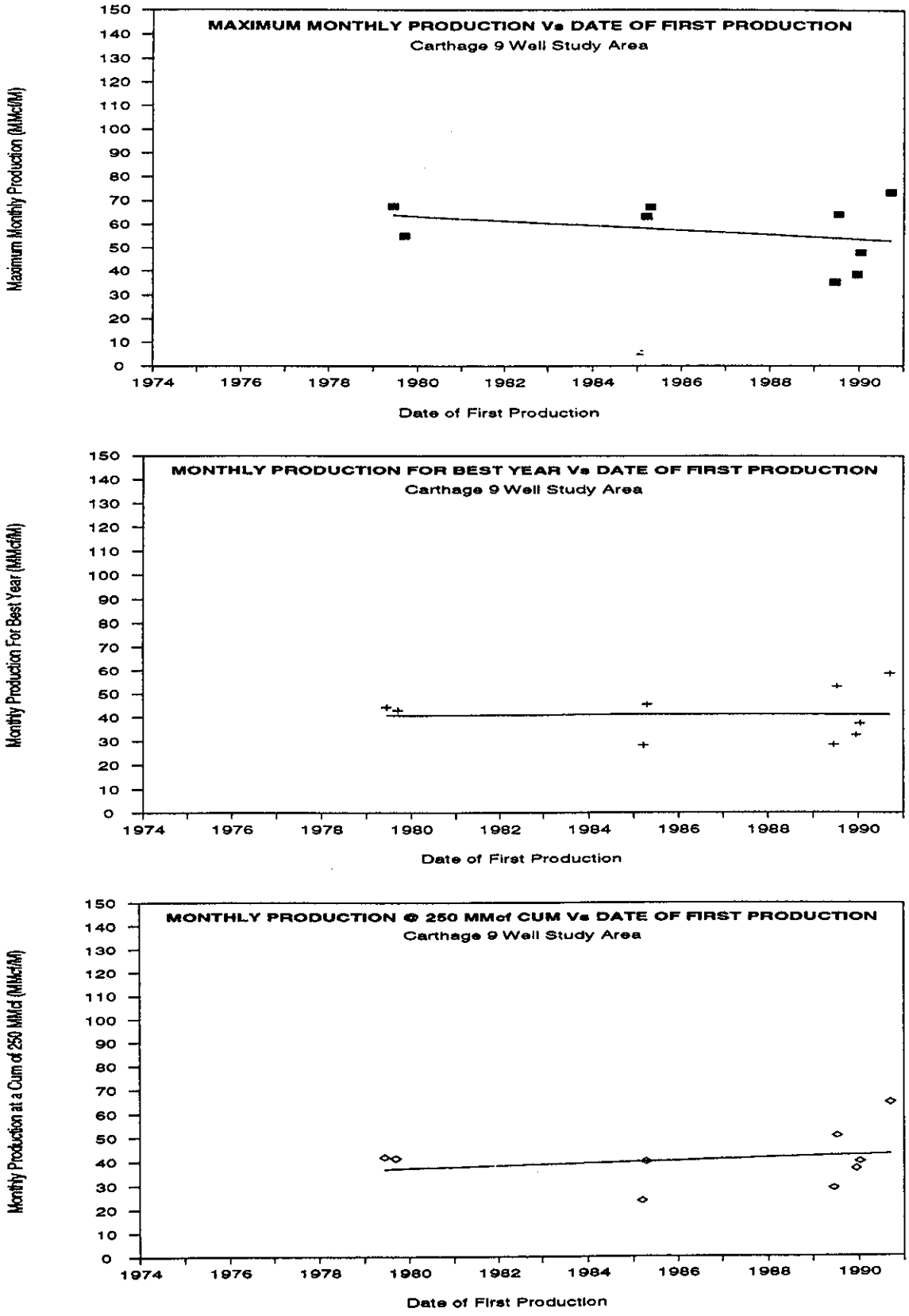

Fig. 7 - Indicator plots for a 9-well, 640 acre study area in the Carthage (Cotton Valley) Field.

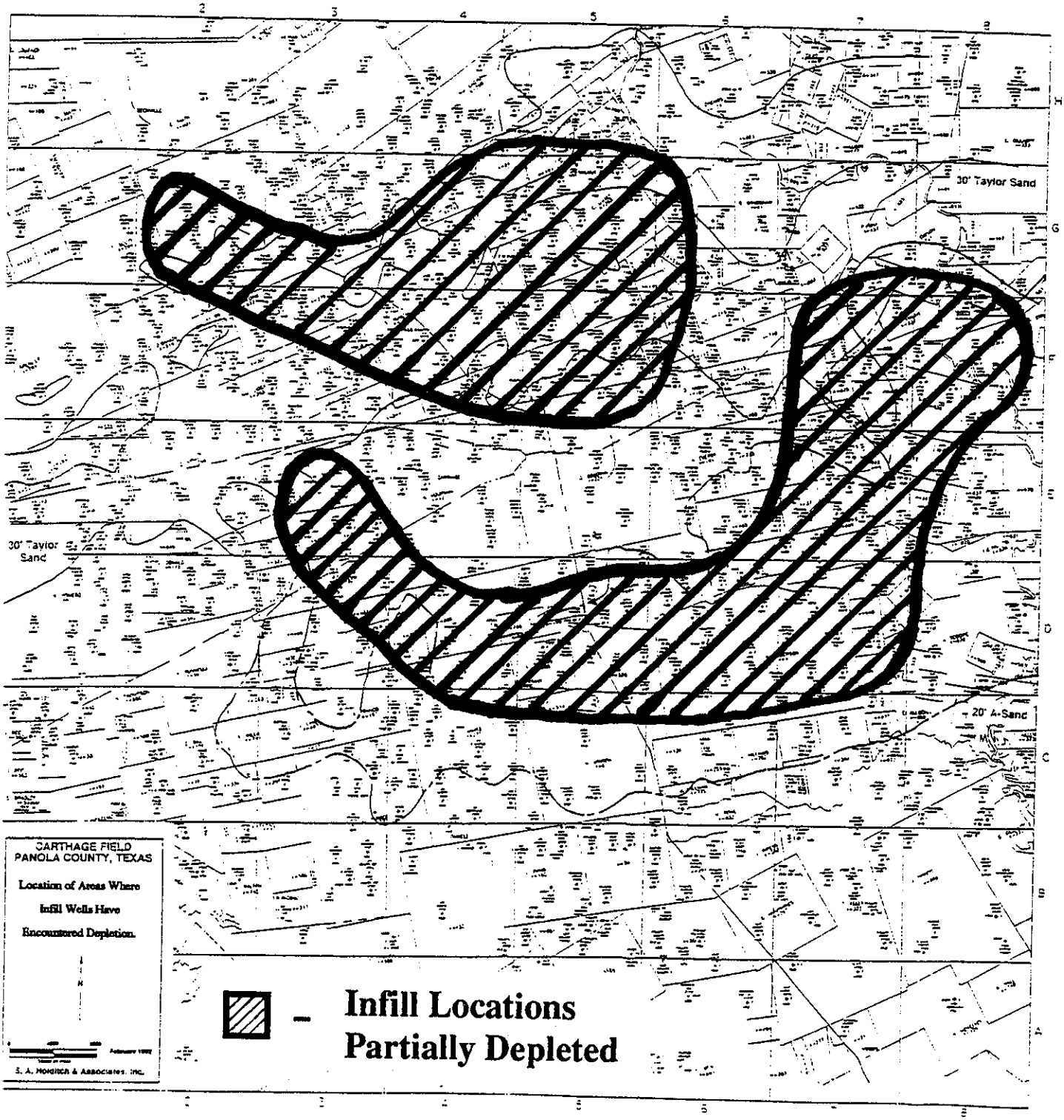

Fig. 8 - Base map of Carthage (Cotton Valley) Field showing areas where infill wells indicate partial depletion. This map is centered on the field and contains all but a few fringe wells.

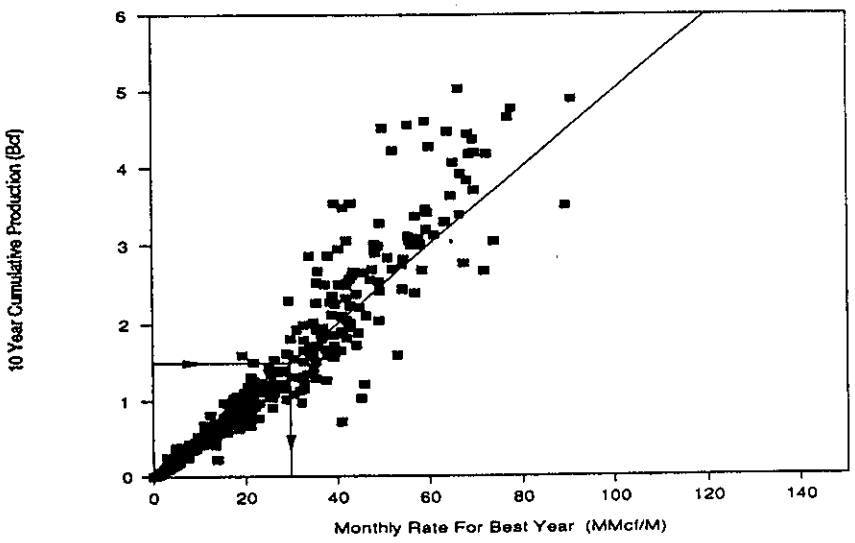

Fig. 9 - Relationship between 10-year cumulative production and the "Best Year" performance indicator for all wells in the Carthage (Cotton Valley) Field with 10 years or more of production.

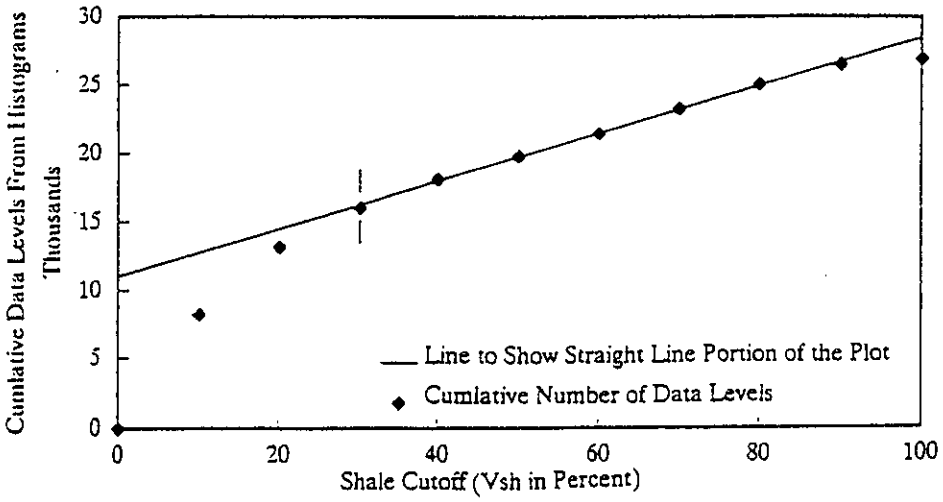

Fig. 10 - Determination of shale volume cutoff for Carthage (Cotton Valley) Field.

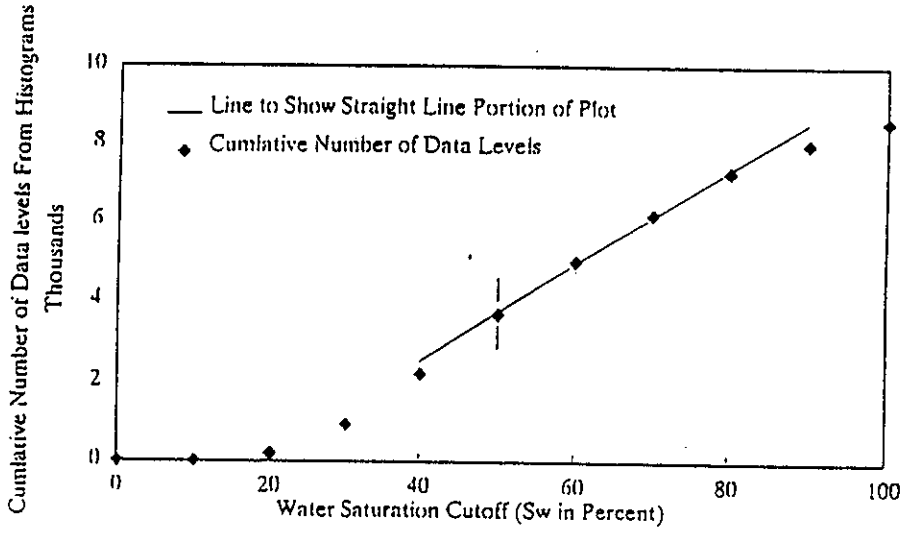

Fig. 11 - Determination of water saturation cutoff for Carthage (Cotton Valley) Field.

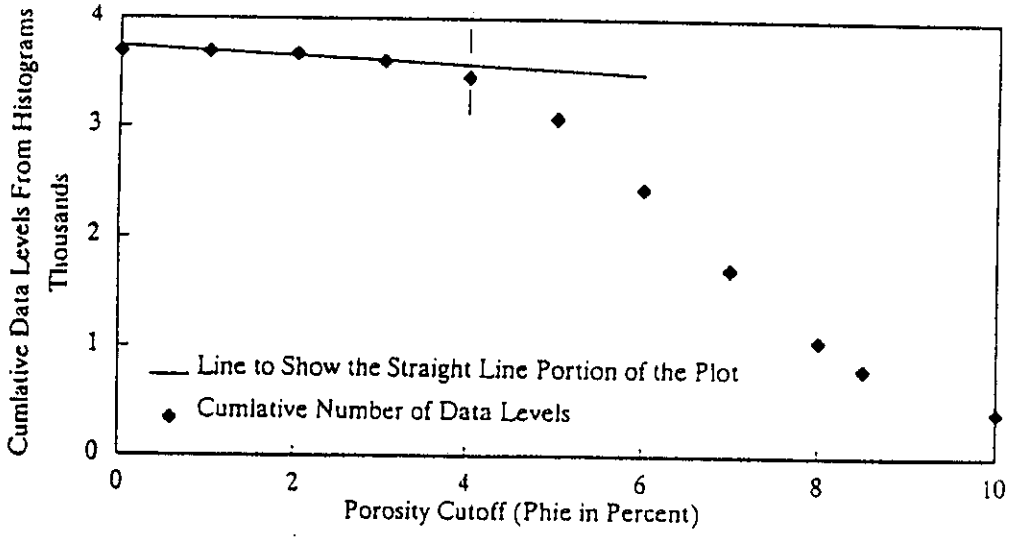

Fig. 12 - Determination of porosity cutoff for Carthage (Cotton Valley) Field.

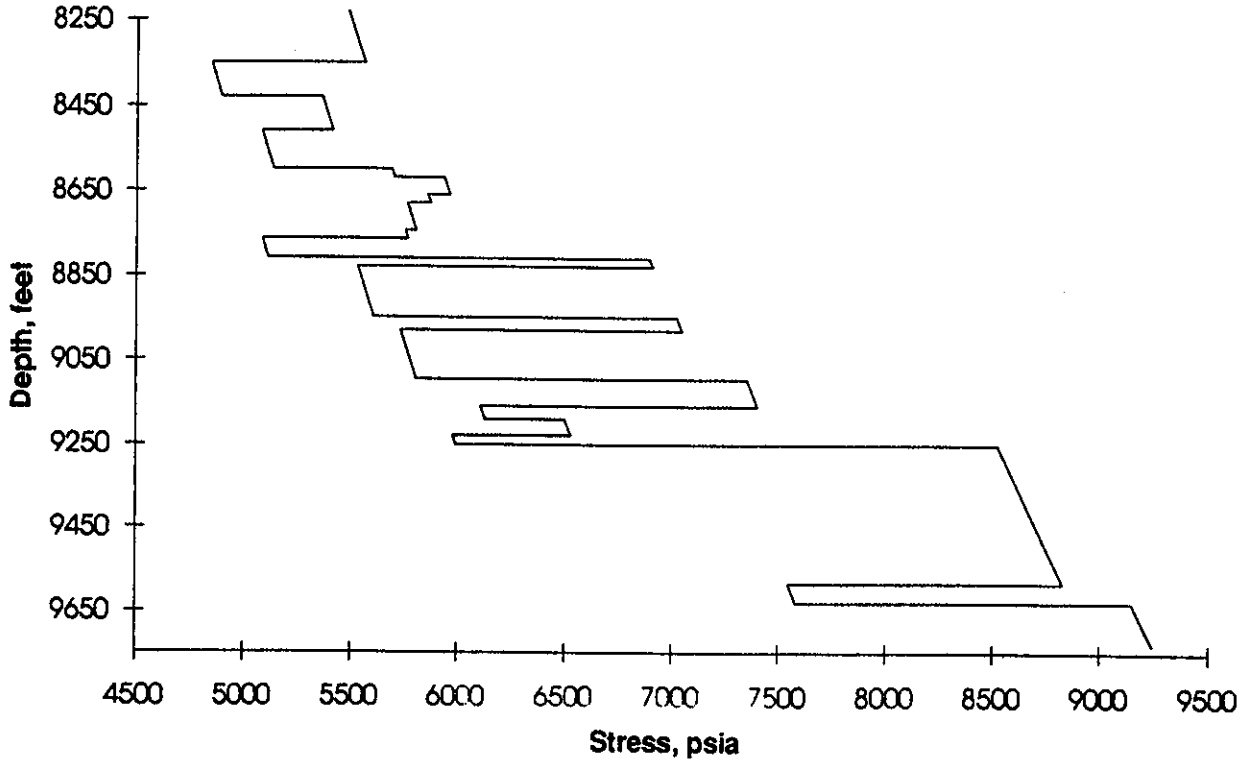

Fig. 13 - Stress profile for a typical Carthage (Cotton Valley) Field well.

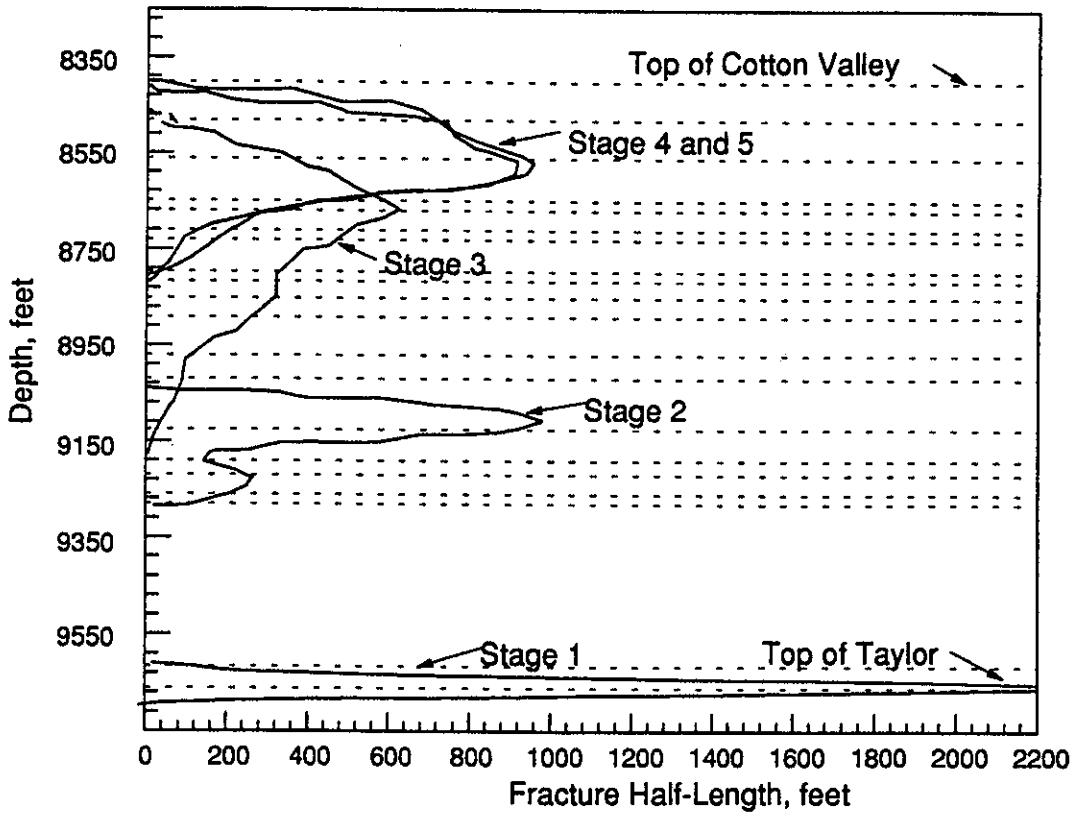

Fig. 14 - Calculated propped fracture dimensions for the 5-stage, massive hydraulic fracture treatment in the well in Fig. 13.

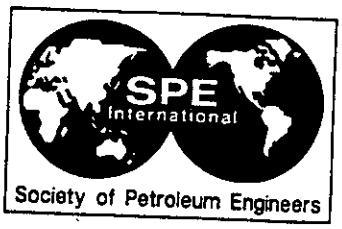

SPE 27931

3-D Reservoir Simulation Results of a 25-Square-Mile Study Area n the Kansas Hugoton Gas Field

R.J. Oberst, Mobil E&P U.S. Inc.; P.P. Bansal and M.F. Cohen, Mobil E&P Technical Center; nd T.C. Ryan, Mobil E&P U.S. Inc.

PE Members

his paper was prepared for presentation at the SPE Mid-Continent Gas Symposium held in Amarillo, Texas, 22-24 May 1994.

ABSTRACT

he Hugoton Gas Field is the largest gas field in the lower 48 tates and represents a significant portion of the domestic gas roduction and reserve base in North America. The gas bearing hase Group is characterized as a heterogeneous, multi-layered, o-crossflow system with over 5,925 producing wells in Kansas lone.

his paper reports the results of a three dimensional (3-D) servoir simulation model that predicts the behavior of this ulti-layered system under various producing scenarios. The 28 ell pattern model covers a 25 square mile representative portion f the field called the "Nix area". The area was initially mulated in 1985 to primarily study the potential benefits of fill drilling. This earlier work is the fundamental blueprint om which today's current model is built. It was felt that by corporating aspects of the previous study into the current odel, it would provide a unique baseline to compare and ntrast the earlier predictions against new data and our increased derstanding of the Hugoton field, some seven years and proximately 1,660 infill wells later. The current model also ntains two new replacement wells and an observation well that ve been drilled since 1985. In addition, individual layer essure data has been gathered along with the additional 10 ars of production and pressure data which has occurred since e first study. Using the new model, various prediction runs re made to project each well's future deliverability, ultimate covery and determine each individual layer's abandonment pressure, with or without infill drilling.

Results from the study indicate that the remaining life of the Kansas portion of the Hugoton field to be at least 40 to 50 years under existing producing conditions. The major gas producing layers will abandon at average bottomhole reservoir pressures ranging from 30-40 psia, while the tighter, less productive layers abandoning between 140-210 psia, regardless of infill drilling or not. This will result in an expected ultimate recovery of between 90%-92% of the initial gas-in-place for the major producing layers, and between 58%-68% ultimate recovery in the tightest layers. The study also indicates that due to the laterally continuous nature of the geologic layers, infill drilling will result in only a period of reserve acceleration, with no significant, incremental reserves being developed.

INTRODUCTION

This simulation study is an extension of a series of larger, fieldwide projects undertaken to accurately quantify the effects of infill drilling in the Kansas portion of the Hugoton field. In April 1986, the basic proration order[1] governing production from the Kansas Hugoton field was modified by the Kansas Corporation Commission (KCC) to allow operators the option to drill and produce a second or infill well, on any unit which contained 480 acres or greater spacing. This increased density decision was based upon geologic and engineering evidence presented by operators in the 1985 infill hearings. The testimony suggested the possibility that between 3.5-5.0 Tcf of additional gas might be recovered by infill drilling. It was assumed that the

ferences and illustrations at end of paper

second well would be required to effectively and efficiently drain the unit in a manner as to recover all possible reserves at the time of abandonment. This conclusion was made based upon geological and engineering studies, but without the benefit of actual production data from any infill wells.

In an effort to better understand and predict the future behavior of the Kansas Hugoton field, an exhaustive full-field geologic mapping and reservoir characterization project was performed prior to the current simulation work. As part of the overall study, the foam drilled Nix #1-4 observation well was drilled and tested to determine the level of depletion in each layer.

Results from the studies provided valuable input into the construction and development of the current 3-D model. The simulator's history match utilized the critical layer pressures, full-life completion histories, official annual and bi-annual state deliverability tests, and 48 years (1945-1993) of monthly production data for all wells in the study area.

This paper demonstrates that through a 3-D reservoir model, derived from extensive geologic and reservoir data, valid predictions can be made for the Kansas Hugoton field under a variety of future production scenarios. These include evaluating the merits of future proration changes which would affect the withdrawal rates from the reservoir, as well as quantifying the degree of reserve acceleration and lack of incremental reserves associated with infill drilling in the Kansas Hugoton gas field.

Background

Production from the largest gas field in the United States began in December 1922, as the first gas well was drilled in Seward County, Kansas. The gas portion of field extends over 14 different counties located in southwest Kansas and the Oklahoma, Texas panhandles (see Fig. 1). Excluding the Texas oil leg portion of the field, it is approximately 180 miles long and varies from 10 to 60 miles in width. The Oklahoma portion is referred to as the Guymon-Hugoton and the Texas portion is referred to as the Texas Hugoton gas field. The Kansas portion of the Hugoton gas field is approximately 70 percent depleted with 21 Tcf of gas already produced and another 7-8 Tcf remaining.

Geologic Studies

There have been a number of geologic articles published within industry literature describing the deposition and lithology of the Hugoton[2] and Guymon-Hugoton[3] gas fields. The Hugoton reservoir is of Permian age rock with gas production coming from the various carbonate layers of the Chase Group. The reservoir consists of a vertical series of alternating gas-bearing carbonates, separated by layers of impermeable shale and silty shales. Productive layers within the Chase are from top to bottom: the Herington, Upper and Lower Krider, Winfield, Towanda, Upper and Lower Fort Riley, and Wreford (see Fig. 2). In Kansas, the majority of the gas production comes from the Towanda, Winfield, and one or the other Upper or Lower Krider and Fort Riley layers. These layers are all laterally continuous and correlatable across the entire field with no definable, absolute barriers to horizontal flow. The Kansas portion of the Hugoton field lies on a north-northeast strike and dips gently to the southeast. Initial reservoir pressure is estimated to be 484 psia at a datum depth of 2,576 feet, with an average reservoir thickness of approximately 400 feet.

Following the KCC infill order in 1986, an extensive geologic effort was undertaken to describe the reservoir and identify areas within the field which would have the highest potential for developing additional reserves due to infill drilling. In 1989-1990, a full-field geologic mapping study[4] was performed on the Kansas portion of the Hugoton field. This study involved a select group of geologists and petrophysicists who correlated layers from over 8,100 wells and then performed detailed petrophysical log and core analysis on a subset of these wells, in order to develop a comprehensive picture of the field's stratigraphic framework and facies distributions. Their work served to establish the overall reservoir quality and determine the volumetric initial gas-in-place (IGIP) for the Kansas Hugoton field. Results from their study indicated that the total volumetrically derived, IGIP for all producing carbonate layers in Kansas Hugoton to be 31.1 Tcf. This was based upon detailed log and core analysis, along with the development of a proprietary porosity algorithm. Their work resulted in the development of a comprehensive series of structure, thickness, porosity, permeability and water saturation maps for each layer. Volumetrics were then computed over the 4,164 governmental sections studied within Kansas resulting in section by section IGIP volumes for every layer across the Kansas Hugoton field.

Reservoir Studies

The detailed mapping study was followed by an extensive reservoir characterization project[5] performed during 1990-1991. This task force worked to determine the reservoir's performance based IGIP before and after infill drilling. Individual well and composite P/z vs. cumulative production plots were generated for all wells in the field. Results from the summation of the individual well analysis and the full field composite plots indicate a performance based IGIP for Kansas Hugoton to be approximately 30.1 Tcf. From an overall standpoint, the volumetric and performance analysis are in close agreement, thus making the possibility of significant additional gas recovery from infill drilling unlikely.

In addition to this reservoir characterization work, other companies have also been active in conducting reservoir studies on the Hugoton field. Phillips Petroleum Company[6-10] has presented a very comprehensive series of papers exploring the actual performance of infill wells in Kansas Hugoton and the potential that infill drilling would have in Guymon-Hugoton.

Numerical Simulation

Numerical simulation consists of mathematically describing a reservoir's distinct geologic and fluid flow characteristics and then representing that information as a series of attributes assigned to some pattern of interconnecting grid cells. In order to mimic the dynamics of a producing hydrocarbon reservoir, and depending on the complexity of the simulator, it then linerarizes the non-linear two-phase or three-phase flow equations and solves for the fluid flux material balance occurring within each grid cell for every step in time. Numerical simulation can be an extremely valuable tool to predict the phenomena and future behavior of hydrocarbon reservoirs.

Previous Model

As technical foundation for the original infill hearing in 1985, a 25 square mile area surrounding the Nix #1 well was modelled using a Mobil proprietary simulator called ALPURS[11]. The ALPURS (ALl PURpose Simulator) model was a three-dimensional, fully implicit, two-phase black oil model built to forecast the future production rate and ultimate recovery in the Nix area for both the 25 well and 50 well infill cases. It was constructed from a localized study of the geologic and reservoir characteristics for the 7x7 section area surrounding the Nix #1. The reservoir description was obtained from log and core analysis, which resulted in a log porosity-permeability correlation and a series of maps detailing the structure, thickness, porosity, horizontal and vertical permeability, and initial water and residual gas saturations for every producing layer in the study area. The larger 7x7 section maps were then resampled in order to build the 5x5 model.

Before actual construction of the pattern model, a single well radial model was built for the Nix #1 well. This model was used for verifying the intended geologic layering, areal grid sizes, and purposed handling of wellbore stimulation parameters, necessary to accurately duplicate the response of the 72-hour state buildup tests, prior to scale up of the larger pattern model.

After validating the appropriate parameters for the history match from the single well model, the study area grids were transformed into an I,J,K coordinate system for the pattern model. The model utilized a 23x23x10 layer grid system, with eight active layers and a separated reservoir option active between layers 4 and 5. This option was used to represent the presence of the Odell Shale which is located between the Lower Krider and Winfield layers. Due to a distinct change in permeability between the upper and lower portions of the Towanda, this layer was separated into two layers (Upper & Lower Towanda - layers 7 and 8) for modelling purposes. Based upon the geologic description, layers in the I and J dimensions (x and y directions) were modelled as laterally continuous throughout, with no barriers to horizontal flow. A zero flux boundary condition was placed at the edges of the 5x5 area with a gas-water contact set at 2,880 feet. The relative permeability data used in the model were based upon special core analysis performed on core obtained from Nix #1-3 well. Initially, the total volume of gas-in-place based on log analysis was 214 Bcf for the Nix 5x5 study area. This volume was subsequently reduced to 172 Bcf, in order to match the well's historical pressure performance. This 20 percent reduction (42 Bcf) in IGIP could have been the result of 1) errors in the log analysis, 2) gas migration away from the study area before it was developed, or 3) the gas was "hidden" and not in pressure communication with the producing wells, thus becoming the target for infill drilling.

The model was then history matched by comparing the simulator's predicted pressures against each well's historical pressure and rate performance from 1945 to 1983. Predictions of future reservoir performance under the 25 well (640 acre) and 50 well (320 acre) densities were then made to quantify the effects of infill drilling.

Predictions from the 1985 model were subject to the following assumptions:

1) Each of the 25 infill wells were perforated in all active layers and every layer received a successful fracture-stimulation which yielded a -4.0 skin throughout the wellbore.
2) The total maximum production from all wells in the study area would not exceed a rate of 3.0 Bcf/year.
3) Minimum bottom hole flowing pressure was 20 psia with a minimum production rate of 10 Mscf/d per well.

Results from the earlier model indicated that the maximum total gas production expected from the Nix area would be 162.1 Bcf for the 50 well case by the year 2048, compared to 161.6 Bcf being produced from the original 25 wells in the year 2084. This indicated a possible maximum benefit of 36 years of acceleration with only an additional 0.5 Bcf of incremental reserves attributed to the extra 25 infill wells. These predictions were largely the result of the first assumption, which was that each infill well would be completed from top to bottom and receive a -4.0 skin in every layer. In light of the actual

performance of the 1600+ infill wells to date, this assumption was optimistic. In order to avoid any undue optimism in the current model, infill wells were assigned the same completion and layer skins as their respective parent (original) well.

Current Model

As stated earlier, the 1985 model was used as the template for the current 3-D pattern model (see Fig. 3). The current work was modelled using Mobil's new proprietary simulator called PEGASUS. In reviewing the 1985 geologic description, it was confirmed that the earlier petrophysical description was adequate to represent the degree of areal variation occurring within each layer. In reviewing the porosity logs from the 1985 study, it was detected that a rather poor quality log was used in the northwest corner of the model for the Herington (layer 1). This log was originally used for control in the 1985 description, but was rejected for inclusion in the 1989 fieldwide volumetric study. Consequently, the IGIP for the current model was modified slightly by changing the porosity in the Herington layer. This was done in order to match the model's IGIP for the Herington layer with the results from the full field mapping study. The current model now has an IGIP of 175.5 Bcf. Also, since there was no evidence found from the mapping study for the existence of any horizontal flow barriers, all layers were left as laterally continuous throughout with only limited vertical communication occurring via hydraulic fractures and backflow in the wellbores. The same individual layer relative permeability curves were used again, along with the assumption that the initial water saturation values were equal to the interstitial water saturations except for in the Upper and Lower Fort Riley, and that the gas-water contact was still at 2,880 feet. The density of water used was 62.653 lb/ft^3, along with a gas specific gravity of 0.69 and a reservoir temperature of 95° degrees fahrenheit.

Completion Data

Since the 1985 study, two replacement wells were drilled in the Nix area. Figure 4 shows the I,J location for all Hugoton wells in the Nix 5x5 study area. Well W51144 (lease code number assigned by the KCC) was plugged and abandoned in February, 1987 and replaced by well W51243. Likewise, well W55246 was plugged in March, 1990 and replaced by well W55529. Both wells necessitated replacement due to casing integrity problems and declining gas production. Initial 72-hour state surface shut-in pressures recorded for these two wells were 172.5 psig and 124.2 psig respectively. Also, well W76260 was drilled deeper by 40 feet in July, 1990 and is now completed down through the Towanda (layers 7 and 8).

In conjunction with the replacement well activity, a large number of hydraulic fracture treatments were performed in the Nix area between 1986 and 1990. Various stimulations jobs were done on another 13 wells in the model area. The various fracture stimulation treatments were modelled by slightly increasing the wellbore penetration length and negative skins in the appropriate layers.

Observation Well

As part of the 1991 reservoir characterization project, a plan was initiated to obtain individual layer to validate and improve the 1985 simulation. In June, 1992 the Nix #1-4 observation well[12] was drilled and completed in the Nix 5x5 study area. An exception location was sought from the KCC to place the observation well as physically close as possible to the lease lines in the southwest corner of the unit. This was done to obtain pressure data from the edge of the drainage radius of the four surrounding original wells, thus maximizing the potential for measuring the communication between the wells. In addition, by placing the observation well in the center of the surrounding four wells, this provided a measurement of the maximum pressure gradients present in each layer. It was felt that if the observation well could find any layers with initial or near virgin pressures, this would help confirm the theory of "unconnected" gas pockets. The observation well was conventionally drilled with a water-based mud system down to the top of the Chase. In order to minimize the skin damage at the formation face, the drilling mud was then switched to a disposal foam system and the well was drilled down into the middle of the Herington layer. Tandem electronic gauges were run in the hole, followed by a retrievable packer set above the gauges to isolate the zone for test. A extended drill stem test (DST) was conducted to measure the drawdown and buildup pressures and determine the layer's average pressure. After each test was completed, the gauges were retrieved and pressure transient analysis was performed to validate the test results before drilling into the next zone. All subsequent tests were performed in the same manner.

Table 1 lists the individual layer pressures data obtained from the observation well. These pressures were incorporated into the current model and compared against the same cell pressures predicted from the base case (25 wells) run in the 1985 simulation. The comparison showed that even after adjusting for the difference between the forecasted and actual production from 1984 to 1992, the earlier model still predicted a more uniform depletion, (less differential depletion between the various low and high permeability layers) than what was measured during the DST's. This difference demonstrated how important the individual layer pressure data was in achieving the desired accuracy and proper material balance for the current model.

History Match

As stated earlier, 48 years of monthly production data, annual/bi-annual 72-hour buildup tests and the individual layer pressures were used in the history match. The 72-hour surface shut-in pressures were converted to bottomhole conditions and used to match against the predicted pressures. Reservoir regions were assigned to each well for the purpose of calculating the bottomhole pressures. These regions were defined by the well's completion interval and areal drainage seen during the 72-hour buildup tests. A valid history match was obtained by adjusting the wellbore parameters (penetration length, permeability and layer skin factors) to properly account for the drainage and interference effects, along with matching the correct individual layer pressures (differential depletion in each layer). As stated earlier, the 1985 model's IGIP of 214 Bcf had to be reduced by 20 percent to 172 Bcf, in order to match the observed individual well pressure data. The current model has 175.5 Bcf for IGIP which was based upon matching the individual layer DST data and comparison with the updated volumetrics using a 4% porosity and 80% water saturation cutoff for the Nix area.

Figures 5 and 6 show the two replacement well's pressure profile and resulting history match. In order to trace the location of the intended wells declining average pressure through time, the two wells were introduced in the model at 1945 (T_i=0) but were given a zero production rate (Q_i=0). The replacement wells were then "turned on" at the time they were physically drilled. By tracing the well's declining pressure profile through time, this demonstrated the possible pressure range that an infill well might encounter. Figure 7 shows the final history match for the Nix #1 (center well) in the pattern model.

Individual well and a composite P/z verses cumulative production plot were made for all wells in the Nix study area. Figure 8 is a P/z composite plot which compares the historical pressure data against the model's total system hydrocarbon-weighted average pressure for the entire 25 sections in the Nix area. By comparing the individual well averaged data, against the "true" total system hydrocarbon-weighted depletion curve, it can provide a reasonable estimate of the total recoverable reserves expected from the study area. By a straight line extrapolation of the averaged historical depletion curve to an estimated 20 psig (34.4 psia) abandonment pressure, a reasonable estimate of approximately 150 Bcf in ultimate recovery can be expected from the Nix area. This estimate is in close agreement with the total gas recovery predicted from the various model runs. Caution should be used however when interpreting this type of performance data by itself, since the wells are in communication and can interfere with each other. Also, since the 72-hour shut-in pressures are averaged and slightly understates the "total system average pressure", the resulting analysis should be recognized as an acceptable approximation (not absolute) for the total IGIP and should be substantiated with volumetric analysis if available.

Original and Infill Well Predictions

The current Nix 3-D pattern model was used to predict the future deliverability and ultimate recovery from both the original and infill well cases using various "offtake" or production scenarios. The 25 well (640 acre spacing) case was simulated from 1945 to 2053 (108 years), with forecasted production starting in 1993. This case established a "base case" of future production under current operating conditions. The minimum rate constraint (economic limit) was set at 35 Mscf/d, which was higher than the 1985 model rate of 10 Mscf/d. The 35 Mscf/d rate also helped to established a realistic "time frame" in which to produce the remaining reserves in the study area. Another run was made using the 10 Mscf/d minimum rate, but showed an enormous length of future producing life, with essential no additional gas being produced. For the base case, the minimum bottomhole flowing pressure was set at 35 psia, to investigate the sensitivity of future production resulting from limited facility upgrades to the gathering systems. If any wells failed to produce at their forecasted rates, the simulator would attempt to cut the rate to an acceptable rate that the well was capable of. If the well failed to flow above the minimum rate, it was plugged and abandoned with no further development on the unit. For the non-infilled, base case (NI1), each well was assigned it's highest 3-month average capacity from the previous year. Cumulative recovery for the Nix area using the 25 well base case is 153.2 Bcf.

A second non-infill case (NI2) was modelled using a total field (Nix 5x5) production rate of 20MMscf/d and allowing the simulator to allocate the production based up individual well's calculated capacity. This case represented possible increases in allowable assignments due to reducing the field's deliverability standard pressure. This case demonstrated the possible increases in deliverability and possible acceleration of reserves from the 25 wells (640 acre density).

Finally, a third case (NI3) was modelled similar to the base case, except the bottomhole flowing pressure constraint was changed from 35 psia to 15 psia, to simulate the anticipated future facility upgrades needed to reduce line pressures in Hugoton. These upgrades to the gathering systems will ultimately have to occur before abandonment of the field. This "high case" served to establish an upper limit for the expected deliverability, ultimate recovery and acceleration possible from the 25 well (640 acre spacing).

For the infill case (INF1), all infill wells were placed in the southeast corners of the section, except for in the northeast corner section where it was placed in the upper right hand corner because of the presence of the replacement well. As stated

earlier, the current model has all 25 infill wells assigned with the same completion intervals and skins as their respective original wells currently have. This was done to reflect the current fracture technology available and not purposely overstate the potential from infill drilling. The 50 well (320 acre density) infill case was modelled for the same period as the other cases, with the wells receiving the same initial 3-month average capacity rate that their original wells have. Is essence, this case shows the effects of "doubling" the production in Hugoton, if that were physically possible. For this case, the same 35 Mscf/d minimum rate and 35 psia minimum bottomhole flowing pressure constraints were used as in the base case.

Figure 9 is a comparison of the 25 well base case (NI1) and the 50 well infill (INF1) case. Notice that by doubling the well density and gas rate, this yields only about 10 years of increased production, after which the production level drops off dramatically compared to the 25 well case. Since the total cumulative recovery for the two cases is essentially the same, the "true" benefit of blanket infill drilling is acceleration. Figure 10 is a summary plot showing various prediction cases and their resulting effects on gas rate and cumulative production. Table 2 lists the expected percent recovery per layer for both the non-infill and infill cases. This clearly demonstrates that infill drilling will be no more effective in reducing the abandonment pressure in tight layers than the original wells have. Comparing the 25 well base case against the 50 well infill case, it shows that over the next 60 years a total incremental recovery of only 1% of IGIP or 0.064 Bcf per infill well, should be expected from blanket infill drilling. In fact, the non-infill compression case demonstrates that higher recoveries can be obtained from just lowering the gathering system's line pressure, rather than by drilling a second well on every unit.

Conclusions

The following conclusions can be made for the 25 square mile Nix study area, as well as for the other major gas producing units or "fairway" portion of the Kansas Hugoton gas field.

1. Through a valid 3-D reservoir model, the following accurate predictions can be made about the future producing life of the Kansas Hugoton Gas Field.
   A. The future remaining life to be at least 40-50 years under existing withdrawal rate conditions.
   B. The major gas producing layers will abandon at reservoir pressures between 30-40 psia, with the tighter, less productive layers between 140-210 psia, with or without infill drilling.
   C. This will result in an expected ultimate recovery between 90%-92% of the IGIP for the major gas producing layers, with or without infill drilling. By adding additional compression to the original wells, this can increase recovery from 90%-92% to 92%-94% of IGIP fro the major producing layers.
   D. Blanket infill drilling results in a period of increased production and reserve acceleration with no significant, fieldwide incremental reserves being developed.

2. The 3-D reservoir model can accurately represent the reservoir heterogeneity, differential depletion and producing capability of this layered, no-cross flow reservoir.

3. A valid history match was obtained by matching the individual well state test data and individual layer pressures measured in the observation well. The DST data provided a direct measurement of the drainage status in each of the layers, which showed strong evidence that:
   A. The major producing zones are in good lateral communication and being adequately depleted.
   B. The maximum distance from surrounding wells found no "pockets" of virgin or anything close to initial pressure.

4. The model accurately predicted the two replacement wells declining reservoir pressure through time. These replacement wells can be used as a direct corollary for predicting what initial pressures that infill wells would encounter.

5. All 25 wells (640 acre spacing) are in pressure communication with each other and experience interference caused by hydraulic fracture stimulations performed on the laterally continuous geologic layers.

Nomenclature

IGIP	=	Initial gas-in-place, Bcf, e^6m^3
NF	=	no measurable flow during drill stem test
P_{abd}	=	hydrocarbon weighted average layer abandonment pressure, psia, kpa
P_i	=	initial layer pressure at time of drill stem test, psia, kpa
P_{max}	=	maximum pressure measured from cased hole, psia, kPa
Q_i	=	initial gas rate, Mcf/d, m^3/d
Rem. GIP	=	Remaining gas-in-place, Bcf, e^6m^3
RF	=	recovery factor (Cum Gas Produced / IGIP), percent
SIBHP	=	shut-in bottomhole pressure, psia, kPa
T_i	=	initial simulation time, years (1945 = 0)
z	=	gas deviation factor, dimensionless

Acknowledgments

The authors thank Mobil Exploration and Producing U.S., Inc. for permission to publish this paper. We gratefully acknowledge the contributions of the numerous engineers and geologists who performed the original 1985 simulation work in Kansas Hugoton. We would also like to recognize K.R. Poulton, J.V. Pelster and especially L.J. Reimer for their efforts during the current simulation project.

References

1. Kansas Corporation Commission Order Docket No. C164, July 18, 1986.

2. Garlough, J.L. and Taylor, G.L.: "Hugoton Gas Field, Grant, Haskell, Morton, Stevens, and Seward Counties, Kansas and Texas County, Oklahoma", in Levorson, A.I (ed.): Stratigraphic Type Oil Fields, American Association of Petroleum Geologists, Tulsa (1941) 78-104.

3. Siemers, W.T. and Ahr, W.H.: "Reservoir Facies, Pore Characteristics, and Flow Units - Lower Permian, Chase Group, Guymon-Hugoton Field, Oklahoma", paper SPE 20757 presented at the 1990 Annual SPE Fall Meeting, New Orleans, September 23-26.

4. Gwinner, D.M., Laude, L.S., Olmos, J.L., Quirein, J.A., and Reimer, L.J.: "Improved Reservoir Characterization by Integration of Petrophysics, Geology, and Core Analysis: An Example from the Hugoton Field, Kansas", paper SPWLA TT presented at the 1991 SPWLA 32nd Annual Logging Symposium, Midland, June 16-19.

5. Ryan, T.C., Oberst, R.J., and Hansen, C.D.: "Analysis of Infill Drilling in Kansas Hugoton," paper SPE 27921 to be presented at the 1994 Mid-Continent Gas Symposium, Amarillo, May 22-24.

6. McCoy, T.F., Fetkovich, M.J., Needham, R.B., and Reese, D.E.: "Analysis of Kansas Hugoton Field Infill Drilling, Part I: Total Field Results Analyzed by Operator," paper SPE 20756 presented at the 1990 Annual SPE Fall Meeting, New Orleans, September 23-26.

7. Fetkovich, M.J., Needham, R.B., and McCoy, T.F.: "Analysis of Kansas Hugoton Infill Drilling, Part II: Twelve Year Performance History of Five Replacement Wells," paper SPE 20779 presented at the 1990 Annual SPE Fall Meeting, New Orleans, September 23-26.

8. Ebbs, D.J., Works, A.M., and Fetkovich, M.J.: A Field Case Study of Replacement Well Analysis Guymon-Hugoton Field, Oklahoma," paper 20755 presented at the 1990 Annual SPE Fall Meeting, New Orleans, September 23-26.

9. Fetkovich, M.J., Ebbs, D.J, and Voelker, J.J. "Development of a Multiwell, Multilayer Model to Evaluate Infill Drilling Potential in the Oklahoma Hugoton Field," paper SPE 20778 presented at the 1990 Annual SPE Fall Meeting, New Orleans, September 23-26.

10. McCoy, T.F., Reese, D.E., Fetkovich, M.J., Needham, R.B., and Freeman, B.E.: "Analysis of Kansas Hugoton Field Infill Drilling, Part III-1993 Update and Infill Well Case Histories," paper SPE 26189 presented at the 1993 Gas Technology Symposium, Calgary, June 28-30.

11. Bansal, P.P., Harper, J.L., McDonald, A.E., Moreland, E.E., Odeh, A.S., and Trimble, R.H.: "A Strongly Coupled, Fully Implicit, Three Dimensional, Three Phase Reservoir Simulator," paper SPE 8329 presented at the 54th Annual Fall Technical Conference of the SPE-AIME (1979), Las Vegas, September 23-26.

12. Ryan, T.C., Sweeney, M.J., Scott, B.D., Jamieson, W.H., and Tanigawa, J.J.: "Individual Layer Transient Tests in Low Pressured, Multi-Layered Reservoirs," paper SPE 27928 to be presented at the 1994 Mid-Continent Gas Symposium, Amarillo, May 22-24.

SI Metric Conversion Factors

acre	x	4.046873	E-01	=	ha
ft	x	3.048*	E-02	=	m^3
ft^3	x	2.831685	E-02	=	m^3
°F		(°F-32)/1.8		=	°C
lbm	x	4.535924	E-01	=	kg
mile	x	1.609344*	E+00	=	km
psi	x	6.894757	E+00	=	kPa

*Conversion factor is exact.

Nix #1-4 Observation Well (Sec. 25-T33S-R36W)

Kansas Hugoton Gas Field - Nix Study Area

Reservoir Layers			Drillstem Test Results	
	DEPTH (Feet)	NAME (Model #)	Pi (Psia)	FLOW (Mcf/d)
HUGOTON FIELD (CHASE GROUP)		Sumner Sh.		
	2634	Herington (1)	254	33
	2658	Paddock Sh. (2)		
	2666	Upper Krider (3)	348*	NF
	2691	Lower Krider (4)	144	34
	2740	Odell Sh. (Sep. Resv.)		NF
	2748	Winfield (5)	158	141
	2785	Gage Sh. (6)		NF
	2808	Towanda Upper & Lower (7&8)	172	33
	2875	Fort Riley Upper & Lower (9&10)	Not Tested - Below GWC	

NF = No Measureable Flow During DST

* Pmax. from later Cased Hole Test

Table 1

Pattern Model Simulation Results

Kansas Hugoton Gas Field - Nix Study Area (Case Comparisons Yrs. 1993 - 2053)

	1945		1993		Base Case (NI1)	Infill Case (INF1)	Compression Case (NI3)
Layer	IGIP (Bcf)	% Total IGIP (%)	Rem. GIP (Bcf)	Rec. Factor (%)	*35/35 Constraints Rem. GIP / Pabd / RF (Bcf / Psia / %)	*35/35 Constraints Rem. GIP / Pabd / RF (Bcf / Psia / %)	*35/15 Constraints Rem. GIP / Pabd / RF (Bcf / Psia / %)
Herington	17.7	10	10.3	42	5.8 / 165 / 67	5.0 / 143 / 68	5.6 / 159 / 68
U. Krider	5.3	3	3.9	26	2.2 / 207 / 58	2.2 / 206 / 59	2.2 / 206 / 58
L. Krider	59.9	34	17.9	70	5.9 / 51 / 90	5.7 / 49 / 90	4.5 / 39 / 92
Winfield	32.5	18	10.1	69	3.3 / 52 / 90	3.0 / 48 / 91	2.6 / 40 / 92
U. Towanda	6.5	4	2.2	66	0.6 / 46 / 91	0.5 / 42 / 92	0.5 / 35 / 92
L. Towanda	47.1	27	14.3	70	3.9 / 43 / 92	3.8 / 40 / 92	2.7 / 30 / 94
U.F. Riley	5.9	3	1.8	69	0.5 / 46 / 92	0.5 / 43 / 92	0.3 / 34 / 95
L.F. Riley	0.6	0	0.2	67	0.1 / 63 / 83	0.0 / 59 / 90	0.0 / 51 / 90
Total System	175.5	100	60.6	65	22.3 / 65 / 87	20.7 / 60 / 88	18.4 / 54 / 90

Table 2

HUGOTON FIELD - STRATIGRAPHIC COLUMN

SYSTEM	AGE	GROUP	FORMATION	MEMBER	LAYER
PERMIAN	WOLFCAMPIAN	CHASE	WELLINGTON	HOLLENBERG (LS)	HOLLENBERG
			NOLANS (LS)	HERINGTON (LS)	HERINGTON
				PADDOCK (SH)	PADDOCK
				KRIDER (LS)	UPPER KRIDER
					LOWER KRIDER
			ODELL (SH)		ODELL
			WINFIELD (LS)	CRESSWELL (LS)	WINFIELD
				GRANT (SH)	
				STOVALL (LS)	
			DOYLE (SH)	GAGE (SH)	GAGE
				TOWANDA (LS)	TOWANDA
				HOLMESVILLE (SH)	HOLMESVILLE
			BARNESTON (LS)	FORT RILEY (LS)	UPPER FORT RILEY
				OKETO (SH)	LOWER FORT RILEY
				FLORENCE (LS)	
			MATFIELD (SH)	BLUE SPRINGS (SH)	MATFIELD
				KINNEY (LS)	
				WYMORE (SH)	
			WREFORD (LS)	SCHROYER (LS)	WREFORD
				HAVENSVILLE (SH)	
				THREEMILE (LS)	

Fig. 2

Hugoton Gas Field - Nix Study Area

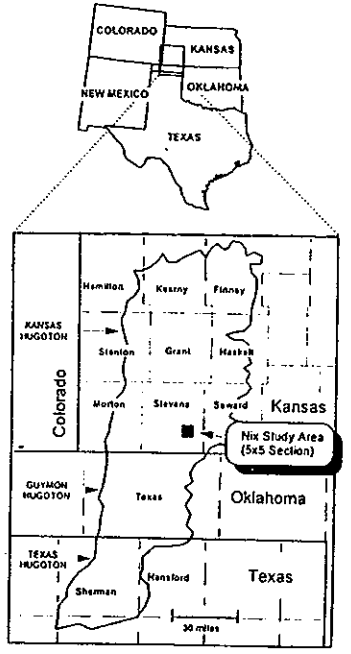

Fig. 1

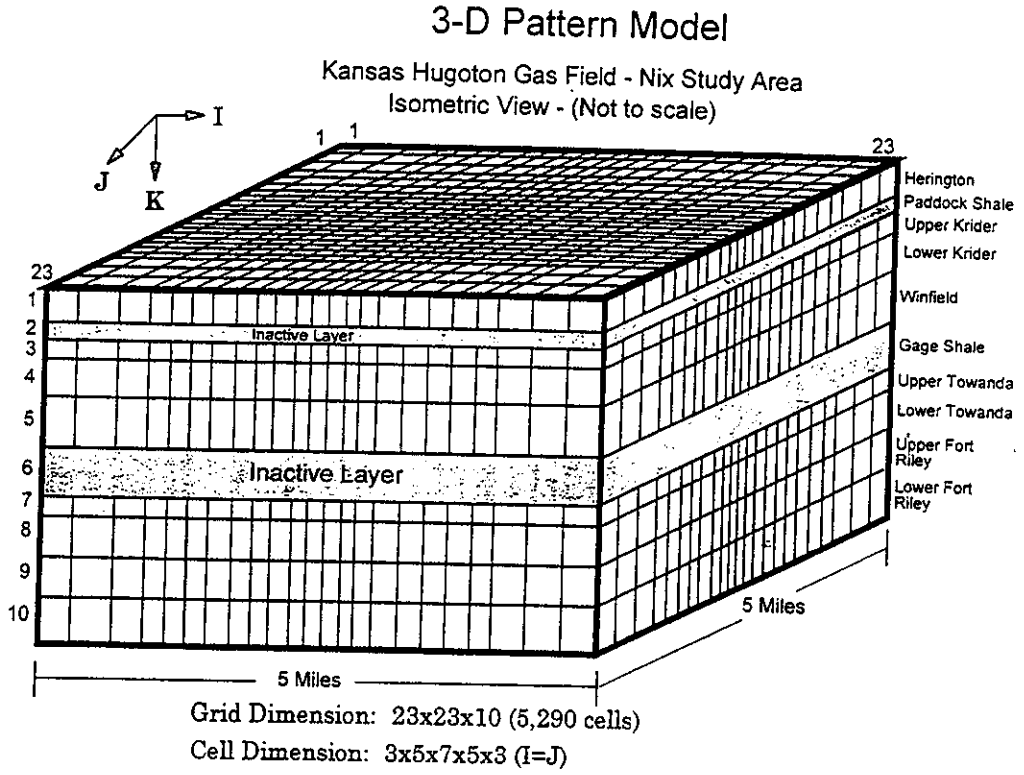
3-D Pattern Model
Kansas Hugoton Gas Field - Nix Study Area
Isometric View - (Not to scale)
I
J
K
1
1
23
23
1
2
3
4
5
6
7
8
9
10
Inactive Layer
Inactive Layer
Herington
Paddock Shale
Upper Krider
Lower Krider
Winfield
Gage Shale
Upper Towanda
Lower Towanda
Upper Fort Riley
Lower Fort Riley
5 Miles
5 Miles
Grid Dimension: 23x23x10 (5,290 cells)
Cell Dimension: 3x5x7x5x3 (I=J)

Fig. 3

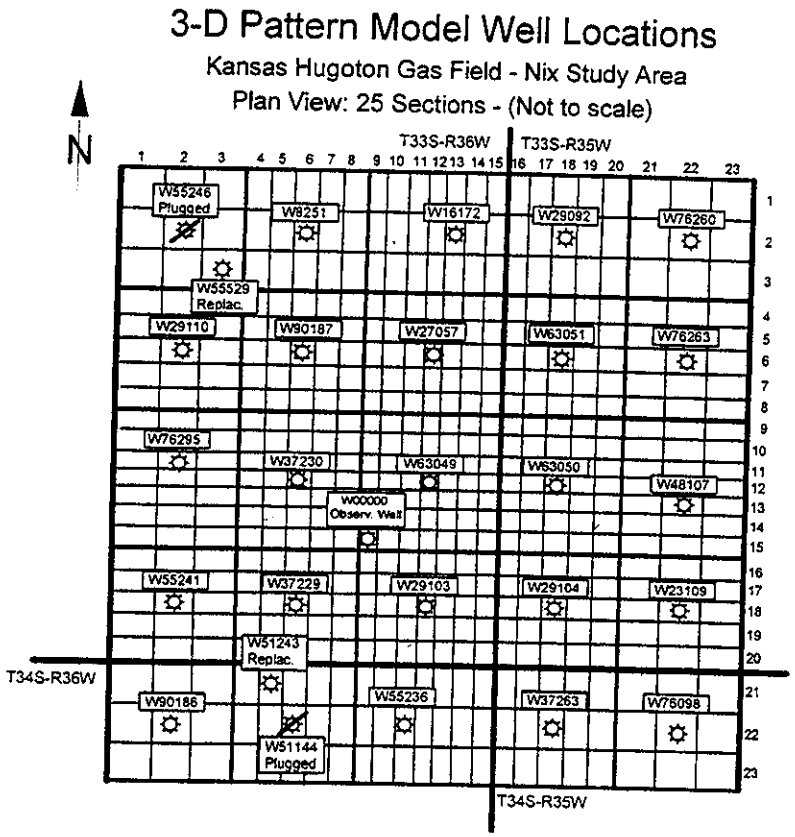
3-D Pattern Model Well Locations
Kansas Hugoton Gas Field - Nix Study Area
Plan View: 25 Sections - (Not to scale)
N
T33S-R36W
T33S-R35W
T34S-R36W
T34S-R35W
W55246 Plugged
W8251
W16172
W29092
W76260
W55529 Replac.
W29110
W90187
W27057
W63051
W76263
W76295
W37230
W63049
W63050
W48107
W00000 Observ. Well
W55241
W37229
W29103
W29104
W23109
W51243 Replac.
W90186
W55236
W37263
W76098
W51144 Plugged

Fig. 4

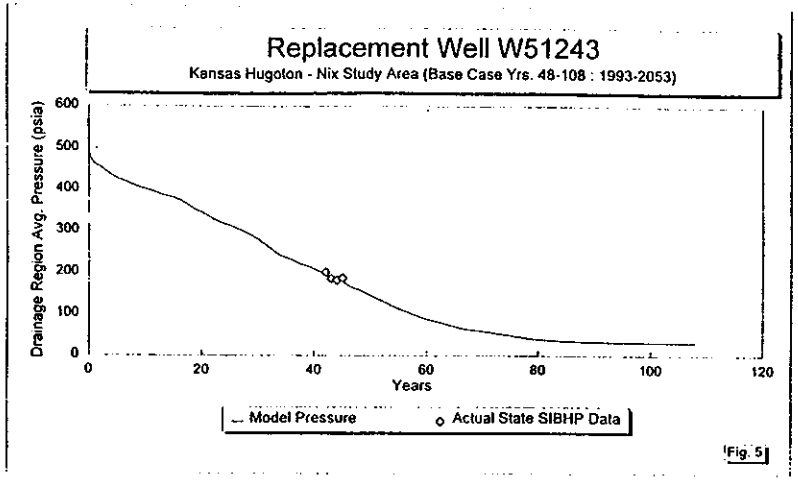
Replacement Well W51243
Kansas Hugoton - Nix Study Area (Base Case Yrs. 48-108 : 1993-2053)
Drainage Region Avg. Pressure (psia)
Years
Model Pressure
Actual State SIBHP Data
Fig. 5

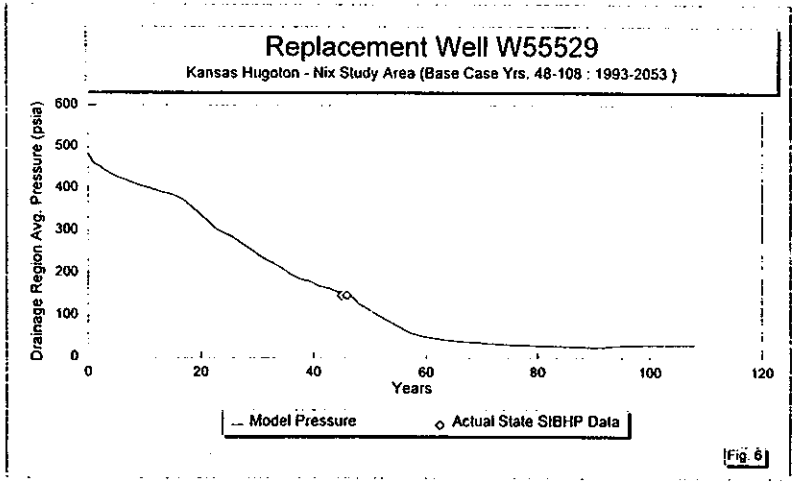
Replacement Well W55529
Kansas Hugoton - Nix Study Area (Base Case Yrs. 48-108 : 1993-2053)
Drainage Region Avg. Pressure (psia)
Years
Model Pressure
Actual State SIBHP Data
Fig. 6

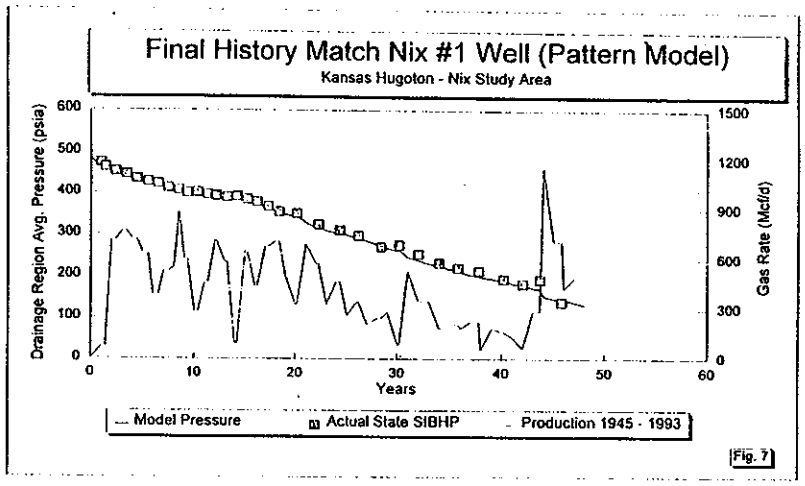
Final History Match Nix #1 Well (Pattern Model)
Kansas Hugoton - Nix Study Area
Drainage Region Avg. Pressure (psia)
Gas Rate (Mcf/d)
Years
Model Pressure
Actual State SIBHP
Production 1945 - 1993
Fig. 7

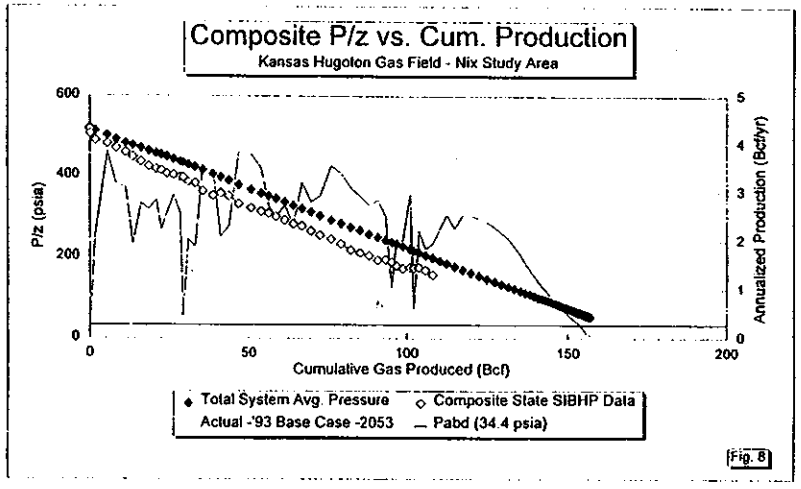
Composite P/z vs. Cum. Production
Kansas Hugoton Gas Field - Nix Study Area
P/z (psia)
Annualized Production (Bcf/yr)
Cumulative Gas Produced (Bcf)
Total System Avg. Pressure
Composite State SIBHP Data
Actual -'93 Base Case -2053
Pabd (34.4 psia)
Fig. 8

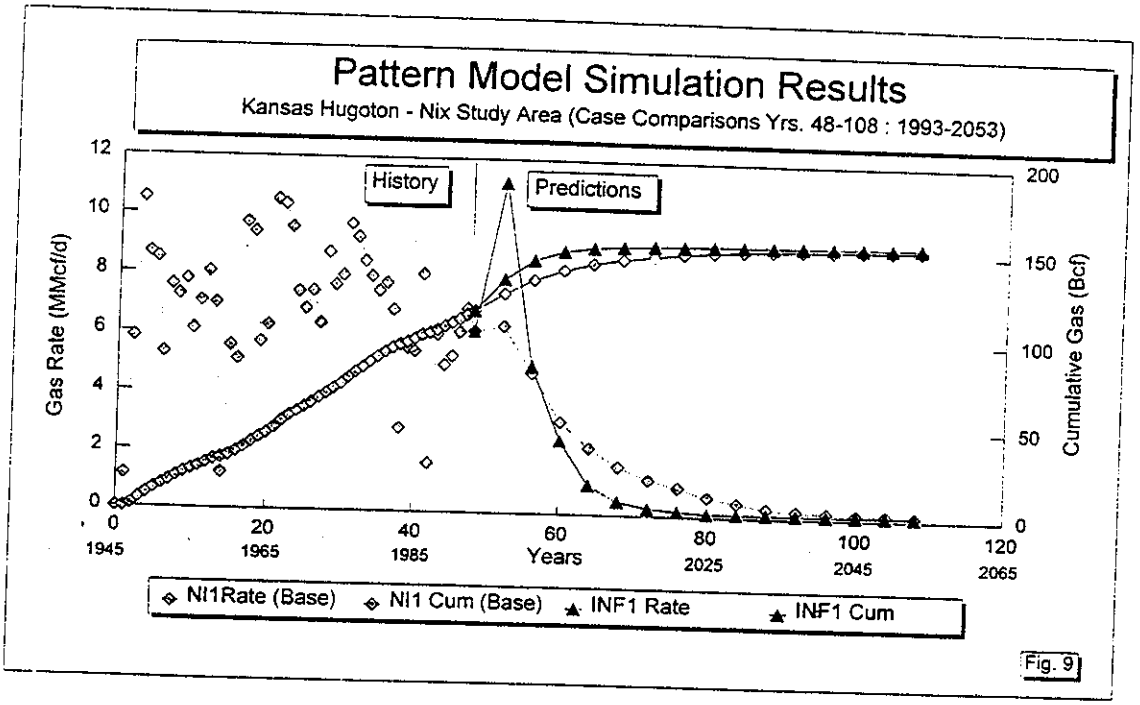
Pattern Model Simulation Results
Kansas Hugoton - Nix Study Area (Case Comparisons Yrs. 48-108 : 1993-2053)
History
Predictions
Gas Rate (MMcf/d)
Cumulative Gas (Bcf)
Years
1945
1965
1985
2025
2045
2065
NI1Rate (Base)
NI1 Cum (Base)
INF1 Rate
INF1 Cum
Fig. 9

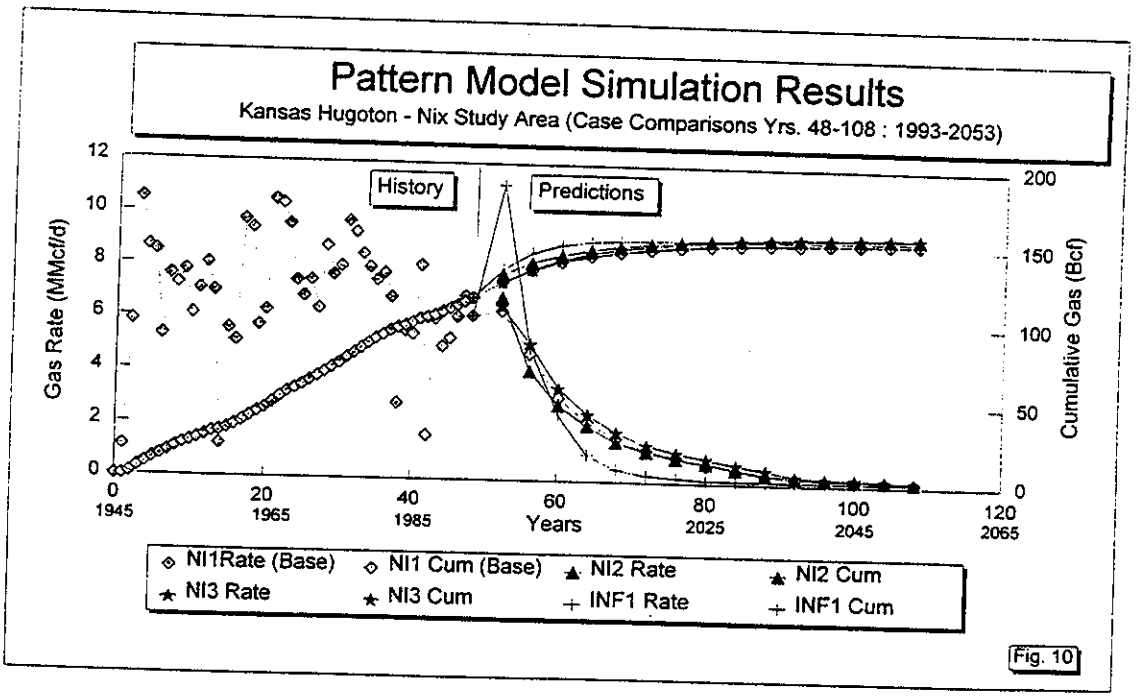
Pattern Model Simulation Results
Kansas Hugoton - Nix Study Area (Case Comparisons Yrs. 48-108 : 1993-2053)
History
Predictions
Gas Rate (MMcf/d)
Cumulative Gas (Bcf)
Years
1945
1965
1985
2025
2045
2065
NI1Rate (Base)
NI1 Cum (Base)
NI2 Rate
NI2 Cum
NI3 Rate
NI3 Cum
INF1 Rate
INF1 Cum
Fig. 10

Reserves Determination Using Type-Curve Matching and EMB Methods in the Medicine Hat Shallow Gas Field

S.L.West, SPE, and **P.J.R. Cochrane**, SPE, Imperial Oil Resources Ltd.

Summary

Tight, shallow gas reservoirs in the Western Canada basin present a number of unique challenges in determining reserves accurately. Traditional methods such as decline analysis and material balance are inaccurate owing to the formation's low permeabilities and poor pressure data. The low permeabilities cause long transient periods that are not separated easily from production decline with conventional decline analysis, resulting in lower confidence in selecting the appropriate decline characteristics (exponential or harmonic), which effects recovery factors and remaining reserves significantly. Limited, poor-quality pressure data and commingled production from the three producing zones results in nonrepresentative pressure data and hence inaccurate material-balance analysis. This paper presents two new methods of reserve evaluation that address the problems described above for tight, shallow gas in the Medicine Hat field. The first method applies type-curve matching, which combines the analytical pressure solutions of the diffusivity equation (transient) with the empirical decline equation. The second method is an extended material balance (EMB), which incorporates the gas deliverability theory to allow selection of appropriate p/z derivatives without relying on pressure data. Excellent results were obtained when these two methods were applied to 10 properties that gather gas from 2300 wells. The two independent techniques resulted in similar production forecasts and reserves, confirming their validity. They proved to be valuable, practical tools in overcoming the various challenges of tight, shallow gas and in improving the accuracy in gas-reserves determination in the Medicine Hat field.

Introduction

Reserves determination for tight, shallow gas reservoirs in the Western Canada basin has relied on such traditional methods as conventional decline analysis and material balance.[1,2] However, these reservoirs and their operations have characteristics that potentially result in inaccurate predictions of future rates and remaining reserves with conventional techniques.

The Medicine Hat field is a tight, shallow gas reservoir producing from multiple highly interbedded, silty sand formations with poor permeabilities of < 1 md, and often < 0.1 md. This poor permeability is the main characteristic of these reservoirs that affects conventional decline analysis. Owing to these low permeabilities, and in part to commingled multilayer production effects, wells experience long transient periods before they begin experiencing pseudo-steady-state flow that represents the decline portion of their lives. One of the principal assumptions often neglected when conducting decline analysis is that pseudo steady state must have been achieved. The initial transient production trend of a well or group of wells is not indicative of the long-term decline of the well. Distinguishing the transient production of a well from its pseudo-steady-state production is often difficult, and this can lead to errors in determining the decline characteristic (exponential, hyperbolic, or harmonic) of a well. **Fig. 1** shows the production history from a tight, shallow gas well and illustrates the difficulty in selecting the correct decline. Another characteristic of tight, shallow gas reservoirs that affects conventional decline analysis is that constant reservoir conditions, an assumption required for conventional decline analysis, do not exist because of increasing drawdown, changing operating strategies, erratic development, and deregulation.

Material balance is affected by tight, shallow gas reservoirs because the pressure data is limited, of poor quality, and nonrepresentative of a majority of the wells. Because the risk of drilling dry holes is low and drillstem tests (DST's) are not cost-effective in development of shallow gas, DST data are very limited. Reservoir pressures are recorded only for government designated "control" wells, which account for only 5% of all wells. Shallow gas produces from multiple formations, and production from these formations is typically commingled, exhibiting some degree of pressure equalization. Unfortunately, the control wells are segregated by tubing/packers, and consequently, the control-well pressure data is not representative of most commingled wells. In addition, pressure monitoring has been very inconsistent. Varied measurement points (downhole or wellhead), inconsistent shut-in times, and different analysis types (e.g., buildup and static gradient) make quantitative pressure-tracking difficult. As **Fig. 2** shows, both these problems result in a scatter of data, which makes material balance extremely difficult.

Because of these difficulties, we evaluated two new methods to determine their merit and practicality in determining tight, shallow gas reserves. Both methods are enhancements of conventional techniques. We chose the first method to address the problems encountered by conventional decline analysis and the second method to address the problems encountered by conventional material balance. The two new methods investigated were (1) advanced decline analysis, which consists of type-curve matching with Fetkovich[3] log-log dimensionless curves, and (2) EMB, which incorporates the gas deliverability equation to choose the most accurate p/z slope. Both methods were used to calculate reserves because neither application had been attempted before and because uncertainty existed concerning whether one of the methods was superior for tight, shallow gas.

Field Description

The Medicine Hat shallow gas field of southeastern Alberta, Canada is among the most extensive gas pools in the world (**Fig. 3**), covering 1.6×10^6 ha [4.0 million acres]. Although discovered accidentally in 1883 when drilling for fresh water, the shallow gas pools were not actively developed until the early 1960's. Currently, > 18 000 gas wells are producing at a total rate of 22 000 km^3/d [800 MMcf/D]. The Medicine Hat shallow gas field produces from three clastic formations namely: Milk River, Medicine Hat, and Second White Specks. All three are Upper Cretaceous, marine or shallow marine sandstones and siltstones encountered at approximate drill depths of 300, 450 and 600 m [1,000, 1,500, 2,000 ft].

Rock properties are fairly uniform across the pool, with porosities ranging from 15% to 25% and matrix permeabilities typically < 1 md. Gas is of biogenic origin, is sweet and dry, and has a composition that is ≈96% methane. The gas is trapped downdip of water in the gently dipping ($< 1°$) northeastern flank of the Sweetgrass Arch that straddles the border of Montana and Alberta. Initial reservoir pressures for the three formations are 3500, 4500, and 6000 kPa [500, 650, and 850 psia], respectively. Connate water is mobilized as the pressure decreases. Consequently, small amounts of water accumulate in the wellbore over time that necessitates regular cleanouts of the wellbores.

The gas is gathered, compressed, and dehydrated before being sent to a sales line. Compressor suction pressures are ≈150 to 700 kPa [≈20 to 100 psig]. Generally, very little pressure loss occurs in

Original SPE manuscript received for review Oct. 10, 1994. Revised manuscript received March 14, 1995. Paper accepted for publication March 15, 1995. Paper (SPE 28609) first presented at the 1994 SPE Annual Technical Conference and Exhibition held in New Orleans, Sept. 25–28.

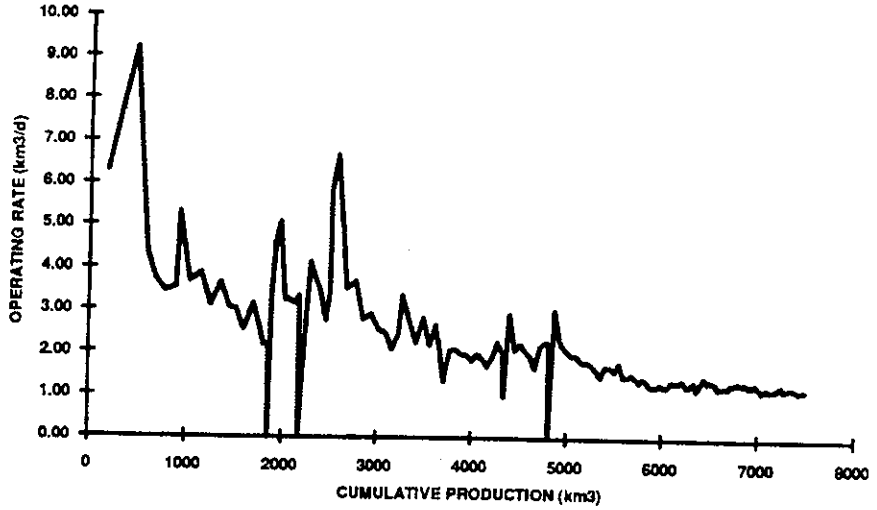

Fig. 1—Production history for a typical Medicine Hat property.

the gathering lines. Because the formations are areally extensive, the field is broken into hundreds of properties that are defined by gathering systems rather than by reservoir boundaries. We evaluated 10 of these properties (2300 wells) in this study.

Wells in the Medicine Hat shallow gas area are generally cased, perforated, and fractured in one, two, or all three formations as ownerships vary not only areally but between formations. The Milk River and Medicine Hat formations are usually produced commingled. Historically, the Second White Specks formation has been segregated from the other two; recently, however, commingled production from all three formations has been approved. Spacing for shallow gas is usually two to four wells per section.

As a result of the poor reservoir quality and low pressures, well productivity is very low. Initial rates rarely exceed 20 km^3/d [700 Mcf/D]. Current average production per well is ≈ 1.5 km^3/d [50 Mcf/D] for a three-formation completion.

Conventional Techniques

Decline Analysis. Decline analysis in the petroleum industry is largely based on the work of Arps.[4] Arps investigated the application of decline analysis to oil and gas well production. His work resulted in the empirical rate-time equation (see Appendix A of Ref. 5):

$$q(t)/q_i = 1/(1 + bD_i t)^{1/b}. \quad \ldots\ldots\ldots\ldots\ldots\ldots\ldots\ldots (1)$$

The exponent b characterizes the decline as harmonic ($b = 1$), hyperbolic ($0 < b < 1$), or exponential ($b = 0$). Note that for the exponential case, the equation is expressed as

$$q(t)/q_i = 1/\left(\exp D_i t\right). \quad \ldots\ldots\ldots\ldots\ldots\ldots\ldots\ldots (2)$$

Conventional decline analysis uses a graphical approach to evaluate exponential- and harmonic-decline characteristics. Rearranging Eq. 2 will show that exponential decline has a unique characteristic in that it is a straight-line relationship for a log-q-vs.-t plot. Similarly, harmonic decline has a straight-line relationship for a log-q-vs.-log-t plot.

For decline analysis to yield maximum accuracy, the main assumption is that reservoir conditions must remain constant. In the Medicine Hat field, this presents a problem owing to changing bottomhole pressures and changing transient/pseudo-steady-state flow regimes.

Material Balance. For volumetric (constant-volume) gas reservoirs, reserves can be predicted accurately by use of conventional material-balance analysis. Material balance, more correctly a volumetric balance, equates the initial volume of a reservoir to its volume at some later time in its life under a different set of conditions. For a bounded gas reservoir with no waterdrive, cumulative volume of gas produced is proportional to the reservoir pressure corrected for the nonideality of gas (see Appendix B of Ref. 5); i.e.

$$p/z = (p_i/z_i) - mG_p. \quad \ldots\ldots\ldots\ldots\ldots\ldots\ldots\ldots (3)$$

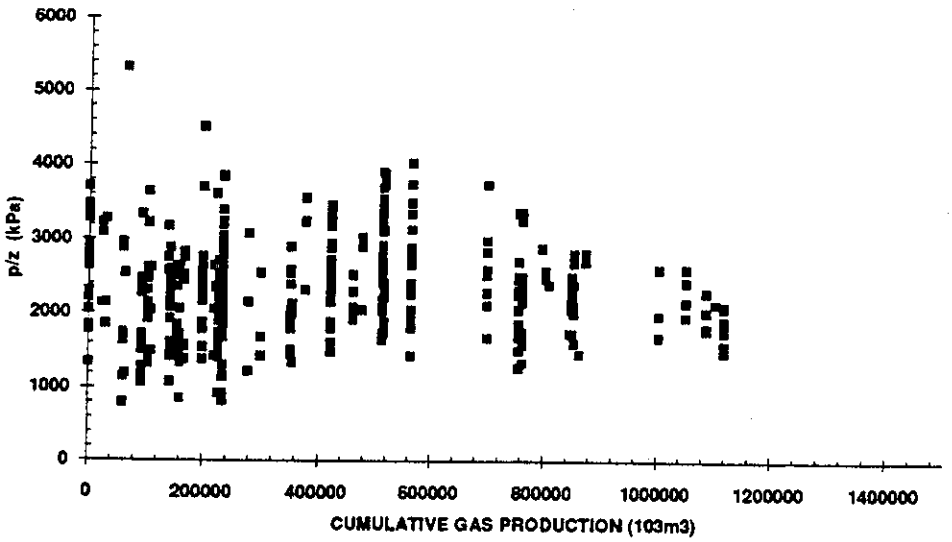

Fig. 2—Pressure data scatter for a typical Medicine Hat property.

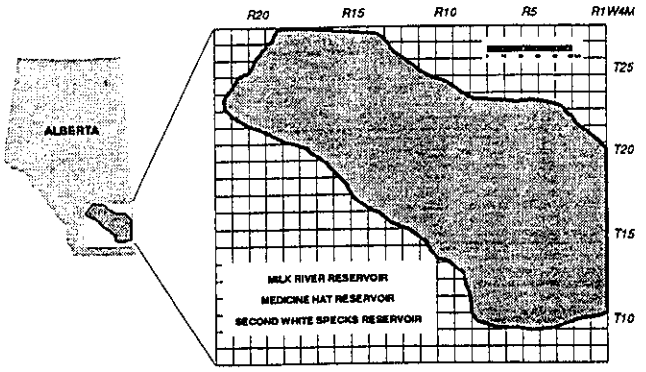

Fig. 3—Medicine Hat shallow gas area.

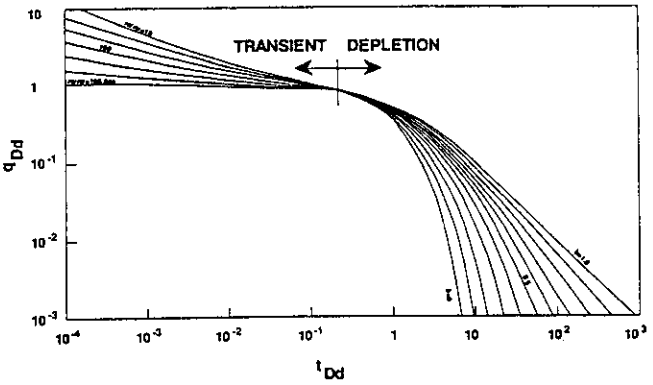

Fig. 4—Composite of analytical and empirical type curves (after Ref. 3).

Eq. 3 results in a straight-line relationship for p/z and G_p with a slope of m. Ultimate reserves can then be estimated with a given abandonment pressure.

An important assumption required for material balance is that the reservoir pressure can be represented by a single value. In the Medicine Hat field this presents a complex problem when producing from multiple low-permeability formations.

Application of Enhanced Techniques

Type-Curve Matching. Fetkovich[3] introduced advanced decline analysis in 1973. He combined the analytical pressure solutions of the diffusivity equation (reflecting the early-time transient period) with Arps'[4] empirical equations (later depletion period) to yield a series of composite log-log dimensionless curves (Appendix C of Ref. 5 gives specific dimensionless equations). In this manner, the entire production data for a well can be used. **Fig. 4** shows these curves. The curves representing transient behavior are on the left and empirical Arps curves are on the right.

Type-curve matching provides two important advantages over conventional decline analysis. First, these curves allow transient behavior to be identified. This ensures that only the pseudo-steady-state or decline portion of the production history is used in forecasting. This is an important advantage for shallow gas because a substantial transient period exists. Second, the decline portion is divided into multiple hyperbolic curves. Unlike conventional decline analysis, type-curve matching allows the data to be fit more easily to a set of hyperbolic curves rather than just to the usual exponential or harmonic behavior.

Another advantage of type-curve matching (which was not required in this study) is its ability to perform transient analysis. Transient analysis provides a means of calculating such reservoir parameters as permeability, skin, PV, and drainage radius in a manner similar to pressure buildup analysis, without having to shut in production.

Until recently, type-curve matching was onerous and time consuming. However, computer software has automated type-curve matching, now making it a feasible option for the reserves evaluation. It provides a simplified means of accurately matching historical production data to a best-fit transient and decline type curve to generate forecasts and reserves. With a match selected, forecasts and reserves are calculated. **Fig. 5** shows a typical type-curve analysis.

To avoid calculating individual reserves for each of the 2300 wells, wells were grouped by formation and by date on production. This simplification was verified on a test group by ensuring that the reserves from the group of wells yielded the same results as the sum of the individual well reserves. These groupings were used for each of the 10 properties, and the results of the groupings combined to give a property production forecast. Also, to estimate the reservoir decline characteristics more accurately, the rates were normalized to reflect changes in the bottomhole flowing pressure (BHFP).

EMB. The EMB technique is essentially an iterative process for obtaining a suitable p/z-vs.-G_p line for a reservoir where pressure data is inadequate. It combines the principles of volumetric gas depletion with the gas-deliverability equation. The deliverability equation for radial flow of gas describes the relationship between the pressure differential in the wellbore and the gas flow rate from the well:

$$q(t) = C(t)\left[p_R(t)^2 - p_{wf}(t)^2\right]^n. \quad \ldots\ldots\ldots\ldots\ldots\ldots (4)$$

Owing to the very low production rates from the wells in Medicine Hat shallow gas, a laminar flow regime exists and $n = 1$. The terms making up the coefficient C in Eq. 4 are either fixed reservoir parameters (kh, r_e, r_w, and T_R) that do not vary with time or terms that fluctuate with pressure, temperature, and gas composition (μ_g and z).

$$C = 0.703 \times 10^{-3} k_g h / \left\{zT_R\mu_g\left[\ln(0.606 r_e/r_w)\right]\right\}. \quad \ldots\ldots (5)$$

[Note that the performance coefficient also contains an adjustment factor to convert external boundary pressure, p_e, to an average reservoir pressure, $\overline{p_R}$. The derivation of the deliverability equation is based on the p_e not $\overline{p_R}$, and the adjustment factor is $\ln(0.606\ r_e/r_w)/\ln(0.472 r_e/r_w)$]. Typically, formation temperature and gas compositions do not change significantly in a dry-gas reservoir, so these properties are mainly pressure dependent.

Because the original reservoir pressure in these shallow formations is low, the differences between initial and abandonment pressures is not significant and the variation in the pressure-dependent terms over time can be assumed negligible. C may be considered constant for a given Medicine Hat shallow gas reservoir over its life. With these simplifications for shallow gas, the deliverability equation becomes

$$q(t) = C\left[p_R(t)^2 - p_{wf}(t)^2\right]. \quad \ldots\ldots\ldots\ldots\ldots\ldots (6)$$

The sum of the instantaneous production rates with time will yield the relationship between G_p and reservoir pressure, similar to the material-balance equation. By use of this common relationship, with the unknowns being p_R and C, the EMB method involves iterating to find the correct p/z-vs.-G_p relationship to give a constant C with time. With the assistance of a computer spreadsheet, the method is applied as outlined in the following.

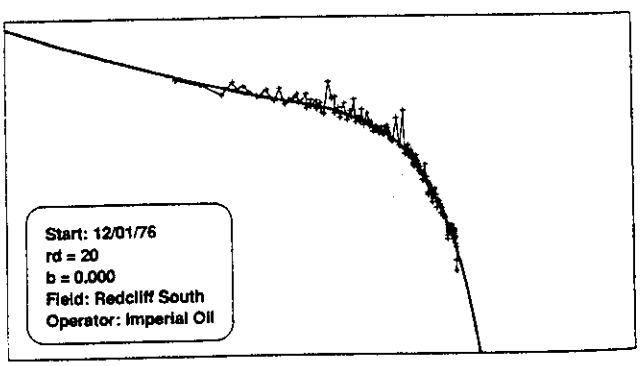

Fig. 5—Medicine Hat production data matched to a type curve.

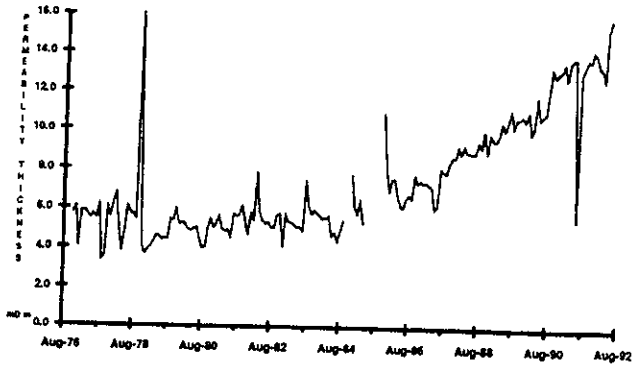

Fig. 6—Example of an invalid *p/z*-vs.-G_p relationship; *kh* is not constant.

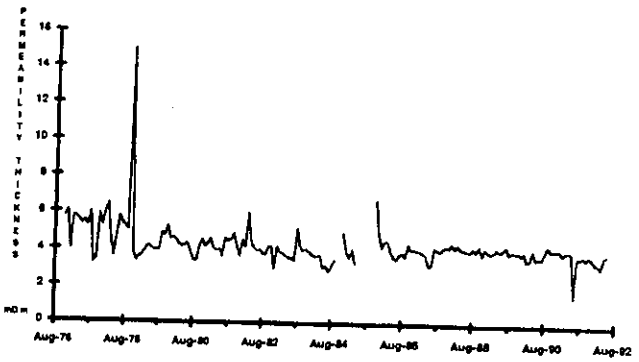

Fig. 7—Example of a successful EMB solution; flat *kh* profile.

1. An initial estimate for the *p/z* variation with G_p is made by guessing an initial pressure, p_i, and a linear slope, m, for the reservoir.
2. Starting at the initial production date for the property, a reservoir-pressure-vs.-time relationship is established with the estimated *p/z* slope because actual cumulative production, G_p, vs. time is known.
3. Knowing production rates, q, and BHFP's, p_{wf}, for each monthly time interval and having estimated reservoir pressures, p_R, from Step 2, C is calculated for each time interval with Eq. 5.
4. C is plotted against time. If C is not constant (i.e., the plot is not a horizontal line), a new *p/z*-vs.-G_p relationship is guessed and the process repeated.
5. Once a constant C solution is obtained, the representative *p/z* relationship has been defined for reserves determination.

Use of the EMB method in the Medicine Hat shallow gas makes the fundamental assumptions (1) that the gas pool depletes volumetrically (i.e. no water influx) and (2) that all wells behave like an average well with the same deliverability constant, turbulence constant, and BHFP, which is a reasonable assumption given the number of wells in the area, the homogeneity of the rocks, and the observed well production trends.

In the EMB evaluation, wells for each property were grouped according to producing interval so that the actual production from the wells could be related to a particular reservoir pressure trend. When calculating the coefficient, C, a total C based on grouped production was calculated and then divided by the number of wells producing in a given time interval to give an average C value. The average C value was used to calculate an average permeability/thickness, $\overline{kh}$, for comparison with actual *kh* data obtained through buildup analysis for the reservoir. For that reason, *kh* vs. time was plotted instead of C vs. time in the method. **Figs. 6 and 7** show some typical results of the EMB analysis. Fig. 6 shows a *kh*-vs.-time profile indicative of an incorrect *p/z*-vs.-G_p guess, and Fig. 7 shows a flat *kh*-vs.-time profile indicating a valid *p/z*-vs.-G_p relationship.

Once a suitable EMB solution was determined, reserves were evaluated by developing a production forecast rather than by defining an abandonment pressure. This was primarily because abandonments for Medicine Hat shallow gas are governed by economic production rates rather than by flowing pressures. In addition, developing a production forecast allowed for comparison with the forecasts obtained with the Fetkovich[3] type-curve analysis. The EMB production forecast was developed by using the calculated constant performance coefficient, C, along with a forecast bottomhole flowing pressure, $p_{wf}(t)$, and the calculated reservoir pressure, $p_R(G_p)$, to determine a production rate for each time interval. **Fig. 8** shows a history match and corresponding production forecast for one of the shallow gas well groupings analyzed.

Results

Type-Curve Matching. Type-curve matching was successful in addressing the problems encountered when estimating reserves with conventional decline analysis for Medicine Hat shallow gas.

The expectation that long transients would be observed for Medicine Hat shallow gas was confirmed by type-curve matching. The transient times averaged 0.5 to 1.5 years. Often, new transient regimes occur as a result of changes in the reservoir, such as commingling, cleanouts, or long shut-ins. The software program used in this evaluation allowed easy reinitialization of the production data to identify these transients and thereby obtain type curves that reflected the changes accurately.

Having identified the true-decline portion of the production history, we determined that the wells and well groupings with long pseudo-steady-state production could clearly be characterized as exponential ($b = 0$). This was an important result because it resolved the uncertainty of the decline characteristic for Medicine Hat shallow gas. In some instances, we observed that the decline was steeper than the exponential curve. This might be attributed to excessive water loading in the wellbores owing to insufficient cleanouts.

Grouping wells by producing formation and "on-production" date proved to be successful. Wells grouped together were found to show minimal loss in accuracy when type-curve analysis was applied in comparison with the sum of the individual well analyses. This reduced the number of type-curve matches required and increased the method's practicality.

The main difficulty encountered in applying the type-curve method was in matching the production to a particular Arps[4] decline characteristic when wells or groups of wells had not been on production long enough to establish significant pseudo-steady-state decline. In these cases, we assumed that they would exhibit exponential behavior because all the other wells and groupings had exhibited this characteristic.

EMB. EMB was very effective in estimating the most representative *p/z* relationship and in determining reserves for the Medicine Hat field where the pressure data were unreliable.

We observed that the C-vs.-time curve was very sensitive to the *p/z* slope. This increased the confidence in the final chosen *p/z* relationship. Generally, a flat C-vs.-time plot could be obtained for the entire life of the well groups analyzed. When this was not the case, emphasis was placed on late-time data because the potential for inaccuracies in

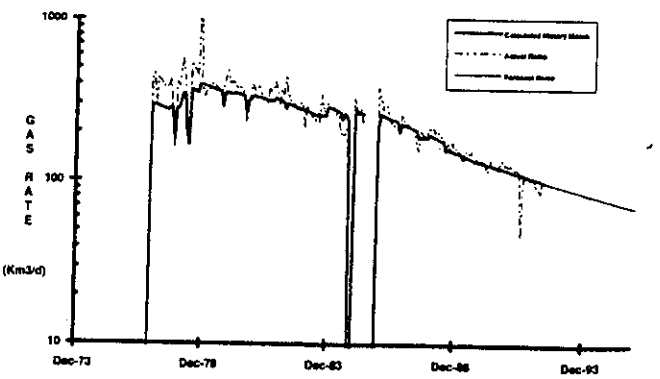

Fig. 8—Example of an EMB production history match.

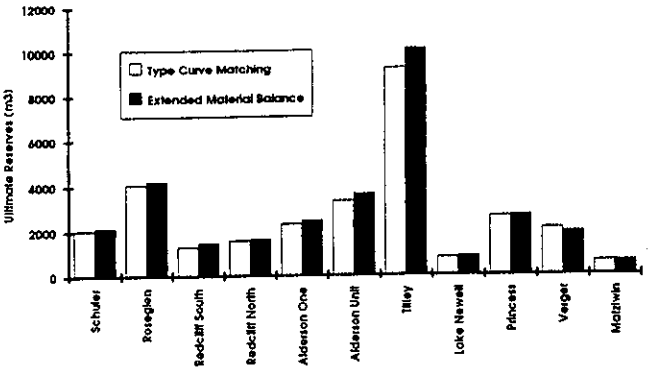

Fig. 9—Comparison of reserves calculated with each method for the 10 Medicine Hat properties.

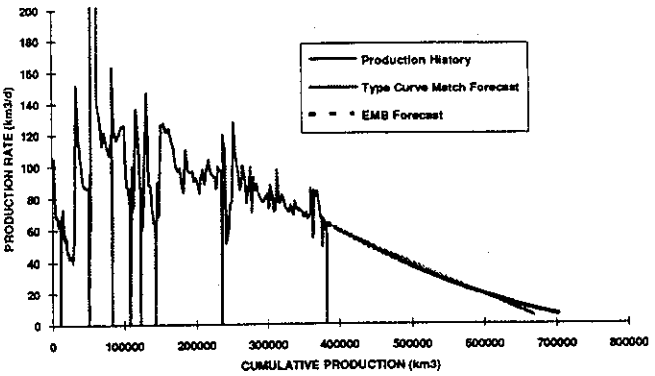

Fig. 10—Comparison of production forecast calculated with each method for one Medicine Hat property.

early-time data was higher. Production forecasts that resulted from EMB were observed to be slightly hyperbolic in nature.

Very good results were achieved when calculated kh and estimated p_i from the EMB method were compared with actual values calculated in the buildup analyses available. Similarly, calculated C values compared favorably with those from any available absolute-open-flow data. These checks proved to be a useful way to verify the accuracy of the p/z solution selected.

Grouping wells by formations proved to be practical and accurate. Ultimate reserves obtained from the small groupings were found to be virtually identical to those obtained from a larger group made up of the sum of the smaller groups.

The main difficulties with EMB were estimating the parameters and assumptions that go into the calculations and determining p_{wf}, which is more critical to EMB than to type-curve matching.

Comparison of Methods. The two methods generated similar production forecasts that resulted in ultimate economic reserves that differed on average by only 7%. **Fig. 9** summarizes the ultimate reserves comparisons for the 10 properties evaluated. EMB generally provided higher reserve estimates than type-curve matching did. **Fig. 10** illustrates the comparison between the production forecasts from each method for one of the Medicine Hat shallow gas properties.

Fig. 10 shows the slight difference in decline characteristics; type-curve matching resulted in exponential decline, whereas EMB forecasts were typically slightly hyperbolic in nature. Fekovitch[3,6] discussed the effect of backpressure on the type of decline for a volumetric gas reservoir. By combining the gas-deliverability equation with the material-balance relationship between pressure and production, we can show that for laminar flow ($n = 1$) with $p_R^2 \gg p_{wf}^2$, a hyperbolic decline characteristic with an Arps b factor of 0.5 would be expected. Therefore, both type-curve matching and EMB provided characteristics that supported the theoretically expected decline for such a reservoir. However, we can also show that if p_{wf} is not negligible in comparison to p_R, as is the case for shallow gas, a decline with b tending towards zero would be expected. The difference in the decline characteristic is minimal and has very little effect on the resulting ultimate reserves determined by each technique.

Both methods are independent, but they are similar in that both are based on production data that constitute the most reliable data source for the shallow gas properties. Subsequent to this reserves study conducted in 1992, comparisons between actual and forecasted volumes have been made. Generally, the comparisons have been excellent (within 5%), with the exceptions being the result of changes in operating conditions that differed from the assumptions made at the time of the evaluation.

Both methods were not only accurate in evaluating reserves, but could be applied practically. In addition, both methods were computer based, which facilitated working with large volumes of data; grouping wells further simplified data handling.

Although the reserves obtained from the two methods were similar, reserves from one method were ultimately selected rather than averaging the two. The technique chosen for each property depended on the individual characteristics of the property and how these were addressed by each method. Type-curve matching was chosen as the more accurate method (1) when long periods of pseudo-steady-state production were observed that allowed a decline to be matched easily; (2) where flowing pressure data was insufficient or nonrepresentative for a property because type-curve matching is less sensitive to p_{wf} than EMB; and (3) in properties where wells are commingled part way through their producing lives because this essentially creates a new transient and the resulting decline represents a different "reservoir" (i.e., a different set of producing zones).

EMB was chosen as the more accurate method (1) in properties where a significant portion of pseudo-steady-state production has not yet developed because EMB does not need a decline trend to obtain a forecast; (2) when fluctuations in well count are frequent, especially in the more recent history because EMB accounts for well-count variations by evaluating an "average well" characteristic (therefore, properties with a large number of abandonments in the last few years of production were handled more accurately by EMB); and (3) where frequent changes in operating practices occur that can be modeled (e.g., changes in cleanout procedures, stimulation, and compressors).

Conclusions

1. Both methods proved to be practical and more accurate techniques-for determining reserves in Medicine Hat shallow gas than conventional decline analysis or material balance. The two independent techniques resulted in similar production forecasts and reserves, confirming their validity and the confidence in the results.
2. Type-curve matching for Medicine Hat shallow gas solved the problem associated with separating the transient from the decline portion of the production history to identify the type of decline.
3. EMB proved to be successful for low-pressure, volumetric gas reservoirs in selecting the most representative p/z slope without pressure data.
4. Both techniques could have potential applications beyond shallow, tight gas reservoirs and should be considered as additional reserves-evaluation methods, with consideration given to the assumptions.
5. The importance and utility of these methods should be of particular significance for reservoirs that lack reliable pressure data and reservoirs that experience long transient behavior.

Nomenclature

b = hyperbolic exponent
B_g = gas FVF
B_{gi} = initial gas FVF
C = gas performance coefficient
D = decline rate
D_i = initial decline rate
G = original gas in place, L^3, m^3
G_p = cumulative gas production, L^3, m^3
h = thickness, L, m
k = permeability, L^2, md
k_g = effective permeability to gas, L^2, md

m = slope
n = exponent of backpressure curve
p = pressure, m/Lt^2, kPa
p_e = pressure at reservoir boundary, m/Lt^2, kPa
p_i = initial pressure, m/Lt^2, kPa
p_R = reservoir pressure, m/Lt^2, kPa
p_{wf} = BHFP, m/Lt^2, kPa
$q(t)$ = flow rate at time t, L^3/t, m^3/d
q_i = initial flow rate, L^3/t, m^3/d
q_D = dimensionless flow-rate functions
q_{dD} = Fetkovich dimensionless flow-rate functions
r_d = r_e/r_w
r_e = drainage radius, L, m
r_w = well radius, L, m
t = time, t
t_D = dimensionless flow-rate functions
t_{dD} = Fetkovich dimensionless flow-rate functions
T_R = reservoir temperature, T
z = gas deviation factor
z_i = initial gas deviation factor
μ_g = gas viscosity, m/Lt

Superscript

$\bar{}$ = average

Acknowledgment

We thank Imperial Oil Resources Ltd. for permission to publish this paper.

References

1. Warren, A.: "Southeastern Alberta Shallow Gas Pools Reserves and Performance Data," ERCB report, Alberta Energy Resources Conservation Board (1981) 1–18.
2. Martin, I. and Yeung, G.C.: "The Medicine Hat Gas Field—100 Years After Discovery," *J. Cnd. Petr. Tech.* (Sept.–Oct. 1991) **30**, No. 5, 66.
3. Fetkovich, M.J.: "Decline-Curve Analysis Using Type Curves," *JPT* (June 1980) 1065; *Trans.*, AIME, **269**.
4. Arps, J.J.: "Analysis of Decline Curves," *Trans.*, AIME (1945) 228.
5. West, S.L. and Cochrane, P.J.: "Reserves Determination Using Type-Curve Matching and Extended Material Balance Methods in the Medicine Hat Field," paper SPE 28609 presented at the 1994 SPE Annual Technical Conference and Exhibition, New Orleans, Sept. 25–28.
6. Fetkovich, M.J. *et al.*: "Decline-Curve Analysis Using Type Curves—Case Histories," *SPEFE* (Dec. 1987) 637; *Trans.*, AIME, **283**.

SI Metric Conversion Factors

acre	×4.046 873	E−01 = ha
ft	×3.048*	E−01 = m
ft^3	×2.831 685	E−02 = m^3
md	×9.869 233	E−04 = μm^2
psi	×6.894 757	E+00 = kPa

*Conversion factor is exact.

Suzanne L. West is a senior reservoir engineer with Imperial Oil Resources Ltd. in Calgary, Alta., and is currently the technical leader of the Southern Gas Development team. Since joining Imperial in 1987, she has held various reservoir development positions. West holds a BS degree in chemical engineering from the U. of Calgary. **P.J.R. Cochrane** is a reservoir engineer with Imperial Oil Resources, currently working in Cold Lake, Alta. Previously, he worked on shallow gas development for the Medicine Hat field and waterflood management of the Norman Wells oil field. Cochrane holds a BS in mechanical engineering from Queens U.

West

Cochrane

Annotated Bibliography

Rock and Fluid Properties

Gold, D.K., McCain, W.D., and Jennings, J.W.: "An Improved Method for the Determination of the Reservoir-Gas Specific Gravity for Retrograde Gases," *JPT* (July 1989) 747; *Trans.*, AIME, **287.**

This paper presents a method to estimate reservoir-gas specific gravity for retrograde-gas reservoirs from field production data. Terms are included to account for the additional gas production from the low-pressure separator and stock tank as well as for the vapor equivalent of the primary separator liquid. Correlations are developed from 234 laboratory fluid analyses to allow easy computation of gas gravity with only the data typically available from field operations. The improved accuracy of gas-gravity estimates with this technique is important when determining reservoir-fluid withdrawal in retrograde-gas reservoirs.

Jones, S.C.: "Using the Inertial Coefficient, β, To Characterize Heterogeneity in Reservoir Rock," paper SPE 16949 pre-sented at the 1987 SPE Annual Technical Conference and Exhibition, Dallas, 27–30 September.

This paper presents data indicating that deviations in the proportionalities between the inertial coefficient and characteristic length are functions of permeability heterogeneity. These deviations are quite evident in reservoir samples as small as a core plug. The deviations from proportionality increase as either the permeability heterogeneity increases and/or the permeability decreases. The authors conclude that permeability heterogeneity is a significant factor in explaining scatter in correlations involving beta in prior work.

Ward, J.S. and Morrow, N.R.: "Capillary Pressures and Gas Relative Permeabilities of Low-Permeability Sandstone," *SPEFE* (September 1987) 345.

A high-speed centrifuge combined with desorption isotherms was used to measure capillary pressures in low-permeability sandstones across a wide range of water saturations. Very high capillary pressures of up to 800 psi were measured and attributed to the clay content and small pore throats in tight sandstones. The repeatability of test results was better for air displacing decane than for air displacing water, with some hysteresis effects noted. No irreducible water saturation could be found. The relative permeability data were insufficient to draw general conclusions.

Wells, J.D. and Amaefule, J.O.: "Capillary Pressure and Permeability Relationships in Tight Gas Sands," paper SPE 13879 presented at the 1985 SPE/DOE Symposium on Low Permeability Gas Reservoirs, Denver, Colorado, 19–22 May.

This paper presents an improved relationship between the Swanson parameter (which involves capillary pressure) and permeability for sandstones below 10 md. The new technique is an extension of both the Thomeer and Swanson procedures. Mercury capillary pressures are found to be as much as 10 times centrifuge air/brine capillary pressures in tight sands leading to optimistic cleanup times when the mercury pressures are used. Gas/water relative permeabilities computed from mercury injection data are found to lead to higher water/gas ratios than relative permeabilities computed from air/brine data.

General Material Balance

Humphreys, N.V.: "The Material-Balance Equation for a Gas-Condensate Reservoir With Significant Water Vaporization," paper SPE 21514 presented at the 1991 SPE Gas Technology Symposium, Houston, 23–25 January.

The development of a modified form of the gas material-balance equation is presented for the case of gas-condensate fluid with a large component of vaporized water. Failure to account for the effects of a condensate fluid with vaporized water can yield significant error in interpretation when the dry-gas material-balance equation is used. In particular, analysis of the p/z vs. G_p behavior of a gas-condensate fluid with vaporized water yields an upward deviation away from the expected straight-line trend and, ultimately, a slight downturn of this trend. This behavior can be easily confused with the case of a water-drive gas reservoir. The author presents the new material-balance equation as a plotting function and provides illustrative field examples of its application.

Rodgers, J.S., Boykin, R.S., and Coble, L.E.: "Nonstatic Pressure History Analyses for Gas Reservoirs," *SPEJ* (April 1983), 209.

This work provides a solution for the particular case of using nonstatic reservoir pressures in the analysis and interpretation of well-performance data. The method proposed uses a nonlinear regression solution of the material-balance equation for a gas reservoir with water influx/water production coupled with the pseudosteady-state gas flow equation. Validation of this method was provided with several numerical simulation examples.

Water Influx

Al-Hashim, H.S. and Bass, D.M. Jr.: "Effect of Aquifer Size on the Performance of Partial Waterdrive Gas Reservoirs," *SPERE* (May 1988) 380.

The concept of a moving gas/water contact (GWC) in a waterdrive gas reservoir is studied to evaluate the effect of this behavior on ultimate gas recovery. This work assumes a simplified radial-flow geometry, and several simulated performance cases are used to investigate the effect of a moving GWC on gas recovery. The authors conclude that, for essentially every case, the pressure in the unsteady-state water-influx equation must be corrected to the original GWC or analysis/prediction errors of up to 100% can occur.

Brinkman, F.P.: "Increased Gas Recovery From a Moderate Waterdrive Reservoir," *JPT* (December 1981) 2475.

The concept of accelerated "blowdown" in waterdrive gas reservoirs is advocated to increase gas recovery from gas reservoirs in the U.S. gulf coast region. The author uses a field case example (Lovells Lake field, Texas) to illustrate this point. Validation of the blowdown concept is implied from the observation of pressure drawdowns measured in the water-invaded zones of the reservoir. The recovery mechanism is assumed to be the percolation of previously trapped gas through the water-invaded zones.

Chen, C.C., Chu, W.C., and Sadighi, S.: "Pressure-Transient Testing of Gas Reservoirs With Edgewater–Drive," *SPEFE* (December 1996) 251.

A pressure-transient analysis method is presented for a two- or three-zone radial composite reservoir model, where this model is used to represent the case of an edge-waterdrive process. In this scenario, the properties of one (or two) of the outer composite regions are varied to model fluid influx. Type-curve solutions are provided for the analysis and interpretation of well test data, and simulated and field data cases are used to provide validation of this approach. The authors present guidelines and generalized conclusions for the interpretation of various features, such as mobility contrasts and reservoir boundaries.

Gajdica, R.J., Wattenbarger, R.A., and Startzman, R.A.: "A New Method of Matching Aquifer Performance and Determining Original Gas in Place," *SPERE* (August 1988) 985.

The behavior of waterdrive gas reservoirs can be modeled with an "aquifer influence function" (AIF), where the AIF is a flow solution for the aquifer, which is then coupled to the gas material-balance equation by means of boundary pressures (predicted by the AIF). The simultaneous solution of the AIF and gas material-balance equation is performed with a linear programming (or LP) technique. The LP technique was selected because constraints on the AIF's are relatively easy to incorporate. The authors demonstrate the LP procedure on more than 30 field cases and conclude that the AIF method (with LP) is more robust than the conventional (steady- and unsteady-state) methods.

Hower, T.L. and Jones, R.E.: "Predicting Recovery of Gas Reservoirs Under Waterdrive Conditions," paper SPE 22937 presented at the 1991 SPE Annual Technical Conference and Exhibition, Dallas, 6–9 October.

This work presents a parametric study that focuses on newly defined parameters derived to incorporate the key factors influencing gas recovery in waterdrive gas reservoirs. For example, a "dimensionless" time variable is defined to represent the behavior of the W_e/G parameter. The authors reduce this dimensionless time to a simple "performance parameter," $kh/(q_g m_w)$, which is assumed to define the entire performance of the p/z vs. G_p behavior for a waterdrive gas reservoir. Simulated examples are used to provide validation of the $kh/(q_g m_w)$ parameter.

Sills, S.R.: "Improved Material-Balance Regression Analysis for Waterdrive Oil and Gas Reservoirs," *SPERE* (May 1996) 127.

A new material-balance procedure is proposed for the case of a gas reservoir with water influx/water production that uses a new definition of a combined aquifer/reservoir expansion term. This formula provides a single plotting function that can be applied to oil and gas reservoirs under either volumetric or waterdrive conditions. The method is demonstrated for a field example, including a detailed discussion of the technique and an error analysis.

Abnormally Pressured Reservoirs

Ambastha, A.K.: "Evaluation of Material Balance Analysis Methods for Volumetric, Abnormally-Pressured Gas Reservoirs," *J. Cdn. Pet. Tech.* (October 1993) 19.

This paper compares several material balance methods for abnormally pressured gas reservoirs where constant effective system compressibility is assumed. The methods are grouped into two categories: 1) those that assume compressibility is known and attempt to find original gas-in-place (OOIP); and 2) those that attempt to determine compressibility and OOIP simultaneously. In the first category are the methods proposed by Hammerlindl, Ramagost and Farshad, Begland and Whitehead, and Fetkovich. In the second category, the methods proposed by Roach, Bernard, and Ambastha are discussed. The author concludes that the Roach method is particularly sensitive to errors in the initial pressure estimate. An error in this estimate can cause the appearance of a changing effective-system compressibility. He also concludes that the type-curve matching he proposed in an earlier paper does not provide unique estimates of both effective compressibility and original gas-in-place (OGIP). Finally, as an example of the application of several of the methods, the methods of Hammerlindl, Roach, Ramagost and Farshad, and Ambastha are applied to the Anderson "L" reservoir.

Bernard, W.J.: "Reserves Estimation and Performance Prediction for Geopressured Gas Reservoirs," *J. Pet. Sci. and Eng.*, (1987) **1**, No. 1, 15.

This paper presents a simple model for geopressured gas reservoirs that accounts for rock and water compressibility, water influx from a limited aquifer, or steady-state water influx from shale. These different effects all exhibit the same pressure behavior, making it impossible to infer the type of drive from the shape of the p/z plot. The proposed model is applied to 13 U.S. gulf coast reservoirs that had been depleted or were nearing depletion. For each reservoir, an apparent rock compressibility is calculated, assuming that rock compressibility and gas expansion were the only mechanisms of pressure support. The resulting apparent rock compressibilities ranged from 0 to 36 microsips. Also computed are the aquifer size necessary to account for the observed reservoir behavior, assuming a normal rock compressibility of 4 microsips. The average aquifer size was 1.4 times the reservoir size, with the largest being only four times the reservoir size. The author concluded that such limited aquifers may remain undetected, resulting in the well being mistakenly identified as depletion drive.

Bourgoyne, A.T.: "Shale Water as a Pressure-Support Mechanism in Gas Reservoirs Having Abnormal Formation Pressure," *J. Pet. Sci. and Eng.*, (1990) **3**, No. 4, 305.

This paper addresses shale compaction as a possible pressure-support mechanism in abnormally pressured gas reservoirs. The author begins with a discussion of the shale properties relevant to shale compaction as a support mechanism. The most important of these properties are shale permeability and compressibility. Shale porosity and water viscosity are also shown to be important. The paper presents a numerical model developed to predict gas-reservoir performance while accounting for shale compaction. The model accounts for vertical flow of water out of a shale zone into the adjacent sandstone. It takes into account the pressure dependence of both the shale permeability and compressibility. The model is applied to two field cases from the literature to illustrate that shale properties within the range of published data are adequate to account for the observed pressure behavior. The model successfully accounts for the observed behavior of the NS2B reservoir of the North Ossun field, Lafayette, Louisiana, as well as that of a south Louisiana Miocene reservoir by use of shale properties that are within the range of published results. However, the range of published shale properties also includes values that would provide no significant pressure support. The paper provides an example calculation showing how shale properties can be incorporated into the extrapolation of early p/z behavior to estimate OGIP. This method is suitable for hand calculation and assumes that shale properties are known or can be estimated.

Ramagost, B.P. and Farshad, F.F.: "p/z Abnormally Pressured Gas Reservoirs," paper SPE 10125 presented at the 1981 SPE Annual Technical Conference and Exhibition, San Antonio, Texas, 5–7 October.

This paper presents a graphical method for estimating original gas-in-place for an abnormally pressured gas reservoir. The method takes into account both formation and water compressibility. In order to use the method, the formation compressibility must be known. The method is based on an extension of the standard p/z straight line analysis for conventional depletion–drive gas reservoirs. To use the method, a graph of $(p/z)\{1-[\Delta p(c_w S_w + c_f)/(1-S_w)]\}$ vs. the cumulative gas produced, G_p, is prepared. The best straight line is then drawn through the data. The line is then extrapolated to obtain the OGIP, G, from the x intercept as in the conventional p/z vs. G_p analysis method. The authors illustrate the use of the proposed method by applying it to three abnormally pressured gas reservoirs in the U.S. gulf coast region.

Production Data Analysis

Blasingame, T.A. and Lee, W.J.: "The Variable-Rate Reservoir Limits Testing of Gas Wells," paper SPE 17708 presented at the 1988 SPE Gas Technology Symposium, Dallas, 13–15 June.

This paper presents a method of estimating drainage area and shape factor from bottomhole pressures and rates for gas wells. The method is applicable only after the initial pressure transient has reached all boundaries. The equations presented do not take into account geopressured gas reservoirs or non-Darcy flow. Three field examples that use this method are included, and results generated are compared with those from other analysis techniques. The drainage area for a gas well can be estimated for both homogeneous and vertically fractured reservoirs with this method. In addition, the shape factor can be estimated for homogeneous reservoirs and the reservoir/fracture shape factor and the fracture half-length can be estimated for vertically fractured wells.

Mohaghegh, S., Bilgesu, H.I., and Ertekin, T.: "Production Decline Curves for Low-Pressure Gas Reservoirs Undergoing Simultaneous Water Production," *SPEFE* (March 1995) 57.

Production decline curves for low-pressure gas reservoirs undergoing simultaneous water production are presented in this paper. The curves are for radial-flow geometry with closed outer boundary and well located in the center of the drainage area. Two-phase flow of gas and water is incorporated into the curves. These decline curves are for low-pressured gas reservoirs (less than 2,000 psia) where the gas viscosity/compressibility product is constant. The decline curves presented were generated by a two-phase, one-dimensional, radial numerical simulator. The curves generated were tested against two different independent numerical models with good agreement. In addition, the new curves were compared with previously published single-phase decline curves with the expected result that the single-phase curves predict higher rates than would be expected if two-phase flow exists.

Spivey, J.P. and Frantz, J.H. Jr.: "History-Matching Production Data Using Analytical Solutions for Linearly Varying Bottomhole Pressure," paper SPE 29167 presented at the 1994 SPE Eastern Regional Conference and Exhibition, Charleston, West Virginia, 8–10 November.

This paper presents analytical solutions for history matching gas-well production data with linearly varying bottomhole pressure. A previously presented method that used constant-pressure analytical solutions resulted in the generation of a spike in production rate for each assumed step decrease in bottomhole flowing pressure. These spikes generally are not apparent in field data owing to the practice of slowly and smoothly decreasing bottomhole flowing pressure. The paper concludes that linear pressure solutions can be superimposed to model varying pressure histories. To use these analytical solutions for gas-well production, the producing pressure and producing time are adjusted to account for pressure-dependent gas properties. The solutions presented were used to history match rate/time behavior for a field example. Rate/time predictions were also history matched by use of a constant flowing pressure analytical solution and incorporating three– and seven–step superposition. The new solutions were found to match actual performance better and required fewer superposition terms.

Spivey, J.P., *et al.*: "Integral Type Curves for Advanced Decline-Curve Analysis," paper SPE 24301 presented at the 1992 SPE Mid-Continent Gas Symposium, Amarillo, Texas, 13–14 April.

A new family of type curves is presented in this paper for use in advanced decline-curve analysis. The new curves contain dimensionless production rate and dimensionless cumulative production vs. dimensionless time and are plotted on a single log-log type curve. These curves have two advantages: (1) the cumulative curve smooths production data and (2) matching both the rate/time and cumulative-time data should be easier and therefore more unique if both curves are matched simultaneously. To use these analytical solutions for gas-well production, the adjusted cumulative production is defined as the integral of rate with respect to adjusted time. The adjusted time calculation is used to account for pressure-dependent gas properties. The paper demonstrates that the new curves can be used for either oil or gas wells having a varying bottomhole pressure history by use of the plotting functions presented in the paper. Three synthetic data sets were generated and the results matched to the new curves. Properties estimated from the type curve match agreed well with the properties used to generate the test cases. Two field examples, an oil and a gas well, were matched with the new type curves and the results presented to show the utility of these curves.

Deliverability

Chase, R.W. and Anthony, T.M.: "A Simplified Method for Determining Gas-Well Deliverability," *SPERE* (August 1988) 1090.

The authors propose a modification of the Mishra and Caudle procedure for calculating dimensionless inflow-performance-relationship (IPR) curves for gas wells. They define two IPR curves: one for predicting flow rate as a function of flowing bottomhole pressure at a given current average reservoir pressure, and the second for predicting future deliverability as average reservoir pressure declines. The resulting IPR curves are based on the use of pressure-squared analysis and account for non-Darcy flow. The authors compare their proposed method with those of Mishra and Caudle and the conventional multipoint test method. In general, they found the proposed method gave results that were very close to those of Mishra and Caudle and somewhat lower than those from the conventional multipoint method. The authors caution that the proposed method be used only for pressures less than 2,000 psi and that the Mishra and Caudle method be used for pressures greater than 2,000 psi.

Green, W.R.: "Analyzing the Performance of Gas Wells," *JPT* (July 1983) 1378.

This paper is a thorough review of the three basic components of gas-well evaluation: inflow performance curves, outflow performance curves, and tubing performance curves. The overview is easy to understand and will refresh experienced engineers and instruct novices. The inflow performance section discusses the most widely used performance relationship based on the difference between the squares of the average and flowing wellbore pressure raised to power n and an empirical constant. Also illustrated is the dependence of the empirical constant on such reservoir properties as permeability and thickness as well as on gas properties. The outflow performance section combines the IPR with vertical pressure drops to define outflow performance relationships on the basis of the surface tubing pressure. The author discusses the dependence of the outflow performance curves on multiphase flow and tubular sizes. One important point is the definition of the "flow point," which is the minimum possible sustainable gas rate. The tubing performance section illustrates how to use estimates of the vertical pressure drop as a function of flow rate in combination with the IPR to compute production rates as functions of surface flowing pressure and tubing sizes.

Mishra, S. and Caudle, B.H.: "A Simplified Procedure for Gas Deliverability Calculations Using Dimensionless IPR Curves," paper SPE 13231 presented at the 1984 SPE Annual Technical Conference and Exhibition, Houston, 16–19 September.

Mishra and Caudle discuss the development of dimensionless IPR curves based on real gas pseudopressure and relationships presented by Vogel for oil wells. This paper is a natural progression to the approach presented by Green (in the paper referenced above) for the inflow performance analysis. A general dimensionless IPR curve is presented that should be applicable to many gas wells. The authors validated the use of a single relationship with a sensitivity analysis that investigated variations in permeability, pressure, drainage area/shapes, and gas gravity. They provide a procedure to apply the dimensionless relationship to actual well conditions.

Reservoir Characterization

Meehan, D.N. and Verma, S.K.: "Improved Reservoir Characterization in Low-Permeability Reservoirs with Geostatistical Models," paper SPE 28608 presented at the 1994 SPE Annual Technical Conference and Exhibition, New Orleans, 25–28 September.

A case history is used to illustrate the use of a high-resolution, fine-grid geostatistical model of the Cotton Valley sandstones of the Carthage field to predict the distribution of reservoir properties used as input to a reservoir simulation model. The improved simulation model matched long-term pressure-buildup data much better and predicted incremental gas recovery by infill drilling much more accurately than those based on simpler models. The authors provide a review of the geostatistical approach to evaluate the variation in reservoir properties as a function of depth and areal position. The result of the evaluation was a mathematical model used to predict porosity, water saturation, and shale content as functions of the position of cells within a geostatistical model. These estimates were then used to estimate permeability within each cell. The fine-grid, 385,875-cell geostatistical model was scaled up to reduce the number of cells to 40,000 for input to a reservoir simulation model. The reservoir simulation model was matched to actual well performance by adjusting the permeability in the model near hydraulically fractured wells and the overall permeability level between wells. Once calibrated, the model was used to forecast gas production rates and volumes from the existing and infill wells.

Wellbore Performance

Coleman, S.B., *et al.*: "Understanding Gas-Well Loadup Behavior," *JPT* (March 1991) 334; *Trans.*, AIME, **291.**

This paper presents a theoretical model of gas-well loadup behavior. The model combines reservoir inflow performance, wellbore outflow performance, and a wellbore mass balance. The model predicts liquid holdup, liquid-column height, gas flow rate, sandface pressure, and wellhead flowing pressure (WHFP) as functions of time as a well loads up while producing below its critical rate. To verify their model, the authors conducted a series of tests by deliberately inducing loadup in several different wells and monitoring the flowing rates and pressures as loadup occurred. The authors found that the field data matched the theoretical predictions reasonably well. They also found that it was difficult to measure the liquid influx rate accurately for wells that were producing at or below the critical rate. In addition, the rate of liquid influx had a major influence on the time required for a well to load up and die. Wells with little fluid production took several days to die, while wells that made large volumes of liquid would die within a few hours after reaching their critical rate.

Coleman, S.B., *et al.*: "The Blowdown-Limit Model," *JPT* (March 1991) 339; *Trans.*, AIME, **291.**

The blowdown limit is defined as the static reservoir pressure at which a gas reservoir is no longer capable of unloading a well's natural loadup fluids without external energy. This paper proposes a blowdown-limit model comprising three criteria: (1) either the sandface pressure must increase or the wellhead pressure decrease to overcome the loadup-induced hydrostatics and allow reservoir flow; (2) the transient reservoir flow rate must be high enough so that the initial wellbore velocities move the wellbore flow regime from bubble flow to slug flow; and (3) the transient reservoir flow rate must remain above the critical rate long enough to remove the fluid remaining after the initial slug is removed. Predictions from the blowdown-limit model were compared with the results of several field tests. These field tests showed that a superficial gas velocity of 5 to 10 ft/sec must be attained to initiate slug flow and that the critical rate must be sustained for 3 hours (for the wells in the study) to achieve a successful blowdown.

Coleman, S.B., *et al.*: "A New Look at Predicting Gas-Well Loadup," *JPT* (March 1991) 329; *Trans.*, AIME, **291.**

This paper provides an update to the classic work by Turner *et al.* There are two obvious sources of liquid that may cause wellbore loading: liquids condensing in the wellbore and free liquids flowing into the wellbore. The paper re-examines the critical-rate theory on which Turner *et al.*'s work is based through comparison with field data. The authors conducted a series of tests to determine the rate and WHFP at which loadup would begin. For each test, the WHFP was increased systematically until the onset of loadup occurred. The authors also built a production chart database of gas wells experiencing loadup, then analyzed the charts to determine rate and WHFP at the onset of loadup. Because the work by Turner *et al.* considered WHFP's higher than 500 psi, the focus was on wells with WHFP's of less than 500 psi. The authors concluded that a 20% upward correction recommended by Turner *et al.* was not necessary. They also found that the critical rate is not affected by liquid/gas ratios up to 22.5 bbl/MMscf and that wells exhibiting slugging behavior do not obey the liquid-droplet model. The most important variables controlling the critical rate are the wellbore diameter and pressure.

Peffer, J.W., Miller, M.A., and Hill, A.D.: "An Improved Method for Calculating Bottomhole Pressures for Flowing Gas Wells With Liquid Present," *SPEPE* (November 1988) 643; *Trans.*, AIME, **285.**

This paper presents a method for calculating bottomhole pressures from wellhead measurements in gas wells with liquid present in the well stream. This method accounts for both condensate and water production, treating the gas/liquid system as a homogeneous mixture. The specific gravity of the mixture is calculated from the gravities of the liquids and the producing gas/liquid ratio. The gas flow rate is also adjusted to account for the presence of condensate in the flow stream. The predictions from this method are compared with those from two different sets of field data and with predictions from a two-phase flow model. The authors found that using an absolute roughness of 0.0018 in. gave better results than the value of 0.0006 in. proposed by Cullender and Smith, reducing the average error from −2.2% to −0.04%. With these modifications, the proposed method was found to give lower overall errors in predicted bottomhole pressure than the two-phase flow model for a wide range of gas-condensate well conditions.

Case Histories

Ancell, K.L. and Manhart, T.A.: "Secondary Gas Recovery From a Waterdrive Gas Reservoir: A Case Study," paper SPE 16944 presented at the 1987 SPE Annual Technical Conference and Exhibition, Dallas, 27–30 September.

This paper presents a reservoir simulation study of the Northeast Hitchcock field in south Texas. At the time of the study (1986), this partial waterdrive gas field had reached the end of its primary productive life and was being considered for enhanced (secondary) gas recovery. The proposed enhancement included lowering the reservoir pressure through increased water production, thereby expanding the gas phase beyond the residual gas saturation and liberating additional gas for production. The simulation study indicated that this process could increase gas recovery from 66 to 88% of in-place gas in the Northeast Hitchcock field if the reservoir pressure were lowered from 3,950 to approximately 1,000 psia. The simulator also computed that primary recovery could have been increased from 66 to 76% of gas-in-place had gas producers been continued as water producers after waterout rather than being plugged.

Berkenpas, P.G.: "The Milk River Shallow Gas Pool: Role of the Updip Water Trap and Connate Water in Gas Production from the Pool," paper SPE 22922 presented at the 1991 SPE Annual Technical Conference and Exhibition, Dallas, 6–9 October.

This case history presents arguments to explain the existence of productive gas reservoirs located downdip from permeable aquifers in the Milk River gas field of southern Alberta, Canada. A review of the geology and evidence of the gas-in-place distribution is presented. The author explains the downdip gas trapping with a model that considers a gently sloping, fully water-saturated reservoir with quality grading from lower permeability downdip to higher permeability updip. Three components—buoyancy, interfacial tension, and pressure—are included in the model. Gas was trapped by small pore throats in the model, causing high interfacial tension forces that exceeded buoyancy forces. The mathematical model also explained behavior observed in physical sandpacks created to investigate the trapping mechanisms.

Cason, L.D. Jr.: "Waterflooding Increases Gas Recovery," *JPT* (October 1989) 1102.

This paper presents the theory of and use of water injection in a low-pressure gas reservoir to aid recovery, and reports the results of a case history that describes the method. The case history is for the Discorbis 1 reservoir in the Duck Lake field of southern Louisiana. Water injection was initiated at a point when reservoir pressure fell below 1,000 psia and was continued for 11 years. Before water injection began, this reservoir had experienced limited water influx, as evident from a concave downward p/z plot. Water injection into this reservoir increased recovery by 25 Bcf, or about 3.6% of OGIP. Theoretical calculations for a purely depletion-drive gas reservoir show that water injection could increase production from 5 to 16% of OGIP, depending on initial and abandonment conditions. The paper recommends that a unified method of analysis, where all possible producing mechanisms are considered, should be used for all gas reservoirs. It is important to realize that water injection performs much in the same manner as compression and therefore becomes a matter of project economics, which for the case presented in this paper is positive.

Fetkovich, M.J., Ebbs, D.J. Jr., and Voelker, J.J.: "Development of a Multiwell, Multilayer Model To Evaluate Infill Drilling Potential in the Oklahoma Hugoton Field," paper SPE 20778 presented at the 1990 SPE Annual Technical Conference and Exhibition, New Orleans, 23–26 September.

Constructing a simulation model for a layered/no-crossflow dry-gas reservoir and identifying the important history-matching parameters for that model are the subjects addressed by this paper. Generating suitable production forecasts with and without infill drilling was the purpose of the model described. This case-history paper is one of five papers written concurrently covering various aspects of potential infill drilling in the Oklahoma Hugoton field. The model was history matched by use of the official state gas-well tests and by individual layer pressures taken by an expendable well after the layers had differentially depleted. The model covered 12 sections, and results presented clearly show the dangers of modeling a large field with a single-well model. The primary conclusion of the study showed that no incremental reserves were generated by infill drilling from one to two wells per section, although gas production can be accelerated. Also, the model shows that the long producing life of the Oklahoma Hugoton gas field is a result of the layered/no-crossflow nature of the reservoir. An important point of the study is the use of an economic limit as the parameter to terminate both the original and infill production forecasts rather than choosing an arbitrary time or well-life cutoff.

Gunter, G.W. and Jones, J.R.: "Developing Gas Reservoir Descriptions Through Multiwell Performance History Matching: Case Histories From Oklahoma's Anadarko Basin," paper SPE 24895 presented at the 1992 SPE Annual Technical Conference and Exhibition, Washington, DC, 4–7 October.

This paper describes a full-field simulation of a 31-well layered gas field producing from the Red Fork in Oklahoma's Anadarko basin. The field occurred at a depth of 11,500 ft and exhibited an average permeability of 1.25 md; it had an initial reservoir pressure of 10,300 psia. This work focused on the importance of matching nonlinear P_{bh}/z vs. cumulative production data from individual wells to characterize differential layer depletion and the effects of offset production within each layer. Ultimately, the history-matched simulator was used to evaluate infill locations, optimize reservoir management, and monitor competitive lease-line positions. Four infill wells were drilled on the basis of the results of the study.

Hinn, R.L. Jr., Glenn, J.M., and McNichol, K.C.: "Case History: Use of a Multiwell Model To Optimize Infill Development of a Tight Gas Sand Reservoir," paper SPE 14659 presented at the 1986 SPE East Texas Regional Meeting, Tyler, Texas, 21–22 April.

This paper describes the use of both a single- and a multiwell simulation model to predict infill-drilling results in the Cotton Valley, a low-permeability gas reservoir. The Cotton Valley reservoir exists in the Blocker, Carthage, Dirgin, Henderson North, Tatum, and Woodlawn fields of east Texas. At the time this paper was written, most of the fields were drilled on a spacing of one well per 640 acres. Large sand-fracture stimulations are used in the Cotton Valley. The paper concludes that most of the fracture half-lengths determined from post-fracture analysis are less than that calculated from design premises. The simulation study was undertaken to determine the incremental rates and reserves from infill drilling. The paper discusses two types of models used in this study: a single well two-dimensional (2D) model and a three-dimensional (3D) multiwell model. Although the 2D model could give satisfactory results, the paper concludes that significant error can result when interwell drainage effects are ignored. The 3D simulation model could account for this interwell drainage; it generated more appropriate production forecasts of incremental rates and reserves. A further conclusion is that infill drilling in a low-permeability reservoir can result in both incremental reserves and rate acceleration.

Hower, T.L. and Decker, M.K.: "Identifying Recompletion Candidates in Stratified Gas Reservoirs," paper SPE 24307 presented at the 1992 SPE Mid-Continent Gas Symposium, Amarillo, Texas, 13–14 April.

This paper represents a case history of a recompletion and redrilling program in the Mesaverde gas reservoir in the San Juan basin. The paper concludes that the Mesaverde is a layered/no-crossflow reservoir that had been poorly completed with the standard practice of using nitroglycerin for stimulation. This stimulation technique had left several individual layers not effectively open to flow. The paper describes a performance analysis technique that uses the shape of the material balance plot, p/z vs. Gp. On the basis of the shape of the plot, recompletion candidates were identified in this field. This technique could be used elsewhere. Setting of casing through the entire productive interval and stimulating layers individually was shown to yield large increases in rate and reserves. For a group of 14 side-track wells, the average rate increased from 26 to 635 Mscf/D. It was determined that redrilling wells was easier operationally and yielded a more favorable gas price. For a group of eight redrills, reserves were added for less than U.S. $0.20/Mcf.

Hower, T.L., Lewis, D.R., and Owens, R.W.: "Recovery Optimization in a Multireservoir Offshore Gas Field With Water Influx," paper SPE 24865 presented at the 1992 SPE Annual Technical Conference and Exhibition, Washington DC, 4–7 October.

This paper documents a case history of a reservoir-simulation-based analysis of an offshore gulf coast gas field containing nine reservoirs produced through eight wells. The authors illustrate the design of an optimized development plan to increase gas reserves based on reservoir characterization through simulation, history matching of past pressure and production performance, and prediction of future recovery for a variety of well-completion schemes, operation scenarios, and economic constraints. Those wishing for an overview of the application of reservoir simulation in waterdrive gas reservoirs should read this paper. The authors concentrate on one series of sandstones that contain one-third of the field's gas reserves. The existence of waterdrive behavior is documented by classic material-balance relationships. Classic evaluation methods were not easily applied because of both vertical and lateral permeability variations that resulted in a variable gas/water contact (GWC). An interesting result was that recovery was maximized by producing downdip water wells at relatively high water-production rates to retard the advance of the GWC. The authors also showed that high gas-production rates were not as successful at increasing reserves because of the accelerated advance of the GWC through high-permeability rocks.

Levey, R.A. *et al.*: "Stratigraphic Compartmentalization Within Gas Reservoirs: Examples From Fluvial-Deltaic Reservoirs of the Texas Gulf Coast," *Bull.*, South Texas Geological Soc. (October 1992) 7.

The authors present three brief case histories of resource additions from Stratton field, Nueces, Kleberg, and Jim Wells counties, Texas. In a mature field in a heterogeneous gas reservoir, reserve growth potential can be divided into five categories: new infield reservoirs, untapped reservoir compartments, incompletely drained reservoir compartments, bypassed reservoirs, and deeper pool reservoirs. This paper gives examples from Stratton field of three of these categories. In the first example, a new well was drilled to a deeper target in the middle of a 320-acre area without any wells. Analysis of the openhole log revealed a new infield reservoir at near initial pressure. OGIP for this reservoir was estimated to be 2.6 Bcf. The second example shows the impact of closely spaced completions in heterogeneous reservoirs. Analysis of pressure data from four new completions indicated the presence of at least three untapped reservoir compartments within a 1-sq-mile area. The incremental resource attributed to these compartments was estimated at 1 Bcf/compartment. The third example showed that even incompletely drained reservoir compartments can provide significant resource additions. In this case, an offset well was drilled 1,100 ft away following abandonment of the initial completion after it had produced 1.6 Bcf. Although the initial pressure for the offset well in the second compartment was only one-third the original reservoir pressure, it was elevated relative to the abandonment pressure in the first compartment. The incremental resource for this case was estimated to be 2 Bcf.

McCoy, T.F. *et al.*: "Analysis of Kansas Hugoton Infill Drilling: Part III—1993 Update and Infill Well Case Histories," paper SPE 26189 presented at the 1993 SPE Gas Technology Symposium, Calgary, 28–30 June.

This paper is a review of the first 1,513 infill wells completed in the 5,889-well Kansas Hugoton field. The majority of the infill drilling occurred 40 years after the initial development on 640-acre spacing, with the infills constituting a second well on each section. Several case histories compare the production and pressure performance of specific wells with that of their older companion wells. The authors conclude that no additional gas in place is encountered by the infill wells and that higher pressures and deliverabilities in the infill wells reflect better stimulation practices and normal pressure gradients in the fully communicated reservoir.

McCoy, T.F. *et al.*: "Analysis of the Kansas Hugoton Infill Drilling Program," *JPT* (June 1992) 714; *Trans.*, AIME, **293.**

This paper reviews the pressure and production performance of five replacement wells and 659 infill wells in the Kansas Hugoton field. The five replacement wells, drilled in 1977 to determine infill potential, encountered layer pressures and deliverabilities that closely matched the offsetting companion wells, indicating no new reserves from the infill wells, only acceleration. The companion wells were shut in for 10 years while the replacement wells were produced. The companion-well pressures closely tracked periodic shut-in pressures in the replacement wells, indicating complete communication. A similar statistical comparison of the 659 infills (each a second well on a section) returned similar results. The authors conclude that higher infill pressures were a result of normal pressure gradients in the reservoir and that higher deliverabilities apparently were incorrect because of a systematic problem in the method used for "official" deliverabilities.

SI Metric Conversion Factors

acre × 4.046 856	E−01 = ha
bbl × 1.589 873	E−01 = m^3
ft × 3.048*	E−01 = m
ft^3 × 2.831 685	E−02 = m^3
in. × 2.54*	E+00 = cm
md × 9.869 233	E−04 = μm^2
psi × 6.894 757	E+00 = kPa
sq mile × 2.589 988	E+00 = km^2

Bibliography

Abdul-Majeed, G.H. and Al-Assal, J.R.: "Graphical Method for Estimating Original Gas-In-Place in Waterdrive Gas Reservoirs," *J. Pet. Res.* (June 1987) **6**, No. 1, 45.

Agarwal, R.G., Carter, R.D., and Pollock, C.B.: "Evaluation and Performance Prediction of Low-Permeability Gas Wells Stimulated by Massive Hydraulic Fracturing," *JPT* (March 1979) 362; *Trans.*, AIME, **267.**

Aguilera, R., and Franks, L.N.: "Isochronal Testing of a Naturally Fractured Gas Reservoir: A Case History," *J. Cdn. Pet. Tech.* (October 1993) **32**, No. 8, 25.

Akibayashi, S. and Zhou, P.: "The Production Performance of the Water-Dissolved Natural Gas Reservoir," paper OSEA 88170 presented at the 1988 SPE Offshore Southeast Asia Conference, Singapore, 2–5 February.

Al-Blehed, M., Sayyouh, M.H., and Desouky, S.M.: "New Approach Estimates Viscosity of Natural Gases," *Pet. Eng. Intl.* (July 1991) 57.

Al-Hashim, H.S. and Bass, D.M.: "Effect of Aquifer Size on the Performance of Partial Waterdrive Gas Reservoirs," *SPERE* (May 1988) 380.

Al Khatib, M.A. and Sadik, A.S.: "Design and Techniques of Testing and Evaluation of Deep Khuff Wells," paper SPE 13682 presented at the 1985 SPE Middle East Oil Show, Bahrain, 11–14 March.

Alcocer, C.F. *et al.*: "A Model for Development, Sensitivity Analysis, and Optimization of Gas Reservoirs With and Without Aquifer: Part I. The Model and Solution Technique," paper SPE 17498 presented at the 1988 SPE Permian Basin Oil and Gas Recovery Conference, Midland, Texas, 10–11 March.

Alcocer, C.F. *et al.*: "A Model for Development, Sensitivity Analysis, and Optimization of Gas Reservoirs With and Without Aquifer: Part II. The Sensitivity Analysis," paper SPE 17499 presented at the 1988 SPE Permian Basin Oil and Gas Recovery Conference, Midland, Texas, 10–11 March.

Allen, D.C.K., Sargeant, D.A., and King, N.B.S.: "Australian Northwest Shelf Gas Project—Risk Management and Potential Rewards," paper 110 presented at the 1988 Gastech LNG/LPG Intl. Conference, Kuala Lumpur, 18–21 October.

Ambastha, A.K.: "Analysis of Material-Balance Equations for Gas Reservoirs," paper CIM 90-36 presented at the 1990 Petroleum Soc. of CIM/SPE International Technical Meeting, Calgary, 10–13 June.

Ambastha, A.K.: "Evaluation of Material-Balance Analysis Methods for Volumetric Abnormally Pressured Gas Reservoirs," *J. Cdn. Pet. Tech.* (October 1993) **32**, No. 8, 19.

Ambastha, A.K.: "A Type-Curve Matching Procedure for Material-Balance Analysis of Production Data From Geopressured Gas Reservoirs," *J. Cdn. Pet. Tech.* (September–October 1991) **30**, No. 5, 61.

Ambastha, A.K., and van Kruijsdijk, C.P.J.W.: "Effects of Input Data Errors on Material-Balance Analysis for Volumetric, Gas, and Gas-Condensate Reservoirs," paper CIM 93-04 presented at the 1993 Annual Technical Meeting of the Petroleum Soc. of CIM, Calgary, 9–12 May.

Aminian, K., Ameri, S., Beg, N., and Yost, A.B. II: "Production Forecasting for Gas Wells Under Variable Conditions," paper SPE 16939 presented at the 1987 SPE Annual Technical Conference and Exhibition, Dallas, 27–30 September.

Aminian, K., Ameri, S., and Hyman, M.D.: "Production Decline Type Curves for Gas Wells Producing Under Pseudo-Steady-State Conditions," paper SPE 15933 presented at the 1986 Eastern Regional Conference, Columbus, Ohio, 12–14 November.

Aminian, K. et al.: "Gas-Well Production Decline in Multiwell Reservoirs," *JPT* (December 1990) 1573; *Trans.*, AIME **289.**

Aminian, K. *et al.*: "Predicting Gas-Well Performance Under Altered Conditions," paper SPE 17060 presented at the 1987 SPE Eastern Regional Meeting, Pittsburgh, Pennsylvania, 21–23 October.

Aminian, K., Ameri, S., and Hyman, M.D.: "Production History Analysis in Predicting "Dry" Gas Well Performance," *J. Pet. Sci. Eng.* (March 1989) **2**, no. 1, 13.

Ammer, J.R., Sawyer, W.K., and Drophin, M.J.: "Practical Methods for Detecting Production Mechanisms in Tight Gas Reservoirs," paper SPE 12864 presented at the 1984 SPE Unconventional Gas Recovery Symposium, Pittsburgh, Pennsylvania, 13–15 May.

Ancell, K.L., and Manhart, T.A.: "Secondary Gas Recovery From a Waterdrive Gas Reservoir: A Case Study," paper SPE 16944 presented at the 1987 SPE Annual Technical Conference and Exhibition, Dallas, 27–30 September.

Ancell, K.L. and Trousil, P.M.: "Remobilization of Natural Gas Trapped by Encroaching Water," paper SPE 20753 presented at the 1990 SPE Annual Technical Conference and Exhibition, New Orleans, 23–26 September.

Arastoopour, H. and Chen, S.T.: "Sensitivity Analysis of Key Reservoir Parameters in Gas Reservoirs," paper SPE 21515 presented at the 1991 SPE Gas Technology Symposium, Houston, 22–24 January.

Arastoopour, H., Chen, S.T., and Hariri, M.H.: "Analysis of Flow of Gas and Water in a Fractured and Nonfractured Low-Permeability Reservoir Under Production," paper SPE 16948 presented at the 1987 SPE Annual Technical Conference and Exhibition, Dallas, 27–30 September.

Arastoopour, H., Chen, S.T., and Hariri, M.H.: "Analysis of Flow of Gas and Water in a Low Permeability Reservoir," *Energy Sources* (1988) **10**, No. 3, 183.

Arcaro, D.P. and Bassiouni, Z.A.: "Technical and Economic Feasibility of Enhanced Gas Recovery in the Eugene Island Field By Use of the Coproduction Technique," *JPT* (May 1987) 585.

Arthur, J.E., Chhina, H.S., and Temeng, K.O.: "Material-Balance Modeling and Performance Prediction of a Composite Gas Reservoir," paper SPE 26194 presented at the 1993 SPE Gas Technology Symposium, Calgary, 28–30 June.

Au, A.D., Franks, L.N., and Aguilera, R.: "Simulation of a Gas Naturally Fractured Reservoir: A Case History," paper SPE 22920 presented at the 1991 SPE Annual Technical Conference and Exhibition, Dallas, 6–9 October.

Aziz, R.M.: "Deliverability Projection Model for Overpressured Gas-Condensate Reservoirs," paper SPE 13706 presented at the 1985 SPE Middle East Oil Show, Bahrain, 11–14 March.

Baldwin, J.O.: "Prediction of Deliverability From a Multiwell Gas Reservoir," paper SPE 9322 presented at the 1980 SPE Annual Technical Conference and Exhibition, Dallas, 21–24 September.

Baldwin, J.O., Kirchner, W.D., and Kennedy, J.H.: "Gas Reservoir Simulation Using Semi-Implicit Rates With Multiple Compressor Stations," paper SPE 10116 presented at the 1981 SPE Annual Technical Conference and Exhibition, Dallas, 5–7 October.

Barker, G. and Vincent, P.: "Geological and Reservoir Engineering Considerations for the North Rankin Gas Recycling Project," *Australian Petroleum Exploration Assn. J.* (1988) **28**, Pt. 1, 54.

Bastian, P.A.and Sherman, J.B.: "The Analysis of a Hydraulically Fractured, Low Permeability Gas Reservoir Using Numerical Simulation," *SPE Advanced Technology Series* (July 1993) 172.

Beck, F.E. and Lee, R.L.: "A Method for Determination of Permeability, Skin, and Turbulence Factor From an Open-Flow Potential Test," paper SPE 18270 presented at the 1988 SPE Annual Technical Conference and Exhibition, Houston, 2–5 October.

Begland, T.F. and Whitehead, W.R.: "Depletion Performance of Volumetric High-Pressured Gas Reservoirs," *SPERE* (August 1989) 279; *Trans.*, AIME, **287.**

Berkenpas, P.G.: "The Milk River Shallow Gas Pool: Role of the Updip Water Trap and Connate Water in Gas Production From the Pool," paper SPE 22922 presented at the 1991 SPE Annual Technical Conference and Exhibition, Dallas, 6–9 October.

Bernard, W.J.: "Reserves Estimation and Performance Prediction for Geopressured Gas Reservoirs," *J. Pet. Sci. Eng.* (August 1987) 15.

Bernard, W.J.: "Reservoir Engineering Concepts in Abnormal Formation Environments," *Studies in Abnormal Pressures*, W.H. Fertl, R.E. Chapman, R.F. Hotz (eds.), *Developments in Petroleum Science*, Elsevier Scientific, New York City (1994) **39**, 93–105.

Blasingame, T.A. and Lee, W.J.: "The Variable-Rate Reservoir Limits Testing of Gas Wells," paper SPE 17708 presented at the 1988 SPE Gas Technology Symposium, Dallas, 13–15 June.

Blasingame, T.A., McCray, T.L., and Lee, W.J.: "Decline-Curve Analysis for Variable Pressure Drop/Variable Flow Rate Systems," paper SPE 21513 presented at the 1991 SPE Gas Technology Symposium, Houston, 22–24 January.

Blasingame, T.A., Poston, S.W., and Hedberg, W.H.: "Evaluation of Reserves for a Number of Small, Partially Shut-In Gas Fields in Northern Tennessee," SPE 16853 presented at the 1987 SPE Annual Technical Conference and Exhibition, Dallas, 27–30 September.

Bourgoyne, A.T. Jr.: "Shale Water as a Pressure Support Mechanism in Gas Reservoirs Having Abnormal Formation Pressure," *J. Pet. Sci. Eng.* (January 1990) **3**, No. 4, 305.

Bowers, B.: "Gas Reservoir Performance Monitoring," paper 81-32-51 presented at the 1981 Annual Technical Meeting of the Petroleum Soc. of CIM, Calgary, 3–6 May.

Brar, G.S. and Aziz, K.: "Analysis of Modified Isochronal Tests To Predict the Stabilized Deliverability Potential of Gas Wells Without Using Stabilized Flow Data," *JPT* (February 1978) 297; *Trans.*, AIME, **265.**

Brigham, W.E.: "Estimating Reservoir Parameters From the Gas Backpressure Equation," *SPERE* (May 1988) 649.

Brinkman, F.P.: "Increased Gas Recovery From a Moderate Waterdrive Reservoir," *JPT* (December 1981) 2475; *Trans.*, AIME, **271.**

Bruns, J.R., Fetkovich, M.J., and Meitzen, V.C.: "The Effect of Water Influx on *p/z*-Cumulative Gas Production Curves," *JPT* (March 1965) 287.

Camacho-Velazquez, R., Vazquez-Cruz, M., and Padilla-Sixto, R: "New Results on Decline Curves Considering Non-Darcy Flow Effects," paper SPE 24058 presented at the 1992 SPE Western Regional Meeting, Bakersfield, California, 30 March–1 April.

Carter, R.D.: "Characteristic Behavior of Finite Radial and Linear Gas Flow Systems—Constant Terminal Pressure Case," paper SPE 9887 presented at the 1981 SPE/DOE Low Permeability Gas Reservoir Symposium, Denver, Colorado, 27–29 May.

Carter, R.D.: "Type Curves for Finite Radial and Linear Gas-Flow Systems: Constant-Terminal-Pressure Case," *SPEJ* (October 1985) 719; *Trans.*, AIME, **279.**

Cason, L.D. Jr.: "Waterflooding Increases Gas Recovery," *JPT* (October 1989) 1102; *Trans.*, AIME, **287.**

Chase, R.W. and Alkandari, H.: "Prediction of Gas Well Deliverability From Just a Pressure Buildup or Drawdown Test," paper SPE 26915 presented at the 1993 SPE Eastern Regional Meeting, Pittsburgh, Pennsylvania, 2–4 November.

Chase, R.W. and Anthony, T.: "A Simplified Method for Determining Gas-Well Deliverability," *SPERE* (August 1988) 1090.

Chierici, G.L. *et al.*: "Production Mechanism of Abnormally High-Pressured Gas Reservoirs," paper IGU/A4-76 presented at the 1976 IGU World Gas Conference, London, 7–11 June.

Chierici, G.L., Gottardi, G.A., and Guidorzi, R.P.: "Forecasting Gas Reservoir Behavior With Identified Models," *Rev. Inst. Franc. Pet.* (September–October 1986) **41,** No. 5, 637.

Chierici, G.L. *et al.*: "Waterdrive From Interbedded Shale Compaction in Superpressured Gas Reservoirs—A Model Study," *JPT* (June 1978) 937.

Clark, D.G., le Foll, P., and Harding, A.: "Some Practical Considerations for Southern North Sea Gas Testing: An Integrated Approach," paper SPE 13983 presented at the 1985 SPE Offshore Europe Conference, Aberdeen, 10–13 September.

Clinton, L., and Carlson, N.R.: "Significance of Turbulent Pressure Loss for the Deliverability of a Perforated Gas Well," paper Z presented at the SPWLA 1985 Annual Logging Symposium, Dallas, 17–20 June.

Coleman, S.B. and Clay, H.B.: "The Blowdown-Limit Model," *JPT* (March 1991) 339; *Trans.*, AIME, **291.**

Coleman, S.B. *et al.*: "Applying Gas-Well Loadup Technology," *JPT* (March 1991) 344.

Coleman, S.B. *et al.*: "A New Look at Predicting Gas-Well Loadup," *JPT* (March 1991) 329; *Trans.*, AIME, 291.

Coleman, S.B. *et al.*: "Understanding Gas-Well Loadup Behavior," *JPT* (March 1991) 329.

Colleary, W.M., Hulme, J.R., and Al-Haddad, S.M.: "Defining Waterdrive Gas Reservoirs: Problems in Data Acquisition and Strategies in Evaluation," paper no. 3RC-26, presented at the 3D U.S. DOE Reservoir Characterization Conference, Tulsa, Oklahoma 3–5 November 1991.

Collier, R.S., Monash, E.A., and Hultquist, P.F.: "Modeling Natural Gas Reservoirs—A Simple Model," *SPEJ* (October 1981) 521; *Trans.*, AIME, **271.**

Cronquist, C.: "Turtle Bayou—1936–1983: Case History of a Major Gas Field in South Louisiana," *JPT* (November 1984) 1941; *Trans.*, AIME, **277.**

Das, A.K. and Tiab, D.: "A Techno-Economic Model for Shallow Gas Reservoirs Under Partial Water Drive," *Proc.*, First Oklahoma Energy Center and UNITAR Intl. Conference, R.F. Meyer (ed.), Gulf Publishing Co., Houston (1986) 315.

Davidson, D.A. and Snowdon, D.M.: "Beaver River Middle Devonian Carbonate: Performance Review of a High-Relief, Fractured Gas Reservoir With Water Influx," *JPT* (December 1978) 1672.

Dogru, A.H. and Knapp, R.M.: "The Reliability of the Predicted Performance of Natural Gas Reservoirs Using Reservoir Parameters From Well-Test Data Containing," paper SPE 5343 presented at the 1975 SPE Rocky Mountain Regional Meeting, Denver, Colorado, 7–9 April.

Doherty, M.G. *et al.*: "Methane Production From Geopressured Aquifers," *JPT* (July 1982) 1591; *Trans.*, AIME, **273.**

Dougherty, E.L. and Chang, J.: "Determining Optimal Capacity and Recovery From Gas Reservoirs: Impact of Permeability Contrast, Tubing Size, and Compressor," paper SPE 26145 presented at the 1993 SPE Gas Technology Symposium, Calgary, 28–30 June.

Duda, J.R. and Aminian, K.: "Type Curves for Predicting Production Performance From Horizontal Wells in Low-Permeability Gas Reservoirs," paper SPE 18993 presented at the 1989 SPE Joint Rocky Mountain Regional/Low Permeability Reservoir Symposium and Exhibition, Denver, Colorado, 6–9 March.

Duggan, J.O. and Langston, R.B.: "Gas-Well Completions Into Low-BHP Reservoirs Add Reserves," paper SPE 17762 presented at the 1998 SPE Gas Technology Symposium, Dallas, 13–15 June.

Durrani, A.J. *et al.*: "The Rejuvenation of 30-year-old McAllen Ranch Field: An Application of Crossfunctional Team Management," *JPT* (December 1994) 1065.

Dyck, W.C. and Moore, R.M.: "Low-Pressure Gas Field Operations in Leman," paper SPE 28889 presented at the 1994 SPE European Petroleum Conference, London, 25–27 October.

Engineer, R.: "Cal Canal Field, California: Case History of a Tight and Abnormally Pressured Gas Condensate Reservoir," paper SPE 13650 presented at the 1985 SPE California Regional Meeting, Bakersfield, California, 27–29 March.

Erarsian, S., Ayan, C., and Lee, W.J.: "Non-Darcy Flow Behavior in Partially Penetrating Gas Wells," paper SPE 21401 presented at the 1991 Middle East Oil Show, Bahrain, 2–5 March.

Erba, M. *et al.*: "A Multidisciplinary Study Aimed at Optimizing Reservoir Management in a Gas Field With Over 30 Years of Production History," paper SPE 26657 presented at the 1993 SPE Annual Technical Conference and Exhibition, Houston, 3–6 October.

Evans, E.V. and Evans, R.D.: "The Influence of an Immobile or Mobile Saturation on Non-Darcy Compressible Flow of Real Gases in Propped Fractures," *JPT* (October 1988) 1343.

Evans, R.D. and Lekia, S.D.L: "A Reservoir Simulation Study of Naturally Fractured Lenticular Tight Gas Sand Reservoirs," *J. Energy Res. Tech.* (December 1990) **112,** No. 4, 231.

Fasanino, G. *et al.*: "Inverse Modeling in Gas Reservoirs," paper SPE 15592 presented at the 1986 SPE Annual Technical Conference and Exhibition, New Orleans, 5–8 October.

Fetkovich, M.J., Fetkovich, E.J., and Fetkovich, M.D.: "Useful Concepts for Decline-Curve Forecasting, Reserve Estimation, and Analysis," *SPERE* (February 1996) 13.

Fetkovich, M.J., Reese, D.E., and Whitson, C.H.: "Application of a General Material Balance for High-Pressure Gas Reservoirs," paper SPE 22921 presented at the 1991 SPE Annual Technical Conference and Exhibition, Dallas, October 6–9.

Fetkovich, M.J. *et al.*: "Depletion Performance of Layered Reservoirs Without Crossflow," *SPEFE* (September 1990) 310; *Trans.*, AIME, **289.**

Firoozabadi, A. and Katz, D.L.: "Analysis of High-Velocity Gas Flow Through Porous Media," *JPT* (February 1979) 211.

Fraim, M.L. and Wattenbarger, R.A.: "Gas Reservoir Decline-Curve Analysis Using Type Curves With Real Gas Pseudopressure and Normalized Time," *SPEFE* (December 1987) 671.

Folefac, A.N., Issa, R.I., and Wall, C.G.: "Study of Well Deliverability in Waterdrive Gas Reservoirs," paper SPE 19260 presented at the 1989 SPE Offshore Europe Conference, Aberdeen, 5–8 September.

Gajdica, R.J., Wattenbarger, R.A., and Startzman, R.A.: "A New Method of Matching Aquifer Performance and Determining Original Gas in Place," *SPERE* (August 1988) 985.

Gao, C. and Lee, W.J.: "Modeling Commingled Reservoirs With Pressure-Dependent Properties and Unequal Pressures in Different Layers," paper SPE 26665 presented at the 1993 SPE Annual Technical Conference and Exhibition, Houston, 3–6 October.

Golaz, P., Sitbon, A.J.A., and Delisle, J.G.: "Case History of the Meillon Gas Field," *JPT* (August 1990) 1032.

Gold, D.K., McCain, W.D. Jr., and Jennings, J.W.: "An Improved Method for the Determination of the Reservoir-Gas Specific Gravity for Retrograde Gases," *JPT* (July 1989) 747; *Trans.*, AIME, **287.**

Greene, W.R.: "Analyzing the Performance of Gas Wells," *JPT* (July 1983) 1378; *Trans.*, AIME, **275.**

Guardia, M.A. and Hackney, R.M.: "A Practical Approach to Original Gas-in-Place Estimation: Development of the South Wilburton Field," paper SPE 22925 presented at the 1991 SPE Annual Technical Conference and Exhibition, Dallas, 6–9 October.

Gunter, G.W. and Jones, J.R.: "Developing Gas Reservoir Descriptions Through Multiwell Performance History Matching: Case Histories From Oklahoma's Anadarko Basin," paper SPE 24895 presented at the 1992 SPE Annual Technical Conference and Exhibition, Washington, DC, 4–7 October.

Hadinoto, N., Raghavan, R., and Thomas, G.W.: "Determination of Gas-Well Deliverability of Vertically Fractured Wells," paper SPE 6136 presented at the 1976 SPE Annual Technical Conference and Exhibition, New Orleans, 3–6 October.

Hales, H.B.: "Pressure-Decline Analysis for Prediction of Gas Reservoir Volumes," *JPT* (November 1981) 2261; *Trans.*, AIME, **271.**

Harrington, A.G., Lee, B.Y.Q., and Taylor, P.S.: "Application of Type-Curve Techniques to Decline Analysis and Forecasting of Gas Wells," paper SPE 16936 presented at the 1987 SPE Annual Technical Conference and Exhibition, Dallas, 27–30 September.

Hinn, R.L. Jr., Glenn, J.M., and McNichol, K.C.: "Case History: Use of a Multiwell Model To Optimize Infill Development of a Tight-Gas-Sand Reservoir," *JPT* (July 1988) 881.

Holditch, S.A.: "Factors Affecting Water Blocking and Gas Flow From Hydraulically Fractured Gas Wells," *JPT* (December 1979) 1515.

Holditch, S.A. and Morse, R.A.: "The Effects of Non-Darcy Flow on the Behavior of Hydraulically Fractured Gas Wells," *JPT* (October 1976) 1169.

Holditch, S.A., Lee, W.J., and Gist, S.R.: "An Improved Technique for Estimating Permeability, Fracture Length, and Fracture Conductivity From Pressure-Buildup Tests in Low-Permeability Gas Wells," *JPT* (May 1983) 981; *Trans.*, AIME, **275.**

Holditch, S.A., *et al.*: "The Optimization of Well Spacing and Fracture Length in Low-Permeability Gas Reservoirs," paper SPE 7496 presented at the 1978 SPE Annual Technical Conference and Exhibition, Houston, 1–3 October.

Hossain, M., Cady, G.V., and Honarpour, M.M.: "Simulation of Real Gas Flow Through Finite-Conductivity Fractures," paper SPE 12919 presented at the 1984 SPE Rocky Mountain Meeting, Casper, Wyoming, 21–23 May.

Hower, T.L. and Collins, R.E.: "Detecting Compartmentalization in Gas Reservoirs Through Production Performance," paper SPE 19790 presented at the 1989 SPE Annual Technical Conference and Exhibition, San Antonio, Texas, 8–11 October.

Hower, T.L. and Jones, R.E.: "Predicting Recovery of Gas Reservoirs Under Waterdrive Conditions," paper SPE 22937 presented at the 1991 SPE Annual Technical Conference and Exhibition, Dallas, 6–9 October.

Hower, T.L. and Owens, R.E.: "Reservoir Management of a Gulf Coast Waterdrive Gas Field," presented at the 1992 Intl. Gas Research Conference, sponsored by Gas Research Inst., Intl. Gas Union, American Gas Assn., and U.S. Dept. of Energy, Orlando, Florida, 16–19 November.

Hower, T.L., Bergeson, I., and Decker, M.K.: "Identifying Recompletion Candidates in Stratified Gas Reservoirs," paper SPE 24307 presented at the 1992 SPE Mid-Continent Gas Symposium, Amarillo, Texas, 12–14 April.

Hower, T.L. *et al.*: "Recovery Optimization in a Multireservoir Offshore Gas Field With Water Influx," paper SPE 24865 presented at the 1992 SPE Annual Technical Conference and Exhibition, Washington, DC, 4–7 October.

Humphreys, N.V.: "The Material-Balance Equation for a Gas-Condensate Reservoir With Significant Water Vaporization," paper SPE 21514 presented at the 1991 SPE Gas Technology Symposium, Houston, 23–25 January.

Hunter, J.L. *et al.*: "Cotton Valley Production Enhancement Team Points Way to Full Gas Production Potential," paper SPE 24887 presented at the 1992 SPE Annual Technical Conference and Exhibition, Washington, DC, 4–7 October.

Iledare, O.O.: "Modeling the Discovery of New Natural Gas Reserves," paper SPE 19322 presented at the 1989 SPE Eastern Regional Meeting, Morgantown, West Virginia, 24–27 October.

Iledare, W.O.: "Use of Least Squares To Estimate Gas-Well Gas Recoverable Reserves and First-Year Gas Production," paper SPE 27943 presented at the 1994 SPE Mid-Continent Gas Symposium, Amarillo, Texas, 22–24 May.

Ireland, M.M., and Robinson, J.B.: "Reserve Predictions From Production Testing in Geopressured Gas Reservoirs," paper SPE 16958 presented at the 1987 SPE Annual Technical Conference and Exhibition, Dallas, 27–30 September.

Jackson, M.L.W. and Ambrose, W.A.: "Influence of Reservoir Heterogeneity on Gas-Resource Potential for Geologically Based Infill Drilling, Brooks and I-92 Reservoirs, Frio Formation, South Texas," *Trans.*, Gulf Coast Assn. of Geological Societies (1989) **39,** 127.

Janahi, I.A. and Dakessian, B.A.: "Development of the Knuff Gas Reservoir, Bahrain Field," paper SPE 13679 presented at the 1985 SPE Middle East Oil Show, Bahrain, 11–14 March.

Jirik, L.A., Howard, W.E., and Sadler, D.L.: "Identification of Bypassed Gas Reserves Through Integrated Geological and Petrophysical Techniques: A Case Study in Seeligson Field, Jim Wells County, South Texas," paper SPE 21483 presented at the 1991 SPE Gas Technology Symposium, Houston, 22–24 January.

Johnston, J.L. and Lee, W.J.: "Identification of Productive Layers in Low-Permeability Gas Wells," *JPT* (November 1992) 1240; *Trans.*, AIME, **293.**

Johnston, J.L., Lee, W.J., and Blasingame, T.A.: "Estimating the Stabilized Delivery of a Gas Well Using the Rawlins and Schellhardt Method: An Analytical Approach," paper SPE 23440 presented at the 1991 SPE Eastern Regional Meeting, Lexington, Kentucky, 22–25 October.

Jones, F.O. Jr. and Owens, W.W.: "A Laboratory Study of Low-Permeability Gas Sands," *JPT* (September 1980) 1631; *Trans.*, AIME, **269.**

Jones, S.C.: "Using the Inertial Coefficient, β, To Characterize Heterogeneity in Reservoir Rock," paper SPE 16949 presented at the 1987 SPE Annual Technical Conference and Exhibition, Dallas, 27–30 September.

Kabir, C.S. and Hasan, A.R.: "Prefracture Testing in Tight-Gas Reservoirs," *SPEFE* (April 1986) 128.

Kazemi, H.: "Low-Permeability Gas Sands," *JPT* (October 1982) 2229; *Trans.*, AIME, **273.**

Keating, J.F., Wattenbarger, R.A., and Chen, H.Y.: "Original Gas-in-Place and Decline Curves From Early Stabilized Rate/Time Data," paper SPE 27666 presented at the 1994 SPE Permian Basin Oil and Gas Recovery Conference, Midland, Texas, 16–18 March.

Koederitz, L.F., Joseph, J.A., and Numbere, D.T.: "Estimating Maximum Gas Rates for Darcy-Type Flow," paper CIM 86-37-38 presented at the 1986 Annual Technical Meeting of the Petroleum Soc. of CIM, Calgary, 8–11 June.

Layne, M.A., Numbere, D.T., and Koederitz, L.F.: "Future Performance Prediction for Waterdrive Gas Reservoirs," paper SPE 26669 presented at the 1993 SPE Annual Technical Conference and Exhibition, Houston, 3–6 October.

Lee, R.L., Tek, M.R., and Logan, R.W.: "Effect of Turbulence on Transient Flow of Real Gas Through Porous Media," *SPEFE* (March 1987) 108; *Trans.*, AIME, **283.**

Lee, W.J.: "Pressure-Transient Test Design in Tight Gas Formations," *JPT* (October 1987) 1185.

Lee, W.J. and Hopkins, C.W.: "Characterization of Tight Reservoirs," *JPT* (November 1994) 956; *Trans.*, AIME, **297.**

Lee, W.J. *et al.*: "Estimating Formation Permeability From Single-Point Flow Data," paper SPE 12847 presented at the 1984 SPE/DOE/GRI Unconventional Gas Recovery Symposium, Pittsburgh, Pennsylvania, 13–15 May.

Levey, R.A. *et al.*: "Natural Gas Reserve Replacement Through Infield Reserve Growth: An Example From Stratton Field, Onshore Texas Gulf Coast Basin," paper 3RC-62 presented at the 1991 U.S. DOE Reservoir Characterization Technology Conference, Tulsa, Oklahoma, 3–5 November.

Levey, R.A. *et al.*: "Stratigraphic Compartmentalization Within Gas Reservoirs: Examples From Fluvial-Deltaic Reservoirs of the Texas Gulf Coast," *South Texas Geol. Soc. Bull.* (October 1992) **33,** No. 2, 7.

Lewis, R.C.: "Reserve Determination Using Pseudosteady-State Techniques in a High-Pressure Sour Gas Field: A Case History," paper SPE 14363 presented at the 1985 SPE Annual Technical Conference and Exhibition, Las Vegas, Nevada, 22–25 September.

Lin, C. and Mattar, L.: "Determination of Stabilization Factor and Skin Factor From Isochronal and Modified Isochronal Tests," *J. Cdn. Pet. Tech.* (March–April 1982) 89.

Lin, Z.S. and Finley, R.J.: "Reservoir Engineering Properties and Production Characteristics of Selected Tight-Gas Fields, Travis Peak Formation, East Texas," paper SPE 13901 presented at the 1985 SPE/DOE Joint Symposium on Low Permeability Reservoirs, Denver, 19–22 May.

Lord, M.E. and Collins, R.E.: "Detecting Compartmented Gas Reservoirs Through Production Performance," paper SPE 22941 presented at the 1991 SPE Annual Technical Conference and Exhibition, Dallas, 6–9 October.

Lord, M.E. *et al.*: "A Compartmented Simulation System for Gas Reservoir Evaluation With Application to Fluvial Deposits in the Frio Formation, South," paper SPE 24308 presented at the 1992 SPE Mid-Continent Gas Symposium, Amarillo, Texas, 12–14 April.

Maley, S.: "The Use of Conventional Decline-Curve Analysis in Tight Gas Well Applications," paper SPE 13898 presented at the 1985 SPE/DOE Joint Symposium on Low Permeability Reservoirs, Denver, Colorado, 19–22 May.

Martin, I. and Young, G.C.: "The Medicine Hat Gas Field: 100 Years After Discovery," paper 90–19 presented at the 1990 Annual Technical Meeting of the Petroleum Soc. of CIM, Calgary, 10–13 June.

Mattar, L. and Adegbesan, K.O.: "Prediction of Pressure Drawdown in Gas Reservoirs Using a Semi-Analytical Solution of the Nonlinear Gas Flow Equation," paper CIM 80-31-39, presented at the 1980 Annual Technical Meeting of the Petroleum Soc. of CIM, Calgary, 25–28 May.

Mattar, L. and Lin, C.: "Validity of Isochronal and Modified Isochronal Testing of Gas Wells," paper SPE 10126 presented at the 1981 SPE Annual Technical Conference and Exhibition, Dallas, 5–7 October.

McCain, W.D. Jr. *et al.*: "A Tight Gas Field Study: Carthage (Cotton Valley) Field," paper SPE 26141 presented at the 1993 SPE Gas Technology Symposium, Calgary, 28–30 June.

McCoy, T.F. *et al.*: "Analysis of Kansas Hugoton Infill Drilling: Part I—Total Field Results," paper SPE 20756 presented at the 1990 SPE Annual Technical Conference and Exhibition, New Orleans, 23–26 September.

McCoy, T.F. *et al.*: "Analysis of the Kansas Hugoton Infill-Drilling Program," *JPT* (June 1992) 714; *Trans.*, AIME, **293.**

McCoy, T.F. *et al.*: "Analysis of Kansas Hugoton Infill Drilling: Part 3—1993 Update and Infill Well Case Histories," paper SPE 26189 presented at the 1993 SPE Gas Technology Symposium, Calgary, 28–30 June.

Meehan, D.N. and Verma, S.K.: "Improved Reservoir Characterization in Low-Permeability Reservoirs With Geostatistical Models," *SPERE* (August 1995) 157.

Mercer, J.C. and Frohne, K.H.: "Production Characterization of Tight Lenticular Gas Sands in the Rulison Area of Western Colorado," paper SPE 15248 presented at the 1986 SPE Unconventional Gas Technology Symposium, Louisville, Kentucky, 18–21 May.

Mijnsson, F.C.J. and Maskall, R.C.: "The Leman Field: Hunting for the Remaining Gas," paper SPE 28880 presented at the 1994 SPE Europe Petroleum Conference, London, 25–27 October.

Mishra, S. and Caudle, B.H.: "Simplified Procedure for Gas Deliverability Calculations Using Dimensionless IPR Curves," paper SPE 13231 presented at the 1984 SPE Annual Technical Conference and Exhibition, Houston, 16–19 September.

Mohaghegh, S. and Ertekin, T.: "Production and Pressure Decline Curves for Wet Gas Sands With Closed Outer Boundaries," paper SPE 23442 presented at the 1991 SPE Eastern Regional Conference and Exhibition, Lexington, Kentucky, 23–25 October.

Mohaghegh, S., Bilgesu, H.I., and Ertekin, T: "Production Decline Curves for Low-Pressure Gas Reservoirs Undergoing Simultaneous Water Production," *SPEFE* (March 1995) 57.

Moltz, A.K.: "Modeling a Repressured Waterdrive Gas Reservoir," *JPT* (April 1993) 314.

Moore, P.J.R.: "Barque and Clipper: Well-Test Analysis in Low-Permeability Fractured Gas Reservoirs," paper SPE 18966 presented at the 1989 SPE Joint Rocky Mountain Regional/Low Permeability Reservoirs Symposium and Exhibition, Denver, Colorado, 6–8 March.

Morton, J. and Malavazos, M.: "A Probabilistic Method for Estimating Reserves in Heterogeneous Gas Reservoirs," *Petroleum Exploration Soc. of Australia J.* (June 1992) **20,** 63–69.

Narahara, G.M. and Holditch, S.A.: "Improved Rock Property Measurements Using Core From the Travis Peak Formation," paper SPE 17730 presented at the 1988 SPE Gas Technology Symposium, Dallas, 13–15 June.

Neal, D.B. and Mian, M.A.: "Early-Time Tight Gas Production Forecasting Technique Improves Reserves and Reservoir Description," *SPEFE* (March 1989) 25.

Newman, G.H.: "Pore-Volume Compressibility of Consolidated, Friable, and Unconsolidated Reservoir Rocks Under Hydrostatic Loading," *JPT* (February 1973) 129.

Nilssen, B.H.: "Troll High-Rate Production Test, Planning and Execution," paper SPE 16555 presented at the 1987 SPE Offshore Europe Conference, Aberdeen, 8–11 September.

Oberst, R.J. *et al.*: "3D Reservoir Simulation Results of a 25-sq-mile Study Area in the Kansas Hugoton Gas Field," paper SPE 27931 presented at the 1994 SPE Mid-Continent Gas Symposium, Amarillo, Texas, 22–24 May.

Ohkuma, H. *et al.*: "An Analysis of Reservoir Mechanics of Geopressured Geothermal Aquifers—the Brazoria County Prospect," *Proc.*, Fourth U.S. Gulf Coast Geopressured-Geothermal Energy Conference: Research and Development, M.H. Dorfman and W.L. Fisher (eds.), Center for Energy Studies, U. of Texas, Austin, Texas (1979) **2,** 907.

Oren, P.E., Lee, R.L., and Tek, M.R.: "The Effects of Wellbore Storage, Skin, and Turbulence Intensity on Early-Time Transient Flow of Real Gas Through Porous Media," *SPEFE* (September 1988) 547.

Pascal, H.: "Advances in Evaluating Gas-Well Deliverability Using Variable Rate Tests Under Non-Darcy Flow," paper SPE 9841 presented at the 1981 SPE/DOE Symposium on Low Permeability, Denver, Colorado, 27–29 May.

Pathak, P. *et al.*: "Java Sea Gas Reservoir Development Design," paper SPE 28788 presented at the 1994 SPE Asia Pacific Oil and Gas Conference, Melbourne, Australia, 7–10 November.

Peffer, J.W., Miller, M.A., and Hill, A.D.: "An Improved Method for Calculating Bottomhole Pressures in Flowing Gas Wells With Liquid Present," *SPEPE* (November 1988) 643; *Trans.*, AIME, **285.**

Piper, L.D., McCain, W.D. Jr., and Corredor, J.H.: "Compressibility Factors for Naturally Occurring Petroleum Gases," paper SPE 26668 presented at the 1993 SPE Annual Technical Conference and Exhibition, Houston, 3–6 October.

Posaner, F.M. and Goldthorpe, W.H.: "The Development and Early Performance of the North Rankin Field," *Australian Petroleum Exploration Assn. J.* (1986) **26,** Pt. 1, 420.

Poston, S.W. and Chen, H.Y.: "Case History Studies: Abnormally Pressured Gas Reservoirs," paper SPE 18857 presented at the 1989 SPE Production Operations Symposium, Oklahoma City, Oklahoma, 13–14 March.

Poston, S.W. and Chen, H.Y.: "The Simultaneous Determination of Formation Compressibility and Gas in Place in Abnormally Pressured Reservoirs," paper SPE 16227 presented at the 1987 SPE Production Operations Symposium, Oklahoma City, Oklahoma, 8–10 March.

Poston, S.W., Chen, H.Y., and Akhtar, M.J.: "Differentiating Between Formation Compressibility and Water-Influx Effects in Overpressured Gas Reservoirs," *SPERE* (August 1994) 183.

Poston, S.W. *et al.*: "Differentiating Between Formation Compressibility and Water Influx Effects in Geopressured Gas Reservoirs," paper presented at the 1992 Intl. Gas Research Conference sponsored by Gas Research Inst., Intl. Gas Union, American Gas Assn., and U.S. Dept. of Energy, Orlando, Florida, 16–19 November.

Poston, S.W. *et al.*: "Using the Isochronal, Transient Pressure Analysis Method To Calculate Gas Reserves," paper presented at the 1992 Intl. Gas Research Conference sponsored by Gas Research Inst., Intl. Gas Union, American Gas Assn., and U.S. Dept. of Energy, Orlando, Florida, 16–19 November.

Prasad, R.K. and Rogers, L.A.: "Superpressured Gas Reservoirs: Case Studies and a Generalized Tank Model," paper SPE 16861 presented at the 1987 SPE Annual Technical Conference and Exhibition, Dallas, 27–30 September.

Purvis, R.A.: "Analysis of Production-Performance Graphs," paper CIM 84-35-50 presented at the 1984 Annual Technical Meeting of the Petroleum Soc. of CIM and the Canadian Assn. of Drilling Engineers, Calgary, 10–13 June.

Raghavan, R.: "Theory and Application of Gas Well-Test Analysis," Tulsa U. and American Gas Assn. *Natural Gas Resources Development in Mid-Continent Basins Proc.*, Tulsa, Oklahoma (1980) 83–173.

Ramagost, B.R. and Farshad, F.F.: "*p/z* Abnormally Pressured Gas Reservoirs," paper SPE 10125 presented at the 1981 SPE Annual Technical Conference and Exhibition, San Antonio, Texas, 4–7 October.

Randolph, P.L., Hayden, C.G., and Anhaiser, J.L.: "Maximizing Gas Recovery From Strong Waterdrive Reservoirs," paper SPE 21486 presented at the 1991 SPE Gas Technology Symposium, Houston, 22–24 January.

Riley, H.G. and Willcox, P.J.: "Performance Matching for a North Sea Gas Field," paper SPE 5535 presented at the 1975 SPE Annual Technical Conference and Exhibition, Dallas, 28 September–1 October.

Robinson, B.M., Holditch, S.A., and Lee, W.J.: "A Case Study of the Wilcox (Lobo) Trend in Webb and Zapata Counties, Texas," *JPT* (December, 1986) 1355; *Trans.*, AIME, **281.**

Rodgers, J.S., Boykin, R.S., and Coble, L.E.: "Nonstatic Pressure History Analyses for Gas Reservoirs," *SPEJ* (April 1983) 209; *Trans.*, AIME, **275.**

Rose, W.: "Decline-Curve Analyses Revisited," *Math. Geol.* (1990) **22,** No. 8, 1051.

Rymers, D.M., Shobe, E.G., and Yu, J.P.: "Decline-Curve Applications in Oil and Gas Property Evaluation," *Geobyte* (1987) **2,** No. 2, 36.

Saleh, S.T.: "A Model for Development and Analysis of Gas Reservoirs With Partial Waterdrive," paper SPE 18289 presented at the 1988 SPE Annual Technical Conference and Exhibition, Houston, 2–5 October.

Sayyouh, M.H.: "A Modified Model for Estimating Initial and Gas Reservoir Reserves," *Energy Sources* (1990) **12,** No. 1, 65.

Schmidt, S.H., Caudle, B.H., and Miller, M.A.: "Gas-Well Decline Analysis Incorporating Real-Gas Behavior and Non-Darcy Flow," paper SPE 15521 presented at the 1986 SPE Annual Technical Conference and Exhibition, New Orleans, 5–8 October.

Scholes, W.A.: "Maui No. 1 in New Zealand," *Pet. Rev.* (July 1993) **47,** No. 558, 328.

Shagroni, M.A. and Bass, D.M.: "Effect of Formation Compressibility and Edge Water on Gas Field Performance," *Proc.*, 14th Intersociety Energy Conversion Engineering Conference, Boston (1979) **1,** 983.

Shah, R.C.: "Interpreting Gas Well Flow Test—A New Approach," Oil and Natural Gas Commission *Bull.* (December 1982) 19, No. 2, 151–160.

Shariff, A.J.: "An Approach for Determining the Drainage Boundary of the Gas Wells Producing From Low-Permeability Gas Reservoirs," paper SPE 15230 presented at the 1986 SPE Unconventional Gas Technology Symposium, Louisville, Kentucky, 18–21 May.

Sharpe, G.F. and Van Kirk, C.W.: "A Reservoir Engineering Study of an Overpressured, Partial Waterdrive Gas Field in Southern Louisiana," paper SPE 12044 presented at the 1983 SPE Annual Technical Conference and Exhibition, San Francisco, 5–8 October.

Sills, S.R.: "Improved Material-Balance Regression Analysis for Waterdrive Oil and Gas Reservoirs," *SPERE* (May 1996) 127.

Sinha, M.K.: "Estimating Reservoir Abandonment Pressure: A General Guideline," *Pet. Eng. Intl.* (July 1978) **50,** No. 7, 32.

Sippel, M.A. and Levey, R.A.: "Gas Reserve Growth Analysis of Fluvial-Deltaic Reservoirs in the Frio and Vicksburg Formations Located in the Stratton Field, Onshore Texas Gulf Coast," paper SPE 22919 presented at the 1991 SPE Annual Technical Conference and Exhibition, Dallas, 6–9 October.

Smith, R.K., Sawyer, W.K., and Esposito, P.R.: "The Effect of Anisotropy and Vertical Fracture Penetration on Production Decline Curves for Low-

Permeability Gas Wells," paper SPE 10369 presented at the 1981 SPE Eastern Regional Meeting, Columbus, Ohio, 4–6 November.
Soemarso, C.: "The Effects of Production Rates and Some Reservoir Parameters on Recovery in a Strong Waterdrive Gas Reservoir," *Proc.*, Eighth Indonesian Petroleum Assn. Annual Convention, Jakarta (1979), 327.
Spivey, J.P. and Frantz, J.H. Jr.: "History-Matching Production Data Using Analytical Solutions for Linearly Varying Bottomhole Pressure," paper SPE 29167 presented at the 1994 SPE Eastern Regional Meeting, Charleston, West Virginia, 8–10 November.
Spivey, J.P. and Lee, W.J.: "Production Data Analysis for Wells Which Have Been Subject to Periodic Curtailment," paper SPE 26182 presented at the 1993 SPE Gas Technology Symposium, Calgary, 28–30 June.
Spivey, J.P. and Lee, W.J.: "Use of Pseudotime: Wellbore Storage and the Middle-Time Region," paper SPE 15229 presented at the 1986 SPE Unconventional Gas Technology Symposium, Louisville, Kentucky, 18–21 May.
Spivey, J.P. *et al.*: "Integral Type Curves for Advanced Decline-Curve Analysis," paper SPE 24301 presented at the 1992 SPE Mid-Continent Gas Symposium, Amarillo, Texas, 13–14 April.
Spoldi, S.: "Unsteady State Gas Field Deliverability Model," paper CIM 81-32-46 presented at the 1981 Annual Technical Meeting of the Petroleum Soc. of CIM, Calgary, 3–6 May.
Stright, D.H. Jr.: "Decline-Curve Analysis in Fractured Low-Permeability Gas Wells in the Piceance Basin," paper SPE 11640 presented at the 1983 SPE/DOE Symposium on Low Permeability Gas Reservoirs, Denver, Colorado, 13–16 March.
Strubhar, M.K., Strubhar, M.K., and Fitch, J.L.: "Simplified Performance Prediction Method for Vertically Fractured Gas Wells," paper SPE 6021 presented at the 1976 SPE Annual Technical Conference and Exhibition, New Orleans, 3–6 October.
Sullivan, S.A., Poston, S., and Piper, L.D.: "Using Short-Term Pressure Buildup Tests for Reserves Estimation in Tight Gas Reservoirs," paper SPE 17707 presented at the 1988 SPE Gas Technology Symposium, Dallas, 13–15 June.
de Swaan, A: "Development of the Critical Gas Saturation," *JPT* (May 1981) 907.
Sweeney, M.J. and Sites, O.A.: "Integrated Approach to Gas Well Deliverability Analysis, Hugoton Field," *SPEPF* (November 1995) 265.
Syfan, F.E. Jr. and Robinson, B.M.: "Production Analysis and Reservoir Simulation Identify Infill Drilling Potential in Previously Produced Basins," paper SPE 25476 presented at the 1993 SPE Production Operations Symposium, Oklahoma City, Oklahoma, 21–23 March.
Targac, G.W., Wattenbarger, R.A., and Startzman, R.A.: "Analyzing Aquifers Associated With Gas Reservoirs Using AIF's and Type Curves," *SPEFE* (September 1990) 255.
Teumer, P. and Voight, H.D.: "Evaluation of Capacity and Gas-Yield of Low-Porous and Low-Permeable Reservoirs," paper SPE 20950 presented at the 1990 SPE European Petroleum Conference, The Hague, The Netherlands, 21–24 October.
Thompson, J.K.: "Use of Constant-Pressure, Finite-Capacity Type Curves for Performance Prediction of Fractured Wells in Low-Permeability Reservoirs," paper SPE 9839 presented at the 1981 SPE/DOE Low Permeability Gas Reservoirs Symposium, Denver, 27–29 May.
Thrasher, T.S.: "Gas-Well Deliverability Monitoring: Case Histories," *SPEPF* (August 1995) 177.
Tilling, G.M. and Manning, G.E.: "The Rejuvenation of Hewett Field," paper OTC 6118 presented at the 1989 Offshore Technology Conference, Houston, 1–4 May.
Trick, M.D. *et al.*: "Gas Field Deliverability Forecasting: A Coupled Reservoir Simulator and Surface Facilities Model," paper CIM 94-62 presented at the 1994 Annual Technical Meeting of the Petroleum Soc. of CIM, Calgary, 12–15 June.
Ubani, E.A. and Ray, R.M.: "On the Performance of Noncontinuous Tight Gas Sands," paper SPE 17728 presented at the 1988 SPE Gas Technology Symposium, Dallas, 13–15 June.
van Beek, F. and Troost, P.J.P.M.: "Groningen Gas Field: A Case History of a Giant Gas Field," *JPT* (July 1979) 815.
Van Kruijsdijk, C.P.J.W. and Niko, H.: "Alternatives for Draining Tight Naturally Fractured Gas Reservoirs: Horizontal Hole Drilling vs. Massive Hydraulic Fracturing," paper SPE 18339 presented at the 1988 SPE European Petroleum Conference, London, 16–19 October.
Van Nieuwland, A.J.F.M.: "Planning and Design of the Optimum Depletion of the Groningen Gas Field," paper presented at the 1990 Gas Processors' Assn. Convention, Phoenix, Arizona, 12–13 March.
Vik, S.A.: "The Importance of Proper Measurements for Well-Test Analysis of a High-Permeability Gas Reservoir," *Proc.*, Norwegian Inst. of Technology North Sea Oil and Gas Reservoirs Symposium, Graham & Trotman, London (1987).
Vu, T.D., Chen, H.Y., and Poston, S.W.: "Using Short-Term Pressure Buildup Tests To Calculate Gas Reserves," paper SPE 20111 presented at the 1990 SPE Permian Basin Oil and Gas Recovery Symposium, Midland, Texas, 8–9 March.
Wadsley, A.W. and Ferguson, W.I.: "Gas Production Optimization With Emphasis on Southern North Sea Fields," paper presented at the 1988 Offshore Conference and Exhibition Ltd., Aberdeen, 22–24 March.
Walsh, M.P., Ansah, J., and Raghavan, R.: "The New, Generalized Material Balance as an Equation of a Straight Line: Part 1—Applications to Undersaturated, Volumetric," paper SPE 27684 presented at the 1994 SPE Permian Basin Oil and Gas Recovery Conference, Midland, Texas, 16–18 March.
Walsh, M.P., Ansah, J., and Raghavan, R.: "New, Generalized Material Balance as an Equation of a Straight Line: Part 2—Applications to Saturated and Nonvolumetric Reservoirs," paper SPE 27728 presented at the 1994 SPE Permian Basin Oil and Gas Recovery Conference, Midland, Texas, 16–18 March.
Ward, J.S. and Morrow, N.R.: "Capillary Pressures and Gas Relative Permeabilities of Low-Permeability Sandstone," *SPEFE* (September 1987) 345.
Warren, A.: "Alberta's Small Gas-Pool Reserves," *J. Cdn. Pet. Tech.* (July–August 1990) **29**, No. 4, 34.
Wattenbarger, R.A. *et al.*: "Estimating Aquifer Size, Shape, and Flow Properties From Aquifer Influence Functions," *Geobyte* (February 1988) **3**, No. 1, 22.
Weingarten, J.S. and Perkins, T.K.: "Prediction of Sand Production in Gas Wells: Methods and Gulf of Mexico Case Studies," *JPT* (July 1995) 596.
Weinmeister, M.: "Calculating Recoverable Gas-in-Place From Volumetric Data," *Shale Shaker* (May–June 1989) **39**, No. 6, 123.
Wells, J.D. and Amaefule, J.O.: "Capillary Pressure and Permeability Relationships in Tight Gas Sands," paper SPE 13879 presented at the 1985 SPE/DOE Low Permeability Reservoirs Symposium, Denver, 19–22 May.
West, S.L. and Cochrane, P.J.R.: "Reserves Determination Using Type-Curve Matching and EMB Methods in the Medicine Hat Shallow Gas," *SPERE* (May 1995) 82.
Willcox, P.J. and Riley, H.G.: "Performance Matching for a North Sea Gas Field," paper SPE 5535 presented at the 1975 SPE Annual Technical Conference and Exhibition, Dallas, 28 September–1 October.
Wright, B.K. and Hawkes, R.V.: "Case Study Production Optimization Shunda Rundle B Pool," paper SPE 18965 presented at the 1989 SPE Rocky Mountain Regional/Low Permeability Reservoirs Symposium and Exhibition, Denver, 6–8 March.
Yale, D.P. *et al.*: "Application of Variable Formation Compressibility for Improved Reservoir Analysis," paper SPE 26647 presented at the 1993 SPE Annual Technical Conference and Exhibition, Houston, 3–6 October.

Permeability Gas Wells," paper SPE 10369 presented at the 1981 SPE Eastern Regional Meeting, Columbus, Ohio, 4–6 November.

Soemarso, C.: "The Effects of Production Rates and Some Reservoir Parameters on Recovery in a Strong Waterdrive Gas Reservoir," *Proc.*, Eighth Indonesian Petroleum Assn. Annual Convention, Jakarta (1979), 327.

Spivey, J.P. and Frantz, J.H. Jr.: "History-Matching Production Data Using Analytical Solutions for Linearly Varying Bottomhole Pressure," paper SPE 29167 presented at the 1994 SPE Eastern Regional Meeting, Charleston, West Virginia, 8–10 November.

Spivey, J.P. and Lee, W.J.: "Production Data Analysis for Wells Which Have Been Subject to Periodic Curtailment," paper SPE 26182 presented at the 1993 SPE Gas Technology Symposium, Calgary, 28–30 June.

Spivey, J.P. and Lee, W.J.: "Use of Pseudotime: Wellbore Storage and the Middle-Time Region," paper SPE 15229 presented at the 1986 SPE Unconventional Gas Technology Symposium, Louisville, Kentucky, 18–21 May.

Spivey, J.P. *et al.*: "Integral Type Curves for Advanced Decline-Curve Analysis," paper SPE 24301 presented at the 1992 SPE Mid-Continent Gas Symposium, Amarillo, Texas, 13–14 April.

Spoldi, S.: "Unsteady State Gas Field Deliverability Model," paper CIM 81-32-46 presented at the 1981 Annual Technical Meeting of the Petroleum Soc. of CIM, Calgary, 3–6 May.

Stright, D.H. Jr.: "Decline-Curve Analysis in Fractured Low-Permeability Gas Wells in the Piceance Basin," paper SPE 11640 presented at the 1983 SPE/DOE Symposium on Low Permeability Gas Reservoirs, Denver, Colorado, 13–16 March.

Strubhar, M.K., Strubhar, M.K., and Fitch, J.L.: "Simplified Performance Prediction Method for Vertically Fractured Gas Wells," paper SPE 6021 presented at the 1976 SPE Annual Technical Conference and Exhibition, New Orleans, 3–6 October.

Sullivan, S.A., Poston, S., and Piper, L.D.: "Using Short-Term Pressure Buildup Tests for Reserves Estimation in Tight Gas Reservoirs," paper SPE 17707 presented at the 1988 SPE Gas Technology Symposium, Dallas, 13–15 June.

de Swaan, A: "Development of the Critical Gas Saturation," *JPT* (May 1981) 907.

Sweeney, M.J. and Sites, O.A.: "Integrated Approach to Gas Well Deliverability Analysis, Hugoton Field," *SPEPF* (November 1995) 265.

Syfan, F.E. Jr. and Robinson, B.M.: "Production Analysis and Reservoir Simulation Identify Infill Drilling Potential in Previously Produced Basins," paper SPE 25476 presented at the 1993 SPE Production Operations Symposium, Oklahoma City, Oklahoma, 21–23 March.

Targac, G.W., Wattenbarger, R.A., and Startzman, R.A.: "Analyzing Aquifers Associated With Gas Reservoirs Using AIF's and Type Curves," *SPEFE* (September 1990) 255.

Teumer, P. and Voight, H.D.: "Evaluation of Capacity and Gas-Yield of Low-Porous and Low-Permeable Reservoirs," paper SPE 20950 presented at the 1990 SPE European Petroleum Conference, The Hague, The Netherlands, 21–24 October.

Thompson, J.K.: "Use of Constant-Pressure, Finite-Capacity Type Curves for Performance Prediction of Fractured Wells in Low-Permeability Reservoirs," paper SPE 9839 presented at the 1981 SPE/DOE Low Permeability Gas Reservoirs Symposium, Denver, 27–29 May.

Thrasher, T.S.: "Gas-Well Deliverability Monitoring: Case Histories," *SPEPF* (August 1995) 177.

Tilling, G.M. and Manning, G.E.: "The Rejuvenation of Hewett Field," paper OTC 6118 presented at the 1989 Offshore Technology Conference, Houston, 1–4 May.

Trick, M.D. *et al.*: "Gas Field Deliverability Forecasting: A Coupled Reservoir Simulator and Surface Facilities Model," paper CIM 94-62 presented at the 1994 Annual Technical Meeting of the Petroleum Soc. of CIM, Calgary, 12–15 June.

Ubani, E.A. and Ray, R.M.: "On the Performance of Noncontinuous Tight Gas Sands," paper SPE 17728 presented at the 1988 SPE Gas Technology Symposium, Dallas, 13–15 June.

van Beek, F. and Troost, P.J.P.M.: "Groningen Gas Field: A Case History of a Giant Gas Field," *JPT* (July 1979) 815.

Van Kruijsdijk, C.P.J.W. and Niko, H.: "Alternatives for Draining Tight Naturally Fractured Gas Reservoirs: Horizontal Hole Drilling vs. Massive Hydraulic Fracturing," paper SPE 18339 presented at the 1988 SPE European Petroleum Conference, London, 16–19 October.

Van Nieuwland, A.J.F.M.: "Planning and Design of the Optimum Depletion of the Groningen Gas Field," paper presented at the 1990 Gas Processors' Assn. Convention, Phoenix, Arizona, 12–13 March.

Vik, S.A.: "The Importance of Proper Measurements for Well-Test Analysis of a High-Permeability Gas Reservoir," *Proc.*, Norwegian Inst. of Technology North Sea Oil and Gas Reservoirs Symposium, Graham & Trotman, London (1987).

Vu, T.D., Chen, H.Y., and Poston, S.W.: "Using Short-Term Pressure Buildup Tests To Calculate Gas Reserves," paper SPE 20111 presented at the 1990 SPE Permian Basin Oil and Gas Recovery Symposium, Midland, Texas, 8–9 March.

Wadsley, A.W. and Ferguson, W.I.: "Gas Production Optimization With Emphasis on Southern North Sea Fields," paper presented at the 1988 Offshore Conference and Exhibition Ltd., Aberdeen, 22–24 March.

Walsh, M.P., Ansah, J., and Raghavan, R.: "The New, Generalized Material Balance as an Equation of a Straight Line: Part 1—Applications to Undersaturated, Volumetric," paper SPE 27684 presented at the 1994 SPE Permian Basin Oil and Gas Recovery Conference, Midland, Texas, 16–18 March.

Walsh, M.P., Ansah, J., and Raghavan, R.: "New, Generalized Material Balance as an Equation of a Straight Line: Part 2—Applications to Saturated and Nonvolumetric Reservoirs," paper SPE 27728 presented at the 1994 SPE Permian Basin Oil and Gas Recovery Conference, Midland, Texas, 16–18 March.

Ward, J.S. and Morrow, N.R.: "Capillary Pressures and Gas Relative Permeabilities of Low-Permeability Sandstone," *SPEFE* (September 1987) 345.

Warren, A.: "Alberta's Small Gas-Pool Reserves," *J. Cdn. Pet. Tech.* (July–August 1990) **29,** No. 4, 34.

Wattenbarger, R.A. *et al.*: "Estimating Aquifer Size, Shape, and Flow Properties From Aquifer Influence Functions," *Geobyte* (February 1988) **3**, No. 1, 22.

Weingarten, J.S. and Perkins, T.K.: "Prediction of Sand Production in Gas Wells: Methods and Gulf of Mexico Case Studies," *JPT* (July 1995) 596.

Weinmeister, M.: "Calculating Recoverable Gas-in-Place From Volumetric Data," *Shale Shaker* (May–June 1989) **39,** No. 6, 123.

Wells, J.D. and Amaefule, J.O.: "Capillary Pressure and Permeability Relationships in Tight Gas Sands," paper SPE 13879 presented at the 1985 SPE/DOE Low Permeability Reservoirs Symposium, Denver, 19–22 May.

West, S.L. and Cochrane, P.J.R.: "Reserves Determination Using Type-Curve Matching and EMB Methods in the Medicine Hat Shallow Gas," *SPERE* (May 1995) 82.

Willcox, P.J. and Riley, H.G.: "Performance Matching for a North Sea Gas Field," paper SPE 5535 presented at the 1975 SPE Annual Technical Conference and Exhibition, Dallas, 28 September–1 October.

Wright, B.K. and Hawkes, R.V.: "Case Study Production Optimization Shunda Rundle B Pool," paper SPE 18965 presented at the 1989 SPE Rocky Mountain Regional/Low Permeability Reservoirs Symposium and Exhibition, Denver, 6–8 March.

Yale, D.P. *et al.*: "Application of Variable Formation Compressibility for Improved Reservoir Analysis," paper SPE 26647 presented at the 1993 SPE Annual Technical Conference and Exhibition, Houston, 3–6 October.

ISBN 1-55563-084-7